Juan Rodríguez-Hernández ·
Aitziber L. Cortajarena *Editors*

# Design of Polymeric Platforms for Selective Biorecognition

Springer

# Design of Polymeric Platforms for Selective Biorecognition

Juan Rodríguez-Hernández • Aitziber L. Cortajarena
Editors

# Design of Polymeric Platforms for Selective Biorecognition

Springer

*Editors*
Juan Rodríguez-Hernández
Institute of Polymer Science & Technology
Madrid
Spain

Aitziber L. Cortajarena
IMDEA Nanociencia and CNB-CSIC-
IMDEA Nanociencia Associated Unit
"Unidad Nanobiotecnología"
Madrid
Spain

ISBN 978-3-319-17060-2 ISBN 978-3-319-17061-9 (eBook)
DOI 10.1007/978-3-319-17061-9

Library of Congress Control Number: 2015935637

Springer Cham Heidelberg New York Dordrecht London


Printed on acid-free paper

Springer International Publishing AG Switzerland is part of Springer Science+Business Media (www.springer.com)

# Contents

# Contributors

**Maria Askildsen** Queensland Micro- and Nanotechnology Centre, Griffith University, Nathan, QLD, Australia

School of Engineering (Environmental), Griffith University, Nathan, QLD, Australia

**Daniel Citterio** Department of Applied Chemistry, Keio University, Kohoku-ku, Yokohama, Japan

**Robert C. Collins** Physical Sciences Department, Esatern Connecticut State University, Willimantic, CT, USA

**Aitziber L. Cortajarena** Instituto Madrileño de Estudios Avanzados en Nanociencia (IMDEA-Nanociencia), CNB-CSIC-IMDEA Nanociencia Associated Unit Unidad de Nanobiotecnología, Madrid, Madrid, Spain

**Guillaume Delaittre** Institute of Toxicology and Genetics, Karlsruhe Institute of Technology, Eggenstein-Leopoldshafen, Hermann-von-Helmholtz-Platz 1, Germany

Institute for Chemical Technology and Polymer Chemistry, Karlsruhe Institute of Technology, Karlsruhe, Engesserstrasse 18, Germany

**Nicolas Delorme** Department of Physics, IMMM—Université du Maine, Le Mans, France

**Ehsan Eftekhari** Queensland Micro- and Nanotechnology Center and School of Engineering, Griffith University, Nathan, QLD, Australia

**Nikolaj Gadegaard** Division of Biomedical Engineering, School of Engineering, University of Glasgow, Glasgow, UK

**Róbert E. Gyurcsányic** Department of Inorganic and Analytical Chemistry, MTA-BME "Lendület" Chemical Nanosensors Research Group, Budapest University of Technology and Economics, Budapest, Hungary

**Terence G. Henares** Department of Applied Chemistry, Keio University, Kohoku-ku, Yokohama, Japan

**I-Chi Lee** Graduate Institute of Biochemical and Biomedical Engineering, Chang Gung University, Kwei-Shan, Tao-Yuan, Taiwan

**Kin Fong Lei** Graduate Institute of Medical Mechatronics, Chang Gung University, Kwei-Shan, Tao-Yuan, Taiwan 333

Department of Mechanical Engineering, Chang Gung University, Kwei-Shan, Tao-Yuan, Taiwan

**Tim C. Lei** Department of Electrical Engineering, University of Colorado Denver, Denver, USA

**Qin Li** Queensland Micro- and Nanotechnology Centre, Griffith University, Nathan, QLD, Australia

School of Engineering (Environmental), Griffith University, Nathan, QLD, Australia

**Serena Molina** Macromolecular Department, Institute of Polymer Science and Technology (ICTP-CSIC), Madrid, Spain

**Alexandra Muñoz-Bonilla** Departamento de Química-Física Aplicada, Facultad de Ciencias, Universidad Autónoma de Madrid, Madrid, Spain

**Rodrigo Navarro** Macromolecular Department, Institute of Polymer Science and Technology (ICTP-CSIC), Madrid, Spain

**Rasmus H. Pedersen** Division of Biomedical Engineering, School of Engineering, University of Glasgow, Glasgow, UK

**Mónica Pérez-Perrino** Glycosystems Laboratory, Instituto de Investigaciones Químicas (IIQ), CSIC-Universidad de Sevilla, Seville, Spain

**Paul M. Reynolds** Division of Biomedical Engineering, School of Engineering, University of Glasgow, Glasgow, UK

**Juan Rodríguez-Hernández** Department of Chemistry and Properties of Polymers, Institute of Polymer Science and Technology (ICTP-CSIC), Madrid, Spain

**Frieder W. Scheller** Fraunhofer Institute for Biomedical Engineering IBMT, Potsdam, Germany

**John M. Stormonth-Darling** Division of Biomedical Engineering, School of Engineering, University of Glasgow, Glasgow, UK

**Koji Suzuki** Department of Applied Chemistry, Keio University, Kohoku-ku, Yokohama, Japan

**Kentaro Yamada** Department of Applied Chemistry, Keio University, Kohoku-ku, Yokohama, Japan

**Aysu Yarmana** Institute of Biochemistry and Biology, University of Potsdam, Potsdam, Germany

# Chapter 1
# Selective Biorecognition on Polymer Surfaces: General Issues

**Juan Rodríguez-Hernández and Aitziber L. Cortajarena**

## 1.1 Biorecognition: Few Concepts

Biorecognition, or molecular recognition, can be defined as the process in which biological molecules interact. This process is the basis of all biological interactions and therefore a key to sustain living systems. In spite of the paramount importance of these processes, the answers of many questions are still unresolved, as illustrated by Wilchek et al. [1]. For instance, how proteins can recognize other proteins, how receptors recognize specific ligands, or how antibodies recognize antigens has been the center of multiple studies but some of the molecular mechanisms of those interactions are not fully clear yet. The large amount of work developed in understanding biorecognition processes have been realized from different points of view. While several groups attempted to focus on protein–protein or protein–ligand interactions from a biophysical and structural perspective, others focused on complex interaction networks involved in signal transduction pathways both in vivo and in vitro. Equally, protein–nucleic acid, protein–carbohydrate, protein–lipid, and even protein–solvent interactions have been investigated extensively. In spite of the multiple aspects that need further research, several aspects are currently understood and will be briefly described within this section.

Two key aspects of the biomolecular interactions are the binding *affinity* and the *specificity*. On the one hand, the *affinity* defines how tight is the interaction between two specific biological molecules and is characterized by a particular binding energy. The latter can be calculated by the combination of all the forces that contribute

J. Rodríguez-Hernández (✉)
Department of Chemistry and Properties of Polymers, Institute of Polymer Science and Technology (ICTP-CSIC), Juan de la Cierva 3, 28006 Madrid, Madrid, Spain
e-mail: rodriguez@ictp.csic.es

A. L. Cortajarena
Instituto Madrileño de Estudios Avanzados en Nanociencia (IMDEA-Nanociencia), CNB-CSIC-IMDEA Nanociencia Associated Unit Unidad de Nanobiotecnología, Cantoblanco, 28049 Madrid, Madrid, Spain
e-mail: aitziber.lopezcortajarena@imdea.org



J. Rodríguez-Hernández, A. L. Cortajarena (eds.), *Design of Polymeric Platforms for Selective Biorecognition,* DOI 10.1007/978-3-319-17061-9_1

**Table 1.1** Range of binding affinities in biomolecular interactions

| Biomolecular interaction | Interaction type | Binding affinity (Kd) (M) |
|---|---|---|
| Avidin–biotin | Protein–small molecule | $10^{-15}$ |
| Antibody–Antigen | Protein–epitope (peptides, sugars, phospholipids, small molecules) | $<10^{-7}$ |
| Aptamer–cocaine | DNA–small molecule | $10^{-6}$ |
| DNA–DNA | DNA–DNA | $10^{-7}$ (10 base pairs) |
| Glucose–concanavalin A | Protein–sugar | $10^{-3}$ |
| Integrins–RGD and GFOGER sequences | Protein–peptide | $10^{-5}$–$10^{-3}$ |

to a defined interaction. Biomolecular interactions present a wide range of binding affinities. The binding affinity constant (Kd) inversely related to the affinity can range from fM-pM in the systems with higher binding affinity such as enzyme–substrate complexes, biotin–avidin system to mM affinities in weak interactions usually related with transient complexes. Table 1.1 shows representative examples of the wide range of binding affinities in natural systems.

On the other hand, the binding *specificity* can be defined as the selectivity of one molecule for a ligand in preference to related ligand molecules. Binding specificity is fundamental for the maintenance of the balance of interactions within living systems. For instance, the cellular milieu is a complex media where many molecules are present; therefore, the binding specificity of the different elements is critical for the balance of the molecular interactions networks that preserve the cell homeostasis.

In a complex cell system, both the binding affinity and the binding specificity, together with the concentration of the different components of a simple interaction network, play interrelated roles that affect the final outcome.

For example, molecule A can bind in the same binding site either molecule X or molecule Y with a 100 times higher affinity for the molecule X (Kd 1 μM) (Fig. 1.1). One can encounter different situations just by changing the concentration of the two ligand molecules in the environment in which: (1) the A molecules only bind molecule at equal concentrations of X and Y X; (2) the A molecules bind equally X and Y when the concentration of Y is 100 times the concentration of X; (3) the A molecule binds only molecule Y, even when the molecule A is more specific for X molecule if there is large excess of the molecule Y compared to X. This example illustrates the different regulation levels to modulate the complex biorecognition interactions. Additional complexity might be incorporated by allosteric effects in which the binding of one ligand to a site results in a conformational change in the target molecule that modulates its affinity for a second ligand molecule.

In addition to the two important considerations described above, the understanding of biorecognition interactions requires the evaluation of the nature of the interactions. In effect, biorecognition is based on a variety of non-covalent interactions and on the structure of the biomolecules. Non-covalent interactions can include H-bonds, dipolar interactions, electrostatic interactions, hydrophobic interactions,

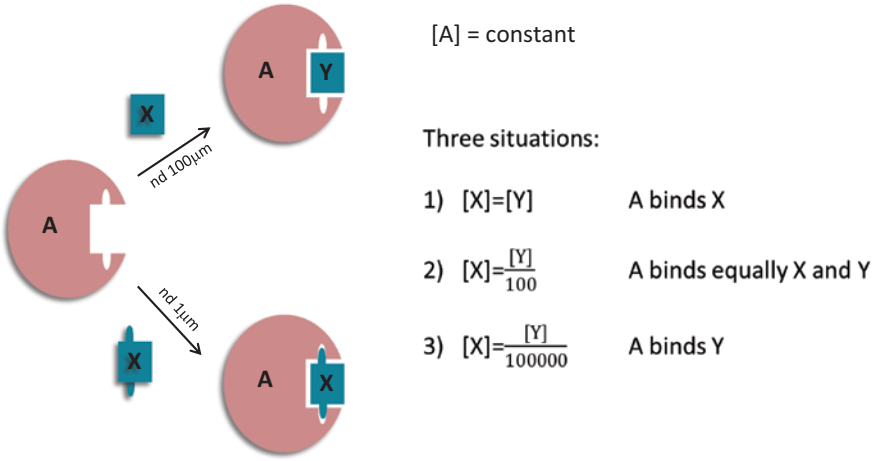


**Fig. 1.1** Biorecognition binding affinity and specificity. Molecule *A* binds two ligands *X* and *Y* with different affinities: Kd of 1 μM for molecule *X* and 100 μM for molecule *Y*. Even though the molecule *A* has significantly tighter affinity for molecule *X*, the fraction of *A* molecules bound to *X* or *Y* can change completely depending on the relative concentrations of the ligand molecules

van der Waals forces, cation–π interactions, and π–π stacking. Moreover, usually the biorecognition processes are driven by a combination of a large number of different weak interactions between two molecules. Those interactions are therefore complex to predict, even if the energetics of the individual components is known. In addition to non-covalent interactions, shape complementarity has been evidenced to also take part in biorecognition processes [2].

Biorecognition interactions can be on one hand transient and very dynamic; usually these interactions are involved in regulatory processes in cells. On the other hand, these interactions can be very tight such as the interactions that hold the two strands of the DNA double helix together, even though it can also be opened by proteins such as helicases that break the H-bonds between the DNA strands. In general, biomolecular interactions are regulated by a subtle balance between many interactions.

The interactions exhibited between two biomolecules can also be defined as *dynamic or static* (Fig. 1.2). In *static interactions* the two molecules bind without a conformational change of any of the components. In this type of interactions the recognition site is shaped to specifically recognize a molecule, or molecules. *On the contrary, dynamic interactions* are more complicated and can comprise a variety of recognition modes. The common aspect is that the molecular recognition includes a conformation change. This can be a simple rearrangement of a binding pocket to accommodate the ligand or can be a more complex allosteric effect in which the binding of the first ligand to one binding site induces a structural change that affects the association of a second ligand to the same or another binding site. These allosteric effects can be positive, negative, double, triple, and include all the range of potential combinations.

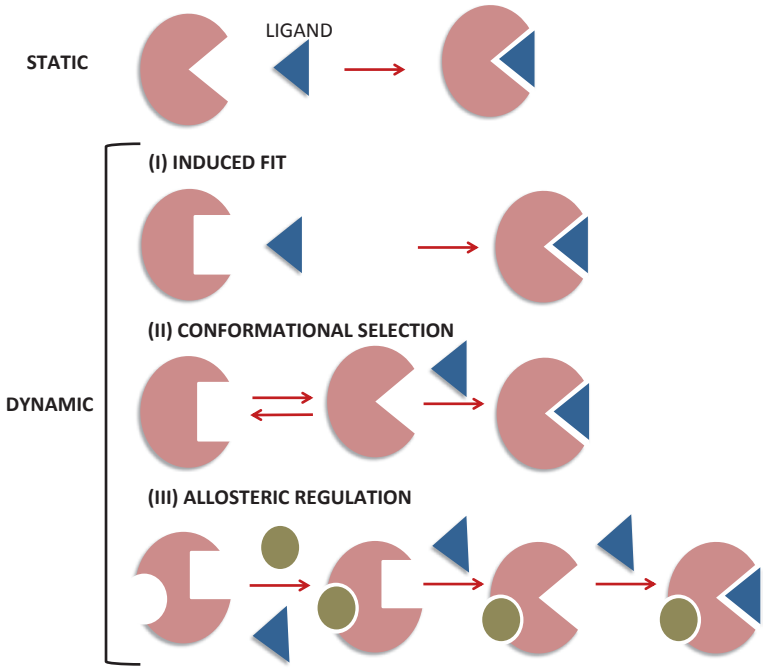


**Fig. 1.2** Schematic representation of static and dynamic recognition mechanisms

Here we want to present the fact that biomolecular recognition can be as simple as the recognition between two base pairs, which occurs in the DNA to a very complicated system that can lead to complex molecular machines made of multiple components such as the bacterial flagellar motor [3]. Nowadays and thanks to many years of research in the field of biomolecular interactions, studying the biophysics and the structural basis of countless interactions, we have started to unravel the great complexity of biorecognition.

## 1.2 Biorecognition Plays a Key Role in Living Systems

The complexity of biorecognition as mentioned before is all encoded in the natural living systems. Biorecognition is mediated for an array of different biomolecules, including nucleic acids, proteins, sugars, lipids, and small biomolecules. Therefore, all the cellular functions rely on biorecognition events. More over on the balance of many biorecognition events that take place at the same time in the intracellular environment and are all interrelated in a delicate equilibrium.

For example during the protein biosynthesis inside cells, the different amino acids are linked in a sequence to form protein chains that fold with a define structure that will encode a specific function. This complex process is carried out by the

**Fig. 1.3** *C. elegans* interactome map, showing 5500 protein interactions among 3000 proteins. Each *dot* represents a protein and each *line* between them represents a protein–protein interaction [6]

ribosome, a large biomolecule inside the cells composed at the same time by many ribosomal proteins and ribosomal nucleic acid (rRNA). The ribosomes recognize the messenger RNA sequence and translate it into a protein sequence. For this translation process the ribosome has to recognize in a concerted way many different molecules including coding mRNA, aminocyl tRNA molecules that carry the different amino acids, ATP molecules that provide energy, and different regulatory proteins such as initiation factors [4, 5].

Biorecognition processes vary in complexity and thus the investigation of such processes can be difficult. For instance, to illustrate this complexity we show a map of the protein–protein interaction network, or interactome of a simple multicellular organism, the worm *Caenorhabditis elegans* (Fig. 1.3). The figure shows the large number of potential interactions and the multiple interaction partners for each protein. In addition to the evident complexity of those biological networks of interactions, there is an extra level of complexity encoded by different binding affinities and specificities and the dynamics of those interactions.

The complexity of all biomolecular interactions in a single cell, considering not only proteins but also nucleic acids, sugars, lipids, and small molecules, is enormous, and the failure of one of these interactions might cause severe diseases, even death.

## 1.3 Application of Biorecognition to Synthetic Systems

Due to the large array of biorecognition interactions in vivo, we can take advantage of a broad range of to generate synthetic complex systems with defined properties. More precisely, natural biorecognition interactions can be selected based on the specific needs in terms of affinity, specificity, modularity, and dynamics of the interaction needed. In addition, different biomolecules also give a selection window for experimental conditions in terms of temperature, pH, and osmolarity in

which the selected interaction is stable. Finally, the key features of the biomolecular interactions can be modulated by design to generate biorecognition systems with optimized properties for particular applications [7–12].

The development of synthetic components with molecular recognition capabilities is a current center of interest for many different targets. As will be depicted throughout this book, biomolecular scaffolds with molecular recognition elements, i.e., those employed in synthetic approaches, can be classified in four different types: proteins and peptides, nucleic acids, small organic molecules, and synthetic polymers [13]. Special scientific attention is currently being paid to these systems, and the technology of producing and improving novel molecular recognition elements is rapidly evolving [14–17]. As a result, today, specific biorecognition molecules have been adapted in different synthetic devices for different applications, including diagnostic testing and biosensing. In addition, such systems have been employed for therapeutic purposes by assisting drug delivery or modulating genetic expression [18–20].

## 1.4 Biorecognition at Surfaces

The biorecognition in biological systems is mostly in solution, but within the living systems there are many key recognition events that take place on immobilized systems such as the 2D biological membranes. The particular effects on biorecognition of immobilized systems need to be considered for the successful applications of those systems. For example, one key problem of biorecognition on surfaces is the establishment of efficient mass transport between the bulk solution with the ligand and the surface with the recognition moiety. If the mass transfer is not efficient, a concentration gradient of the ligand will be generated in the solution. This effect needs to be considered for each system and will depend on the interaction affinity, the number of binding sites on the surface, and the concentration of the ligand in solution [21, 22].

Another limitation that would apply only for kinetic studies is the deviation from first order biding kinetics observed in the surface binding processes. These deviations might be due to the heterogeneity of the immobilized binding sites and their orientation on the surface [23]. The density of binding sites immobilized on the surfaces is also critical and should be considered when using biorecognition on surfaces. High density of the ligands might induce avidity effects when multivalent ligands are used. The avidity of a multivalent interaction is the accumulated affinity of different interactions, and can be considered as a functional affinity. Avidity can be a problem to avoid, or an advantage to be used to convert a low affinity interaction into a high avidity one.

## 1.5 About this Book

Within this context, this book aims to provide a general overview of the strategies that can be employed to prepare micro- and nanostructured polymeric substrates with biorecognition capabilities. In addition, we illustrate biorecognition processes occurring on surfaces, their particular features, and their potential applications.

Chapter 2 establishes the criteria from the point of view of the design of a particular platform introducing the major strategies that are discussed further in detail throughout the different chapters.

Chapter 3 focuses on the description of the molecules that can be incorporated into the platforms, and the basis of the distinct molecular biorecognition processes, including the development of affinity and specificity. This chapter establishes the basis for a knowledge-based selection of biorecognition molecules tailored for the different applications.

Chapter 4 describes the chemical approaches that can be followed to anchor biomolecules to polymeric surfaces. In effect, chemical and physical approaches to modify polymeric surfaces to immobilize biomolecules are thoroughly described.

The following chapters are devoted to the fabrication of different structures and simultaneously biofunctionalization of such polymer surfaces in view of their use in biorecognition processes. In this concern, Chap. 5 introduces the preparation of gradient polymeric surfaces. In these surfaces, a particular variable varies gradually from one extreme to the opposite of the material. Micro/nanoscale structuration, chemical functionality or surface mechanical properties are aspects that will be discussed in detail. Finally, this chapter describes how these materials can be fabricated in view of use in applications such as cell sensing.

Chapters 6 and 7 explore two closely related strategies to pattern polymer surfaces with micro- and nanometer scale resolution. On the one hand, Chap. 6 focuses on the description of the polymer replication techniques in which a master stamp is brought into contact with the polymer; as a result of the pressure applied, the polymer adopts the form imposed by the stamp. On the other hand, Chap. 7 describes the lithographic approaches including conventional lithography and nonconventional (soft lithography or printing processes) lithography, electron beam lithography, and focused ion beam that allows the preparation of surfaces with topographies at the nanoscale.

Inkjet printing that enables the precise deposition of very small droplets of liquids in a well-defined and user-controlled position of a particular substrate is depicted in Chap. 8. More precisely, in this chapter, the preparation of biorecognition surfaces by immobilization of DNAs, enzymes, or antibodies of various polymeric surfaces with high precision is analyzed.

Porous interfaces with controlled pore distribution and size have also been employed for biorecognition purposes. In Chap. 9, a particular approach to prepare porous surfaces with pores sizes ranging between 20 nm and 20 μm is described. The approach employed, known as Breath Figures, also permits the control over the

chemical composition of the pores and thus the precise immobilization of biomolecules with biorecognition capabilities.

Chapter 10 describes the preparation of polymer brushes, i.e., the immobilization (covalent or not) of polymer chains onto surfaces. Polymer brushes can be designed to include different biorecogntion sites such as RGD or GFOGER sequences that enable the protein recognition. Moreover, cell adhesion and immobilization of proteins is reviewed.

Using microfluidic systems with functional patterned surfaces is also an interesting strategy to construct polymeric platforms with final recognition capabilities. Microfluidic devices have great potential to be widely used as a great diagnostic technique of many diseases, especially in remote areas where well-equipped biochemical labs and trained technicians are generally not available. A detailed description of microfluidic systems is provided in Chap. 11.

Colloidal structures arranged on polymeric surfaces can serve to create different surface patterns. In Chap. 12, apart from the description of the fundamentals of formation of colloidal templates, a large number of the patterns analyzed involve biomolecules that can be precisely distributed.

Chapters 13 and 14 are devoted to sophisticated systems to obtain biorecognition platforms. Chapter 13 resorts to the preparation of a 3D polymeric structure prepared by using a target analyte acting as template, i.e., the so-called molecular imprinting. Upon copolymerization of the monomer mixture, the removal of the analyte provides binding sites which are complementary in size and shape to the analyte and thus allow their rebinding. This strategy, in comparison with other approaches, provides not only the selectivity due to the chemical functionality but also shape selectivity. Chapter 14 focuses on the tip-based strategies to finely control the deposition of biomolecules using an atomic force microscopy (AFM) tip. This nanofabrication approach, also known as tip-based nanofabrication, is described in detail in three variations: dip-pen nanolithography, nanoshaving, and nanografting.

Finally, Chapter 15 presents an overview of the major issues that remain unresolved as well as the future trends for the development of more performant polymer surfaces with biorecognition capabilities. In particular, biocompatibility of the interfaces, stability as well as binding specificity are current challenges that require further investigation.

## References

1. Wilchek, M.; Bayer, E.A.; Livnah, O. Essentials of biorecognition: The (strept)avidin–biotin system as a model for protein–protein and protein–ligand interaction. *Immunology Letters* **2006**, *103*, 27–32.
2. Williams, D.H.; Stephens, E.; O'Brien, D.P.; Zhou, M. Understanding noncovalent interactions: Ligand binding energy and catalytic efficiency from ligand-induced reductions in motion within receptors and enzymes. *Angewandte Chemie-International Edition* **2004**, *43*, 6596–6616.
3. Lee, L.K.; Ginsburg, M.A.; Crovace, C.; Donohoe, M.; Stock, D. Structure of the torque ring of the flagellar motor and the molecular basis for rotational switching. *Nature* **2010**, *466*, 996–1000.

4. Nierhaus, K.H.; Wilson, D. *Protein synthesis and ribosome structure*. Wiley: 2004.
5. Rodnina, M.V.; Wintermeyer, W.; Green, R. *Ribosomes structure, function, and dynamics: Structure, function, and dynamics*. Springer: 2011.
6. Blow, N. Systems biology: Untangling the protein web. *Nature* **2009**, *460*, 415–418.
7. Levy, M.; Ellington, A.D. Directed evolution of streptavidin variants using in vitro compartmentalization. Chemistry & Biology 2008, 15, 979–989.
8. Adams, J.; Nelson, B.; Sidhu, S. Recombinant genetic libraries and human monoclonal antibodies. In Human monoclonal antibodies, Steinitz, M., Ed. Humana Press: 2014; Vol. 1060, pp 149–170.
9. Grove, T.Z.; Cortajarena, A.L.; Regan, L. Ligand binding by repeat proteins: Natural and designed. Current Opinion in Structural Biology 2008, 18, 507–515.
10. Schreiber, G.; Fleishman, S.J. Computational design of protein–protein interactions. *Current Opinion in Structural Biology* **2013**, *23*, 903–910.
11. Grigoryan, G.; Reinke, A.W.; Keating, A.E. Design of protein-interaction specificity gives selective bzip-binding peptides. *Nature* **2009**, *458*, 859–864.
12. Schueler-Furman, O.; Wang, C.; Bradley, P.; Misura, K.; Baker, D. Progress in modeling of protein structures and interactions. *Science* **2005**, *310*, 638–642.
13. Zhao, M.; Wu, T.; Xiao, X.; Liu, Y.; Su, X. New advances in molecular recognition based on biomolecular scaffolds. *Analytical and Bioanalytical Chemistry* **2013**, *405*, 5679–5685.
14. Thomas, J.R.; Hergenrother, P.J. Targeting rna with small molecules. *Chemical Reviews* **2008**, *108*, 1171–1224.
15. Vendrell, M.; Zhai, D.; Er, J.C.; Chang, Y.-T. Combinatorial strategies in fluorescent probe development. *Chemical Reviews* **2012**, *112*, 4391–4420.
16. Bui, B.T.S.; Haupt, K. Molecularly imprinted polymers: Synthetic receptors in bioanalysis. *Analytical and Bioanalytical Chemistry* **2010**, *398*, 2481–2492.
17. Haupt, K. Biomaterials plastic antibodies. *Nature Materials* **2010**, *9*, 612–614.
18. Holliger, P.; Hudson, P.J. Engineered antibody fragments and the rise of single domains. *Nature Biotechnology* **2005**, *23*, 1126–1136.
19. Keefe, A.D.; Pai, S.; Ellington, A. Aptamers as therapeutics. *Nature Reviews Drug Discovery* **2010**, *9*, 537–550.
20. Reichert, J.M. Antibody-based therapeutics to watch in 2011. *Mabs* **2011**, *3*, 76–99.
21. Gervais, T.; Jensen, K.F. Mass transport and surface reactions in microfluidic systems. *Chemical Engineering Science* **2006**, *61*, 1102–1121.
22. Schuck, P.; Zhao, H. The role of mass transport limitation and surface heterogeneity in the biophysical characterization of macromolecular binding processes by spr biosensing. In *Surface plasmon resonance*, Mol, N.J.; Fischer, M.J.E., Eds. Humana Press: 2010; Vol. 627, pp 15–54.
23. Svitel, J.; Boukari, H.; Van Ryk, D.; Willson, R.C.; Schuck, P. Probing the functional heterogeneity of surface binding sites by analysis of experimental binding traces and the effect of mass transport limitation. *Biophysical Journal* **2007**, *92*, 1742–1758.

# Chapter 2
# Patterning and Functionalization of Polymeric Surfaces

**Juan Rodríguez-Hernández**

## 2.1 Introduction

The design of polymeric biointerfaces is crucial since interfaces [1] are directly involved in the connection of a synthetic material and a particular biomolecule, microorganism, or cell. A large amount of work has been carried out in order to identify those aspects that need to be considered during the surface design. As a result of this effort, today it is generally admitted that parameters such as topology, surface morphology, physical structure, chemical and biological composition as well as their particular distribution on the surface play a key role on the interaction with the biological environment.

In spite of the limited complexity that can be achieved in synthetic materials in comparison with the intricate features found in nature and that can hardly be mimicked from a synthetic point of view, several innovative and challenging concepts have been developed in the materials design. Recent advances include the preparation of nanoscale patterns in a controlled manner or the precision obtained by the surface modification approaches that, among others, allow the selective and sensitive detection [2–5]. Within this context, the aim of this chapter is to introduce and provide a general overview over the polymer surface characteristics that can be modified from a synthetic point of view in order to fabricate materials with biorecognition capabilities. The first section of this chapter will summarize the key features required for an engineered material to exhibit recognition and specificity in their interactions. The following sections will briefly introduce the main approaches to both functionalize and pattern polymer interfaces focusing on the most recent advances. It is out of the scope of this chapter to exhaustively cover the technologies but rather present the alternatives that will be developed in the corresponding chapters.

J. Rodríguez-Hernández (✉)
Chemistry and Properties of Polymeric Materials Department, Institute of Polymer Science and Technology (ICTP-CSIC), Madrid, Spain
e-mail: rodriguez@ictp.csic.es



J. Rodríguez-Hernández, A. L. Cortajarena (eds.), *Design of Polymeric Platforms for Selective Biorecognition,* DOI 10.1007/978-3-319-17061-9_2

## 2.2 Surface Design of Materials that Interact with Biological Systems

Even if it is already 20 years old, Ratner's work counts among the pioneers in the engineering of biomaterials with recognition and specificity. The base was already established at that time but some issues still remain [6]. In their work, Ratner reported the criteria that a material need to satisfy in order to be of potential interest in biorelated applications. These criteria included the design of receptor-based recognition reactions, the appropriate characterization of the material, the presence of recognition sites with high specificity, or the absence of nonspecific interactions. In addition, the materials employed should be reasonably robust (sterilizable and storable) and should be manufacturable in view of a commercial development.

Polymers are excellent candidates as biomaterials for different reasons. First, they can be manufacturable and exhibit a wide variety of mechanical properties from rigid to rather soft thus being adaptable to the final material application. In addition, they can be robust and can be sterizable and storable. Finally, as depicted below, commercially available inert polymeric materials can be functionalized in multiple ways thus providing a wide range of opportunities to finely tune the surface chemistry. For instance, the immobilization of a biomolecule to the surface of a polymer has been evidenced to provide specificity to biomaterials [7]. Proteins, active peptide sequences, carbohydrates, and DNA have been either covalently or non-covalently anchored to polymer surfaces. Moreover, different approaches can be employed to prepare surfaces that inhibit nonspecific interactions, for instance by modifying the surface with fluoropolymers, silicones, hydrogels, or poly(ethylene oxide) among others [8].

Equally, the rapid advances in the field of microtechnology and nanotechnology have constantly overcome the limits of the patterning techniques and permit the structuration of surfaces at the nanometer scale. Precise patterning of biomolecules on surfaces with nanometer resolution is currently a center of interest in view of its potential use in a wide variety of applications such as molecular diagnostics or the fabrication of nanobiochips and nanobiosensors but also may offer unique opportunities to perform fundamental studies in molecular and cell biology.

In summary, as depicted by Alves et al. [9], the great versatility of polymer surfaces allows us to prepare surfaces with a variable chemical composition, properties, and processing techniques. As a consequence, there are multiple available techniques that permit to vary the spatial arrangement of chemical and topographic moieties (Fig. 2.1). We can distinguish between changes perpendicular to the surface (i.e., the *Z*-direction) or in the surface plane (*X*–*Y* direction). Variations perpendicular to the surface include the treatments to vary the topography of the interface either increasing the surface roughness (i.e., patterning with random structural motifs) or patterning in an ordered manner introducing regular motifs. In addition to variations on the surface topography the surface chemical composition can be equally modified by using different methodologies. Hence, layer by layer deposition, attachment of chemical or biochemical compounds or grafting macromolecules with smart capabilities or including biomolecules are among the methods employed to modify the surface chemical composition (see following sections).

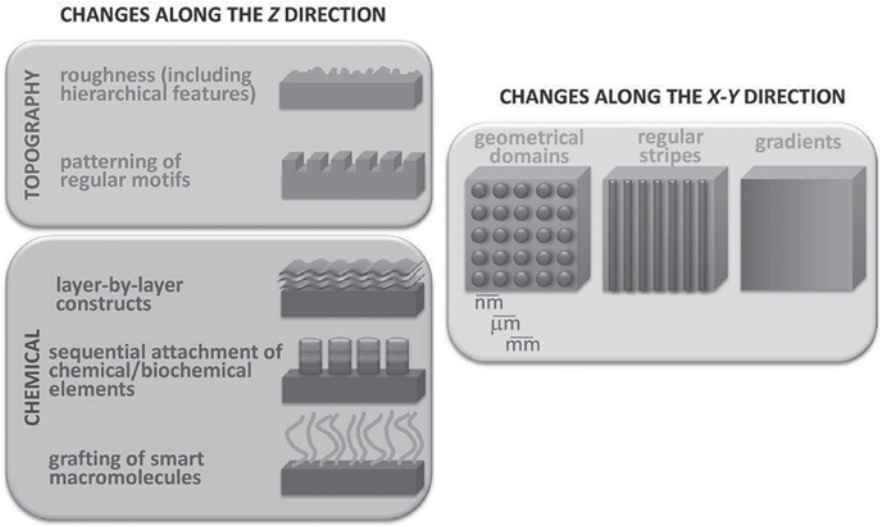


**Fig. 2.1** Possibilities to vary both surface morphology and chemistry of polymer surfaces by producing changes either on the *Z* or the *X*–*Y* direction. (Reproduced with permission from [9])

Besides, changes can be introduced along the *X*–*Y* direction, i.e., precise distribution of both the topographical motifs and functional molecules on the surface plane at different length scales ranging from nanometers to millimeters or even the formation of gradient polymer surfaces.

This chapter will then be devoted to introduce of the approaches existing in order to chemically modify polymer surfaces and also to provide a short overview over the most significant methodologies that are available to control the topography and the surface distribution of the biomolecules. These aspects are the center of this book and will be thoroughly discussed in the corresponding chapters.

## 2.3 Specific Functionalization of Surfaces and Precision Immobilization

The surface of a particular template, in order to be employed in biorelated applications, requires the control of the surface chemical composition. In general, commercially available polymeric materials are hydrophobic and usually inert. This limits their use since, even though the bulk properties are the appropriate biological processes need of particular interfaces. Moreover, the most basic approach that synthesizes surfaces exhibiting specificity and recognition involves immobilization of biological molecules at the surface of a biomaterial [6].

General approaches to modify the surface of a polymer are depicted in Fig. 2.2. In general, independent of the approach employed, three different steps are required. The first step is related to the selection of a particular polymer depending

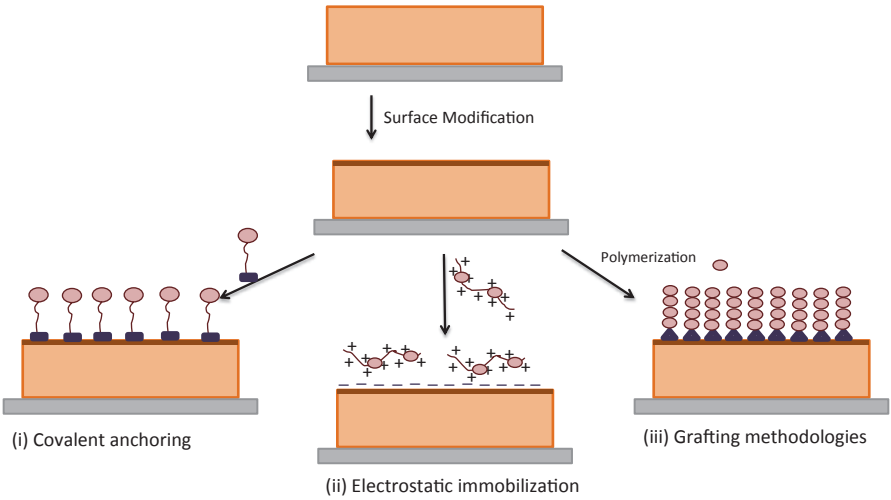


**Fig. 2.2** Illustrative approaches to immobilize bioactive compounds (BACs) using **(i)** covalent anchoring, **(ii)** electrostatic immobilization of polyelectrolytes, or **(iii)** grafting from the surface functional groups

on the mechanical properties searched that depends, in turn, on the final use of the material. Provided that the polymer has the required mechanical properties, the surface requires an additional functionalization step. Finally, the functional groups created at the surface are employed to anchor the bioactive compound (BAC) using different alternatives. Among others, Fig. 2.2 describes the use of organic chemistry to covalently anchor the compound, the immobilization by means of electrostatic interactions or the use of grafting-from polymerization techniques.

There is a broad literature devoted to the different approaches that can be employed to immobilize BACs [1, 9–25]. It is outside of the scope of the chapter to include an exhaustive summary of the approaches reported but we aim rather to provide a general overview of this field focusing on those methods that are currently most extended.

### *2.3.1 Surface Treatments to Chemically Modify the Polymer Interface*

Initial methods of surface functionalization focused on the increase of, among others, wettability and adhesion of hydrophobic interfaces. Among these approaches, flame or corona treatments have been extensively employed to create hydrophilic functional groups at the interface [26]. Nevertheless, two main drawbacks have limited their use for biorelated applications. First of all, these functionalization methods are generally difficult to reproduce; upon the surface treatment, the composition is a mixture of different chemical functional groups that may vary depending on

the duration of the treatment; and a control over the density of functional groups at the surface is difficult to achieve. Later efforts were thus focused on the control over these three parameters. As a result, today there exist several approaches that improve, at least to some extent, these initial methods.

**Wet Chemical Surface Modifications** Wet chemical treatments refer to those approaches in which a liquid reagent is brought in contact with the surface to be treated. Typically, a strong acid or base is employed to create oxygen containing groups. Among the acids, employed chromic acid, potassium permanganate, or mixtures of different acids (e.g., chromium trioxide-sulfuric acid) have been used to treat PP [22, 27] or PE [14, 28, 29]. Strong bases are able to modify polymers such as poly(methyl methacrylate) (PMMA) producing carboxylic functional groups at the surface [30]. Other wet treatments include the use of aminolysis [11, 31] to create primary amines on different polyurethanes, polysaccharides, poly(lactic acid), or PMMA [32] or the use of elementary metal (e.g., sodium to generate double bonds in polytetrafluoroethylene (PTFE) materials) [19].

Wet treatments are interesting to treat surfaces with particular surface shapes and geometries in which the liquid compound could penetrate. However, two main drawbacks need to be considered. On the one hand, the reproducibility is largely dependent on the polymer employed and its molecular characteristics (molecular weight, polydispersity, and crystallinity). On the other hand, the use of hazardous chemicals limits its expansion from a laboratory into an industrial scale [33].

**Self-Assembled Monolayers** Self-assembled monolayers refer to the immobilization of organosilane derivatives onto inorganic substrates by chemical reaction and simultaneous formation of a self-organized silane monolayer. In this approach, the hydroxyl groups of a particular inorganic surface (glass, silicon wafers) are employed to covalently anchor chlorosilanes (Fig. 2.3). The large variety of chrolosilanes commercially available allows us to prepare surfaces with a large variety of functional groups (–R). Several extensive reviews cover all the aspects of self-assembled monolayer ranging from formation to the final application [34, 35].

**Surface Polymer Coatings** Different approaches that were developed during the past provide a large range of methods, these days, to deposit coatings on polymer surfaces for biomedical purposes. For instance, coatings have been deposited from the vapor phase by using laser-based processes [37], plasma [38, 39] and hot filament polymerization [40] as well as chemical vapor deposition (CVD) polymerization [41, 42].

A particularly interesting approach is the preparation of bioactive surfaces by means of reactive coatings [43–45]. Reactive coatings permit the functionalization of polymeric surfaces with a rather broad variety of chemical groups allowing the immobilization of different biomolecules such as proteins [46] and sugars [47].

**Plasma Treatments** Plasmas have been defined as the fourth state of matter and consist of highly excited atomic, molecular, ionic, and radical species [48]. Plasma is typically obtained when gases are energized into energetic states by radio frequency (rf), microwave, or electrons from a hot-filament discharge. Plasma is a

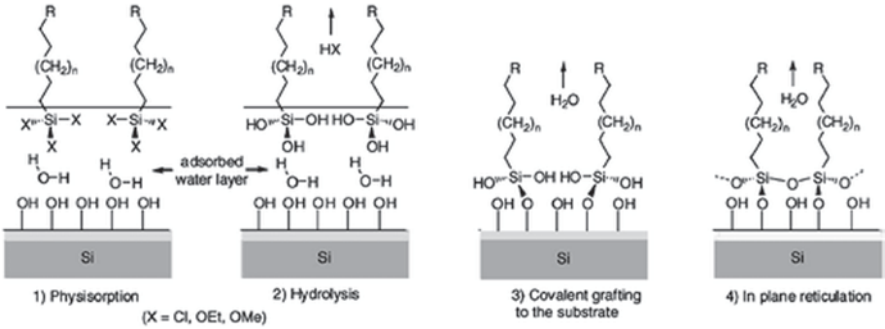


**Fig. 2.3** Formation of self-assembled monolayers on silicon wafers. (Reproduced with permission from [36])

highly unusual and reactive chemical environment in which a lot of plasma–surface reactions occur. The high density of ionized and excited species in the plasma can change the surface properties of normally inert materials. In this sense, depending on the gas employed, different surface properties, e.g., surfaces with variable surface energy and chemical surface composition, can be obtained. For instance, oxygen plasma treatments increase the surface energy of polymers, whereas fluorine plasma treatments decrease the surface energy of the polymer treated. Thus, a control over the plasma treatment allows us to obtain materials with surface energetics, which improve the adhesion strength, surface and coating properties, or biocompatibility. Moreover, the use of a gas is particularly interesting to provide an effective surface modification in materials with complex shapes, can be monitored quite accurately using in situ plasma diagnostic devices and, therefore, are rather reliable, reproducible, and relatively inexpensive.

As mentioned later, the surface modification needs to be accompanied of a particular chemical distribution. This requirement has associated the use of patterning techniques. Plasma techniques are compatible with masking techniques to enable surface patterning [11, 12], a process that is commonly used in the microelectronics industry.

**Photon Irradiation** Photon irradiation includes the use of UV or IR sources either to create chemical and physical surface changes or when the applied power increases to induce the ablation of the material. Surface chemical modification using photons has been largely employed to produce chemical changes. For instance, irradiation of PTFE with ArF laser provokes the surface defluorination and oxidation [49]. In the case of other polymers, such as poly(ethylene teretphtalate), large deoxidation is observed upon loss of CO and $CO_2$ [49] whereas in polypropylene, intense oxidation is observed even using rather soft conditions producing oxygen containing functional groups upon UV laser irradiation in ozone [50]. Finally in polyimides, surface degradation as a consequence of a complete denitrification was observed at higher fluence using UV-pulsed irradiation [51].

**Ion-Beam Modification of Polymer Surfaces** Ion-beam irradiations of polymers have associated different types of chemical reactions: reduction, oxidation, crosslinking, ion-implantation, loss of heteroatoms, and loss of aromacity via ring opening [26, 52]. The frequency of each reaction largely depends on the experimental conditions such as type of ions and the energy employed for the treatment, the nature of the polymer to be modified, or the beam dose. It has to be mentioned that ion beam modifications have been also employed to create textures and patterns on polymer surfaces that should improve the adhesion among others. For this reason, this method has been extensively used with fluoropolymers with low surface energy and poor adhesion.

One of the key points to be considered in this approach is the nature of the polymer, which is an important factor in determining the product of the surface modification. In effect, the same treatment conditions employed for two different polymers may produce completely different results. For example, oxygen and argon ion bombardment of polystyrene and polypropylene causes oxidation and partial crosslinking, whereas in the case of poly(ethylene terephthalate) crosslinking occurs to a larger extent in comparison with oxidation [53, 54].

**Surface Segregation of Polymeric Additives** Surface segregation is a phenomenon common to all classes of materials. From the thermodynamical point of view, segregation phenomena are driven by the tendency of the system studied to decrease its enthalpy through, for example, lowering the number of unfavorable bulk contacts. Additionally to enthalpy, in polymeric melts, entropy can also serve as a significant additional driving force for surface segregation [55–57]. The presence of a surface introduces a boundary condition that reduces the number of total configurations available to the chain and hence the entropy of the system. Therefore, chain ends preferentially segregate to the surface in absence of strong interactions [58, 59], and lower molar mass components are preferentially oriented to the surface in bimodal polymer blends as well [60]. On the other hand, the energy of the functional groups present in the chain has an influence on the segregation process. Examples can be found in the literature where, for example,ω–functionalized polystyrene showed a large surface excess of chain ends for materials terminated with low surface energy groups such as fluorocarbons [60], but a surface depletion of ends for systems terminated with carboxylic [61] or amine groups [57, 62].

### *2.3.2 Alternatives to Immobilize Depending on the Nature of the Chemical Bonds Involved*

Depending on the nature of the interactions established between the biomolecule and the functionalized surface, three different alternatives can be employed to immobilize them (Fig. 2.4). When both surface and biomolecule possess charged functional groups, for instance, in an aqueous solution at a particular pH, electrostatic interactions (A) can be employed to immobilize them both on surfaces with opposite similar surface charge. For the latter, an intermediate, typically a divalent ion,

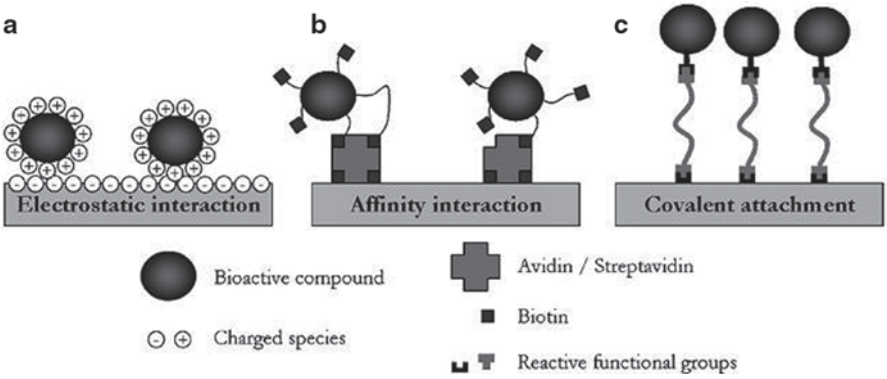


**Fig. 2.4** Types of interactions involved in the biomolecule immobilization. Non-covalent: electrostatic (**a**) and affinity interactions (**b**). Covalent attachment of bioactive compounds (BACs) (**c**). (Reproduced with permission from [33])

needs to be immobilized first. Conjugation, i.e., taking advantage of selective interactions between two biomolecules, can serve equally to immobilize biomolecules on surfaces (B). An illustrative example is depicted in Fig. 2.4. In this case, Avidin is immobilized onto a support and selective recognizes and attach Streptavidin. Finally, the third approach consists of the coupling of a biomolecule to a functional surface by covalent chemical reaction (C).

#### 2.3.2.1 Immobilization Using Electrostatic Interactions

Non-covalent attachment of BACs is generally accomplished by either hydrophobic interactions, physical entrapment, or by electrostatic interactions as depicted in Fig. 2.4. Concerning the case of electrostatic interactions, for instance, Xu et al. [63] studied the protein adsorption and cell adhesion on charged (cationic and anionic) 2-methacryloyloxyethyl phosphorylcholine (MPC) copolymer surfaces. Similarly, opposite electrostatic interactions have been successfully employed to anchor negatively charged DNA, protein complexes or positively charged proteins onto either protonated amine functionalized surfaces or negatively charged supports, respectively [21, 24, 64–66]. In addition to the immobilization of the oppositely charged, a particular interesting strategy has been developed by Vega et al. [67] in which carboxylate-rich tobacco mosaic virus (TMV) has been immobilized onto carboxylic acid functionalized monolayers. For this purpose, the authors first immobilized divalent Zn ions onto the carboxylic acid groups at the surface and next, they attached the TMV, at the surface.

Successive deposition of multiple polyelectrolyte layers has also been employed to modify polymer surfaces. The layer-by-layer (LbL) technique was reported first by Decher et al. for the fabrication of polymer multilayers constructed mainly through electrostatic interaction [68–75]. The scope and applicability of this LbL assembly has been largely extended due to the possibility to introduce molecularly

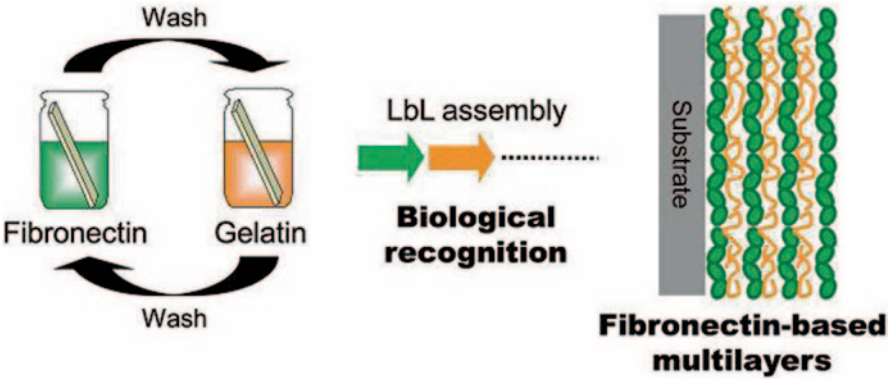


**Fig. 2.5** Schematic illustration of the layer-by-layer (*LbL*) assemblies construction using biological recognition. *Fibronectin* (FN) and *gelatin* (FN domain interactive protein) were selected for *biological recognition* assemblies. (Reproduced with permission from [77])

regular conformations of polymers or proteins within the layers and by employing weak interactions such as biological recognition [76]. More precisely, Matsusaki et al. [77] reported the preparation of multilayers based on fibronectin (FN) using biologically specific recognition (Fig. 2.5). FN is a highly flexible multifunctional glycoprotein and is well known to interact with not only a variety of ECM proteins and glycosaminoglycans (GAGs) such as collagen, gelatin, heparin, and fibrin, but also the integrin receptor on the cell membrane.

#### 2.3.2.2 Immobilization Using Electrostatic Interactions

A particular case of non-covalent interactions is related with the employment of affinity interactions between a pair of ligand-receptor molecules to modify the chemical composition of the surface. Biotin-Avidin and Streptavidin-Biotin complexes are among the most extended pairs employed due to their particularly strong binding force compare with other non-covalent forces [78] and the highly specific molecular recognition interaction between both biomolecules [79]. For instance, Haussling et al. studied the chemisorption of biotin-functionalized organic mercaptans on gold surfaces that were able to recognize streptavidin from aqueous solutions [80]. Equally, Hyun et al. [79] took advantage of the Dip-pen nanolithography to immobilize biotin onto chemically activated self-assembled nanopatterns. Streptavidin was subsequently attached to biotin providing a nanostructured platform with biorecognition capabilities.

#### 2.3.2.3 Covalent Immobilization on Functionalized Surfaces

In the literature, two main approaches have been employed to anchor a biomolecule onto a polymer surfaces. The simplest case concerns an initial surface modification

that can be directly employed to covalently anchor molecules or macromolecules onto the functional groups present at the surface (see Fig. 2.6). This immobilization requires specific functional groups at the surface, able to react with those present in the compound to be covalently attached. Typical functional groups employed to introduce biomolecules, include thiols, carboxylic acids, hydroxyl, primary amines, or aldehydes. Moreover, these coupling reactions are typically carried out by using crosslinking agents that favor the anchoring reaction to occur with higher yields [33, 81, 82] or by employing click chemistry reactions [83].

An extensively employed approach takes advantage of UV treatments to introduce functional groups in different polymers. For instance, UV irradiation on PMMA has been employed to create carboxylic acid functional groups that can react by primary amines by means of standard amide formation chemistry. In particular, Situma et al. [84, 85] have employed this strategy to fabricate DNA arrays for the detection of low abundant point mutations. Similarly in the case of polystyrene, UV treatments activate the surface and can be further employed to immobilize biomolecules such as proteins and enzymes [86].

An alternative to the direct chemical reaction or a single bioactive molecule by using orthogonal chemistry on functional polymer surfaces concern the case of the use of the surface functional groups to covalently anchor macromolecules thus leading to what is known as "polymer brushes." Even though it is possible to fabricate polymer brushes by physisorption [88–92], generally, the fabrication of polymer brushes is accomplished by covalent immobilization of the polymer chains. Polymer brushes are immobilized onto polymeric surfaces either by using grafting-from or grafting-onto methodologies [93]. In the grafting-to approach, end-functionalized macromolecules react with an appropriately functionalized substrate. On the contrary, the grafting-from approach consists of the polymerization from immobilized functional groups or initiators present at the polymer surface. The latter permits the elaboration of brushes with higher chain density and controllable polymer chain lengths when using controlled polymerization techniques such as ATRP, RAFT, or TEMPO. The functionalization can be achieved by the following two different strategies, i.e., by direct grafting of functional monomers incorporated during the polymerization step or by post-derivatization of the grafted chains.

An alternative to the surface treatments consists of the use of a functional polymer to prepare the material that will, thus, contain functional groups at the surface (see Fig. 2.6). These functional groups can be further employed to immobilize the biomolecule by direct chemical reaction or by the introduction of a linker. Polymers that inherently possess reactive groups include hydroxyl-funcionalized polymers such as poly(hydroxyethyl methacrylate), [94] poly(vinyl alcohol) [95], or poly(propylene fumarate) [96], carboxylic acid containing polymers such as poly(1-(2-carboxyethyl)pyrrole) [97] and polyethylene terephthalate (PET) [98].

In some situations, the presence of the interface limits the yield of the immobilization reaction. In these cases, the use of a spacer or linker may favor the covalent attachment of the bioactive molecule. Moreover, a second advantage of tethering a BAC is related to the improvement of the bioactivity. In effect, tethering reduces steric hindrance and shields the effect of hydrophobic surfaces that have been demonstrated to induce denaturation. A broad literature has been devoted to the

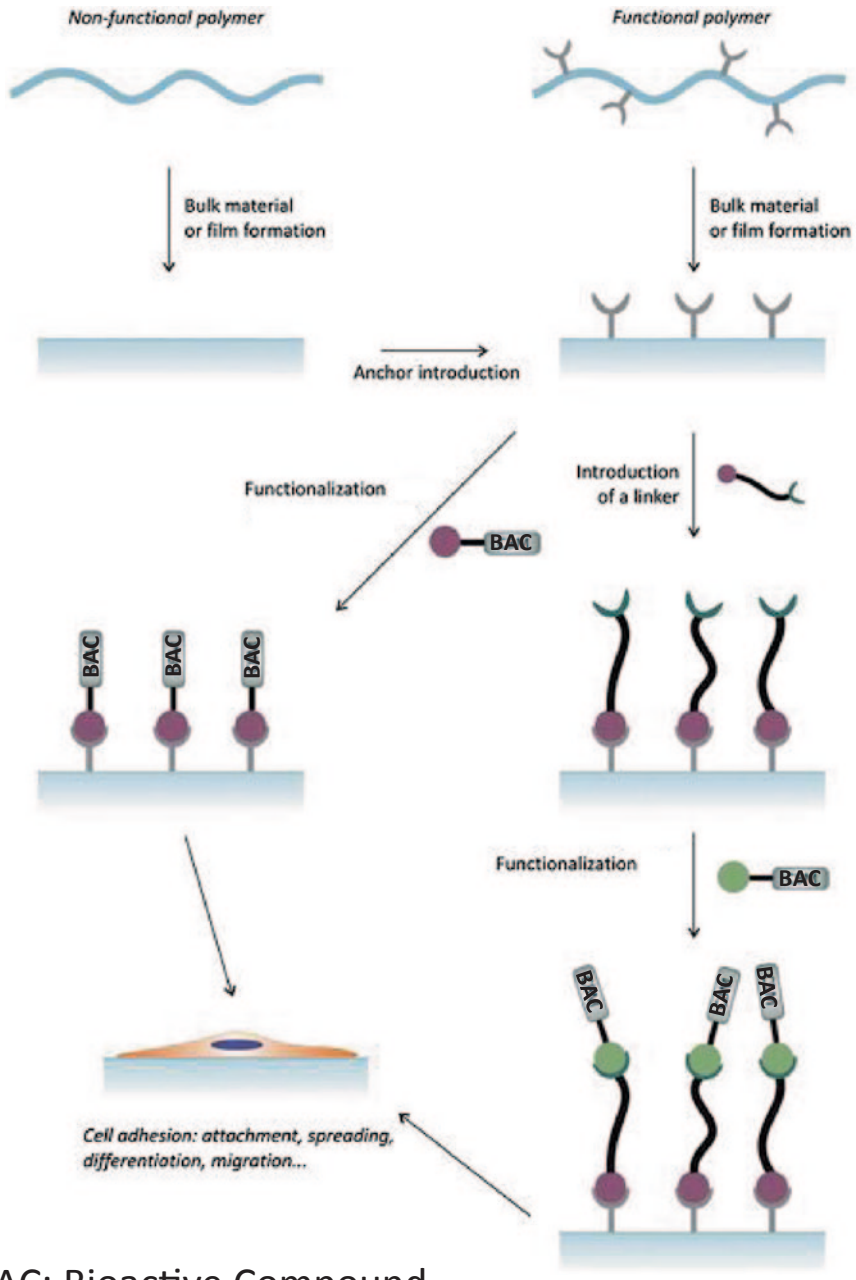


**Fig. 2.6** Modification strategies for the incorporation of bioactive compounds (*BACs*) onto synthetic polymer surfaces. (Figure adapted with permission from [87])

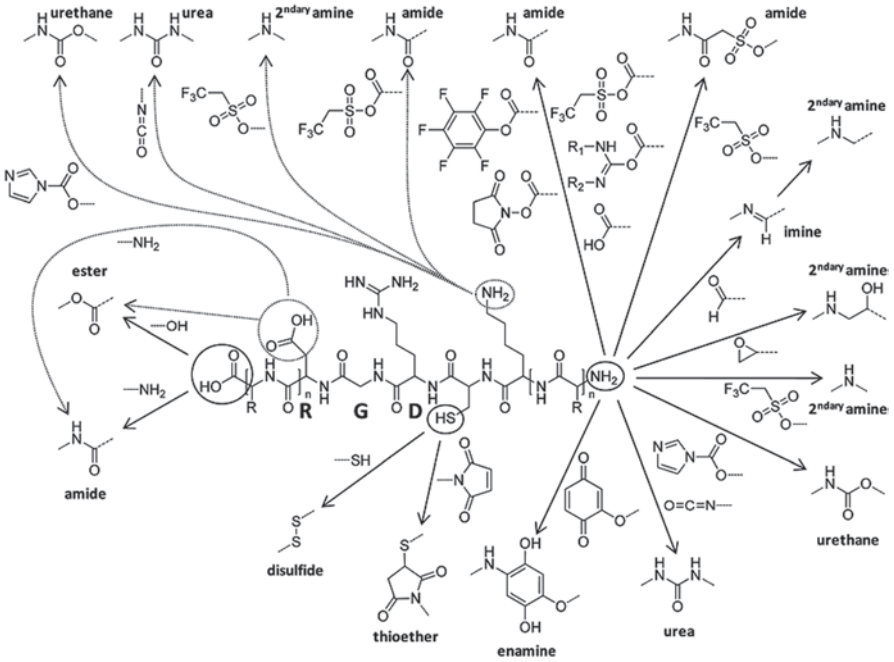


**Fig. 2.7** Coupling chemistries employed for attachment of cell-binding peptides onto a surface or to a linker prior to surface attachment. (Reproduced with permission from [87])

study of the influence of the linker on the biorecognition processes. Typically, linkers are bifunctional molecules with identical or different chemical groups. As an example, polypeptides can be immobilized via their N-termini onto aminated surfaces by using a glutaraldehyde as a spacer [99, 100]. Similarly, diisocyanates can be employed to attach polypeptides onto hydroxyl-functionalized surfaces [101–103]. In summary, Fig. 2.7 provides a general overview of the coupling chemistries that can be employed to immobilize a particular RGD sequence onto a linker [87].

In some cases, the surface functional groups require an additional modification step in which particular chemical groups are immobilized onto the polymeric surface. The latter will serve to attach the biomolecule. As an example of this procedure in Fig. 2.8, the strategy employed by Sun and Önneby is depicted. These authors first hydrolyzed the surface of a polycaprolactone (PCL) by using aqueous sodium hydroxide, thus leading to a modified surface composed of a mixture of hydroxyl and carboxylic acid groups. In a second step, the selective modification of the carboxylic acid groups by using coupling agents, enabled the modification of the surface with a thiol-end terminated RGD peptide. [104]. A recent review extensively covers the chemical methods indicating that they can be employed to functionalize polymer interfaces using small binding motifs [87]. More precisely, they classify the approaches depending on the polymeric material employed, the functional group present at the surface, and the mode of introduction.

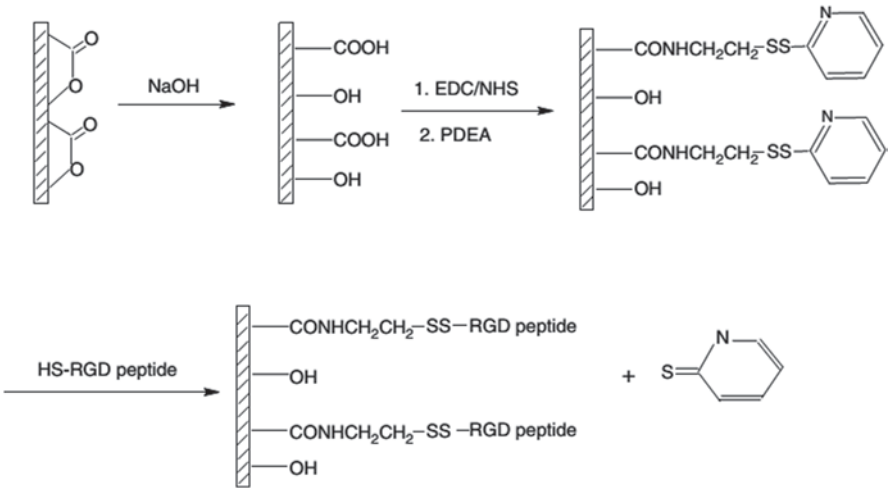


**Fig. 2.8** Surface carboxylation of polycaprolactone (PCL) via base hydrolysis and subsequent attachment of cell-recognizing peptide. *HS* thiol, *RGD* arginine-glycine-aspartic acid (Reproduced with permission from [104])

### *2.3.3 Immobilized Molecules and Applications Pursued*

There exists a large variety of BACs depending on the final application of the interface. Some of the most relevant and recently reported biomolecules immobilized in polymer surfaces and their potential applications are included in Table 2.1.Thus, immobilization of enzymes [105–110] has been employed to prepare biosensors [19], bioreactors [111, 112], or microanalytical devices [113]. Oligonucleotides immobilized on surfaces [114–116] have been demonstrated to be useful in the preparation of DNA microarrays [18, 85] and biosensors [117]. Peptides [12, 100, 118] and antibodies [119–123] exhibit interesting properties for the elaboration of biosensors [124], in tissue engineering [100, 125], or for the preparation of antimicrobial surfaces [126]. Finally, polysaccharides [127, 128] due to their role on cell to cell recognition processes have also been largely employed as a model for biorecognition processes [129, 130], the preparation of antimicrobial surfaces [20, 131], or to prepare hemocompatible materials [132, 133].

## 2.4 Approaches for Surface Patterning

Advances in micro- and nanofabrication offer unique opportunities to construct nanoengineering structures with dimensions in the nanoscale, i.e., below 100 nm. Today, a variety of nano- and microfabrication approaches are available that have largely contributed to fulfill the requirements for a multitude of applications in

**Table 2.1** Biomolecules immobilized onto surfaces and potential applications of the resulting surfaces

| Immobilized recognition molecule | Applications literature |
|---|---|
| Polysaccharides | Protein [129, 130, 134] and molecular recognition processes [135], cell-adhesion [136], cell patterning, tissue engineering [137], fabrication of biosensors [138], separation of stereoisomers [139], diagnosis [140]. |
| Enzymes | Biosensors [19] and sensing [141, 142], microanalytical devices [113], antimicrobial packaging [143], catalysis [144] and bioreactors [145], treatment of environmental pollutants [146] and biofuel cells [147]. See also [148–150] |
| Peptides and proteins | Elaboration of biosensors [124], protein-based diagnostics and therapeutics [17], immunoassays,[151] protein [152] and cellular microarrays [153], restricted cell attachment [154], spatially controlled cell adhesion [155] |
| Antibodies | Immunoassay chip [16, 123, 156], immuno [157, 158] and biosensors,[23, 159] protein recognition [160], specific cell adhesion [161], generation of functional nanoarrays [162] |
| Aptamers | Biosensors [163–169], clinical diagnostics [170–175], biomolecules detection [176, 177], artificial receptors [178] controlled cell catch and release [179], cell targeting and imaging [180] |
| Oligonucleotides | Preparation of DNA microarrays [18, 85, 181, 182] and biosensors [117, 183–186], biochips for disease diagnosis [187], recognition, control de bacterial expression [188], attach nanoparticles [189] |

the field of nanobiotechnology [13, 21, 190–205]. As a consequence of the large amount of techniques and methods reported to fabricate nanostructured polymer interfaces, a general classification is admitted dividing them into two main categories: "Top-down" and "bottom-up" methodologies. As defined by Biswas et al. [206], a top-down approach corresponds to "using nanofabrication tools that are controlled by external experimental parameters to create nanoscale structures/functional devices with the desired shapes and characteristics starting from larger dimensions and reducing them to the required values." On the other hand, they defined bottom-up approaches as those that pretended to have "molecular or atomic components built up into more complex nanoscale assemblies or directed self-assemblies based on complex mechanisms and technologies."

A large amount of literature can be found covering the fabrication approaches following these two different methodologies. The following chapters of this book are intended to provide a precise and brief overview of different alternatives that have been employed to fabricate structured and functional platforms with potential in biorelated applications and in particular for biorecognition purposes. Herein, we will limit our discussion to briefly summarize the most recent techniques giving a rather large overview of the techniques available.

### 2.4.1 Lithography: Recent Advances

Lithography is probably the most extended top-down approach to generate micro- and nanostructures on polymer surfaces [207]. Lithographic approaches include various alternatives such as photolithography, soft-lithography, beam-lithography, embossing and printing lithography, or scanning-probe lithography. More recent advances make use of living organisms including bacteria [208] and cells [10] to pattern polymer surfaces.

**Photolithography** The principle of this technique consists of the selective removal of particular surface areas upon suffering an external stimulus in general using a mask with the desired pattern [209]. Typically, two different strategies have been depicted. The first approach generally uses a light source (UV lamp, electron beam, or X-rays) or any other stimulus to crosslink the directly exposed areas whereas the areas under the mask remain unreacted. Thus, in a subsequent development step, for instance, by washing the surface with an appropriate solvent the noncross-linked areas can be easily removed (negative-tone imaging). In a second alternative, the exposure directs the formation of more soluble areas than can be removed by using a developer. This is, for instance, the case of photoacid generators [210–212]. Advances in photolithography have been directed to reduce the lateral dimensions of the patterns generated. For this purpose, different alternatives either by using enhancement resolution techniques [213–218] or the development of novel photo-resists allowed to reduce the size of the moieties down to sub-100 nm [212].

Whereas initially the use of photolithography to pattern polymer surfaces was somehow limited to the availability of particular masks, new fabrication methodologies have appeared that enable the formation of more complex 3D surface structures [219]. Some of these examples are summarized in Fig. 2.1 (Fig. 2.9).

**Soft Lithography** Soft lithography is a low-cost and high-throughput methodology that employs an elastomeric material, typically PDMS, as a stamp to transfer the pattern from the master to a particular material [194, 220, 221]. This technique, as a consequence of the particularly well contact between the stamp and the surface can generate well-defined patterns over large areas. Moreover, the flexibility of the stamp allows us to use curved interfaces as well. By using this approach, proteins and cells have been anchored in a controlled manner [222].

**Imprinting–Embossing–Injection Molding** The principle of imprint lithography [194, 207, 223, 224] also known as hot embossing is that a hard mold containing nano- or microscale features on its surface is used to deform a thermoplastic polymer above the glass transition temperature deposited on the wafer substrate under controlled temperature and pressure. These two factors are crucial since an increase in the temperature of the polymer reduces the viscosity of the material so that pressure application causes the polymer melt to flow into the cavities of the mold. The subsequent cooling of the system freezes the pattern on the target surface. As a result, a negative copy of the master is obtained. In injection, molding is a variant of the imprinting method where a polymer melt is injected at high pressure into a cavity where it cools down and therefore became rigid [225, 226].

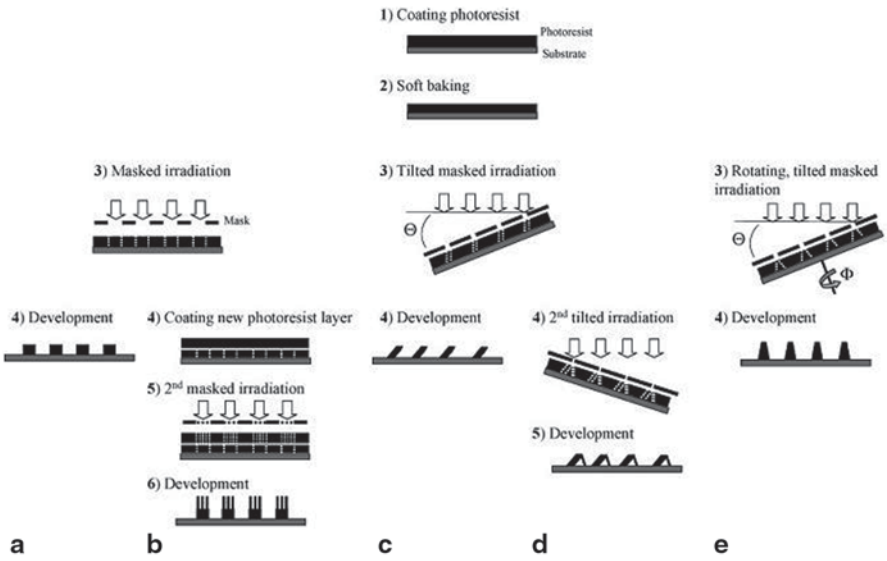


**Fig. 2.9** Photolithographic structuring methods using masked irradiation and a negative photoresist material: **a** HAR patterning by single exposure, **b** hierarchical patterning by layer-by-layer (LbL) coating and exposure, **c** tilted patterning by single inclined exposure, **d** interconnected patterns by double inclined exposure, **e** tapered patterns by rotating tilted exposure. (Reproduced with permission from [219])

*Advances in Lithography: Towards Nanolithographic Techniques* A crucial issue in the final use of a particular artificial biological surface is the resolution of the surface pattern. In effect, nanostructured arrays of biomolecules permit among others the fabrication of smaller biochips, an increase in the selectivity of the platform with a reduction of the sample volume employed, or throughput screening for molecular diagnostics [227]. In this concern, the nanometer scale resolution of the most recent lithographic approaches has largely contributed to improve the quality of the surface patterns. Figure 2.10 provides an overview of the lithographic alternatives capable of achieving nanometer resolution.

**(A)–(E) Scanning Probe Nanolithography** Scanning probe lithography (SPL) involves different techniques in which a nanoscopic tip is brought in contact with a surface [228]. The tip moves across the plane and generates a particular pattern by interacting with the surface. The equipment employed to carry out SPL is a scanning tunneling microscope with permits to control the movements of the tip with nanometer resolution. Within this patterning approach, several methodologies have been developed with some particularities including dip-pen nanolithography, nanoshaving, nanografting, electrochemical, and thermal nanolithography [229].

*Dip-Pen Nanolithography* In this technique, an AFM tip is employed to distribute materials from a solution to the surface (Fig. 2.10 (A) and (B)). This process requires an inking step of the tip with the appropriate solution prior to the transfer to the substrate. The surface pattern originated varies from nanometer dots upon

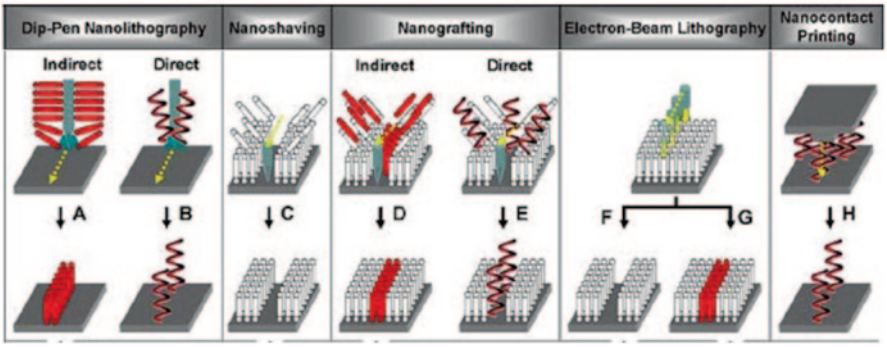


**Fig. 2.10** Schematic representation of the main lithographic techniques employed to indirectly or directly immobilize biomolecules on surfaces with nanometer-scale resolution. (Reproduced with permission from [227])

punctual contact and removal of the tip or lines, if the tip moves across the surface. In addition to the pattern originated from a static or dynamic deposition process, the resolution of the moieties depends also on the water-meniscus properties, the tip geometry, the chemical nature of both ink and substrate, the tip-substrate contact time, and the writing rate [21, 197, 198].

Two alternatives have been investigated to pattern biomolecules onto surface by DPN, i.e., direct and indirect DPN. On the one hand, the indirect method DPN is used to create arrays of functional organic molecules that serve to immobilize the desired biomolecule in these particular positions. This strategy has been employed among others to immobilize DNA [64, 65] and negatively charged membrane protein complexes [66] on amino-functionalized surfaces. Equally, carboxylic functional groups were employed to anchor proteins such as immunoglobulin G, lysozyme, or retronectin [21, 24].

On the other hand, the direct method allows the direct patterning of the biomolecules. Dip-pen nanolithography has been employed among others to direct-write proteins on modified silicon oxide surfaces [230, 231] or to immobilize DNA [232] by modifying the AFM tips chemically.

Both strategies have particular advantages and disadvantages. For instance, direct patterning avoids nonspecific binding and allows the formation or multicomponent arrays. However, direct patterning is more challenging in order to preserve the activity of the biomolecule during the transfer onto the surface. In particular, biomolecule transfer depends on several aspects including the humidity or the affinity of the template [227].

*Nanoshaving and Nanografting* Nanoshaving resorts to the use of the AFM tip to remove a resist material, thus creating nanometer size structures (Fig. 2.10(C)) [227, 233]. Instead, nanografting (Fig. 2.10(D) and (E)) is accomplished by shaving a particular surface replacing the removed materials with a second molecule exhibiting larger affinity for the substrate [234, 235]. These two techniques have been employed to direct the assembly of thiolated peptide nanotubes [236] and also proteins on gold substrates [237, 238].

**(F)–(G) Electron Beam Nanolithography** This approach includes the creation of low-dimensional structures in resistance that are subsequently transferred to the substrate material by etching (Fig. 2.10 (F)) [206]. E-beam lithography can produce surface patterns with higher resolution in comparison with conventional photolithography. The advantage of e-beam lithography lies in the fact that it overcomes the diffraction limit of light that helps create features in the nanometer range. In addition, this process does not require the use of any mask typically employed in photolithography.

**(H) Nanoimprint Lithography** Nanoimprinting allows the fabrication of patterned substrates with features below 40 nm by using a stamp (coated with a solution containing the biomolecule) that is put in contact with a substrate [239, 240]. This strategy generally employed for the fabrication of micrometer size surface patterns has been developed in order to achieve nanometer scale patterns. For this purpose, two different alternatives are available. The first concerns the reduction of the pattern size of typical PDMS stamps with micrometer size features. The second is related to the use of stamps other than PDMS like polyolefin plastomers, including hard PDMS [241], polyolefin plastomers (POPs) [242], poly (ethylene)/PMMA composite stamps [243], perfluoropolyethers [244], domed stamps [245], and PMMA stamps [246]. By using this approach, lines of different proteins with lateral resolution below 100 nm has been achieved [245, 247].

### *2.4.2 Inkjet Printing*

Inkjet printing is an attractive technology to control the biomolecule deposition having additionally important advantages such as low cost, simplicity, high resolution, speed, reproducibility, flexibility, and low amount of waste generated [248]. These capabilities have transformed initially this office-limited technology into an important tool for mass fabrication. Inkjet printing basically involves the ejection of a precise amount of ink (solute dissolved/dispersed in a solvent) in a chamber. An applied external voltage in the chamber causes a liquid drop to eject from a nozzle. The droplet falls due to action of gravity and is deposited on a substrate.

Several methods can be compared to inkjet printing since they attempt to achieve a similar purpose: drop casting, contact printing, pneumatic dispensing, screen printing, and spin coating. Although all these methods follow a similar concept, i.e., controlled deposition of a liquid on a substrate, inkjet printing has important advantages due to the flexible spatial control of the material deposition process. For a detailed description over the inkjet process and a general view of its applications, the readers are referred to [249].

In particular, inkjet printing has been employed, among others, for the fabrication of biosensors and biodevices [250], to control the deposition of proteins on surfaces [251] or the preparation of (bio)chemical sensing devices [248].

### 2.4.3 Self-Assembled Monolayers

Self-assembled monolayers (SAMs) consist, generally, in the surface immobilization of organosilanes onto inorganic supports [34, 35]. As a result of the wide variety of commercially available organosilanes having different functional groups, SAMs have been employed to tailor the material surfaces in order to obtain control both over the molecular composition and thus the interfacial surface properties [81]. As a consequence, SAMs provide interesting properties that have been exploited for different bioapplications. SAMs have been, for instance, used to evaluate the effect of the abovementioned surface properties (surface charge, wettability, and topography) on protein adsorption and cell behavior including adhesion and spreading [252–256].

### 2.4.4 Surface Instabilities to Pattern Surfaces

In contrast to the use of, in some cases, highly sophisticated tools required by the abovementioned techniques, surface instabilities produced by different mechanisms take advantage of the inherent properties of polymers to induce particular surface patterns. Some of the surface instabilities are well known since decades but novel and old known instability mechanisms have been only recently extended their use to pattern polymer surfaces. This recent interest relies on the rich and complex patterns obtained as a result of self-organizing processes that are rather difficult if not impossible to fabricate by using traditional patterning techniques [204, 205, 257–259].

Among the approaches to obtain patterned interphases by means of surface instabilities the formation of functional porous films as a consequence of simultaneous solvent evaporation and water vapor condensation, also known as breath figures [260–264] has been one of the most explored methods to prepare supports for biorelated applications [265–268].

### 2.4.5 Molecular Imprinting

The fabrication of molecularly imprinting polymers (MIPs) is a particular technique that combines chemical functionality with surface modification of polymers. MIPs consist of artificial polymeric receptors with the ability to specially bind a particular target molecule. For that purpose, MIP aims to create artificial recognition cavities employing as a host synthetic polymer [269–275]. The base of this concept is, thus, the fabrication of recognition sites where a guest molecule can be attracted. A typically employed strategy involves the choice of a template molecule that is, during a polymerization step, entrapped within the structure. Therefore, the template involved is crucial for the final recognition process. Moreover, the complex to be polymerized is usually composed of functional monomers capable of interacting with the template employed and a crosslinking agent that will stabilize the 3D

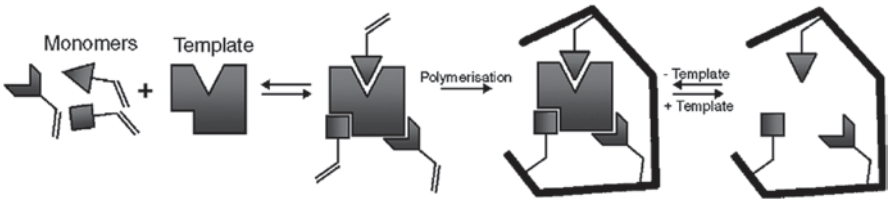


**Fig. 2.11** Schematic generalization of the molecular imprinting process. (Reproduced with permission from [282])

structure created. Finally, the template is removed by means of an extraction step providing sites with particular shape and functionality, i.e., a molecularly imprinted polymer. As depicted in a recent review [276], a molecular imprinted platform can be generated in multiple ways depending, for instance, in the nature of the force of the host–guest interactions. These can involve either strong covalent interactions between the monomers and the template [277] or weak non-covalent interactions [270, 278, 279]. In addition, alternatives to these two possibilities, other methodologies include the stoichiometric non-covalent approach [10; 280], the semicovalent (combination) approach [281], imprinting ionic species or metal-ion-mediated imprinting [276, 282, 283] (Fig. 2.11).

### *2.4.6 Miscellaneous Approaches for Surface Patterning or Approaches Combining Different Techniques*

In addition to the methods for surface functionalization and patterning described below, there are numerous studies in which, rather than using a particular approach, two or more techniques are involved in the fabrication of platforms with biorecognition capabilities [284–287].

Examples of fabrication approaches that involve different techniques are, for instance, the preparation of nanostripe surface structure by multilayer film deposition combined with micropatterning, [199], the sue of SPL using self-assembled monolayers [288, 289], or the employment of enzyme nanoarchitectonics [290].

## 2.5 Conclusions

Patterning and functionalization of polymer surfaces have come a long way and today, a rather large variety of methodologies permit the micro/nanostructuration of functional biomolecules. In view of the application of biopatterning in different fields ranging from the preparation of biosensors to the fabrication of platforms for selective catalysis or the understanding of the processes that regulate the biorecognition (protein–protein, protein–cell interactions, …), there is a strong interest among the scientist to further improve the patterning techniques.

In this concern, this book will further develop some of the most promising methodologies briefly summarized in this chapter focusing on the role of these platforms in biorecognition processes.

## References


1. Castner, D.G. and B.D. Ratner, *Biomedical surface science: Foundations to frontiers*. Surface Science, 2002. **500**(1–3): p. 28–60.
2. Shekhawat, G., S.H. Tark, and V.P. Dravid, *MOSFET-embedded microcantilevers for measuring deflection in biomolecular sensors*. Science, 2006. **311**(5767): p. 1592–1595.
3. Cui, Y., et al., *Nanowire nanosensors for highly sensitive and selective detection of biological and chemical species*. Science, 2001. **293**(5533): p. 1289–1292.
4. Christman, K.L., V.D. Enriquez-Rios, and H.D. Maynard, *Nanopatterning proteins and peptides*. Soft Matter, 2006. **2**(11): p. 928–939.
5. Demidov, V.V., *Nanobiosensors and molecular diagnostics: a promising partnership*. Expert Review of Molecular Diagnostics, 2004. **4**(3): p. 267–268.
6. Ratner, B.D., *The engineering of biomaterials exhibiting recognition and specificity*. Journal of Molecular Recognition, 1996. **9**(5–6): p. 617–625.
7. Chen, H., et al., *Biocompatible polymer materials: Role of protein–surface interactions*. Progress in Polymer Science, 2008. **33**(11): p. 1059–1087.
8. Kingshott, P., et al., *Surface modification and chemical surface analysis of biomaterials*. Current Opinion in Chemical Biology, 2011. **15**(5): p. 667–676.
9. Alves, N.M., et al., *Controlling Cell Behavior Through the Design of Polymer Surfaces*. Small, 2010. **6**(20): p. 2208–2220.
10. Alexander, C. and E.N. Vulfson, *Spatially functionalized polymer surfaces produced via cell-mediated lithography*. Advanced Materials, 1997. **9**(9): p. 751–755.
11. Alfonso, I. and V. Gotor, *Biocatalytic and biomimetic aminolysis reactions: useful tools for selective transformations on polyfunctional substrates*. Chemical Society Reviews, 2004. **33**(4): p. 201–209.
12. Appendini, P. and J.H. Hotchkiss, *Surface modification of poly(styrene) by the attachment of an antimicrobial peptide*. Journal of Applied Polymer Science, 2001. **81**(3): p. 609–616.
13. Ariga, K., J.P. Hill, and Q. Ji, *Layer-by-layer assembly as a versatile bottom-up nanofabrication technique for exploratory research and realistic application*. Physical Chemistry Chemical Physics, 2007. **9**(19): p. 2319–2340.
14. Bag, D.S., V.P. Kumar, and S. Maiti, *Chemical modification of LDPE film*. Journal of Applied Polymer Science, 1999. **71**(7): p. 1041–1048.
15. Blawas, A.S. and W.M. Reichert, *Protein patterning*. Biomaterials, 1998. **19**(7–9): p. 595–609.
16. Darain, F., K.L. Gan, and S.C. Tjin, *Antibody immobilization on to polystyrene substrate-on-chip immunoassay for horse IgG based on fluorescence*. Biomedical Microdevices, 2009. **11**(3): p. 653–661.
17. Delamarche, E., *Microcontact Printing of Proteins*, in *Nanobiotechnology*. 2005, Wiley-VCH Verlag GmbH & Co. KGaA. p. 31–52.
18. Fixe, F., et al., *Functionalization of poly* (*methyl methacrylate*) (*PMMA*) *as a substrate for DNA microarrays*. Nucleic Acids Research, 2004. **32**(1).
19. Glodek, J., et al., *Derivatization of fluorinated polymers and their potential use for the construction of biosensors*. Sensors and Actuators B-Chemical, 2002. **83**(1–3): p. 82–89.
20. Hu, S.G., C.H. Jou, and M.C. Yang, *Surface grafting of polyester fiber with chitosan and the antibacterial activity of pathogenic bacteria*. Journal of Applied Polymer Science, 2002. **86**(12): p. 2977–2983.

21. Lee, K.B., et al., *Protein nanoarrays generated by dip-pen nanolithography*. Science, 2002. **295**(5560): p. 1702–1705.
22. Tao, G.L., et al., *Surface functionalized polypropylene: Synthesis, characterization, and adhesion properties*. Macromolecules, 2001. **34**(22): p. 7672–7679.
23. Volcke, C., et al., *Protein pattern transfer for biosensor applications*. Biosensors and Bioelectronics, 2010. **25**(6): p. 1295–1300.
24. Zhang, H., et al., *Biofunctionalized nanoarrays of inorganic structures prepared by dip-pen nanolithography*. Nanotechnology, 2003. **14**(10): p. 1113–1117.
25. Zhang, J. and Y. Han, *Active and responsive polymer surfaces*. Chemical Society Reviews, 2010. **39**(2): p. 676–693.
26. Pethrick, R.A., *Polymer surface modification and characterization, edited by Chi-Ming Chan. Carl Hanser Verlag, Munich, Vienna, New York, 1993.*
27. Sheng, E., et al., *Effects of the chromic-acid etching on propylene polymer surfaces*. Journal of Adhesion Science and Technology, 1995. **9**(1): p. 47–60.
28. Eriksson, J.C., et al., *Characterization of kmno4 h2so4-oxidized polyethylene surfaces by means of esca and 45ca2 + adsorption*. Journal of Colloid and Interface Science, 1984. **100**(2): p. 381–392.
29. Bandopadhay, D., A.B. Panda, and P. Pramanik, *Surface modification of LDPE film by chemical processes with Ni2 + and ammonium persulfate*. Journal of Applied Polymer Science, 2001. **82**(2): p. 406–415.
30. Holmberg, K. and H. Hyden, *methods of immobilization of proteins to polymethylmethacrylate*. Preparative Biochemistry, 1985. **15**(5): p. 309–319.
31. Zhu, Y., Z. Mao, and C. Gao, *Aminolysis-based surface modification of polyesters for biomedical applications*. Rsc Advances, 2013. **3**(8): p. 2509–2519.
32. Zhu, Y.B., et al., *Endothelium regeneration on luminal surface of polyurethane vascular scaffold modified with diamine and covalently grafted with gelatin*. Biomaterials, 2004. **25**(3): p. 423–430.
33. Goddard, J.M. and J.H. Hotchkiss, *Polymer surface modification for the attachment of bioactive compounds*. Progress in Polymer Science, 2007. **32**(7): p. 698–725.
34. Ulman, A., *Formation and structure of self-assembled monolayers*. Chemical Reviews, 1996. **96**(4): p. 1533–1554.
35. Whitesides, G.M. and P.E. Laibinis, *Wet chemical approaches to the characterization of organic surfaces: self-assembled monolayers, wetting, and the physical-organic chemistry of the solid-liquid interface*. Langmuir, 1990. **6**(1): p. 87–96.
36. Dejeu, J., et al., *Improvement of Robotic Micromanipulations Using Chemical Functionalisations*, in *Precision Assembly Technologies and Systems*, S. Ratchev, Editor. 2010. p. 215–221.
37. Chrisey, D.B., et al., *Laser Deposition of Polymer and Biomaterial Films*. Chemical Reviews, 2003. **103**(2): p. 553–576.
38. Schiller, S., et al., *Chemical Structure and Properties of Plasma-Polymerized Maleic Anhydride Films*. Chemistry of Materials, 2001. **14**(1): p. 235–242.
39. Calderon, J.G. and R.B. Timmons, *Surface Molecular Tailoring via Pulsed Plasma-Generated Acryloyl Chloride Polymers: Synthesis and Reactivity*. Macromolecules, 1998. **31**(10): p. 3216–3224.
40. Mao, Y. and K.K. Gleason, *Hot Filament Chemical Vapor Deposition of Poly(glycidyl methacrylate) Thin Films Using tert-Butyl Peroxide as an Initiator*. Langmuir, 2004. **20**(6): p. 2484–2488.
41. Lahann, J., *Vapor-based polymer coatings for potential biomedical applications*. Polymer International, 2006. **55**(12): p. 1361–1370.
42. Lahann, J., *Reactive polymer coatings for biomimetic surface engineering*. Chemical Engineering Communications, 2006. **193**(11): p. 1457–1468.
43. Bally, F., et al., *Co-immobilization of Biomolecules on Ultrathin Reactive Chemical Vapor Deposition Coatings Using Multiple Click Chemistry Strategies*. Acs Applied Materials & Interfaces, 2013. **5**(19): p. 9262–9268.

44. Nandivada, H., et al., *Reactive polymer coatings that "click"*. Angewandte Chemie-International Edition, 2006. **45**(20): p. 3360–3363.
45. Nandivada, H., et al., *Reactive Polymer Coatings for Biological Applications*. Polymers for Biomedical Applications, 2008. **977**: p. 283–298.
46. Lahann, J., et al., *Universal approach towards r-Hirudin derivatives with high anti-thrombin activity based on chemical differentiation of primary amino groups*. Macromolecular Bioscience, 2002. **2**(2): p. 82–87.
47. Nandivada, H., H.Y. Chen, and J. Lahann, *Vapor-based synthesis of poly (4-formyl-p-xylylene)-co-(p-xylylene) and its use for biomimetic surface modifications*. Macromolecular Rapid Communications, 2005. **26**(22): p. 1794–1799.
48. Chu, P.K., et al., *Plasma-surface modification of biomaterials*. Materials Science & Engineering R-Reports, 2002. **36**(5–6): p. 143–206.
49. Chtaib, M., et al., *Polymer surface reactivity enhancement by ultraviolet arf laser irradiation—an x-ray photoelectron-spectroscopy study of polytetrafluoroethylene and polyethyleneterephthalate ultraviolet treated surfaces*. Journal of Vacuum Science & Technology a-Vacuum Surfaces and Films, 1989. **7**(6): p. 3233–3237.
50. Rabek, J.F., et al., *Photoozonization of polypropylene oxidative reactions caused by ozone and atomic oxygen on polymer surfaces*. Acs Symposium Series, 1988. **364**: p. 187–200.
51. Chtaib, M., et al., *Polyimide surface degradation—x-ray photoelectron spectroscopic study under uv-pulsed laser irradiation*. Acs Symposium Series, 1990. **440**: p. 161–169.
52. Marletta, G., *Ion-Beam Modification of Polymer Surfaces for Biological Applications*, in *Materials Science with Ion Beams*, H. Bernas, Editor. 2010. p. 345–369.
53. Dunn, D.S., J.L. Grant, and D.J. McClure, *texturing of polyimide films during o-2/cf4 sputter etching*. Journal of Vacuum Science & Technology a-Vacuum Surfaces and Films, 1989. **7**(3): p. 1712–1718.
54. Grant, J.L., D.S. Dunn, and D.J. McClure, *argon and oxygen sputter etching of polystyrene, polypropylene, and poly(ethylene-terephthalate) thin-films*. Journal of Vacuum Science & Technology a-Vacuum Surfaces and Films, 1988. **6**(4): p. 2213–2220.
55. Kellogg, G.J., et al., *Observed surface energy effects in confined diblock copolymers*. Physical Review Letters, 1996. **76**(14): p. 2503–2506.
56. Walton, D.G. and A.M. Mayes, *Entropically driven segregation in blends of branched and linear polymers*. Physical Review E, 1996. **54**(3): p. 2811–2815.
57. Jalbert, C., et al., *Molecular-weight dependence and end-group effects on the surface-tension of poly(dimethylsiloxane)*. Macromolecules, 1993. **26**(12): p. 3069–3074.
58. Hunt, M.O., et al., *End-functionalized polymers.1. Synthesis and characterization of perfluoroalkyl-terminated polymers via chorosilane derivatives*. Macromolecules, 1993. **26**(18): p. 4854–4859.
59. Linton, R.W., et al., *Time-of-flight secondary-ion mass-spectrometric analysis of polymer surfaces and additives*. Surface and Interface Analysis, 1993. **20**(12): p. 991–999.
60. Hopkinson, I., et al., *Investigation of surface enrichment in isotopic mixtures of poly(methyl methacrylate)*. Macromolecules, 1995. **28**(2): p. 627–635.
61. Elman, J.F., et al., *A neutron reflectivity investigation of surface and interface segregation of polymer functional end-groups*. Macromolecules, 1994. **27**(19): p. 5341–5349.
62. Jalbert, C.J., et al., *Surface depletion of end-groups in amine-terminated poly(dimethylsiloxane)*. Macromolecules, 1994. **27**(9): p. 2409–2413.
63. Xu, Y., M. Takai, and K. Ishihara, *Protein adsorption and cell adhesion on cationic, neutral, and anionic 2-methacryloyloxyethyl phosphorylcholine copolymer surfaces*. Biomaterials, 2009. **30**(28): p. 4930–4938.
64. Nyamjav, D. and A. Ivanisevic, *Alignment of long DNA molecules on templates generated via dip-pen nanolithography*. Advanced Materials, 2003. **15**(21): p. 1805–1809.
65. Nyamjav, D. and A. Ivanisevic, *Templates for DNA-templated Fe3O4 nanoparticles*. Biomaterials, 2005. **26**(15): p. 2749–2757.
66. Valiokas, R., et al., *Selective recruitment of membrane protein complexes onto gold substrates patterned by dip-pen nanolithography*. Langmuir, 2006. **22**(8): p. 3456–3460.

67. Vega, R.A., et al., *Nanoarrays of single virus particles*. Angewandte Chemie-International Edition, 2005. **44**(37): p. 6013–6015.
68. Decher, G. and J.D. Hong, *buildup of ultrathin multilayer films by a self-assembly process.1. Consecutive adsorption of anionic and cationic bipolar amphiphiles on charged surfaces*. Makromolekulare Chemie-Macromolecular Symposia, 1991. **46**: p. 321–327.
69. Decher, G., et al., *Layer-by-layer adsorbed films of polyelectrolytes, proteins or dna*. Abstracts of Papers of the American Chemical Society, 1993. **205**: p. 334–POLY.
70. Hong, J.D., et al., *Layer-by-layer deposited multilayer assemblies of polyelectrolytes and proteins—from ultrathin films to protein arrays*, in *Trends in Colloid and Interface Science Vii*, P. Laggner and O. Glatter, Editors. 1993. p. 98–102.
71. Decher, G., et al., *New nanocomposite films for biosensors—layer-by-layer adsorbed films of polyelectrolytes, proteins or dna*. Biosensors & Bioelectronics, 1994. **9**(9–10): p. 677–684.
72. Ladam, G., et al., *Protein adsorption onto auto-assembled polyelectrolyte films*. Biomolecular Engineering, 2002. **19**(2–6): p. 273–280.
73. Voegel, J.C., G. Decher, and P. Schaaf, *Polyelectrolyte multilayer films in the biotechnology field*. Actualite Chimique, 2003(11–12): p. 30–38.
74. Richert, L., et al., *Improvement of stability and cell adhesion properties of polyelectrolyte multilayer films by chemical cross-linking*. Biomacromolecules, 2004. **5**(2): p. 284–294.
75. Izquierdo, A., et al., *Dipping versus spraying: Exploring the deposition conditions for speeding up layer-by-layer assembly*. Langmuir, 2005. **21**(16): p. 7558–7567.
76. Matsusaki, M., et al., *Layer-by-Layer Assembly Through Weak Interactions and Their Biomedical Applications*. Advanced Materials, 2012. **24**(4): p. 454–474.
77. Matsusaki, M., et al., *Fabrication of celtular multilayers with nanometer-sized extracellular matrix films*. Angewandte Chemie-International Edition, 2007. **46**(25): p. 4689–4692.
78. Moy, V.T., E.L. Florin, and H.E. Gaub, *intermolecular forces and energies between ligands and receptors*. Science, 1994. **266**(5183): p. 257–259.
79. Hyun, J., et al., *Molecular recognition-mediated fabrication of protein nanostructures by dip-pen lithography*. Nano Letters, 2002. **2**(11): p. 1203–1207.
80. Häußling, L., et al., *Surface functionalization and surface recognition: Plasmon optical detection of molecular recognition at self assembled monolayers*. Makromolekulare Chemie. Macromolecular Symposia, 1991. **46**(1): p. 145–155.
81. Faucheux, N., et al., *Self-assembled monolayers with different terminating groups as model substrates for cell adhesion studies*. Biomaterials, 2004. **25**(14): p. 2721–2730.
82. Desai, S., et al., *Tailor-made functional surfaces: potential elastomeric biomaterials I*. Journal of Biomaterials Science-Polymer Edition, 2003. **14**(12): p. 1323–1338.
83. Norberg, O., et al., *Photo-Click Immobilization of Carbohydrates on Polymeric Surfaces-A Quick Method to Functionalize Surfaces for Biomolecular Recognition Studies*. Bioconjugate Chemistry, 2009. **20**(12): p. 2364–2370.
84. Situma, C., et al., *UV patterning of high density oligonugleotide microarrays in poly(methyl) methacrylate (PMMA) microfluidic devices*. Abstracts of Papers of the American Chemical Society, 2004. **228**: p. U118–U118.
85. Situma, C., et al., *Fabrication of DNA microarrays onto poly(methyl methacrylate) with ultraviolet patterning and microfluidics for the detection of low-abundant point mutations*. Analytical Biochemistry, 2005. **340**(1): p. 123–135.
86. Nahar, P., A. Naqvi, and S.F. Basir, *Sunlight-mediated activation of an inert polymer surface for covalent immobilization of a protein*. Analytical Biochemistry, 2004. **327**(2): p. 162–164.
87. Delaittre, G., et al., *Chemical approaches to synthetic polymer surface biofunctionalization for targeted cell adhesion using small binding motifs*. Soft Matter, 2012. **8**(28): p. 7323–7347.
88. Parsonage, E., et al., *Adsorption of poly(2-vinylpyridine) poly(styrene) block copolymers from toluene solutions*. Macromolecules, 1991. **24**(8): p. 1987–1995.
89. Marra, J. and M.L. Hair, *interactions between 2 adsorbed layers of poly(ethylene oxide) polystyrene diblock copolymers in heptane toluene mixtures*. Colloids and Surfaces, 1989. **34**(3): p. 215–226.

90. Guzonas, D., D. Boils, and M.L. Hair, *surface force measurements of polystyrene-block-poly(ethylene oxide) adsorbed from a nonselective solvent on mica*. Macromolecules, 1991. **24**(11): p. 3383–3387.
91. Hair, M.L., D. Guzonas, and D. Boils, *adsorption of polystyrene-b-poly(ethylene oxide) on mica—scaling concepts*. Macromolecules, 1991. **24**(1): p. 341–342.
92. Guzonas, D.A., et al., *Role of block size asymmetry on the adsorbed amount of polystyrene-b-poly(ethylene oxide) on mica surfaces from toluene*. Macromolecules, 1992. **25**(9): p. 2434–2441.
93. Zhao, B. and W.J. Brittain, *Polymer brushes: surface-immobilized macromolecules*. Progress in Polymer Science, 2000. **25**(5): p. 677–710.
94. Massia, S.P. and J.A. Hubbell, *covalently attached grgd on polymer surfaces promotes biospecific adhesion of mammalian-cells*. Annals of the New York Academy of Sciences, 1990. **589**: p. 261–270.
95. Matsuda, T., et al., *Development of a novel artificial matrix with cell adhesion peptides for cell culture and artificial and hybrid organs*. ASAIO transactions/American Society for Artificial Internal Organs, 1989. **35**(3): p. 677–9.
96. Lee, J.W., et al., *Estimation of cell proliferation by various peptide coating at the PPF/DEF 3D scaffold*. Microelectronic Engineering, 2009. **86**(4–6): p. 1451–1454.
97. Lee, J.W., et al., *Carboxylic acid-functionalized conductive polypyrrole as a bioactive platform for cell adhesion*. Biomacromolecules, 2006. **7**(6): p. 1692–1695.
98. Biltresse, S., M. Attolini, and J. Marchand-Brynaert, *Cell adhesive PET membranes by surface grafting of RGD peptidomimetics*. Biomaterials, 2005. **26**(22): p. 4576–4587.
99. Gabriel, M., et al., *Direct grafting of RGD-motif-containing peptide on the surface of polycaprolactone films*. Journal of Biomaterials Science-Polymer Edition, 2006. **17**(5): p. 567–577.
100. Hu, Y.H., et al., *Porous polymer scaffolds surface-modified with arginine-glycine-aspartic acid enhance bone cell attachment and differentiation in vitro*. Journal of Biomedical Materials Research Part A, 2003. **64A**(3): p. 583–590.
101. Sanchez, M., et al., *Synthesis of hemocompatible materials.1. Surface modification of polyurethanes based on poly(chloroalkylvinylether)s by rgd fragments*. Clinical Materials, 1994. **15**(4): p. 253–258.
102. Guan, J.J., et al., *Biodegradable poly(ether ester urethane)urea elastomers based on poly(ether ester) triblock copolymers and putrescine: synthesis, characterization and cytocompatibility*. Biomaterials, 2004. **25**(1): p. 85–96.
103. Kondoh, A., K. Makino, and T. Matsuda, *2-dimensional artificial extracellular-matrix—bioadhesive peptide-immobilized surface design*. Journal of Applied Polymer Science, 1993. **47**(11): p. 1983–1988.
104. Sun, H. and S. Onneby, *Facile polyester surface functionalization via hydrolysis and cell-recognizing peptide attachment*. Polymer International, 2006. **55**(11): p. 1336–1340.
105. Goddard, J.M., J.N. Talbert, and J.H. Hotchkiss, *Covalent attachment of lactase to low-density polyethylene films*. Journal of Food Science, 2007. **72**(1): p. E36–E41.
106. Dominick, W.D., et al., *Covalent immobilization of proteases and nucleases to poly(methylmethacrylate)*. Analytical and Bioanalytical Chemistry, 2003. **376**(3): p. 349–354.
107. Biederman, H., et al., *Characterization of glow-discharge-treated cellulose acetate membrane surfaces for single-layer enzyme electrode studies*. Journal of Applied Polymer Science, 2001. **81**(6): p. 1341–1352.
108. Rejikumar, S. and S. Devi, *immobilization of beta-galactosidase onto polymeric supports*. Journal of Applied Polymer Science, 1995. **55**(6): p. 871–878.
109. Gonzalez-Saiz, J.M. and C. Pizarro, *Polyacrylamide gels as support for enzyme immobilization by entrapment. Effect of polyelectrolyte carrier, pH and temperature on enzyme action and kinetics parameters*. European Polymer Journal, 2001. **37**(3): p. 435–444.

110. Godjevargova, T., R. Dayal, and I. Marinov, *Simultaneous covalent immobilization of glucose oxidase and catalase onto chemically modified acrylonitrile copolymer membranes*. Journal of Applied Polymer Science, 2004. **91**(6): p. 4057–4063.
111. Bahulekar, R., N.R. Ayyangar, and S. Ponrathnam, *polyethyleneimine in immobilization of biocatalysts*. Enzyme and Microbial Technology, 1991. **13**(11): p. 858–868.
112. Qu, H.Y., et al., *Stable microstructured network for protein patterning on a plastic microfluidic channel: Strategy and characterization of on-chip enzyme microreactors*. Analytical Chemistry, 2004. **76**(21): p. 6426–6433.
113. Henry, A.C., et al., *Surface modification of poly(methyl methacrylate) used in the fabrication of microanalytical devices*. Analytical Chemistry, 2000. **72**(21): p. 5331–5337.
114. Fixe, F., et al., *One-step immobilization of aminated and thiolated DNA onto poly(methylmethacrylate) (PMMA) substrates*. Lab on a Chip, 2004. **4**(3): p. 191–195.
115. Fuentes, M., et al., *Directed covalent immobilization of aminated DNA probes on aminated plates*. Biomacromolecules, 2004. **5**(3): p. 883–888.
116. Tran, L.D., et al., *A polytyramine film for covalent immobilization of oligonucleotides and hybridization*. Synthetic Metals, 2003. **139**(2): p. 251–262.
117. Ketomaki, K., et al., *Hybridization properties of support-bound oligonucleotides: The effect of the site of immobilization on the stability and selectivity of duplex formation*. Bioconjugate Chemistry, 2003. **14**(4): p. 811–816.
118. Niu, X.F., et al., *Arg-gly-Asp (RGD) modified biomimetic polymeric materials*. Journal of Materials Science & Technology, 2005. **21**(4): p. 571–576.
119. Sebra, R.P., et al., *Surface grafted antibodies: Controlled architecture permits enhanced antigen detection*. Langmuir, 2005. **21**(24): p. 10907–10911.
120. Chang, C.-C., et al., *Comparative Assessment of Oriented Antibody Immobilization on Surface Plasmon Resonance Biosensing*. Journal of the Chinese Chemical Society, 2013. **60**(12): p. 1449–1456.
121. Jackson, J.M., et al., *UV activation of polymeric high aspect ratio microstructures: ramifications in antibody surface loading for circulating tumor cell selection*. Lab on a Chip, 2014. **14**(1): p. 106–117.
122. Feyssa, B., et al., *Patterned Immobilization of Antibodies within Roll-to-Roll Hot Embossed Polymeric Microfluidic Channels*. Plos One, 2013. **8**(7).
123. Sung, D., et al., *High-density immobilization of antibodies onto nanobead-coated cyclic olefin copolymer plastic surfaces for application as a sensitive immunoassay chip*. Biomedical Microdevices, 2013. **15**(4): p. 691–698.
124. Chebil, S., et al., *Polypyrrole functionalized with new copper complex as platform for His-tag antibody immobilization and direct antigen detection*. Sensors and Actuators B-Chemical, 2013. **185**: p. 762–770.
125. Shin, H., S. Jo, and A.G. Mikos, *Biomimetic materials for tissue engineering*. Biomaterials, 2003. **24**(24): p. 4353–4364.
126. Goddard, J.M. and J.H. Hotchkiss, *Tailored functionalization of low-density polyethylene surfaces*. Journal of Applied Polymer Science, 2008. **108**(5): p. 2940–2949.
127. Kim, Y.J., et al., *Surface characterization and in vitro blood compatibility of poly(ethylene terephthalate) immobilized with insulin and/or heparin using plasma glow discharge*. Biomaterials, 2000. **21**(2): p. 121–130.
128. Byun, Y., H.A. Jacobs, and S.W. Kim, *heparin surface immobilization through hydrophilic spacers—thrombin and antithrombin-iii binding-kinetics*. Journal of Biomaterials Science-Polymer Edition, 1994. **6**(1): p. 1–13.
129. de Leon, A.S., et al., *Control of the chemistry outside the pores in honeycomb patterned films*. Polymer Chemistry, 2013. **4**(14): p. 4024–4032.
130. Munoz-Bonilla, A., et al., *Fabrication of Honeycomb-Structured Porous Surfaces Decorated with Glycopolymers*. Langmuir, 2010. **26**(11): p. 8552–8558.
131. Yang, J.M., et al., *Wettability and antibacterial assessment of chitosan containing radiation-induced graft nonwoven fabric of polypropylene-g-acrylic acid*. Journal of Applied Polymer Science, 2003. **90**(5): p. 1331–1336.

132. Yang, M.C. and W.C. Lin, *Protein adsorption and platelet adhesion of polysulfone membrane immobilized with chitosan and heparin conjugate*. Polymers for Advanced Technologies, 2003. **14**(2): p. 103–113.
133. Xu, F.J., et al., *Heparin-coupled poly(poly(ethylene glycol) monomethacrylate)-Si(111) hybrids and their blood compatible surfaces*. Biomacromolecules, 2005. **6**(3): p. 1759–1768.
134. Toyoshima, M., et al., *Biological specific recognition of glycopolymer-modified interfaces by RAFT living radical polymerization*. Polymer Journal, 2010. **42**(2): p. 172–178.
135. Reynolds, M., et al., *Influence of ligand presentation density on the molecular recognition of mannose-functionalised glyconanoparticles by bacterial lectin BC2 L-A*. Glycoconjugate Journal, 2013. **30**(8): p. 747–757.
136. Massia, S.P., J. Stark, and D.S. Letbetter, *Surface-immobilized dextran limits cell adhesion and spreading*. Biomaterials, 2000. **21**(22): p. 2253–2261.
137. Reddy, R.M., A. Srivastava, and A. Kumar, *Monosaccharide-Responsive Phenylboronate-Polyol Cell Scaffolds for Cell Sheet and Tissue Engineering Applications*. Plos One, 2013. **8**(10).
138. Bertok, T., et al., *Electrochemical lectin based biosensors as a label-free tool in glycomics*. Microchimica Acta, 2013. **180**(1–2): p. 1–13.
139. Vega, E., et al., *Synthesis of chiral mesoporous silicas with oligo(saccharide) surfaces and their use in separation of stereoisomers*. Journal of Colloid and Interface Science, 2011. **359**(2): p. 542–544.
140. Kejik, Z., et al., *Selective recognition of a saccharide-type tumor marker with natural and synthetic ligands: a new trend in cancer diagnosis*. Analytical and Bioanalytical Chemistry, 2010. **398**(5): p. 1865–1870.
141. Tseng, T.T.C., J. Yao, and W.-C. Chan, *Selective enzyme immobilization on arrayed microelectrodes for the application of sensing neurotransmitters*. Biochemical Engineering Journal, 2013. **78**: p. 146–153.
142. Palacio, M.L.B. and B. Bhushan, *Enzyme adsorption on polymer-based confined bioinspired biosensing surface*. Journal of Vacuum Science & Technology A, 2012. **30**(5).
143. Muriel-Galet, V., et al., *Covalent Immobilization of Lysozyme on Ethylene Vinyl Alcohol Films for Nonmigrating Antimicrobial Packaging Applications*. Journal of Agricultural and Food Chemistry, 2013. **61**(27): p. 6720–6727.
144. Khosravi, A., et al., *Magnetic labelled horseradish peroxidase-polymer nanoparticles: a recyclable nanobiocatalyst*. Journal of the Serbian Chemical Society, 2013. **78**(7): p. 921–931.
145. Fang, Y., et al., *Polymer materials for enzyme immobilization and their application in bioreactors*. Bmb Reports, 2011. **44**(2): p. 87–95.
146. Dai, Y., et al., *Electrospun Nanofiber Membranes as Supports for Enzyme Immobilization and Its Application*. Progress in Chemistry, 2010. **22**(9): p. 1808–1818.
147. Wang, Z.-G., et al., *Enzyme immobilization on electrospun polymer nanofibers: An overview*. Journal of Molecular Catalysis B-Enzymatic, 2009. **56**(4): p. 189–195.
148. Ansari, S.A. and Q. Husain, *Potential applications of enzymes immobilized on/in nano materials: A review*. Biotechnology Advances, 2012. **30**(3): p. 512–523.
149. Talbert, J.N. and J.M. Goddard, *Enzymes on material surfaces*. Colloids and Surfaces B: Biointerfaces, 2012. **93**(0): p. 8–19.
150. Tran, D.N. and K.J. Balkus, Jr., *Perspective of Recent Progress in Immobilization of Enzymes*. Acs Catalysis, 2011. **1**(8): p. 956–968.
151. Leung, K.C.F., et al., *Immunoassays using polypeptide conjugate binders with tuned affinity*. Expert Review of Molecular Diagnostics, 2010. **10**(7): p. 863–867.
152. Groll, J., et al., *Ultrathin Coatings from Isocyanate Terminated Star PEG Prepolymers: Patterning of Proteins on the Layers*. Langmuir, 2005. **21**(7): p. 3076–3083.
153. Welle, A., et al., *Photo-chemically patterned polymer surfaces for controlled PC-12 adhesion and neurite guidance*. Journal of Neuroscience Methods, 2005. **142**(2): p. 243–250.
154. Thissen, H., et al., *Nanometer thickness laser ablation for spatial control of cell attachment*. Smart Materials and Structures, 2002. **11**(5): p. 792.

155. Tan, J.L., et al., *Simple approach to micropattern cells on common culture substrates by tuning substrate wettability*. Tissue Engineering, 2004. **10**(5–6): p. 865–872.
156. Yang, M., et al., *Lab-on-a-chip for carbon nanotubes based immunoassay detection of Staphylococcal Enterotoxin B (SEB)*. Lab on a Chip, 2010. **10**(8): p. 1011–1017.
157. Puertas, S., et al., *Improving immunosensor performance through oriented immobilization of antibodies on carbon nanotube composite surfaces*. Biosensors & Bioelectronics, 2013. **43**: p. 274–280.
158. Sai, V.V.R., et al., *Immobilization of antibodies on polyaniline films and its application in a piezoelectric immunosensor*. Analytical Chemistry, 2006. **78**(24): p. 8368–8373.
159. Skottrup, P.D., M. Nicolaisen, and A.F. Justesen, *Towards on-site pathogen detection using antibody-based sensors*. Biosensors & Bioelectronics, 2008. **24**(3): p. 339–348.
160. Moreira, F.T.C., et al., *Smart plastic antibody material (SPAM) tailored on disposable screen printed electrodes for protein recognition: Application to myoglobin detection*. Biosensors & Bioelectronics, 2013. **45**: p. 237–244.
161. Zhang, M., et al., *Immobilization of anti-CD31 antibody on electrospun poly(epsilon-caprolactone) scaffolds through hydrophobins for specific adhesion of endothelial cells*. Colloids and Surfaces B-Biointerfaces, 2011. **85**(1): p. 32–39.
162. Badelt-Lichtblau, H., et al., *Genetic Engineering of the S-Layer Protein SbpA of Lysinibacillus sphaericus CCM 2177 for the Generation of Functionalized Nanoarrays*. Bioconjugate Chemistry, 2009. **20**(5): p. 895–903.
163. Chakraborty, B., et al., *Rational design and performance testing of aptamer-based electrochemical biosensors for adenosine*. Journal of Electroanalytical Chemistry, 2009. **635**(2): p. 75–82.
164. Cheng, A.K.H., D. Sen, and H.-Z. Yu, *Design and testing of aptamer-based electrochemical biosensors for proteins and small molecules*. Bioelectrochemistry, 2009. **77**(1): p. 1–12.
165. Han, K., Z. Liang, and N. Zhou, *Design Strategies for Aptamer-Based Biosensors*. Sensors, 2010. **10**(5): p. 4541–4557.
166. He, P., et al., *Label-free electrochemical monitoring of vasopressin in aptamer-based microfluidic biosensors*. Analytica Chimica Acta, 2013. **759**: p. 74–80.
167. Wang, R.E., et al., *Aptamer-Based Fluorescent Biosensors*. Current Medicinal Chemistry, 2011. **18**(27): p. 4175–4184.
168. Khung, Y.L. and D. Narducci, *Synergizing nucleic acid aptamers with 1-dimensional nanostructures as label-free field-effect transistor biosensors*. Biosensors & Bioelectronics, 2013. **50**: p. 278–293.
169. Su, S., et al., *Microgel-based inks for paper-supported biosensing applications*. Biomacromolecules, 2008. **9**(3): p. 935–941.
170. Luo, Y., et al., *Dual-Aptamer-Based Biosensing of Toxoplasma Antibody*. Analytical Chemistry, 2013. **85**(17): p. 8354–8360.
171. Sekhon, S.S., et al., *Advances in pathogen-associated molecules detection using Aptamer based biosensors*. Molecular & Cellular Toxicology, 2013. **9**(4): p. 311–317.
172. Wang, T., et al., *The diagnostic application of aptamer based on polyacrylamide gel electrophoresis and gray analysis*. Journal of Gastroenterology and Hepatology, 2013. **28**: p. 383–383.
173. Sharma, S., et al., *Nucleic acid aptamer based glycan binders for analytical and diagnostic tools*. Irish Journal of Medical Science, 2013. **182**: p. S139–S139.
174. Hong, P., W. Li, and J. Li, *Applications of Aptasensors in Clinical Diagnostics*. Sensors, 2012. **12**(2): p. 1181–1193.
175. Balamurugan, S., et al., *Surface immobilization methods for aptamer diagnostic applications*. Analytical and Bioanalytical Chemistry, 2008. **390**(4): p. 1009–1021.
176. Wang, Y., K.-Y. Pu, and B. Liu, *Anionic Conjugated Polymer with Aptamer-Functionalized Silica Nanoparticle for Label-Free Naked-Eye Detection of Lysozyme in Protein Mixtures*. Langmuir, 2010. **26**(12): p. 10025–10030.
177. Yoon, H., et al., *A novel sensor platform based on aptamer-conjugated polypyrrole nanotubes for label-free electrochemical protein detection*. Chembiochem, 2008. **9**(4): p. 634–641.

178. Danielsson, B., *Artificial receptors*, in *Biosensing for the 21st Century*, R. Renneberg and F. Lisdat, Editors. 2008. p. 97–122.
179. Zhang, Z., et al., *Programmable Hydrogels for Controlled Cell Catch and Release Using Hybridized Aptamers and Complementary Sequences*. Journal of the American Chemical Society, 2012. **134**(38): p. 15716–15719.
180. Li, Z., et al., *Aptamer-conjugated dendrimer-modified quantum dots for cancer cell targeting and imaging*. Materials Letters, 2010. **64**(3): p. 375–378.
181. Jafari, R., et al., *Development of oligonucleotide microarray involving plasma polymerized acrylic acid*. Thin Solid Films, 2009. **517**(19): p. 5763–5768.
182. Sethi, D., et al., *Polymer supported synthesis of aminooxyalkylated oligonucleotides, and some applications in the fabrication of microarrays*. Bioorganic & Medicinal Chemistry, 2009. **17**(15): p. 5442–5450.
183. Shishkanova, T.V., et al., *Functionalization of PVC membrane with ss oligonucleotides for a potentiometric biosensor*. Biosensors & Bioelectronics, 2007. **22**(11): p. 2712–2717.
184. Yan, F., et al., *Label-free DNA sensor based on organic thin film transistors*. Biosensors & Bioelectronics, 2009. **24**(5): p. 1241–1245.
185. Levicky, R. and A. Horgan, *Physicochemical perspectives on DNA microarray and biosensor technologies*. Trends in Biotechnology, 2005. **23**(3): p. 143–149.
186. Marie, R., et al., *Immobilisation of DNA to polymerised SU-8 photoresist*. Biosensors & Bioelectronics, 2006. **21**(7): p. 1327–1332.
187. Patnaik, S., et al., *Engineered Polymer-Supported Synthesis of 3 '-Carboxyalkyl-Modified Oligonucleotides and Their Applications in the Construction of Biochips for Diagnosis of the Diseases*. Bioconjugate Chemistry, 2012. **23**(3): p. 664–670.
188. Cottenye, N., et al., *Oligonucleotide Nanostructured Surfaces: Effect on Escherichia coli Curli Expression*. Macromolecular Bioscience, 2008. **8**(12): p. 1161–1172.
189. Andersson, M., et al., *Surface attachment of nanoparticles using oligonucleotides*. Colloids and Surfaces B-Biointerfaces, 2004. **34**(3): p. 165–171.
190. Ariga, K., et al., *Challenges and breakthroughs in recent research on self-assembly*. Science and Technology of Advanced Materials, 2008. **9**(1).
191. Sakakibara, K., J.P. Hill, and K. Ariga, *Thin-Film-Based Nanoarchitectures for Soft Matter: Controlled Assemblies into Two-Dimensional Worlds*. Small, 2011. **7**(10): p. 1288–1308.
192. Ariga, K., et al., *Nanoarchitectonics: A Conceptual Paradigm for Design and Synthesis of Dimension-Controlled Functional Nanomaterials*. Journal of Nanoscience and Nanotechnology, 2011. **11**(1): p. 1–13.
193. Acharya, S., J.P. Hill, and K. Ariga, *Soft Langmuir-Blodgett Technique for Hard Nanomaterials*. Advanced Materials, 2009. **21**(29): p. 2959–2981.
194. Gates, B.D., et al., *New approaches to nanofabrication: Molding, printing, and other techniques*. Chemical Reviews, 2005. **105**(4): p. 1171–1196.
195. Li, L., et al., *Achieving lambda/20 Resolution by One-Color Initiation and Deactivation of Polymerization*. Science, 2009. **324**(5929): p. 910–913.
196. Schmid, G.M., et al., *Step and flash imprint lithography for manufacturing patterned media*. Journal of Vacuum Science & Technology B, 2009. **27**(2): p. 573–580.
197. Chung, S.W., et al., *Top-down meets bottom-up: Dip-pen nanolithography and DNA-directed assembly of nanoscale electrical circuits*. Small, 2005. **1**(1): p. 64–69.
198. Ginger, D.S., H. Zhang, and C.A. Mirkin, *The evolution of dip-pen nanolithography*. Angewandte Chemie-International Edition, 2004. **43**(1): p. 30–45.
199. Ando, Y., et al., *Fabrication of nanostripe surface structure by multilayer film deposition combined with micropatterning*. Nanotechnology, 2010. **21**(9).
200. Marrian, C.R.K. and D.M. Tennant, *Nanofabrication*. Journal of Vacuum Science & Technology A, 2003. **21**(5): p. S207–S215.
201. Yaman, M., et al., *Arrays of indefinitely long uniform nanowires and nanotubes*. Nature Materials, 2011. **10**(7): p. 494–501.
202. Liddle, J.A. and G.M. Gallatin, *Lithography, metrology and nanomanufacturing*. Nanoscale, 2011. **3**(7): p. 2679–2688.

203. Smith, J.C., et al., *Nanopatterning the chemospecific immobilization of cowpea mosaic virus capsid*. Nano Letters, 2003. **3**(7): p. 883–886.
204. Schaffer, E., et al., *Electrically induced structure formation and pattern transfer*. Nature, 2000. **403**(6772): p. 874–877.
205. Thurn-Albrecht, T., et al., *Overcoming interfacial interactions with electric fields*. Macromolecules, 2000. **33**(9): p. 3250–3253.
206. Biswas, A., et al., *Advances in top–down and bottom–up surface nanofabrication: Techniques, applications & amp; future prospects*. Advances in Colloid and Interface Science, 2012. **170**(1–2): p. 2–27.
207. Acikgoz, C., et al., *Polymers in conventional and alternative lithography for the fabrication of nanostructures*. European Polymer Journal, 2011. **47**(11): p. 2033–2052.
208. Aherne, A., et al., *Bacteria-mediated lithography of polymer surfaces*. Journal of the American Chemical Society, 1996. **118**(36): p. 8771–8772.
209. Lan, H. and H. Liu, *UV-Nanoimprint Lithography: Structure, Materials and Fabrication of Flexible Molds*. Journal of Nanoscience and Nanotechnology, 2013. **13**(5): p. 3145–3172.
210. Ito, H., *Development of new advanced resist materials for microlithography*. Journal of Photopolymer Science and Technology, 2008. **21**(4): p. 475–491.
211. Moon, S.-Y. and J.-M. Kim, *Chemistry of photolithographic imaging materials based on the chemical amplification concept*. Journal of Photochemistry and Photobiology C-Photochemistry Reviews, 2007. **8**(4): p. 157–173.
212. Nishikuboand, T. and H. Kudo, *Recent Development in Molecular Resists for Extreme Ultraviolet Lithography*. Journal of Photopolymer Science and Technology, 2011. **24**(1): p. 9–18.
213. Wallraff, G.M. and W.D. Hinsberg, *Lithographic Imaging Techniques for the Formation of Nanoscopic Features*. Chemical Reviews, 1999. **99**(7): p. 1801–1822.
214. Brunner, T.A., *Why optical lithography will live forever*. Journal of Vacuum Science & Technology B, 2003. **21**(6): p. 2632–2637.
215. Ito, T. and S. Okazaki, *Pushing the limits of lithography*. Nature, 2000. **406**(6799): p. 1027–1031.
216. Willson, C.G. and B.C. Trinque, *The evolution of materials for the photolithographic process*. Journal of Photopolymer Science and Technology, 2003. **16**(4): p. 621–627.
217. Rothschild, M., et al., *Liquid immersion lithography: Why, how, and when*? Journal of Vacuum Science & Technology B, 2004. **22**(6): p. 2877–2881.
218. Gil, D., et al., *Immersion lithography: New opportunities for semiconductor manufacturing*. Journal of Vacuum Science & Technology B, 2004. **22**(6): p. 3431–3438.
219. del Campo, A. and E. Arzt, *Fabrication approaches for generating complex micro- and nanopatterns on polymeric surfaces*. Chemical Reviews, 2008. **108**(3): p. 911–945.
220. Xia, Y.N. and G.M. Whitesides, *Soft lithography*. Annual Review of Materials Science, 1998. **28**: p. 153–184.
221. Rogers, J.A. and R.G. Nuzzo, *Recent progress in soft lithography*. Materials Today, 2005. **8**(2): p. 50–56.
222. Kane, R.S., et al., *Patterning proteins and cells using soft lithography*. Biomaterials, 1999. **20**(23–24): p. 2363–2376.
223. Kaufmann, T. and B.J. Ravoo, *Stamps, inks and substrates: polymers in microcontact printing*. Polymer Chemistry, 2010. **1**(4): p. 371–387.
224. Ruiz, S.A. and C.S. Chen, *Microcontact printing: A tool to pattern*. Soft Matter, 2007. **3**(2): p. 168–177.
225. Amellal, K., et al., *Injection-molding of medical plastics—a review*. Advances in Polymer Technology, 1994. **13**(4): p. 315–322.
226. Chen, Z.B. and L.S. Turng, *A review of current developments in process and quality control for injection molding*. Advances in Polymer Technology, 2005. **24**(3): p. 165–182.
227. Mendes, P.M., C.L. Yeung, and J.A. Preece, *Bio-nanopatterning of surfaces*. Nanoscale Research Letters, 2007. **2**(8): p. 373–384.

228. Xie, Z., et al., *Polymer Nanostructures Made by Scanning Probe Lithography: Recent Progress in Material Applications*. Macromolecular Rapid Communications, 2012. **33**(5): p. 359–373.
229. Rosa, L.G. and J. Liang, *Atomic force microscope nanolithography: dip-pen, nanoshaving, nanografting, tapping mode, electrochemical and thermal nanolithography*. Journal of Physics-Condensed Matter, 2009. **21**(48).
230. Lim, J.H., et al., *Direct-write dip-pen nanolithography of proteins on modified silicon oxide surfaces*. Angewandte Chemie-International Edition, 2003. **42**(20): p. 2309–2312.
231. Lee, M., et al., *Protein nanoarray on Prolinker ™ surface constructed by atomic force microscopy dip-pen nanolithography for analysis of protein interaction*. Proteomics, 2006. **6**(4): p. 1094–1103.
232. Demers, L.M., et al., *Direct patterning of modified oligonucleotides on metals and insulators by dip-pen nanolithography*. Science, 2002. **296**(5574): p. 1836–1838.
233. Wendel, M., et al., *Nanolithography with an atomic-force microscope for integrated fabrication of quantum electronic devices*. Applied Physics Letters, 1994. **65**(14): p. 1775–1777.
234. Liu, G.Y., S. Xu, and Y.L. Qian, *Nanofabrication of self-assembled monolayers using scanning probe lithography*. Accounts of Chemical Research, 2000. **33**(7): p. 457–466.
235. Xu, S. and G.Y. Liu, *Nanometer-scale fabrication by simultaneous nanoshaving and molecular self-assembly*. Langmuir, 1997. **13**(2): p. 127–129.
236. Banerjee, I.A., et al., *Thiolated peptide nanotube assembly as arrays on patterned Au substrates*. Nano Letters, 2004. **4**(12): p. 2437–2440.
237. Nuraje, N., et al., *Biological bottom-up assembly of antibody nanotubes on patterned antigen arrays*. Journal of the American Chemical Society, 2004. **126**(26): p. 8088–8089.
238. Zhao, Z.Y., P.A. Banerjee, and H. Matsui, *Simultaneous targeted immobilization of anti-human IgG-coated nanotubes and anti-mouse IgG-coated nanotubes on the complementary antigen-patterned surfaces via biological molecular recognition*. Journal of the American Chemical Society, 2005. **127**(25): p. 8930–8931.
239. Schift, H., *Nanoimprint lithography: An old story in modern times? A review*. Journal of Vacuum Science & Technology B, 2008. **26**(2): p. 458–480.
240. Guo, L.J., *Nanoimprint lithography: Methods and material requirements*. Advanced Materials, 2007. **19**(4): p. 495–513.
241. Michel, R., et al., *A novel approach to produce biologically relevant chemical patterns at the nanometer scale: Selective molecular assembly patterning combined with colloidal lithography*. Langmuir, 2002. **18**(22): p. 8580–8586.
242. Csucs, G., et al., *Microcontact Printing of Macromolecules with Submicrometer Resolution by Means of Polyolefin Stamps*. Langmuir, 2003. **19**(15): p. 6104–6109.
243. Nakamatsu, K., et al., *Nanoimprint and nanocontact technologies using hydrogen silsesquioxane*. Journal of Vacuum Science & Technology B, 2005. **23**(2): p. 507–512.
244. Rolland, J.P., et al., *Solvent-resistant photocurable "liquid teflon" for microfluidic device fabrication*. Journal of the American Chemical Society, 2004. **126**(8): p. 2322–2323.
245. Renault, J.P., et al., *Fabricating arrays of single protein molecules on glass using microcontact printing*. Journal of Physical Chemistry B, 2003. **107**(3): p. 703–711.
246. Pla-Roca, M., et al., *Micro/nanopatterning of proteins via contact printing using high aspect ratio PMMA stamps and NanoImprint apparatus*. Langmuir, 2007. **23**(16): p. 8614–8618.
247. Li, H.W., et al., *Nanocontact printing: A route to sub-50-nm-scale chemical and biological patterning*. Langmuir, 2003. **19**(6): p. 1963–1965.
248. Komuro, N., et al., *Inkjet printed (bio)chemical sensing devices*. Analytical and Bioanalytical Chemistry, 2013. **405**(17): p. 5785–5805.
249. Singh, M., et al., *Inkjet Printing—Process and Its Applications*. Advanced Materials, 2010. **22**(6): p. 673–685.
250. Gonzalez-Macia, L., et al., *Advanced printing and deposition methodologies for the fabrication of biosensors and biodevices*. Analyst, 2010. **135**(5): p. 845–867.
251. Delaney, J.T., P.J. Smith, and U.S. Schubert, *Inkjet printing of proteins*. Soft Matter, 2009. **5**(24): p. 4866–4877.

252. Ito, Y., *Surface micropatterning to regulate cell functions*. Biomaterials, 1999. **20**(23–24): p. 2333–2342.
253. Webb, K., V. Hlady, and P.A. Tresco, *Relationships among cell attachment, spreading, cytoskeletal organization, and migration rate for anchorage-dependent cells on model surfaces*. Journal of Biomedical Materials Research, 2000. **49**(3): p. 362–368.
254. Kapur, R. and A.S. Rudolph, *Cellular and cytoskeleton morphology and strength of adhesion of cells on self-assembled monolayers of organosilanes*. Experimental Cell Research, 1998. **244**(1): p. 275–285.
255. Jenney, C.R., et al., *Human monocyte/macrophage adhesion, macrophage motility, and IL-4-induced foreign body giant cell formation on silane-modified surfaces in vitro*. Journal of Biomedical Materials Research, 1998. **41**(2): p. 171–184.
256. Sukenik, C.N., et al., *Modulation of cell-adhesion by modification of titanium surfaces with covalently attached self-assembled monolayers*. Journal of Biomedical Materials Research, 1990. **24**(10): p. 1307–1323.
257. Wu, N. and W.B. Russel, *Micro- and nano-patterns created via electrohydrodynamic instabilities*. Nano Today, 2009. **4**(2): p. 180–192.
258. Schaffer, E., et al., *Electrohydrodynamic instabilities in polymer films*. Europhysics Letters, 2001. **53**(4): p. 518–524.
259. Gentili, D., et al., *Applications of dewetting in micro and nanotechnology*. Chemical Society Reviews, 2012. **41**(12): p. 4430–4443.
260. Bunz, U.H.F., *Breath Figures as a Dynamic Templating Method for Polymers and Nanomaterials*. Advanced Materials, 2006. **18**(8): p. 973–989.
261. Muñoz-Bonilla, A., M. Fernández-García, and J. Rodríguez-Hernández, *Towards hierarchically ordered functional porous polymeric surfaces prepared by the breath figures approach*. Progress in Polymer Science, 2014. **39**(3): p. 510–554.
262. Bai, H., et al., *Breath figure arrays: Unconventional fabrications, functionalizations, and applications*. Angewandte Chemie—International Edition, 2013. **52**(47): p. 12240–12255.
263. Escalé, P., et al., *Recent advances in honeycomb-structured porous polymer films prepared via breath figures*. European Polymer Journal, 2012. **48**(6): p. 1001–1025.
264. Hernández-Guerrero, M. and M.H. Stenzel, *Honeycomb structured polymer films via breath figures*. Polymer Chemistry, 2012. **3**(3): p. 563–577.
265. Nishida, J., et al., *Preparation of self-organized micro-patterned polymer films having cell adhesive ligands*. Polymer Journal, 2002. **34**(3): p. 166–174.
266. Ting, S.R.S., et al., *Lectin recognizable biomaterials synthesized via nitroxide-mediated polymerization of a methacryloyl galactose monomer*. Macromolecules, 2009. **42**(24): p. 9422–9434.
267. Escalé, P., et al., *Synthetic route effect on macromolecular architecture: from block to gradient copolymers based on acryloyl galactose monomer using RAFT polymerization*. Macromolecules, 2011. **44** (15): p. 5911–5919.
268. Stenzel, M.H., T.P. Davis, and A.G. Fane, *Honeycomb structured porous films prepared from carbohydrate based polymers synthesized via the RAFT process*. Journal of Materials Chemistry, 2003. **13**(9): p. 2090–2097.
269. Mosbach, K., *The promise of molecular imprinting*. Scientific American, 2006. **295**(4): p. 86–91.
270. Ye, L. and K. Mosbach, *The technique of molecular imprinting—Principle, state of the art, and future aspects*. Journal of Inclusion Phenomena and Macrocyclic Chemistry, 2001. **41**(1–4): p. 107–113.
271. Ye, L. and K. Mosbach, *Molecular imprinting: Synthetic materials as substitutes for biological antibodies and receptors*. Chemistry of Materials, 2008. **20**(3): p. 859–868.
272. Holliger, P. and H.R. Hoogenboom, *artificial antibodies and enzymes—mimicking nature and beyond*. Trends in Biotechnology, 1995. **13**(1): p. 7–9.
273. Balamurugan, S. and D.A. Spivak, *Molecular imprinting in monolayer surfaces*. Journal of Molecular Recognition, 2011. **24**(6): p. 915–929.
274. Nicholls, I.A. and J.P. Rosengren, *Molecular imprinting of surfaces*. Bioseparation, 2001. **10**(6): p. 301–305.

275. Sharma, P.S., et al., *Surface development of molecularly imprinted polymer films to enhance sensing signals*. Trac-Trends in Analytical Chemistry, 2013. **51**: p. 146–157.
276. Hillberg, A.L. and M. Tabrizian, *Biomolecule imprinting: Developments in mimicking dynamic natural recognition systems*. IRBM, 2008. **29**(2–3): p. 89–104.
277. Wulff, G., *Molecular imprinting in cross-linked materials with the aid of molecular templates—a way towards artificial antibodies*. Angewandte Chemie-International Edition in English, 1995. **34**(17): p. 1812–1832.
278. Wang, H.Y., T. Kobayashi, and N. Fujii, *Molecular imprint membranes prepared by the phase inversion precipitation technique*. Langmuir, 1996. **12**(20): p. 4850–4856.
279. Arshady, R. and K. Mosbach, *synthesis of substrate-selective polymers by host-guest polymerization*. Macromolecular Chemistry and Physics-Makromolekulare Chemie, 1981. **182**(2): p. 687–692.
280. Wulff, G. and R. Schonfeld, *Polymerizable amidines—Adhesion mediators and binding sites for molecular imprinting*. Advanced Materials, 1998. **10**(12): p. 957–959.
281. Kirsch, N., et al., *Sacrificial spacer and non-covalent routes toward the molecular imprinting of "poorly-functionalized" N-heterocycles*. Analytica Chimica Acta, 2004. **504**(1): p. 63–71.
282. Sellergren, B. and C.J. Allender, *Molecularly imprinted polymers: A bridge to advanced drug delivery*. Advanced Drug Delivery Reviews, 2005. **57**(12): p. 1733–1741.
283. Sellergren, B., *Molecularly imprinted polymers, man made mimics of antibodies and their applications in Analytical Chemistry*. Techniques and Instrumentation in Analytical Chemistry. Vol. 23. 2001, Amsterdam: Elsevier.
284. Gong, J., et al., *Micro- and Nanopatterning of Inorganic and Polymeric Substrates by Indentation Lithography*. Nano Letters, 2010. **10**(7): p. 2702–2708.
285. Nie, Z. and E. Kumacheva, *Patterning surfaces with functional polymers*. Nature Materials, 2008. **7**(4): p. 277–290.
286. Woodson, M. and J. Liu, *Functional nanostructures from surface chemistry patterning*. Physical Chemistry Chemical Physics, 2007. **9**(2): p. 207–225.
287. Tsai, I.Y., A.J. Crosby, and T.P. Russell, *Surface patterning*, in *Cell Mechanics*, Y.L. Wang and D.E. Discher, Editors. 2007. p. 67–87.
288. Fuierer, R.R., et al., *Patterning mesoscale gradient structures with self-assembled monolayers and scanning tunneling microscopy based replacement lithography*. Advanced Materials, 2002. **14**(2): p. 154–157.
289. Kramer, S., R.R. Fuierer, and C.B. Gorman, *Scanning probe lithography using self-assembled monolayers*. Chemical Reviews, 2003. **103**(11): p. 4367–4418.
290. Ariga, K., et al., *Enzyme nanoarchitectonics: organization and device application*. Chemical Society Reviews, 2013. **42**(15): p. 6322–6345.

# Chapter 3
# Biorecognition Molecules: Types and Molecular Basis and Development of Specificity

**Robert E. Collins and Aitziber L. Cortajarena**

## 3.1 Introduction

As introduced in Chap. 1 many biomolecules are involved in molecular recognition processes. These molecules include proteins, peptides, and nucleic acids. In the current chapter we introduce in detail the different recognition molecules found in nature. The chapter analyzes the recognition processes that they mediate and the key aspects of such recognition, including affinity and specificity. Finally, we hint about the tools that can be used in order to modify and expand the natural biorecognition diversity. The chapter aims to provide an overview of the biomolecular complexity and the array of biorecognition functions available in nature or by design, focusing mostly into the two major recognition moieties: proteins and peptides and nucleic acids. We cover some of the biorecognition pairs that are used in the applications described in the following book chapters.

Most importantly, we aim to provide the basis for a thoughtful selection of appropriate biorecognition moieties to add functionality to different polymeric platforms considering the final application.

A. L. Cortajarena (✉)
Instituto Madrileño de Estudios Avanzados en Nanociencia (IMDEA-Nanociencia), CNB-CSIC-IMDEA Nanociencia Associated Unit Unidad de Nanobiotecnología, Cantoblanco, 28049 Madrid, Madrid, Spain
e-mail: aitziber.lopezcortajarena@imdea.org

R. E. Collins
Physical Sciences Department, Esatern Connecticut State University, 83 Windham St, Willimantic, CT 06226, USA
e-mail: collins.r.e@gmail.com



J. Rodríguez-Hernández, A. L. Cortajarena (eds.), *Design of Polymeric Platforms for Selective Biorecognition*, DOI 10.1007/978-3-319-17061-9_3

## 3.2 Proteins

Proteins, also called polypeptides, are genetically encoded linear polymers built from 20 standard amino acids. An amino acid contains an invariant backbone, which consists of a carbon flanked by an amine and a carboxylic acid group. This carbon attaches to the variable amino acid side chains, which include charged, polar and nonpolar groups. Following dehydration during amino acid synthesis, a planar peptide bond is formed. The resulting amide grants each amino acid residue in the polymer a hydrogen bond donating and accepting group. Although the lowest energy state of some proteins is an extended unstructured form, most either assemble colinearly with other polypeptides (e.g., collagen), or fold into a compact state. Assembly and folding is typically driven by the so-called "hydrophobic effect," the sequestration of hydrophobic amino acid side chains away from water, in order to minimize the entropically disfavored ordering of water around groups with which it cannot interact. Folding maximizes the hydrogen bonding of main chain and side chain polar groups. Although the peptide bond is planar, other bonds in the protein can rotate in all conformations that do not result in clashes with other atoms. Predicting protein structure de novo solely from sequence remains difficult and has unpredictable results.

Proteins are critical to life, serving as catalysts, structural supports, carriers, sensors, and scaffolds. In this chapter, we focus on proteins that have been utilized as binding platforms. Excluding covalent modification of proteins, protein–protein, or protein–ligand binding is driven by the same fundamental forces that drive protein folding: hydrogen bond formation, ionic bonding, the hydrophobic effect, and van der Walls interactions. Ionic bonds are generally (mis)taken to mean the interactions of the monovalent positively and negatively charged side chains. Aromatic hydrophobic side chains have recently been recognized to have quadrupolar ionic nature, as the pi orbitals above and below aromatic rings are negatively charged, leaving the ring edges positively charged. This can provide a quite unique hydrophobic-yet-charged interaction interface seen, for example, in nicotine binding to acetylcholine receptor and proteins that bind methylated lysines [1, 2]. The presence of ions at interfaces, and metal coordination chemistry is another consideration, as polyvalent cations are observed in protein–protein and protein–ligand interfaces, and have been included in design strategies of polymeric assemblies and scaffolds [3–8]. Although the forces are the same, the frequencies of amino acid pairings differ in protein cores and protein–protein interfaces. Ionic bonds and hydrophobic interactions, in particular, tryptophan-proline pairs, tend to be overrepresented in the latter [9].

At any given protein recognition site, any or all of these bond types may be present. One might predict respective bond energies to sum evenly. In this case, interface size would directly correlate with binding strength. The previously exposed surface area that is buried when proteins interact does, in fact, correlate with affinity up to a certain size; however, at any given size of buried area, there is an enormous range of actual binding affinities, from very weak to quite strong interactions [10]. Clearly, not all interactions are equal. Considerations of the difficulty of accurately

modeling the affinities of interactions have been extensively reviewed elsewhere [11]. The four primary noncovalent bond types above are listed roughly in descending order of strength; however, local environments can alter bond strength. For example, an ionic bond in a desolvated protein–protein interface is shielded from water, and therefore binds with much greater strength than a solvent-exposed one. This may, in part, explain why interfaces with the same buried surface area and similar amino acid content can have affinities ranging across many orders of magnitude. Binding free energy "hot-spots" that have unexpectedly large contributions to binding affinities have been identified in natural complexes, and are a desirable but elusive target in designed interfaces. Although different residue types (primarily charged or aromatic amino acids) have been found in hot-spots, protection from solvent by other residues is the feature that best appears to typify hot-spots [12–14].

*Affinity, Avidity, and Specificity* Affinity is a measure of strength of binding of a molecule to its ligand. The affinity of a protein interaction with its ligand is quantified as a dissociation constant (Kd), in molar units (M). Quantitatively, Kd values can be determined as the ratio of the off-rate constant (how quickly the protein dissociates from bound ligand) and the on-rate constant (how quickly the protein binds ligand). Alternatively, at equilibrium, Kd is the concentration of ligand that results in equal concentrations of free protein and complex. As the inverse of an association constant, it describes the susceptibility of a complex to dissociation. Lower values indicate tighter binding. As described in Chap. 1, physiological binding constants can range from the femtomolar to the millimolar. Complexes with femtomolar affinities are long lived, for example, biotin-streptavidin complexes exhibit a half-life of 35 h under physiological conditions [15]. Assuming diffusion-limited on-rates, complexes with millimolar affinities will have millisecond half-lives at best.

While affinity properly refers to the binding of a single ligand to a single protein, avidity is considered with multivalent binding. Avidity is the cumulative effects of multiple affinities working together. In order for multivalent complexes to dissociate, each subunit must simultaneously reach the "off" state. Avidity is sometimes referred to as functional affinity, in that the association and dissociation of multiple binding units and their ligands can be measured. Avidity has been noted in the generation of engineered antibodies, where single-chain fragments (scFV) are selected for, and then are later reassembled into IgG class antibodies, which have two binding sites, or are simply dimerized into "diabodies." In these cases, the Kd values for the affinity of the scFV (single unit) are hundreds to thousands times weaker than the avidity of the diabody or antibody) [16]. With high starting affinities, bivalent or higher order binding soon becomes practically irreversible. The degree to which functional avidity assays can, therefore, obscure the true underlying affinity has led to criticisms against these techniques (especially with indirect assays) [17]. Nevertheless, it is clear that conversion of monovalent binders to polyvalent binders may boost effectiveness when engineering binding scaffolds for a target.

Specificity, as opposed to affinity and avidity, lacks a formal quantifiable unit. It is simply the binding of one ligand to the exclusion of others. Specificity can be experimentally assessed, for example by pull down, where hopefully one ligand and

not many is isolated from the cellular milieu. In protein design, engineering, and selection, specificity often seems to come about through the selection of functional high affinity binders. The perfection of a binding site for one ligand should tend to physically and chemically gate out others. Moreover, truly nonspecific binders may be lost in purification or fail to behave in selection assays. In the following sections, we highlight the development of high affinity binding platforms, and a few cases where specificity was assessed and enhanced.

In the case studies we present in this chapter, as high-affinity binders are progressively selected and refined, structural features that promote binding emerge. More surface area is buried, and more fruitful bonds emerge, particularly in the satisfaction of constrained hydrogen bond distances and geometries. Side chains become better positioned, requiring less rearrangement (and entropic penalty) to bind. Finally, solvent excluding seals emerge around hot-spot residues, guaranteeing their full, uninterrupted binding energies.

## *3.2.1 Common Natural Protein Recognition*

As efforts to use proteins as polymeric platforms for recognition, and as therapeutic agents began, the first source of tools were naturally occurring proteins. As detailed in Chap. 1, the affinities of the protein ligand interactions found in nature range from the transient to the near permanent. This is according to the physiological role of the protein itself. Interactions of cellular signaling processes must be short lived, so that when a signal is terminated, those complexes transmitting that signal dissociate and return to a resting state. Antibody–antigen complexes should remain intact until immune processes are recruited and complete their job. In this section, we highlight some of the most commonly used naturally occurring protein–ligand interactions.

### 3.2.1.1 Streptavidin–Biotin

Streptavidin is a protein isolated from bacteria that binds the small molecule biotin with one of the strongest noncovalent interactions known ($K_d = 10^{-14}$ M). This remarkable affinity is achieved through an extensive network of hydrogen bonds with the polar moieties of biotin and hydrophobic and van der Waals interactions mediated by conserved tryptophans packing against biotin (Fig. 3.1b). These interactions are reinforced by the closing of a loop over the pocket. For streptavidin to release biotin, concerted loop movement, solvation of apolar surfaces, and the breaking of the hydrogen bond network must occur [23, 24].

Because of the high affinity and specificity of this interaction, the biotin–streptavidin interaction is often used in scaffold engineering and protein isolation. Biotin can be synthetically attached to DNA, RNA, or proteins in vitro, and in vivo, proteins can be tagged with biotin acceptor peptides which are posttranslationally

modified with biotin in the presence of biotin ligases [25–27]. A small peptide sequence has also been selected for streptavidin affinity in the absence of biotin [28, 29]. Additionally, engineered streptavidins of varying affinities and valence (monomers, tetramers, monovalent tetramers) have been developed, allowing control of scaffold design [30, 31]. These features have been used to generate biosensors, facilitate nanotube assembly in controlled orientation, and the controlled assembly of extended protein lattices, for example [3, 32, 33].

#### 3.2.1.2 Antibody–Antigen

Antibodies are the protein products of the adaptive immune system that exist as either secreted or cell-bound forms. Antibody diversity is far greater than the number of genes in a genome. This diversity comes about by combination of several genetic cassettes and somatic mutation of the sequence in those cassettes. Antibodies (Fig. 3.1a) consist of conserved structural regions and variable antigen-binding regions. Typically, antibodies used in research are IgG, which contain two binding sites per antibody complex (Fab) (Fig. 3.1a), but other antibody classes contain more. Upon introduction of an antigen, the basal diversity of the immune system allows weak recognition of an antigen. Cells displaying antibodies that recognize the antigen are stimulated to proliferate, and their antibodies further diversify. The expansion and diversification of successful binders is termed affinity maturation, and this term has been adopted to describe synthetic selection processes that proceed by genetic diversification and selection of superior binders [34]. Figure 3.2 depicts methods for the affinity maturation process. In short, loose contacts are replaced by more fruitful, direct interactions that bury additional hydrophobic surface area, and protect inner binding contacts that may constitute a solvent-shielded “hot-spot.”

Antibodies are typically generated in one of two ways. Polycolonal antibodies are the product of all cell lineages that recognize an antigen. An animal is injected with antigen (often in one primary and several booster injections). Following development of high-affinity antibodies, serum is harvested, and antibodies purified. Polyclonal antibodies may recognize different sites on a large antigen, and will range in affinities. Conversely, monoclonal antibodies are produced by a single cell lineage. An animal (typically mouse) is injected with antigen, and immortal hybridoma cell lines are generated from the animal’s spleen cells. Cloning of antibody producing cells allows for isolation of a single antibody against the antigen.

Protocols for the chemical modification of antibodies are abundant and have nearly a 60 year history. Additionally, in the design of antibody-based binding scaffolds, antibody-binding modules have been borrowed from bacteria that use them as countermeasures to the adaptive immune system. Protein A is derived from *Staphylococcus aureus* and has high affinity for the conserved (Fc) region of most antibodies. Protein G is produced by Streptococcal species and has Fc and Fab affinities. Physiologically, these block conserved regions of antibodies from their normal immune functions, but antigen binding should be unimpaired. Both are used in antibody purification and immobilization [35, 36].

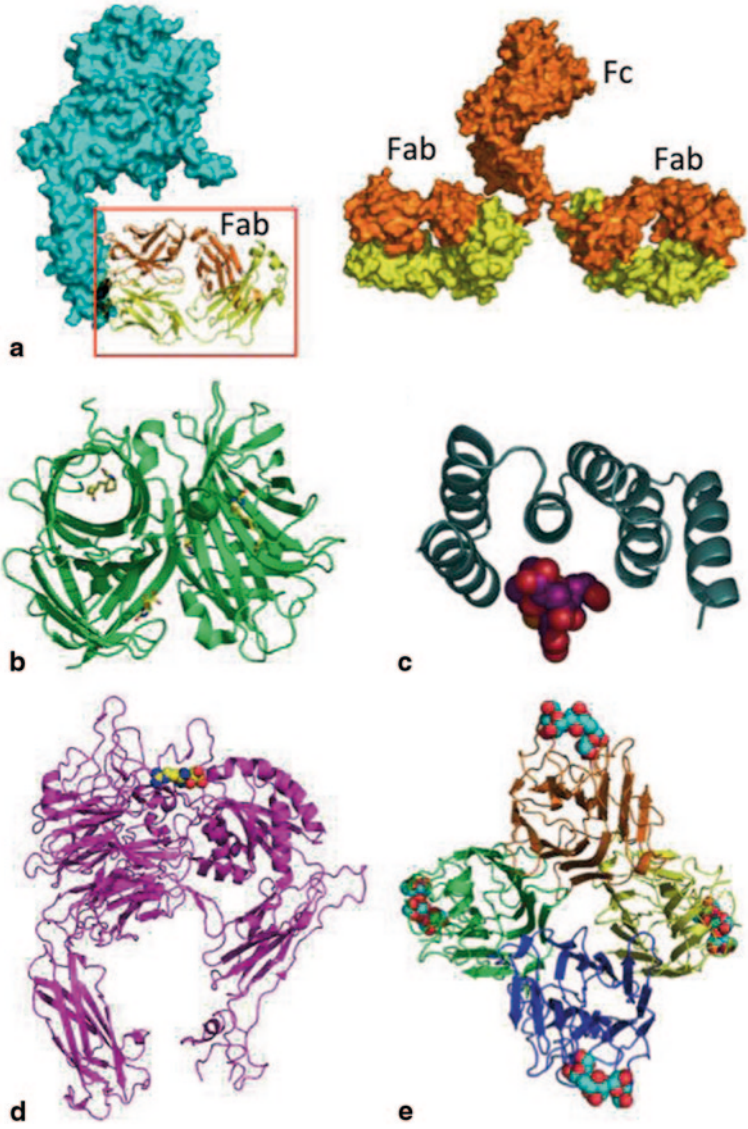


**Fig. 3.1** Collection of structures that represent different types of biorecognition interactions mediated by proteins. **a** Crystal structure of Herceptin monoclonal antibody antigen-binding fragment (Fab) represented as *ribbons* in *yellow* and *orange* for the light and heavy chains respectively. The structure shows the Herceptin antibody bound to the extracellular region of Her2 shown as cyan surface (PDB ID: 1N8Z) [18]. The *right panel* shows the structure of a complete antibody with the light and heavy chains displayed as *yellow* and *orange* surfaces, respectively. The two antigen recognition regions Fab, and the constant region (Fc) are shown. The Herceptin anti-Her2 antibody example represents a high affinity interaction between two proteins with a dissociation constant of 0.1 nM. Heceptin is commonly used in breast cancer treatment. **b** Crystal structure of

Human antibodies against therapeutic targets are desirable as drugs (called biologics), as they should avoid immune responses to nonhuman immunoglobins (Fig. 3.1a). As conventional development of human or humanized antibodies would be impossible, in vitro approaches were developed. Libraries of the isolates variable fragments of an antibody (scFv) were expressed on the surface of phage (viruses that infect bacteria) or bacteria. Physical isolation of successful binders was followed by rounds of diversification and reisolation. The result produced antibodies with affinities comparable to antibodies produced by affinity maturation in vivo. When reconstituted into antibodies, even higher apparent affinity (avidity) was observed. The highly successful biologic Humira (human monoclonal antibody in rheumatoid arthritis) was developed by this approach [37–40].

#### 3.2.1.3 Integrin–RGD

Proteins that contain the Arg-Gly-Asp peptide sequence (RGD) are recognized by the integrins that serve as receptors for them and constitute a major recognition system for cell adhesion [41]. The RGD sequence is the cell attachment site of a large number of adhesive extracellular matrix, blood, and cell surface proteins, and nearly half of the over 20 known integrins recognize this sequence in their adhesion protein ligands. The integrin-binding activity of adhesion proteins can be reproduced by short synthetic peptides containing the RGD sequence (Fig. 3.1d). The binding affinity of this interaction is relatively low with dissociation constant values of $10^{-5}$–$10^{-3}$ M. The structural basis of the interaction provides insights on the promiscuity of RGD-binding integrins [42]. Many ligands are shared by this subset of integrins, but the ligand affinity varies, presumably reflecting the fit of the ligand RGD conformation with the specific α-β integrin binding pockets. RDG is a ubiquitous adhesion sequence, therefore numerous new biomaterials and surfaces coated with RGD peptides have been used to control the cell adhesion in vitro and in vivo.

---

the streptavidin-biotin complex. The streptavidin protein is a tetramer shown in *green ribbons*. Each barrel binds one biotin molecule the small biotin molecules (one per streptavidin barrel) are shown as *yellow sticks*. (PDB ID: 1MK5) [19]. This interaction represents a high affinity interaction with a dissociation constant of $K_d = 10^{-14}$ M between a protein and a small molecule. **c** Crystal structure of a small designed protein binding module in complex with its target peptide. The designed tetratricopeptide repeat (*TPR*) module is shown in *green* as *ribbon* representation. The target C-terminal Hsp90 peptide is shown as *spheres* in *purple* (PDB ID: 3KD7) [20]. This is an example of a low affinity interaction with micromolar dissociation constant and therefore a short half-live, these interactions mediate transient and dynamic interactions. **d** Crystal structure of the integrin-RGD peptide biorecognition complex. The Integrin alpha 5 chain head piece recognition fragment is shown as *magenta ribbon* and the RGD peptide shown in *yellow spheres* (PBD ID: 3VI4) [21]. **e** Crystal structure of the lectin Concanavalin A in complex with sugar ligands. The four subunits of the Concanavalin A tetramer are shown in different colors: *green*, *blue*, *orange*, and *yellow*. Each subunit binds through specific hydrogen bonds and van der Waals interactions a trimannoside molecule shown as *cyan spheres*. PDB ID: 1CVN) [22]

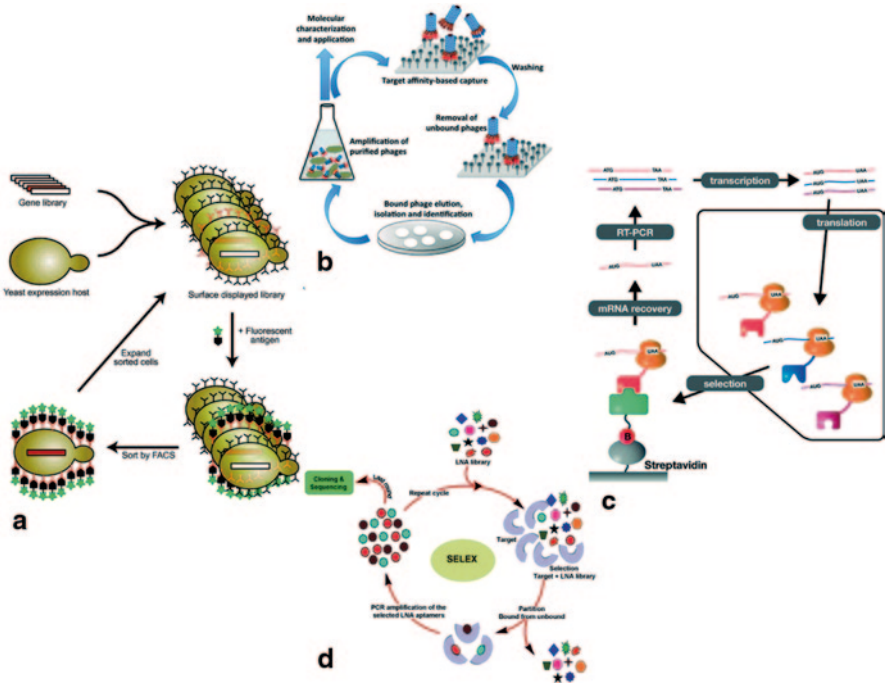


**Fig. 3.2** Examples of the most commonly used methods for in vitro evolution methods for selection of high-affinity binders. **a** Schematic of yeast display technology, in which a protein of interest is expressed on the surface of yeast. From a library of potential ligand molecules high-affinity protein ligands can be isolated [52]. Iterative rounds of cell sorting by fluorescence activated cell sorting (*FACS*) and expansion by cell culture are applied to yield enrichment of binders from a combinatorial library. The cells recovered are expanded and subjected to multiple rounds of FACS/expansion. Figure reproduced from [53]. **b** Schematic of phage display technique for affinity-based selection of protein–protein, protein–peptide, and protein–DNA interactions. A protein or library of variants of a protein of interest is displayed on the surface of phage. The phages displaying the proteins are then screened against the target molecule of interest. After several screening and amplification rounds new or high-affinity ligands can be developed. Figure reproduced from [54]. **c** Schematic representation of ribosome-display selection methodology. A DNA of the library encoding the protein variants of interest is transcribed in vitro and the resulting mRNA is used for in vitro translation to synthesize the encoded proteins. The absence of the stop codon at the end of the protein results in the protein connected to the tRNA. The mRNA-ribosome-protein ternary complexes are used for affinity selection on an immobilized target. The genetic information of binders is rescued by RT-PCR yielding a PCR product. After several cycles highly specific and pure binders are selected [55]. Figure reproduced from [56]. **d** Schematic of systematic evolution of ligands by exponential enrichment (*SELEX*). SELEX is used for the selection of nucleic acids including single-stranded DNA, RNA, or aptamers that specifically bind to a target ligand. Synthetic libraries of nucleic acids are screened to select for nucleic acids that bind the target molecule. After several cycles of selection and PCR-amplification specific high affinity binders are identified. Figure reproduced from [57]

#### 3.2.1.4 Lectins

Lectins are proteins that bind carbohydrates and mediate cell to cell contacts. These contacts are strong by the combination of many individual lectins–sugar weak and specific interactions. Similarly, these interactions can open many doors in their use in biotechnology and for the generation of specific biorecognition surfaces [43–45]. For example, concanavalin A (ConA) is a commercially available lectin that binds specifically to defined glycosyl moieties found in various sugars, glycoproteins, and glycolipids (Fig. 3.1e). ConA is widely used as a tool in sugar biorecognition, detection, and sensing applications [46-49]. Recent works on the carbohydrate–lectin recognition mechanisms open the door to the efficient design of new lectin-based sugar recognition modules [50, 51].

### *3.2.2 Engineering to Expand the Binding Repertoire and Affinity of Natural Scaffolds*

Protein engineers soon exhausted the natural repertoire of protein–ligand in their designs, and sought to engineer new ones. In this section, we describe approaches that take a protein scaffold from nature, and functionalize it with new amino acids that allow binding to a new target. Typically, this is done by repeatedly generating large libraries of variants and selecting for increasingly high-affinity binders. Figure 3.2 summarizes methods used to accomplish this goal. Successful binding proteins displayed on the surfaces of phage, bacteria, or yeast, or attached to ribosomes, can be physically isolated by binding to immobilized ligand. Proteins displayed on cells can be mixed with fluorescent ligand and sorted in a fluorescent activated cell sorter (FACS). As the gene that produced the protein is coisolated in all cases, DNA sequences are obtained, allowing for determination of successful substitutions across many clones, and serves as a foundation for the next round of variation and selection.

Scaffold choice itself is important. Scaffolds with sufficient surface area to bury and, in particular, ones with loops that project into their target, seem to frequent studies that successfully isolate high-affinity binders. Stable scaffolds that express well, that are stable, and that are structurally predictably are desirable. To this end, consensus sequence design has been used. Many sequences of the same domain are aligned, and the consensus construct is generated. Consistent with the evolutionary hypothesis that the most conserved residues are responsible for structural cohesion of the domain, these consensus designs are often extremely stable, even more so than their natural counterparts [58–60]. The least-conserved hypervariable positions are what define the different binding functions of each member of the protein family, and are, therefore, varied in the libraries in order to obtain novel functions (Fig. 3.1c).

Another deliberate design feature that improves binding is the incorporation of charges complimentary to the ligand being bound. Long-range electrostatic interac-

tions apparently attract and position the ligand before the specific interactions of the binding site lock it in. On rates, and therefore affinities, are dramatically increased in electrostatically optimized systems of very different folds [61–63].

The success of these approaches cannot be understated. Several scaffolds have emerged into mature technologies with commercial and even some clinical success. They demonstrate antibody-like affinities in the nanomolar to picomolar range. Their specificities are precise. Further, they can be engineered with modules coupled together for avidity effects. Modules with different affinities can be coupled for bi- or multi-specific binding.

The basis of higher and lower affinity binders are not fully understood, but the structural biology work on many biorecognition complexes has provided valuable information to decipher the key elements in the biorecognition interactions. Figure 3.3 provides detailed structural comparison between high- and low-affinity binders.

Affibodies are based on a Protein A scaffold. This is a helical bundle which originally had positions on two alpha helices randomized. Selection primarily has been performed by rounds of phage display (Fig. 3.2b). Affibodies have been commercialized, resulting in over 200 publications with applications ranging from protein capture and purification to enzyme inhibition to a clinical trial for an anti-Her2neu imaging reagent [66–70].

DARPins (designer ankyrin repeat proteins) are based on a consensus ankyrin repeat scaffold. A single ankyrin repeat is typically 33 amino acids and consists of a β-turn, followed by two antiparallel α-helices and a loop leading to the next repeat. Hydrophobic and polar interactions within a repeat, and with neighboring repeats, form a stable, extended hydrophobic core mediated by the stacking of the α-helices, while the more flexible loops project out [58, 71, 72]. Like other consensus designs, DARPins are very stable [58]. Their ability to accept any residue type in loop positions has allowed the development of DARPin libraries, from which high-affinity binders of therapeutic and diagnostic targets have been selected by ribosome display (Fig. 3.2c; [73–75]).

Adnectins are based on a fibronectin iii fold, resulting in antibody-like loops projecting out of a core comprised of sheets. They have been selected by a variety of methods including yeast display (Fig. 3.2a) and phage display (Fig. 3.2b). Adnectins are commercialized and have entered clinical trials [76–78]. Many other scaffolds have been designed and selected for novel binding affinities. The goal of this review is to highlight a few cases and their development. Other scaffolds, design principles, and structural considerations [79] have been extensively reviewed elsewhere [80].

#### 3.2.2.1 Computationally Designed Proteins

Rather than randomizing the amino acids on a scaffold, the Baker lab has selected scaffolds to complement a computer-designed binding site [65]. DIG (digoxigenin), a drug and easily incorporated DNA/RNA modification commonly used by mo-

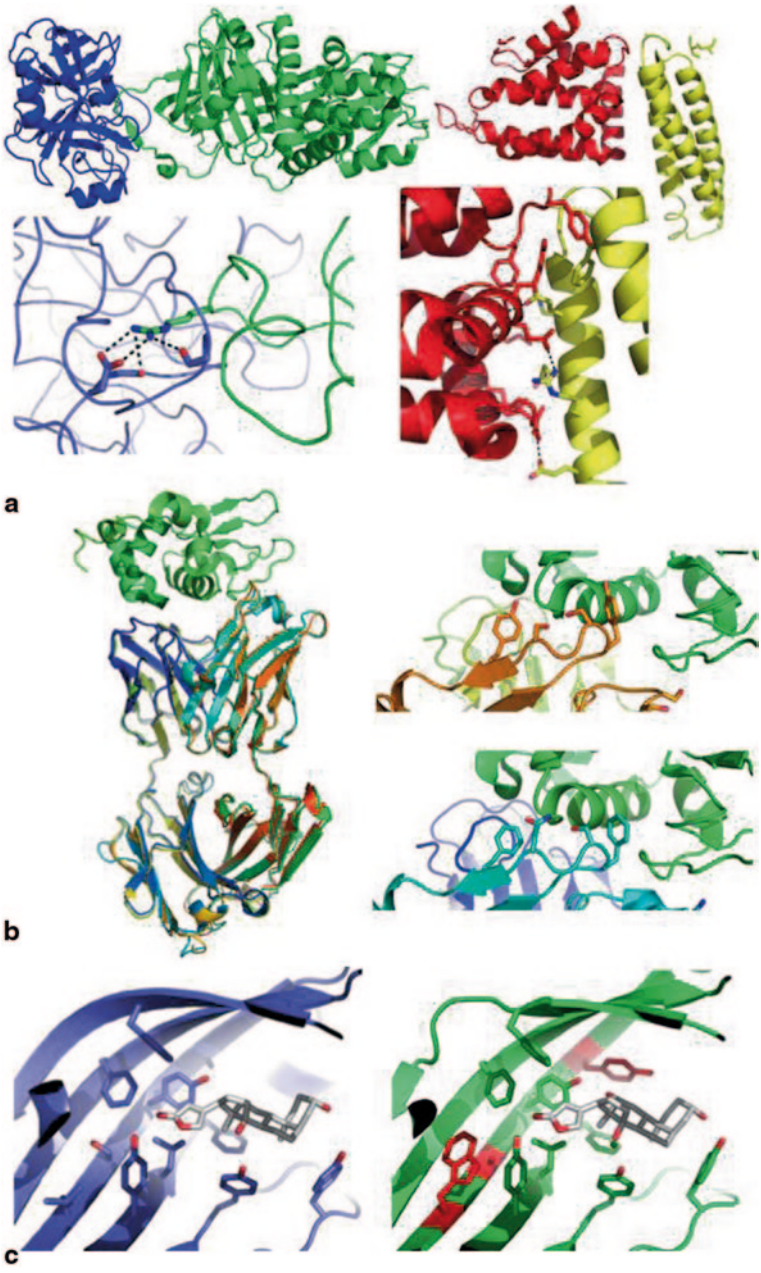


**Fig. 3.3** Structural comparisons of higher and lower affinity binders. **a** A potential natural hot-spot versus surface binding is apparent when comparing the natural protein–protein complexes in proteinase–proteinase inhibitors (PDB ID: 1OPH) and a SNARE-adaptor complex (PDB ID: 2V8S). Both are protein complexes that bury almost the same surface area (1359 and 1333 $Å^2$), respectively. The two complexes have similar hydrophobic content at their interfaces. However, 1OPH

lecular biologists was selected as a target. “Disembodied” amino acids were aligned with DIG and optimized for binding using the ROSETTA program. Potential scaffolds from the protein database were computationally screened for their ability to harbor the desired amino acids in favored orientations. Designer proteins comprised of the selected amino acids mated to the scaffold were generated, and selected using surface display on yeast and fluorescent-activated cell sorting. From an initial affinity of ~10 μM, additional rounds of design, randomization, and selection resulted in pM to low nM affinities (Fig. 3.3c). Specificity for DIG versus other steroids of similar shapes and chemistry was developed by positive designs that inserted residues incompatible with binding undesirable ligands. Although the Baker lab sampled known protein backbone conformations in this study, it seems totally de novo protein designs are imminent [81].

### *3.2.3 Peptides*

Peptides are distinct from proteins in their small size and general lack of folding or even secondary structure. Specific high-affinity interactions do not necessarily require protein-sized molecules. For example, antibody epitopes that mediate nanomolar binding with precise specificity can be as short as 6 amino acids. The biotin acceptor peptide (described in 2.1.1) has high affinity and specificity for streptavidin. The short lengths of peptides allow comprehensive sequence libraries to be generated. Peptide binding can be selected for by panning phage-display libraries. Libraries of random or near random sequence can also be queried as fusions to proteins in yeast-two hybrids or functional screens. Alternatively, libraries can be plated on glass, generating peptide microarrays. In these microarrays, target binding to immobilized peptides of known identity can be directly detected [82]. Peptides selected for binding are often referred to as “aptamers”, which can cause some

(*left*) features binding 4000 times tighter than seen in 2V85 (*right*). A potential hot-spot (*inset*) is formed by a salt bridge. This interaction is clearly isolated from bulk solvent by surrounding polar and hydrophobic interactions. The SNARE-adaptor complex features as many interactions along long helices, but side chain and main chain interactions are solvent adjacent. Values from [10]. **b** During antibody affinity maturation, antibody affinity for lysozyme (*green left*) improved 36 times, resulting in nanomolar affinities. Only a few of the amino acid substitutions that occur during affinity maturation are at the antibody–antigen interface (shown as *sticks*). The immature (*right top*, PDB ID: 1NDM) and fully matured (*right bottom*, PDB ID: 1NDG) complexes bury a similar solvent-accessible surface area (overlay, *left*). The major change observed is due to the mutation of a noncontact residue that allows a key loop to move closer to the antigen. This allows replacement of tyrosines that participate in loose water-mediated hydrogen bond networks with phenylalanine that directly bind the antigen, burying additional nonpolar surface area and protecting a neighboring hot-spot. Other substitutions in the same region provide some additional contacts [64]. **c** Selection of a picomolar affinity small molecule (DIG) binding (*right*, PDB ID: 4J9A proceeded through lower affinity units (*left*, PDB ID: 4J8T). Substitutions are colored *red*. A 16–28X improvement in affinity cannot be accounted for by the single substitution that contacts DIG. Noncontact mutations, in particular a leu to trp substitution help position binding residues in optimal geometries, and lock them into binding conformations, decreasing the entropic and kinetic penalty on binding affinity if residues need to reorient prior to binding [65]

confusion as DNA and RNA modules are also called aptamers in some contexts. Peptide aptamers have been generated to inhibit cellular processes and to act as biosensors and diagnostics ([83], reviewed in [84]). Interestingly, peptides have been developed with specificity and fairly high affinity for different surfaces, including polystyrene, carbon nanotubes, and glass [85].

## 3.3 Nucleic Acids

Nucleic acids in addition to their fundamental role to encode the genetic information in living systems have some intrinsic features that make them useful biorecognition molecules. The Watson–Crick base pairing between G and C and A and T bases by hydrogen bonds permits the formation of stable double-stranded nucleotide chains (Fig. 3.4a). These interactions are very specific and follow very simple rules with only 4 blocks A, T, G, and C and two possible interactions G–C and A–T, therefore can be easily used to engineer and program interactions based on the DNA base pairing.

In order to generate different binding specificities, nucleic acids present less chemical functionality than proteins but large libraries of oligonucleotides with different sequences can be generated relatively easily. In addition to the simple base pair complementarity, nucleic acids can fold into complex three-dimensional structures (Fig. 3.4b, 3.4c). Those structures have been shown to be able to bind specific target molecules (Fig. 3.4c; [86, 87]). Large libraries of nucleotide sequences will potentially encode binding molecules to almost any potential target. Advanced selection tools including Systematic Evolution of Ligands by EXponential Enrichment (SELEX) are used to select from complex libraries DNA molecules that bind specifically the different targets of interest (Fig. 3.2d; [88]). Aptamers are small single-stranded nucleic acids that fold in defined structure (Fig. 3.4d). High-affinity aptamers have been developed to bind a wide variety of molecules and even complex systems such as live cells [82, 89]. The affinity and specificity of those molecules can be evolved and selected to match the desired properties. The expansion of the natural repertoire of nucleotides by the introduction of unnatural nucleotides can increase the functionality and affinity of aptamers by providing additional chemical and structural diversity beyond that available with modified natural nucleotides [90].

In addition, to use nucleic acids as stapling and binding molecules, there are new advanced technologies for the generation of complex structures based on the assembly of DNA molecules exploiting the same simple base paring complementarity [91]. Nowadays using these methodologies, that include the DNA origami, scientist can create almost any type of DNA-based shapes [92]. The DNA structures could be functionalized primarily through selective attachment of functional groups, such as biotin [93–95]. These novel technologies will allow not only to generate complex biorecognition platforms but also to pattern chemical reactions at the surfaces.

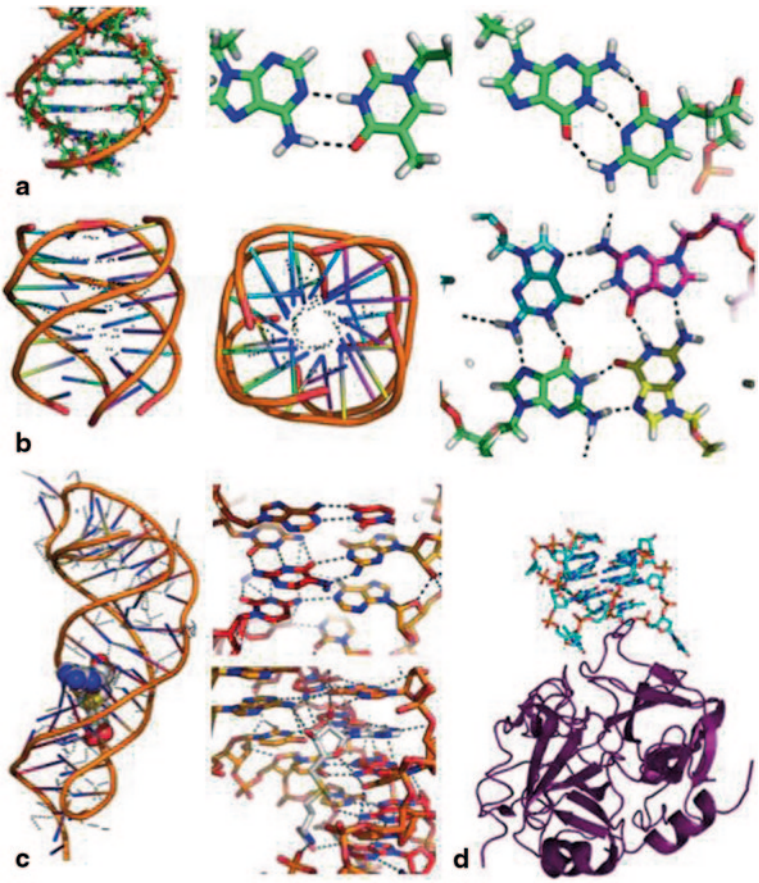


**Fig. 3.4** Nucleic acids-based interactions. **a** A typical B-DNA helix and Watson–Crick A:T and G:C base pairs. (PDB ID: 2VAH). Hydrogen bonds are drawn as *black dashed lines*. Bases stack in a regular orientation, and traditional geometries are observed. **b** Quadruplex DNA from side on and top orientations. (PDB ID: 139D). Base pairing in quadruplex DNA is extensive, and involves additional hydrogen bonds not seen in double stranded DNA helices. **c** The S-adenosylmethionine binding domain of an RNA riboswitch (PDB ID: 2QWY). S-adenosylmethionine is rendered with *grey* carbons. The structure is an RNA helix formed by one RNA that loops back on itself. Non-Watson–Crick base pairs stabilize the binding site (*upper right*). S-adenosylmethionine binding includes extensive hydrogen bond with the nucleotides, and base stacking of the adenosine ring (*lower right*). **d** Crystal structure of an aptamer, a structure oligonucleotide, recognizing its molecular target. The figure shows the overall structure of the best-known aptamer, the thrombin-binding aptamer (*TBA*) in complex with thrombin. Thrombin molecule is representedin *purple*. TBA molecule is represented on *top* as *cyan sticks* (PDB ID: 3QLP) [96]

## 3.4 Summary and Conclusions

In summary, the natural variety of molecular recognition modules provides a wide tool-set for encoding and grafting specific biorecognition activities into polymeric surfaces. The versatility of the modules permits the construction of biorecognition platforms with unique binding properties in terms of affinity and specificity. The key aspects of biorecognition including binding affinity, avidity, and specificity, need to be comprehended and considered for the selection of the optimal molecular pairs for each application. The fast development of biomolecular engineering techniques is expanding the natural diversity even more and allows exploring a new landscape of molecules. The near future will deliver a complete new collection of tailored interactions and biorecognition molecules with fine-tuned properties that will allow scientist to build biorecognition systems "à *la carte*".

## References

1. Dougherty, D.A. The cation-pi interaction. Acc Chem Res, 2013, 46, 885–893.
2. Hughes, R.M.; Wiggins, K.R.; Khorasanizadeh, S.; Waters, M.L. Recognition of trimethyllysine by a chromodomain is not driven by the hydrophobic effect. Proc Natl Acad Sci U S A 2007, 104, 11184–11188.
3. Sinclair, J.C.; Davies, K.M.; Venien-Bryan, C.; Noble, M.E. Generation of protein lattices by fusing proteins with matching rotational symmetry. Nat Nanotechnol 2011, 6, 558–562.
4. Salgado, E.N.; Radford, R.J.; Tezcan, F.A. Metal-directed protein self-assembly. 2010, 43, 661–672.
5. Mejías, S.H.; Sot, B.; Guantes, R.; Cortajarena, A.L. Controlled nanometric fibers of self-assembled designed protein scaffolds. Nanoscale 2014, 6, 10982–10988.
6. Sinclair, J.C. Constructing arrays of proteins. Curr Opin Chem Biol 2013, 17, 946–951.
7. Bozic, S.; Doles, T.; Gradisar, H.; Jerala, R. New designed protein assemblies. Curr Opin Chem Biol 2013, 17, 940–945.
8. Gradisar, H.; Bozic, S.; Doles, T.; Vengust, D.; Hafner-Bratkovic, I.; Mertelj, A.; Webb, B.; Sali, A.; Klavzar, S.; Jerala, R. Design of a single-chain polypeptide tetrahedron assembled from coiled-coil segments. Nature chemical biology 2013, 9, 362–366.
9. Yan, C.; Wu, F.; Jernigan, R.L.; Dobbs, D.; Honavar, V. Characterization of protein-protein interfaces. Proteins 2007, 27, 59–70.
10. Chen, J.; Sawyer, N.; Regan, L. Protein-protein interactions: General trends in the relationship between binding affinity and interfacial buried surface area. *Protein Sci* **2013**, *22*, 510–515.
11. Kastritis, P.L.; Bonvin, A.M. On the binding affinity of macromolecular interactions: Daring to ask why proteins interact. *J. R. Soc. Interface*. **2013**, *10*, 20120835
12. Bogan, A.A.; Thorn, K.S. Anatomy of hot spots in protein interfaces. *J Mol Biol* **1998**, *280*, 1–9.
13. Desrosiers, D.C; Peng, Z.Y. A binding free energy hot spot in the ankyrin repeat protein gabpbeta mediated protein-protein interaction. *J Mol Biol* **2005**, *354*, 375–384.
14. Keskin, O.; Ma, B.; Nussinov, R. Hot regions in protein–protein interactions: The organization and contribution of structurally conserved hot spot residues. *J. Mol. Biol.* **2005**, *345*, 1281–1294.

15. Chilkoti, A.; Tan, P.H.; Stayton, P.S. Site-directed mutagenesis studies of the high-affinity streptavidin-biotin complex: Contributions of tryptophan residues. *Proc Natl Acad Sci U S A* **1995**, *92*, 1754–1758
16. Rudnick, S.I.; Adams, G.P. Affinity and avidity in antibody-based tumor targeting. *Cancer Biother Radiopharm*, **2009**, *24*, 155–161.
17. Mattes, M.J. Binding parameters of antibodies: Pseudo-affinity and other misconceptions. *Cancer Immunol Immunother* **2005**, *54*, 513–516.
18. Cho HS; Mason K; Ramyar KX; Stanley AM; Gabelli SB; Denney DW Jr; DJ., L. Structure of the extracellular region of her2 alone and in complex with the herceptin fab. *Nature* **2003**, *421*, 756–760.
19. Hyre DE; Le Trong I; Merritt EA; Eccleston JF; Green NM;Stenkamp RE; PS., S. Cooperative hydrogen bond interactions in the streptavidin-biotin system. *Protein Sci* **2006**, *15*, 459–467.
20. Cortajarena, A.L.; Wang, J.; Regan, L. Crystal structure of a designed tpr module in complex with its peptide-ligand. *Febs J* **2010**, *277*, 1058–1066.
21. Nagae, M.; Re, S.; Mihara, E.; Nogi, T.; Sugita, Y.; Takagi, J. Crystal structure of α5β1 integrin ectodomain: Atomic details of the fibronectin receptor. *J Cell Biol* **2012**, *197*, 131–140.
22. Naismith, J.H.; Field, R.A. Structural basis of trimannoside recognition by concanavalin a. *J Biol Chem* **1996**, *271*, 972–976.
23. Weber, P.C.; Ohlendorf, D.H.; Wendoloski, J.J.; Salemme, F.R. Structural origins of high-affinity biotin binding to streptavidin. *Science* **1989**, *243*, 85–88.
24. DeChancie, J.; Houk, K.N. The origins of femtomolar protein-ligand binding: Hydrogen-bond cooperativity and desolvation energetics in the biotin-(strept)avidin binding site. *Journal of the American Chemical Society* **2007**, *129*, 5419–5429.
25. Cronan, J.E., Jr.; Reed, K.E. Biotinylation of proteins in vivo: A useful posttranslational modification for protein analysis. *Methods in enzymology* **2000**, *326*, 440–458.
26. Chapman-Smith, A.; Cronan, J.E. Jr. In vivo enzymatic protein biotinylation. *Biomolecular engineering* **1999**, *16*, 119–125.
27. de Boer, E.; Rodriguez, P.; Bonte, E.; Krijgsveld, J.; Katsantoni, E.; Heck, A.; Grosveld, F.; Strouboulis, J. Efficient biotinylation and single-step purification of tagged transcription factors in mammalian cells and transgenic mice. *Proceedings of the National Academy of Sciences of the United States of America* **2003**, *100*, 7480–7485.
28. Schmidt, T.G.; Skerra, A. One-step affinity purification of bacterially produced proteins by means of the "strep tag" and immobilized recombinant core streptavidin. *Journal of chromatography. A* **1994**, *676*, 337–345.
29. Schmidt, T.G.; Koepke, J.; Frank, R.; Skerra, A. Molecular interaction between the strep-tag affinity peptide and its cognate target, streptavidin. *Journal of molecular biology* **1996**, *255*, 753–766.
30. Howarth, M.; Chinnapen, D.J.; Gerrow, K.; Dorrestein, P.C.; Grandy, M.R.; Kelleher, N.L.; El-Husseini, A; Ting, A.Y. A monovalent streptavidin with a single femtomolar biotin binding site. *Nature methods* **2006**, *3*, 267–273.
31. Wu, S.C.; Wong, S.L. Engineering soluble monomeric streptavidin with reversible biotin binding capability. *J Biol Chem* **2005**, *280*, 23225–23231.
32. Lyonnais, S.; Goux-Capes, L.; Escude, C.; Cote, D.; Filoramo, A.; Bourgoin, J.P. DNA-carbon nanotube conjugates prepared by a versatile method using streptavidin-biotin recognition. *Small* **2008**, *4*, 442–446.
33. Chen, H.M.; Lin, C.W. Hydrogel-coated streptavidin piezoelectric biosensors and applications to selective detection of strep-tag displaying cells. *Biotechnology progress* **2007**, *23*, 741–748.
34. Sundberg, E.J. Structural basis of antibody-antigen interactions. *Methods in molecular biology* **2009**, *524*, 23–36.
35. Graille, M.; Stura, E.A.; Corper, A.L.; Sutton, B.J.; Taussig, M.J.; Charbonnier, J.B.; Silverman, G.J. Crystal structure of a staphylococcus aureus protein a domain complexed with the fab fragment of a human igm antibody: Structural basis for recognition of b-cell receptors and

superantigen activity. *Proceedings of the National Academy of Sciences of the United States of America* **2000**, *97*, 5399–5404.
36. Sjobring, U.; Bjorck, L.; Kastern, W. Streptococcal protein g. Gene structure and protein binding properties. *J Biol Chem* **1991**, *266*, 399–405.
37. Marks, J.D.; Hoogenboom, H.R.; Bonnert, T.P.; McCafferty, J.; Griffiths, A.D.; Winter, G. By-passing immunization. Human antibodies from v-gene libraries displayed on phage. *Journal of molecular biology* **1991**, *222*, 581–597.
38. Hawkins, R.E.; Russell, S.J.; Winter, G. Selection of phage antibodies by binding affinity. Mimicking affinity maturation. *Journal of molecular biology* **1992**, *226*, 889–896.
39. Vaughan, T.J.; Williams, A.J.; Pritchard, K.; Osbourn, J.K.; Pope, A.R.; Earnshaw, J.C.; McCafferty, J.; Hodits, R.A.; Wilton, J.; Johnson, K.S. Human antibodies with sub-nanomolar affinities isolated from a large non-immunized phage display library. *Nat Biotechnol* **1996**, *14*, 309–314.
40. Vaughan, T.J.; Osbourn, J.K.; Tempest, P.R. Human antibodies by design. *Nat Biotechnol* **1998**, *16*, 535–539.
41. Rouslahti, E. Rgd and other recognition sequences for integrins. *Annu Rev Cell Dev Biol*. **1996**, *12*, 697–715.
42. Takagi, J. Structural basis for ligand recognition by rgd (arg-gly-asp)-dependent integrins. *Biochemical Society transactions* **2004**, *32*, 403–406.
43. Yu K; Creagh AL; Haynes CA; JN., K. Lectin interactions on surface-grafted glycostructures: Influence of the spatial distribution of carbohydrates on the binding kinetics and rupture forces. *Anal. Chem.* **2013**, *85*, 7786–7793.
44. Gabius HJ; Siebert HC; André S; Jiménez-Barbero J; H., R. Chemical biology of the sugar code. *Chembiochem*. **2004**, *7:5*, 740–764.
45. Wittmann V; Pieters RJ. Bridging lectin binding sites by multivalent carbohydrates. *Chem. Soc. Rev.* **2013**, *42*, 4492–4503.
46. García R; Rodríguez R; Montesino R; Besada V; González J; JA., C. Concanavalin a- and wheat germ agglutinin-conjugated lectins as a tool for the identification of multiple n-glycosylation sites in heterologous protein expressed in yeast. *Anal. Biochem* **1995**, *231*, 342–348.
47. Cella LN; Chen W; Myung NV; A., M. Single-walled carbon nanotube-based chemiresistive affinity biosensors for small molecules: Ultrasensitive glucose detection. *J. Am. Chem. Soc.* **2010**, 14.
48. Duke J; Janer L; M., C. Sem visualization of glycosylated surface molecules using lectin-coated microspheres. *J Electron Microsc Tech* **1985**, *2*, 173–174.
49. Schiefer HG;Krauss H;Brunner H;U, G. Ultrastructural visualization of surface carbohydrate structures on mycoplasma membranes by concanavalin a. *J Bacteriol* **1975**, *124*, 1598–1600.
50. Ponader D; Maffre P; Aretz J; Pussak D; Ninnemann NM; Schmidt S; Seeberger PH; Rademacher C; Nienhaus GU; L., H. Carbohydrate-lectin recognition of sequence-defined hetero-multivalent glycooligomers. *J. Am. Chem. Soc.* **2014**, *136*, 2008–2016.
51. Sato Y; Yoshioka K; Murakami T; Yoshimoto S; O., N. Design of biomolecular interface for detecting carbohydrate and lectin weak interactions. *Langmuir* **2012**, *28*, 1846–1851.
52. Boder, E.; Wittrup, D. Yeast surface display for screening combinatorial polypeptide libraries. *Nature biotechnology* **1997**, *15*, 553–557.
53. Boder ET; Raeeszadeh-Sarmazdeh M; JV., P. Engineering antibodies by yeast display. *Arch Biochem Biophys*. **2012**, *526*, 99–106.
54. Singh A; Poshtiban S; S., E. Recent advances in bacteriophage based biosensors for food-borne pathogen detection. *Sensors* **2013**, *13*, 1763–1786.
55. Hanes, J.; Plückthun, A. In vitro selection and evolution of functional proteins by using ribosome display. *Proc Natl Acad Sci U S A* **1997**, *94*, 4937–4942.
56. Kanamori, T.; Fujino, Y.; Ueda, T. Pure ribosome display and its application in antibody technology. *Biochim Biophys Acta* **2014**, *1844*, 1925–1932.
57. Veedua, R.N.; Wengel, J. Locked nucleic acid nucleoside triphosphates and polymerases: On the way towards evolution of lnaaptamers. *Mol. BioSyst.* **2009**, *5*, 797–792.

58. Kohl, A.; Binz, H.K.; Forrer, P.; Stumpp, M.T.; Pluckthun, A.; Grutter, M.G. Designed to be stable: Crystal structure of a consensus ankyrin repeat protein. *Proceedings of the National Academy of Sciences of the United States of America* **2003**, *100*, 1700–1705.
59. Jarymowycz, V.A.; Cortajarena, A.L.; Regan, L.; Stone, M.J. Comparison of the backbone dynamics of a natural and a consensus designed 3-tpr domain. *Journal of biomolecular NMR* **2008**, *41*, 169–178.
60. Wezner-Ptasinska, M.; Krowarsch, D.; Otlewski, J. Design and characteristics of a stable protein scaffold for specific binding based on variable lymphocyte receptor sequences. *Biochimica et biophysica acta* **2011**, *1814*, 1140–1145.
61. Kajander, T.; Sachs, J.N.; Goldman, A.; Regan, L. Electrostatic interactions of hsp-organizing protein tetratricopeptide domains with hsp70 and hsp90: Computational analysis and protein engineering. *J Biol Chem* **2009**, *284*, 25364–25374.
62. Selzer, T.; Albeck, S.; Schreiber, G. Rational design of faster associating and tighter binding protein complexes. *Nature structural biology* **2000**, *7*, 537–541.
63. Schreiber, G.; Fersht, A.R. Rapid, electrostatically assisted association of proteins. *Nature structural biology* **1996**, *3*, 427–431.
64. Li Y; Li H; Yang F; Smith-Gill SJ; RA., M. X-ray snapshots of the maturation of an antibody response to a protein antigen. *Nat Struct Biol* **2003**, *10*, 482–488.
65. Tinberg, C.E.; Khare, S.D.; Dou, J.; Doyle, L.; Nelson, J.W.; Schena, A.; Jankowski, W.; Kalodimos, C.G.; Johnsson, K.; Stoddard, B.L., *et al*. Computational design of ligand binding proteins with high affinity and selectivity. *Nature* **2013**, *501*, 212–216.
66. Orlova, A.; Magnusson, M.; Eriksson, T.L.; Nilsson, M.; Larsson, B.; Hoiden-Guthenberg, I.; Widstrom, C.; Carlsson, J.; Tolmachev, V.; Stahl, S., *et al*. Tumor imaging using a picomolar affinity her2 binding affibody molecule. *Cancer research* **2006**, *66*, 4339–4348.
67. Ahlgren, S.; Orlova, A.; Wallberg, H.; Hansson, M.; Sandstrom, M.; Lewsley, R.; Wennborg, A.; Abrahmsen, L.; Tolmachev, V.; Feldwisch, J. Targeting of her2-expressing tumors using 111in-aby-025, a second-generation affibody molecule with a fundamentally reengineered scaffold. *Journal of nuclear medicine: official publication, Society of Nuclear Medicine* **2010**, *51*, 1131–1138.
68. Wahlberg, E.; Lendel, C.; Helgstrand, M.; Allard, P.; Dincbas-Renqvist, V.; Hedqvist, A.; Berglund, H.; Nygren, P.A.; Hard, T. An affibody in complex with a target protein: Structure and coupled folding. *Proceedings of the National Academy of Sciences of the United States of America* **2003**, *100*, 3185–3190.
69. Nord, K.; Gunneriusson, E.; Ringdahl, J.; Stahl, S.; Uhlen, M.; Nygren, P.A. Binding proteins selected from combinatorial libraries of an alpha-helical bacterial receptor domain. *Nat Biotechnol* **1997**, *15*, 772–777.
70. Nord, K.; Nord, O.; Uhlen, M.; Kelley, B.; Ljungqvist, C.; Nygren, P.A. Recombinant human factor viii-specific affinity ligands selected from phage-displayed combinatorial libraries of protein a. *European journal of biochemistry/ FEBS* **2001**, *268*, 4269–4277.
71. Mosavi, L.K.; Cammett, T.J.; Desrosiers, D.C.; Peng, Z.Y. The ankyrin repeat as molecular architecture for protein recognition. *Protein science: a publication of the Protein Society* **2004**, *13*, 1435–1448.
72. Mosavi, L.K.; Minor, D.L., Jr.; Peng, Z.Y. Consensus-derived structural determinants of the ankyrin repeat motif. *Proceedings of the National Academy of Sciences of the United States of America* **2002**, *99*, 16029–16034.
73. Binz, H.K.; Amstutz, P.; Kohl, A.; Stumpp, M.T.; Briand, C.; Forrer, P.; Grutter, M.G.; Pluckthun, A. High-affinity binders selected from designed ankyrin repeat protein libraries. *Nat Biotechnol* **2004**, *22*, 575–582.
74. Zahnd, C.; Pecorari, F.; Straumann, N.; Wyler, E.; Pluckthun, A. Selection and characterization of her2 binding-designed ankyrin repeat proteins. *The Journal of biological chemistry* **2006**, *281*, 35167–35175.
75. Boersma, Y.L.; Chao, G.; Steiner, D.; Wittrup, K.D.; Pluckthun, A. Bispecific designed ankyrin repeat proteins (darpins) targeting epidermal growth factor receptor inhibit a431 cell proliferation and receptor recycling. *The Journal of biological chemistry* **2011**, *286*, 41273–41285.

76. Lipovsek, D. Adnectins: Engineered target-binding protein therapeutics. *Protein engineering, design & selection: PEDS* **2011**, *24*, 3–9.
77. Khan, J.A.; Camac, D.M.; Low, S.; Tebben, A.J.; Wensel, D.L.; Wright, M.C.; Su, J.; Jenny, V.; Gupta, R.D.; Ruzanov, M., *et al*. Developing adnectins that target src co-activator binding to pxr: A structural approach toward understanding promiscuity of pxr. *Journal of molecular biology* **2015**.
78. Ackermann, M.; Morse, B.A.; Delventhal, V.; Carvajal, I.M.; Konerding, M.A. Anti-vegfr2 and anti-igf-1r-adnectins inhibit ewing's sarcoma a673-xenograft growth and normalize tumor vascular architecture. *Angiogenesis* **2012**, *15*, 685–695.
79. Gilbreth, R.N.; Koide, S. Structural insights for engineering binding proteins based on non-antibody scaffolds. *Current opinion in structural biology* **2012**, *22*, 413–420.
80. Hosse, R.J.; Rothe, A; Power, B.E. A new generation of protein display scaffolds for molecular recognition. *Protein science: a publication of the Protein Society* **2006**, *15*, 14–27.
81. MacDonald, J.T.; Maksimiak, K.; Sadowski, M.I.; Taylor, W.R. De novo backbone scaffolds for protein design. *Proteins* **2010**, *78*, 1311–1325.
82. Tombelli, S.; Mascini, M. Aptamers as molecular tools for bioanalytical methods. *Curr Opin Mol Ther*. **2009**, *11*, 179–188.
83. Reverdatto, S.; Rai, V.; Xue, J.; Burz, D.S.; Schmidt, A.M.; Shekhtman, A. Combinatorial library of improved peptide aptamers, clips to inhibit rage signal transduction in mammalian cells. *PloS one* **2013**, *8*, e65180.
84. Colas, P. The eleven-year switch of peptide aptamers. *Journal of biology* **2008**, *7*, 2.
85. Aubin-Tam, M.E.; Appleyard, D.C.; Ferrari, E.; Garbin, V.; Fadiran, O.O.; Kunkel, J.; Lang, M.J. Adhesion through single peptide aptamers. *The journal of physical chemistry. A* **2011**, *115*, 3657–3664.
86. Ellington, A.D.; Szostak, J.W. In vitro selection of rna molecules that bind specific ligands. *Nature* **1900**, *346*, 818–822.
87. Kimoto, M.; Yamashige, R.; Matsunaga, K.; Yokoyama, S.; Hirao, I. Generation of high-affinity DNA aptamers using an expanded genetic alphabe. *Nature biotechnology* **2013**, *31*, 453–457.
88. Tuerk C; L., G. Systematic evolution of ligands by exponential enrichment: Rna ligands to bacteriophage t4 DNA polymerase. *Science* **1990**, *249*, 505–510.
89. Bunka DH; PGl., S. Aptamers come of age – at last. *Nat Rev Microbiol*. **2006**, *4*, 588–596.
90. Kimoto, M.; Yamashige, R.; Matsunaga, K.; Yokoyama, S.; Hirao, I. Generation of high-affinity DNA aptamers using an expanded genetic alphabet. *Nat Biotechnol* **2013**, *31*, 453–457.
91. Seeman, N.C. Synthesis from DNA of a molecule with the connectivity of a cube. *Nature* **1991**, *350*, 631–633.
92. Rothemund, P.W.K. Folding DNA to create nanoscale shapes and patterns *Nature* **2006**, *440*, 297–302
93. Busuttil K;Rotaru A;Dong M;Besenbacher F; KV., G. Transfer of a protein pattern from self-assembled DNA origami to a functionalized substrate. *Chem Comm* **2013**, *49*, 1927–1929.
94. Voigt NV; Tørring T; Rotaru A; Jacobsen MF; Ravnsbaek JB; Subramani R; Mamdouh W; Kjems J; Mokhir A; Besenbacher F, *et al*. Single-molecule chemical reactions on DNA origami. *Nat Nanotechnol* **2010**, *5*, 200–203.
95. Wang R; Nuckolls C; SJ., W. Assembly of heterogeneous functional nanomaterials on DNA origami scaffolds. *Angew Chem* **2012**, *51*, 11325–11327.
96. Krauss, R.; Merlino, A.; Giancola, C.; Randazzo, A.; Mazzarella, L.; Sica, F. Thrombin–aptamer recognition: A revealed ambiguity. *Nucleic Acids Res* **2011**, *39*, 7858–7867.

# Chapter 4
# Modification of Polymer Surfaces for Biofunctionalization

**Guillaume Delaittre**

## 4.1 Introduction

Molecular recognition is central to biological processes where it is usually the first step toward a cascade of events. Despite many years of intense research, still little is understood on how most biorecognition events actually operate. For instance, many questions remain unanswered on how proteins recognize one another, for the specific criteria of antibody-antigen binding, on the extent of (un)specificity in binding events, or on small molecule-based biorecognition, among others. Some systems are better understood than others. For instance, the biotin/avidin complex is, without a doubt, the most widely known biorecognition system since its discovery in the 1940s [1] as it features the strongest binding constant known to date ($K_D = 10^{-14}$–$10^{-15}$ M) [2]. It was consequently ubiquitously employed in many areas spreading out of the pure biological field. Nevertheless, even for such a popular system, it took many years to understand its mechanism [2] and to even manipulate it [3, 4]. Therefore, biorecognition is not only a wide field of research on its own but is also vastly employed as a tool—with the few systems that are understood to a minimal extent—in other fields such as biotechnology or materials science.

In any case, immobilization of one binding partner onto a solid substrate is an important technique. Indeed, on the one hand, this technique is used for identification of unknown binding partners in screening methods such as peptide microarrays [5]. On the other hand, known complementary binding partners are involved in biopurification [6], biosensors [7, 8], bioassays such as ELISA [9, 10], biomaterials for cell biology or tissue engineering through integrin-binding peptides [11], targeted

G. Delaittre (✉)
Institute of Toxicology and Genetics, Karlsruhe Institute of Technology, Hermann-von-Helmholtz-Platz 1, 76344 Eggenstein-Leopoldshafen, Germany
e-mail: guillaume.delaittre@kit.edu

Institute for Chemical Technology and Polymer Chemistry, Karlsruhe Institute of Technology, Engesserstrasse 18, 76131 Karlsruhe, Germany



J. Rodríguez-Hernández, A. L. Cortajarena (eds.), *Design of Polymeric Platforms for Selective Biorecognition,* DOI 10.1007/978-3-319-17061-9_4

delivery via biological ligands such as folic acid [12, 13], as well as in pure materials science to bring together entities that are covalently linked to either of them [14, 15] such as in the classic case of streptavidin-coated surfaces serving as docking sites for biotinylated molecules [16] or even to construct extremely complex nanoarchitectures, as in the case of DNA supramolecular assemblies [17]. Some techniques combine both approaches, i.e., exploiting a known biorecognition pair in combination with molecular biology tools to detect, extract, and study unknown biomolecules and often their complexes. For instance, tandem affinity purification consecutively utilizes IgG- and calmodulin-functionalized beads to purify multiprotein complexes expressed in native conditions [18].

Prior to immobilization of one of the biorecognition partners, the presence of reactive groups on the surface of the material is necessary. One can distinguish three major classes of materials: metals, ceramics, and polymers. The first two are hard and either ductile and conductive, or brittle and nonconductive, while polymers are light and can possess any of these features, depending on their chemical composition. Thus, polymers offer a significantly wider range of applications than metals and ceramics. Depending on the targeted application, one can choose among an overwhelming variety of reported and even commercial polymers. Premade (commercial) polymers are usually inert, for obvious reasons. This implies that surface modification will usually be necessary in order to covalently bind recognition motifs. This is certainly the easiest option when one has limited chemical facility access or chemistry skills. Alternatively, one can indeed opt for fabricating an advanced polymeric material through specific monomer design or simply mixing different monomers in the so-called "copolymerization" method. Thus, in these cases, it is not only possible to tune the mechanical properties of the bulk material but also to introduce functionality, including at the surface. This chapter, however, only focuses on the surface modification route—as it is the most commonly employed one—and especially on studies leading to surface biofunctionalization. For examples of prefunctionalization methods, the reader may refer to the existing literature [11, 19–21]. Importantly, conducting polymers, albeit major players in polymer-based biosensors, [22] are not described here as their surface functionalization is predominantly the result of a prefunctionalization approach either through the use of a functional (co)monomer [23–25] or via a doping method (i.e., blending of the conducting polymer with a functional nonconductive counterpart) [26], certainly due to the fact that direct backbone functionalization would lower their conductivity [27].

It must be noted that polymer coatings onto inorganic materials (e.g., polymer brushes, spin-coated or chemical-vapor deposited polymer films) will generally not be treated here as these methods do not exploit the polymer bulk properties cited above. Only cases with widely used polymers involved are mentioned as the chemical surface modification may be translated to bulk systems. Furthermore, we only present methods leading to covalent immobilization of biorecognition units, as opposed to noncovalent adsorption. Finally, this chapter does not aim at being comprehensive as there is an immense body of published work on the modification of polymers (for bio-related purposes) but rather intends to provide an overview of the basic methods to introduce surface functionality into polymeric substrates that are initially devoid of it.

## 4.2 General Aspects of the Modification of Polymeric Substrates

It is possible to distinguish two main categories of postpolymerization surface modification. In the first case, the modification is carried out by placing the polymer in contact with a solution containing chemicals, which modifies the chemical structure of the outermost layer of the material. Usually, the depth of modification depends on the exposure time, the harshness of the treatment, and the susceptibility of the polymer toward the employed chemicals. In the second case, physical methods are employed to generate reactive species at the surface of the materials, and often (but not always) in the gaseous environment of a close chamber where the polymer sample is placed. In this case, it is usually the method that acts as a determining factor for the extent of modification, rather than the specific polymer. In the following sections, we thus describe the most common routes employed to introduce the initial (primary) reactive handles into polymeric materials and sort them according to two main categories, namely, wet chemical methods or physical chemical methods. We then explain the subsequent steps that can be taken to immobilize recognition units.

## 4.3 Introduction of Primary Reactive Groups by Wet Chemical Methods

A major aspect regarding the employment of wet chemical methods (pure or in combination with physical activation) is typically the resistance of polymers to solvents. Indeed, the user will often desire to maintain the surface roughness of the initial material, or at least the bulk integrity (i.e., prevent the complete dissolution), and therefore will be limited in terms of possible solvents and reagents (which usually need to be dissolved) by the nature of the polymer. Generally, polar polymers such as poly(meth)acrylates, poly(meth)acrylamides, or polyesters are not soluble in solvents with a very low polarity index (e.g., pentane, hexane) and apolar polymers such as polystyrene are not soluble in polar solvents. But the picture is quite more complicated than this simple statement as substituents within a same class of polymers can have a dramatic effect on solubility and, sometimes, solvents may not molecularly dissolve the polymer but would at least induce swelling. The chemical resistance of some important polymers can actually be correlated to their low propensity to interact with solvents. For instance, elevated temperatures are required to dissolve polyethylene (PE) in “strong” solvents such as aromatic hydrocarbons or chlorinated solvents. Poly(tetrafluoroethylene) (PTFE) is generally considered as insoluble as only high-molecular-weight (per)fluoroalkanes can dissolve it (close to its melting temperature). These two polymers are among the most chemically inert ones. Therefore, wet chemical methods will be employed when it is possible to dissolve the reagents necessary to carry out the surface modification in a solvent which does not provoke extensive swelling on the bulk material. This greatly reduces the leeway.

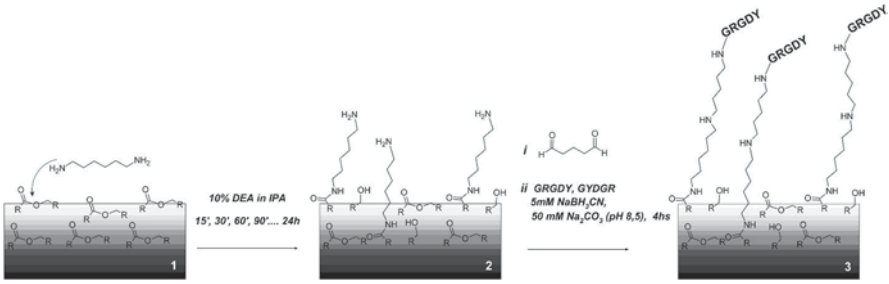


**Fig. 4.1** Aminolysis/amination of poly(ε-caprolactone) surface by hexanediamine and subsequent glutaraldehyde-mediated peptide functionalization [29]

As a general rule, it actually is safe to state that the combination of most common organic solvents with most common polymers is not judicious. The safest organic solvents are probably the low-molecular-weight alcohols, particularly methanol and ethanol, but swelling cannot be excluded. Therefore, water is the solvent of choice for wet chemical treatment. Wet chemical treatments are generally highly dependent on the chemical structure of the polymer to modify, particularly on the presence of chemical groups that can be altered using chemicals. This implies that for each type of polymeric surface, a limited range of chemistries are available.

Without a doubt, hydrolysis and aminolysis have been the most popular solution-based methods to introduce reactive groups at the surface of polymeric materials. Obviously, only polymers that are able to undergo such degradations are concerned. This typically includes polyesters such as poly(ε-caprolactone) (PCL), poly(lactic acid) (PLA), and poly(lactic acid-*co*-glycolic acid) (PLGA). PCL is commonly treated with isopropanol solutions of diamines such as ethylenediamine (EDA) or hexanediamine (HDA), which induces a transamidification reaction and leave free amines on the surface (Fig. 4.1) [28−31]. The extent of surface functionalization, that is, the density of surface-displayed amines, depends on the temperature and duration of immersion. Nevertheless, satisfying results can be obtained at room temperature, even in water [32]. In one case, SEC characterization was utilized to prove the overall integrity of the polymer after aminolysis, thereby, demonstrating that the bulk material was intact [32]. For a specific study, it was shown that the density of surface-bound amines increased dramatically in the first 30 min, followed by a slight decrease and stabilization. At the same time, surface roughness evaluated by AFM increased for treatments longer than 30 min. The authors also witnessed rapid weight loss and drop in elastic modulus between 45–90 min with a further stabilization. These phenomena probably occur due to the formation and dissolution of oligomers. All in all, although not mentioned in this study, it is likely that the depletion of amines leads to a termination of the aminolysis process, which means that without standardized experiments (sample surface area and thickness), it is rather complicated to extract absolute values and only trends should be considered.

Aminolysis/transamidification has also been performed on PLA and PLGA. Probably due to the higher concentration of ester bonds in these (co)polymers as compared to PCL, which possesses a longer alkyl spacer, short exposure times are enough to reach the maximum effect [33]. A treatment as brief as 2 min at room temperature with a 6% w/v solution of HDA in isopropanol (i.e., 1 M amine) was efficient to introduce amines in an amount sufficient for further bioconjugation [34]. In the case of more sensitive PLGA materials such as microporous scaffolds, the slightest surface alteration can lead to a drastic change of the porosity. As a consequence, a treatment of only 10 s at room temperature with a 0.075 g $mL^{-1}$ diamino-poly(ethylene glycol) solution in isopropanol (1500 g $mol^{-1}$, i.e., 0.1 M amine) revealed adequate [35]. As another member of the polyester family, poly(ethylene terephthalate) (PET) was also reported to undergo controlled aminolysis. Particularly, PET fibers were treated with a set of four amines exhibiting various chain lengths and alkyl or ethoxy spacers, nondiluted or in methanolic or aqueous solutions, at different temperatures and times [36]. The weight loss and the morphology of the fibers were monitored by gravimetry and by the use of scanning electron and atomic force microscopes, respectively, while the amount of grafted amines was measured by colorimetry. Overall, a temperature reaction of 50 °C with a 1 M methanolic amine solution was claimed to be the best compromise. Aminolysis/transamidification was also performed onto poly(methyl methacrylate) (PMMA) using diamines. In this case, the ester groups are lateral groups, which should not lead to an extensive degradation of the polymer [37, 38]. In this context, a method where these diamino linkers were first converted to their monoanion by treatment with *n*-butyl lithium was also reported by Soper and McCarley [39]. For more details on polymethacrylate surface modification for biosensors, the review of Djordjevic in the context of optical biosensors is recommended [40].

Hydrolysis has been in lesser use than aminolysis, probably because it yields species (i.e., hydroxyl and carboxyl) that are less reactive and usually require further activation or the presence of catalysis for further coupling. Although acid hydrolysis is possible, base-catalyzed hydrolysis is preferred as it is proceeds faster. In addition, the former may induce bulk hydrolysis, at least in the case of PLA, [41] rather than surface-confined modification. Only strong acid treatments may be efficient but they would also lead to extended morphological changes at the surface. PCL [42, 43] as well as PLA [44] and PLGA [33] were treated with sodium hydroxide solutions. Again, temperature and concentration are the determining parameters regarding the reaction rate [42] and the increase of surface roughness [44]. Hydrolysis with an ethanolic sodium hydroxide solution on a PMMA substrate was directly compared to aminolysis in terms of subsequent surface functionalization and it clearly showed that the latter was more efficient [37]. In some cases, hydrolysis of the PMMA surface was performed as a preliminary step before amidification, particularly when using polymeric amines such as poly(ethyleneimine) and poly(allylamine) [38]. Saturated sodium hydroxide aqueous solutions were also efficiently employed to produce carboxylic acids at the surface of commercial PMMA investigated for DNA microarrays [45].

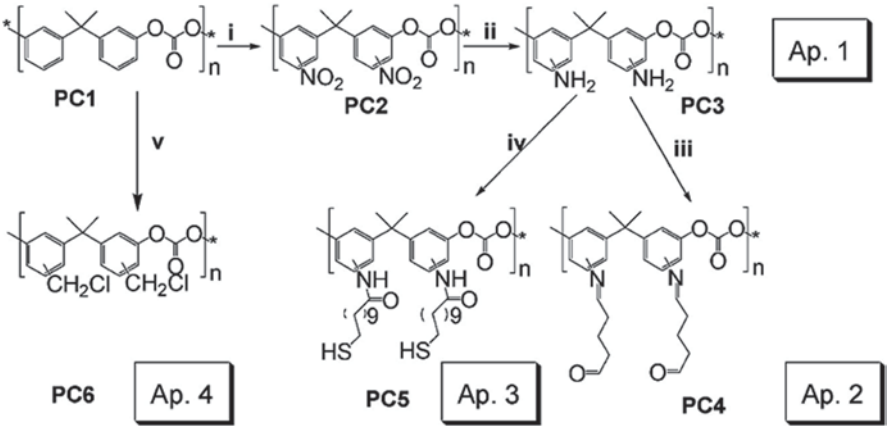


**Fig. 4.2** Various methods to introduce reactive groups at the surface of polycarbonate substrates through initial aromatic substitutions [53]

A few other methods have been reported to enrich the surface of PET materials in hydroxyl and carboxyl groups, which otherwise are only present as end groups. Marchand-Brynaert reported an oxidation procedure to convert hydroxyl termini into carboxyl groups in PET microporous membranes by exposure to a potassium permanganate in sulfuric acid at 60 °C [46, 47], following assessment of diverse methodologies to maintain the porous structure [48]. In addition, Hubbell showed that the aromatic ring present in the PET repeating unit could be exploited to introduce further hydroxyl groups by treatment with an aqueous solution of formaldehyde and acetic acid at 20–37 °C for 4–8 h [49, 50].

Polycarbonate (PC) is an attractive polymer as it is transparent, has a high temperature and impact resistance, and can be thermoformed. This is advantageous for studies requiring well-defined topography and geometry, such as emulating blood vessels for instance [51]. PC is also the constituting material of compact discs (CDs) and has thus been considered in this very form to be an ideal platform for screening [52]. Therefore, Maquieira studied two routes to impart surface reactivities to CDs with the aim of immobilizing oligonucleotides for DNA detection (Fig. 4.2) [53]. The first method was based on a Friedel–Crafts alkylation with chlorodimethylether catalyzed by zinc(II) chloride, in cyclohexane at 60 °C for 2 h. These conditions were found to be the best compromise between a reasonable extent of functionalization and the conservation of the physical properties. Longer times and higher temperatures lead to increase in roughness and even cracking. It was noted that this method proved to be efficient for further attachment of aminated DNA strands and is particularly attractive as after only one treatment step the CDs are ready for biofunctionalization. However, the requirement for organic solvents and highly toxic chlorodimethylether lowers the attractiveness of this route. Indeed, the second alternative consisted of a nitration/reduction sequence to attach amine groups to the aromatic rings of PC, all performed in aqueous solutions (of nitric acid and sodium

borohydride, respectively). Nevertheless, we also found in our laboratory that this method was sometimes not conclusive for more fragile specimens of PC, such as porous thin membranes, as cracking also occurred [54].

Polyethersulfone (PES) is another interesting polymer as it is a highly chemical resistant, semitransparent thermoplastic, and sometimes replaces PC in more demanding applications. Its backbone is also made of multiple aromatic rings, this time connected together via sulfone and ether groups. Therefore, Marra employed a Friedel–Crafts alkylation procedure similar to Maquieira's to halogenate the polymer surface using chlorodimethylether with tin(IV) chloride as the Lewis acid catalyst [55]. This exact same procedure was developed earlier by Higuchi in the frame of poly(*N*-vinylpyrrolidone) grafting onto PES [56].

PTFE and other perfluorinated polymers are usually considered nonreactive and are widely used for biomedical applications. Strong reducing agents are, nevertheless, able to alter PTFE. Often, alkali metals are employed but yield blackened products. Importantly, McCarthy reported a procedure in which a benzoin dianion formed by reaction of benzoin with potassium *tert*-butoxide in deoxygenated dimethyl sulfoxide or *N*-methylpyrrolidone was able to reduce the surface of PTFE in a more controlled manner, producing films with a metallic visual aspect [57, 58]. This process was later used by Hubbell in order to produce insaturations at the surface of PTFE, which were then modified to immobilize cell-adhesive peptides [50]. Another protocol for introducing surface insaturations, initially reported by McCarthy [59] and later employed by Shoichet [60] for poly(tetrafluoroethylene-*co*-hexafluoropropylene) (FEP), was exploited by Gabriel on the PTFE homopolymer [61]. In this case the (strong) reducing agent is sodium naphthalide, which must be prepared fresh by stirring sodium and naphthalene together in dry tetrahydrofuran as the resulting product degrades in presence of water.

Finally, a very important polymer that has been used to a lesser extent in the frame of biorecognition is polydimethysiloxane (PDMS). For instance, we can mention the report of Sheardown who grafted a polymethylsiloxane layer to introduce Si–H groups that can later be involved in palladium-catalyzed hydrosilylation [62]. For further possible procedures, the reader may refer to reviews dealing with the surface modification of PDMS for microfluidic [63] and biomedical [64] applications. A typical alternative is oxidation to create silanol groups amenable to further silanization, as in the case of silicon wafers.

## 4.4 Introduction of Primary Reactive Groups by Physical Chemical Methods

The introduction of functional groups at the surface of a material using physical methods is significantly less substrate-dependent than that with wet chemical procedures and usually relies on the employed reagents (elemental gases or small molecules) rather than the chemical structure of the polymeric surface. An important difference between wet chemical and "dry" physical chemical methods is that in the

latter case, the surface topography is generally less altered, at least for compared treatment times leading to similar degrees of functionality. Nevertheless, these physical methods often present the disadvantage of simultaneously generating a broad range of species rather than a precisely defined single species and of requiring specialized equipment.

Plasma-induced modifications are the most widely employed techniques. Other methods include ozone treatment, as well as UV- or electron beam-based methods. Importantly, physical treatments generally allow spatially resolved modification due to the radiative nature of these modifications. Typically, a simple masking procedure with a blocking grid is sufficient [65–67].

### *4.4.1 Plasma-Based Modifications*

Plasmas basically originate from the ionization of gases. They can be created via different methods, the most popular—at least in the area of surface modification for biorelated applications—being glow discharge, a nonthermal process. In that case, the plasma is generated by applying a radio-frequency electrical field into a gas-filled container. Plasma procedures are easily transferable from one polymer to another, only requiring optimization in some cases [68]. Depending on the gas or liquid vapors introduced in the plasma chamber as well as on other potentially coupled energy sources, plasma treatments can be categorized as follows:

- Direct plasma treatment (DP) utilizing nondepositing gases, commonly argon, nitrogen, or oxygen, or small molecule vapors [68]
- Plasma (grafting) polymerization, also named plasma-enhanced chemical vapor deposition (PECVD), employing vapors of diverse molecules, typically enes [69]
- Plasma-immersion ion implantation (PIII), which is based on a direct plasma treatment setup coupled to a high voltage pulse generator (Fig. 4.3) [70]

These three treatments result in rather different functionalities on the surface:

- DP will introduce elementary functional groups by oxidation directly on the treated polymer surface such as hydroxyls, aldehydes/ketones, carboxyls, or amines, depending on the nature of the gas [68]. DP treatment is usually not extremely stable over time: it was for instance commonly observed that it resulted in a sharp decrease of water contact angle (increase of hydrophilicity) in comparison to the native materials but that the hydrophobicity slowly increased when samples were exposed to air or water [72, 73].
- PECVD yields a thin polymeric layer grafted on the modified substrate and the functionality directly arises from the employed monomers. Obviously, milder plasma-generating conditions will preserve functionality to a higher extent [69]. PECVD usually leads to stable functionalization over time.
- PIII is reported to produce unpaired electrons inside the material, these electrons slowly migrating to the surface enabling radical-based grafting. [74]. The activated substrate procedure maintains a bonding ability of several months, if for instance freeze-dried.

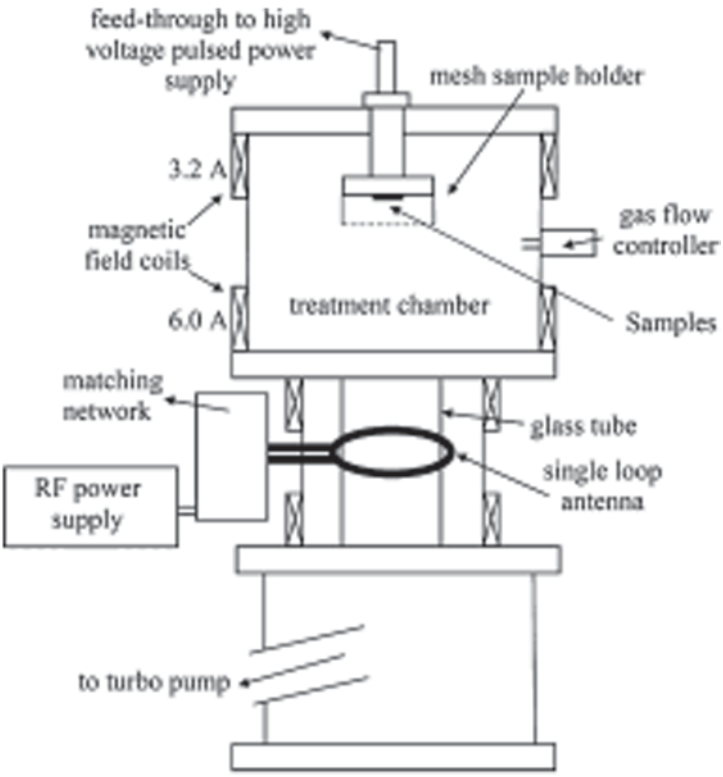


**Fig. 4.3** Schematic diagram of a PIII treatment system [71]

Below, we explain in detail the sort of reactive groups that are produced in each method, depending on the employed gas/vapor phase. How these primary groups are further exploited in order to bring biorecognition units onto the surface is described later in Sect. 4.5.

#### 4.4.1.1 Direct Plasma Treatment (DP)

In DP, flows of inert gases such as argon and nitrogen have been employed at low pressure. These two gases present great advantages in terms of safety of storage and handling. After such plasma exposure, the polymeric samples are usually exposed to air or even to pure oxygen in order to generate oxygen-based reactive species such as carboxylic acid or peroxides. Callens [75], Ho [71], Maeji [76], and Yin [77] have done so on PCL, PE, polyvinylidene difluoride (PVDF) [78], and PP, respectively. Nitrogen additionally leads to the introduction of amines [71, 79].

Oxygen, which is clearly more hazardous than argon or nitrogen, has been extensively utilized as the plasma source in DP. Quite obviously, it generates a mixture of species ranging from oxygen radicals and anions to hydroxyls, carbon-

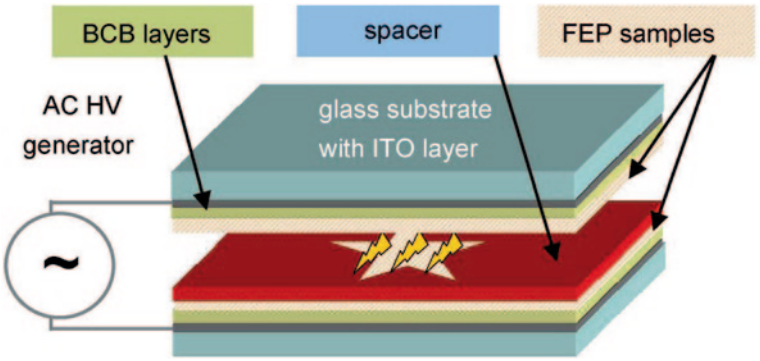


**Fig. 4.4** Schematic setup for surface modification of two polymer samples at a time, which are sandwiched between two indium tin oxide (ITO) coated glass slides covered with the dielectric benzocyclobutene (BCB) and separated by a patterned spacer-mask [89]

yls, carboxyls, and peroxides that can be exploited in a range of chemistries with the final aim of immobilizing biomolecule ligands. Oxygen plasma was applied to numerous polymeric substrates. For instance, it has proven particularly useful to introduce functionality at the surface of vinyl polymers: polyolefins [80, 81] and their copolymers such as cyclic olefin (co)polymers (COP or COC) [72, 73, 82, 83], and PS-*b*-poly(ethylene-*co*-butylene)-*b*-PS (SEBS) [84], as well as their perfluorinated counterparts, for example, PTFE [73]. Interestingly, carbon dioxide seems to yield similar species, as reported by Vassile for PVDF functionalizations [79]. Polymers made by step-growth polymerization were also treated with oxygen plasma: polyesters such as PET [73], PLA [85, 86], and its copolymers [87]; polycarbonates [73]; poly(ether carbonate urethane) [88]. PDMS usually undergoes plasma oxidation similarly to silicon wafers, thereby producing silanol (Si-OH) groups [73].

A unique method, not involving low molecular gas pressure but air at atmospheric pressure was reported by Graz [89]. The plasma is generated by dielectric barrier discharges (DBD), a process first reported by Siemens in the nineteenth century [90]. The setup consists of a sandwich procedure where two polymeric films—in the present case FEP—can be treated at once if placed between two metal electrodes generating a high voltage alternating current with at least one insulating film in the discharge gap (Fig. 4.4). This process leads to the formation of weakly ionized plasma. In such a setup, patterning is also possible by placing a mask between the two polymeric substrates. Not only the presence of oxygen species such as aldehydes, but also of nitrogen species, was evidenced on the surface of the DBD-treated FEP films.

As mentioned above, DP can also be utilized in the presence of chemical vapors. For instance, Aebischer employed a mixture of helium and methanol vapors to create hydroxyl groups at the surface of FEP substrates [65, 91]. More commonly, polymeric materials were exposed to ammonia plasma for the specific grafting of amino

groups on PP [78, 79], PVDF [92], polyesters such as poly(3-hydroxybutyrate-*co*-3-hydroxyvalerate) [93], or PLA [94], and poly(ether ester urethane)s [95].

Friedrich had recourse to bromoform ($HCBr_3$) as the plasma source in order to introduce bromide groups at the surface of PE and PP, species later involved in nucleophilic substitutions [80].

Finally, DP can also result in the formation of grafted polymer but after additional thermal or radiative activation of DP-generated species in presence of radically polymerizable monomers. This process is called postplasma-grafting and will not be distinguished from DP as the same primary species (e.g., peroxides) are also present in DP processes. Corresponding examples of secondary functionalization will be detailed in Sect. 4.5.

#### 4.4.1.2 Plasma Polymerization or Plasma-Enhanced Chemical Vapor Deposition (PECVD)

DP suffers from the requirement for renewed optimization for each polymer to be treated [68], although far less than in the case of wet procedures. However, plasma polymerization exhibits a higher transferability. PECVD can be considered a covalent coating method that relies to a large excess onto the nature of the radically polymerizable monomers present in the vapor phase (Fig. 4.5). It is applicable not only to polymers but also to metals and ceramics. The relative mildness of the process is important with regards to functional substituents of the vinyl monomers. A customarily applied method is shortening the plasma duty cycle by pulsing periods interspersed with "off" times during which the polymerization continues to proceed. In some cases, continuous wave conditions can still be applied during a short initiation period.

By far, carboxylic acid-containing monomers, and particularly acrylic acid (AA), have been graft-polymerized the most, onto a variety of polymeric materials: PE and PP [80], PS [97], PLA [98−100], polyurethanes [98]. Urban reported a PECVD-based method where he used maleic anhydride (MAnh) in place of AA [101]. MAnh is a special monomer owing to the fact that it is not able to homopolymerize. Therefore in that study, a monolayer of maleic acid—that can be hydrolyzed to yield two carboxylic acid functions—was certainly formed onto PE and PP substrates.

Usually, carboxylic acids require activation for subsequent conjugation reactions. A recent alternative has been explored via the plasma polymerization of pentafluorophenyl methacrylate, first on silicon substrates [102, 103] and then on PS [96].

Allyl monomers were not forgotten in the area of PECVD where they are rather popular to introduce alcohol and amine groups. Allyl alcohol (AllOH) as well as allylamine ($AllNH_2$) were graft-polymerized by Friedrich onto PP and PE [80]. Eberhart covalently attached poly($AllNH_2$) onto PCL and PLA [104], so did Sheardown with P(AllOH) onto PDMS [105]. Klee utilized a protected, hydrolyzable version of AllOH, namely vinyl acetate (VAc) [106].

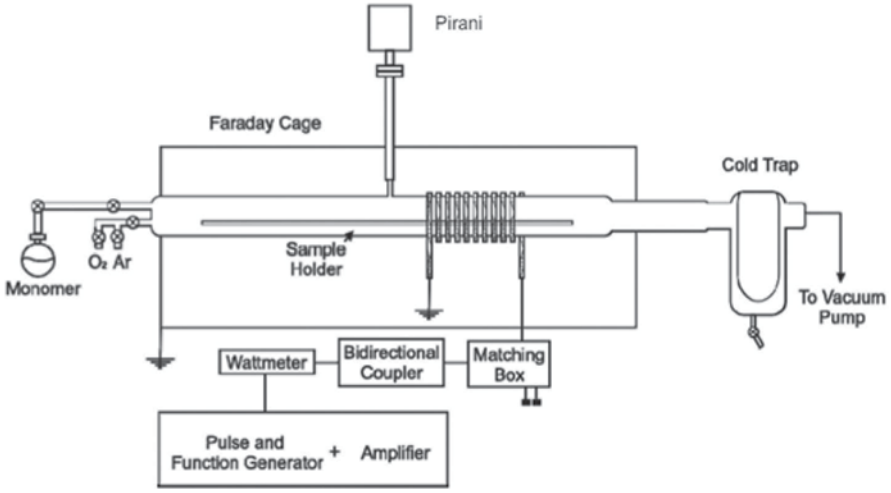


**Fig. 4.5** Schematic diagram of a plasma reactor employed for plasma-enhanced chemical vapor deposition (PECVD) and its electrical components [96]

#### 4.4.1.3 Plasma-Immersion Ion Implementation (PIII)

PIII has been extensively employed in the frame of bioconjugation by the team of Bilek [107, 108]. Although PIII certainly yields similar species as classic DP, it is usually employed in order to exploit the radicals that are formed along with these oxygen and nitrogen species. It is usually referred to as a linker-free method for biomolecules, particularly enzymes, which can be immobilized without intermediate procedures [109]. The treated substrates generally become hydrophilic (as in DP, which confirms the previous statement on the similarity of produced species) but seem to retain this character for extended period of time, which results in prolonged protein activity albeit this absence of linker that could regulate protein-surface interaction and prevent denaturation. In the frame of PIII, inert gas plasmas have generally been used: nitrogen onto PE [71, 74, 110, 111], PTFE [74, 112, 113], PMMA [74], PS [74, 114], and PC [115] as well as argon onto PE [71] and PS [116].

In a different approach, Choi employed PIII together with a masked irradiation to pattern implanted areas that would yield peroxide surface patterns after exposure to air for 24 h [117].

### *4.4.2 Ozone Treatment*

Ozone treatment is related to plasma techniques in the fact that it also relies on a reactive gas phase. Early studies on the action of ozone onto PE films evidenced the formation of oxidation products similar to those produced by oxygen plasma, i.e., hydroxyls, carbonyls, and carboxyls [118, 119]. For instance, Diaz-Quijada investigated the ozone treatment for the fabrication of DNA microarrays on COP

and PMMA [45]. The activation of ozone by UV was also investigated and demonstrated a higher degree of modification, unfortunately yielding an increase of autofluorescence of the substrates, which can be detrimental for applications involving spectroscopic methods.

### *4.4.3 Photoirradiation*

Light-based techniques can play a major role in the area of surface modification, as they allow facile temporal and spatial control [54, 120−122]. Notably, they usually do not require harsh chemicals as in the case of wet chemical modifications, and avoid the requirement for vacuum techniques as in plasma-based techniques or for hazardous gases such as ozone. An exception to that is however the UV activation of a mercury- and ammonia-containing chamber to introduce amines at the surface of FEP fibers [123].

The incorporation of photoreactive species in the polymer itself is out of the scope of this chapter, therefore the following described examples concern the use of soluble photoactive moieties yielding a direct grafting onto the surface. The first class of such studies is devoted to UV-induced polymerization, which is conceptually very similar to PECVD: radicals are created in the surroundings of and onto the surface in presence of radically polymerizable monomers. This process has been carried out using either gaseous or liquid monomer formulations.

For instance, Kessler reported the direct grafting of acrylated integrin ligand peptides—precisely, cyclic RGD—on PMMA in the presence of camphorquinone acting as a radical source, in solution, and under UV light [124, 125]. The same team also reported the grafting polymerization of photoisomerizable cyclic RGD peptide-based acrylamides at the surface of PMMA without the use of a photoinitiator. In that case, the PMMA films were first irradiated for 2 h at 254 nm, in order to create surface-bound radicals [126].

Albertsson reported a similar strategy using benzophenone for gas-phase grafting polymerization with acrylamide, vinylpyrrolidone, and MAnh [127]. The vapor pressure of the monomers had an influence on the grafting yield: the higher, the better. As we suggested in the case of PEVCD reported by Urban, MAnh yielded a low grafting density, for which impossible homopolymerization was here explicitly designated as the cause. While this study did not involve subsequent biofunctionalization, the method was adapted by other teams for this purpose. For instance, Xu graft-polymerized acrylic acid on PP [128]. In that case, PP membranes were first soaked in a solution of benzophenone and dried before placing them in an aqueous solution of AA and irradiating them.

Larsen also utilized a benzophenone derivative (benzoyl benzylamine hydrochloride, BzBAm) to create protein-repellent coatings from a solution of PEG and BzBAm [129]. In this case, no polymerizable monomer is present, but benzophenone derivatives are known to readily abstract hydrogen from hydrocarbons and create radicals. This feature was thus exploited for a second step of functionalization to graft, directly on the passivating layer, an enzyme as well as an antibody,

which both maintained activity. Tan reported a few years before a rather similar method exploiting the hydrogen abstraction ability of benzophenone—with the coupling of 4-benzoylbenzoic acid and an RDG peptide followed by its direct UV-induced grafting of the latter onto poly(carbonate urethane)s [130].

Yang reported another simple UV-induced grafting method. His team found that irradiation of a phenol solution in acetone resulted in the attachment of the aromatic compound onto polymeric surfaces, via a mechanism involving the triplet state of acetone [131]. This method is compatible with several functional groups (sulfonic and carboxylic acids, amine, thiol). In the case which interests us, bromo-4-hydroxyacetophenone was chosen to introduce bromine groups at the surface of PP in a spatially resolved way using a metallic mask [132].

Isopropylthioxanthone (ITX) is a common photoinitiator, which was used by Yin to grow polymer brushes at the surface of PE and PS. Particularly, methacrylated microperoxidase and poly(L-lysine) could be copolymerized from the surface of PE films and PS well plates, respectively. The method relies on two steps: (i) the UV-induced grafting of ITX onto the polymer surface proceeding by hydrogen abstraction and coupling with the newly formed polymer-bound radical and (ii) the visible light-induced formation on an equilibrium between ITX-bound species and propagating radicals next along with the ITX intermediate radical. This mechanism somehow resembles that of photoinduced reversible-deactivation radical polymerization such as nitroxide-mediated photopolymerization [133].

Finally, photogeneration of highly reactive species, nitrenes and carbenes, able to insert into C–H bonds was utilized as a simple means to introduce not only chemical groups but also, more commonly, directly the biorecognition ligand. The most employed class of precursors is that of *p*-azidophenyl derivatives, which form nitrenes upon UV irradiation. Many *p*-azidophenyl-functionalized peptide systems have been reported for grafting onto PS [134], PET [134] poly(vinyl alcohol) [135], poly(ester carbonate)s [135], and polyurethanes [136]. A biotin derivative was also described for the functionalization of the epoxy-based photoresist SU-8 (Fig. 4.6) [137]. Lee also had recourse to this method to immobilize a brominated compound for further surface-initiated atom-transfer polymerization from COC. Chevolot opted for a related method based on the generation of carbenes from diazirine-functionalized mono- and disaccharides for PS surface functionalization [138].

### *4.4.4 Electron-Beam Irradiation*

Electron-beam irradiation (eBeam) was seldom used on polymeric materials in the context of biorecognition-based systems. It has nevertheless been employed extensively for the patterning/crosslinking of PEG derivatives directly involved in bioconjugation/biorecognition [139]. eBeam is performed to create radicals at the surface of a polymeric material. Albertsson has for instance shown that it is possible to treat topographically patterned PCL substrates with eBeam and maintain the morphology of the sample [140]. The irradiated samples could be stored without loss of reactivity by immediate immersion into liquid nitrogen. A simple subsequent exposure to a deoxygenated solution of acrylic acid allowed surface grafting polymerization. Quite

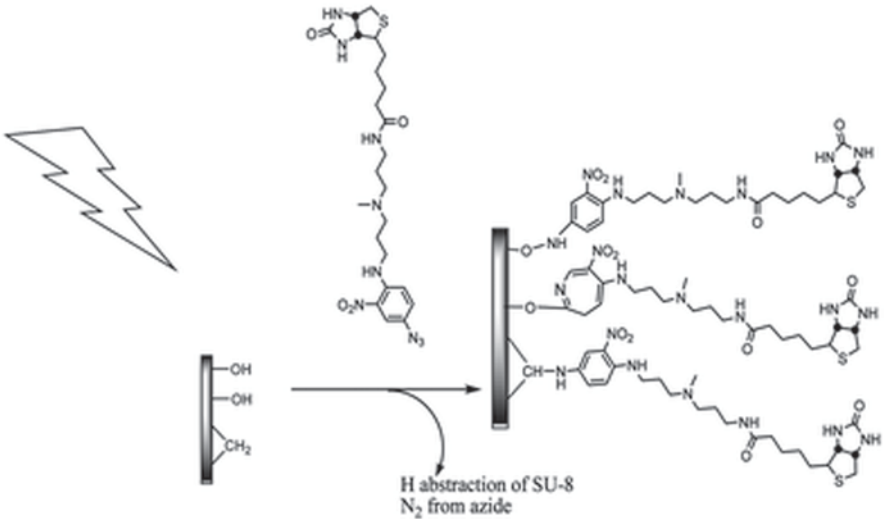


**Fig. 4.6** UV-induced grafting of a *p*-azidophenyl-functionalized biotin [137]

differently, Okano proceeded to the direct eBeam of solutions of *N*-isopropylacrylamide and a carboxyl-functionalized analogue to yield patterned crosslinked layers through masked irradiation onto tissue culture polystyrene dishes [67].

## 4.5 Subsequent Surface Functionalization Methods and Attachment of Biorecognition Modules

Depending on the chemical groups introduced through methods described in Sect. 4.3 and 4.4, several synthetic routes open. In the following, the description of these routes is ordered according to the type of functional group present on the surface after the initial treatment, irrespective of the method employed to achieve this state.

### *4.5.1 Oxygen Species*

Through the use of oxygen DP, diverse oxygen species are produced at the surface of a polymer. We detail their derivatization one by one below but it is perhaps interesting to first mention that Friedrich reported the global conversion of these groups into alcohols through the application of strong reductants such as $B_2H_6$/$H_2O_2$, $LiAlH_4$, or vitride/NaOH [80]. Sheardown did the same with sodium borohydride [105].

#### 4.5.1.1 Peroxides

Surface-bound peroxides are generally exploited for a subsequent grafting-polymerization procedure. This can be triggered either by UV exposure [75, 77, 87] or by thermal treatment [76, 117] in presence of the monomer solution. UV sources usually employed are in the UVA range and irradiation is performed for a few tens of minutes. Thermal treatment occurs in the 65–75 °C range for a few hours. Again, as in PECVD, AA is the most widely utilized monomer [87, 117]. After polymerization, peptide coupling reagents such as 1-ethyl-3-(3-dimethylaminopropyl)-carbodiimide (EDC) and *N*-hydroxysuccinimide (NHS) are employed to immobilize amino containing bioligands [87]. Copolymerization of styrene and MAnh to yield alternating copolymers that can be hydrolyzed to yield carboxylic acids was reported [76]. Amine-containing monomers such as 2-aminoethyl methacrylate [75] and 2-methacryloyloxyethyl phosphorylcholine [77] were also used. Sometimes inhibitors such as Mohr's salt are added to the monomer mixture to prevent solution-phase homopolymerization and promote exclusive grafting [141].

#### 4.5.1.2 Alcohols

There are many ways surface-bound alcohols can be derivatized to ultimately lead to biomolecular immobilization. In many reports, silanization is employed. 3-(aminopropyl)triethoxysilane is clearly the most popular reagent, yielding aminated surfaces that can then react further with aldehydes (such as glutaraldehyde [80] or reduced dextran [82]) or activated esters [85]. Through silanization atom-transfer radical polymerization (ATRP) initiators have also been introduced at the surface of PP, to yield brushes of poly(ethylene glycol) methacrylate (PEGMA) and glycidyl methacrylate (GMA) copolymers, whose epoxide rings were then exploited for amine-based protein attachment [81]. An interesting route was reported by Chiari with the use of a copolymer bearing silane side chains (as well as either NHS ester or epoxide groups) that could be coupled to oxidized surfaces for DNA microarraying (Fig. 4.7) [73].

Hydroxyl groups can also be reacted with diisocyanates to produce isocyanate surfaces that can be used as such for coupling with amine-containing biomolecules or again converted into amines by hydrolysis [80]. Esterification using acyl chloride was also performed to introduce a chloromethylbenzyl group which could potentially serve as an ATRP initiator but was actually converted to a dithiocarbamate (also called photoiniferter) instead, in order to perform UV-initiated "living" polymerization of PEGMA and AA, followed by IgG immobilization mediated by EDC/NHS [83]. Carbodiimidazole and tresyl chloride activations supplied handles for peptide immobilization through their N-terminus, forming urethane linkages, [65] and secondary amine and amide linkages, [105] respectively. Finally, Klee reported a protocol involving benzoquinone as a bridging molecule between the hydroxyl groups of hydrolyzed PVAc and the N-terminus of peptides [106].

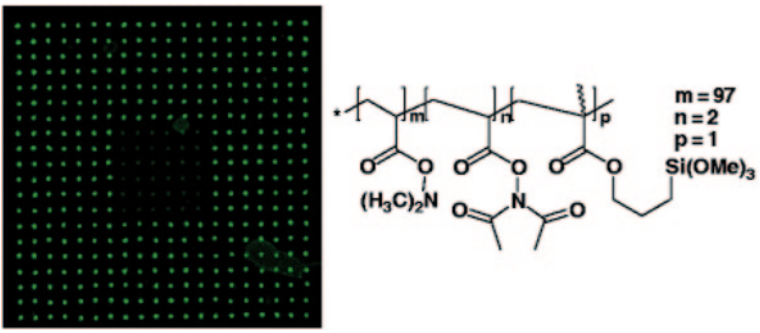


**Fig. 4.7** (*Left*) Oligonucleotide hybridization experiment on a cyclic olefin (co)polymers (COC) surface treated by $O_2$ plasma, coated with an *N*-hydroxysuccinimide (NHS) ester-containing silane copolymer, functionalized with a 5′-$NH_2$-functionalized DNA strand, and incubated with a Cy3-labeled complementary oligonucleotide. (*Right*) Chemical structure of the coating copolymer. Adapted from [73]

Bromination of surface hydroxyl groups on plasma-oxidized SEBS could be achieved by HBr/H2SO4 treatment in order to perform surface-initiated ATRP [84].

#### 4.5.1.3 Carbonyls

Carbonyl groups such as aldehydes and ketones have been less considered than other oxygen species although they can lead to interesting materials, as it is possible to reverse the immobilization of amine-containing (bio)molecules via the labile Schiff base adduct. Actually, most reports involving carbonyl-amine coupling describe the permanent fixation of this linkage by reduction using sodium cyanoborohydride (Fig. 4.8) [72, 89].

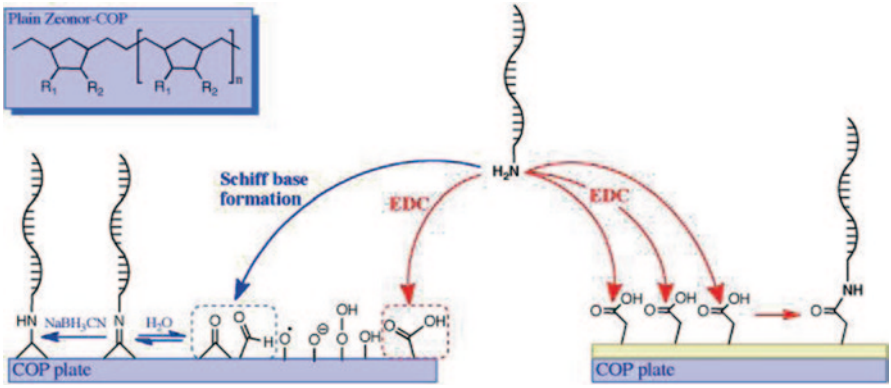


**Fig. 4.8** Chemical structure of a cyclic olefin (co)polymers (COP; inset) and functional groups generated on the surface of oxidized COP (*left*) and graft-polymerized acrylic acid (AA; *right*), as well as possible chemistries to immobilize amine-terminated DNA [72]

#### 4.5.1.4 Carboxylic Acids and Activated Esters

The derivatization of carboxylic acids offers much less variations. Basically, one method has been generally applied and relies on peptide coupling chemistry through the ubiquitous EDC/NHS couple (Fig. 4.8) [67, 72, 77, 88, 128, 140]. Sometimes the sulfonated variant of NHS is used to increase water solubility [86].

In most cases, the so-formed NHS-activated ester serves as a direct reactive site for biomolecule immobilization: peptides, [67, 86, 88] proteins, [67, 77] or aminated DNA strands [72].

In other cases, the NHS ester serves as an intermediate handle to incorporate another functional bioconjugation-amenable group via an amino derivative: 2-(2-pyridinyldithio)-ethanamine for thiol exchange immobilization of cysteine-containing peptides, [140] or propargyl amine for attachment of azidosugars involved in lectin recognition by *click* chemistry [128]. Urban also published a procedure to introduce alkyne groups but via acyl chloride formation and subsequent reaction with propargyl amine [101].

There are otherwise very few examples of activated ester directly introduced by a surface treatment. Borros showed that protein covalent immobilization could readily be achieved after the PECVD of pentafluorophenyl methacrylate without any additional treatment [96].

### *4.5.2 Amines*

Besides the surprising examples of direct protein attachment onto amino groups without any catalyst or previous activation, [142, 143] amines have been reacted with bifunctional linkers to bridge surfaces and biomolecules. A very popular linker is glutaraldehyde which possesses two aldehyde groups, thereby allowing attachment of peptides and proteins through their N-termini [94]. Diisocyanates have also been used for the same purpose but present the disadvantage of being less stable, requiring a rapid bioconjugation event [92, 95].

Increasingly popular are nowadays hetero bifunctional linkers, such as succinimidyl-4-(*N*-maleimidomethyl)cyclohexane-1-carboxylate (SMCC) [123] or NHS-PEG-maleimide, [93] which allow site-selective immobilization of polypeptides through rare cysteine residues by Michael addition on virtually any aminated substrate.

### *4.5.3 Halides*

Albeit less common in polymer surface modifications, halides may gain a broader interest as they can be involved in a range of reactions. For instance, Friedrich derivatized the bromide group formed during bromoform plasma treatment of PE

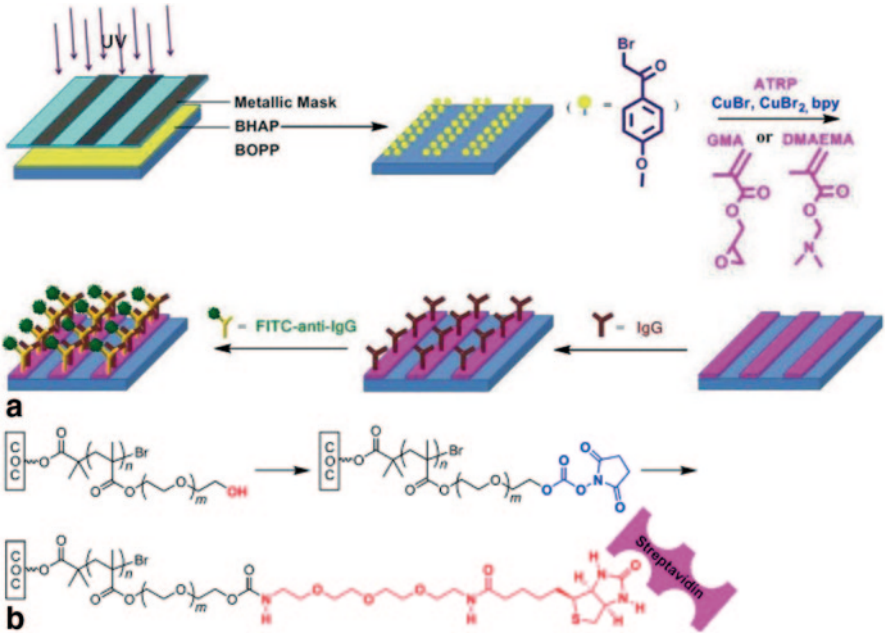


**Fig. 4.9** **a** Schematic illustration of the surface-initiated *ATRP* of *GMA* (or *DMAEMA*) on *PP* functionalized by acetone-mediated UV grafting and subsequent protein immobilization [132]. **b** Formation of biotin-functionalized antifouling brushes onto *COC* after nitrene-mediated UV grafting [144]. *COC* cyclic olefin (co)polymers, *ATRP* atom-transfer radical polymerization, *GMA* glycidyl methacrylate

and PP into alcohols, by Williamson ether synthesis with a diol, and into amines by a nucleophilic substitution with diamines [80].

Halides are also commonly involved in radical-mediated processes such as ATRP. For example, Yang exploited the UV-grafted bromo-4-hydroxyacetophenone as an ATRP initiator to grow PGMA brushes and subsequently ring-open the epoxide side-chains to anchor IgG (Fig. 4.9a) [132]. Lee employed a similar strategy to grow brushes of poly(hydroxyPEGMA), followed by activation of the pendant hydroxyl groups by *N,N′*-disuccinimidyl carbonate, and coupling of amino-biotin (Fig. 4.9b) [144].

### *4.5.4 Insaturations*

Insaturations resulting from strong reductant treatment on perfluorinated films usually are converted into alcohols. This can be done by oxidation using a hydroboration/oxidation sequence [50, 60, 61]. Alternatively, insaturations can give rise to carboxyl groups by direct oxidation in potassium chlorate/sulfuric acid [60].

## 4.6 Conclusion and Outlook

In this chapter, we have tried to cover as much as possible the range of chemical modifications, which have been carried out at the surface of commercial polymeric materials that are relevant for the field of biorecognition. Lately, physical methods seem to have taken the lead in that area for the introduction of primary reactive groups, owing to the easier access to advanced surface characterization techniques, such as X-ray photoelectron spectroscopy, FT-IR spectroscopy, or water-contact angle, that allow a better understanding of these processes. Of particular interest is that the surfaces are usually well-conserved in terms of topology, particularly with photoirradiation [145].

An aspect that has not been very much alluded to in the present literature review is that of passivation. Passivation is the key to biorecognition, in order to avoid non-specific adsorption [146, 147]. This is particularly true for biosensing applications where reduction of the background is essential to allow a decrease in detection limit down to the attomolar range. Over the last decade, there have been many advances in terms of designing such surfaces, particularly thanks to the advance in controlled polymerization methods allowing the grafting of dense hydrophilic polymer brushes [148−151]. Controlled radical polymerization processes [152−155] have thus a great future for the design of high-quality biochips, biosensors, and biomaterials as they are tolerant to a wide range of functionalities and can be combined with advanced photochemical strategies for patterning [120−122].

## References

1. Gyorgy, P.; Rose, C. S.; Eakin, R. E.; Snell, E. E.; Williams, R. J. Egg-White Injury As the Result of Nonabsorption or Inactivation of Biotin. *Science* **1941**, *93*, 477–478.
2. DeChancie, J.; Houk, K. N. The Origins of Femtomolar Protein–Ligand Binding: Hydrogen-Bond Cooperativity and Desolvation Energetics in the Biotin–(Strept)Avidin Binding Site. *J. Am. Chem. Soc.* **2007**, *129*, 5419–5429.
3. Holmberg, A.; Blomstergren, A.; Nord, O.; Lukacs, M.; Lundeberg, J.; Uhlén, M. The biotin-streptavidin interaction can be reversibly broken using water at elevated temperatures. *Electrophoresis* **2005**, *26*, 501–510.
4. Chivers, C. E.; Crozat, E.; Chu, C.; Moy, V. T.; Sherratt, D. J; Howarth, M. A streptavidin variant with slower biotin dissociation and increased mechanostability. *Nat. Methods* **2010**, *7*, 391–393.
5. Breitling, F.; Nesterov, A.; Stadler, V.; Felgenhauer, T.; Bischoff, F. R. High-density peptide arrays. *Mol. BioSyst*. **2009**, *5*, 224–234.
6. Hage, D. S.; Anguizola, J. A.; Bi, C.; Li, R.; Matsuda, R.; Papastavros, E.; Pfaunmiller, E.; Vargas, J.; Zheng, X. Pharmaceutical and biomedical applications of affinity chromatography: Recent trends and developments. *J. Pharm. Biomed. Anal.* **2012**, *69*, 93–105.
7. Liedberg, B.; Nylander, C.; Lunström, I. Surface plasmon resonance for gas detection and biosensing. *Sensors and Actuators* **1983**, *4*, 299–304.
8. Do, T.; Ho, F.; Heidecker, B.; Witte, K.; Chang, L; Lerner, L. A rapid method for determining dynamic binding capacity of resins for the purification of proteins. *Protein Expression Purif.* **2008**, *60*, 147–150.
9. Engvall, E.; Perlmann, P. Enzyme-linked immunosorbent assay (ELISA) quantitative assay of immunoglobulin G. *Immunochemistry* **1971**, *8*, 871–874.

10. Van Weemen, B. K.; Schuurs, A. H. W. M. Immunoassay using antigen—enzyme conjugates. *FEBS Lett*. **1971**, *15*, 232–236.
11. Delaittre, G.; Greiner, A. M.; Pauloehrl, T.; Bastmeyer, M.; Barner-Kowollik, C. Chemical approaches to synthetic polymer surface biofunctionalization for targeted cell adhesion using small binding motifs. *Soft Matter* **2012**, *8*, 7323–7347.
12. Stella, B.; Arpicco, S.; Peracchia, M. T.; Desmaële, D.; Hoebeke, J.; Renoir, M.; D'Angelo, J.; Cattel, L.; Couvreur, P. Design of folic acid-conjugated nanoparticles for drug targeting. *J. Pharm. Sci.* **2000**, *89*, 1452–1464.
13. Low, P. S.; Henne, W. A.; Doorneweerd, D. D. Discovery and Development of Folic-Acid-Based Receptor Targeting for Imaging and Therapy of Cancer and Inflammatory Diseases. *Acc. Chem. Res.* **2007**, *41*, 120–129.
14. Li, M.; Wong, K. K. W; Mann, S. Organization of Inorganic Nanoparticles Using Biotin–Streptavidin Connectors. *Chem. Mater.* **1998**, *11*, 23–26.
15. Lee, J.; Govorov, A. O.; Kotov, N. A. Bioconjugated Superstructures of CdTe Nanowires and Nanoparticles: Multistep Cascade Förster Resonance Energy Transfer and Energy Channeling. *Nano Lett*. **2005**, *5*, 2063–2069.
16. Morais, S.; Marco-Moles, R.; Puchades, R.; Maquieira, A. DNA microarraying on compact disc surfaces. Application to the analysis of single nucleotide polymorphisms in Plum pox virus. *Chem. Commun.* **2006**, 2368–2370.
17. McLaughlin, C. K.; Hamblin, G. D.; Sleiman, H. F. Supramolecular DNA assembly. *Chem. Soc. Rev.* **2011**, *40*, 5647–5656.
18. Rigaut, G.; Shevchenko, A.; Rutz, B.; Wilm, M.; Mann, M; Seraphin, B. A generic protein purification method for protein complex characterization and proteome exploration. *Nat. Biotechnol.* **1999**, *17*, 1030–1032.
19. Goddard, J. M.; Hotchkiss, J. H. Polymer surface modification for the attachment of bioactive compounds. *Prog. Polym. Sci.* **2007**, *32*, 698–725.
20. Hersel, U.; Dahmen, C.; Kessler, H. RGD modified polymers: biomaterials for stimulated cell adhesion and beyond. *Biomaterials* **2003**, *24*, 4385–4415.
21. Reynhout, I. C.; Delaittre, G.; Kim, H.-C.; Nolte, R. J. M.; Cornelissen, J. J. L. M. Nanoscale organization of proteins via block copolymer lithography and non-covalent bioconjugation. *J. Mater. Chem. B* **2013**, *1*, 3026–3030.
22. Ates, M. A review study of (bio)sensor systems based on conducting polymers. *Mater. Sci. Eng., C* **2013**, *33*, 1853–1859.
23. Haddour, N.; Cosnier, S.; Gondran, C. Electrogeneration of a Poly(pyrrole)-NTA Chelator Film for a Reversible Oriented Immobilization of Histidine-Tagged Proteins. *J. Am. Chem. Soc.* **2005**, *127*, 5752–5753.
24. Xie, H.; Luo, S.-C.; Yu, H.-h. Electric-Field-Assisted Growth of Functionalized Poly(3,4-ethylenedioxythiophene) Nanowires for Label-Free Protein Detection. *Small* **2009**, *5*, 2611–2617.
25. Sosnowska, M.; Pieta, P.; Sharma, P. S.; Chitta, R.; Kc, C. B.; Bandi, V.; D'Souza, F; Kutner, W. Piezomicrogravimetric and Impedimetric Oligonucleotide Biosensors Using Conducting Polymers of Biotinylated Bis(2,2′-bithien-5-yl)methane as Recognition Units. *Anal. Chem.* **2013**, *85*, 7454–7461.
26. Song, H. K.; Toste, B.; Ahmann, K.; Hoffman-Kim, D.; Palmore, G. T. R. Micropatterns of positive guidance cues anchored to polypyrrole doped with polyglutamic acid: A new platform for characterizing neurite extension in complex environments. *Biomaterials* **2006**, *27*, 473–484.
27. Guimard, N. K.; Gomez, N.; Schmidt, C. E. Conducting polymers in biomedical engineering. *Prog. Polym. Sci.* **2007**, *32*, 876–921.
28. Santiago, L. Y.; Nowak, R. W.; Peter Rubin, J.; Marra, K. G. Peptide-surface modification of poly(caprolactone) with laminin-derived sequences for adipose-derived stem cell applications. *Biomaterials* **2006**, *27*, 2962–2969.
29. Causa, F.; Battista, E.; Della Moglie, R.; Guarnieri, D.; Iannone, M.; Netti, P. A. Surface Investigation on Biomimetic Materials to Control Cell Adhesion: The Case of RGD Conjugation on PCL. *Langmuir* **2010**, *26*, 9875–9884.

30. Zhang, H.; Hollister, S. Comparison of bone marrow stromal cell behaviors on poly(caprolactone) with or without surface modification: studies on cell adhesion, survival and proliferation. *J. Biomater. Sci., Polym. Ed.* **2009**, *20*, 1975–1993.
31. Gabriel, M.; Nazmi, K.; Dahm, M.; Zentner, A.; Vahl, C.-F; Strand, D. Covalent RGD Modification of the Inner Pore Surface of Polycaprolactone Scaffolds. *J. Biomater. Sci., Polym. Ed.* **2012**, *23*, 941–953.
32. Gabriel, M.; Van Nieuw Amerongen, G. P.; Van Hinsbergh, V. W. M.; Van Nieuw Amerongen, A. V.; Zentner, A. Direct grafting of RGD-motif-containing peptide on the surface of polycaprolactone films. *J. Biomater. Sci., Polym. Ed.* **2006**, *17*, 567–577.
33. Croll, T. I.; O'Connor, A. J.; Stevens, G. W.; Cooper-White, J. J. Controllable Surface Modification of Poly(lactic-co-glycolic acid) (PLGA) by Hydrolysis or Aminolysis I: Physical, Chemical, and Theoretical Aspects. *Biomacromolecules* **2004**, *5*, 463–473.
34. Ning, C.; Yingxue, G.; Kerm Sin, C.; Vincent, C.; Kin, L. Adhesion dynamics of porcine esophageal fibroblasts on extracellular matrix protein-functionalized poly(lactic acid). *Biomed. Mater.* **2008**, *3*, 015014.
35. Rohman, G.; Baker, S. C.; Southgate, J.; Cameron, N. R. Heparin functionalisation of porous PLGA scaffolds for controlled, biologically relevant delivery of growth factors for soft tissue engineering. *J. Mater. Chem.* **2009**, *19*, 9265–9273.
36. Bech, L.; Meylheuc, T.; Lepoittevin, B.; Roger, P. Chemical surface modification of poly(ethylene terephthalate) fibers by aminolysis and grafting of carbohydrates. *J. Polym. Sci., Part A: Polym. Chem.* **2007**, *45*, 2172–2183.
37. Patel, S.; Thakar, R. G.; Wong, J.; McLeod, S. D.; Li, S. Control of cell adhesion on poly(methyl methacrylate). *Biomaterials* **2006**, *27*, 2890–2897.
38. Bai, Y.; Koh, C. G.; Boreman, M.; Juang, Y.-J.; Tang, I. C.; Lee, L. J; Yang, S.-T. Surface Modification for Enhancing Antibody Binding on Polymer-Based Microfluidic Device for Enzyme-Linked Immunosorbent Assay. *Langmuir* **2006**, *22*, 9458–9467.
39. Henry, A. C.; Tutt, T. J.; Galloway, M.; Davidson, Y. Y.; McWhorter, C. S.; Soper, S. A.; McCarley, R. L. Surface Modification of Poly(methyl methacrylate) Used in the Fabrication of Microanalytical Devices. *Anal. Chem.* **2000**, *72*, 5331–5337.
40. Hosseini, S.; Ibrahim, F.; Djordjevic, I.; Koole, L. H. Recent advances in surface functionalization techniques on polymethacrylate materials for optical biosensor applications. *Analyst* **2014**, *139*, 2933–2943.
41. Tsuji, H.; Nakahara, K. Poly(L-lactide). IX. Hydrolysis in acid media. *J. Appl. Polym. Sci.* **2002**, *86*, 186–194.
42. Sun, H.; Önneby, S. Facile polyester surface functionalization via hydrolysis and cell-recognizing peptide attachment. *Polym. Int.* **2006**, *55*, 1336–1340.
43. Xu, F. J.; Wang, Z. H.; Yang, W. T. Surface functionalization of polycaprolactone films via surface-initiated atom transfer radical polymerization for covalently coupling cell-adhesive biomolecules. *Biomaterials* **2010**, *31*, 3139–3147.
44. Punet, X.; Mauchauffé, R.; Giannotti, M. I.; Rodríguez-Cabello, J. C.; Sanz, F.; Engel, E.; Mateos-Timoneda, M. A.; Planell, J. A. Enhanced Cell-Material Interactions through the Biofunctionalization of Polymeric Surfaces with Engineered Peptides. *Biomacromolecules* **2013**, *14*, 2690–2702.
45. Diaz-Quijada, G. A.; Peytavi, R.; Nantel, A.; Roy, E.; Bergeron, M. G.; Dumoulin, M. M.; Veres, T. Surface modification of thermoplastics-towards the plastic biochip for high throughput screening devices. *Lab Chip* **2007**, *7*, 856–862.
46. Boxus, T.; Touillaux, R.; Dive, G.; Marchand-Brynaert, J. Synthesis and evaluation of RGD peptidomimetics aimed at surface bioderivatization of polymer substrates. *Bioorg. Med. Chem.* **1998**, *6*, 1577–1595.
47. Marchand-Brynaert, J.; Detrait, E.; Noiset, O.; Boxus, T.; Schneider, Y.-J.; Remacle, C. Biological evaluation of RGD peptidomimetics, designed for the covalent derivatization of cell culture substrata, as potential promoters of cellular adhesion. *Biomaterials* **1999**, *20*, 1773–1782.
48. Boxus, T.; Deldime-Rubbens, M.; Mougenot, P.; Schneider, Y.-J.; Marchand-Brynaert, J. Chemical assays of end-groups displayed on the surface of poly(ethylene terephthalate) (PET) films and membranes by radiolabeling. *Polym. Adv. Technol.* **1996**, *7*, 589–598.

49. Massia, S. P.; Hubbell, J. A. Covalently attached GRGD on polymer surfaces promotes biospecific adhesion of mammalian cells. *Ann. N. Y. Acad. Sci.* **1990**, *589*, 261–70.
50. Massia, S. P.; Hubbell, J. A. Human endothelial cell interactions with surface-coupled adhesion peptides on a nonadhesive glass substrate and two polymeric biomaterials. *J. Biomed. Mater. Res.* **1991**, *25*, 223–42.
51. Hebeiss, I.; Truckenmuller, R.; Giselbrecht, S.; Schepers, U. Novel three-dimensional Boyden chamber system for studying transendothelial transport. *Lab Chip* **2012**, *12*, 829–834.
52. Kido, H.; Maquieira, A.; Hammock, B. D. Disc-based immunoassay microarrays. *Anal. Chim. Acta* **2000**, *411*, 1–11.
53. Bañuls, M.-J.; García-Piñón, F.; Puchades, R.; Maquieira, Á. Chemical Derivatization of Compact Disc Polycarbonate Surfaces for SNPs detection. *Bioconjug. Chem.* **2008**, *19*, 665–672.
54. Hirschbiel, A. F.; Geyer, S.; Yameen, B.; Welle, A.; Nikolov, P.; Giselbrecht, S.; Scholpp, S.; Delaittre, G.; Barner-Kowollik, C. Photolithographic Patterning of 3D-Formed Polycarbonate Films for Targeted Cell Guiding. *Adv. Mater.* **2015**, *27,* 2621–2626.
55. Lin, Y.-C.; Brayfield, C. A.; Gerlach, J. C.; Rubin, J. P.; Marra, K. G. Peptide modification of polyethersulfone surfaces to improve adipose-derived stem cell adhesion. *Acta Biomater.* **2009**, *5*, 1416–1424.
56. Higuchi, A.; Shirano, K.; Harashima, M.; Yoon, B. O.; Hara, M.; Hattori, M.; Imamura, K. Chemically modified polysulfone hollow fibers with vinylpyrrolidone having improved blood compatibility. *Biomaterials* **2002**, *23*, 2659–2666.
57. Costello, C. A.; McCarthy, T. J. Surface modification of poly(tetrafluoroethylene) with benzoin dianion. *Macromolecules* **1984**, *17*, 2940–2942.
58. Costello, C. A.; McCarthy, T. J. Surface-selective introduction of specific functionalities onto poly(tetrafluoroethylene). *Macromolecules* **1987**, *20*, 2819–2828.
59. Bening, R. C.; McCarthy, T. J. Surface modification of poly(tetrafluoroethylene-co-hexafluoropropylene): introduction of alcohol functionality. *Macromolecules* **1990**, *23*, 2648–2655.
60. Tong, Y. W.; Shoichet, M. S. Peptide surface modification of poly(tetrafluoroethylene-co-hexafluoropropylene) enhances its interaction with central nervous system neurons. *J. Biomed. Mater. Res.* **1998**, *42*, 85–95.
61. Gabriel, M.; Dahm, M.; Vahl, C. F. Wet-chemical approach for the cell-adhesive modification of polytetrafluoroethylene. *Biomed. Mater.* **2011**, *6*, 035007.
62. Mikhail, A. S.; Jones, K. S.; Sheardown, H. Dendrimer-grafted cell adhesion peptide–modified PDMS. *Biotechnol. Prog.* **2008**, *24*, 938–944.
63. Zhou, J.; Ellis, A. V.; Voelcker, N. H. Recent developments in PDMS surface modification for microfluidic devices. *Electrophoresis* **2010**, *31*, 2–16.
64. Abbasi, F.; Mirzadeh, H.; Katbab, A.-A. Modification of polysiloxane polymers for biomedical applications: a review. *Polym. Int.* **2001**, *50*, 1279–1287.
65. Ranieri, J. P.; Bellamkonda, R.; Bekos, E. J.; Gardella, J. A., Jr.; Mathieu, H. J.; Ruiz, L.; Aebischer, P. Spatial control of neuronal cell attachment and differentiation on covalently patterned laminin oligopeptide substrates. *Int. J. Dev. Neurosci.* **1994**, *12*, 725–35.
66. Sugawara, T.; Matsuda, T. Photochemical surface derivatization of a peptide containing Arg-Gly-Asp (RGD). *J. Biomed. Mater. Res.* **1995**, *29*, 1047–52.
67. Hatakeyama, H.; Kikuchi, A.; Yamato, M.; Okano, T. Patterned biofunctional designs of thermoresponsive surfaces for spatiotemporally controlled cell adhesion, growth, and thermally induced detachment. *Biomaterials* **2007**, *28*, 3632–3643.
68. Coad, B. R.; Jasieniak, M.; Griesser, S. S.; Griesser, H. J. Controlled covalent surface immobilisation of proteins and peptides using plasma methods. *Surf. Coat. Technol.* **2013**, *233*, 169–177.
69. Alf, M. E.; Asatekin, A.; Barr, M. C.; Baxamusa, S. H.; Chelawat, H.; Ozaydin-Ince, G.; Petruczok, C. D.; Sreenivasan, R.; Tenhaeff, W. E.; Trujillo, N. J.; Vaddiraju, S.; Xu, J.; Gleason, K. K. Chemical Vapor Deposition of Conformal, Functional, and Responsive Polymer Films. *Adv. Mater.* **2010**, *22*, 1993–2027.
70. Conrad, J. R.; Radtke, J. L.; Dodd, R. A.; Worzala, F. J.; Tran, N. C. Plasma source ion-implantation technique for surface modification of materials. *J. Appl. Phys.* **1987**, *62*, 4591–4596.

71. Ho, J. P. Y.; Nosworthy, N. J.; Bilek, M. M. M.; Gan, B. K.; McKenzie, D. R.; Chu, P. K.; dos Remedios, C. G. Plasma-Treated Polyethylene Surfaces for Improved Binding of Active Protein. *Plasma Processes Polym*. **2007**, *4*, 583–590.
72. Gubala, V.; Le, N. C. H.; Gandhiraman, R. P.; Coyle, C.; Daniels, S.; Williams, D. E. Functionalization of cyclo-olefin polymer substrates by plasma oxidation: Stable film containing carboxylic acid groups for capturing biorecognition elements. *Colloids Surf., B* **2010**, *81*, 544–548.
73. Zilio, C.; Sola, L.; Damin, F.; Faggioni, L.; Chiari, M. Universal hydrophilic coating of thermoplastic polymers currently used in microfluidics. *Biomed. Microdevices* **2014**, *16*, 107–114.
74. Bilek, M. M. M.; Bax, D. V.; Kondyurin, A.; Yin, Y.; Nosworthy, N. J.; Fisher, K.; Waterhouse, A.; Weiss, A. S.; dos Remedios, C. G.; McKenzie, D. R. Free radical functionalization of surfaces to prevent adverse responses to biomedical devices. *Proc. Natl. Acad. Nat. USA* **2011**, *108*, 14405–14410.
75. De Cooman, H.; Desmet, T.; Callens, F.; Dubruel, P. Role of radicals in UV-initiated post-plasma grafting of poly-ε-caprolactone: An electron paramagnetic resonance study. *J. Polym. Sci., Part A: Polym. Chem.* **2012**, *50*, 2142–2149.
76. Muir, B. W.; Barden, M. C.; Collett, S. P.; Gorse, A.-D.; Monteiro, R.; Yang, L.; McDougall, N. A.; Gould, S.; Maeji, N. J. High-throughput optimization of surfaces for antibody immobilization using metal complexes. *Anal. Biochem.* **2007**, *363*, 97–107.
77. Song, L.; Zhao, J.; Jin, J.; Ma, J.; Liu, J.; Luan, S.; Yin, J. Fabricating antigen recognition and anti-bioadhesion polymeric surface via a photografting polymerization strategy. *Mater. Sci. Eng., C* **2014**, *36*, 57–64.
78. Ameduri, B. From Vinylidene Fluoride (VDF) to the Applications of VDF-Containing Polymers and Copolymers: Recent Developments and Future Trends. *Chem. Rev.* **2009**, *109*, 6632–6686.
79. Pâslaru, E.; Baican, M. C.; Hitruc, E. G.; Nistor, M. T.; Poncin-Epaillard, F; Vasile, C. Immunoglobulin G immobilization on PVDF surface. *Colloids Surf., B* **2014**, *115*, 139–149.
80. Friedrich, J.; Kühn, G.; Mix, R.; Hoffmann, K.; Resch-Genger, U. Tailoring of Polymer Surfaces with Monotype Functional Groups of Variable Density Using Chemical and Plasma Chemical Processes. In *Characterization of Polymer Surfaces and Thin Films*; Grundke, K., Stamm, M., Adler, H.-J., Eds.; Springer Berlin Heidelberg, 2006; Vol. 132; pp 62–71.
81. Li, C.; Jin, J.; Liu, J.; Xu, X.; Yin, J. Improving hemocompatibility of polypropylene via surface-initiated atom transfer radical polymerization for covalently coupling BSA. *RSC Adv*. **2014**, *4*, 24842–24851.
82. Jonsson, C.; Aronsson, M.; Rundstrom, G.; Pettersson, C.; Mendel-Hartvig, I.; Bakker, J.; Martinsson, E.; Liedberg, B.; MacCraith, B.; Ohman, O.; Melin, J. Silane-dextran chemistry on lateral flow polymer chips for immunoassays. *Lab Chip* **2008**, *8*, 1191–1197.
83. Ma, J.; Luan, S.; Song, L.; Jin, J.; Yuan, S.; Yan, S.; Yang, H.; Shi, H; Yin, J. Fabricating a Cycloolefin Polymer Immunoassay Platform with a Dual-Function Polymer Brush via a Surface-Initiated Photoiniferter-Mediated Polymerization Strategy. *ACS Appl. Mater. Interfaces* **2014**, *6*, 1971–1978.
84. Hou, J.; Shi, Q.; Stagnaro, P.; Ye, W.; Jin, J.; Conzatti, L.; Yin, J. Aqueous-based immobilization of initiator and surface-initiated ATRP to construct hemocompatible surface of poly (styrene-b –(ethylene-co-butylene)-b-styrene) elastomer. *Colloids Surf., B* **2013**, *111*, 333–341.
85. Petersen, S.; Wulf, K.; Schunemann, S.; Teske, M.; Schmitz, K. P; Sternberg, K. Biofunctionalization of Polymer Implant Surfaces: From Drug Delivery to Stable Surface Functionality. *Biomed. Tech*. **2013**.
86. Paletta, J. R. J.; Bockelmann, S.; Walz, A.; Theisen, C.; Wendorff, J. H.; Greiner, A.; Fuchs-Winkelmann, S.; Schofer, M. D. RGD-functionalisation of PLLA nanofibers by surface coupling using plasma treatment: influence on stem cell differentiation. *J. Mater. Sci. Mater. Med.* **2010**, *21*, 1363–1369.
87. Wen, F.; Wong, H. K.; Tay, C. Y.; Yu, H.; Li, H.; Yu, T.; Tijore, A.; Boey, F. Y. C.; Venkatraman, S. S.; Tan, L. P. Induction of Myogenic Differentiation of Human Mesenchymal Stem Cells Cultured on Notch Agonist (Jagged-1) Modified Biodegradable Scaffold Surface. *ACS Appl. Mater. Interfaces* **2014**, *6*, 1652–1661.

88. Wang, F.; Li, Z.; Lannutti, J. L.; Wagner, W. R.; Guan, J. Synthesis, characterization and surface modification of low moduli poly(ether carbonate urethane)ureas for soft tissue engineering. *Acta Biomater*. **2009**, *5*, 2901–2912.
89. Graz, I.; Ebner, A.; Bauer, S.; Romanin, C.; Gruber, H. Micropatterned atmospheric pressure discharge surface modification of fluorinated polymer films for mammalian cell adhesion and protein binding. *Appl. Phys. A: Mater. Sci. Process*. **2008**, *92*, 547–555.
90. Kogelschatz, U.; Eliasson, B.; Egli, W. From ozone generators to flat television screens: history and future potential of dielectric-barrier discharges. *Pure Appl. Chem.* **1999**, *71*, 1819–1828.
91. Ranieri, J. P.; Bellamkonda, R.; Bekos, E. J.; Vargo, T. G.; Gardella, J. A.; Aebischer, P. Neuronal cell attachment to fluorinated ethylene propylene films with covalently immobilized laminin oligopeptides YIGSR and IKVAV. II. *J. Biomed. Mater. Res.* **1995**, *29*, 779–785.
92. Heuts, J.; Salber, J.; Goldyn, A. M.; Janser, R.; Möller, M.; Klee, D. Bio-functionalized star PEG-coated PVDF surfaces for cytocompatibility-improved implant components. *J. Biomed. Mater. Res., Part A* **2010**, *92A*, 1538–1551.
93. Wang, Y.-Y.; Lü, L.-X.; Shi, J.-C.; Wang, H.-F.; Xiao, Z.-D; Huang, N.-P. Introducing RGD Peptides on PHBV Films through PEG-Containing Cross-Linkers to Improve the Biocompatibility. *Biomacromolecules* **2011**, *12*, 551–559.
94. Hu, Y.; Winn Shelley, R.; Krajbich, I.; Hollinger Jeffrey, O. Porous polymer scaffolds surface-modified with arginine-glycine-aspartic acid enhance bone cell attachment and differentiation in vitro. *J. Biomed. Mater. Res., Part A* **2003**, *64*, 583–90.
95. Guan, J.; Sacks, M. S.; Beckman, E. J.; Wagner, W. R. Biodegradable poly(ether ester urethane)urea elastomers based on poly(ether ester) triblock copolymers and putrescine: synthesis, characterization and cytocompatibility. *Biomaterials* **2004**, *25*, 85–96.
96. Cifuentes, A.; Borrós, S. Comparison of Two Different Plasma Surface-Modification Techniques for the Covalent Immobilization of Protein Monolayers. *Langmuir* **2013**, *29*, 6645–6651.
97. Ito, Y.; Kajihara, M.; Imanishi, Y. Materials for enhancing cell adhesion by immobilization of cell-adhesive peptide. *J. Biomed. Mater. Res.* **1991**, *25*, 1325–1337.
98. Yanagi, M.; Kishida, A.; Shimotakahara, T.; Matsumoto, H.; Nishijima, H.; Akashi, M.; Aikou, T. Experimental study of bioactive polyurethane sponge as an artificial trachea. *Asaio J.* **1994**, *40*, M412–8.
99. Jung, H.; Ahn, K.-D.; Han, D.; Ahn, D.-J. Surface characteristics and fibroblast adhesion behavior of RGD-immobilized biodegradable PLLA films. *Macromol. Res.* **2005**, *13*, 446–452.
100. Jung, H. J.; Park, K.; Kim, J.-J.; Lee, J. H.; Han, K.-O.; Han, D. K. Effect of RGD-immobilized dual-pore poly(L-lactic acid) scaffolds on chondrocyte proliferation and extracellular matrix production. *Artificial Organs* **2008**, *32*, 981–989.
101. Pearson, H. A.; Urban, M. W. Simple click reactions on polymer surfaces leading to antimicrobial behavior. *J. Mater. Chem. B* **2014**, *2*, 2084–2087.
102. Francesch, L.; Garreta, E.; Balcells, M.; Edelman, E. R.; Borrós, S. Fabrication of Bioactive Surfaces by Plasma Polymerization Techniques Using a Novel Acrylate-Derived Monomer. *Plasma Processes Polym*. **2005**, *2*, 605–611.
103. Francesch, L.; Borros, S.; Knoll, W.; Förch, R. Surface Reactivity of Pulsed-Plasma Polymerized Pentafluorophenyl Methacrylate (PFM) toward Amines and Proteins in Solution. *Langmuir* **2007**, *23*, 3927–3931.
104. Carlisle, E. S.; Mariappan, M. R.; Nelson, K. D.; Thomes, B. E.; Timmons, R. B.; Constantinescu, A.; Eberhart, R. C.; Bankey, P. E. Enhancing hepatocyte adhesion by pulsed plasma deposition and polyethylene glycol coupling. *Tissue Engineering* **2000**, *6*, 45–52.
105. Aucoin, L.; Griffith, C. M.; Pleizier, G.; Deslandes, Y.; Sheardown, H. Interactions of corneal epithelial cells and surfaces modified with cell adhesion peptide combinations. *J. Biomater. Sci., Polym. Ed.* **2002**, *13*, 447–462.
106. Breuers, W.; Klee, D.; Höcker, H.; Mittermayer, C. Immobilization of a fibronectin fragment at the surface of a polyetherurethane film. *J. Mater. Sci.: Mater. Med.* **1991**, *2*, 106–109.
107. Hirsh, S. L.; Bilek, M. M. M.; Bax, D. V.; Kondyurin, A.; Kosobrodova, E.; Tsoutas, K.; Tran, C. T. H.; Waterhouse, A.; Yin, Y.; Nosworthy, N. J.; McKenzie, D. R.; dos Remedios, C. G.; Ng, M. K. C.; Weiss, A. S. Ion implanted, radical-rich surfaces for the rapid covalent immobilization of active biomolecules. *AIP Conf. Proc.* **2013**, *1525*, 364–369.

108. Bilek, M. M. M. Biofunctionalization of surfaces by energetic ion implantation: Review of progress on applications in implantable biomedical devices and antibody microarrays. *Appl. Surf. Sci.* **2014**, *310*, 3–10.
109. Bilek, M. M.; McKenzie, D. R. Plasma modified surfaces for covalent immobilization of functional biomolecules in the absence of chemical linkers: towards better biosensors and a new generation of medical implants. *Biophys. Rev.* **2010**, *2*, 55–65.
110. Nosworthy, N. J.; Ho, J. P. Y.; Kondyurin, A.; McKenzie, D. R.; Bilek, M. M. M. The attachment of catalase and poly-l-lysine to plasma immersion ion implantation-treated polyethylene. *Acta Biomater*. **2007**, *3*, 695–704.
111. Nosworthy, N. J.; Kondyurin, A.; Bilek, M. M. M.; McKenzie, D. R. Ion implantation treatment of beads for covalent binding of molecules: Application to bioethanol production using thermophilic beta-glucosidase. *Enzym. Microb. Technol.* **2014**, *54*, 20–24.
112. Kondyurin, A.; Nosworthy, N. J.; Bilek, M. M. M. Attachment of horseradish peroxidase to polytetrafluorethylene (teflon) after plasma immersion ion implantation. *Acta Biomater*. **2008**, *4*, 1218–1225.
113. Bax, D. V.; McKenzie, D. R.; Weiss, A. S.; Bilek, M. M. M. The linker-free covalent attachment of collagen to plasma immersion ion implantation treated polytetrafluoroethylene and subsequent cell-binding activity. *Biomaterials* **2010**, *31*, 2526–2534.
114. Hirsh, S. L.; Nosworthy, N. J.; Kondyurin, A.; dos Remedios, C. G.; McKenzie, D. R.; Bilek, M. M. M. Linker-free covalent thermophilic [small beta]-glucosidase functionalized polymeric surfaces. *J. Mater. Chem.* **2011**, *21*, 17832–17841.
115. Kosobrodova, E.; Mohamed, A.; Su, Y.; Kondyurin, A.; dos Remedios, C. G.; McKenzie, D. R.; Bilek, M. M. M. Cluster of differentiation antibody microarrays on plasma immersion ion implanted polycarbonate. *Mater. Sci. Eng., C* **2014**, *35*, 434–440.
116. MacDonald, C.; Morrow, R.; Weiss, A. S.; Bilek, M. M. M. Covalent attachment of functional protein to polymer surfaces: a novel one-step dry process. *J. R. Soc. Interface* **2008**, *5*, 663–669.
117. Jung, C.-H.; Hwang, I.-T.; Kuk, I.-S.; Choi, J.-H.; Oh, B.-K.; Lee, Y.-M. Poly(acrylic acid)-Grafted Fluoropolymer Films for Highly Sensitive Fluorescent Bioassays. *ACS Appl. Mater. Interfaces* **2013**, *5*, 2155–2160.
118. Beachell, H. C.; Nemphos, S. P. Oxidative degradation of polyethylene. *J. Polym. Sci.* **1956**, *21*, 113–124.
119. Cooper, G. D.; Prober, M. The action of oxygen corona and of ozone on polyethylene. *J. Polym. Sci.* **1960**, *44*, 397–409.
120. Dietrich, M.; Delaittre, G.; Blinco, J. P.; Inglis, A. J.; Bruns, M; Barner-Kowollik, C. Photoclickable Surfaces for Profluorescent Covalent Polymer Coatings. *Adv. Funct. Mater.* **2012**, *22*, 304–312.
121. Pauloehrl, T.; Delaittre, G.; Winkler, V.; Welle, A.; Bruns, M.; Börner, H. G.; Greiner, A. M.; Bastmeyer, M; Barner-Kowollik, C. Adding Spatial Control to Click Chemistry: Phototriggered Diels–Alder Surface (Bio)functionalization at Ambient Temperature. *Angew. Chem. Int. Ed.* **2012**, *51*, 1071–1074.
122. Richter, B.; Pauloehrl, T.; Kaschke, J.; Fichtner, D.; Fischer, J.; Greiner, A. M.; Wedlich, D.; Wegener, M.; Delaittre, G.; Barner-Kowollik, C.; Bastmeyer, M. Three-Dimensional Microscaffolds Exhibiting Spatially Resolved Surface Chemistry. *Adv. Mater.* **2013**, *25*, 6117–6122.
123. Shaw, D.; Shoichet, M. S. Toward Spinal Cord Injury Repair Strategies: Peptide Surface Modification of Expanded Poly(Tetrafluoroethylene) Fibers for Guided Neurite Outgrowth In Vitro. *J Craniofac Surg*. **2003**, *14*, 308–316.
124. Kantlehner, M.; Finsinger, D.; Meyer, J.; Schaffner, P.; Jonczyk, A.; Diefenbach, B.; Nies, B.; Kessler, H. Selective RGD-Mediated Adhesion of Osteoblasts at Surfaces of Implants. *Angew. Chem. Int. Ed.* **1999**, *38*, 560–562.
125. Kantlehner, M.; Schaffner, P.; Finsinger, D.; Meyer, J.; Jonczyk, A.; Diefenbach, B.; Nies, B.; Hölzemann, G.; Goodman, S. L; Kessler, H. Surface Coating with Cyclic RGD Peptides Stimulates Osteoblast Adhesion and Proliferation as well as Bone Formation. *ChemBioChem* **2000**, *1*, 107–114.

126. Auernheimer, J.; Dahmen, C.; Hersel, U.; Bausch, A; Kessler, H. Photoswitched Cell Adhesion on Surfaces with RGD Peptides. *J. Am. Chem. Soc.* **2005**, *127*, 16107–16110.
127. Edlund, U.; Källrot, M.; Albertsson, A.-C. Single-Step Covalent Functionalization of Polylactide Surfaces. *J. Am. Chem. Soc.* **2005**, *127*, 8865–8871.
128. Wang, C.; Ren, P.-F.; Huang, X.-J.; Wu, J.; Xu, Z.-K. Surface glycosylation of polymer membrane by thiol-yne click chemistry for affinity adsorption of lectin. *Chem. Commun.* **2011**, *47*, 3930–3932.
129. Larsen, E. K. U.; Mikkelsen, M. B. L.; Larsen, N. B. Facile Photoimmobilization of Proteins onto Low-Binding PEG-Coated Polymer Surfaces. *Biomacromolecules* **2014**, *15*, 894–899.
130. Li, J.; Ding, M.; Fu, Q.; Tan, H.; Xie, X; Zhong, Y. A novel strategy to graft RGD peptide on biomaterials surfaces for endothelization of small-diamater vascular grafts and tissue engineering blood vessel. *J. Mater. Sci.: Mater. Med.* **2008**, *19*, 2595–2603.
131. Xu, J.; Ma, Y.; Xie, J.; Xu, F. J.; Yang, W. Functionalization of polymeric surfaces by simple photoactivation of Cï£¿H bonds. *J. Polym. Sci., Part A: Polym. Chem.* **2011**, *49*, 2755–2760.
132. Li, C. Y.; Xu, F. J.; Yang, W. T. Simple Strategy to Functionalize Polymeric Substrates via Surface-Initiated ATRP for Biomedical Applications. *Langmuir* **2012**, *29*, 1541–1550.
133. Guillaneuf, Y.; Bertin, D.; Gigmes, D.; Versace, D.-L.; Lalevée, J.; Fouassier, J.-P. Toward Nitroxide-Mediated Photopolymerization. *Macromolecules* **2010**, *43*, 2204–2212.
134. Huebsch, J. B.; Fields, G. B.; Triebes, T. G.; Mooradian, D. L. Photoreactive analog of peptide FN-C/H-V from the carboxy-terminal heparin-binding domains of fibronectin supports endothelial cell adhesion and spreading on biomaterial surfaces. *J. Biomed. Mater. Res.* **1996**, *31*, 555–567.
135. Mizutani, M.; Arnold, S. C.; Matsuda, T. Liquid, Phenylazide-End-Capped Copolymers of ε-Caprolactone and Trimethylene Carbonate: Preparation, Photocuring Characteristics, and Surface Layering. *Biomacromolecules* **2002**, *3*, 668–675.
136. Lin, Y.-S.; Wang, S.-S.; Chung, T.-W.; Wang, Y.-H.; Chiou, S.-H.; Hsu, J.-J.; Chou, N.-K.; Hsieh, K.-H.; Chu, S.-H. Growth of endothelial cells on different concentrations of Gly-Arg-Gly-Asp photochemically grafted in polyethylene glycol modified polyurethane. *Artificial Organs* **2001**, *25*, 617–621.
137. Ortega, F. J.; Banuls, M.-J.; Sanza, F. J.; Laguna, M. F.; Holgado, M.; Casquel, R.; Barrios, C. A.; Lopez-Romero, D.; Maquieira, A.; Puchades, R. Development of a versatile biotinylated material based on SU-8. *J. Mater. Chem. B* **2013**, *1*, 2750–2756.
138. Chevolot, Y.; Martins, J.; Milosevic, N.; Léonard, D.; Zeng, S.; Malissard, M.; Berger, E. G.; Maier, P.; Mathieu, H. J.; Crout, D. H. G.; Sigrist, H. Immobilisation on polystyrene of diazirine derivatives of mono- and disaccharides: biological activities of modified surfaces. *Bioorg. Med. Chem.* **2001**, *9*, 2943–2953.
139. Kolodziej, C. M.; Maynard, H. D. Electron-Beam Lithography for Patterning Biomolecules at the Micron and Nanometer Scale. *Chem. Mater.* **2011**, *24*, 774–780.
140. Sun, H.; Wirsen, A.; Albertsson, A.-C. Electron beam-induced graft polymerization of acrylic acid and immobilization of arginine-glycine-aspartic acid-containing peptide onto nanopatterned polycaprolactone. *Biomacromolecules* **2004**, *5*, 2275–2280.
141. Bozzi, A.; Chapiro, A. Synthesis of perm-selective membranes by grafting acrylic acid into air-irradiated Teflon-FEP films. *Int. J. Radiat. Appl. Instrum. C Radiat. Phys. Chem.* **1988**, *32*, 193–196.
142. Sipehia, R.; Chawla, A. S.; Chang, T. M. S. Enhanced albumin binding to polypropylene beads via anhydrous ammonia gaseous plasma. *Biomaterials* **1986**, *7*, 471–473.
143. Sipehia, R.; Chawla, A. S.; Daka, J.; Chang, T. M. S. Immobilization of enzymes on polypropylene bead surfaces by anhydrous ammonia gaseous plasma technique. *J. Biomed. Mater. Res.* **1988**, *22*, 417–422.
144. Jeong, S. P.; Hong, D.; Kang, S. M.; Choi, I. S.; Lee, J. K. Polymeric Functionalization of Cyclic Olefin Copolymer Surfaces with Nonbiofouling Poly(oligo(Ethylene Glycol) Methacrylate). *Asian J. Org. Chem.* **2013**, *2*, 568–571.
145. Barish, J. A.; Goddard, J. M. Topographical and chemical characterization of polymer surfaces modified by physical and chemical processes. *J. Appl. Polym. Sci.* **2011**, *120*, 2863–2871.

146. Kochkodan, V.; Johnson, D. J.; Hilal, N. Polymeric membranes: Surface modification for minimizing (bio)colloidal fouling. *Adv. Colloid Interface Sci*. **2014**, *206*, 116–140.
147. Yang, R.; Asatekin, A.; Gleason, K. K. Design of conformal, substrate-independent surface modification for controlled protein adsorption by chemical vapor deposition (CVD). *Soft Matter* **2012**, *8*, 31–43.
148. Leckband, D.; Sheth, S.; Halperin, A. Grafted poly(ethylene oxide) brushes as nonfouling surface coatings. *J. Biomater. Sci., Polym. Ed.* **1999**, *10*, 1125–1147.
149. Hucknall, A.; Rangarajan, S.; Chilkoti, A. In Pursuit of Zero: Polymer Brushes that Resist the Adsorption of Proteins. *Adv. Mater.* **2009**, *21*, 2441–2446.
150. Tauhardt, L.; Kempe, K.; Gottschaldt, M.; Schubert, U. S. Poly(2-oxazoline) functionalized surfaces: from modification to application. *Chem. Soc. Rev.* **2013**, *42*, 7998–8011.
151. Schlenoff, J. B. Zwitteration: Coating Surfaces with Zwitterionic Functionality to Reduce Nonspecific Adsorption. *Langmuir* **2014**, *30*, 9625–9636.
152. Handbook of RAFT Polymerization; Barner-Kowollik , C., Ed.; Wiley-VCH Verlag GmbH & Co. KGaA, 2008.
153. Moad, G.; Rizzardo, E.; Thang, S. H. Toward Living Radical Polymerization. *Acc. Chem. Res.* **2008**, *41*, 1133–1142.
154. Braunecker, W. A.; Matyjaszewski, K. Controlled/living radical polymerization: Features, developments, and perspectives. *Prog. Polym. Sci.* **2007**, *32*, 93–146.
155. Nicolas, J.; Guillaneuf, Y.; Lefay, C.; Bertin, D.; Gigmes, D.; Charleux, B. Nitroxide-mediated polymerization. *Prog. Polym. Sci.* **2013**, *38*, 63–235.

# Chapter 5
# Polymer Gradient Surfaces for Biomedical Applications

**Paul M. Reynolds and Nikolaj Gadegaard**

## 5.1 Introduction

### *5.1.1 Background*

Biological systems interact with artificial polymeric materials in a complex, multi-stage, and iterative process of sensing and response [1]. The biological response at the cellular level to polymeric substrates has been studied at great length. However, this is often done on individual samples with a homogeneous feature. This results in experiments which are limited only to samples that the investigator can imagine — leaving potentially interesting samples or sample combinations hidden from use. Subtle variations in surface properties can have a drastic impact on cell response, and therefore a considered and careful approach must be employed in surface design and fabrication. Following the example set by combinatorial chemistry and high-throughput screening (HTS) applied to drug discovery by the pharmaceutical industry in the 1990s, [2] researchers are increasingly turning to similar methodologies in biomaterial design [3−10]. This involves creating high content samples for exploring the full sample space, usually taking the form of a highly multiplexed array platform, or a continuous variation of a single material property as a gradient. Creating such dense sample formats presents a series of unique challenges in both their fabrication and implementation. In the case of surface modification for biomedical applications, platforms must be created which offer broad variations in surface properties, and they must also be designed in such a way as to allow meaningful interpretation of often complex responses.

Gradients seem to offer the ideal solution in terms of manufacture and sample variation. Gradients may be fabricated in 2D or 3D, however whilst 3D studies are generally considered to be more representative of the in vivo architecture of most

N. Gadegaard (✉) · P. M. Reynolds
Division of Biomedical Engineering, School of Engineering,
University of Glasgow, Glasgow, UK
e-mail: Nikolaj.Gadegaard@glasgow.ac.uk



J. Rodríguez-Hernández, A. L. Cortajarena (eds.), *Design of Polymeric Platforms for Selective Biorecognition,* DOI 10.1007/978-3-319-17061-9_5

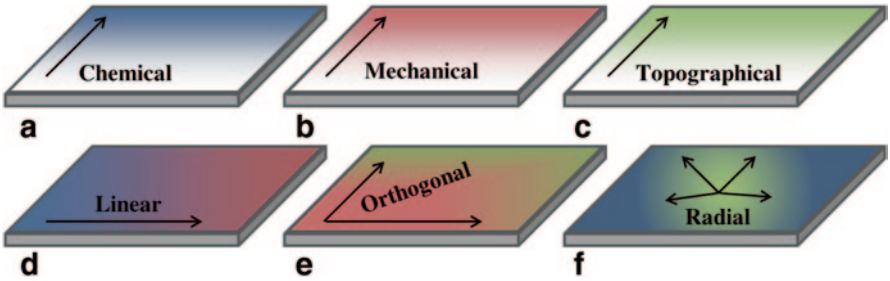


**Fig. 5.1** Cells sense their environment through three main 'columns' of sensing: chemical, mechanical, and topographical. **a** Chemical gradients range from a simple change in surface energy, to surface modification with proteins, functional molecules, or peptides. **b** Mechanical gradients are a modulation of a mechanical property such as the Young's modulus of a substrate. **c** Topographical gradients present a variation of surface structure, which have been shown to be a powerful manipulator of biological response. **d**, **e**, **f** These gradients of surface properties can be combined into linear **d** orthogonal **e** or radial gradients **f** which elicit the interplay between two material factors in a biological response

biological systems, they present problems in terms of fabrication, data acquisition, and data analysis. For this reason, studies investigating cellular response to engineered surface cues are predominantly carried out in 2D in vitro systems. The use of semiconductor fabrication techniques, which have consistently increased in resolution since their inception [11] has allowed 2D surface patterning at length scales which now approach that of single molecules, and surpassed that of the single cell many years ago [12]. Chemical, mechanical, and topographical features of a polymeric surface have all been shown to be capable of independently affecting cell behaviour and response to an engineered surface [1]. Gradients of each surface property can be fabricated independently or orthogonally to one another to create multiplexed parameter variations on a single substrate, Fig. 5.1.

Ease of fabrication, data analysis, and interpretation makes the use of linear gradients most favourable. Single properties may be varied in a single direction, Fig. 5.1a–c, or multiple may be varied in opposite directions to create a bidirectional linear gradient, Fig. 5.1d. Orthogonal variation of two parameters serves to create as many possible combinations of two surface parameters as possible. Radial gradients have surface properties which change continuously from a central point outwards, and are most often used when fabrication makes use of diffusion-based processes from a single point source [4, 13]. These gradients are least favourable due to the difficulties associated with mapping cell response to corresponding surface properties.

### *5.1.2 Gradient and Array Platforms*

The distinction between gradient and array formats as HTS methods is an important one. A gradient is a continuous variation of a feature, such as structural dimension

or surface chemistry. This feature changes 'continuously' from one value to another, however its resolution is essentially defined by its nature—a gradient of chemistry may only change spatially in so much as its molecular structure allows. Arrays, however, are discrete variations in a surface parameter, separated or congruent on a single sample. These areas may be completely isolated from one another, or may exist on a single substrate and used in an open environment. Essentially, then, based on the property in question, an array might have a fine enough resolution so as to offer a working resolution which is comparable with a continuous gradient.(Fig. 5.2)

The key difference in understanding their use and implementation is that cells or molecules are free to move along or adsorb across a gradient platform, with cell motility yielding further information about how they interact with the surface. In an array platform, this is not possible—as cells or biomolecules interact with sample conditions which are isolated from each other, or at least separated spatially. There are benefits to each of these methods, and the impact of gradient or array formats should be carefully considered. Whether a continuous gradient or a microarray platform should be used must be taken into consideration, with Hook et al. suggesting that gradients are most useful in optimisation of surface properties, whereas microarray platforms are preferable in the discovery of new cell-material interactions[5]. Nonetheless, gradients represent a significant improvement on discrete material tests for screening the relative change in properties such as adsorption of nanoparticles or proteins, and cell behaviour itself.

The continuous nature of gradients can present a problem in experimental design, in that artefacts such as cell migration along the gradient and cell–cell communication across it are a unique part of the biological response. Instead some groups choose to prioritise the use of microarray platforms as these provide distinct variations in material properties and therefore produce data which is easier to interpret. These difficulties are offset by advantages such as a lower cell number and culture media usage—reduced biological variation between conditions and reduced sample material usage—these are significant advantages when working with rare or problematic biological specimens/materials.

### *5.1.3 Cell-Surface Interactions*

Polymer surfaces can broadly be divided into three groups, based on their apparent mode of action, Fig. 5.1. They may provide topographical cues via their micro- and nanoscale architecture. Surfaces may also provide chemical cues which may comprise biomolecules directly tethered to the surface, or a tuned wettability which modulates protein adsorption. Finally, their mechanical properties such as stiffness and rigidity can direct biological activity. Here, we will present a series of emerging fabrication techniques which allow the creation of high content gradient platforms for all three classifications, including combinations of the three.

Preparing and characterising individual samples with different properties is a time consuming and costly approach to finding polymer materials which are fit for purpose. Including multiple conditions on a single sample, in the form of either

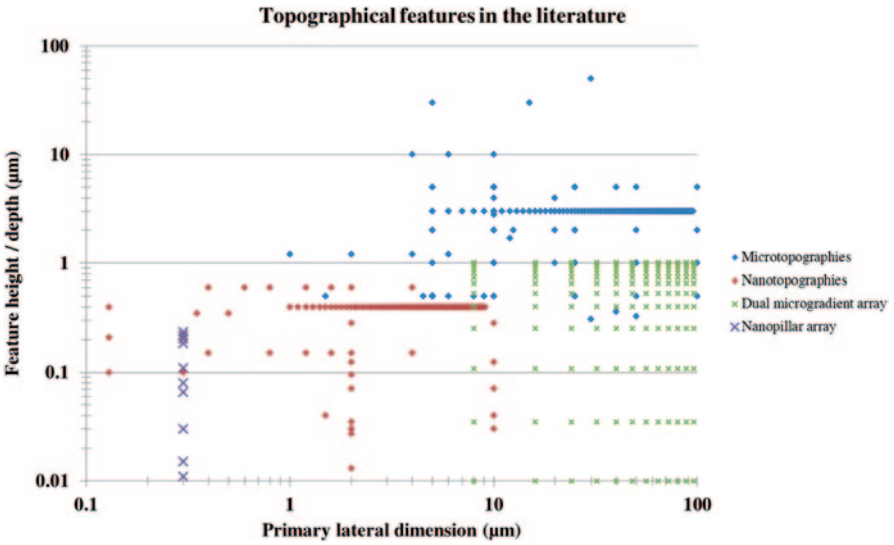


**Fig. 5.2** **a** Graphical understanding of the literature. Collated data from 25 papers with at least 50 citations which use structured polymer microtopographies [14−24] or nanotopographies [25−38] to drive cellular response. We have chosen to focus only on structures produced by common semiconductor fabrication techniques, so as to simplify data comparison—as each study was conducted with certain feature dimensions in terms of feature height and lateral dimensions. Commonly, each paper is represented by one or two single points due to the limitations of fabricating individual, homogeneous samples. Alongside these datapoints, we have included work from our lab (nanopillar array [39] and dual microgradient array [40]) which seeks to more fully explore the sample space by using gradients of topographical features. Continuous variation of nanopillar height was used to investigate the differential response of fibroblast and endothelial cells to the surface, *blue* [39]. Furthermore, we have demonstrated the use of dual topographical gradients—variation of microgroove depth, with orthogonally varied microgroove pitch, *green* [40]. This demonstrates the ability of gradient platforms to more fully cover the sample space, rather than limiting results to a small subset of individually fabricated samples

arrays or continuous gradients, can greatly expedite the characterisation of biological response to it. High-content libraries of topographical motifs have been demonstrated as powerful tools for the discovery of optimal surface topographies, with a single 2 × 2 cm chip containing 2176 distinct geometric patterns generated algorithmically by combining three primitive shapes, fabricated by photolithography, and applied to the analysis of human mesenchymal stromal cells to these geometric combinations [41]. Simon and Gibson compiled an excellent review on combinatorial approaches to biomaterial design including both array and gradient formats [3]. Numerous other review articles are available for further reading [4−10]. Genzer et al. present a compilation of 24 innovative gradient fabrication methodologies, covering a broad range of functionalization methods for both polymeric and inorganic substrates. [4] Inorganic substrates such as silicon are often used as a substrate, which is functionalized with bioactive molecules. Whilst incompatible with direct applications in biological systems, the use of such substrates enables

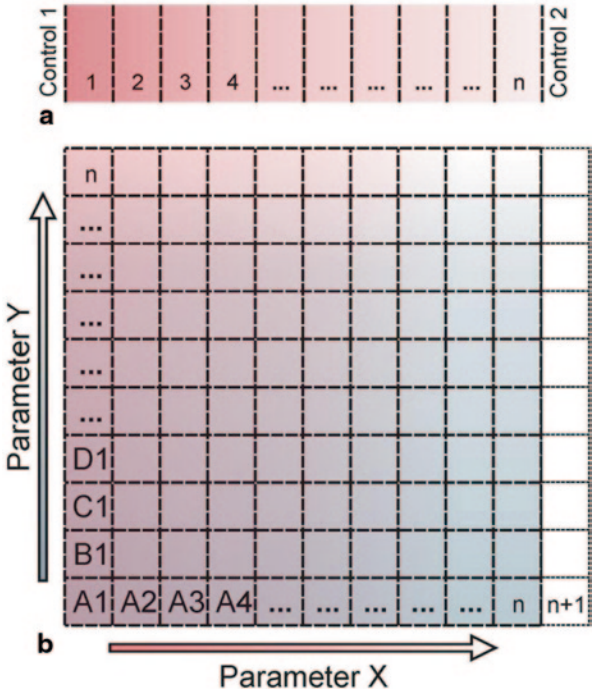


**Fig. 5.3** Continuously varied surface parameters must be discretised for analysis. Cell culture studies have a theoretical maximum resolution of the spread of a single cell along the gradient axis. Whilst modern scanning stage microscopes and automated image analysis software makes this possible, the most common approach in the literature is to divide linear or 2D gradients into subunits of size L/n, where L is the total gradient length and n is the number of subunits. This yields an inherent variation in a single subunit, which is often presented as a uniform value in the literature, masking underlying variation in surface properties and therefore cell response. A square imaging array, captured with a camera which has a rectangular field of view will also be disproportionately loaded in each datapoint with variation in one axis versus the other. Both linear gradients, **a**, and multidimensional gradients, **b**, must be divided into subunits for image analysis

the screening of biological response to a variation in functionalization, which may then be translated onto compatible bulk materials [42]. In fact, the use of thin film polymer coatings alleviates the need for bulk materials to be fully compatible with prospective applications.

Besides discussing the three cues listed above, we will also address how such gradient substrates are evaluated. Commonly, they are simply discretised and analysed in a similar fashion to arrayed samples or platforms. In this respect, the use of gradients may seem counterproductive, if high resolution variations in surface parameters are simply reduced to single instance of a parameter, Fig. 5.3. The strength of parameter gradients lies in the fact that a spatially discretised gradient may include surface parameters which may not have been included in a spatially discretised array. In addition, fabrication of a wide range of surface parameters in a single process may be faster and more reliable than fabrication of individual samples.

Despite increasing resolution of surface characterisation techniques allowing a finer determination of the variation of a given property along a gradient, the literature does little to address the methodologies used to segment biological results on gradients. The default spatial unit of measurement is frequently found to simply be the width of an image frame, for example images captured at ×10 magnification are commonly 800–1000 μm in width. These images become individual datapoints, when in reality they contain an intrinsic variation across them, depending on the spatial rate of change of the underlying gradient. This results in a quantisation of the gradient in a semi-arbitrary fashion, and is particularly inflexible to tolerances in the imaging method. For example, using a motorised stage to capture congruent images across a linear or 2D gradient relies strongly on accurately aligning the substrate and ensuring uniformity in imaging locations across samples.

The location of controls in investigations making use of gradient surfaces also merits some consideration. A surface gradient may occupy a given sample space, with blank control regions surrounding it. Our work on gradients of nanopillar height has shown differences in cell phenotype on flat regions which are adjacent to tall nanopillars versus short nanopillars [39]. Local migratory behaviours and cell–cell interactions influence cell response at these adjacent regions, as can be seen in Fig. 5.10 as an increase in cell number adjacent to one end of the linear gradient. Such effects, most prominent when comparing flat regions to a section of the gradient, must be considered as also having an influence on the patterned regions themselves. This can lead to situations whereupon scale up of a region of the gradient, after identifying it as driving a positive cellular response, a homogeneous sample covered in the same pattern does not elicit the same response. This inherent tendency for cross talk between cells on gradient platforms must be considered when interpreting results. Expansion of individual gradient points into larger homogeneous areas may not produce the same biological response, perhaps indicating that the complex gradient environment has a strong effect on the experiment.

### *5.1.4 Gradient Fabrication*

In most cases, uniformity and homogeneity represent the gold standard in sample fabrication for biomedical engineering studies. Variability between experimental materials is recognised as a source of irreproducible results, slowing and distorting studies of cell-material interactions. As a result, there has been a vast deal of effort invested in ensuring that sample fabrication schemes are consistent and reproducible. This has meant that until relatively recently, there was little work available on the controlled fabrication of *nonuniform* gradient substrates. There has, however, been a recent increase in the reporting of new methods for the fabrication of gradient surfaces—encompassing chemical, topographical, and mechanical modifications of a range of materials [5, 43, 44]. Such samples are viable alternative to groups of individual samples as they can provide a more complete variation in a property, such as hydrophobicity. Conducting a full experiment on a single sample also reduces problems associated with biological variability between large numbers of samples.(Fig. 5.4)

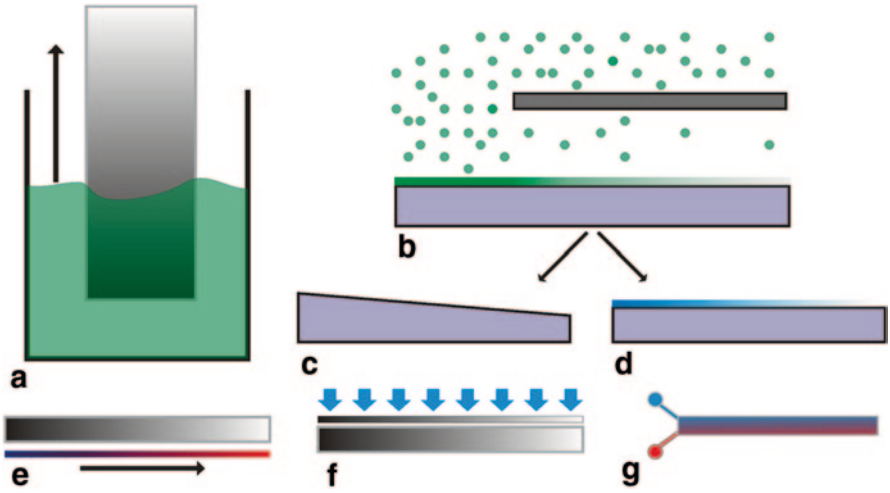


**Fig. 5.4** Polymer gradient fabrication techniques. **a** Sample immersion and removal from a solution of monomer, solvent, or etchant—creating a gradient based on retraction rate. **b** Plasma polymerisation excited by RF glow discharge under a diffusion mask, yielding a decrease in monomer concentration into the channel which translates into a variation in deposited film thickness or chemical composition. Plasma polymer gradients may be used in their deposited state, **b**, as wettability gradients [45, 46], or they may be used as sacrificial masks in a dry etching process to transfer a gradient of etch depth into a substrate. **c** [39, 40] Monomers with reactive groups such as carboxyl [47] or amine groups may be functionalised after deposition with biomolecules such as proteins or short chain peptides [48]. **d**. **e** Polymer microspheres annealed on a temperature gradient have a continuously varying crystallinity across the sample [49–51]. **f** Greyscale lithography or localised UV irradiation can be used to deliver a gradient of light across a photoactive substrate [42, 52]. **g** Microfluidic mixing devices allow precise mixing of monomer solutions or suspensions of biomolecules into gradients on a surface [53–57].

Polymer gradients may be classified in terms of properties such as their mode of interaction with a biological system, their dimensionality, and their range (either steep or shallow). An overview of fabrication methods are presented below in Table 5.1.

## 5.2 Chemical Gradients

Chemical modification or tuning of a surface may take two forms; either guiding the way in which proteins and biomolecules interact and adsorb on the surface, or directly tethering biomolecules to the surface so as to present an artificially engineered interface. Ultimately, both methods affect cell response by the same means, whereby interrogation of the surface properties by a cell is changed. Density, type, and structure of adsorbed proteins have all been shown to influence cell behaviour and can be prepared by various methods. Plasma treatment of polymer surfaces—either the modification of a bulk polymer surface, or deposition of a polymer film,

**Table 5.1** An overview of fabrication methods for gradients of surface chemistry, topography, and mechanical properties

| | Fabrication method | Gradient type | Length scale | Speed | Ref |
|---|---|---|---|---|---|
| Chemical | Plasma polymerisation under a diffusion mask | Wettability/surface functionalization | Up to 20 mm | Moderate | [47, 58–61] |
| | Microfluidic mixing of component solutions | Surface functionalization | 10 μm to 1 mm | Slow | [53–57] |
| | Substrate movement through a vessel | Wettability/surface functionalisation | Up to 10 mm | Fast | [62–64] |
| Topographical | Direct write lithography | Micro or nano | Up to 10 mm | Slow | [18] |
| | Grey scale lithography | Micropatterning | Up to 10 mm | Fast | [42, 52] |
| | Annealing on a temperature gradient | Surface roughness/feature depth | Up to 10 mm | Moderate | [50, 65] |
| | Plasma polymer thickness gradient, used as sacrificial etch masks | Feature depth | Up to 10 mm | Moderate | [39, 40] |
| Mechanical | Curing under UV or thermal gradients, multilayer lithography | Elastic modulus | Up to 10 mm | Moderate | [66, 67] |
| | Microfluidic mixing | Elastic modulus | 10 μm to 1 mm | Slow | [53] |

has been used extensively to tune the biological response of a surface. Cell adhesion to polymer surfaces may be enhanced or inhibited by glow discharge treatment through tuning of the water contact angle (WCA)—with a WCA of 70° appearing to be the optimal value for cell adhesion. Beyond modification of the surface energy many methods have been reported to create continuous variations in chemistry on a surface, with varying levels of complexity. As most existing chemical modifications are done in a homogeneous manner across a surface, adapting these methods to spatially vary the chemical modification is essential. This can be done by physically moving the sample through a solution [62–64], intricate mixing of reagents on a sample using microfluidics [53–57], annealing or curing a surface coating on a temperature gradient [51, 65], or plasma polymer deposition using either knife edge electrodes or through a series of apertures [68].

### 5.2.1 Wettability Gradients

Deposition of plasma polymer films through a diffusion mask can be used to tune the density of functional groups on a surface or to vary the hydrophobicity of a surface [46, 48, 59, 69]. By limiting the concentration of the monomer across the sample by covering the area, deposition rates can be varied along the diffusion mask. These films yield a conformal, pinhole free coating which can then be processed to covalently link biomolecules to its surface. Alternatively, the surface may be physically masked with a barrier held in close proximity, which is then gradually moved away, yielding a variation of plasma exposure time. Whilst this method has a more involved setup due to the requirement of building a mechanically actuated barrier inside a radio frequency discharge chamber, it is more flexible than deposition by diffusion gradient, as the rate and manner of movement can be tailored to produce various gradients. Such a mechanical barrier can readily be constructed from e.g. LEGO parts [70;Fig. 5.5].

Plasma polymer films are especially attractive due to the variety and scope for uses after the initial outlay on construction of the necessary processing equipment. Reaction chambers themselves are fairly simple to construct, generally consisting of a vacuum chamber, some means of exciting a plasma, for example copper band electrodes or parallel plate electrodes along with a radio frequency generator, and a monomer inlet with flow control [71–73]. Various monomers are available for deposition by plasma polymerisation, including hexane, acrylic acid, and allylamine among others [74–78]. Deposition of these polymers creates thin film coatings with unique properties for biomedical applications. Plasma polymerisation techniques are particularly amenable to the creation of gradients, with the use of a simple diffusion mask as shown in Fig. 5.6.

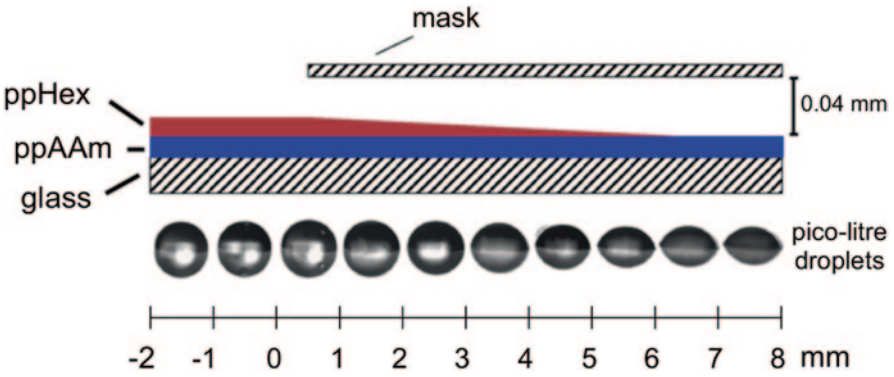


**Fig. 5.5** Schematic of the experimental setup used to prepare a shallow diffusion gradient. The hexane plasma diffuses under the mask from the left-hand side onto a plasma polymerised allylamine coated glass slide while all the other edges are sealed. Representative images of the water contact angle (WCA) droplets used for the WCA analysis are inset. (Figure adapted from [59], with permission from Elsevier)

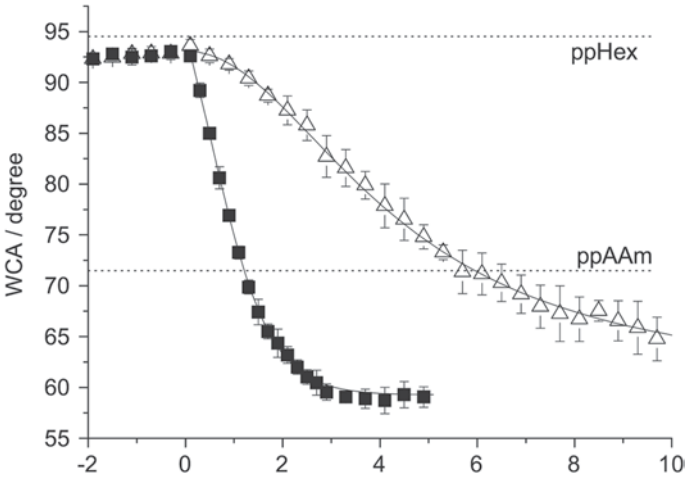


**Fig. 5.6** Water contact angle (WCA) along the steep (*square*) and shallow (*triangle*) gradients averaged over 15 measurements. The WCA decreases when going from ppHex (*left*) to ppAAm (*right*). The masked area starts at 0 mm and proceeds to the right of the graph (*positive values*). In the gradient zone the data was fitted with a sigmoidal curve. Error bars represent the standard deviation between 15 measurements from three gradients. (Figure adapted from [59], with permission from Elsevier)

The range and profile of plasma polymer gradients may be tuned by the proximity of the mask depicted in Fig. 5.6 to the sample surface. The larger the gap through which the monomer gas can diffuse, the shallower and longer the resultant gradient. Zelzer et al. deposited a gradient of plasma polymerised hexane (ppHex) over a uniform film of plasma polymerised allylamine (ppAAm), Fig. 5.7. By varying the spacing between the diffusion mask and the substrate they were able to create both steep and shallow gradients of surface energy, which they used to assess the impact of surface wettability on cell adhesion, spreading, and proliferation. Surface roughness of the plasma polymer film was measured by atomic force microscope (AFM) across the gradient, changing from an root-mean-squared (rms) roughness of 0.37–0.38 nm, reinforcing that changes in cell behaviour were in response to surface wettability rather than any topographical cue.(Fig. 5.7)

### *5.2.2 Biomolecular Gradients*

Density of cell binding ligands and other biomolecules on the surface also play a critical role in cell behaviour, and gradients can be created by various methods. Adsorption of extra cellular matrix (ECM) proteins to a predefined gradient or the direct coupling of ligand binding motifs such as RGD peptides have been demonstrated. The ability to control gradients and density of ligand binding motifs represents a powerful tool in creating ‘artificial’ ECM environments to control cell

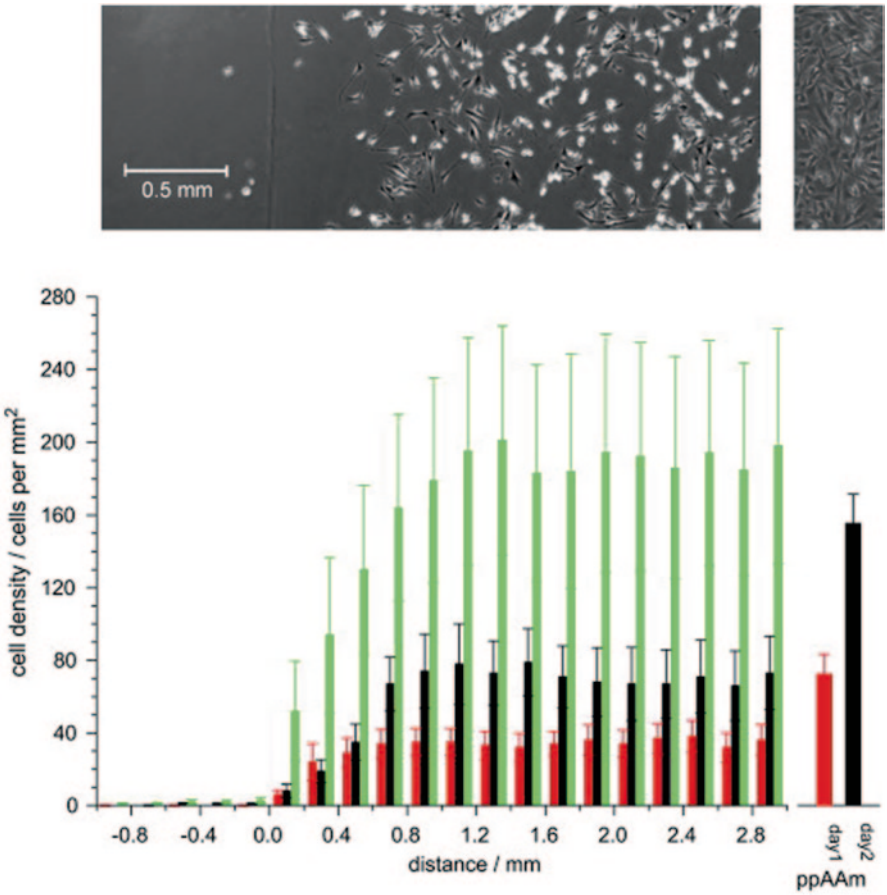


**Fig. 5.7** Average cell density across a gradient of wettability. Plasma polymerised allylamine deposited under a diffusion mask has a varied water contact angle over 3 mm. Clear differences in cell morphology can be seen across this gradient in brightfield imaging, *top*. The *lower* figure shows cell response over time, at 1 (*red*), 2 (*black*), and 3 (*green*) days, highlighting the variation in cell density as the hydrophilicity of the surface is continuously varied. (Figure adapted from [59], with permission from Elsevier)

behaviour [42, 79]. Furthermore, microfluidic approaches have also been used to create gradients of common extracellular matrix proteins, for the investigation of cell migration [54, 80; Fig. 5.8].

Both steep and shallow short range chemical gradients may be fabricated by diffusive processes in microfluidic channels, Fig. 5.7, based on the relative concentration of monomer solutions [55]. Parallel channels containing varying concentrations create a stepped gradient at the inlets, which diffuses to form a smooth gradient over a distance of 20 mm. These parallel flows are formed in a gradient generator channel arrangement, which can create a modulated mix of any two input monomer solutions. The gradient profile is dependent of tuning the flow rate of

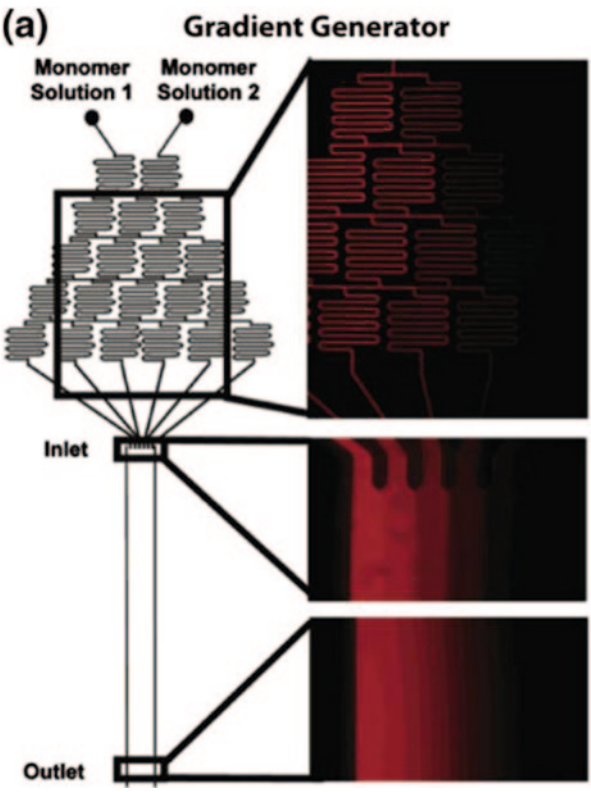


**Fig. 5.8** Chemical gradients can be produced using microfluidic platforms. Hydrogels with a semi continuous variation in composition between two monomers across a channel, adapted from [55], with permission from The American Chemical Society

both monomer solutions—fast monomer flow does not provide sufficient time for a complete diffusion gradient to form, whereas slow monomer flow results in truncating of the gradient range due to excess diffusive mixing. Hydrogel networks with a variation in adhesive ligands (e.g., RGDS) tethered throughout were fabricated by this method. The authors also demonstrated gradients of crosslinking density and hydrogel thickness fabricated through this method. Gradients of adhesive ligands fabricated by this method demonstrated spatial variation of endothelial cell attachment across a 900 μm gradient. Specific ECM protein gradients spanning 500 μm have been created on microstructured substrates [80], whilst similar gradient hydrogels were fabricated by mould casting and photocuring, increasing the gradient dimensions to over 6 cm [81].

Besides surface bound biomolecular gradients, soluble chemical factor gradients have also been created in polymeric microfluidic devices [82]. Mosadegh et al. developed a microfluidic device which generates several chemical gradient conditions on a single platform in flow free microchambers. Polydimethylsiloxane (PDMS) membranes allow the diffusion of chemical gradients whilst protecting cells from shear forces associated with other soluble gradient platforms presented in the literature. There is little or no consideration given to the initial seeding of

cells on gradient platforms by the literature, with this study being a rare exception. Taking care to ensure a homogeneous distribution, either upon seeding cells on a surface gradient, or applying a chemical gradient to the culture environment, is of paramount importance. The majority of experiments conducted on gradients use metrics which depend on uniform initial cell seeding. Cell attachment, chemotaxis, durotaxis, migratory behaviours, and morphological characteristics are all heavily influenced by local cell density. It is possible that uneven initial application of cells may distort results, with certain areas of the gradient appearing to enhance cell attachment and proliferation when in fact they were simply seeded with more cells in the first instance. The use of short range or steep gradients mitigates this risk somewhat, however long range gradients over a few millimetres in length are vulnerable to inhomogeneous cell seeding across the entire gradient area.

## 5.3 Topographical Gradients

Micro- and nanoscale surface structuring can be used to modify cell behaviour at an interface. Contact guidance, the phenomena in which cells conform to topographical features, can be used to drive cell morphology into a given shape. Polarisations of the cell body, as well as restriction of cell area to a defined size have been extensively demonstrated by differing methods [83]. In order to better understand the impact of geometric cues in cell behaviour, continuous gradient assays are being used to screen cellular response across the full parameter space. The questions raised surrounding the topographical control of cell behaviour have driven the development of new fabrication techniques to create gradients of feature size, pitch, and depth. Etching of plasma polymer films deposited under a diffusion mask [39, 40] and annealing of nanoimprinted gratings on a temperature gradient [51, 84] have been used to create gradients in feature height on a surface and subsequently assess the impact of feature height on cellular contact guidance and migratory behaviours. Greyscale lithography, which varies the intensity of exposure to create varied depth profiles in a photoresist can be used to create topographical gradients, however such methods are sensitive to changes in processing conditions [85]. Direct spatial positioning of a ultraviolet (UV) source provides more reproducible and tuneable control of depth profiles in a photocurable polymer, however this comes at the cost of lateral resolution [86].

### *5.3.1 Micro- and Nanopatterned Surfaces*

Fabrication of micro- and nanoscale topographies for biomedical engineering borrows a host of techniques from the semiconductor industry, which has driven increasing resolution in lithographic techniques down to the nanometre over the past decades. This has delivered biomedical engineers a toolbox of surface patterning

techniques, along with some new methods developed specifically to address biological questions. Patterns are generally defined by either direct write (e.g., electron beam lithography (EBL)) or mask based photolithographic approaches. These create topographical features which drive cell behaviour through contact guidance, or spatial distribution of biomolecules or ECM proteins to precisely control cell adhesion to the substrate [22, 26, 87–93].

Micro- and nanogrooves have been shown to direct cellular alignment to a polymeric substrate [24, 94, 95], with various gradient platforms being developed making use of capillary force lithography [18], direct write patterning [15], and plasma polymer deposition [40]. Evidence of cell migration and response to the underlying gradient topography has been demonstrated in the directional migration of fibroblasts along anisotropic grooved substrates [18]. Ultraviolet assisted capillary force lithography was used to create a mould with ridges which were 1 μm in width and 400 nm tall, upon which poly(urethane acrylate) (PUA) films were cast. The spacing between ridges was increased in 100 nm increments across the pattern, creating a linear gradient of pitch. Cell shape and motility was studied at five positions across the gradient, which was relatively steep with average groove width changing from 2.6 to 8.6 μm across a 500 μm pattern, with an absolute variation in groove width across the pattern from 1 to 9.1 μm. These five analysis positions therefore incorporate a substantial range of groove widths into a single datapoint. Cell polarisation and elongation are more pronounced on narrower grooves. Cell migration speeds were optimal at intermediate ridge widths, with cells appearing to migrate towards these intermediate regions from both narrow and wide areas. This indicates that individual cells were capable of sensing and responding to small variations of topographical dimensions underneath them. Sun et al. demonstrated a depth gradient in both groove and ridge polarity, fabricated in polystyrene (PS), polymethylmethacrylate (PMMA), and dimethacrylate (DMA) to separate the effects of surface chemistry and topography on cell alignment [96]. This study found that surface topography had a more prominent impact on cell alignment than surface chemistry for the two materials examined.

Plasma polymerisation has predominantly found use in the creation of chemical coatings and gradients, which may also be functionalized with biomolecules to tune cellular response to a surface. Our group has developed several new applications in micro- and nanofabrication processes, including direct patterning of ppHex films by EBL [97] and use of ppHex as an etch mask for reactive ion etching (RIE) processes [39, 40]. Gradients of plasma polymer thickness, generated by deposition under a diffusion mask (Fig. 5.4c), were deposited across prefabricated etch masks for both nanopillar and microgroove arrays. Upon etching in an RIE process, the variation in film thickness across the etch mask results in a greater etch depth at the thinnest end of the ppHex gradient. Etch rates and material selectivities may be tuned to create a shallow or steep variation in feature height in the prefabricated pattern.(Figs. 5.9, 5.10)

Nanospun fibre meshes represent a bridging between 2D and 3D synthetic environments. Ramalingam et al demonstrated a method of creating a gradient of composition in the final fibre mesh across centimetre length scales [98]. This new technique is applicable to any electrospun polymer, and may be used as either a

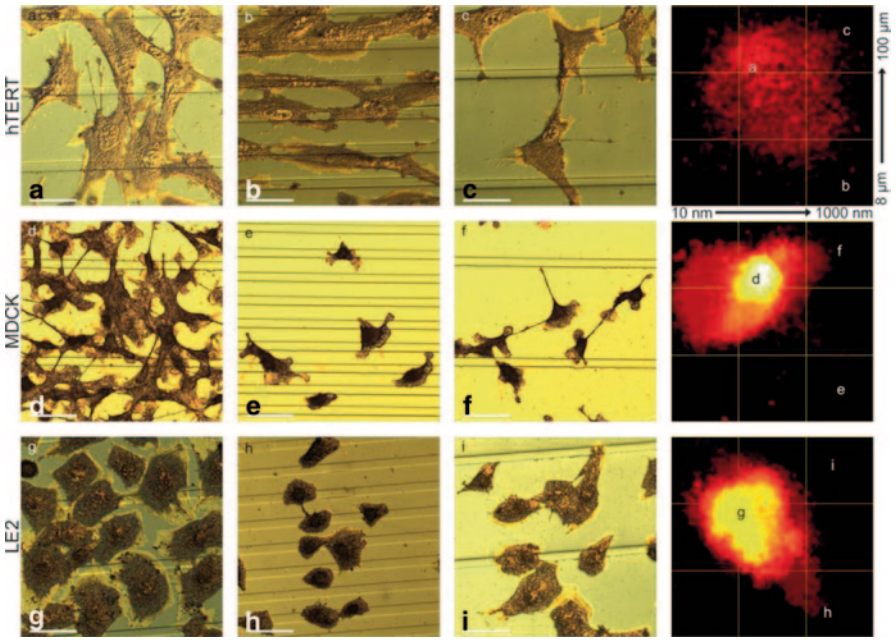


**Fig. 5.9** **a–i** Microscopy images showing clear morphological changes in response to three distinct regions of the dual topography gradient after 72 h, for the three cell types screened. Certain combinations of groove depth and pitch elicit a cell specific response in the fibroblast type hTERT cells when compared to the response of the endothelial (LE2) and epithelial (MDCK) cells. Pseudo-coloured heat maps show the cell coverage over the full 10× 10 mm topography, constructed by scanning and averaging six Coomassie stained samples. A clear 'hot spot' can be seen for the epithelial and endothelial cell types. Scale bar: 50 µm. (Figure adapted from [40], with permission from John Wiley and Sons)

screening tool to determine ideal blend compositions for a given purpose, or to generate tissue engineering scaffolds for interfacial tissues such as cartilage.

Predominantly, gradients have been fabricated for use to investigate a single cell type, protein or nanoparticle behaviour on a single surface—with homogeneous chemical, topographical, and mechanical properties. For example, fibroblast cells adhere and proliferate rapidly on short polymer phase separated nanotopographies, however this effect is reduced as the nanostructure height increases from 13 to 95 nm to the point where the effect of the topography is reversed [99, 100]. These topographical effects on cell behaviour are not one and the same for all cell types, or geometrical arrangements of nanofeatures of the same length scale. Comparison of the behaviour of fibroblast cells with that of endothelial cells on the same nanostructured array showed an opposite response for each cell type [31].

Our group has increased the information gained from a single experiment by culturing two cell types simultaneously on a nanotopographical gradient, so as to assess the interplay and competition between different cell types and the relative impact of a continuous variation of nanopillar height, Fig. 5.7. As nanopillar height

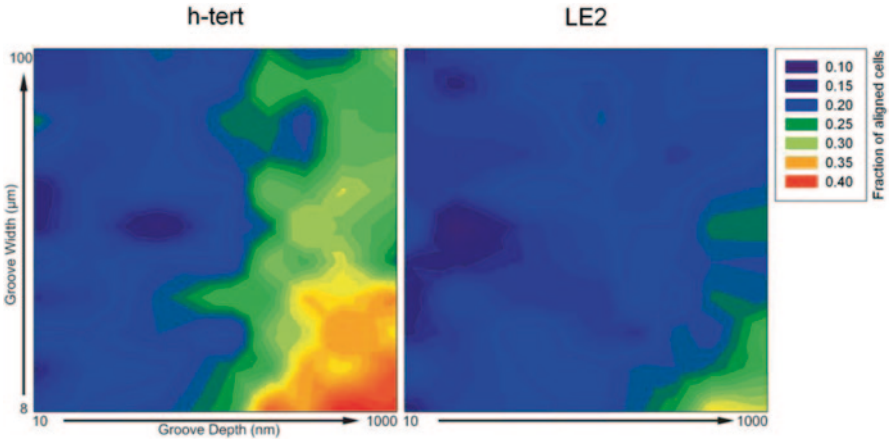


**Fig. 5.10** Cellular alignment on the dual gradient topography as a fraction of the total number of cells. **a** hTERT fibroblast type cells exhibit a high degree of alignment to the groove axis where the distance between grooves is lower, and if the grooves are over 500 nm deep. Cells were considered to have aligned to the topography if the major axis of an elliptical fit to their shape lay within ± 15° of the groove axis. **b** LE2 epithelial type cells show some level of alignment at narrower groove pitches, presumably driven by contact inhibition, however, the higher rate of fibroblast alignment is clear. Sixteen percent of cells on the nonstructured region around the topography fell within this alignment range as expected (30° acceptance over 180°). The groove pitch increases in 0.5 μm steps from 8 to 100 μm, while groove depth increases from under 10 nm to over 1 μm. (Figure adapted from [40], with permission from John Wiley and Sons)

increases from < 10 to 250 nm, the ratio of each cell type in the coculture varies—indicating a cell type specific impact of the nanotopography on cell behaviour. An enrichment of LE2 endothelial cells is evident, whilst hTERT fibroblast cells are simultaneously depleted as the gradient changes from a flat surface to 100 nm tall pillars [39]. A concurrent reduction in total cell number at extreme heights indicates that whilst nanopillar arrays may enrich endothelial populations, there is an upper limit at which their effect becomes detrimental. This reinforces the effectiveness of gradient platforms in optimisation of surfaces which have already been identified as driving the desired biological response.(Fig. 5.11)

### *5.3.2 Surface Roughness*

Whilst sophisticated micro- and nanolithographic techniques have been used to drive cellular behaviour at polymeric surfaces, less precise methods have also been successfully demonstrated as being capable of driving cell behaviour. A continuous gradient of surface roughness in cast epoxy resins revealed higher cell densities on partly roughened surfaces over flat or very rough surfaces—demonstrating the ability of gradient platforms to optimise surface properties [101; Fig. 5.12].

Gradients of surface roughness have also been created in various polymers by applying a temperature gradient across the sample. Poly L lactic acid (PLLA)

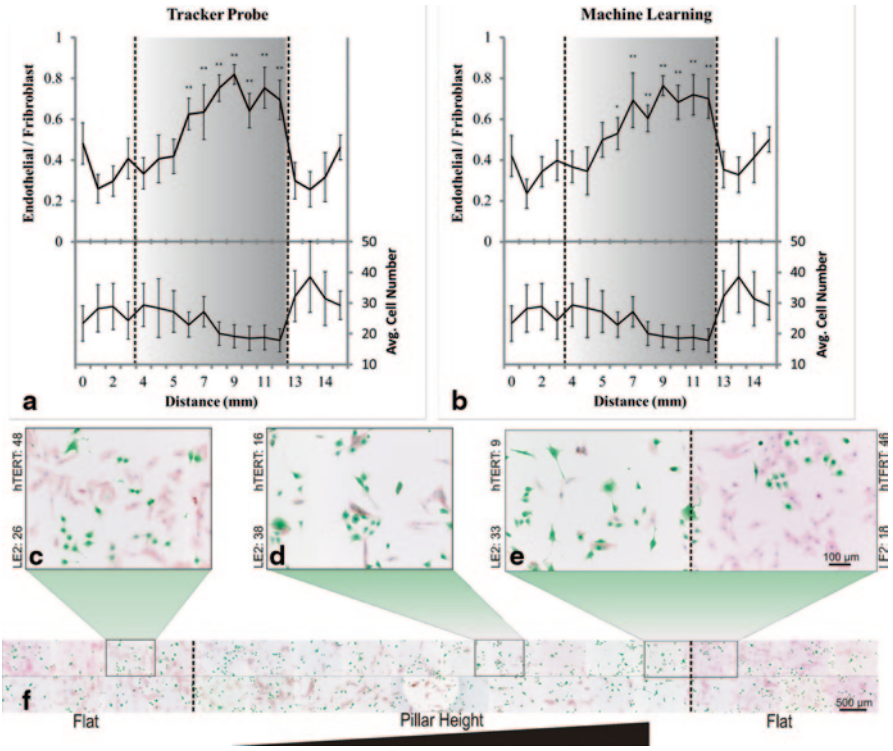


**Fig. 5.11** Response of fibroblast (hTERT-BJ1) and endothelial (LE2) cells in coculture to a gradient of nanopillar height is shown. The ratio of endothelial/fibroblast cells after 96 h culture was calculated by **a** direct labelling of the subpopulations with CellTracker probes and **b** applying machine learning to cell morphology and nucleus data to predict cell type; greyscale background gradient represents increasing pillar height from left to right with *dashed line* indicating the nanopillar-flat boundary. Statistically, each datapoint was compared to the 'baseline' flat region, $*p<0.01$, $**p<0.001$. Images **c**–**e** show cellular response at various points across the nanogradient sample **f** From this analysis, we can suggest that a nanopillar height in excess of 75 nm is sufficient to induce a statistically significant change in the ratio of endothelial/fibroblast cells on the nanopattern, however as pillar height increases the average number of cells per frame was found to fall. (Figure adapted from [39], with permission of The American Chemical Society)

crystallinity was continuously varied across a sample by an underlying gradient of annealing temperature [50]. This created a surface roughness gradient with rms roughness values ranging from 0.5 to 13 nm. The total gradient length is not specified, however the method of annealing on a temperature gradient appears to produce a step change in surface roughness rather than a continuously varying gradient, Fig. 5.11c. Alternatively, gradients of surface roughness yielding a gradient of wettability have been achieved by coating a surface in PS polymer nanospheres, then applying a temperature gradient from ambient to above the glass transition temperature of PS [51]. In doing so, the polymer nanospheres experience higher temperatures in one direction, which results in a variation of melting and reflow across the sample. Spheres which are not exposed to any heat remain spherical,

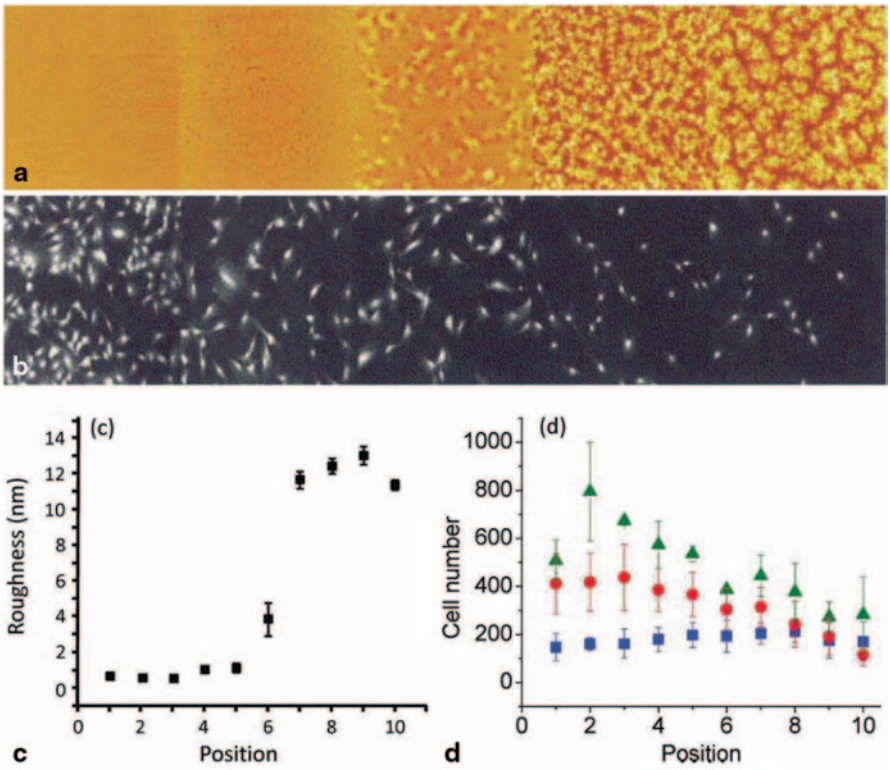


**Fig. 5.12** Montage of representative images of PLLA morphology from AFM data (**a** field of view in each image is 20 nm), and corresponding cell count from fluorescent microscopy (**b**, field of view in each image is 1500 mm). Modification of PLLA crystallinity across a millimetre scale by annealing on a temperature gradient yields a continuum of variation in the nanoscale structure of the surface, a. MCT3T3-E1 pre-osteoblast cell adhesion was inhibited at increasing levels of roughness. Graph **c** shows average measured roughness as a function of library position. Graph **d** plots average cell number as a function of library position after culturing for 1 (*blue*), 3 (*red*), and 5 (*green*) days. Initial cell attachment is consistent across the gradient substrate, with cell density increasing differentially on areas with lower surface roughness over prolonged culture times. (Figure adapted from [50], with permission from Elsevier)

creating prominent features in the surface. With increasing temperature across the sample, the spheres melt and reflow into less defined structures—creating a long range gradient of surface roughness. Still more control can be achieved: rather than simply annealing polymers on a temperature gradient to create a change in topography, methods utilising stress relaxation in a partially cross linked visco-elastic thin film have been demonstrated [49]. This method employs a combination of soft lithography and differential heating to imprint a uniform structure with nonuniform thermal cross linking of the substrate polymer film. Upon demoulding of the stamp, the temperature dependent stress induced in the film results in a variation in feature amplitude across the pattern.

## 5.4 Mechanical Gradients

### *5.4.1 Rigidity Gradients*

The mechanical properties of a material signal the stiffness of the local environment to adherent cells, and have been shown to drive differentiation [102], migration [103, 104], and apoptosis [105]. Local variations in stiffness exist within the tissues of the body, and form a key migratory signal for so called durotaxis along a gradient of stiffness [106]. Stiffness of the local environment plays a key role in cell behaviour, and gradients of substrate rigidity have been created in both PDMS and hydrogel materials with stiffness gradients from 'soft' to 'hard' with compressive moduli ranging from kilopascals to megapascals respectively. This enables studies which span a biologically relevant stiffness gradient, from soft tissues such as the brain with an elastic modulus of approximately 10 kPa, to hard tissues which approach the MPa range such as collagenous bone [102]. Chatterjee et al. showed 3D encapsulation of cells in a poly(ethylene glycol) dimethacrylate (PEGDM) hydrogel with a varied compressive modulus from 10 to 300 kPa, which they achieved through modified monomer concentration across the sample [81]. Osteoblasts cultured within the hydrogel exhibited differentiation lineage commitment which was determined by the stiffness of their local environment—depositing calcified matrix in regions of higher stiffness.

Greyscale lithography was used to create radial gradients of compliance in photocurable polyacrylamide gels. These gradients were relatively shallow, transitioning from a Young's modulus of 11 kPa in the centre to 2.5 kPa at the edge over a radius of 9 mm [85]. The authors demonstrated that vascular smooth muscle cell motility is influenced by the underlying substrate stiffness, with cells migrating from soft to stiff regions of the substrate and eventually accumulating on stiff regions of the substrate. In fact, cell spreading, polarisation, and motility were all found to increase on gels with uniform stiffness values—whereas cell durotaxis was found to be independent of local stiffness values, and driven by the magnitude of the gradient from soft to stiff [66]. This work demonstrates that minor fluctuations in substrate stiffness can have a drastic impact on cell response, and highlight that any mechanical heterogeneity in supposedly homogeneous surfaces can impact cell behaviour.

Gradients of elasticity are present in physiological contexts such as in muscle, but can also result from pathological conditions. Vincent et al. utilised multiple techniques to generate stiffness gradients in polyacrylamide gels of with shallow and steep rates of change, corresponding to both physiological and pathological states respectively [107, 108]. Steep polymer gradients designed to mimic pathological states had lateral rate of change of between 10 and 40 Pa/μm, for example a myocardial infarction establishes gradients of approximately 8.5 Pa/μm [108]. Shallow gradients had a lateral rate of change of approximately 1 Pa/μm. Step changes in stiffness were also included in the study in the form of 100 μm wide strips of stiff polymer, interspersed with 500 μm wide strips of soft polymer.(Fig. 5.13)

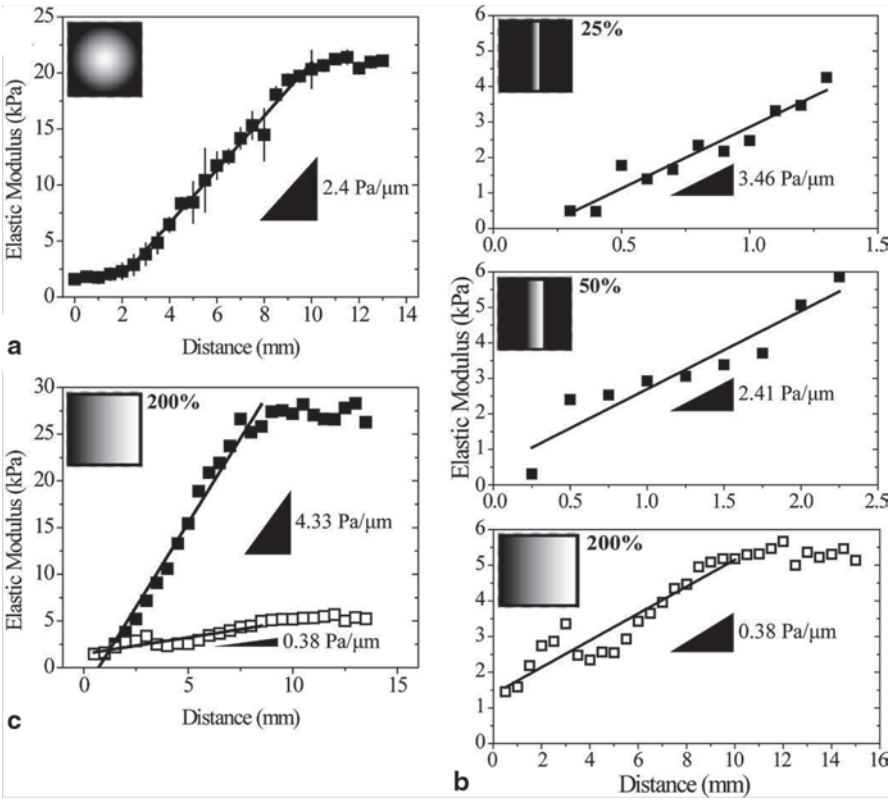


**Fig. 5.13** **a** Gradients generated using a radially symmetric mask and a solution containing 10% acrylamide, 0.3% bis-acrylamide, and 0.5% irgacure as the initiator. $n = 4$ gels **b** Gradients produced with the same polymer solution (10% acrylamide, 0.1% bis-acrylamide) but using photomasks where the opacity gradient was scaled to 25%, 50%, or 200% of the distance used in Fig. 5.1 **b**ii, $n = 1$. **c** Two different gradients made with the same photomask but different polymer solutions. Closed squares: 10% acrylamide and 0.3% bis-acrylamide, open squares: 10% acrylamide, 0.1% bis-acrylamide, $n = 1$. Insets **a**–**c** Photomask images used for gradient fabrication with indicated photomask gradient distance relative to the photomask in Fig. 5.1 **b**ii. (Adapted from [108], reproduced with permission from John Wiley and Sons)

## 5.5 Combinatorial Gradient Platforms

As cellular response to an engineered surface is complex, and depends on the synergistic effects of multiple properties, creating combined gradients in a single platform can speed up discovery. Combined gradients also allow the relative impact and importance of two distinct surface properties to be investigated at once, as depicted in Fig. 5.3b. Orthogonally positioned gradients of topography and chemistry have been demonstrated in the investigation of multiple surface properties.

Deposition of two allylamine plasma polymer gradients positioned orthogonally, using different polymerisation parameters, were used to create a dual gradient of

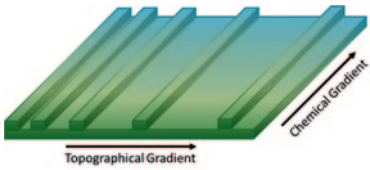


**Fig. 5.14** A dual gradient of topography and chemistry. Microgroove pitch increases in one direction, whilst wettability increases in the perpendicular direction. (Reproduced from [16], with permission from John Wiley and Sons)

amine functionality on a polypropylene membrane [109]. Wettability was assessed by WCA measurements, showing a range across the sample of 33–96°. Fibroblast cells showed extensive elongation and polarisation at a local WCA of 64.5 ± 9.3°, with cell proliferation increasing dramatically as the WCA fell to 25.4°. Further to their functionality as wetabillity gradients, the high density of amine functional groups present in allylamine plasma polymers makes attachment of biomolecules to create more complex gradients possible [110].

Alignment of fibroblast cells to a microgroove substrate with an orthogonally deposited gradient of surface wettability allowed the relative impact of the two distinct cues to be investigated by [16]. Cell coverage and relative alignment to the grooves was analysed after a period of 3 days culture, showing cell alignment to narrow microgrooves was independent of the local WFA.

Dual chemical gradients have been demonstrated in poly(2-hydroxyethyl methacrylate) (PHEMA) which resists the surface adhesion of ECM proteins such as fibronectin [111]. Orthogonal gradients of PHEMA molecular weight and grafting density resulted in a variation of dry thickness across the substrate, and qualitative changes in fibroblast adhesion and morphology.(Fig. 5.14)

Gradients of ECM protein concentration have been superimposed over prefabricated topographical structures in PMMA by a microfluidic approach [80]. Comelles et al. report steep fibronectin concentration gradients of 0.5 $pmol \cdot cm^{-2} \cdot mm^{-1}$ which are 40 times higher than previously reported gradients on PMMA substrates [112]. This study used homogeneous topographical patterns, however topographical gradients would also be applicable to this method as used in Fig. 5.15. These gradients of fibronectin molecules, and therefore gradients of adhesive ligand density, effectively control cell adhesion processes—yielding differential cell adhesion and focal contact formation dependent on gradient slope and absolute density.

## 5.6 Gradient Characterisation

Characterisation of gradients represents a further challenge in effectively applying them to biomedical applications. Many metrology and analysis techniques are currently configured for larger, homogeneous sample areas and are therefore

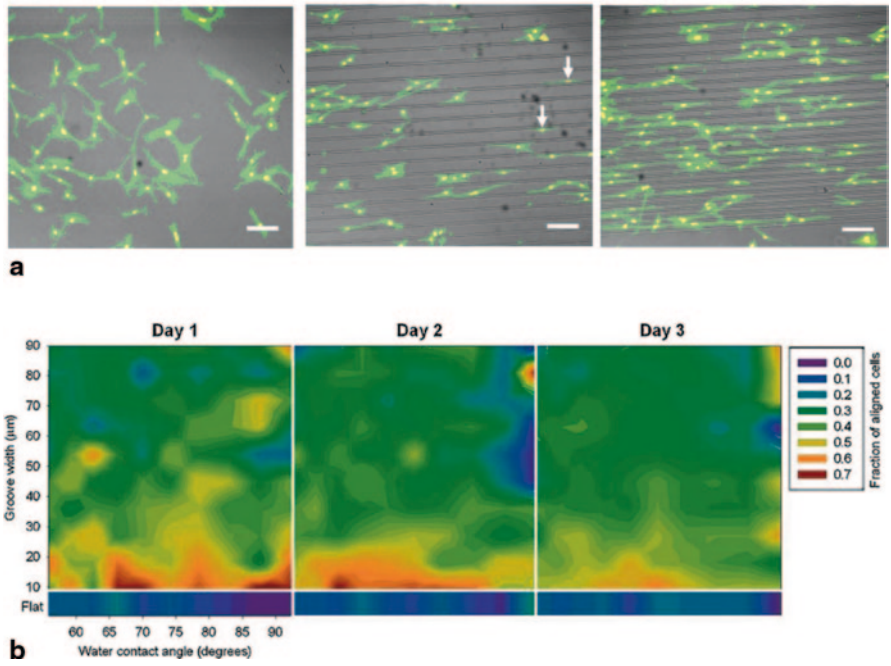


**Fig. 5.15** Cell morphology and orientation on orthogonal gradient samples. **a** Typical cell morphology on flat and grooved surfaces at day three. The corresponding WCA range for the three images is approximately between 55° and 58°. Scale bar: 100 μm. F-actin fibres in the cytoskeleton were stained using FITC-labelled phalloidin; the nuclei were stained with propidium iodide. **b** Cell alignment on surfaces with orthogonal gradients after 1, 2, and 3 days culture. Cells with an orientation angle less than 10° were defined as aligned, whereas cells with 0° and 90° were classed as being parallel and perpendicular to the groove, respectively. Cell orientations were classified in nine intervals of 10° each, i.e., 0°–10°, 10°–20°, etc. For randomly oriented cells, approximately 11% of the whole population was oriented within each one of nine orientation intervals. Data is average of 3 repeats for each image. Each square graph (*grooved area*) and rectangular graph (*flat area*) represents 10 × 10 mm and 10 × 1 mm areas, respectively. The flat and grooved areas are from the same sample. (Adapted from [16], with permission from John Wiley and Sons)

unsuitable for use in a situation where parameters continuously vary spatially. To that end, picolitre volume WCA analysis, Time-of-Flight Secondary Ion Mass Spectrometry (ToF-SIMS), and optical techniques have been developed to fully characterise gradient surfaces [52]. Mangindaan et al. presented a comprehensive analysis of wettability gradients produced on polypropylene under a diffusion mask in $SF_6$ plasma [113]. Here, they fabricated a surface with a wide ranging wettability gradient (115° WCA over 10 mm) and fully characterised the plasma-polymer interactions, creating a mathematical model which enables the prediction of wettability based on etch mask design.(Fig. 5.16)

The development of new fabrication methodologies has understandably driven the development of new characterisation methodologies to better determine and quantify the exact properties of these unique surface modifications with sufficient resolution and sensitivity. Analysis of surface energy by measuring the WCA has

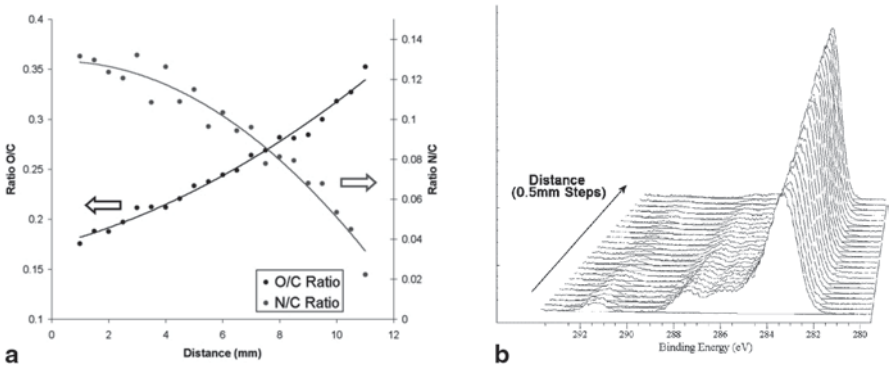


**Fig. 5.16** Spatial analysis of chemical gradients by XPS. O/C and N/C ratios as a function of position along an amine-acid chemical gradient, *left*. This shows a changing surface concentration of amine and acid chemistry in opposite directions on the surface. C1s region of a trifluoroethanol derivatised octadiene-acrylic acid chemical gradient, *right*. The reactivity of the surface has been spatially controlled. (Figure adapted from [114], reproduced with permission from The Royal Society of Chemistry)

been refined from microliter volumes on single homogeneous samples through to picolitre volume measurements using automated fluid dispensing and motorised sample stages. This yields millimetre resolution across gradients of surface energy. [59, 70, 84, 115] Chemical composition of the surface may also be analysed using classical techniques such as X-ray photoelectron spectroscopy (XPS) and secondary ion mass spectrometry, where placement and control of the excitation source may be scanned across the gradient surface to yield a readout of its changing properties [114, 116]. Whittle et al. achieved 0.5 mm resolution in XPS analysis of the chemical composition of plasma polymer gradients on glass substrates, including analysis after derivatisation of the deposited chemical groups. Characterisation resolution, in this case, is still limited by the spot size of the XPS tool used, and a continuously varying surface will have inherent differences across a 500 μm analysis region. Cells themselves are often approximately 10–30 μm in size, therefore increased resolution in gradient characterisation is imperative if cell response is to be attributed to a given surface parameter. Other techniques offer increased resolution, such as Fourier transform infrared spectroscopy (FTIR) [117, 118] for chemical gradients or AFM for topographical gradients. Increased resolution, however, increases the burden of acquiring large measurement datasets of slowly changing parameters over a large area.

## 5.7 Conclusions and Outlook

Gradient platforms represent an effective method of generating a wide range of properties on a single substrate. These allow for the systematic investigation of cellular response to given values or combinations of surface properties. Included in such continuous gradients are more possible values between the initial and final

value, ensuring that the full parameter space is explored, rather than simply one or two possibilities. It is this potential to uncover optimal parameters that has driven the increasing use of gradient platforms in biomaterials research over the past decade. This growing interest has seen the development of over 30 novel techniques for the fabrication of polymeric gradient materials, with new approaches continuing to emerge.

Key to harnessing these powerful and information rich platforms will be similar advances in both characterisation and analysis. As parameters such as surface chemistry are varied continuously over millimetre scale gradients, many surface characterisation techniques cannot capture the fine spatial variation. Techniques such as XPS and WCA measurements have been refined to increase their lateral resolution through motorised stages, smaller spot/drop sizes respectively and automated data acquisition.

Analysis of cell culture experiments on gradient platforms has, however, lagged behind developments of new fabrication and characterisation techniques. We have attempted to take a high content approach, using automated software to screen and characterise cell response based on morphological characteristics [39]. There are significant opportunities to refine the analysis of cell response to gradient substrates beyond simply capturing microscopy data at various points on the gradient. Bringing the full toolset used to interpret cellular response to homogeneous samples across to gradient platforms represents the next step in harnessing the true power of gradient platforms to screen and optimise cellular response.

## References

1. Stevens, M. M.; George, J. H. Exploring and Engineering the Cell Surface Interface. *Science* **2005**, *310*, 1135–1138.
2. Geysen, H. M.; Schoenen, F.; Wagner, D; Wagner, R. Combinatorial Compound Libraries for Drug Discovery: An Ongoing Challenge. *Nat. Rev. Drug Discov.* **2003**, *2*, 222–230.
3. Simon, C. G.; Lin-Gibson, S. Combinatorial and High-Throughput Screening of Biomaterials. *Adv. Mater.* **2011**, *23*, 369–387.
4. Genzer, J.; Bhat, R. R. Surface-Bound Soft Matter Gradients. *Langmuir* **2008**, *24*, 2294–2317.
5. Hook, A. L.; Anderson, D. G.; Langer, R.; Williams, P.; Davies, M. C.; Alexander, M. R. High Throughput Methods Applied in Biomaterial Development and Discovery. *Biomaterials* **2010**, *31*, 187–198.
6. Ankam, S.; Teo, B. K. K.; Kukumberg, M.; Yim, E. K. F. High Throughput Screening to Investigate the Interaction of Stem Cells with Their Extracellular Microenvironment. *Organogenesis* **2013**, *9*, 128–142.
7. Morgenthaler, S.; Zink, C.; Spencer, N. D. Surface-Chemical and -Morphological Gradients. *Soft Matter* **2008**, *4*, 419.
8. Singh, M.; Berkland, C.; Detamore, M. S. Strategies and Applications for Incorporating Physical and Chemical Signal Gradients in Tissue Engineering. *Tissue Eng. Part B* **2008**, *14*.
9. Suk, M.; Khang, G; Bang, H. Gradient Polymer Surfaces for Biomedical Applications. *Prog. Polym. Sci.* **2008**, *33*, 138–164.
10. Edalat, F. E.; Bae, H.; Manoucheri, S.; Min Cha, J; Khademhosseini, A. Engineering Approaches Toward Deconstructing and Controlling the Stem Cell Environment. *Ann. Biomed. Eng.* **2012**, *40*, 1301–1315.

11. Voldman, J.; Gray, M. L.; Schmidt, M. a. Microfabrication in Biology and Medicine. *Annu. Rev. Biomed. Eng.* **1999**, *1*, 401–425.
12. Weibel, D. B.; Diluzio, W. R.; Whitesides, G. M. Microfabrication Meets Microbiology. *Nat. Rev. Microbiol.* **2007**, *5*, 209–218.
13. Wu, J.; Mao, Z.; Tan, H.; Han, L.; Ren, T; Gao, C. Gradient Biomaterials and Their Influences on Cell Migration. *Interface Focus* **2012**, *2*, 337–355.
14. Altomare, L.; Gadegaard, N.; Visai, L.; Tanzi, M. C.; Farè, S. Biodegradable Microgrooved Polymeric Surfaces Obtained by Photolithography for Skeletal Muscle Cell Orientation and Myotube Development. *Acta Biomater*. **2010**, *6*, 1948–1957.
15. Kim, D.-H.; Seo, C.-H.; Han, K.; Kwon, K. W.; Levchenko, A; Suh, K.-Y. Guided Cell Migration on Microtextured Substrates with Variable Local Density and Anisotropy. *Adv. Funct. Mater.* **2009**, *19*, 1579–1586.
16. Yang, J.; Rose, F. R. a. J.; Gadegaard, N.; Alexander, M. R. A High-Throughput Assay of Cell-Surface Interactions Using Topographical and Chemical Gradients. *Adv. Mater.* **2009**, *21*, 300–304.
17. Kolind, K.; Dolatshahi-Pirouz, A.; Lovmand, J.; Pedersen, F. S.; Foss, M; Besenbacher, F. A Combinatorial Screening of Human Fibroblast Responses on Micro-Structured Surfaces. *Biomaterials* **2010**, *31*, 9182–9191.
18. Kim, D.-H.; Han, K.; Gupta, K.; Kwon, K. W.; Suh, K.-Y; Levchenko, A. Mechanosensitivity of Fibroblast Cell Shape and Movement to Anisotropic Substratum Topography Gradients. *Biomaterials* **2009**, *30*, 5433–5444.
19. Lam, M. T.; Sim, S.; Zhu, X; Takayama, S. The Effect of Continuous Wavy Micropatterns on Silicone Substrates on the Alignment of Skeletal Muscle Myoblasts and Myotubes. *Biomaterials* **2006**, *27*, 4340–4347.
20. Dalby, M. J.; Riehle, M. O.; Yarwood, S. J.; Wilkinson, C. D..; Curtis, A. S. G. Nucleus Alignment and Cell Signaling in Fibroblasts: Response to a Micro-Grooved Topography. *Exp. Cell Res.* **2003**, *284*, 272–280.
21. Meyle, J.; Wolburg, H.; Von Recum, a. F. Surface Micromorphology and Cellular Interactions. *J. Biomater. Appl.* **1993**, *7*, 362–374.
22. Teixeira, A. I.; Abrams, G. a; Bertics, P. J.; Murphy, C. J.; Nealey, P. F. Epithelial Contact Guidance on Well-Defined Micro- and Nanostructured Substrates. *J. Cell Sci.* **2003**, *116*, 1881–1892.
23. Lensen, M. C.; Schulte, V. a.; Salber, J.; Diez, M.; Menges, F.; Möller, M. Cellular Responses to Novel, Micropatterned Biomaterials. *Pure Appl. Chem.* **2008**, *80*, 2479–2487.
24. Miller, C.; Jeftinija, S; Mallapragada, S. Micropatterned Schwann Cell-Seeded Biodegradable Polymer Substrates Significantly Enhance Neurite Alignment and Outgrowth. *Tissue Eng*. **2001**, *7*, 705–715.
25. Wójciak-Stothard, B.; Curtis, A. S. G.; Monaghan, W.; McGrath, M.; Sommer, I.; Wilkinson, C. D. Role of the Cytoskeleton in the Reaction of Fibroblasts to Multiple Grooved Substrata. *Cell Motil. Cytoskeleton* **1995**, *31*, 147–158.
26. Clark, P.; Connolly, P.; Curtis, A. S. G.; Dow, J. a; Wilkinson, C. D. Topographical Control of Cell Behaviour. I. Simple Step Cues. *Development* **1987**, *99*, 439–448.
27. Wójciak-Stothard, B.; Curtis, A. S. G.; Monaghan, W.; MacDonald, K; Wilkinson, C. Guidance and Activation of Murine Macrophages by Nanometric Scale Topography. *Exp. Cell Res.* **1996**, *223*, 426–435.
28. Clark, P.; Connolly, P.; Curtis, A. S. G.; Dow, J. a; Wilkinson, C. D. Cell Guidance by Ultrafine Topography in Vitro. *J. Cell Sci.* **1991**, *99 (Pt 1)*, 73–77.
29. Huang, N. F.; Patel, S.; Thakar, R. G.; Wu, J.; Hsiao, B. S.; Chu, B.; Lee, R. J; Li, S. Myotube Assembly on Nanofibrous and Micropatterned Polymers. *Nano Lett*. **2006**, *6*, 537–542.
30. Dalby, M. J.; Gadegaard, N.; Tare, R.; Andar, A.; Riehle, M. O.; Herzyk, P.; Wilkinson, C. D. W.; Oreffo, R. O. C. The Control of Human Mesenchymal Cell Differentiation Using Nanoscale Symmetry and Disorder. *Nat. Mater.* **2007**, *6*, 997–1003.
31. Csaderova, L.; Martines, E.; Seunarine, K.; Gadegaard, N.; Wilkinson, C. D. W.; Riehle, M. O. A Biodegradable and Biocompatible Regular Nanopattern for Large-Scale Selective Cell Growth. *Small* **2010**, *6*, 2755–2761.

32. Yim, E. K. F.; Darling, E. M.; Kulangara, K.; Guilak, F.; Leong, W. Nanotopography-Induced Changes in Focal Adhesions, Cytoskeletal Organization, and Mechanical Properties of Human Mesenchymal Stem Cells. *Biomaterials* **2011**, *31*, 1–16.
33. Mcmurray, R. J.; Gadegaard, N.; Tsimbouri, P. M.; Burgess, K. V; Mcnamara, L. E.; Tare, R.; Murawski, K.; Kingham, E.; Oreffo, R. O. C.; Dalby, M. J. Nanoscale Surfaces for the Long-Term Maintenance of Mesenchymal Stem Cell Phenotype and Multipotency. *Nat. Mater.* **2011**, 1–8.
34. Yim, E. K. F.; Reano, R. M.; Pang, S. W.; Yee, A. F.; Chen, C. S.; Leong, K. W. Nanopattern-Induced Changes in Morphology and Motility of Smooth Muscle Cells. *Biomaterials* **2005**, *26*, 5405–5413.
35. Yim, E. K. F.; Pang, S. W.; Leong, K. W. Synthetic Nanostructures Inducing Differentiation of Human Mesenchymal Stem Cells into Neuronal Lineage. *Exp. Cell Res.* **2007**, *313*, 1820–1829.
36. Gerecht, S.; Bettinger, C. J.; Zhang, Z.; Borenstein, J. T.; Vunjak-Novakovic, G; Langer, R. The Effect of Actin Disrupting Agents on Contact Guidance of Human Embryonic Stem Cells. *Biomaterials* **2007**, *28*, 4068–4077.
37. Rebollar, E.; Frischauf, I.; Olbrich, M.; Peterbauer, T.; Hering, S.; Preiner, J.; Hinterdorfer, P.; Romanin, C; Heitz, J. Proliferation of Aligned Mammalian Cells on Laser-Nanostructured Polystyrene. *Biomaterials* **2008**, *29*, 1796–1806.
38. Tzvetkova-Chevolleau, T.; Stéphanou, A.; Fuard, D.; Ohayon, J.; Schiavone, P; Tracqui, P. The Motility of Normal and Cancer Cells in Response to the Combined Influence of the Substrate Rigidity and Anisotropic Microstructure. *Biomaterials* **2008**, *29*, 1541–1551.
39. Reynolds, P.; Pedersen, R. H.; Stormonth-Darling, J.; Dalby, M. J.; Riehle, M. O.; Gadegaard, N. Label-Free Segmentation of Co-Cultured Cells on a Nanotopographical Gradient. *Nano Lett*. **2013**, *13*, 570–576.
40. Reynolds, P. M.; Pedersen, R. H.; Riehle, M. O; Gadegaard, N. A Dual Gradient Assay for the Parametric Analysis of Cell-Surface Interactions. *Small* **2012**, *8*, 2541–2547.
41. Unadkat, H. V; Hulsman, M.; Cornelissen, K.; Papenburg, B. J.; Truckenmüller, R. K.; Post, G. F.; Uetz, M.; Reinders, M. J. T.; Stamatialis, D.; van Blitterswijk, C. a; *et al*. An Algorithm-Based Topographical Biomaterials Library to Instruct Cell Fate. *Proc. Natl. Acad. Sci. U. S. A*. **2011**.
42. Gallant, N. D.; Lavery, K. a.; Amis, E. J.; Becker, M. L. Universal Gradient Substrates for "Click" Biofunctionalization. *Adv. Mater.* **2007**, *19*, 965–969.
43. Genzer, J.; Bhat, R. R. Classification of Key Attributes of Soft Material Gradients. In *Soft Matter Gradient Surfaces: Methods and Applications, First Edition*; 2012.
44. Genzer, J. Surface-Bound Gradients for Studies of Soft Materials Behavior. *Annu. Rev. Mater. Res.* **2012**, *42*, 435–468.
45. Alexander, M. R.; Whittle, J. D.; Barton, D.; Short, R. D. Plasma Polymer Chemical Gradients for Evaluation of Surface Reactivity: Epoxide Reaction with Carboxylic Acid Surface Groups. *J. Mater. Chem.* **2004**, *14*, 408.
46. Menzies, D. J.; Cowie, B.; Fong, C.; Forsythe, J. S.; Gengenbach, T. R.; Mclean, K. M.; Puskar, L.; Textor, M.; Thomsen, L.; Tobin, M.; *et al*. One-Step Method for Generating PEG-Like Plasma Polymer Gradients†¯: Chemical Characterization and Analysis of Protein Interactions. *Langmuir* **2010**, *252*, 13987–13994.
47. Lee, J. H.; Pazk, J. O. I. W.; Lee, H. B. Cell Adhesion and Growth on Polymer Surfaces with Hydroxyl Soups Prepared by Water Vapour Plasma Treatment. **1991**, *12*, 443–448.
48. Seo, H. S.; Ko, Y. M.; Shim, J. W.; Lim, Y. K.; Kook, J.-K.; Cho, D.-L.; Kim, B. H. Characterization of Bioactive RGD Peptide Immobilized onto Poly(acrylic Acid) Thin Films by Plasma Polymerization. *Appl. Surf. Sci.* **2010**, *257*, 596–602.
49. Roy, S.; Bhandaru, N.; Das, R.; Harikrishnan, G; Mukherjee, R. Thermally Tailored Gradient Topography Surface on Elastomeric Thin Films. *ACS Appl. Mater. Interfaces* **2014**.
50. Washburn, N. R.; Yamada, K. M.; Simon, C. G.; Kennedy, S. B.; Amis, E. J. High-Throughput Investigation of Osteoblast Response to Polymer Crystallinity†¯: Influence of Nanometer-Scale Roughness on. *Biomaterials* **2004**, *25*, 1215–1224.

51. Zhang, J.; Xue, L; Han, Y. Fabrication Gradient Surfaces by Changing Polystyrene Microsphere Topography. *Langmuir* **2005**, 5–8.
52. Bowen, A. M.; Ritchey, J. A.; Moore, J. S.; Nuzzo, R. G. Programmable Chemical Gradient Patterns by Soft Grayscale Lithography. *Small* **2011**, 3350–3362.
53. Almodóvar, J.; Crouzier, T.; Selimović, Š.; Boudou, T.; Khademhosseini, A; Picart, C. Gradients of Physical and Biochemical Cues on Polyelectrolyte Multilayer Films Generated via Microfluidics. *Lab Chip* **2013**, *13*, 1562–1570.
54. Gunawan, R. C.; Silvestre, J.; Gaskins, H. R.; Kenis, P. J. A.; Leckband, D. E. Cell Migration and Polarity on Microfabricated Gradients of Extracellular Matrix Proteins. *Langmuir* **2006**, *22*, 4250–4258.
55. Burdick, J. A.; Khademhosseini, A; Langer, R. Fabrication of Gradient Hydrogels Using a Microfluidics/ Photopolymerization Process. *Langmuir* **2004**, *20*, 8–11.
56. Julthongpiput, D.; Fasolka, M. J.; Zhang, W.; Nguyen, T.; Amis, E. J. Gradient Chemical Micropatterns: A Reference Substrate for Surface. *Nano Lett*. **2005**, *5*, 1535–1540.
57. Kreppenhofer, K.; Li, J.; Segura, R.; Popp, L.; Rossi, M.; Tzvetkova, P.; Luy, B.; Ka, C. J.; Guber, A. E.; Levkin, P. A. Formation of a Polymer Surface with a Gradient of Pore Size Using a Microfluidic Chip. *Langmuir* **2013**, *29*, 3797–3804.
58. Harding, F. J.; Clements, L. R.; Short, R. D.; Thissen, H.; Voelcker, N. H. Assessing Embryonic Stem Cell Response to Surface Chemistry Using Plasma Polymer Gradients. *Acta Biomater*. **2012**, *8*, 1739–1748.
59. Zelzer, M.; Majani, R.; Bradley, J. W.; Rose, F. R. a J.; Davies, M. C.; Alexander, M. R. Investigation of Cell-Surface Interactions Using Chemical Gradients Formed from Plasma Polymers. *Biomaterials* **2008**, *29*, 172–184.
60. Wells, N.; Baxter, M. a; Turnbull, J. E.; Murray, P.; Edgar, D.; Parry, K. L.; Steele, D. a; Short, R. D. The Geometric Control of E14 and R1 Mouse Embryonic Stem Cell Pluripotency by Plasma Polymer Surface Chemical Gradients. *Biomaterials* **2009**, *30*, 1066–1070.
61. Pitt, W. Fabrication of a Continuous Wettability Gradient by Radio Frequency Plasma Discharge. *J. Colloid Interface Sci*. **1989**, *133*, 223–227.
62. Kim, J.; Carbonell, R. G. Deposition of poly[2-(perfluorooctyl)ethyl Acrylate] from Liquid CO2 High-Pressure Free Meniscus coating—Uniformity and Morphology. *J. Supercrit. Fluids* **2007**, *42*, 129–141.
63. Ueda-yukoshi, T; Matsuda, T. Cellular Responses on a Wettability Gradient Surface with Continuous Variations in Surface Compositions of Carbonate and Hydroxyl Groups. **1995**, 4135–4140.
64. Xu, C.; Wu, T.; Mei, Y.; Drain, C. M.; Batteas, J. D.; Beers, K. L. Synthesis and Characterization of Tapered Copolymer Brushes via Surface-Initiated Atom Transfer Radical Copolymerization. **2005**, 11136–11140.
65. Kennedy, S. B.; Washburn, N. R.; Simon, C. G.; Amis, E. J. Combinatorial Screen of the Effect of Surface Energy on Fibronectin-Mediated Osteoblast Adhesion, Spreading and Proliferation. *Biomaterials* **2006**, *27*, 3817–3824.
66. Isenberg, B. C.; Dimilla, P. a; Walker, M.; Kim, S.; Wong, J. Y. Vascular Smooth Muscle Cell Durotaxis Depends on Substrate Stiffness Gradient Strength. *Biophys. J*. **2009**, *97*, 1313–1322.
67. Kuo, C.-H. R.; Xian, J.; Brenton, J. D.; Franze, K; Sivaniah, E. Complex Stiffness Gradient Substrates for Studying Mechanotactic Cell Migration. *Adv. Mater.* **2012**, *24*, 6059–6064.
68. Zelzer, D. I. M. Plasma Polymer Gradients, University of Nottingham, 2009.
69. Parry, K. L.; Shard, A. G.; Short, R. D.; White, R. G.; Whittle, J. D; Wright, A. ARXPS Characterisation of Plasma Polymerised Surface Chemical Gradients. *Surf. Interface Anal.* **2006**, 1497–1504.
70. Cantini, M.; Sousa, M.; Moratal, D. Non-Monotonic Cell Differentiation Pattern on Extreme Wettability Gradients. *Biomater. Sci.* **2013**, 202–212.
71. Yasuda, H; Gazicki, M. Biomedical Applications of Plasma Polymerization and Plasma Treatment of Polymer Surfaces. *Biomaterials* **1982**, *3*, 68–77.

72. Yasuda, H.; Hsu, T. Some Aspects of Plasma Polymerization Investigated by Pulsed R.F. Discharge. *J. Polym. Sci. Polym. Chem. Ed.* **1977**, *15*, 81–97.
73. Yasuda, H; Hirotsu, T. Critical Evaluation of Conditions of Plasma Polymerization. *J. Polym. Sci. Polym. Chem. Ed.* **1978**, *16*, 743–759.
74. Siow, K. S.; Britcher, L.; Kumar, S.; Griesser, H. J. Plasma Methods for the Generation of Chemically Reactive Surfaces for Biomolecule Immobilization and Cell Colonization—A Review. *Plasma Process. Polym.* **2006**, *3*, 392–418.
75. Van Os, M. T. Surface Modification by Plasma Polymerization: Film Deposition, Tailoring of Surface Properties and Biocompatibility, University of Twente.
76. Smith, T.; Kaelble, D. H.; Hamermesh, C. L. Surface Properties of Metals and Plastic Substrates and Properties of Plasma Polymerized Films on These Substrates Are Reported. *Surf. Sci.* **1978**, *76*, 203–231.
77. Friedrich, J.; Kühn, G.; Mix, R; Unger, W. Formation of Plasma Polymer Layers with Functional Groups of Different Type and Density at Polymer Surfaces and Their Interaction with Al Atoms. *Plasma Process. Polym.* **2004**, *1*, 28–50.
78. Bilek, M. M.; McKenzie, D. R. Plasma Modified Surfaces for Covalent Immobilization of Functional Biomolecules in the Absence of Chemical Linkers: Towards Better Biosensors and a New Generation of Medical Implants. *Biophys. Rev.* **2010**, *2*, 55–65.
79. Luo, W.; Yousaf, M. N. Tissue Morphing Control on Dynamic Gradient Surfaces. *J. Am. Chem. Soc.* **2011**, *133*, 10780–10783.
80. Comelles, J.; Hortiguela, V.; Samitier, J; Martines, E. Versatile Gradients of Covalently Bound Proteins on Microstructured Substrates. *Langmuir* **2012**, *28*, 13688–13697.
81. Chatterjee, K.; Young, M. F.; Simon, C. G. Fabricating Gradient Hydrogel Scaffolds for 3D Cell Culture. *Comb chem High Throughput Screen* **2011**, *14*, 227–236.
82. Mosadegh, B.; Agarwal, M.; Tavana, H.; Bersano-Begey, T.; Torisawa, Y.; Morell, M.; Wyatt, M. J.; O'Shea, K. S.; Barald, K. F; Takayama, S. Uniform Cell Seeding and Generation of Overlapping Gradient Profiles in a Multiplexed Microchamber Device with Normally-Closed Valves. *Lab Chip* **2010**, *10*, 2959–2964.
83. Curtis, A. S. G.; Wilkinson, C. Topographical Control of Cells. *Biomaterials* **1997**, *18*, 1573–1583.
84. Ashley, K. M.; Meredith, J. C.; Amis, E.; Raghavan, D.; Karim, A. Combinatorial Investigation of Dewetting: Polystyrene Thin Films on Gradient Hydrophilic Surfaces. *Polymer (Guildf)*. **2003**, *44*, 769–772.
85. Wong, J. Y.; Velasco, A.; Rajagopalan, P; Pham, Q. Directed Movement of Vascular Smooth Muscle Cells on Gradient-Compliant Hydrogels. **2003**, 1908–1913.
86. Berry, B. C.; Stafford, C. M.; Pandya, M.; Lucas, L. a; Karim, A.; Fasolka, M. J. Versatile Platform for Creating Gradient Combinatorial Libraries via Modulated Light Exposure. *Rev. Sci. Instrum.* **2007**, *78*, 072202.
87. Nakajima, M.; Ishimuro, T.; Kato, K.; Ko, I.; Hirata, I.; Arima, Y; Iwata, H. Combinatorial Protein Display for the Cell-Based Screening of Biomaterials That Direct Neural Stem Cell Differentiation. *Biomaterials* **2007**, *28*, 1048–1060.
88. Xu, F.; Wu, J.; Wang, S.; Durmus, N. G.; Gurkan, U. A.; Demirci, U. Microengineering Methods for Cell-Based Microarrays and High-Throughput Drug-Screening Applications. *Biofabrication* **2011**, *3*, 034101.
89. Khademhosseini, A.; Langer, R.; Borenstein, J.; Vacanti, J. P. Microscale Technologies for Tissue Engineering and Biology. *Proc. Natl. Acad. Sci. U. S. A*. **2006**, *103*, 2480–2487.
90. Alom Ruiz, S.; Chen, C. S. Microcontact Printing: A Tool to Pattern. *Soft Matter* **2007**, *3*, 168.
91. Zhou, X.; Hu, J.; Li, J.; Shi, J.; Chen, Y. Patterning of Two-Level Topographic Cues for Observation of Competitive Guidance of Cell Alignment. *ACS Appl. Mater. Interfaces* **2012**, *4*, 3888–3892.
92. Ferrari, A.; Cecchini, M.; Serresi, M.; Faraci, P.; Pisignano, D; Beltram, F. Neuronal Polarity Selection by Topography-Induced Focal Adhesion Control. *Biomaterials* **2010**, *31*, 4682–4694.

93. Altomare, L.; Riehle, M.; Gadegaard, N.; Tanzi, M. C.; Farè, S. Microcontact Printing of Fibronectin on a Biodegradable Polymeric Surface for Skeletal Muscle Cell Orientation. *Int. J. Artif. Organs* **2010**, *33*, 535–543.
94. Charest, J. L.; García, A. J.; King, W. P. Myoblast Alignment and Differentiation on Cell Culture Substrates with Microscale Topography and Model Chemistries. *Biomaterials* **2007**, *28*, 2202–2210.
95. Fraser, S. a; Ting, Y.-H.; Mallon, K. S.; Wendt, A. E.; Murphy, C. J.; Nealey, P. F. Sub-Micron and Nanoscale Feature Depth Modulates Alignment of Stromal Fibroblasts and Corneal Epithelial Cells in Serum-Rich and Serum-Free Media. *J. Biomed. Mater. Res. Part A* **2008**, *86*, 725–735.
96. Sun, J.; Ding, Y.; Lin, N. J.; Zhou, J.; Ro, H.; Soles, C. L.; Cicerone, M. T; Lin-gibson, S. Exploring Cellular Contact Guidance Using Gradient Nanogratings Jirun. *Biomacromolecules* **2010**, 3067–3072.
97. Pedersen, R. H.; Hamzah, M.; Thoms, S.; Roach, P.; Alexander, M. R; Gadegaard, N. Electron Beam Lithography Using Plasma Polymerized Hexane as Resist. *Microelectron. Eng.* **2010**, *87*, 1112–1114.
98. Ramalingam, M.; Young, M. F.; Thomas, V.; Limin, S.; Chow, L. C.; Miles, W. C.; Simon, C. G. Nanofiber Scaffold Gradients for Interfacial Tissue Engineering Murugan. *J Biomater Appl* **2013**, *27*, 695–705.
99. Dalby, M. J.; Riehle, M. O.; Johnstone, H. J. H.; Affrossman, S.; Curtis, A. S. G. Nonadhesive Nanotopography: Fibroblast Response to Poly(n-Butyl Methacrylate)-Poly(styrene) Demixed Surface Features. *J. Biomed. Mater. Res. A* **2003**, *67*, 1025–1032.
100. Dalby, M. J.; Giannaras, D.; Riehle, M. O.; Gadegaard, N.; Affrossman, S.; Curtis, A. S. G. Rapid Fibroblast Adhesion to 27 nm High Polymer Demixed Nano-Topography. *Biomaterials* **2004**, *25*, 77–83.
101. Kunzler, T. P.; Drobek, T.; Schuler, M.; Spencer, N. D. Systematic Study of Osteoblast and Fibroblast Response to Roughness by Means of Surface-Morphology Gradients. *Biomaterials* **2007**, *28*, 2175–2182.
102. Engler, A. J.; Sen, S.; Sweeney, H. L.; Discher, D. E. Matrix Elasticity Directs Stem Cell Lineage Specification. *Cell* **2006**, *126*, 677–689.
103. Pelham, R. J; Wang, Y.-L. Cell Locomotion and Focal Adhesions Are Regulated by Substrate Flexibility. *Proc. Natl. Acad. Sci.* **1997**, *94*.
104. Lo, C.; Wang, H.; Dembo, M; Wang, Y. Cell Movement Is Guided by the Rigidity of the Substrate. *Biophys. J.* **2000**, *79*, 144–152.
105. Fu, J.; Wang, Y.; Yang, M. T.; Desai, R. A.; Yu, X.; Liu, Z.; Chen, C. S. Mechanical Regulation of Cell Function with Geometrically Modulated Elastomeric Substrates. *Nat. Publ. Gr.* **2010**, *7*, 733–736.
106. Seidi, A.; Ramalingam, M.; Elloumi-Hannachi, I.; Ostrovidov, S.; Khademhosseini, A. Gradient Biomaterials for Soft-to-Hard Interface Tissue Engineering. *Acta Biomater*. **2011**, *7*, 1441–1451.
107. Tse, J. R.; Engler, A. J. Stiffness Gradients Mimicking in Vivo Tissue Variation Regulate Mesenchymal Stem Cell Fate. *PLoS One* **2011**, *6*, e15978.
108. Vincent, L. G.; Choi, Y. S.; Alonso-Latorre, B.; Del Álamo, J. C.; Engler, A. J. Mesenchymal Stem Cell Durotaxis Depends on Substrate Stiffness Gradient Strength. *Biotechnol. J.* **2013**, *8*, 472–484.
109. Mangindaan, D.; Kuo, W.; Wang, M. Two-Dimensional Amine-Functionality Gradient by Plasma Polymerization. *Biochem. Eng. J.* **2013**, *78*, 198–204.
110. Basarir, F.; Cuong, N.; Song, W.-K; Yoon, T.-H. Surface Modification via Plasma Polymerization of Allylamine for Antibody Immobilization. *Macromol. Symp.* **2007**, *249–250*, 61–66.
111. Bhat, B. R. R.; Chaney, B. N.; Rowley, J.; Liebmann-vinson, A; Genzer, J. Tailoring Cell Adhesion Using Surface-Grafted Polymer Gradient Assemblies. *Adv. Mater.* **2005**, *17*, 2802–2807.

112. Lagunas, A.; Comelles, J.; Martı, E; Samitier, J. Universal Chemical Gradient Platforms Using Poly (Methyl Methacrylate) Based on the Biotin—Streptavidin Interaction for Biological Applications. *Langmuir* **2010**, *26*, 14154–14161.
113. Mangindaan, D.; Kuo, W.; Wang, Y; Wang, M. Experimental and Numerical Modeling of the Controllable Wettability Gradient on Poly (Propylene) Created by SF 6 Plasma. *Plasma Process. Polym.* **2010**, *7*, 754–765.
114. Whittle, J. D.; Barton, D.; Alexander, R.; Short, R. D.; Robert, S.; Building, H.; Street, M; Uk, S. A Method for the Deposition of Controllable Chemical Gradients †. *Chem. Commun. (Camb)*. **2003**, 1766–1767.
115. Zelzer, M.; Alexander, M. R.; Russell, N. A. Acta Biomaterialia Hippocampal Cell Response to Substrates with Surface Chemistry Gradients. *Acta Biomater*. **2011**, *7*, 4120–4130.
116. Menzies, D. J.; Jasieniak, M.; Griesser, H. J.; Forsythe, J. S.; Johnson, G.; Mcfarland, G. A.; Muir, B. W. A ToF-SIMS and XPS Study of Protein Adsorption and Cell Attachment across PEG-like Plasma Polymer Fi Lms with Lateral Compositional Gradients. *Surf. Sci.* **2012**, *606*, 1798–1807.
117. Eidelman, N.; Simon, C. G. Blend Composition Gradients by FTIR Microspectroscopy. **2004**, *109*, 219–231.
118. l'Abee, R.; Li, W.; Goossens, H; van Duin, M. Application of FTIR Microscopy in Combinatorial Experimentation on Polymer Blends. *Macromol. Symp.* **2008**, *265*, 281–289.

# Chapter 6
# Polymer Replication Techniques

**John M. Stormonth-Darling, Rasmus H. Pedersen and Nikolaj Gadegaard**

## 6.1 Rationale for Replication

### *6.1.1 Background*

Direct nanopatterning of surfaces using lithographic methods, such as electron beam lithography (EBL) or photolithography, allows unique structures to be defined in a methodical, step-by-step manner that delivers fantastically high-quality results that cannot be obtained by any other means, but is generally unsuitable for mass production or requires substantial infrastructure and financial investment to make it suitable as is the case with optical lithography in the microelectronics industry. A more economical route to create large number of nanostructured devices lies in replication-based technology where a single master may give birth to many clones of itself, eliminating the need to repeat an entire fabrication process. These methods are gaining increasing interest where the resolution limit of optical lithography makes it harder to form the ever smaller structures that are desired [1] and in other emerging application areas that also require nanoscale patterns, but do not have the volume required for the investment in advanced conventional systems. Examples of such applications include substrates for biochemical research such as cell growth, advanced lab-on-a-chip devices, integrated nanophotonic devices and hard disk storage devices. Developments in polymer-based replication technology have also been extensive for applications where conventional fabrication techniques [2] are not well suited such as flexible display systems.

N. Gadegaard (✉) · J. M. Stormonth-Darling · R. H. Pedersen
Division of Biomedical Engineering, School of Engineering,
University of Glasgow, Glasgow, UK
e-mail: Nikolaj.Gadegaard@glasgow.ac.uk

J. M. Stormonth-Darling
e-mail: John.Stormonth-Darling@glasgow.ac.uk



J. Rodríguez-Hernández, A. L. Cortajarena (eds.), *Design of Polymeric Platforms for Selective Biorecognition,* DOI 10.1007/978-3-319-17061-9_6

#### 6.1.1.1 Replication-Based Nanopatterning Techniques

A common type of material used in replication-based fabrication at all length scales is thermoplastic polymers, also known as thermoplasts. Thermoplasts are a class of polymer that are characterised by their reversible temperature-dependant physical characteristics; they may be melted and frozen repeatedly without chemical alteration of their constituent molecular chains. This behaviour is in contrast to thermosetting plastics and other curable materials which form cross-links between their molecular chains when energy is applied by, for example, heat or UV radiation. Thermoplastics can be classified as amorphous (random molecular structure) or semicrystalline (molecules are ordered in a crystalline manner) polymers, or thermoplastic elastomers (rubbery, elastic polymers).

Above its glass transition temperature ($T_g$), an amorphous thermoplastic will move from its solid state to a more malleable one, increasing in malleability until it reaches its melting temperature ($T_m$) when it behaves as a liquid. This easily controlled phase change and the fact that they retain their original characteristics upon refreezing have seen thermoplastic polymers being used in the manufacture of countless products and devices where they are formed into a functional shape by a mould-based process such as thermoforming or injection moulding. Thermoplastic polymers are already ubiquitous in their use as tissue culture labware and may be shaped and patterned in a variety of ways to add more functionality to this already well-defined platform.

A large group of replication-based techniques falls under the banner of nanoimprint lithography [3, 4] (NIL) which, in the case of thermal NIL (T-NIL), is similar to another process known as hot embossing. These processes differ somewhat on a practical and conceptual level, with the former as a lithography (pattern transfer for further processing) technique and the latter as a method of direct patterning into a bulk polymer substrate, and therefore not concerned with the uniformity of residual layers which must be removed to facilitate further pattern transfer. Embossing and NIL processes are parallel by their nature and differ from traditional lithographic processes in that the pattern transfer is mediated by a physical deformation rather than a purely chemical change requiring subsequent development. NIL was first developed by Chou et al. in 1995 [5] and was quite remarkable; from the outset it demonstrated successful replication of 25-nm structures, a figure that was only limited by the patterns on the stamp. Since then, the resolution of NIL has been repeatedly demonstrated to be limited only by the structure of the stamp, the polymer faithfully replicating stamp features even in the sub 10-nm range [6, 7]. In a typical NIL process, a master stamp, previously fabricated by other methods such as photolithography and etching, is brought into contact with the polymer which has been heated above its $T_g$ (this is the case for amorphous polymers, crystalline polymers are characterised by their $T_m$). As pressure is applied, the polymer flows and adopts the physical form imposed by the stamp and after sufficient time the assembly may be cooled and separated, leaving the inverse pattern of the stamp embedded in the polymeric material. This embossed structure may be used as a functional component of further fabrication steps (e.g. as an etch mask) or may itself form a structural

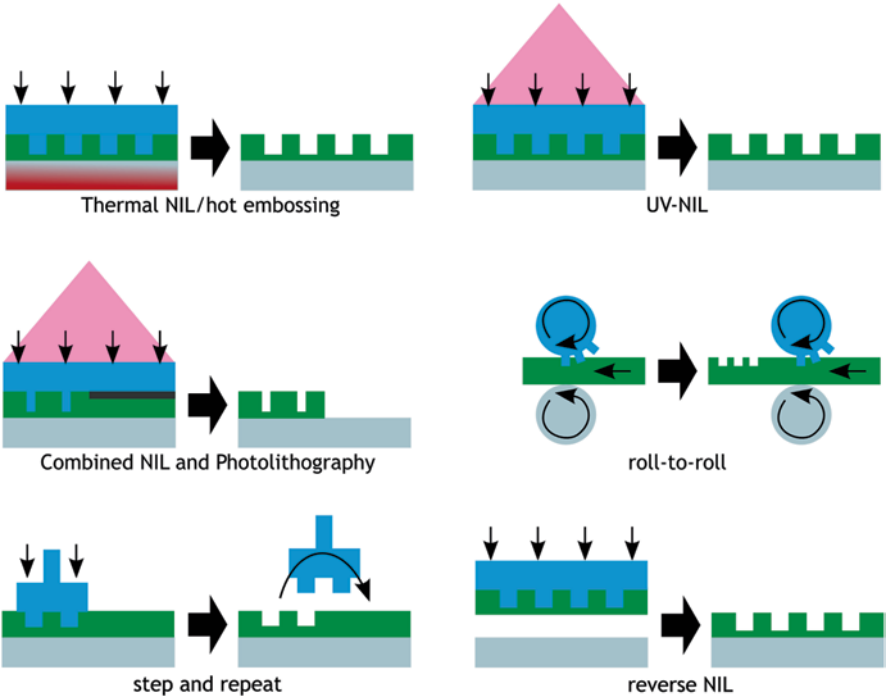


**Fig. 6.1** Illustrations of variations of NIL. Each image shows stamp (*blue*) and substrate (*grey*) position during (*left*) and after (*right*) the imprint. The imprint material is shown as *green*, UV light as *pink* and heat as *red*. *Thin arrows* indicate movement or applied imprint pressure and the *black strip* in the CNP image indicates an opaque region of the nanopatterned photomask/stamp

component of the final outcome. In the former case (which defines the process as a form of lithography, rather than simply embossing), a thin *residual layer* will remain in the area of the substrate that was imprinted, since the polymer cannot fully be displaced from underneath the protrusion. Since the residual layer must be removed in order to gain access to the substrate below, the thickness and uniformity of this layer is a crucial parameter in determining the quality of an achieved imprint. If the uniformity is too low, it will decrease the fidelity of any final pattern due to overetching and may cause device failure. Over the years, several variations of NIL have been developed which are summarised in the text below and schematically depicted in Fig. 6.1.

**Thermal NIL** This technique was used in the first demonstration of nanoimprint by Chou [5]. The resist is a thermoplast, which is a material that behaves similar to a high-viscosity liquid when heated above $T_g$. Thus, imprint is performed by coating a substrate with resist, heating the said substrate above the glass transition and performing the imprint. After completing the imprint, the resist is cooled to below $T_g$, whereby it solidifies, and a stable structure remains after separation. Drawbacks of the T-NIL technique compared to other options include the need of thermal cycling

of the material to possibly high temperatures, and the relatively low throughput that is obtained as a result. Advantages include process simplicity, as well as very relaxed demands on the materials used (stamp, resist, as well as substrate), which opens many options to develop a fabrication process for any given application. T-NIL is covered in more detail as the focus of Sect. 6.2 of this chapter.

**UV-NIL** In UV-nanoimprint [8], the resist is a photosensitive polymer that is initially soft but solidifies when exposed to UV radiation. Thus, replacing the thermal cycling by UV radiation will provide the same end result. Instead of spin coating the resist, it is also possible to use a very low viscosity material (e.g. a monomer) which is dispensed on the substrate immediately before the imprint, with the UV irradiation initiating the polymerisation process [9]. A major drawback of UV-NIL is material restrictions—either stamp or substrate must be UV transparent, and the choice of UV-sensitive materials is not as varied as that of thermoplasts, a fact which may influence postprocessing options by requiring an additional transfer layer. A major advantage is the increase of throughput due to the omission of a thermal cycle.

**Combined Nanoimprint and Photolithography (CNP)** Imprint quality often suffers when attempting to imprint large structures, especially if large and small structures are in close vicinity to each other. In the CNP process, only the nm-scale features, which cannot be fabricated by photolithography, are fabricated on the mould as protrusions. Larger features are created on the transparent mould as an opaque chromium layer. Thereby, in the imprint process, the nm-scale features are transferred by imprint, while the large features are defined in a normal lithography process before separating the wafers [10]. The advantage of this method is the capability of forming high-quality complex patterns in a single step, while the drawbacks include a complicated mould fabrication and a very limited choice of resist materials.

**Step and Repeat** Some modern photolithography systems are steppers, where the mask only contains information about a single die, which can then be transferred sequentially across the substrate surface. The same concept can be applied for nanoimprint, with the stamp being imprinted sequentially over the surface of the substrate. A special case for UV-NIL, has been dubbed step-and-flash imprint lithography (SFIL), whereby a liquid monomer (resist) is dispensed on the substrate prior to each imprint step [9], while the thermal imprint variation is denoted step-and-stamp imprint lithography (SSIL) [11]. The main advantage is the possibility of patterning a full substrate surface with only a small stamp (drastically reducing the cost of stamp fabrication), while the disadvantages include the limitations on device design size and throughput decrease due to the requirement of a large amount of imprints to cover the substrate.

**Roll-to-Roll** Roll-to-roll (R2R) imprint is similar to newspaper printing. Instead of a planar process, the stamp is coated on a cylindrical roller, and the substrate is a flexible plastic film or web. The imprint occurs by rolling the plastic web between the stamp roll and a backside fixation roll. R2R imprint has been demonstrated in thermal [12] as well as UV variations [13]. The main advantage of the technique

is the very high throughput that can be achieved, while a drawback is the severe limitations placed on the stamp and substrate. There are many variations of R2R systems, as well as similar techniques such as sheet-to-sheet and roll-to-plate [14]. These have demonstrated a great deal of success in the patterning of thin polymer films for emerging applications, including lab-on-chip [15], flexible electronics [16] and those requiring large area patterning such as solar photovoltaics [17].

**Reverse NIL** In reverse nanoimprint [18], the stamp is coated with resist prior to the imprint, not the substrate. Otherwise the process is identical to standard imprint. The point of this process is that it enables imprint on a prepatterned substrate, thereby enabling construction of multilayer, 3D structures by successive imprint cycles—something that all other imprint variations cannot produce.

Other replication techniques that operate on a moulding basis include thermoforming, injection moulding and polymer casting. Thermoforming is a thermoplastic processing technique that is used in industrial high-throughput manufacturing above the microscale, and is also capable of producing micro- and nanostructures over curved surfaces by patterning a thin film before heating and pulling it over a larger structure [19, 20]. Injection moulding is a very well-established industrial process that is attracting more and more attention as a mass production nanofabrication solution due to its unparalleled level of throughput and industrial heritage [21, 22]. By forcing hot polymer into a cold mould at high pressure, the injection moulding process eliminates the slow thermal cycling associated with T-NIL and hot embossing and can fabricate nanopatterned parts in a matter of seconds. Injection moulding of micro- and nanostructures is a growing area with great potential and, as such, is the focus of the second half of this chapter.

Casting polymers, such as polydimethylsiloxane (PDMS), are not thermoplastic and take their form in a curing process which can take several hours. PDMS has somewhat customisable elastic properties and is a ubiquitous prototyping material for microstructured devices owing to its intrinsic ease of processing and finds particularly frequent use in the field of microfluidics [23]. In addition to these, the term “soft lithography” describes a family of techniques concerned with patterning *on* the surface rather than *in* it. Microcontact printing is a popular soft lithographic technique where a patterned solid stamp is coated in the printing material before being pressed against another sample to which the material, in the shape of the pattern, is transferred. It has found a great deal of use in patterning functional surfaces for studying cell–substrate interactions [24, 25].

Replication-based fabrication techniques are advantageous, owing to their simplicity, low cost and speed compared to direct patterning processes. When used lithographically (e.g. NIL), they can replace costly techniques like EBL and address the resolution limits of photolithographic patterning too. Polymer replication techniques like hot embossing and injection moulding specialise in the production of monolithic parts that can be of use in optical and microfluidic applications, and the fact that they can be applied to many different materials makes them highly applicable to the patterning of materials for tissue engineering applications, both clinically and in continuing biological research [26].

## 6.2 Hot Embossing and Nanoimprint Lithography

### *6.2.1 Introduction*

This section is concerned with a closer look at T-NIL and, by extension, hot embossing. Essentially they are identical techniques, except the fact that T-NIL is concerned with the facilitation of further processing which is dependent upon the pattern which it defines. This additional requirement means that the residual layer of imprinted material that remains at the former location of stamp protrusions is of some concern in terms of the minimisation of its thickness and the maximisation of its uniformity. This section will not, however, dwell extensively on these differentiating matters.

The section begins with an introduction to polymer physics, explaining the polymer flow beneath the imprint protrusion, before material choices and commercial T-NIL equipment are discussed. Finally, some of the important practical issues to consider when performing T-NIL/embossing are presented. For further background information, the reader is referred to review articles [3, 27] and book chapters [28, 29].

### *6.2.2 Polymer Physics*

In order to understand the thermal nanoimprint process, an overview of simple polymer physics should be given. As already discussed, thermal nanoimprint relies on the deformation of a thermoplastic polymer above the glass transition. When the thermoplast is heated to immediately above the glass transition, it becomes soft, and the storage modulus decreases by several orders of magnitude. In this region, the behaviour is a mixture between viscous flow and elastic deformation. The polymer is said to be in a rubbery state. Heating the polymer further, a flow regime is entered, where the elastic response diminishes, and the storage modules decreases even further. This is known as the flow region. For this reason, imprint is often performed at temperatures 50–80 ° above the glass transition, ensuring that the flow regime is reached.

The most important polymer parameter influencing the flow is the zero-shear viscosity of a polymer above the glass transition, determined by the Williams–Landel–Ferry (WLF) equation:

$$\eta_0(T) = \eta_0(T) e^{\left(\frac{C_1(T-T_0)}{C_2+T-T_0}\right)}, \tag{6.1}$$

where $T_0$ and $\eta_0 T_0$ are the reference temperature and the zero-shear viscosity at the reference, respectively. $C_1$ and $C_2$ are fitting parameters. The polymer viscosity is also influenced by the molecular weight of the polymer, i.e. the chain length. Below a certain critical molecular weight, the viscosity is found to be directly proportional

to the molecular weight. Above the critical point, $\eta_0$ follows a power law, with the exponent almost identical for most common polymers. Thus,

$$\eta_0 \propto \begin{cases} M_\omega & , M_\omega < M_c \\ M_\omega^{3.4\pm0.2} & , M_\omega > M_c \end{cases}. \tag{6.2}$$

Polymer viscosity can vary rapidly in response to temperature change. For example, polymethyl methacrylate (PMMA), a thermoplast commonly used in T-NIL, hot embossing and injection moulding, will exhibit a tenfold change in viscosity for a 20 K change in temperature [28].

The polymer flow behaviour is further complicated by an effect known as *shear thinning*. When a shearing force is applied to a polymer sample, the observed viscosity is found to vary, decreasing with the power law above a certain critical shear rate:

$$\eta(\dot{\gamma}) = \begin{cases} \eta_0 & , \dot{\gamma} < \dot{\gamma}_0 \\ \eta_0 \left( \dfrac{\dot{\gamma}}{\dot{\gamma}_0} \right)^{(1-k)/k} & , \dot{\gamma} > \dot{\gamma}_0 \end{cases}. \tag{6.3}$$

This is a non-Newtonian effect that will often occur in imprint situations. However, it is difficult to incorporate in complex flow models, and most imprint simulation efforts treat the imprint polymer as Newtonian.

To evaluate a proposed imprint process, a model of the required time to imprint a feature of a given size would be desirable. This problem, the sinking of a rigid plate in a liquid of a given viscosity, was first considered by M. J. Stefan as early as 1874 [30]. (Stefan actually considered the inverse situation, but the end result is the same.) In essence, the amount of volume under the imprint feature decreases over time as the feature is lowered. The lost volume must flow out through the available edge area. The situation is shown in Fig. 6.2. The sinking is determined by the applied pressure and surface area of the protrusion, while the flow velocity is dependent on the surface area and the polymer viscosity. Both also depend on the initial amount of polymer present under the protrusion. By balancing these two effects, an equation relating the imprint time with the polymer height can be found, assuming the Newtonian, steady-state flow of an incompressible fluid. For a circular protrusion of radius $R$, the result is

$$t = \frac{3\pi\eta_0 R^4}{4F}\left( \frac{1}{h(t)^2} - \frac{1}{h_0^2} \right), \tag{6.4}$$

whereas for rectangular protrusions, provided the length $L$ is much larger than the width $s$, one finds:

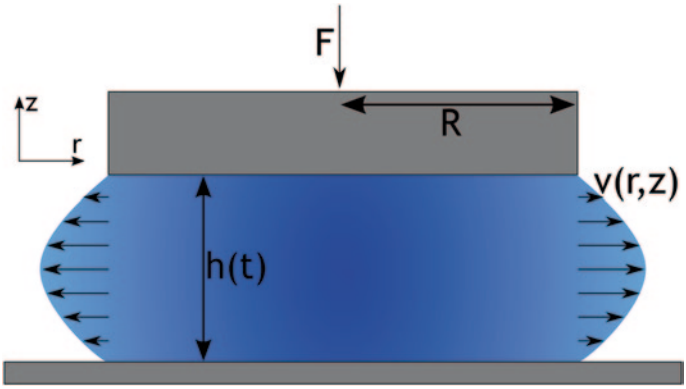


**Fig. 6.2** Polymer flow under an imprint protrusion as described by the Stefan equation

$$t = \frac{\eta_0 L s^4}{2F}\left(\frac{1}{h(t)^2} - \frac{1}{h_0^2}\right). \tag{6.5}$$

In these equations, $F$ is the force applied to the protrusion, $h_0$ is the initial thickness of the polymer and $h(t)$ is the polymer thickness after the given time $t$. Both these equations are referred to as the *Stefan equation*, with the actual meaning easily inferred by context. Of obvious interest is the determination of the time required to complete the imprint, i.e. the time needed until the imprint cavities are filled. This information is not readily available in the Stefan equation, since no information regarding the protrusion height $h_{pr}$ is included (essentially, the derivation assumes $h_{pr} >> R$). However, if the imprint polymer is assumed to be incompressible, a simple mass conservation consideration will provide the answer. Consider a pattern with a total protruding area $A_p$, and the total stamp area $A$. The amount of polymer before initiating the imprint ($h_0$) can then be equated to the amount of polymer after completing the imprint ($h_f$) as:

$$h_0 A = h_f A + h_{pr}(A - A_p) \Leftrightarrow \tag{6.6}$$

$$h_f = h_0 - h_{pr}(1 - v),\ v = \frac{A_p}{A}, \tag{6.7}$$

where the parameter $v$, the *protrusion coverage*, a measure of the density of structures, is introduced. If the protrusion coverage is below 0.5, the stamp is said to be *positive*, otherwise it is *negative*. Equation (6.7) can now be combined with the Stefan equation (Eq. (6.4) or (6.5)) to provide the time to complete the imprint, $t_f$.

When performing such an evaluation, it is important to remember that the force entering the Stefan equation is the force on one individual protrusion. This can

be calculated from the pressure or force provided to the backside of the stamp as (the subscript *p* denotes all protrusions, while the subscript *pr* denotes one single protrusion):

$$F_{pr} = p_{total} A_{pr} = \frac{F_{ext}}{A_p} A_{pr} = F_{ext} \frac{A_{pr}}{vA}. \tag{6.8}$$

Considering the Stefan equation, the most important parameters determining the imprint time are clearly identified as the protrusion size and the temperature (remember from Eq. (6.1), the viscosity varies strongly with temperature), but since the feature size will often be dictated by the device to be fabricated, temperature seems the most important parameter, with the force a secondary concern. When creating models using these equations to predict imprint time, the reality may be rather different from the theoretical results obtained. It is not uncommon for a model to predict imprint time to be a fraction of a second, but for a successful imprint to require several minutes in reality. This discrepancy is primarily attributed to the failure of Eq. (6.8) to accurately predict the protrusion pressure, and due to the design not being homogeneously structured with the given protrusion coverage.

## *6.2.3 Materials and Equipment*

In this section, a discussion on the materials used in hot embossing and T-NIL is given, both regarding the stamp and the resist.

### 6.2.3.1 Stamp Materials

The choice of the stamp material will depend on several factors including cost, available fabrication facilities, the choice of imprint material and substrate, as well as other factors specific to a particular situation. Generally, the requirements of the stamp material are:

- sufficient hardness not to deform during the imprint process,
- possibility of attaching an antistiction layer to the surface and
- limited thermal mismatch to the imprint substrate.

By far, the most widely used materials are silicon and silicon dioxide. These materials are used due to the vast experience in structuring them by conventional methods, and compatibility with the existing equipment and processes. In addition, since the substrates are also usually silicon or glass, no significant thermal mismatch is incurred. The most popular alternative stamp material is nickel, due to the existing standard replication techniques with this material, e.g. LIGA (in German: *lithographie, galvanik und abformung* meaning lithography, electroplating and moulding). More exotic stamp materials, such as silicon carbide [31] or diamond [32], have

also been used. The main advantage of these materials is even greater hardness than silicon or quartz; however, this comes at the cost of a more involved stamp fabrication process. A recent development is the use of a polymer–ceramic composite material [33]. This material, which can be directly structured in an imprint process, can, for example, be used as an intermediate stamp, or daughter mould, thereby reducing the strain on an expensive master stamp, or simply serving to inverse the polarity of the final structure.

#### 6.2.3.2 Antistiction

A common feature of the replication-based micro- and nanofabrication is the use of nonadhesive surface coatings to aid both the filling of moulds and the subsequent demoulding of the replica [34–36]. The possibility of successful release is determined not only by the presence and quality of an antistiction layer but also by the total contact area, i.e. the density and the depth of the imprint features, and by the surface energy of the imprint polymer. Thus, for low-density patterns imprinted in low-surface energy polymers, successful release can be possible even without antistiction coatings; however, this is rare. In most processes, antistiction is required. In addition, in spite of the antistiction layer, the stamp and substrate must be forcefully separated by the insertion of a sharp blade between the wafers. There are two typical failure modes. First, part of the imprinted pattern may be ripped off the substrate and remain on the stamp. In such cases, simply cleaning the stamp and reapplying the antistiction coating is possible. Second, if the surface energy is much too high, the forceful insertion of a blade may cause catastrophic fracture of the stamp and/or substrate. As stamps can often be very expensive to produce, this must of course be avoided, and a high-quality antistiction layer is essential in most nanoimprint processes.

In the NIL or embossing process, nonadhesive coatings can greatly improve results through the reduction of surface energies and resulting interfacial friction that occurs at the critical moment when the master and replica are separated [37]. These forces, which are amplified at higher aspect ratios, can lead to the structural failure of features on both the master and moulded or imprinted product [38]. Fluorosilanes are a popular choice when it comes to antistiction coatings, as they readily form a thin monolayer on silicon-containing substrates (e.g. silicon, quartz, glass and PDMS) and provide a low energy surface [4, 39, 40]. An example of such a material is perfluorodecyltrichlorosilane (FDTS or F-TCS). This chemical molecule consists of a long fluorocarbon chain terminated at one end by a silicon–chlorine end group. When this chemical is introduced in gaseous form to a hydroxylated surface, it covalently bonds to the surface under release of hydrochloric acid gas. In this process, a monolayer surface is formed, chemically bonded to the stamp surface to provide a stable process. Although primarily used for silicon and quartz, it has also been used successfully to improve the release properties of NiO, TiO [34], polyimide [41] and SU-8 moulds [42]. It has also been shown that the introduction of nitrides to fluorocarbons can enhance the durability of nonadhesive coatings [43].

Much of the characterisation of nonadhesive surfaces is performed by water contact angle (WCA) analysis. Measurements of WCAs (or indeed the contact angle made by a drop of any liquid) on surfaces can be an indicator of surface energy and, therefore, replication performance; although any nonplanar micro- or nanoscale surface topography will have a significant effect on the measurement. On a planar surface, a high WCA indicates a low energy which will decrease the potentially damaging forces experienced during separation, and a low angle implies a strong wetting ability which is beneficial to the initial filling of structures. This implies that a good replication surface will display a convenient medium between these two extremes that will depend on physical conditions such as the pattern geometry, viscosity of the replication material and available materials and processes [44].

#### 6.2.3.3 Nanoimprint Materials

There are essentially three classes of imprint materials:

*Conventional thermoplasts* are known thermoplastic polymers, used for decades in thermal-based polymer forming such as injection moulding or hot embossing [45]. Examples are PMMA, polycarbonate (PC), polystyrene (PS) and cyclic olefin copolymer (COC). Such materials are often selected for their ability to dissolve easily in a common solvent (and thus achieve a homogeneous spin-coated thin film), and due to their $T_g$, which is neither too low, leading to unstable structures, nor too high, leading to excessive processing time. The mentioned polymers have approximate $T_g$ of 105 ° (PMMA) [46], 100 ° (PS) [47] and 145 ° (PC) [48], while COCs can be produced in a range of types with $T_g$ as diverse as 80 ° and 180 ° [49]. PMMA has the added advantage of being well known as an EBL resist and is thus already a standard material in many fabrication facilities, and COC attracts particular attention for microfluidic and optical applications due to its chemical resistance and UV transparency.

*Custom-designed resists* are materials developed purely for their use as nanoimprint resists. The common thermoplasts mentioned above are not optimised for thermal nanoimprint. Specific parameters that could be improved are glass transition temperate (should be lower), viscosity at the flow temperature (should be lower) and resistance to dry plasma etching (should be higher). In Europe, the company micro resist technology GmbH, Germany, has been at the forefront of this development, and a wide variety of nanoimprint resists are available. Other suppliers in the market include Tokyo Ohka Kogyo, Japan [50] and Nanonex, USA [51]. In addition, some research labs have used in-house developed resist materials [52, 53].

*Device-specific polymers* are materials selected not due to their properties as pertaining to the imprint situation itself but rather due to the use of the imprinted pattern directly as a part of the final device. A common example is the negative photoresist SU-8, a widely used material in the fabrication of microfluidic systems [54], and also commonly used for on-chip solid-state dye lasers [55].

#### 6.2.3.4 Commercially Available Equipment

The thermal imprint process, at its heart, is relatively simple. Two wafers must be heated up and pressed together. This process should possibly take place in an evacuated atmosphere to avoid air becoming trapped between the two wafers. These requirements are very similar to the requirements in a wafer bonding process, and therefore many commercial machines are simply slightly modified wafer bonders. Many imprint equipment manufacturers offer a range of products with varying feature sets, such as possible substrate sizes and varying degree of automation (e.g. robotic wafer handling). A common feature is that the equipment is also large and bulky, requiring a large amount of space in the laboratory, and complicated installations.

There are a wide range of equipment suppliers in the worldwide market [51, 56–61]. Many of these offer both thermal and UV imprint, with a few options also available for stepper-based imprint. Despite this variation in supply, the method of operation is very similar. The heat for the process is supplied by conduction from metal chucks. This method, while effective and easy to control, is also quite time-consuming, since the thermal mass is high. The pressure is supplied to the stamp by a piston (with some exceptions). This method will often lead to inhomogeneity in the applied pressure due to the piston and the stamp not being completely flat or parallel. See below for a more detailed description of the pressure application process.

### *6.2.4 Practical Process Considerations*

#### 6.2.4.1 Polymer Flow—the Filling of Cavities

When the polymer flows from underneath the imprint feature and into the polymer cavity, it will generally not immediately proceed to flow laterally further into the cavity. Instead, it will climb the walls of the imprint feature and only proceed laterally when the cavity ceiling is reached. This process is described extensively in the literature [28, 62–64]. The mechanics of cavity filling may not be of relevance to the end result, provided the cavities are completely filled. However in many real cases, the cavities may not be completely filled, either intentionally due to a desire to minimise residual layer thickness or as a side effect of a varying protrusion coverage. In these cases, one must be aware that the resulting polymer profile will not be simple depressions in an essentially uniform film, which may complicate the post-imprint process.

Another effect is occasionally observed in large unstructured areas, or in cavities where the polymer flow was not quite enough to completely fill the cavity. Some examples are shown in Fig. 6.3. This effect, dubbed *viscous fingering*, or *flower-like structures*, is caused by pressure instabilities in the polymer, and may be related to the trapping of air in the resist [63, 65].

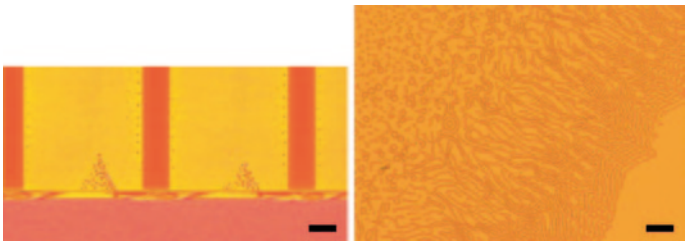

**Fig. 6.3** Illustration of the viscous fingering effect in an almost-filled cavity (*left*) and large unstructured areas (*right*). Scale bars represent 25 µm.

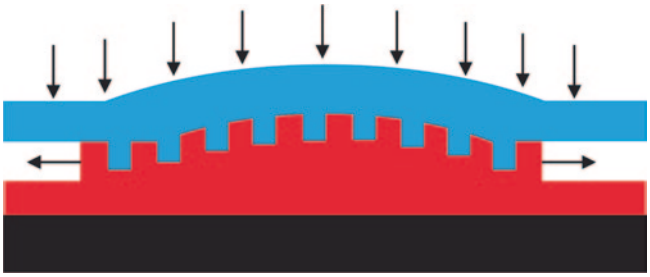

**Fig. 6.4** Illustration of stamp bending in a grating pattern. When the imprint cavities in the centre are filled, the imprint stops. In the edge of the grating, the imprint can continue due to the polymer escaping outside the grating area

#### 6.2.4.2 Stamp Bending

In a simplistic view of an imprint situation, the imprint features will sink uniformly into the polymer under the application of pressure, and then stop when the cavities are filled, thus providing a uniform imprint and a uniform residual layer thickness. The reality is more complicated, the complexities of the polymer flow causing mechanical bending of the stamp. The magnitude of stamp bending will depend heavily on the design and complexity of the imprinted structures, however, even for the simplest structures, it is an effect that cannot be ignored.

Consider Fig. 6.4—a simple, uniform grating to be imprinted. When the imprint is initiated, all grating lines sink into the polymer concurrently. However, problems soon arise. When the cavities become filled, the polymer must seek alternative ways to escape the imprint protrusions. Near the edges of the gratings, the polymer can still escape outside the grating area, and the imprint features continue to sink. In the centre of the grating, the distance to the edge may be so high that the polymer cannot traverse the distance on the timescale of the imprint (essentially, the effective linewidth of the Stefan equation (Eq. (6.4) or (6.5)) increases dramatically). Thus, in this area the imprint essentially stops. As a result, the stamp will bend to accommodate the continuing imprint in the edge regions. The end result is a nonuniformity

in the achieved residual layer, which is undesirable in the case of NIL, but not necessarily relevant for hot embossing. The amount of nonuniformity will, in general, depend on the viscosity of the imprint polymer (lower viscosity means the polymer can easily traverse longer distance), the polymer film thickness (if the polymer is thin enough, the cavities may never be filled at all and if the polymer film is thick, the features at the edge can sink more compared to the centre), the mechanical rigidity of the stamp and the density of structures.

The situation described above will occur even in uniformly structured designs, provided the imprint area is large enough. For nonuniform patterns, stamp bending is a highly pronounced feature of the imprint process. In a complicated pattern, with different areas structured with different densities, the denser areas of the pattern will fill up first, and the sinking of features will essentially stop, while continuing in the less dense areas of the stamp.

A final stamp bending methodology should also be considered. If the stamp contains large unstructured areas, the stamp in these regions may easily bend and come into contact with the polymer, before the imprinted features can sink into the polymer. This effect may decrease the effective pressure for imprint [65].

Several steps may be taken to avoid or diminish stamp bending effects. It may be possible to modify the design to even out protrusion coverage variations, and consequently diminish the effects. For example, if the design consists of some form of circuitry, the operation of the device might not be disturbed by the inclusion of extra stand-alone features in low-density regions. Conversely, the design calls for large structured areas, such as contact pads for electronics or inlet holes for microfluidics. Operation of the device may be unimpeded by changing the pattern to a form of honeycomb structure. If the desired device design cannot be modified to be more suitable for imprint, the process must be designed to limit the stamp bending effects by, for instance, carrying out the imprint at high temperature or long times to allow for the polymer flow to proceed over longer distances, or by using a more rigid stamp to limit the susceptibility to stamp bending.

#### 6.2.4.3 The Imprint Pressure

When using conventional, commercial, full wafer imprint equipment, a high pressure of at least 20 bar is typically applied to form a satisfactory imprint [3, 64, 66–70]. Theoretically, cf. the Stefan equation (6.5), imprint of even several micrometre large features should be completed in less than a second at much lower pressure, say 1–5 bar. So why is it experimentally found that such a high pressure (and, to a lesser extent, time) is required especially when performing imprint on a large scale, i.e. a full 4″ wafer? A number of factors that contribute to this observation are described in the following section.

**Stamp Spring-Back** In the derivation of the Stefan equation, the imprint polymer is described simply as a high-viscosity liquid, however, as already discussed in Sect. 6.2, this is not the case in reality. The flow will be *viscoelastic*, with some semblance of elastic response remaining. In simple terms, the polymer pushes back

on the stamp protrusion, which can be seen as an apparent decrease in the applied pressure if pure viscous flow is assumed.

**Nonoptimal Application of Pressure** When performing calculations based on the Stefan equation, it is assumed that the pressure applied by, for example, pressing the piston is perfectly transferred to the bottom surface of the imprint features. In reality, this will not be the case. For piston-based imprint equipment, the piston surface cannot be made perfectly parallel and in intimate contact with the entire surface. This will lead to inhomogeneity in the application of pressure. This problem can be alleviated by the use of a so-called *compliance layer*, a layer of a soft material placed between the stamp and the piston. This layer serves to homogenise the application of pressure, compensating for the inaccuracy in the application of pressure from the piston. Various materials are in use, including flexible graphite sheets and PDMS [71]. Alternatively, if the imprint pressure is supplied not by a piston but by compressed air (or a different gas) through a flexible membrane, the pressure supplied to the backside will intrinsically be homogeneously distributed. There are a few commercial equipment available based on this principle [51, 61]. Also falling under this header is the possibility of stamp bending bringing non-protruding stamp areas into contact with the polymer, effectively increasing the total protrusion coverage (or, alternatively, decreasing the force available to perform imprint of the desired structures).

**Conformal Contact** Standard silicon wafers are not flat. Across the surface of the wafer, not only is the thickness not constant but the wafer may also bow or taper. In total, a profile variation in the tens of microns range is to be expected from a standard 500-μm wafer [72], which is the material of choice for both stamp and substrate. Thus, when an imprint is to be performed, the initial step in the process is to achieve conformal contact between the stamp and the substrate. Only then can a uniform imprint across the entire surface be achieved.

The exact pressure required to achieve conformal contact is difficult to estimate, however its expected dependence on the properties of the system is likely to be similar to those in the process of simple bending of a membrane. The bending of an ideal plate to obtain a surface profile $u$ (and, conversely, to obtain the opposite result) is found from the equation [73]

$$\nabla^2\nabla^2 u(\mathbf{r}) = \frac{p(\mathbf{r})}{D}, \tag{6.9}$$

where $D$ is the *flexural rigidity*, given from the material properties of Young's modulus $E$ and Poisson's ratio $v$, as well as the plate thickness $h$ as

$$D = \frac{Eh^3}{12(1-v^2)}. \tag{6.10}$$

Representing the surface as a Bessel function of lowest order with a wavelength λ at maximum deflection $w$ at the centre of the plate, one arrives at a solution for the

pressure (assuming uniform pressure application and fixation of the membrane at the rim).

$$p = \frac{16\pi^4 Dw}{\lambda^4} \tag{6.11}$$

Inserting values for a 500-μm-thick silicon plate being deflected 10 μm, and using a wavelength equal to the stamp radius (50 mm) result in a value of $p_{bend} = 26$ mbar.

Note that this equation only described membrane bending. Achieving conformal contact will likely also involve compression of the stamp material. Due to the high stiffness of silicon (E = 170 GPa), even a slight compression will require considerable pressure, and may well be the dominant contribution, considering the low value reached for the bending pressure.

The reduction of the requirement of high imprint pressure is of interest, since it would simplify the imprint equipment (for both piston and compressed air-type machines), and reduce the possibility of stamp or substrate failure due to repeated stress.

Based on Eq. (6.11), there are essentially two avenues available to reduce the process pressure. One is material choice; if one uses a material with a low Young's modulus, the process pressure can be dramatically reduced. This, along with a low-viscosity imprint polymer, is the reason why soft UV imprint can be performed at pressure only barely above ambient [74]. This has been demonstrated in literature, where PDMS was used as a stamp material, or as a handling material for a thin, stiff, top layer containing the features [75, 76]. The other is the membrane thickness, entering cubed in Eq. (6.10). Thus, simply using thinner stamps will reduce the amount of pressure required to achieve conformal contact, the desired effect.

#### 6.2.4.4 The Thermal Cycle—Throughput Improvement

As previously discussed, a major issue that nanoimprint still faces in order to be a successful contender for industrial applications is throughput. In full wafer thermal imprint, the thermal cycle time is often the dominant factor in determining the full imprint cycle time, due to the reliance on thermal conduction from large plates or chucks in order to sufficiently heat the imprint polymer. This in turn leads to long cooling times due to the excessive thermal mass. In practice, cycle times are in the range of 20–60 min per imprint, depending on the polymer choice and the pattern complexity. In photonic-based pattern transfer processes (e.g. deep-UV photolithography), the process is completed in much shorter time, typically a minute or less. In recent years, considerable research has been devoted to reduce thermal cycle times to a more competitive level. By using a custom-designed imprint resist rather than conventional thermoplasts such as PMMA, the $T_g$ and, hence, the required imprint temperature can be considerably reduced, yielding an immediate reduction in cycle time. Imprint at room temperature has also been conceptually demonstrated [77]. Another possibility is to use a thermosetting resist, i.e. a material that is initially

soft but hardens when exposed to temperature. In this way, a constantly hot mould can be employed, removing the need for cooling. In addition, it may be possible to demould the substrate at temperatures even above $T_g$ [78], further reducing the required temperature range.

More radical reduction in process time can involve some way of reducing the thermal mass. If the energy supply for heating is located in the imprint polymer or its immediate vicinity, the required time for heating and especially cooling will be dramatically reduced. Several methods of achieving this have been established in the literature, including joule heating of the stamp [79–81], applying heated fluid as the imprint pressure medium [82] and heating based on infrared radiation [82, 83] or inductive coupling [84]. All of these methods have been demonstrated to decrease the required thermal cycle time to a few minutes, the most effective even to just a few seconds, demonstrating that it is possible to achieve short cycle times in thermal-based nanoimprint. High-quality full wafer imprint, however, remains to be demonstrated with low cycle times. It is in this area the industrial replication technologies like injection moulding can offer a route to true high-throughput fabrication of polymeric nanostructures. The second half of this chapter is dedicated to injection moulding.

## 6.3 Injection Moulding

### *6.3.1 Introduction*

#### 6.3.1.1 Background

Injection moulding technology revolutionised manufacturing in the second half of the twentieth century by making it possible to replicate rapidly the identical parts made from thermoplastic materials from a single-machined mould. While the cost of the initial infrastructure, equipment and a precisely constructed mould might be very high, once the production is up and running, the economies of scale make mass production by injection moulding a solid foundation for an extremely efficient business model. The technology is still widely used today and looks set to dominate industrial production for many years to come.

Injection moulding was put to good use by the music industry in the 1980s with the advent of compact discs, a form of media storage that required cheap, accurate replication of microscale features on a previously unseen scale. More recently, Blu-ray discs have seen commercial injection moulding move to length scales below 150 nm [85]. It is, therefore, an industrially proven method of nanofabrication, but has yet to be widely utilised as such outwith the sphere of optical media. This is despite the fact that researchers have demonstrated successful replication of distinct structures as small as 50 [86], 25 [87] and 5 nm [88]. With so many other applications of polymeric nanostructures, such as nonreflective, superhydrophobic and adhesive surfaces, as well as substrates for biological research into regenerative

medicine, there is a great scope for injection moulding to play a much wider role in realising low-cost mass production for these technologies.

#### 6.3.1.2 The Injection Moulding Process

Injection moulding is conceptually simple and similar to other replication-based processes such as hot embossing and thermoforming. During the injection moulding process, a thermoplastic polymer is heated to around 100 ° above its $T_g$, before it is injected into the mould cavity which is kept 30–50 ° below the polymer's $T_g$. Here the polymer rapidly cools and the moulded part is ejected before the process begins again to produce the next part in a fully automated and unsupervised process. It is this spatial separation of heating and cooling that makes injection moulding such a high-throughput process compared to embossing where these processes occur in the same location; the industrial production of a single CD takes only around 4 s to complete.

### *6.3.2 Injection Moulding Equipment*

#### 6.3.2.1 Injection Moulding Machine

Figure 6.5 shows a schematic of a typical hydraulic injection moulding machine. An injection moulding machine is made up of two distinct units: the injection unit and the clamping unit. The polymer that will eventually be moulded starts its journey in the hopper located to the right of the injection unit in the form of small beads, measuring a few millimetres across, which are gravity fed through the throat into one end of the screw. The barrel is heated by multiple heating bands (four in Fig. 6.6) which increase in temperature from the hopper to the nozzle. A convenient definition for the processing conditions is to define the melt temperature ($T_m$) by the settings of the nozzle heater. A more accurate measurement could be obtained by inserting a thermometer into freshly purged polymer. The cylindrical barrel which houses the screw and the threads of the screw itself has constant diameter along its length, but the central shaft of the screw increases in diameter as it approaches the nozzle, thereby decreasing the gap through which the polymer moves. This combination of increasing temperature, rotational motion and narrowing gap serves to gradually melt, pressurise and mix the polymer to ensure that by the time it reaches the end it is homogeneous in both its temperature and consistency.

Located at the nozzle is a nonreturn valve (see Fig. 6.7) which moves back under the pressure of the polymer as it fills the nozzle cavity, having been pushed through the narrow gaps by the turning screw in a process known as *plasticising*. When the cavity is full, the check ring blocks the progress of any more polymer, the plasticising stops and the next shot is ready for injection. It is important to note that the presence of a previous injection's completed part is required to block the nozzle and allow the polymer for the next shot to build up; without this, the polymer is free to flow out of the end of the nozzle when plasticising is active. The thrust for the injection itself is supplied by the injection cylinder at the far end of the screw.

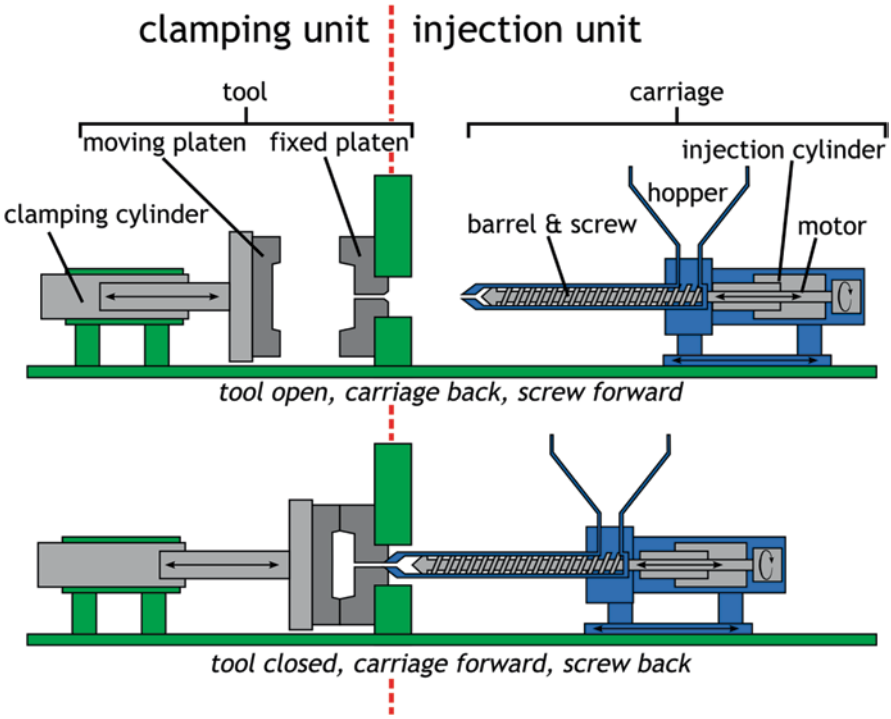


**Fig. 6.5** Schematic of a typical hydraulic injection moulding machine

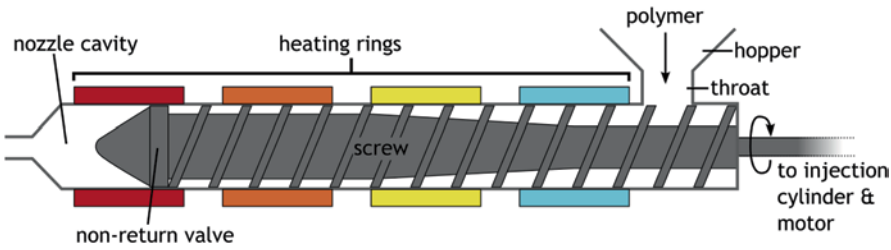


**Fig. 6.6** Schematic diagram of a typical injection moulding machine's barrel

The clamping unit houses the all-important mould, a cavity located at the centre of the tool. The size and shape of this cavity define the size and shape of the moulded part. The tool comprises two halves, the moving platen and the fixed platen, which allow it to be closed while the polymer is injected before reopening so that the final moulded part can be ejected. Tool design and tool making are highly skilled disciplines in their own right and so will only be touched upon lightly in this chapter.

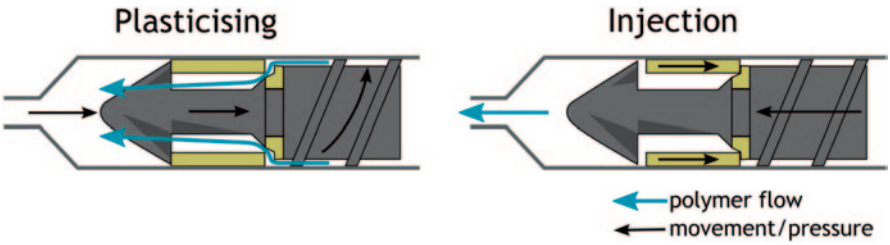


**Fig. 6.7** Operation of a nonreturn valve

## 6.4 Operation

The timeline of a single cycle is illustrated in Fig. 6.8 and described in the following points:

- *mould closing*: the two halves of the mould come together under pressure
- *carriage unit forward*: pressure is built up at the end of the screw
- *injection*: the polymer is pushed into the mould at high speed
- *holding pressure*: the mould is held under pressure so that as the polymer shrinks due to cooling, more may be forced into the mould to ensure a full filling
- *cooling time and plasticising for next cycle*: time delay to allow polymer to freeze; the next shot of polymer is prepared by plasticising with the newly injected part blocking the nozzle, thus allowing the plasticised material to build up
- *carriage unit back*: screw pressure relaxed
- *mould opening*: mould opens with moulded part stuck to inlay side of mould
- *ejection of part*: ejector pins pop out and part falls into collection bucket.

There are many parameters that can be set on the moulding machine. General practice is to start off with the polymer manufacturer's guideline values and then adapt

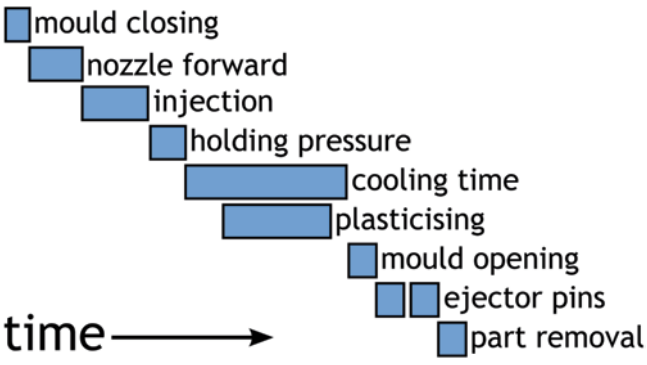


**Fig. 6.8** Timeline of a single injection cycle. Despite being much faster than T-NIL/hot embossing, the thermal cycling (*cooling time*) is still the major limiting factor in cycle time optimisation in injection moulding

conditions based upon the observation of the parts produced. The following parameters are of particular importance:

*Injection speed* directly affects the injection time and injection pressure, and dictates how quickly the polymer is forced into the mould. If it is too slow the polymer may freeze before it has fully filled the mould, leading to an incomplete part, and if it is too high it may result in polymer being forced into unwanted areas of the tool (this is known as *flashing*).

*Tool temperature* affects how quickly the melt cools in the mould: if it is set too low it will result in poor filling, and if it is too high it can lead to an unnecessarily long cooling time or cause the part to not be fully frozen upon mould opening which can cause ejection problems.

*Melt temperature* directly affects the fluidity of the melt at the point of injection. If it is too low it will not flow well enough to fill the mould properly and if it is too high the cooling time may be unnecessarily long or, in extreme cases, the polymer may burn.

*Holding pressure* determines the pressure at which the polymer is held in the mould immediately after injection. As the part cools the polymer shrinks, so holding pressure is required to push more polymer into the cavity to compensate for this shrinkage and ensure that a fully formed part is produced. Too low a value may result in a concave drooping on the nozzle-facing surface of the part which is undesirable when a planar geometry is required.

*Cooling time* is a post-injection, post-holding pressure waiting period during which the tool remains closed so that the part may cool to an acceptable level, ideally the tool temperature. If cooling time is not sufficient the part may come out too hot and deform upon ejection; if it is too long, you are just wasting time.

*Moisture* in certain polymers can affect its physical properties in a detrimental way which can cause a range of quality issues, such as bubbles or streaks appearing in the moulded parts. For this reason, some polymers are dried before use.

### 6.4.1 Tooling for Injection Moulding of Micro- and Nanostructures

The central component of an injection moulding machine is the mould, or tool. It is here where the mould cavity resides and the part is formed. With so many options available for fabricating nanostructured masters, much of the research in the field is focussed on the production and optimisation of the tooling itself. Mould tools used for the production of most plastic products, be they coat hangers or tooth brushes, are generally made by milling large pieces of steel and assembling them together into a single unit containing the cavities, vents and other specific features required for the production of a particular part or parts. The practice of tool making is a precise art where accuracies of tens of micrometres as well as the capacity to fit in as part of an elaborate, multistage, automated mass production process can be required. If the intended product of a tool is to contain micro- or nanoscale features on its surface, certain adaptations must be made to the tool design as these length scales cannot be addressed by metalworking techniques.

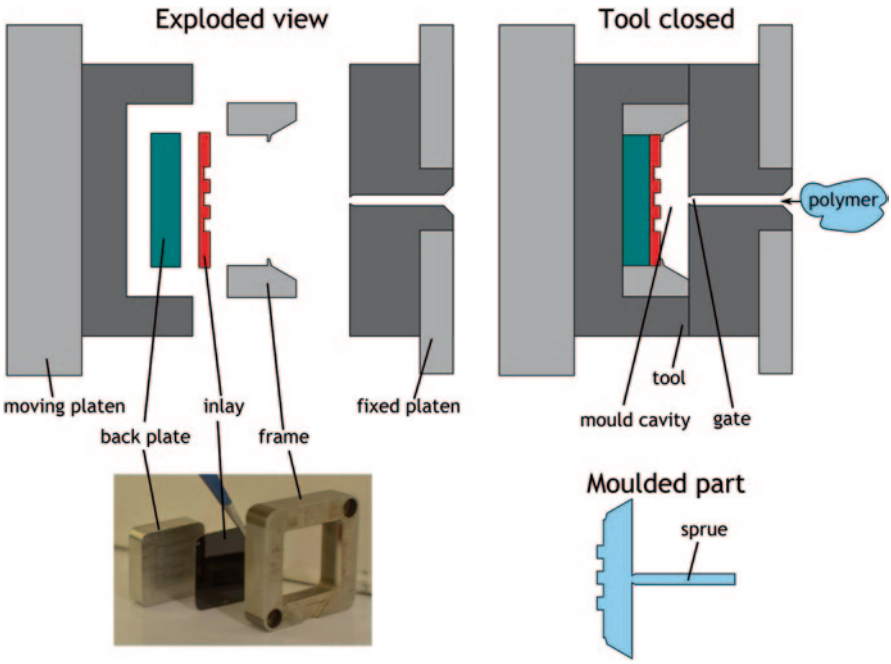


**Fig. 6.9** Schematic diagram and corresponding photograph of one example of an inlay-frame tool design

Tools designed for the injection moulding of micro- and nanostructures often incorporate interchangeable elements known as *inserts*, *stampers* or *inlays*. A good example of this in industry is the fabrication of optical media, where every product has the same macroscopic disk shape, but differently patterned inlays are used to define the content of the data stored on the disk. Since the first compact disks in the 1980s, advances in industrial processes and materials have allowed this format to remain useful by reducing the minimum feature size, from 800 nm (and 1.6 μm track pitch) on a CD to 150 nm (and 320 nm track pitch) on a Blu-ray, thereby enabling mare data to be stored on the same surface area.

The accepted way to nanopattern a single surface of a moulded part (invented to facilitate the production of optical media) is to use an inlay-frame configuration like that shown in Fig. 6.9.

In this configuration, the inlay is a planar substrate which has been patterned in advance by other means. The tool is designed such that the inlay slots into a frame which, in turn, slots into the bulk of the tool, allowing parts of one particular size and shape (or *format*) to be produced with the pattern from the inlay formed on one of its surfaces. The term *tooling* is used to refer to the material(s) of which the inlay is comprised or indeed the inlay itself.

#### 6.4.1.1 Tooling Material

The fabrication of micro- or nanopatterned inlays generally requires a wafer-based approach as would be employed to fabricate structures of this size for any purpose; although milling processes are an option for larger structures [22]. For this reason, the likes of silicon, quartz and III-V materials might seem like an obvious choice with which to fabricate inlays and they have indeed been used to conduct research in the field [86, 89], although the brittle nature of these materials may cause them to shatter under the high pressures of the injection moulding process depending on the specifications of specific equipment and processing parameters [90]. Because of this, nickel, with its durable characteristics, has become a standard tooling material for the injection moulding of micro- and nanostructures [22]. Nickel tooling is commonly formed by a LIGA-like process whereby it is galvanically electroplated against a prefabricated master pattern. The electroplating step is a carefully controlled electrolysis process where patterned target of nickel deposition is the cathode.

As described earlier, the molten polymer is injected into the tool which has its temperature kept below the polymer's $T_g$. As the hot melt makes contact with the tool wall it quickly cools and a skin layer is formed [91]. The formation of the skin layer largely inhibits the ability to produce raised structures (e.g. pillars) at diminishing length scales and increasing aspect ratios. As the polymer melt moves into the patterned holes of the inlay, the surrounding metal conducts the heat away so quickly that the polymer cools below $T_g$ and freezes before it has been able to completely fill the hole. This does not adversely affect the replication of holes like those which pattern optical media, but it does make it difficult, if not impossible, to replicate structures, which stand proud of the surface, which are often desirable for the type of biomimetic and cell engineering applications mentioned earlier. An example of titanium tooling highlights another possible artefact of this problem in which PC broke off inside the inlay's 50-nm holes, causing the replication of 50-nm holes rather than the intended pillars in subsequent shots [86]. Nonetheless, this example did show Ti to be robust and damage free after 50 shots, while the robustness of Ni is surely evidenced by its widespread use in the commercial replication of optical media.

One type of method that had been developed to combat the premature cooling of injected polymer is known as variothermal injection moulding. Variothermal techniques use elaborate mechanisms that will require the incorporation of plumbing or electrical systems in the construction of the tool, with these additions being used to heat and cool the tooling surface at appropriate times to aid the filling of micro- and nanostructures [92, 93]. Variothermal heating with a micro-electro mechanical system (MEMS) heater located behind nickel tooling was shown to improve the filling of 320 nm wide grooves with PC from 20 to 60 nm, but was still short of the 82 nm groove depth [94, 95]. Laser-mediated heating (capable of creating temperature gradients of 300 K/s) was successfully used to fabricate superhydrophobic microstructures in polypropylene (PP) with steel tooling [96] where the structures were conical pillars with a base diameter of around 5 μm and were not replicated

to a high level of uniformity. Yet other ways to implement variothermal injection moulding include heating the tooling surface by electrical induction [97] which has been shown to enhance the filling of COC nanostructures in nickel tooling [98], or by electrifying the actual inlay surface [99] which permitted the formation of nanoscale PP hair-like structures over a 2-min cycle time. Furthermore, a variothermal process may use steam and coolant to respectively heat and cool the tool and has been used to successfully replicate a 46-in. LCD panel in acrylonitrile butadiene styrene (ABS), although the variothermal process added well over a minute to the cycle time [100].

In an infrared-based variothermal approach, nanochannel filling was further aided by the introduction of a heat-resistant polymer layer behind the Ni inlay to further impede the heat transfer to the surrounding tool [101]. This use of heat-retardant material offers a simpler approach to variothermal techniques which has been adopted by a number of researchers. Over several publications [102–105], Yoon et al. document their successes with silicon and hybrid metal–polymer inlays for injection moulding of microscale features. They have shown that inlays made from embossed PC coated with aluminium or titanium allowed injected PS to fill 1–2 μm trenches (depth dimensions are unclear, but do not appear to be more than the width) to twice the depth of fluorinated silicon tooling [105] (work which went on to form the basis of a patent application) [106]. They also showed that PC inlays, somewhat unsurprisingly, suffered deformation during injection moulding with the same polymer, but that polyimide (PI) coated with aluminium was capable of replicating microstructures in PC and PMMA for over 1000 cycles [103]. Polymer–metal tooling has shown similar durability in the form of photolithographically patterned SU-8 microstructures on Ni which showed no sign of damage after 300 replicas with COC [107]; heat retardation was not required in this case. Embossed polymer tooling has other reported successes at the microscale in the form of UV-cured poly(urethane acrylate) (PUA), with additional insulation provided by poly(ethylene terephthalate) (PET), replicating gratings that are 1–10 μm in width and 10 μm in height [108]. At the nanoscale, an embossed polyvinyl alcohol (PVA) film produced features down to 100 nm in size in COC, but required that the adhesive inlay be sacrificially dissolved after each replication, somewhat cancelling out the core advantage of injection moulding as a high-throughput technique [109]. A conceptually similar but more durable (> 1000 cycles) tooling solution comprising PI substrates coated with SU-8 photoresist patterned by NIL provided accurate replication of ~ 100-nm diameter pillars in PC as well as the means to selectively stretch nanopillars to up to 1.4 times their intended height through the simple adjustment of constant tool temperature [110]. Polyether ether ketone (PEEK), a thermoplastic with high $T_m$ (~ 340 °), may also provide a useful thermally insulating tooling solution and has been tested tor compatibility with a range of resins (PP, ABS, PC and COC) [111]. An example of a non-polymeric heat-retardant material, bulk metallic glass, also shows promise as a robust tooling solution that can facilitate the formation of 100–200 nm bumps in PMMA [112].

It is clear that there exist two main schools of thought for how to best tackle the problem of poor mould filling as induced by premature freezing: variothermal and heat retardation. Variothermal techniques offer a means of precise control that could lead to more predictable outcomes, but do not seem to be any more advantageous in that regard in the evidence presented by the current literature. Furthermore, the development of complex heating/cooling systems is time-consuming and costly, and with the exception of the laser heating [96] and induction [97, 98] examples, these solutions caused significant increases in cycle time. The polymeric tooling approach is appealing, not just for its simplicity but also for the fact that it opens up a wealth of alternative inlay material and patterning options (e.g. UV-NIL) that remove the requirement for expensive Ni electroforming and can be adapted to the individual's own fabrication capabilities. With the simple approach, the imagination is free to ponder the nature of the next pattern rather than concentrate on the seemingly unnecessary technicalities of developing a sophisticated variothermal solution.

#### 6.4.1.2 Surface Coatings

The success of injection moulding of micro- and nanoscale features relies as much on smooth demoulding as it does in a nanoimprint or embossing process (see Sect. 6.3.2). As with NIL and embossing, the use of fluorosilanes is a popular method to add nonadhesive properties to tooling. Yoon et al. demonstrated that fluorinated silicon tooling was not only protected from the damaging effects of interfacial friction but also made it possible to almost completely fill 4-μm wide 9.2-μm deep trenches with thermoplastic polyurethane (TPU) where uncoated tooling could not even fill half [113]. These type of coatings have even made it possible to fight the filling problems associated with Ni tooling and permit the replication of 40-nm diameter pillars in COC [114]. Fluorosilane treatment of Ni has also helped to reduce the build-up of injected PC and poly(4-methyl-1-pentene) (PMP) residue for over 15,000 machine cycles in an experiment where molybdenum nitride and tungsten nitride coatings also performed favourably [115]. Elsewhere, chromium and titanium nitrides have shown benefits in terms of tool durability [116], and silicon carbide and diamond-like carbon coated on brass tooling reduced demoulding forces by ~40% in a work which also highlighted that optimum moulding conditions were specific to the coating–resin combination [117]. Similarly, a broad UV-NIL study of five metal nitrides and seven metal oxides saw no single coating performing better than another, suggesting that the most effective release at the demoulding stage must be determined by the specific master–replica material combination rather than by a single mould coating which outperforms all others in all situations [118]. Another systematic study of coatings on nanopatterned heat-retardant tooling with $SiO_2$, $Si_3N_4$, Ti and Ni, all with and without fluorosilane attachment, showed that it was possible to replicate 100-nm diameter pillars with heights of 2 μm (aspect ratio =20:1) in PC [119]. In this work, fluorinated oxide and nitride showed marginally superior performance, but issues of nonuniformity caused by the methods of coating deposition were highlighted.

In other cases of purely metallic coatings, aluminium and titanium on polymeric tooling have been shown to double the filling of microstructures with PS and PC compared to fluorinated silicon with a heat insulating back plate [105, 106]. Aluminium did however show slight peeling on imprinted PI tooling after 1000 cycles with PS, although it still showed superior adhesion reduction at this stage compared to uncoated tooling after only 100 cycles [103]. Gold-coated nickel was reported to be resistant to residue when PMMA was moulded up against it [102], although Ni, as the traditional tooling of choice, is itself not prone to residue build-up or it would unlikely have achieved such status.

It is remarkably clear that nonadhesive surface coatings are a vital addition to any replication-based fabrication process, and while fluorosilanes appear to offer a solution in most situations, they may require some optimisation of their composition [35] or prove inferior to metals in some cases [105]. As has been suggested [118], there is probably no one-coating-fits-all solution, but indicative techniques such as WCA measurements, surface analysis techniques such as X-ray photon spectroscopy (XPS) and energy dispersive X-ray spectroscopy (EDX) and the mathematics of surface energy can guide the way to design and interpret the practical development of potential tooling solutions.

## 6.5 Conclusions

### *6.5.1 Advantages and Limitations*

The advantages of replication-based fabrication are quite clear. It allows devices containing features that are normally very expensive and difficult to create to be replicated accurately at a fraction of the cost and provides a range of material choices for both master and replica. Nanoimprint/embossing techniques are many and varied and can be implemented initially with minimal equipment investment and upscaled with bespoke equipment or one of several commercially available tools. These processes are conceptually simple and practically well understood, but in the case of T-NIL/hot embossing particularly, the time limitations imposed by thermal cycling make such techniques more suited to prototyping or very small volume production at best.

Injection moulding offers a solution to these limitations by enabling rapid replication in large numbers, decreasing cost through improved throughput, while durable tooling can facilitate excellent, long-term reproducibility. It is a well-understood process which is fully established in industry and has the potential to revolutionise the way we make many useful devices that rely on accurately reproduced micro- and nanoscale dimensions.

Essentially, hot embossing and injection moulding offer the same practical outcome, but injection moulding provides vast improvements in throughput, albeit at the expense of initial financial investment in machinery, making hot embossing a more suitable technique for initial prototyping and small-volume production. Hot

embossing may be a more established and accessible nanoreplication technique for these reasons, but there is a large and growing interest in injection moulding that may allow it to establish itself as a mass production nanofabrication technique where the throughput issues of embossing and NIL continue to see them struggle to make an impact commercially.

Besides the challenges in implementing some of the techniques (tooling, materials, anti-stick, etc.) required to realise the potential of injection moulding at the micro- and nanoscale, there are also inherent (technical) limitations to the technique too. Primarily, injection moulding is generally limited to the production of monolithic parts made from thermoplastic polymers; although metal and ceramic injection moulding are possible and conducted at larger length scales, as is the formation of polylithic parts, it still remains the case that the replication of some intricate nanotechnologies, such as integrated circuits, may well be fundamentally beyond the capabilities of injection moulding. It is also the case that most current micro- and nanopatterned tooling solutions focus on the patterning of a single surface of a flat part and the transition to patterning continuously over 3D, potentially curved, surfaces will be far from trivial. It is hard for injection moulding to address thin-film applications due to the difficulty with filling large, thin structures, and, as such, this is an area that may be better addressed by R2R embossing and related techniques.

### *6.5.2 Outlook*

Despite being invented around 20 years ago, there is still much interest in using and further developing the toolbox of NIL-type processes. Although it has not yet been widely adopted for mass production in the microelectronics industry, the desire for the smaller devices may soon make NIL the only option for moving below the resolution limit of even the most optimised optical lithographic process. Injection moulding too, although perhaps not applicable to microelectronics, is nonetheless an incredibly promising means of nanofabrication that is being increasingly recognised as such and motivating a great deal of research [21]. In other fields, the vast range and relative simplicity of the replication-based processes that are available means that the development and adaptation of these techniques is ongoing and driven by the needs of new applications. In this way, the toolkit is only going to grow and provide more useful ways to replicate minute structures for a fraction of the cost of conventional lithography.

With such a broad range of processes available, replication-based fabrication will always have a place where polymer devices are required. Hot embossing is still well used for low-cost prototyping and small-volume production and will continue to provide superior resolution than new prototyping methods, like 3D printing, for the foreseeable future. NIL and derivatives still provide a cheap method for nanoscale parallel pattern transfer, while techniques like injection moulding and R2R NIL provide a route to high-throughput production which is sure to be a commonplace within a few short years. Combined embossing/NIL variants and thermoforming have even found ways to address the patterning of nonplanar surfaces [120],

which could be utilised by injection moulding if these methods can be applied to the tooling.

In terms of polymer replication for microfluidics, tissue engineering and other biology research, a mastery of both hot embossing for prototyping and injection moulding for upscaling the production of experimental devices is highly desirable. Indeed, a recent review [121] highlights high-throughput production as one of the three most important areas in furthering of the field of nanostructured biomaterials and no technique is better equipped to address this need than injection moulding, both in terms of research and the smooth translation to real-world products through industry.

## References

1. Lee, J.-S., Progress in non-volatile memory devices based on nanostructured materials and nanofabrication. Journal of Materials Chemistry, 2011. **21**(37): p. 14097.
2. Madou, M. J., Fundamentals of Microfabrication. 2nd ed. 2002: CRC Press.
3. Schift, H., Nanoimprint lithography: An old story in modern times? A review. Journal of Vacuum Science & Technology B, 2008. **26**(2): p. 458.
4. Guo, L. J., Nanoimprint Lithography: Methods and Material Requirements. Advanced Materials, 2007. **19**(4): p. 495.
5. Chou, S. Y., P. R. Krauss and P. J. Renstrom, Imprint of sub-25 nm vias and trenches in polymers. Applied Physics Letters, 1995. **67**(21): p. 3114.
6. Austin, M. D., H. Ge, W. Wu, M. Li, Z. Yu, D. Wasserman, S. A. Lyon and S. Y. Chou, Fabrication of 5 nm linewidth and 14 nm pitch features by nanoimprint lithography. Applied Physics Letters 2004. **84**: p. 5299.
7. Hua, F., Y. Sun, A. Gaur, M. A. Meitl, L. Bilhaut, L. Rotkina, J. Wang, P. Geil, M. Shim, J. A. Rogers and A. Shim, Polymer Imprint Lithography with Molecular-Scale Resolution. Nano Letters, 2004. **4**(12): p. 2467.
8. Haisma, J., M. V. K. vandenHeuvel and J. vandenBerg Mold-assisted nanolithography: a process for reliable pattern replication. J. Vac. Sci. Tech. B, 1996. **14**(6): p. 4124.
9. Bailey, T. C., S. C. Johnson, S. V. Sreenivasan, J. G. Ekerdt, C. G. Willson and D. J. Resnick, Step and flash imprint lithography: an efficient nanoscale printing technology. Journal of Photopolymer Science and Technology 2002. **15**(3): p. 481.
10. Cheng, X. and L. J. Guo, One-step lithography for various size patterns with a hybrid mask-mold. Microelectronic Engineering 2004. **71**: p. 288.
11. Haatainen, T. and J. Ahopelto, Pattern transfer using step & stamp imprint lithography. Physica Scripta 2003. **67**(4): p. 357.
12. Makela, T., T. Haatainen, P. Majander and J. Ahopelto, Continuous roll to roll nanoimprinting of inherently conducting polyaniline. Microelectronic Engineering 2007. **84**(5–8): p. 877.
13. Guo, L. J. and S. H. Ahn, High-speed roll-to-roll nanoimprint lithography on flexible plastic substrates. Advanced Materials 2008. **20**: p. 2044.
14. Ahn, S. H. and L. J. Guo, Large-Area Roll-to-Roll and Roll-to-Plate Nanoimprint Lithography: A Step toward High-Throughput Application of Continuous Nanoimprinting. ACS Nano, 2009. **3**(8): p. 2304.
15. Vig, A. L., T. Makela, P. Majander, V. Lambertini, J. Ahopelto and A. Kristensen, Roll-to-roll fabricated lab-on-a-chip devices. Journal of Micromechanics and Microengineering, 2011. 21(3).
16. Moonen, P. F., I. Yakimets and J. Huskens, Fabrication of Transistors on Flexible Substrates: from Mass-Printing to High-Resolution Alternative Lithography Strategies. Advanced Materials, 2012. **24**(41): p. 5526.

17. Kumar, P. and S. Chand, Recent progress and future aspects of organic solar cells. Progress in Photovoltaics: Research and Applications, 2012. **20**(4): p. 377.
18. Kehagias, N., V. Reboud, G. Chansin, M. Zelsmann, C. Jeppesen, F. Reuther, C. Schuster, M. Kubenz, G. Gruetzner and C. M. S. Torres, Submicron three-dimensional structures fabricated by reverse contact UV nanoimprint lithography. Journal of Vacuum Science and Technology B 2006. **24**: p. 3002.
19. Heilig, M., S. Giselbrecht, A. Guber and M. Worgull, Microthermoforming of nanostructured polymer films: a new bonding method for the integration of nanostructures in 3-dimensional cavities. Microsystem Technologies-Micro-and Nanosystems-Information Storage and Processing Systems, 2010. **16**(7): p. 1221.
20. Heilig, M., M. Schneider, H. Dinglreiter and M. Worgull, Technology of microthermoforming of complex three-dimensional parts with multiscale features. Microsystem Technologies-Micro-and Nanosystems-Information Storage and Processing Systems, 2011. **17**(4): p. 593.
21. Yang, C., X.-H. Yin and G.-M. Cheng, Microinjection molding of microsystem components: new aspects in improving performance. Journal of Micromechanics and Microengineering, 2013. **23**(9): p. 093001.
22. Giboz, J., T. Copponnex and P. Mélé, Microinjection molding of thermoplastic polymers: a review. Journal of Micromechanics and Microengineering, 2007. **17**(6): p. R96.
23. Zaouk, R., B. Y. Park and M. J. Madou, Fabrication of polydimethylsiloxane microfluidics using SU-8 molds. Methods Mol Biol, 2006. **321**: p. 17.
24. Lee, L. H., R. Peerani, M. Ungrin, C. Joshi, E. Kumacheva and P. W. Zandstra, Micropatterning of human embryonic stem cells dissects the mesoderm and endoderm lineages. Stem cell research, 2009. **2**(2): p. 155.
25. Tee, S.-Y., J. Fu, C. S. Chen and P. A. Janmey, Cell Shape and Substrate Rigidity Both Regulate Cell Stiffness. Biophysical Journal, 2011. **100**(5).
26. Gadegaard, N., S. Thoms, D. S. Macintyre, K. McGhee, J. Gallagher, B. Casey and C. D. W. Wilkinson, Arrays of nano-dots for cellular engineering. Microelectronic Engineering, 2003. **67–68**: p. 162.
27. Guo, L. J., Recent progress in nanoimprint technology and its applications. Journal of Physics D: Applied Physics 2004. **37**: p. R123.
28. Schift, H. and L. J. Heyderman, Nanorheology, in Alternative Lithography, C.M. Sotomayor Torres, Editor. 2003, Kluwer Academic/Plenum: New York.
29. Kristensen, A. and H. Schift. Springer Handbook of Nanotechnology. 2007: Springer.
30. Stefan, M. J., Versuche über die sheinbare adhäsion. Österreichische Akademie der Wissenschaften < Wein > /Mathematisch-Naturwissenschaftliche Klasse, 1874. **2**(69:713): p. 735.
31. Yamada, K., M. Umetami, T. Tamura, Y. Tanaka, H. Kasa and J. Nishii, Antireflective structure imprinted on the surface of optical glass by SiC mold. Applied Surface Science 2009. **255**: p. 4267.
32. Taniguchi, J., Y. Tokano, I. Miyamoto, M. Komoro and H. Hiroshima, Diamond nanoimprint lithography. Nanotechnology, 2002. **13**(5): p. 592.
33. Mühlberger, M., I. Bergmair, A. Klukowska, A. Kolander, H. Leichtfried, E. Platzgummer, H. Loeschner, C. Ebm, G. Grützner and R. Schöftner, UV-NIL with working stamps made from ormostamp. Microelectronic Engineering 2009.
34. Park, S., H. Schift, C. Padeste, B. Schnyder, R. Kotz and J. Gobrecht, Anti-adhesive layers on nickel stamps for nanoimprint lithography. Microelectronic Engineering, 2004. **73–4**: p. 196.
35. Schift, H., S. Saxer, S. Park, C. Padeste, U. Pieles and J. Gobrecht, Controlled co-evaporation of silanes for nanoimprint stamps. Nanotechnology, 2005. **16**(5): p. S171.
36. Schulz, H., F. Osenberg, J. Engemann and H. C. Scheer, Mask fabrication by nanoimprint lithography using anti-sticking layers, in 16th European Conference on Mask Technology for Integrated Circuits and Microcomponents, U.F.W. Behringer, Editor. 2000, Spie-Int Soc Optical Engineering: Bellingham. p. 244.
37. Guo, Y. H., G. Liu, X. L. Zhu and Y. C. Tian, Analysis of the demolding forces during hot embossing. Microsystem Technologies-Micro-and Nanosystems-Information Storage and Processing Systems, 2007. **13**(5–6): p. 411.

38. Matschuk, M., H. Bruus and N. B. Larsen, Nanostructures for all-polymer microfluidic systems. Microelectronic Engineering, 2010. **87**(5–8): p. 1379.
39. Beck, M., M. Graczyk, I. Maximov, E. L. Sarwe, T. G. I. Ling, M. Keil and L. Montelius, Improving stamps for 10 nm level wafer scale nanoimprint lithography. Microelectronic Engineering, 2002. **61–2**: p. 441.
40. Park, S., C. Padeste, H. Schift and J. Gobrecht, Nanostructuring of anti-adhesive layers by hot embossing lithography. Microelectronic Engineering, 2003. **67–68**(0): p. 252.
41. Wu, C. C., S. L. C. Hsu and I. L. Lo, Fabrication and Application of Polyimide Plastic Molds for Nanoimprint Lithography. Journal of Nanoscience and Nanotechnology, 2010. **10**(10): p. 6446.
42. Moresco, J., C. H. Clausen and W. Svendsen, Improved anti-stiction coating of SU-8 molds. Sensors and Actuators B-Chemical, 2010. **145**(2): p. 698.
43. Kim, H. H., S. G. Park, E. H. Lee, S. G. Lee and B. H. O, Durability of nitrided fluorocarbon polymer films for nanoimprint lithography. Thin Solid Films, 2011. **519**(16): p. 5490.
44. Kumar, G., H. X. Tang and J. Schroers, Nanomoulding with amorphous metals. Nature, 2009. **457**(7231): p. 868.
45. Heckele, M. and W. K. Schomburg, Review on micro molding of thermoplastic polymers. Journal of Micromechanics and Microengineering, 2004. **14**: p. R1.
46. Prucker, O., S. Christian, H. Bock, J. Rühe, C. W. Frank and W. Knoll, On the glass transition in ultrathin polymer films of different molecular architecture. Macromolecular Chemistry and Physics 1998. **199**(1435–1444).
47. Forrest, J. A. and K. Dalnoki-Veress, The glass transition in thin polymer films. Advances in Colloid and Interface Science 2001. **94**: p. 167.
48. Cangialosi, D., M. Wübbenhorst, J. Groenewold, E. Mendes, H. Schut, A. van and S. J. Picken, Physical aging of polycarbonate far below the glass transition temperature: Evidence for the diffusion mechanism. Physical Review B, 2004. **70**: p. 224213.
49. Nunes, P. S., P. D. Ohlsson, O. Ordeig and J. P. Kutter, Cyclic olefin polymers: emerging materials for lab-on-a-chip applications. Microfluidics and Nanofluidics 2010. **9**(2–3): p. 145.
50. Tokyo Ohka Kogyo Co., L. http://www.tok.co.jp.
51. Nanonex. www.nanonex.com.
52. Yu, Z., L. Chen, W. Wu, H. Ge and S. Y. Chou, Fabrication of nanoscale gratings with reduced line endge roughness using nanoimprint lithography. Journal of Vacuum Science and Technology B 2003. **21**: p. 2089.
53. Wu, C.-C., S. L.-C. Hsu and W.-C. Liao, A photo-polymerization resist for UV nanoimprint lithography. Microelectric engineering, 2009. **86**: p. 325.
54. Abgrall, P., V. Conedera, H. C. A.-M. Gue and N.-T. Nguyen, SU-8 as a structural material for labs-on-chips and microelectromechanical systems. Electrophoresis, 2007. **28**: p. 4539.
55. Christiansen, M. B. 2009, DTU Nanotech, Technical University of Denmark.
56. EV Group, A. http://www.evgroup.com.
57. Süss Microtec AG, G. http://www.suss.com.
58. Jenoptik Mikrotechnik GmbH, G. http://www.jo-mt.com.
59. Molecular Imprints, I. www.molecularimprints.com.
60. Scivax corporation, J. http://www.scivax.com.
61. Obducat AB, S. http://www.obducat.com.
62. Heyderman, L. J., H. Schift, C. David, J. Gobrecht and T. Schweizer, Flow behaviour of thin polymer films used for hot embossing lithography. Microelectronic Engineering, 2000. **54**(3–4): p. 229.
63. Schift, H., L. J. Heyderman, M. A. der and J. Gobrecht, Pattern formation in hot embossing of thin films. Nanotechnology, 2001. **12**(2): p. 173.
64. Scheer, H.-C. and H. Schulz, A contribution to the flow behaviour of thin polymer films during hot embossing lithography. Microelectronic Engineering 2001. **56**: p. 311.
65. Perret, C., C. Gourgon, F. Lazzarino, J. Tallal, S. Landis and R. Pelzer, Characterization of 8-in. wafers printed by nanoimprint lithography. Microelectronic Engineering 2004. **73–74**: p. 172.

66. Beck, M., F. Persson, P. Carlberg, M. Graczyk, I. Maximov, T. G. I. Ling and L. Montelius, Nanoelectrochemical transducers for (bio-) chemical sensor applications fabricated by nanoimprint lithography. Microelectronic Engineering 2004. **73–74**: p. 837.
67. Lebib, A., Y. Chen, J. Bourneix, F. Carcenac, E. Cambril, L. Couraud and H. Launois, Nanoimprint lithography for a large area pattern replication. Microelectronic Engineering 1999. **46**: p. 319.
68. Heidari, B., I. Maximov and L. Montelius, Nanoimprint at the 6 in. wafer scale. Journal of Vacuum Science and Technology B 2000. **18**(6): p. 3557.
69. Li, M., L. Chen, W. Zhang and S. Y. Chou, Pattern transfer fidelity of nanoimprint lithography on six-inch wafers. Nanotechnology, 2003. **14**(1): p. 33.
70. Schulz, H., M. Wissen and H.-C. Scheer, Local mass transport and its effect on global pattern replication during hot embossing. Microelectronic Engineering 2003. **67–68**: p. 657.
71. Merino, S., H. Schift, A. Retolaza and T. Haatainen, The use of automatic demolding in nanoimprint lithography processes. Microelectronic Engineering 2007. **84**: p. 958.
72. Senturia, S. D., Microsystem Design. 2001: Kluwer Academic.
73. Young, W. C., Roark's Formulas for Stress & Strain. 1989: McGraw-Hill.
74. Plachetka, U., M. Bender, A. Fuchs, B. Vratzov, T. Glinsner, F. Lindner and H. Kurz, Wafer scale patterning by soft UV-nanoimprint lithography. Microelectronic Engineering 2004. **73–74**: p. 167.
75. Khang, D.-Y., H. Kang, T.-I. Kim and H. H. Lee, Low-pressure nanoimprint lithography. Nano Letters 2004. **4**(4): p. 633.
76. Tormen, M., T. Borzenko, G. Schmidt, J. Liu and L. W. Molenkamp, Thermocurable polymers as resists for imprint lithography. Electronics Letters 2000. **36**(11): p. 983.
77. Khang, D.-Y. and H. H. Lee, Wafer-scale sub-micron lithography. Applied Physics Letters 1999. **75**(17): p. 2599.
78. Leveder, T., S. Landis, L. Davoust and C. Gourgon, Optimization of demolding temperature for throughput improvement of nanoimprint lithography. Microelectronic Engineering 2007. **84**: p. 953.
79. Lee, J. C., I. C. Leu, K. L. Lai and M. H. Hon, Hot embossing by joule heating. Journal of Vacuum Science and Technology B 2008. **26**(1): p. 260.
80. Tormen, M., R. Malureanu, R. H. Pedersen, L. Lorenzen, K. H. Rasmussen, C. J. Lüscher, A. Kristensen and O. Hansen, Fast thermal nanoimprint lithography by a stamp with integrated heater. Microelectric Engineering, 2008. **85**(5–6): p. 1229.
81. Kimerling, T. E., W. Liu, B. H. Kim and D. Yao, Rapid hot embossing of polymer microfeatures. Microsystem Technologies 2006. **12**: p. 730.
82. Chang, J.-H. and S.-Y. Yang, Development of fluid-based heating and pressing systems for micro hot embossing. Microsystem Technologies 2005. **11**: p. 396.
83. Grigaliunas, V., S. Tamulevicius, M. Muehlberger, D. Jucius, A. Guobiene, V. Kopustinskas and A. Gudonyte, Nanoimprint lithography using IR laser irradiation. Applied Surface Science 2006. **253**: p. 646.
84. Hong, S.-K., Y.-M. Heo and J. Kang, Replication of polymeric micro patterns by rapid thermal pressing with induction heating apparatus. Proceeding of the 3rd IEEE Int. Conf. on Nano/Micro Engineered and Molecular Systems, January 6–9, 2008, Sanya, China, 2008: p. 911.
85. Pranov, H., H. K. Rasmussen, N. B. Larsen and N. Gadegaard, On the injection molding of nanostructured polymer surfaces. Polymer Engineering & Science, 2006. **46**(2): p. 160.
86. Macintyre, D. and S. Thoms, The fabrication of high resolution features by mould injection. Microelectronic Engineering, 1998. **42**: p. 211.
87. Schift, H., C. David, M. Gabriel, J. Gobrecht, L. J. Heyderman, W. Kaiser, S. Köppel and L. Scandella, Nanoreplication in polymers using hot embossing and injection molding. Microelectronic Engineering, 2000. **53**(1–4): p. 171.
88. Gadegaard, N., S. Mosler and N. B. Larsen, Biomimetic Polymer Nanostructures by Injection Molding. Macromolecular Materials and Engineering, 2003. **288**(1): p. 76.
89. Yoon, S.-h., C. Srirojpinyo, J. S. Lee, J. L. Mead, S. Matsui and C. M. F. Barry. Evaluation of novel tooling for nanoscale injection molding. in Proc. SPIE. 2005.

90. Zhao, J., R. Ong, G. Chen, Y. K. Juay, F. L. Ng, M. W. Lee and C. H. Kua. Development of rapid manufacturing technology of polymer microfluidic devices by micro moulding using silicon mould inserts. in Proceedings of the 6th International Conference on Nanochannels, Microchannels, and Minichannels, Pts a and B. 2008. New York: Amer Soc Mechanical Engineers.
91. Viana, J., Development of the skin layer in injection moulding: phenomenological model. Polymer, 2004. **45**(3): p. 993.
92. Yao, D. and B. Kim, Development of rapid heating and cooling systems for injection molding applications. Polymer Engineering & Science, 2002. **42**(12): p. 2471.
93. Chang, P.-C. and S.-J. Hwang, Experimental investigation of infrared rapid surface heating for injection molding. Journal of Applied Polymer Science, 2006. **102**(4): p. 3704.
94. Kim, Y., Y. Choi and S. Kang, Replication of high density optical disc using injection mold with MEMS heater. Microsystem Technologies, 2005. **11**(7): p. 464.
95. Michaeli, W. and F. Klaiber, Development of a system for laser-assisted molding of micro- and nanostructures. Journal of Vacuum Science & Technology B, 2009. **27**(3): p. 1323.
96. Bekesi, J., J. J. J. Kaakkunen, W. Michaeli, F. Klaiber, M. Schoengart, J. Ihlemann and P. Simon, Fast fabrication of super-hydrophobic surfaces on polypropylene by replication of short-pulse laser structured molds. Applied Physics A-Materials Science & Processing, 2010. **99**(4): p. 691.
97. Keun, P. and L. Sang-Ik, Localized mold heating with the aid of selective induction for injection molding of high aspect ratio micro-features. Journal of Micromechanics and Microengineering, 2010. **20**(3): p. 035002.
98. Kim, S., C.-S. Shiau, B. H. Kim and D. Yao, Injection Molding Nanoscale Features with the Aid of Induction Heating. Polymer-Plastics Technology and Engineering, 2007. **46**(11): p. 1031.
99. Yoo, Y. E., T. H. Kim, D. S. Choi, S. M. Hyun, H. J. Lee, K. H. Lee, S. K. Kim, B. H. Kim, Y. H. Seo, H. G. Lee and J. S. Lee, Injection molding of a nanostructured plate and measurement of its surface properties. Current Applied Physics, 2009. **9**(2, Supplement 1): p. e12.
100. Wang, G., G. Zhao, H. Li and Y. Guan, Research on a New Variotherm Injection Molding Technology and its Application on the Molding of a Large LCD Panel. Polymer-Plastics Technology and Engineering, 2009. **48**(7): p. 671.
101. Lin, H. Y., C. H. Chang and W. B. Young, Experimental Study on the Filling of Nano Structures with Infrared Mold Surface Heating. International Polymer Processing, 2011. **26**(1): p. 73.
102. Yoon, S.-H., P. Palanisamy, P. Padmanabha, J. L. Mead and C. M. F. Barry. Comparison of Tooling Materials in Injection Molding of Microscale Features. in ASME Conference. 2009: ASME.
103. Kim, Y., S.-H. Yoon, J. S. Lee, S. Johnston, J. L. Mead and C. M. F. Barry. Performance of Hybrid Tooling in Micro Injection Molding. in Proc. Ann. Tech. Conf. Soc. Plast. Eng. 2010.
104. Yoon, S.-h., J. Lee, K. Park, J. L. Mead, S. Matsui and C. M. F. Barry. Critical factors for nanoscale injection molding. 2006: SPIE.
105. Yoon, S.-H., P. Padmanabha, J. S. Lee, J. L. Mead, C. M. F. Barry, N.-G. Cha, A. A. Busnaina and K. Park. Evaluation of Metal-Polymer Hybrid Tooling for Micro-Injection Moulding. in Proc. Ann. Tech. Conf. Soc. Plast. Eng. 2008. Milwaukee, WI.
106. Yoon, S.-H., C. M. F. Barry, J. L. Mead, N.-G. Cha and A. A. Busnaina, Methods for Forming Metal-Polymer Hybrid Tooling for Forming Parts Having Micro Features. 2011, University of Massachusetts Lowel, Northeastern University: USA.
107. Hansen, T. S., D. Selmeczi and N. B. Larsen, Fast prototyping of injection molded polymer microfluidic chips. Journal of Micromechanics and Microengineering, 2010. **20**(1): p. 8.
108. Park, S. H., W. I. Lee, S. N. Moon, Y. E. Yoo and Y. H. Cho, Injection molding micro patterns with high aspect ratio using a polymeric flexible stamper. Express Polymer Letters, 2011. **5**(11): p. 950.
109. Kim, S. H., J. H. Jeong and J. R. Youn, Nanopattern insert molding. Nanotechnology, 2010. **21**(20): p. 205302.

110. Stormonth-Darling, J. M. and N. Gadegaard, Injection Moulding Difficult Nanopatterns with Hybrid Polymer Inlays. Macromolecular Materials and Engineering, 2012. **297**(11): p. 1075.
111. Griffiths, C. A., S. Bigot, E. Brousseau, M. Worgull, M. Heckele, J. Nestler and J. Auerswald, Investigation of polymer inserts as prototyping tooling for micro injection moulding. The International Journal of Advanced Manufacturing Technology, 2010. **47**(1–4): p. 111.
112. Zhang, N., C. J. Byrne, D. J. Browne and M. D. Gilchrist, Towards nano-injection molding. Materials Today, 2012. **15**(5): p. 216.
113. Yoon, S.-H., N.-G. Cha, J. S. Lee, J.-G. Park, D. J. Carter, J. L. Mead and C. M. F. Barry, Effect of processing parameters, antistiction coatings, and polymer type when injection molding microfeatures. Polymer Engineering & Science, 2010. **50**(2): p. 411.
114. Matschuk, M. and N. B. Larsen, Injection molding of high aspect ratio sub-100 nm nanostructures. Journal of Micromechanics and Microengineering, 2013. **23**(2): p. 025003.
115. Miikkulainen, V., M. Suvanto, T. A. Pakkanen, S. Siitonen, P. Karvinen, M. Kuittinen and H. Kisonen, Thin films of MoN, WN, and perfluorinated silane deposited from dimethylamido precursors as contamination resistant coatings on micro-injection mold inserts. Surface and Coatings Technology, 2008. **202**(21): p. 5103.
116. Cunha, L., M. Andritschky, K. Pischow, Z. Wang, A. Zarychta, A. S. Miranda and A. M. Cunha, Performance of chromium nitride and titanium nitride coatings during plastic injection moulding. Surface and Coatings Technology, 2002. **153**(2–3): p. 160.
117. Griffiths, C. A., S. S. Dimov, E. B. Brousseau, C. Chouquet, J. Gavillet and S. Bigot, Investigation of surface treatment effects in micro-injection-moulding. The International Journal of Advanced Manufacturing Technology, 2010. **47**(1–4): p. 99.
118. Houle, F. A., S. Raoux, D. C. Miller, C. Jahnes and S. Rossnagel, Metal-containing release layers for use with UV-cure nanoimprint lithographic template materials. Journal of Vacuum Science & Technology B, 2008. **26**(4): p. 1301.
119. Stormonth-Darling, J. M., R. H. Pedersen, C. How and N. Gadegaard, Injection moulding of ultra high aspect ratio nanostructures using coated polymer tooling. Journal of Micromechanics and Microengineering, 2014. **REVISED MANUSCRIPT SUBMITTED**.
120. Senn, T., J. P. Esquivel, N. Sabaté and B. Löchel, Fabrication of high aspect ratio nanostructures on 3D surfaces. Microelectronic Engineering, 2011. **88**(9): p. 3043.
121. Engel, Y., J. D. Schiffman, J. M. Goddard and V. M. Rotello, Nanomanufacturing of biomaterials. Materials Today, 2012. **15**(11): p. 478.

# Chapter 7
# Lithographic Processes for the Design of Biosurfaces

**Nicolas Delorme**

Miniaturization is a key concept that, during the past 20 years, led the microelectronics industry to increase the integration rate up to 100 million transistors per chip, with a minimum size of features close to 100 nm. Today miniaturization plays an increasingly important role for the realization of various types of components used in telecommunication, micro-robotics, chemistry, biology, and biomedical research. For instance, miniaturization of biosensors must benefit to increase in the density of components, decrease in the amount and volume of a sample, improvement in detection limit, and precise control.

Increased effort has been made in the past 10 years to establish fabrication technologies that allow production of structured surfaces with great geometrical complexity and reduced operation time and cost. Manufacturing in miniaturization embraces bottom-up and top-down techniques. Usually the fabrication of complex systems such as platforms for selective recognition requires the association of both approaches. On one side, bottom-up is mainly focused to develop materials in the form of particles or films and concerns mainly methods such as chemical synthesis and self-assembly. On the other side, top-down approaches use processes such as patterning, etching, and deposition.

Lithography was invented in 1796 as a printing technique that allows the creation and reproduction from a limestone of multiple copies of ink drawings. Today lithography is a more general term which includes top-down approaches used to create a chemical or a topographical pattern onto a substrate. The recent progress in microelectronics has allowed the development of effective lithographic method that is able to create, with a compatible industrial throughput, features with a size close to 10 nm. Moreover, conventional lithography was developed for silicon-based materials. Critical issues such as resolution, reliability, speed, and cost need to be considered in developing lithography techniques. In order to reduce the cost inherent to conventional lithography and to allow the structuration of non-silicon-based

N. Delorme (✉)
Department of Physics, IMMM—Université du Maine, Avenue Olivier Messiaen, 72085 Le Mans, France
e-mail: nicolas.delorme@univ-lemans.fr



J. Rodríguez-Hernández, A. L. Cortajarena (eds.), *Design of Polymeric Platforms for Selective Biorecognition,* DOI 10.1007/978-3-319-17061-9_7

material, new lithographic methods (also called unconventional lithography) have arisen [1]. These processes have eliminated the need of clean room environment and offer the possibility to template a wider range of materials such as polymer. These improvements have naturally led the application of these tools in different areas of microelectronics such as the biomedical research.

In nature, many biological interactions rely on the specific placement of biomolecules to dictate and direct complex processes. The ability to site-specifically pattern biomolecules with spatial resolution is a key challenge for biophysical cell studies, microarray analytics, tissue engineering, therapeutics, and high-density biosensor applications [2]. Concerning this field, the two main applications are biosensors and biopatterning. The first one obviously requires improved detection devices by the pursuit of new innovative processes. Reducing the dimensions to nanoscale detection generates a significant increase in sensitivity. Indeed, the concentrations of the order of fM are now detectable with the use of nano-transistors. On the other side, biopatterning consists in depositing biomolecules probes which are capable of detecting in a sample solution of target molecules because of their specific interaction with the latter. Biopatterning of surfaces has been of growing interest in recent years, from both scientific and technological points of view. Such artificial biological surfaces can be tremendously useful in diverse applications, including biochips, biosensors, and fundamental studies of cell biology [3].

Biopatterning not only offers the possibility of smaller biochips with more reaction sites but also smaller test volume and potentially higher sensitivity and throughput screening for molecular diagnostics [4]. For instance, DNA hybridization nanoarrays come with the remarkable ability to rapidly and effectively monitor the expression of thousands of genes used in the diagnosis and treatment of disease [3]. On the other side, protein nanoarrays offer the possibility of developing a rapid global analysis of an entire proteome [5].

The number of biological and medical applications presents many challenging materials design for biopatterning. Indeed, if a spatial positioning of biomolecules on a substrate with nanoscale resolution is required, their native biological functions have to be retained and usually the other regions of the substrate have to be resistive to biomolecules. Recent years have witnessed the advent of several promising strategic methodologies for biopatterning [6]. In this chapter, we review the principle of the prominent lithographic method for the fabrication of polymeric platform for different selective biorecognition methods and their specific application to polymer platform for selective biorecognition.

## 7.1 Conventional Lithography

Conventional lithography is a top-down approach which combines all the methods based on the use of an irradiation source to pattern the surface of a material. These methods are commercially available and hugely used in the industry and particularly in microelectronics [7]. However, for these methods clean room facilities where

**Table 7.1** Resolution throughput and approximate buying cost of conventional lithography techniques

| | Photolithography | EBL | FIB |
|---|---|---|---|
| Resolution (nm) | 200 | 1–20 | 5–30 |
| Throughput | +++ | ++ | + |
| Buying cost (€) | $>5.10^5$ | $>1.10^6$ | $>1.10^6$ |

air is filtered, temperature and humidity are controlled, are needed. This causes a significant increase in the cost of conventional lithography and limits its accessibility. Conventional lithography regroups two different techniques: photolithography and particle beam lithography which including itself electron beam lithography (EBL) and focused ion beam lithography (FIB). As shown by Table 7.1, the choice of the technique depends mainly on the balance between desired resolution and throughput.

### *7.1.1 Photolithography*

Photolithography is a cornerstone of the progress of the semiconductor industry. Indeed, it has allowed the reduction of the size and an increase of the integration density of the integrated circuits with an economically acceptable cost. In the photolithographic process, geometric features drawn on a mask are transferred via electromagnetic illumination onto a substrate (Fig. 7.1). The mask is generally made with a quartz or glass plate coated with a thin layer of chromium presenting the desired geometric features.

The photolithographic process starts with the coating of a planar substrate with a photoresist. The photoresist consists in a polymer matrix transparent to the irradiation wavelength and containing photosensitive compounds. Once coated, the substrate is baked in order to remove the solvents from the resist and improve the resist–substrate adhesion. In the next step, the mask is aligned accurately above the resist and the illumination is performed. Selected parts of the photoresist film are then exposed to the light source that leads to degradation (positive lithography) or cross-linking (negative lithography) of the polymer matrix. Finally, the substrate is immerged into a solvent allowing the differentiation of the exposed and nonexposed areas of the resist. In the case of positive lithography, the irradiation alters the physical and chemical properties of the exposed area such that it can be dissolved in the solvent. In the case of negative lithography, irradiation causes cross-linking of the polymer which becomes less soluble than the nonirradiated part so that the nonirradiated part is eliminated by the solvent rinsing process. Although photolithography is massively present in the microelectronic industry, its use in the elaboration of polymeric substrate for biological application is scarce [5]. For instance photolithography has been used to pattern synthetic and natural polymers for use as two-dimensional (2D) or cell-encapsulating scaffolds [8].

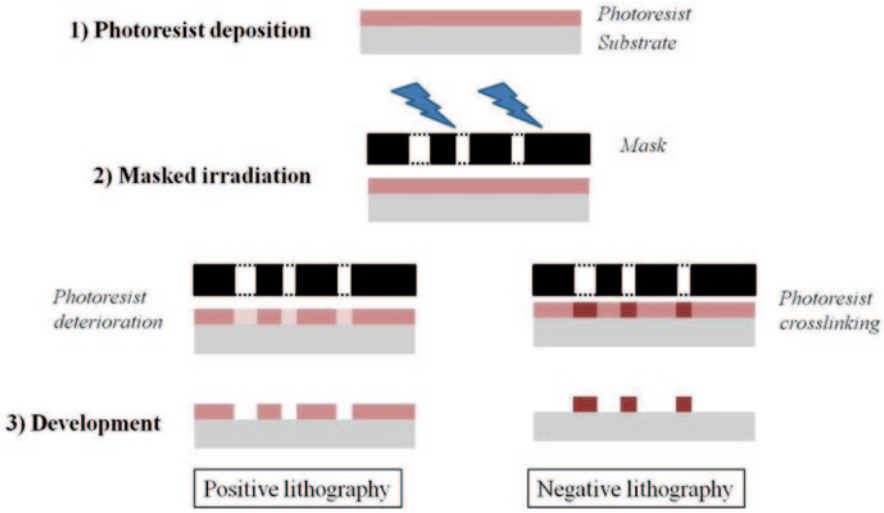


**Fig. 7.1** Principle of the photolithography process

Negative lithography processes require the use of photo-crosslinkable polymer but biocompatible photocrosslinkable polymers are scarce, which limits the use of this process for biomedical applications. However, some teams have used photo-crosslinkable chitosan as a photoresist to create patterns with micrometer resolution of various shapes on glass and tissue culture polystyrene [9]. The advantages of such polymer are that it does not require photoinitiator and forms flexible and biocompatible hydrogel upon short UV exposure. As shown in Fig. 7.2, the process allowed the deposition of cardiac fibroblast on the glass surface and between the lines of cross-linked chitosan. The elongation of the adsorbed cells along the lines can be clearly observed.

Enzyme-based electrodes represent an important class of biosensors which can be used for the detection of energy metabolites (glucose, lactate). Yan et al. have described a photolithographic-based method to immobilize enzyme on gold electrode via a poly(ethylene glycol) (PEG) hydrogel [10]. As shown in Fig. 7.3, a PEG prepolymer is deposited on a glass substrate where gold electrodes were previously deposited by photolithography. The deposition of the cross-linked PEG between the electrodes is performed by aligning a mask with the electrode template, UV irradiating, and water rinsing. The following step is to irradiate an enzyme containing PEG prepolymer, which was deposited over the whole surface, through a second mask (used to deposit the gold electrodes). After water rinsing, the gold electrodes are covered with the enzyme-containing hydrogel which is finally tested successfully for glucose detection.

Positive photolithography was used by Christman et al. to obtain micron and submicron-scale features of aldehyde functionality in polymer films to develop a platform for protein immobilization and assembly. Films containing a pH-reactive

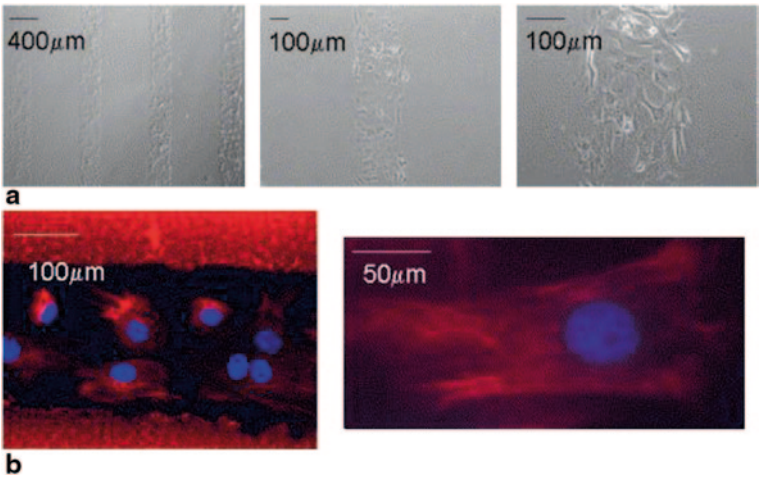


**Fig. 7.2** **a** Optical microscopy image of cardiac fibroblasts seeded on chitosan patterned TCP and maintained for 8 days of culture. The cells attached to the surface of empty lines, elongated and proliferated to confluence. **b** Immunofluorescent staining for filament vimentin (*red*), nuclei (*blue*). Chitosan lines appear *red* [9]

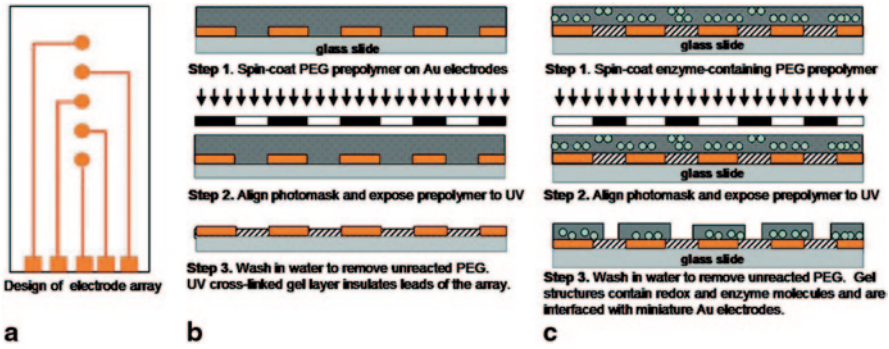


**Fig. 7.3** Schematic of the process used to prepare an enzyme-based gold electrode [10]

polymer and a photoacid generator (PAG) were patterned by exposure to a 365-nm light. Upon PAG activation and hydrolysis of acetals, aldehyde groups can be formed and used to bind protein such as streptavidin [11].

Microelectrode arrays (MEAs) that are able to stimulate and record electrical signals down to the single-cell level have become an indispensable tool in the study of different properties of neural networks. Advancements in these MEA applications require a decrease in the size and spacing between electrodes in order to match the dimensions of neuronal networks, and also the development of flexible MEA (non-silicon-based technology) [12]. Sessolo et al. have recently developed a method to prepare conductive polymer MEAs by photolithography. Here, as shown

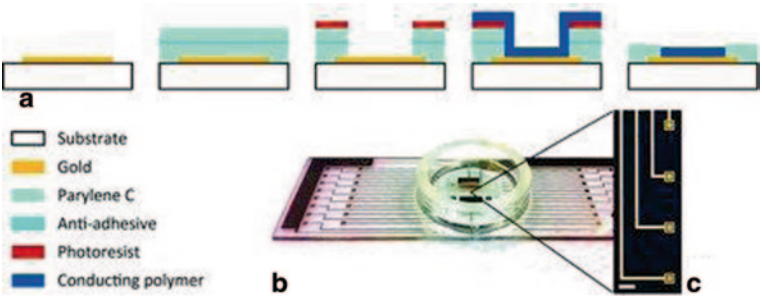


**Fig. 7.4** **a** Fabrication process illustrating the main processing steps. **b** Photograph of MEA fabricated on a microscope slide with a culture chamber ring attached. **c** Optical microscopy image showing the electrodes (scale bar 50 µm) [13]

by Fig. 7.4a photolithography is firstly used to deposit gold structure on the glass substrate and then to topographically template a parylene C layer just before the deposition of the conductive polymer (PEDOT:PSS). In this step, instead of solvent rinsing, the elimination of the nonirradiated parylene C is made by $O_2$ plasma etching. The obtained polymeric platform consists in an array of square electrodes with a side of 20 µm and a center-to-center spacing of 160 µm (Fig. 7.4b), a spatial resolution which allows the monitoring of signal propagation among the adjacent neurons and the recording of the spontaneous electrical activity from rat hippocampus brain slices [13].

The principle of photolithography was also used by Yamazoe et al. to create a micropatterned fibroblast adhesive protein surfaces on cell culture dishes. For this, they simply irradiate an albumin film through a photomask by UV radiation. The irradiation renders the proteins adhesive to cell on patches with a diameter close to 500 µm allowing the localized adsorption of mouse fibroblast cells [14].

*Limitations* The major advantage of photolithography is the ability to fabricate many devices in parallel, making possible the production of very complex circuits in a relatively short time. Limitations of photolithography are its cost and light diffraction, which limit the size of the features that can be made to approximately the wavelength of the used light. Consequently to decrease the structure size, the irradiation source has to be decreased to Deep UV (DUV) or X-ray. The consequences are important since the apparatus (source, lenses…) as well as the masking techniques, as shown by Table 7.2, have to be modified.

**Table 7.2** Nature of the mask as function of the irradiation wavelength

| Irradiation type | Wavelength (nm) | Mask |
|---|---|---|
| UV | 450 | Quartz or glass/Cr |
| DUV | 193 | Mo/Si multilayers |
| X-ray | 0.5 | Au/W on $Si_3N_4$ |

Although, through the decrease of the irradiation wavelength, DUV and X-ray lithography allow a clear improvement of the resolution, the associated high energy is usually too destructive to be employed for polymer material and biomedical applications. Moreover, the cost of such techniques (~10 million €) is clearly a limiting factor for the generalization of their uses. Moreover independently of the used wavelength, one major disadvantage of photolithography is the use of photomasks. Indeed, as illustrated by the previous examples, usually several masks are needed to pattern complex structures and this leads first to an increase of the cost and then to some loss of resolution due to the difficulty of the alignment of the mask with the preexisting templated surface.

## *7.1.2 Particle Beam Lithography*

Particle beam lithography uses high-energy charged particles instead of light to pattern material. Charged particles can be electrons or ions and the associated techniques are called EBL and FIB, respectively. The use of high-particle energy beam (>2 keV) associated with wavelengths < nm eliminates the diffraction problem which limits the resolution of photolithography. And pattern resolution below 10 nm can be obtained. Another advantage of particle beam lithography over photolithography is that it is a direct write technique which does not require the use of a mask. This offers a great flexibility in the feature design.

### 7.1.2.1 Electron Beam Lithography (EBL)

The development of EBL tool started from late 1960s by the modification of a scanning electron microscopy (SEM) [15]. Indeed, in an EBL apparatus the electron beam can be deflected either to scan the substrate surface to produce an image (SEM) or to expose an electron-sensitive resin previously deposited on the surface of the substrate. Most of the time, the resist is made of poly(methyl methacrylate) (PMMA) [16]. As shown in Fig. 7.5, similar to photolithography, the high-energy electrons beam can cause either a cross-linking (negative lithography) or degradation (positive lithography) of the resist. Then the exposed substrate has to be rinsed in a developer solution. EBL offers the ability to pattern features with varying shapes and dimensions (from 10nm to 1mm) [17]. This resolution is determined by the size of the molecules in the resist and by the scattering range of the electrons. Indeed, collision of electrons which generates backscattered or secondary electrons can expose unwanted regions of the resist [18].

Although 40 years after the first development of the technique, most of the work in EBL is still made from SEM with a controllable scanning on PMMA resin [19]; the technique has been recently exploited for patterning biomolecules. Indeed, EBL can be used to modify functionality of conventional lithographic polymer resists

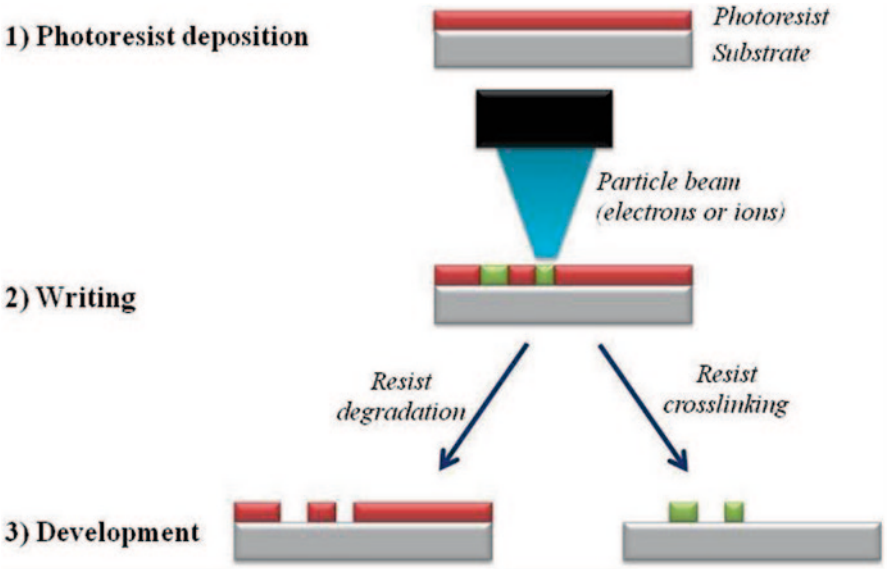


**Fig. 7.5** Principle of the maskless particle beam lithography technique

in order to allow specific biomolecules adsorption [20], or to ablate locally self-assembled monolayers or proteins monolayer [21].

For the patterning of polymer by EBL, most of the works concern the use of PEG as a negative resist [22]. When PEG is exposed to focused electron beams, it cross-links to itself and links to Si surfaces [23]. This method is advantageous in that the features which are formed are resistive to protein adsorption [24]. Christman et al. have used EBL to produce a multicomponent protein nanopatterns [25]. In this work, the end groups of eight-arm PEGs were modified with different proteins (biotin, maleimide, aminooxy, or NTA). The PEG polymer layer was then deposited onto Si substrate by the spin casting method and the desired patterns were created using EBL. The un-crosslinked polymer is finally removed by rinsing the samples with methanol and water. As shown in Fig. 7.6, EBL is interesting for creating structures containing multiplexed biomolecules in three-dimensional (3D) multilayer formats.

EBL can also be used to fabricate simultaneously submicron topographical and chemical patterns, on a biocompatible and biodegradable hydrogel. Dos Reis et al. used EBL to pattern amphoteric poly(amidoamine) (PAA) hydrogel and used it as a substrate for the study of neuronal network [26]. In this work, the hydrogel microstructuring differs from the method used with PEG polymer since it relies on the direct electron beam exposure of dry and already cross-linked hydrogels. From chemical, structural, and morphological analyses they demonstrated that after development, the uppermost PAA layers were ablated, whereas the residual layers showed an amorphous carbon structure (disappearance of–COOH groups and increase of C=C double bonds). A morphologically and chemically modified surface can then be obtained. The template substrate is then successfully used to study the growth of a neuronal network (Fig. 7.7).

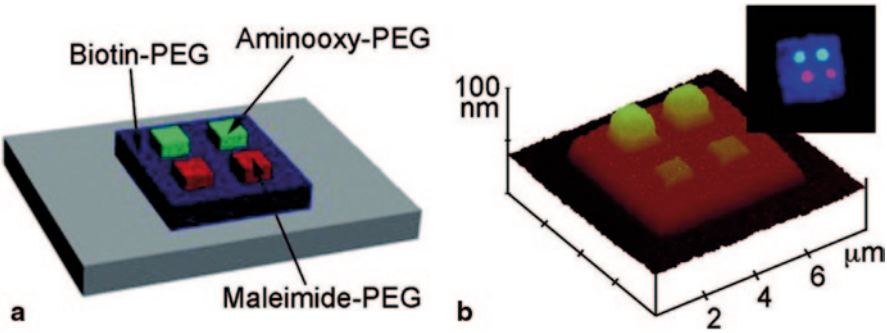


**Fig. 7.6** **a** Schematic showing that 5 µm wide biotin-PEG is first cross-linked to the native oxide of an Si wafer, after which two 1 µm wide maleimide-PEG and two 1 µm wide aminooxy-PEG patterns are then cross-linked on top of the original biotin-PEG pattern. **b** AFM height images of corresponding pattern. Inset: overlay image of a *blue fluorescent* on the biotin-PEG, a *green fluorescent* antibody-stained R-oxoamide myoglobin, and a *red fluorescent* BSA. *AFM* atomic force microscopy [25]

*Limitation* The main limitations of EBL are its low speed due to a point-by-point scanning and its high cost which make it only suitable for small area fabrication and academic research. The high energy of the irradiation limits also the use of EBL for biopatterning. However, its high resolution allows EBL to be widely used for the fabrication of photolithography masks and soft lithography masters.

### 7.1.2.2 Focused Ion Beam (FIB)

During the past decade, the use of FIB systems has become widespread in the fields of materials and micro-nanotechnologies. Indeed, they offer on the same platform the ability to image and to modify locally with a very high resolution (10–30 nm) a wide range of materials and objects [27]. The operation mode of such a system is

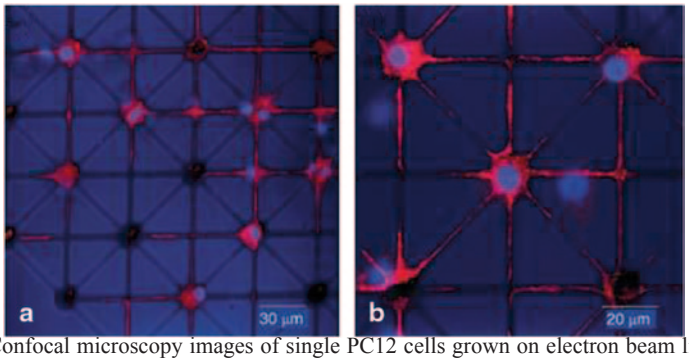


**Fig. 7.7** Confocal microscopy images of single PC12 cells grown on electron beam lithography (EBM)-patterned network of microwells (10 µm diameter) connected by microchannels (1 µm width). The cells are immunostained with DAPI (cell nuclei, *blue*), FITC anti-vinculin antibody (focal contacts, *red*), and TRITC phalloidin (actin filaments, *red*) [26]

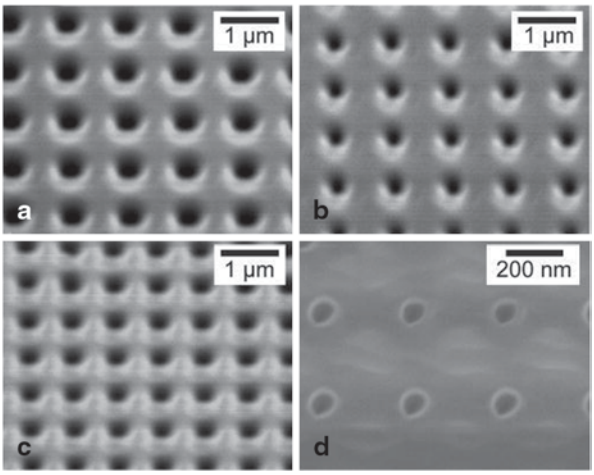


**Fig. 7.8** SEM images of micro/nano through-holes in 500-nm-thick PLLA fabricated with Ga+ FIB [29]

quite similar to that of an SEM, except that the beam is constituted by ions ($Ga^+$, $H^+$, or $He^+$) instead of electrons. Another advantage is that secondary electrons are generated during the ion–material interaction allowing the formation of an image. If the incident ions have sufficient energy, they provide a way to etch the material. In addition, if FIB is combined with a gas flow the technique can also allow the deposition of material [28].

The resolution is usually better for FIB than for EBL because the area of the particle–substrate interaction region is smaller. FIB lithography should be a suitable technique for polymeric material since it does require neither development nor mask. However, FIB lithography in polymers is still at a very early stage of development due to chemical changes induced in the polymer after the irradiation by the high-energy ions, and the localized heating due to the low thermal conductivity of polymeric material [27]. Recently Oyama et al., by controlling the operating conditions, were able to perform high-resolution features on both thick (500 nm) and thin (50 nm) poly(L-lactic acid) (PLLA) films (Fig. 7.8; [29]). However, chemical modification of the surface of the polymer film cannot be avoided and in the case of PLLA the resulting surface is richer in C=C double bonds. Hopefully, such surfaces are known to improve cell adhesion and confirm that FIB can be used to prepare platforms for the studying of cell adhesion [30].

## 7.2 Nonconventional Lithography

Nonconventional lithography techniques include soft lithography and scanning probe lithography. The involved processes are totally different than for conventional lithography which relies on focused energetic beam (light or particle). Indeed for nonconventional lithography, feature size limitation is not imposed by wavelength, but by physical and chemical interactions such as diffusion, capillarity, or

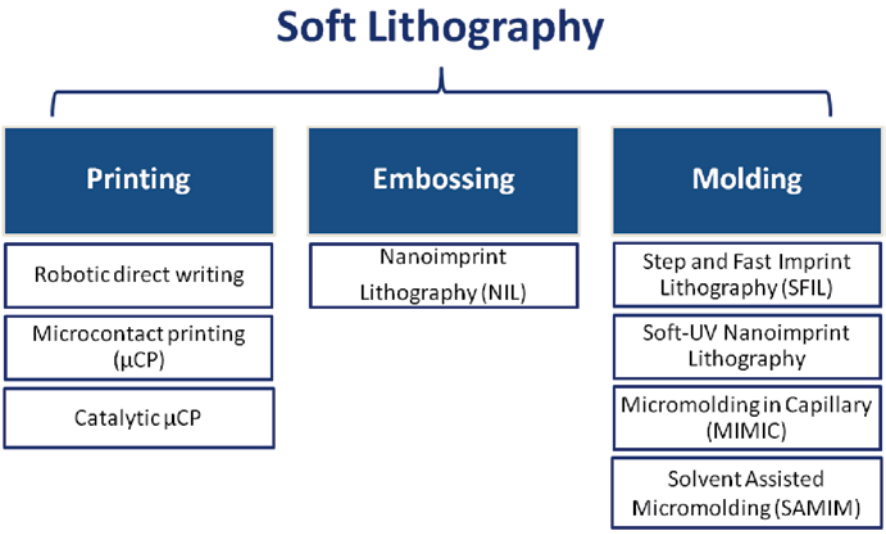


**Fig. 7.9** Principal soft lithography processes used for the preparation of polymeric platform

intermolecular interactions. They offer opportunities for patterning a wide range of substrates, some of which are not patternable with traditional techniques like nonplanar surfaces. Moreover, they have the potential to be of low cost for manufacturing, they are easier to operate and are more easily applicable to biological compatible environment or for the fabrication of chemical patterns [31].

### *7.2.1 Soft Lithography*

Soft lithography refers to a group of techniques based on the use of polymers to replicate and to transfer patterns onto surfaces [32]. These techniques, which do not require expensive clean room processing, can be used with a wide variety of substrates, and enable rapid prototyping of features down to tens of nanometers at a fraction of the cost of traditional lithographic strategies.

The main strength of this technology lies in the ability to reuse a large number of times the same mold made by conventional lithography. This allows reducing and compensating the low speed of EBM. In addition, the wide variety of materials that can be structured and the ability to structure nonplanar and 3D surface make soft lithography a key technology in nanotechnology.

As resumed in Fig. 7.9, most of these techniques can be categorized in three different groups based on different processes: printing, embossing, and replica molding. During the past decade, several methods have been developed inside these groups for biotemplating purposes. Indeed, soft lithographic process offers the possibility to imprinted surfaces or films that offer both geometrical as well as chemical functionality which ensure high selectivity and specificity [33]. Main soft lithog-

raphy procedures and requirements for generating controllable and well-defined biotemplated surfaces are discussed below.

In most of the soft lithography techniques a "soft" polymeric stamp is used instead of the hard mask used in photolithography. Usually poly-dimethysiloxane (PDMS) is used to fabricate the stamp. PDMS is an elastomeric curable polymer which exhibits several attractive properties:

- A flexible backbone which enables accurate replication of relief shapes, a low Young's modulus (~ 750 KPa)
- A low surface energy enabling conformal contact with the substrate without applied pressure and nondestructive release from patterned structures
- An optical transparency which facilitate the alignment procedure
- A commercial availability at low cost

Fabrications of the PDMS stamps are not time consuming. Indeed, they are fabricated by casting (PDMS) silicone elastomer against a master which possesses the desired topography. This master is usually made of silicon and it is fabricated by photolithography or EBL. PDMS is usually used in 10:1 mixture (w/w) of base elastomer/curing agent and thermally cured at 70 °C for 2 h [34]. When using silicon as the master material, a surface treatment is needed to increase its protection against contamination and to favor the demolding of the stamp. Usually functionalization of the master with an alkylsilane or a perfluorosilane is used [35]. As shown in Fig. 7.10, this process allows a good fidelity between the master and the PDMS mold for features > 100 nm.

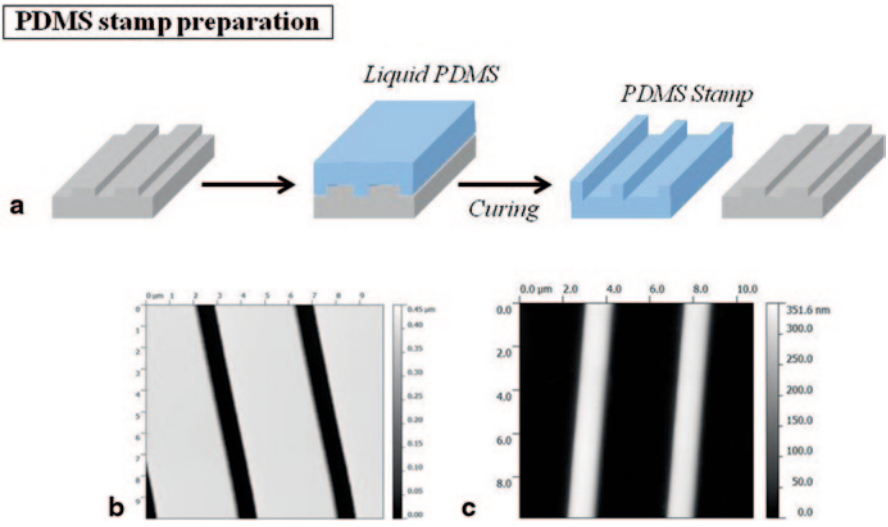


**Fig. 7.10** **a** Schematic PDMS stamp preparation procedure, **b** AFM topographic image of a silicon master template by photolithography, and **c** AFM topographic image of the corresponding PDMS stamp. Unpublished images from author's group

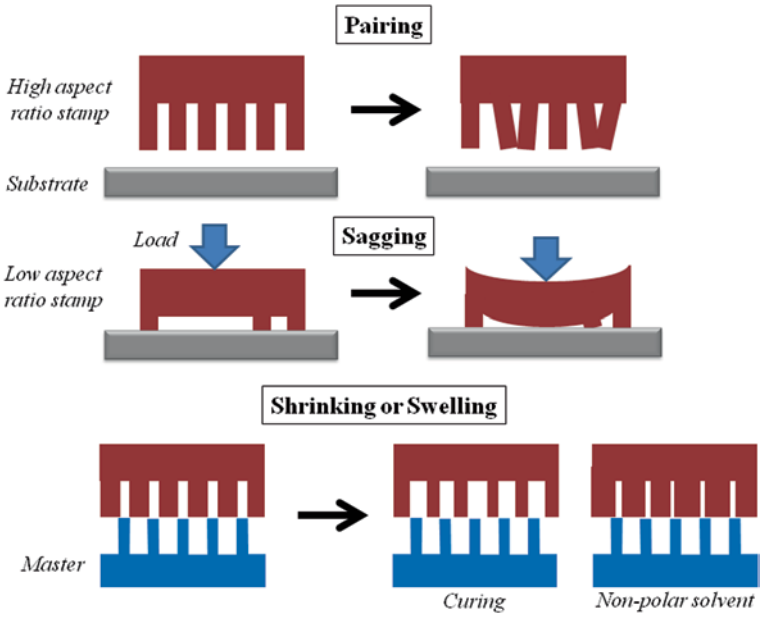


**Fig. 7.11** Limitations of PDMS stamps in soft lithography

While PDMS offers some advantages, there are a number of properties inherent to PDMS which can limit its capabilities in soft lithography. As illustrated by Fig. 7.11, first, its low surface energy and Young's modulus limit the fabrication of features with high aspect ratios due to merging (pairing) and buckling of the relief structures. Second, its high elasticity can lead to deformation during the transfer (sagging). Then, PDMS shrinks by ~1 % after curing and can be readily swelled by some nonpolar solvents [36].

Hopefully, pairing can be limited by increasing the elastic modulus of the PDMS. For instance, hard-PDMS is based on a bimodal mixture of short and long polymer chains which confer better mechanical properties for the stamp [37]. Sagging can be avoided by the use of a thin rigid substrate backplane (such as glass or mica which preserves the stamp flexibility) [38].

#### 7.2.1.1 Printing Process

Lithography by printing is the transfer of a material (ink) from a writing head or a topographically patterned stamp to a surface. The most common printing methods for templating polymer substrate for biological applications are direct write printing and microcontact printing (μCP).

#### 7.2.1.2 Contact and Noncontact Direct Writing

Direct writing approaches remove the need for a mask to achieve surface patterning and rely on the movement of a print head in a defined pattern. Direct write assembly enabled the construction of micro-periodic structures without the need for expensive tooling, dies, or lithographic masks. Contact printing is achieved using a robotic apparatus that first dips a microscale dimension pin into a solution; then, spots the ink onto the substrate surface. Noncontact printing (also called ‘‘inkjet printing”) is achieved by ejecting nanoliter of solution from a microcapillary onto specified positions on a surface [8]. The advantage of this strategy is that common problems with contact printing (contamination of the nose, inhomogeneous spot geometry, and variations in the dispensed volume) can be limited [39]. Such strategies can be applied for the formation of DNA, protein, and cell microarrays [40]. 2D monolayers of a broad range of molecules can be printed on a glass surface using robotic spotting technology [8]. For instance, acrylate monomers with diversified hydrophobicity/hydrophilicity and cross-linking densities were robotically deposited on a non-cell adhesive layer of poly(hydroxyl ethylmethacrylate) on top of conventional glass slides, and then UV polymerized [41]. Almost 500 spots with different composition and with a diameter of 300 μm and a periodicity of 740 μm spots have been deposited. The arrays were further evaluated for their capacity to maintain pluripotency of human stem cells. Hook et al. used robotic contact printer to prepare platform for high-density cell assays [42]. A high-density PEG coating was deposited on glass slides as a background exhibiting low cell attachment properties. Drops of phenylazide modified poly-l-lysine (PLL) were then directly deposited on this background without contact using robotic deposition. UV irradiation of these polymer arrays resulted in the cross-linking of the polymer spots and their covalent attachment to the surface. A second run with the robotic contact printer enabled the deposition of DNA microarrays on top of the polymer microarrays.

3D direct writing techniques by robotic deposition using hydrogels are under development. Several teams have recently presented independent works on the 3D printing of gelatin hydrogels for the attachment and proliferation of cells [43]. Gelatin can be used as “ink” in direct write manufacturing due to temperature induced sol–gel transition characteristics. Above the gelling temperature (around 27 °C) aqueous solution of gelatin exists. As temperature is lowered, the material becomes gel-like. In future, such strategies should find widespread application for tissue engineering, organ printing, and the development of 3D drug discovery platforms.

*Limitations* One of the limitations with contact and noncontact printing is that, although patterned arrays of DNA, proteins, and other molecules are easy to form, there are limited procedures in place to keep the molecules where they are spotted. Resolution of the technique is limited to hundred of microns which is mainly due to the accuracy of the positioning of the writing head and the volume control of the dispensed ink [39].

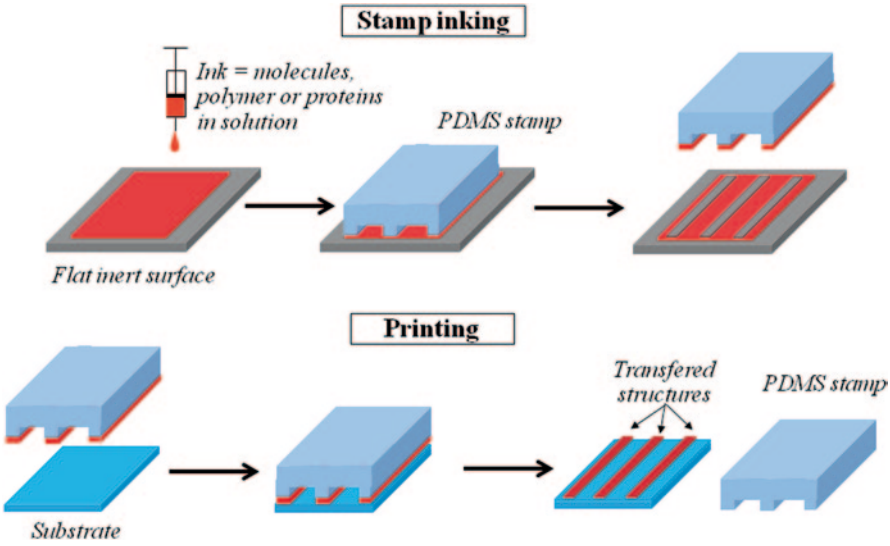


**Fig. 7.12** Schematic of the two-step microcontact printing process (Stamp inking and transfer)

### *7.2.2 Microcontact Printing*

μCP, introduced by the Whitesides group [32], is a process similar to the well-known reprographic techniques. Indeed, from a topographically template master made by conventional lithography, a mold (also called a "stamp") is realized by the deposition and the curing of an elastomeric material (often, PDMS) which after cross-linking provides a matrix (mold) that can then be used to reproduce multiple copies of the initial structures (Fig. 7.10).

To perform the transfer, the PDMS stamp first needs to be "inked" with the solution. The inking consists in placing drops of solution on the structured stamp. Then, the exceeding liquid solution is removed from the stamp surface by a drying procedure under a nitrogen flow. The inking is a key step in μCP because the consistency and nature of the deposited molecule will depend on the quality and the nature of the transfer. As shown in Fig. 7.12, in our laboratory, to obtain a homogeneous inking we first deposit the ink on a flat and inert substrate (usually a flat PDMS substrate). Then the exceeding ink solution is removed and the structured stamp is brought to contact with the deposited ink. This method prevents the inking of the uninteresting zone of the stamp that occurs when the stamp is dipped in a solution. For the printing procedure, molecules adsorbed on the stamp surface are transferred onto the substrate in contact if they have a greater affinity with the substrate than with the stamp. If the contact conditions (load on the stamp, environmental conditions) are controlled, during the contact, molecules will be transferred only from the top of the topographic patterns of the stamp. Finally, the stamp has to be carefully removed in order to leave the template of ink molecules on the substrate.

Initially μCP was largely used for the reproduction of self-assembled monolayer (SAM) patterns on a gold surface by using thiols molecules as an ink [44]. Now microcontact printing has undergone a spectacular evolution since its discovery and can achieve very fine patterning of different kind of inks (thiols, silanes, biomolecules, colloidal particles, and polymers) on a wide variety of substrates (metal, semiconductor, polymers) [36]. The lateral resolution of the chemical pattern can be below 100 nm and depends mainly on the properties of the stamp, the nature of the ink, and the extent of the ink diffusion across the substrate [45]. Many biological materials such as protein or DNA are suitable inks for μCP. The affinity between biomolecules and the stamp has to be carefully checked if one wants to keep the biological activity. Indeed, it was shown that for protein patterning hydrophobic stamps such as pristine PDMS has to be avoided in order to prevent the denaturation of the protein [46]. To render PDMS surface hydrophilic, several processes have been successfully tested such as UV/ozone, $O_2$ plasma treatment or surface functionalization via silane [38].

Feng et al. used substrate films based on poly(N-succinimidylmethacrylate) (PNHSMA) as platforms for biomolecules immobilization with high molecular loading [47]. PEG-NH2 was transferred via μCP and coupled covalently to ester groups exposed at the surface of PNHSMA films. After the transfer and a rinsing procedure, PEG-NH2 region have a thickness below 2 nm. Amino-end-labeled probe DNA was then covalently coupled to PEG-patterned PNHSMA, and followed by a treatment with dye-labeled complete-mismatch target DNA or matching target DNA, respectively. While no fluorescence is observed for the probe DNA–mismatch target DNA combination, the matching DNA strands yielded a well-defined pattern in the microscopy images.

Patterning of cells is of great importance for its potential applications in the therapy of nerve injuries [48] or for tissue engineering [49]. Due to the critical requirements and the great difficulty in some cells cultivation, developing new methods for cells patterning has progressed rapidly in recent years. Buzanska et al. [50] have transferred PLL and fibronectin on petri dishes coated with a plasma polymerized polyethylene oxide-like film to study the adherence and differentiation capacity of neural stem cells. They concluded that compared to other technique to pattern cell such as noncontact spotting, μCP allows densely packed and uniform monolayers of protein patterns to be obtained. Finally they observed that tailoring the geometry of the biopattern enabled directing and monitoring of the neural stem cells. μCP was also used to pattern cells on poly(lactic acid) (PLA) and poly(lactide-co-glycolide) (PLGA) substrates that are routinely used as scaffolds in engineering tissues [51]. Cell-resistant poly-OEGMA polymer was microcontact printed onto the polymeric substrates to create cell-resistant areas. After seeding, NIH 3T3 fibroblasts remain confined within the patterns on the PLGA and PLA films and aligned their actin cytoskeleton along the line patterns (Fig. 7.13).

Hydrogels can also been templated by μCP. For instance, Burnham et al. have patterned a polyacrylamide hydrogel coating containing disulfides with iodoacetyl biotin in order to attach streptavidin [52]. Biotinylated immune complexes and lipid vesicles were finally readily bound to streptavidin-functionalized region.

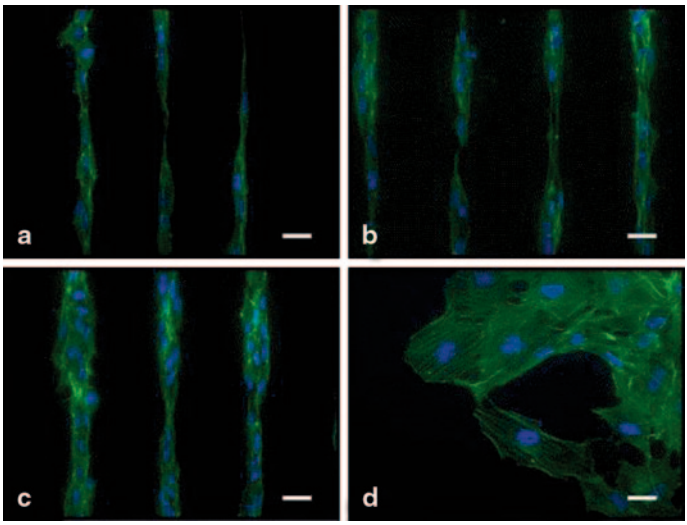


**Fig. 7.13** Alignment of cytoskeleton and nuclei in NIH 3T3 fibroblasts cultured on **a** 10 μm, **b** 20 μm, **c** 30 μm wide lines, and on **d** unpatterned control PLGA substrates after 24 h. Actin microfilaments appeared in *green* and cell nuclei in *blue* (scale bar: 25 μm) [51]

*Limitations* As described previously, pairing or sagging of the PDMS stamp leads to limit the resolution to μCP above 100 nm [53]. For smaller feature sizes harder materials can be used such as composite PDMS [37] or perfluoropolyethers polymers [54]. In addition, even after curing PDMS stamps, they contain traces of residual low-molecular weight PDMS that is likely to be transferred on the substrate during μCP [55]. It was shown that either an oxygen plasma [56] or UV/ozone [57] pretreatment of the stamps limits the transfer of PDMS residues. Finally, due to the hydrophobic nature of PDMS surface, water-soluble inks such as biomolecules do not wet the surface of the stamp. However, oxidation of the surface by either an oxygen plasma or UV/ozone treatment allows the printing of polar inks.

Independent of the stamp, a major limitation of the resolution of μCP arises from the ink diffusion during the contact between the stamp and the substrate. Indeed as a function of the temperature and humidity, inks can diffuse through the ambient vapor phase reaching undesired areas [58]. Ink diffusion can be limited either by the use of high-weight molecules such as polymers [38] or by using catalytic μCP for which the ink is immobilized on the stamp [59].

### *7.2.3 Catalytic μCP*

The PDMS stamp surface can be made catalytically active in order to induce a chemical reaction at the substrate. In such process called catalytic μCP, no ink is needed, and therefore the lateral resolution of the transfer is not limited by ink diffusion.

This inkless strategy was used by several groups to pattern self-assembled surfaces by using either a chemical reaction [60] or a biocatalytic reaction [59]. In this later work, they immobilized exonuclease enzymes on biocompatible poly(acrylamide) stamps and created circular patterned DNA (∅ = 10 µm) both on glass and gold surfaces. More recently we have used a method based on the deposition of a biopolymer layer on a surface and the hydrolysis of this layer by microcontact printing with an immobilized hydrolytic enzyme [34, 61]. Fluorescently labeled poly-L-lysine ($PLL^{FITC}$) was first adsorbed on silicon substrate by spin coating leading to a sub-nm thick homogeneous film over the whole surface. In order to template the PLL film, trypsin was immobilized on a structured PDMS stamp treating the stamp surface with 3-aminopropyltriethoxysilane (APTES). After silanization, the stamp was first immersed in phosphate buffer containing glutaraldehyde and finally immersed in phosphate buffer solution containing trypsin. The PLL film was patterned with trypsin-functionalized stamps that consisted of 1 µm width lines separated by 3 µm. The fluorescence microscopy images (Fig. 7.14) revealed a large scale patterning of the PLL layer due to the degradation of the PLL by the trypsin. The atomic force microscopic (AFM) picture displayed the simultaneous resolution of degradation of the PLL layer (Fig. 7.14c, d and e). The profile of degradation of the PLL layer is steep and no residual material is apparent on the silicon surface.

The patterned PLL surfaces can be used, for instance, to capture ionically cross-linked hydrogel pectin beads [61] or to pattern polyelectrolyte multilayers. Indeed, we applied our patterning strategy using trypsin enzymatic lithography to a pectin/PLL assembly and obtained 1 µm width positively charged chitosan lines separated by 3 µm width line corresponding to the negatively charged PLL [34]. In addition to improvement of the resolution, another advantage offered by our method is that the stamp can be used for the printing of several surfaces without reinking contrary to the standard µCP approach [36].

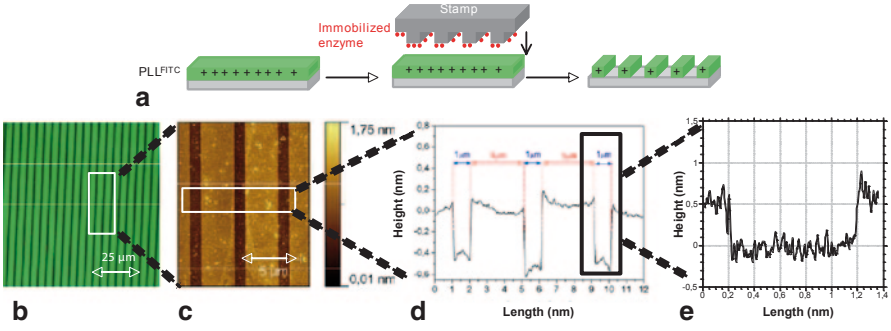


**Fig. 7.14** Schematic representation of the enzymatic microlithography process (**a**), Fluorescence microscopy image of $PLL^{FITC}$ surface patterned by enzymatic microlithography (**b**), AFM topography image of the patterned PLL surface previously created (**c**), lines profile of the corresponding AFM image (**d**), zoom on a single line of the previous profile (**e**) [34]

### 7.2.4 Photocatalytic Lithography

Bearinger et al. have developed an hybrid method between μCP and photolithography [62]. Indeed, they reported the patterning of a poly(propylene sulfide) block copolymer at the submicrometer scale using a porphyrin-based photocatalytic lithography. Porphyrin molecules, used as photocatalyst molecules, are firstly bound to the surface of a patterned PDMS stamp mask which is put in contact with an appropriately sensitive organic resist (here a symmetric triblock poly(propylene sulfide) (PPS)-blockpoly(ethylene glycol) copolymers coated gold substrate). Controlled patterning and removal of the PPS-PEG was achieved by local oxidation via activation of the photocatalyst through the polymeric photomask with red LED light. The biomolecular patterning on micrometer and submicrometer scales was demonstrated by the immobilization of fibronectin on the regions where PPS-PEG were removed and by the grafting of fluorescently labeled IgG [63].

## 7.3 Embossing

### 7.3.1 Nanoimprint Lithography (NIL)

Nanoimprint lithography (NIL) which was firstly introduced by Chou et al. [64], is a low-cost, rapid, and simple fabrication process with a high throughput that offers the possibility to easily pattern polymer substrates. Unlike the conventional methods that mimics the patterns of the mask in the resin by chemical contrast, the mask is replaced by a mold having 3D patterns on its active face (face in contact with the resist). This mold is then pressed into the resist which fills its cavities. For NIL, also called hot embossing, the mold is usually a silicon template prepared by conventional lithography (EBL, FIB, or photolithography). The procedure to obtain a templated structure by NIL is shown in Fig. 7.15. At first, the mold is put in contact with a polymer resist heated well above its glass transition temperature (Tg) to soften the polymeric material [65]. The mold is then pressed with a controlled load onto the deformable polymeric resist to imprint the mold structure. Finally, the mold and the resist are cooled down at $T < Tg$ to allow the separation and the hardening of the transferred structure. After NIL procedure, a thin residual layer of resist is usually left between the protrusions of the mold and the substrate. This residual layer can be removed by reactive ion etching (RIE) but this process can affect the original shape and size of the pattern.

Theoretical resolution of NIL is only linked to the mold resolution. It was shown that NIL is able to transfer features down to 0.4 nm [67] and features with size below 10 nm can be obtained on a relatively larger area ($\varnothing = 20$ cm) [68]. Because of its versatility NIL is one of the most used techniques to template polymeric substrate for biomedical applications.

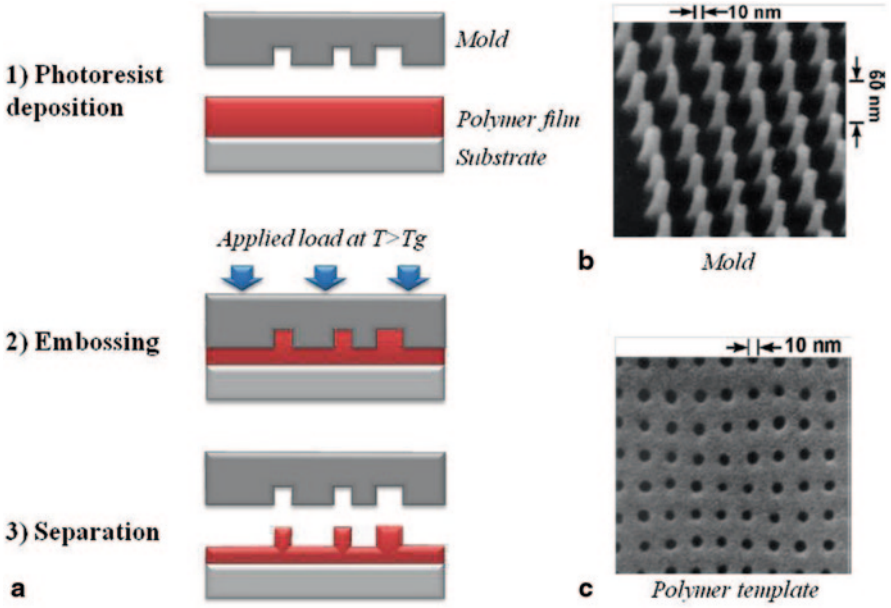


**Fig. 7.15** Thermal-NIL principle (**a**) and SEM images of a high-resolution silicon mold prepared by EBL (**b**), and the corresponding polymer template after NIL process (**c**) [66]

Ohtake et al. fabricated DNA nanopatterning by nanoimprinting a PLL-coated glass. DNA molecules are then immobilized with the amino group of the PLL, and DNA lines of about 700 nm width were obtained [69]. Falconnet et al. [70] used NIL for protein immobilization. They imprinted grooves onto a PMMA-coated $Nb_2O_5$ substrate. The substrate is then immersed into biotin-functionalized poly(L-lysine)-graft-poly(ethylene glycol) (PLL-g-PEG/PEG-biotin). After removing the remained PMMA with acetone, the exposed substrate was passivated with PLL-g-PEG. Finally, streptavidin was immobilized onto the patterned biotin regions and protein patterns with a feature size of 100 nm were obtained. Although in most of the applications the resist is usually made of PMMA polymer, [71] biopolymer can also be used [72]. A non-biofouling amphiphilic comb polymer was physically patterned by NIL process with a modulus-enhanced polyurethane acrylate mold material (Fig. 7.16) [73]. Physically defined nanostructures of the polymer were subsequently functionalized with proteins. As a result, submicrometer-scaled streptavidin patterns were readily constructed over a larger area. These patterns are then used for the immobilization of biotinylated M13 bacteriophages (Fig. 7.16).

When used on thin polymer films [66, 74], NIL can be a simple method to fabricate nanofluidic channels with controllable diameter and height which can be used for DNA detection [75] or DNA stretching study. The technique consists in imprinting a channel template into a thin polymer film on a glass substrate without detachment. A very thin polymer layer is used so that the displaced polymer will not be

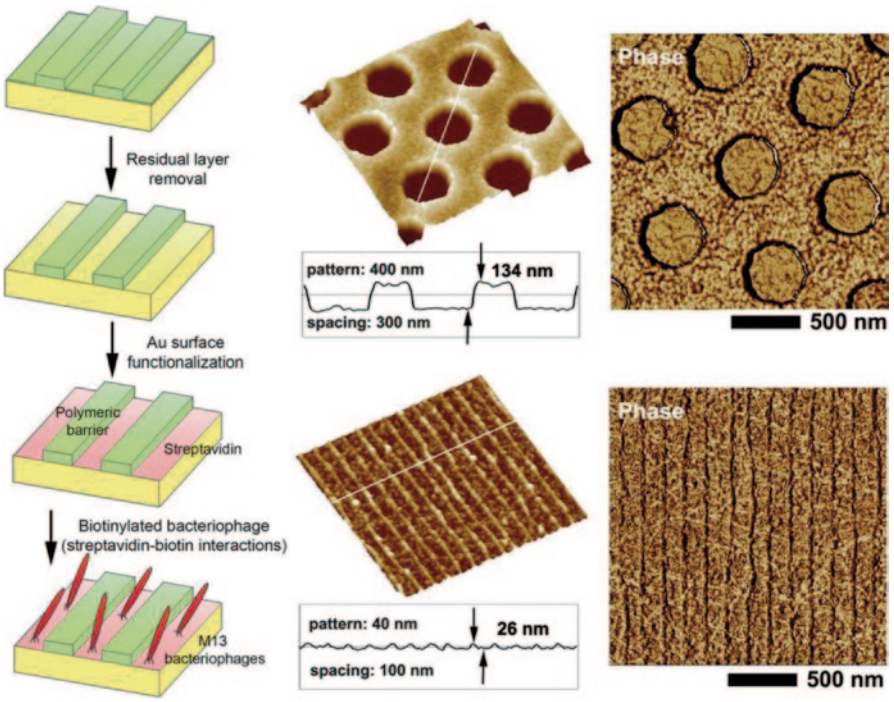


**Fig. 7.16** Schematic diagram of the experimental procedure for the nanopatterning of the proteins (*left*) and atomic force microscopic (*AFM*) images of the two different bacteriophage-bound protein patterns [73]

able to completely fill the trenches on the mold. Uniform nanofluidic channels as small as 75 × 120 nm were obtained by this method.

*Limitations* NIL presents some limitation such as the releasing of the resist from the mold after the separation. Indeed, the resist tend to adhere on the mold even if the mold is treated [28]. As a consequence, the mold has to be regularly cleaned or replaced which limits the use of NIL for industrial production. In addition, parameters such as resist thickness, temperature, or applied load have to be strictly controlled for reproducibility. The materials utilized for NIL generally require large pressures (in the order of 500–5000 kPa) to fill the mold during the imprint step. The high viscosity of the polymer can also have consequences in the filling of the mold such as an incomplete filling of small neighboring features [76]. Finally, substrate imprinting generally requires operating temperatures that are sometimes too high for biopolymers to remain chemically stable [77]. However, NIL is clearly one of the most promising processes for the design of polymeric platform for biorecognition. Besides, MIT's 2003 Technology Review named NIL as one of the "ten breakthrough technologies that will change the world."

## 7.4 Molding

Molding is a well known form for transferring patterns in polymer substrates. A topographically patterned stamp is placed into contact with a precursor of a solid material, which can be a prepolymer or a melt. Once the precursor have filled the stamp cavities, a curing step (thermal or irradiation) is performed to obtain the desired features. This simple approach has been adapted and used as a low-cost and effective method to structure polymeric substrate at the nanoscale. Recent developments of this technique in the biomaterial field concern methods such as step and flash imprint lithography (SFIL), Soft UV nanoimprint lithography, 3D-micromolding technologies (micromolding in capillaries (MIMIC) and solvent-assisted micromolding in capillaries (SAMIM)).

### *7.4.1 Step and Flash Imprint Lithography (SFIL)*

Traditional embossing processes such as NIL require high pressures and temperatures (pressures greater than 10 MPa may be required, and temperatures must be greater than the Tg of the polymer film). This leads to unpredictable distortions in the imprinted structures. In 1999, Willson and Sreenivasan developed SFIL [78] which is a three steps process.

1. A rigid UV-transparent mold (glass, quartz, or PET) which is gently pressed onto a low-viscosity UV-curable liquid which fills the mold cavities.
2. UV-irradiation leads to the polymerization of the liquid which adopts the mold features sizes.
3. The mold and the substrate are separated.

The use of UV irradiation eliminates the heating step of the NIL process and thus allows performing SFIL at room temperature. Moreover, compared to NIL, the mold transparency facilitates the alignment between the mold and the substrate, and thus, better throughputs can be reached [66]. In terms of resolution, SFIL and NIL are comparable [78].

SFIL was used for direct nanopatterning of an silsesquioxane/poly(ethylene glycol) (SSQ/PEG) blend which is a highly stable and robust nonfouling material with nonswelling property and good hydrophilicity [79]. As demonstrated by SEM imaging, the process allows the formation of feature sizes down to 25 nm at room temperature. Xie et al. have recently used SFIL to prepare a platform to study the effect of nanocues on the cell growth direction in primary cortical cell [80]. Before imprinting, a layer of 60 nm antireflective coating was spin coated on a silicon wafer and baked to improve the adhesion of the resist. Then, droplets of liquid imprint resist (height close to 100 nm) were dispensed on the precoated wafer. After leveling the contact force between the quartz template mold (fabricated by EBL) and the substrate, the resist was polymerized by UV exposure. A branched polyethylenimine (PEI) coating is then performed on the surface of the template. The coated template is then ready for the cell seeding with rat primary CTX cells. Results show

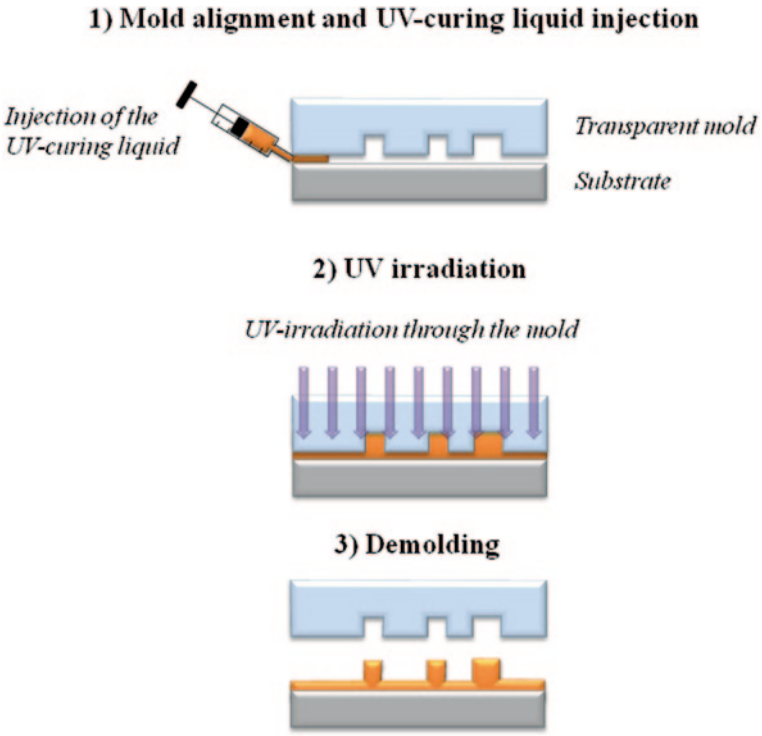


**Fig. 7.17** Schematic of the SFIL process

that patterns with periods between 400 and 600 nm guide the growth of neurites effectively compared to planar surface (Fig. 7.18).

*Limitations* In fact, the current library of UV curing liquid has been designed for microelectronic applications and they are often not compatible with biological systems. Hence, there is a need to develop materials to be used in this emerging field [81]. Indeed, the curing properties of the UV curing liquid material are essential along with the molecularly clean separation of the template from the surface of the nanoimprinted material for repeated use of the template in SFIL. For instance, UV curing liquid must have a low shrinkage during UV curing. Takei et al. have thus recently developed an ecofriendly new UV curing liquid material derived from medicinal drugs for the volume manufacture of biomicrochips [82]. The thickness of the UV curing liquid, as well as the injection speed and the imprinting pressure, have to be accurately controlled to avoid the formation of air bubble at the mold/liquid interface and to ensure a complete resist filling in the stamp nanocavities. The pressure applied during imprinting directly influences the flow of the resist and determines the accuracy of the imprinted nanoscale structures. Finally, because of the need of an interface planarity between the mold and the substrate (as for NIL), SFIL is limited to the template of relatively smaller area regions.

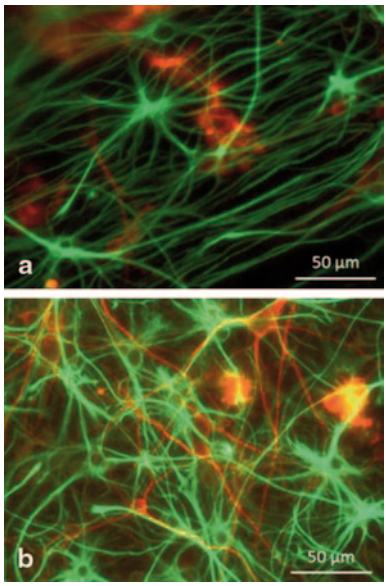


**Fig. 7.18** Immunostaining of cells on PEI-coated samples: (*top*) nanoscaffold with 380 nm ridge width, 600 nm pattern period and (*bottom*) flat glass substrate [80]

### *7.4.2 Soft UV-Nanoimprint Lithography*

Soft UV-NIL has recently been proposed as a means to reduce the cost of master fabrication in SFIL [83]. Indeed, soft UV-NIL uses a flexible transparent stamp usually made of PDMS that can be easily replicated from a unique silicon master mold. Moreover, the flexibility of the polymeric stamp ensures contact with the surface substrate on larger surfaces at low pressures and allow the structuration on curved or flexible substrates [84]. The preparation of the PDMS mold follows the same procedure than for the microcontact printing process which was detailed previously. Because of the softness of the mold, it is easy to make the center area of the mold to bow outwards to contact with the core layer first, then slowly lower down the remaining part of the imprinting mold. In this way, the trapped air bubble can be squeezed out along the pattern, making the patterns void free [83].

Recently, Wang et al. presented the preparation of an optical biosensor built on a low-cost polymer platform by soft UV imprint lithography [85]. For this they used a silicate-based inorganic–organic hybrid polymer (PSQ). At first a low density form of the polymer (PSQ-LL) is spin coated and cured on a silicon substrate to act as the waveguide bottom cladding. Then the core waveguide polymer (PSQ-LH) is spin coated and a PDMS-patterned mold is used to transfer the pattern on the PSQ-LH film by soft UV imprint lithography. Finally, a post baking at 180 °C for 4 h allows full polymerization of the PSQ-LH-structured film and the obtention of a microring resonator (Fig. 7.19). Microring resonators are versatile wavelength-selective elements for which ring length and refractive index-dependent resonant wavelength can be measured [86]. For biosensing, biomolecules binding on the microresonator surface imply a modification of the refractive index and thus a shift of the resonant

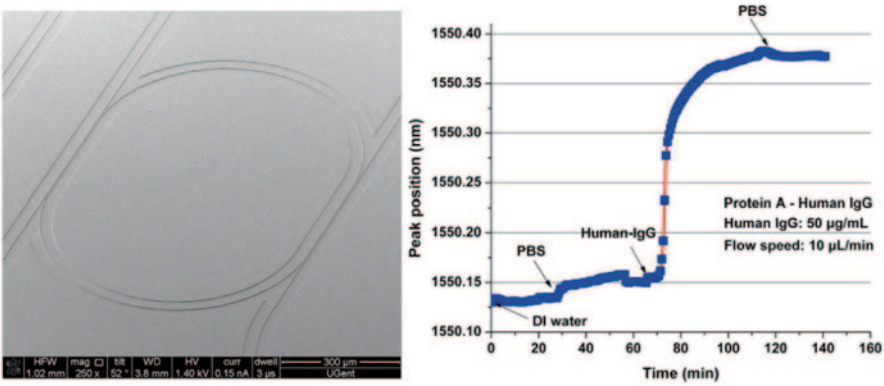


**Fig. 7.19** SEM pictures of the microring resonator (*left*) and evolution of the wavelength resonance during the sensing procedure with protein A as bioreceptors immobilized on the resonator surface (*right*) [85]

wavelength. ([85], #364). In this work, human immunoglobulin G (IgG) and protein A (Staphylococcal protein A) are chosen as an affinity model. Under physiological solution conditions, protein A molecules were coated on the surface of the microring resonator through an incubation process. The efficiency of the system to detect IgG/protein A binding is shown in Fig. 7.19.

*Limitation* The distortion of the flexible mold is a drawback to be solved for high fidelity pattern fabrication in soft UV-NIL. The applied imprint pressure is the main cause for the mold deformation, which leads to inadequate pattern fidelity. On the other hand, a certain amount of imprint pressure is necessary to ensure fast pattern replication, that is, efficient conformal mold contact and sufficient mass transport for a fast filling of mold cavities. Solutions to control the applied pressure have been explored to circumvent this problem [87].

Soft UV-NIL process was modified by Rolland et al. to produce isolated nanoparticles with different shapes and compositions [88]. The difference with traditional soft imprint lithography is that particle replication in nonwetting templates (PRINT) process uses a nonwetting fluorinated materials and surfaces which confines the liquid precursor inside the features of the mold. The highly fluorinated perfluoropolyether (PFPE) material allows for resistance to swelling by organic liquids and very low surface energies, thereby preventing flash layer formation and ease of separation of PFPE molds from the substrates. These enhanced characteristics enable easy removal of the stamp from the molded material, thereby minimizing damage to the nanoscale features. PRINT was used to produce monodisperse, nanometer scale PEG particles in a variety of shapes by molding a PEG-diacrylate liquid monomer followed by room temperature photopolymerization. This process has been used to mold monodisperse microparticles and nanoparticles in various complex shapes (Fig. 7.20) from several polymers (including PLGA, PEG, and proteins) and loaded with a wide variety of therapeutic payloads (including docetaxel, DNA and vaccine) [89].

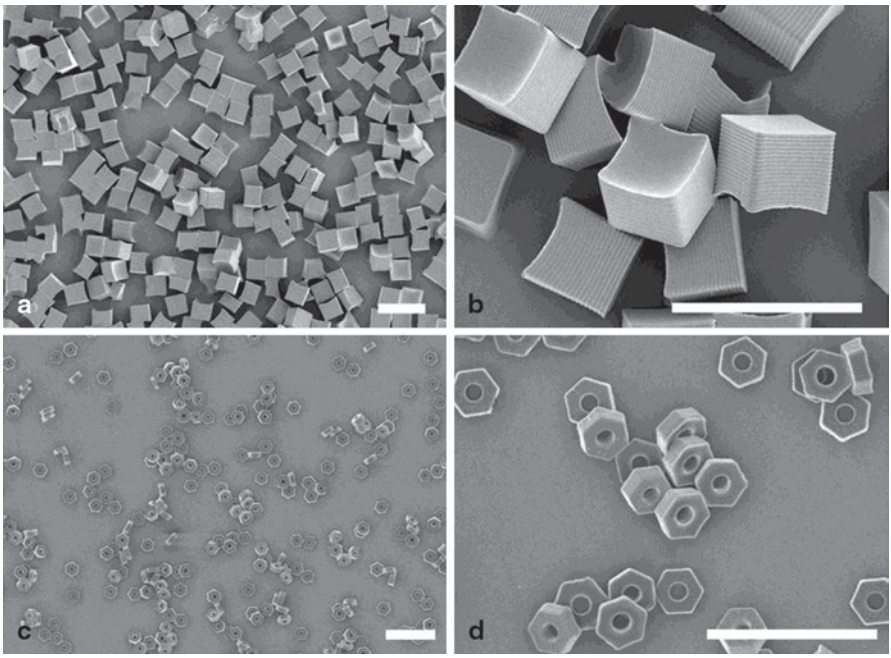


**Fig. 7.20** Cubic (**a, b**) and hexnut (**c, d**) polymer microparticles molded by PRINT technology. Scale bars are 10 μm [90]

**3D Micromolding Technologies** Micromolding in capillaries (MIMIC) is a technique that uses the capillarity phenomenon to fill microfluidic channels with a prepolymer [32]. Such process is close to SFIL except that in that case the stamp is in close contact with the substrate. The prepolymer is deposited at the open ends of the stamp channels, and spontaneously fills the channels, thanks to the capillary force. After curing, the PDMS mold is removed to reveal 3D-patterned microstructures of the polymer. Like the PRINT process and in contrast with SFIL, the advantage of MIMIC is that it can produce isolated features without an interconnecting layer [91].

Several teams have used MIMIC to produce cell patterning on polyelectrolyte multilayer (PEM) surface [92]. Shim et al. placed an $O_2$ plasma oxidized PDMS mold in contact with a cationic polyallylamine hydrochloride/anionic polystyrene sulfonate (PSS/PAH) multilayers. A UV curable PEG-dimethacrylate (PEG-DMA) polymer was placed at the open ends of micromolds and filled spontaneously the void spaces by capillary action. After curing, the PDMS mold is peeled off and a PEG/PEM template surface is obtained. As shown in Fig. 7.21, PEG microstructures serve as a biological barrier to reduce nonspecific binding of cells, whereas PEM surface improves cell immobilization [92c]. More recently, Marel et al. have used MIMIC to prepare PEG-DMA microstructures on a large scale directly on a petri dish surface in order to confine cell in desired geometry [92b].

For that they had to introduce a micro pillar field to prevent the PDMS mold from sagging during the MIMIC procedure. Cell arrays of microcolonies can then

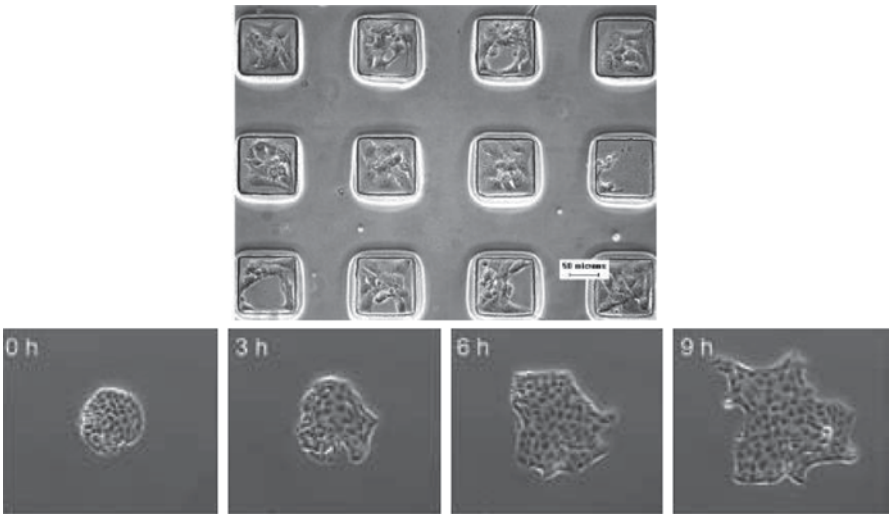


**Fig. 7.21** Optical image of NIH 3T3 fibrobrasts patterned on the polyelectrolyte-patterned region [92c]. Time lapse microscopy images of the evolution of the microstructured MDCKII cells culture growth [92b]

be studied under boundary free growth conditions by lifting-off the PEG-DMA layer (Fig. 7.21). Another 3D-micromolding technique named solvent-assisted micromolding (SAMIM) consists in wetting the stamp surface with a solvent and press it against a polymeric substrate at ambient conditions. The solvent can swell or dissolve the polymer substrate to decrease its Tg and viscosity, and thereby allow the polymer to conform to the elastomeric mold [93]. SAMIM enables the 3D-molding of polymers that cannot be molded by SFIL or NIL, however the resolution is limited by some uncontrolled solvent etching [94].

Due to the difference of chemical properties among the PEMs, it is hard to find a universal chemical method to pattern PEMs. SAMIM such as the compression [95] and imprinting [96] techniques can create physical structures on most of the PEMs. Very recently SAMIM of PEM was performed with a PDMS stamp to treat PSS/poly(diallyldimethylammonium) chloride (PDADMAC) multilayers before or after etching with an NaCl solution [97]. Different patterns were obtained such as double thin lines, meniscus-shaped ridges, and high ridges for which the ridge height was controllable in the range of 25–1100 nm. Due to these patterns, Han et al. demonstrated that migration of smooth muscle cells was restrained by the double-line patterns in a ridge height-dependent manner.

### *7.4.3 Scanning Probe Lithography (SPL)*

SPL exploits the high accuracy of the probe displacement of an Atomic Force Microscopy and its interaction with the substrate to induce mechanical, thermal, or electrical interactions [98].

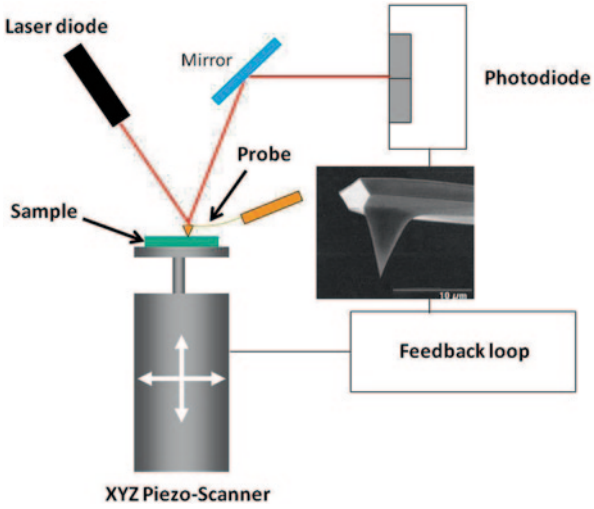


**Fig. 7.22** Schematic representing the principle of an AFM apparatus

### 7.4.3.1 Atomic Force Microscopy (AFM) Principle

An AFM consists of four main elements (Fig. 7.22):

- A probe usually made in silicon, silicon nitride, or Gold with a nanometer-sized apex.
- A detection system that is able to measure the probe displacements (lateral and vertical) accurately. Most of the commercial AFMs today are equipped with a laser diode and a photodiode detection system.
- A piezoelectric scanner that is able to move the probe or the sample with high resolution (< 1 nm).
- An electronic setup with a feedback loop which controls the probe displacement toward the imposed experimental setpoint (probe/sample interaction intensity).

AFM was developed at the end of the 1980s by Binnig et al. [99] as a high-resolution imaging technique of the topography of insulator surfaces which were not measurable by the Nobel Prize winning scanning tunnelling microscope (STM). However, because of its high versatility and the ability to control probe/sample interaction and/or displacement, the technique has been used to modify surface sample at the nanoscale. Since the end of the 1990s, AFM is often used as a technique to remove, modify, or deposit material on a surface [100]. In terms of resolution, SPL is able to fabricate nanometer-scale structures with at least one lateral dimension between the size of an individual atom (for STM-based lithography) and approximately 100 nm on silicon and other surfaces. SPL methods are widely employed for nanopatterning of biomolecules with submicrometer resolution [2]. To fabricate polymeric platform, SPL's most used methods are force lithography which consists in patterning topographically a polymer material with the AFM probe and dip-pen nanolithography which allows the accurate deposition of biomolecules on a substrate.

### 7.4.4 Force Lithography—Nanoscratching

An interesting way of performing nanometer patterns into polymeric material as force lithography which is based on direct indentation of the material by the AFM probe pressed with sufficiently high load conducting to an irreversible plastic deformation. The pattern is formed as a result of the AFM probe motion above the polymer surface with imposed set point force intensity. As expected, the higher the load the deeper will be the scratch. This technique is also called nanoscratching. Modification of a preexisting polymer film to obtain a patterned surface has several benefits over other patterning techniques in that thin polymer film deposition techniques are well established (e.g., spin casting, dip coating, spray coating). The scratching depth is linked to the applied force, to the mechanical properties of the polymer and to the scratching velocity [101]. Like in AFM force versus distance measurements, preliminary calibration of the AFM apparatus is required in order to accurately control the applied force during scratching [102]. The main issue with polymer scratching is the presence of protrusions along the scratch which are due to the material displacement by the probe displacement. Post solvent rinsing can overcome this problem for PMMA but they usually result in a decrease of the pattern resolution [103]. Although several ways have been proposed to limit tip wear and substrate protrusion such as using an oscillating probe, [104] or thermally assisted indentation [105], the protrusion problem cannot be completely suppressed and this problem shortens strongly the list of candidate of polymeric substrates.

For these reasons, although nanoscratching has been performed on thiol self-assembly monolayers to generate protein nanopatterns with lateral dimensions from 10 nm to 1 μm, [106] to our knowledge only few papers treated of nanoscratching of polymer surfaces for biological application. Among these scarce works Muir et al. have used nanoscratching to prepare a template protein-adsorbing surface [107]. As shown in Fig. 7.23, the polymer surface consists in a protein-fouling heptylamine plasma-polymer (HApp) base film and a low-fouling diethylene glycol dimethyl ether plasmapolymer (DGpp) top film. The DGpp film is selectively removed through the use of nanoscratching to expose the underlying HApp film, which provides a protein-adsorbing surface.

### 7.4.5 Dip-Pen Nanolithography (DPN)

DPN is an SPM-based lithographic technique introduced by Mirkin et al. in 1999 [108]. With the use of an AFM probe coated with a molecular ink, one can transfer ink molecules to a substrate surface and draw patterns with nanoscale resolution. In DPN, the AFM probe is dipped in a solution containing the molecule to transfer (Fig. 7.24). The probe is then dried under $N_2$ in order to remove the remaining solvent. Using the AFM apparatus, the probe is brought into soft contact (low load) with the substrate. Under classical room conditions, atmospheric water is going to spontaneously condense and form a water meniscus between the probe and the sub-

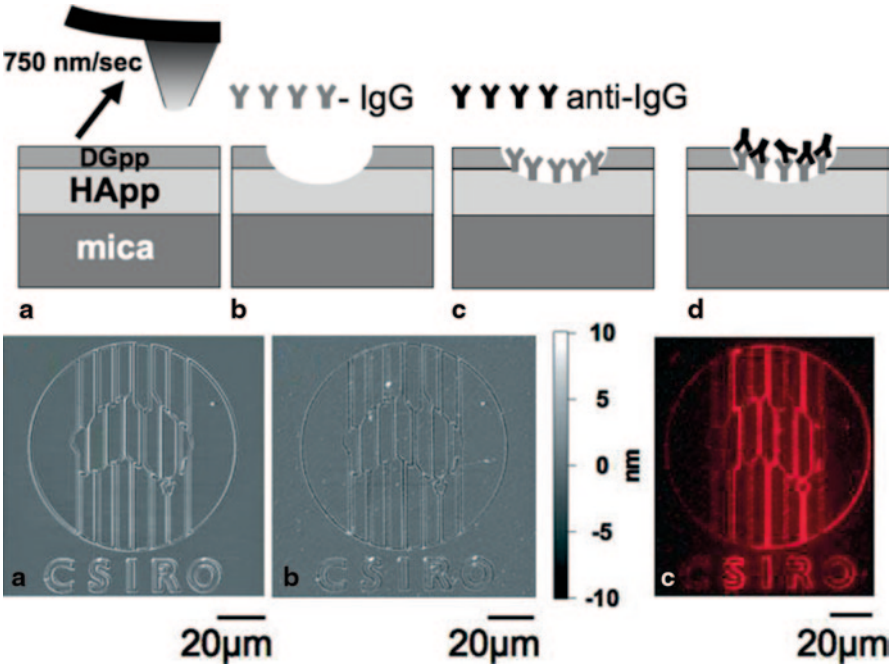


**Fig. 7.23** Schematic diagram illustrating the SPL technique used to produce nanometer-sized protein patterns (*top*). **a** AFM image before protein adsorption (depth of scratches ca. 7 nm, width of scratches ca. 300 nm; *bottom*). **b** AFM image of (**a**) after adsorption of fluorescent. **c** Fluorescence microscopy (*FM*) image of (**a**) after performing an IgG assay using fluorescently labeled anti-IgG [107]

strate [109]. The formation of the water meniscus serves as a channel for molecules to flow from the tip to the substrate.

The resolution of DPN, which is close to 25 nm, [2] is mainly governed by the size of the water meniscus which itself is dependent on humidity, temperature, and AFM probe–sample distance [110]. Other parameters can also modify the quality of the pattern. For instance, we have shown that it was possible by tuning the speed of the AFM tip during the writing process to control the amount of transferred molecules (thiol) on gold substrates [111]. The technique has been widely applied to the transfer of thiol molecules on gold surface [112]. But polymer, [113] protein, silanes, metal salt can also be deposited with nanoscale resolutions on a wide range of substrates (oxide, metal, polymer) [114].

Concerning the deposition of polymer ink by DPN for biomedical applications, to our knowledge only works dealing with PEG hydrogels were published [115]. The choice of polymer ink is limited because the spreading depends strongly on the ink's viscosity [116]. PEG absorbs a large amount of water at high humidity and becomes a viscous liquid which can flow onto the substrate at the tip–substrate contact areas. Jang et al. have recently [117] used a PEG-based ink composed of a (2:1) mixing of high- and low-mass PEG-DMA, a fluorescent dye, and a photoinitiator.

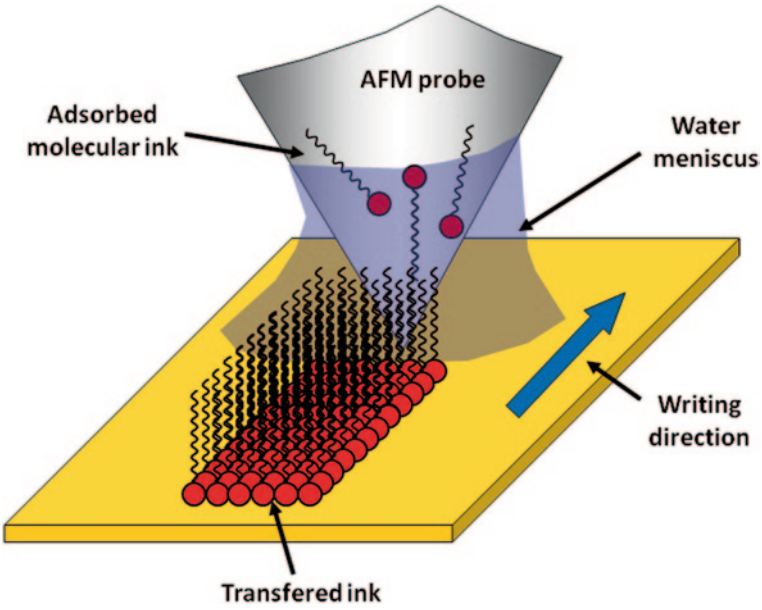


**Fig. 7.24** Schematic of the molecular ink transfer during the DPN process

The deposition was performed using a modified tip composed of 12 parallel pens with a controlled environment (humidity and temperature). The use of the parallel pens system allows the deposition of 3000 hydrogel domains, covering a total area of 800 × 600 µm within 5 min. The microarray was then exposed to UV irradiation to polymerize the PEG hydrogel precursors and form the PEG hydrogels. They have observed that the PEG hydrogel diffusion was controlled from 1.7 to 6.2 µm by printing at different temperature.

Relatively few examples in the literature deal with deposition of biomolecules by DPN on polymeric surfaces. A precursor work was done by Turri et al. in 2010 which used DPN to realize high-density DNA arrays on polystyrene surface (Fig. 7.25; [118]). For this, they deposit acrylamido-functionalized oligonucleotides, directly by DPN (three different types of 23-mer oligonucleotides have been then used as inks, bearing different end groups in the 5′ position). The acrylamide function is used for its high affinity toward the PS surface. The high-density array is then treated with a solution containing the complementary oligonucleotide. Results seem to indicate that that molecular recognition between complementary oligonucleotides was successful. The same team has recently developed this approach to other thermoplastic surfaces [119].

Irvine et al. have prepared dense protein arrays on nitrocellulose which are suitable for disease screening using standard fluorescence detection. As described in Fig. 7.25, capture antibody was used as the DPN ink then the substrate is immersed in a prostate specific antigen (PSA). Finally, the PSAs are fluorescently labeled for the detection. Spot sizes are typically no larger than 8 µm in diameter and limits

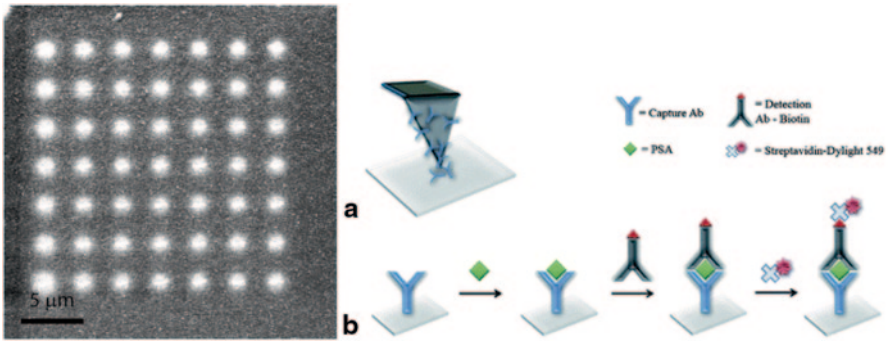


**Fig. 7.25** AFM tapping mode images of acrylamide-terminated oligonucleotides array on polystyrene after hybridization reaction [118] (*left*). Schematic of PSA immunoassay development on nitrocellulose (*right*). DPN is used to pattern the surface with anti-PSA capture antibody (**a**) followed by the exposure to PSA, a biotinylated anti-PSA detection antibody and finally fluorescently-tagged (**b**) [120]

of detection for PSA were found to be comparable with a commercially available enzyme-linked immunosorbant assay (ELISA) kit [120]. DPN was also used to pattern protein (Proteinase K) on PLLA film by agarose-assisted DPN. Once in contact with the PLLA film, enzymatic degradation occurs and creates holes in the film. It was found that while the concentration does not affect the biodegradation, the shape of the patterned protein dots can affect the depth of the biodegraded holes [121].

### *7.4.6 Polymer Pen Lithography*

Polymer pen lithography (PPL) [122] is the meeting of microcontact printing and DPN. Instead of using a hard silicon-based AFM cantilevers to deliver inks onto a surface, PPL utilizes a soft polymer pen array from which the movement is controlled by a scanning probe microscope. The feature size in a PPL experiment not only depends on probe–substrate contact time but also on contact force [123]. The pen array is made in PDMS or hard-PDMS and its preparation as well as the inking of the array follow the procedure described previously for microcontact printing. The polymer pen array is then mounted on a Z piezo scanner which can control accurately the applied load when the contact is made with the substrate. Opposite to DPN, in PPN experiment the pen is made of a permeable material and the solvent required to facilitate molecular transport can come from the environment and/or the pen itself [124]. Recently PPL was used to print initiator molecules on gold substrate followed by growth of poly(glycidyl methacrylate) (PGMA) brushes via surface-initiated atom transfer radical polymerization. The PGMA brushes template are then utilized as platforms for the immobilization of bioactive molecules to form 2D- and 3D-patterned DNA oligonucleotides and protein chips [125].

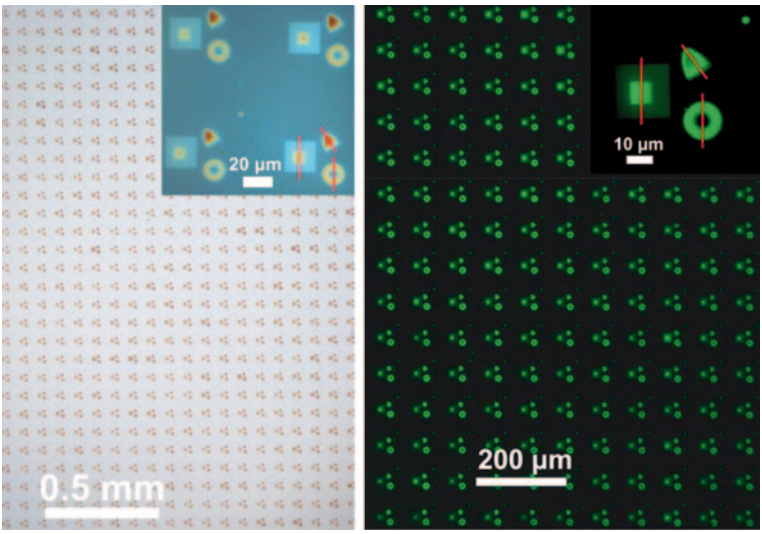


**Fig. 7.26** Optical microscope images of the large area patterned 3D structures of PGMA brushes (*left*). The inset shows a magnified polarized optical image of the 3D patterns. Fluorescent microscope images of the immobilized human IgG/FTIC-labeled antihuman IgG on the 3D-patterned PGMA brushes (*right*) [125]

The feature size of PGMA brushes can be tailored by controlling the contact force and contact time in PPL experiments. Moreover, by controlling the lateral spacing to their neighboring nanobrushes, their morphology evolves from collapsed to stretched structures and arbitrary 3D topographies can be produced (Fig. 7.26) and serve as platform for human IgG/antihuman IgG recognition [126].

As it was previously shown [34, 61], enzyme can be used to create 3D pattern on biopolymer films. In order to increase the resolution of the pattern by limiting the diffusion during the degradation, several teams have developed enzymatic lithography which consists in the covalent immobilization on the AFM probe of the enzyme. When the probe is brought into contact with a particular biomaterial, a high-resolution 3D architecture can be created. This technique has been applied since 1998 [127] to pattern lipid, or to hydrolyse DNA, peptide, and protein [128]. However, the covalent immobilization can lead to the loss of the enzyme activity. To avoid this issue, Ganesh et al. reported the use of PPL to pattern poly(ε-caprolactone) (PCL) films with a lipase B enzyme [129]. Although the protein was not linked to the polymer pen, limited lateral diffusion was observed during the degradation of the PCL film. The authors attribute this result to the strong binding of the enzyme to PCL.

*Limitations* The lower cost of AFM and its versatility make it competitive with conventional lithography. Moreover, SPL, which is a direct write technique, does not need the use of expensive molds. However, high-volume manufacturing is currently impractical due to the slow fabrication speeds resulting from the serial

patterning. Even with serial constraints, SPL could be a valuable technique for mask repair, master fabrication, and prototyping. To overcome limitations in speed, recent developments concern the use of parallel arrays of cantilevers [130]. Another limitation for the wide scale adoption of DPN or PPL is the need for reinking of the tip for the production of large arrays. Works are conducted to produce probe with an ink-tank but they are still under development [131].

## 7.5 Conclusion

In the field of biomolecular recognition, patterning techniques can increase the information density and provide the possibility to develop new generation of biosensors. Conventional and unconvential techniques have enabled the fabrication of 2D and 3D structures ranging from several tens of nanometers to micrometer scales. Many varied patterning techniques have been developed, each with their inherent advantages and limitations which are mentioned in Table 7.3. Currently, photolithography is the most widely used technique due to its several advantages, such as high throughput. On the other hand, the main drawbacks of this technique are the limited resolution due to light diffraction and the limited possibilities of working with preexisting topography and curved substrates. Novel approaches, like EBL or FIB have succeeded to increase the resolution pattern. However, this improvement came with an increase of the operational cost and a loss of throughput.

Recently, soft lithography based on molding, embossing, and printing has created the opportunity to reproduce patterns at low cost over large areas and on nonplanar surfaces. Among these techniques, both NIL and SFIL can offer several advantages such as nanometer-scale resolution and high throughput with a low process cost. However, the procedure (thermal cycling or UV curing) limits the list of candidates of possible substrate. Moreover, these techniques do not allow chemical patterning. μCP as well as DPN are well-established printing methods for biorecognition platform, since they allow biochemical patterning with high resolution and relatively low cost. However, the low throughput must be addressed in order to bring these technologies from laboratories to commercial settings.

Despite all recent progress in patterning, each method has its specific strengths and advantages and cannot meet the requirements of all fabrication needs. The choice of the lithographic technique has to be made by taking into account several parameters:

1. The material to template: plane or curved substrate? nature of the substrate (polymer, metal)?
2. The nature of the template (chemical or topographical or both)
3. The desired resolution
4. The production throughput (laboratory or industrial)

Then of course the choice of the technique is also governed by the accessibility to the techniques especially for the technique requiring clean room facilities.

**Table 7.3** Maximum resolution, advantages, and disadvantages of the principal lithographic techniques used for the preparation of polymeric platforms for biorecognition

| | Maximum resolution (nm) | Advantages | Disadvantages |
|---|---|---|---|
| Photolithography | 200 | Topographical patterns<br>High throughput<br>Parallelization | High cost<br>Low resolution<br>Clean room facilities |
| Electron beam lithograpghy (EBL) | 5–10 | Topographical patterns<br>High throughput<br>Maskless technique | Low throughput<br>High cost<br>Medium deterioration of biomaterial |
| Focused ion beam (FIB) | 5 | Topographical patterns<br>Highest throughput<br>Maskless technique | Low throughput<br>High cost<br>High deterioration of biomaterial |
| Microcontact printing (μCP) | 50 | Chemical patterns<br>Low cost<br>Maskless technique<br>Curved substrate | Low throughput<br>Lower resolution compared to EBL and FIB<br>No topographic pattern except with catalytic μCP |
| Nanoimprint lithography (NIL) | 5 | Topographical patterns<br>High resolution | Small list of polymeric substrate candidate<br>No chemical patterns |
| Step and flash imprint lithography (SFIL) | 10 | Topographical patterns<br>No temperature cycling (NIL) | Few materials available |
| Dip-pen nanolithography (DPN) | 50 | Chemical patterns<br>High resolution | No topographic pattern except with enzymatic nanolithography<br>Low speed |

In the future, for the development of polymeric platform for biorecognition, patterning techniques have to include several aspects. For industrial application, the main objective is to develop patterning techniques that can make the fabrication process simple, fast, and of low consumption. In addition, large-scale fabrication of surface patterns still remains a big challenge.

Although 3D-direct printing represents a first step in this direction, 3D-fabricating techniques have to be developed in order to mimic complex biological environments. For multiple analysis, biosensors require the presence of different templates associated to different chemistry on the same platform . The lithographic technique that is able to answer to the totality of these requirements will probably never exist; however, the combination of different fabrication methods could exist, for the future development of devices and their performances.

## References


1. M. Lundstrom, Science **2003**, 299, 210.
2. H. Tran, K. L. Killops, L. M. Campos, Soft Matter **2013**, 9, 6578.
3. C. M. Niemeyer, C. A. Mirkin, Nanobiotechnology: Concepts, Applications and Perspectives, WILEY-VCH, **2004**.
4. C. Lin, Y. Liu, H. Yan, Nano Letters **2007**, 7, 507.
5. M. Dubey, K. Emoto, H. Takahashi, D. G. Castner, D. W. Grainger, Advanced Functional Materials **2009**, 19, 3046.
6. A. M. Ross, J. Lahann, Journal of Polymer Science Part B: Polymer Physics **2013**, 51, 775.
7. N. Nie, E. Kumacheva, Nature Mat **2008**, 7, 277.
8. H. Bae, H. Chu, F. Edalat, J. M. Cha, S. Sant, A. Kashyap, A. F. Ahari, C. H. Kwon, J. W. Nichol, S. Manoucheri, B. Zamanian, Y. Wang, A. Khademhosseini, Journal of Tissue Engineering and Regenerative Medicine **2014**, 8, 1.
9. J. M. Karp, Y. Yeo, W. Geng, C. Cannizarro, K. Yan, D. S. Kohane, G. Vunjak-Novakovic, R. S. Langer, M. Radisic, Biomaterials **2006**, 27, 4755.
10. J. Yan, V. A. Pedrosa, A. L. Simonian, A. Revzin, *ACS Applied Materials & Interfaces* **2010**, *2*, 748.
11. K. L. Christman, M. V. Requa, V. D. Enriquez-Rios, S. C. Ward, K. A. Bradley, K. L. Turner, H. D. Maynard, *Langmuir* **2006**, *22*, 7444.
12. R. A. Green, N. H. Lovell, G. G. Wallace, L. A. Poole-Warren, *Biomaterials* **2008**, *29*, 3393.
13. M. Sessolo, D. Khodagholy, J. Rivnay, F. Maddalena, M. Gleyzes, E. Steidl, B. Buisson, G. G. Malliaras, *Advanced Materials* **2013**, *25*, 2135.
14. H. Yamazoe, T. Uemura, T. Tanabe, *Langmuir* **2008**, *24*, 8402.
15. O. C. Wells, *Introduction to electron beam technology*, Wiley, **1962**.
16. M. Hatzakis, *Journal of The Electrochemical Society* **1969**, *116*, 1033.
17. A. N. Broers, A. C. F. Hoole, J. M. Ryan, *Microelectronic Engineering* **1996**, *32*, 131.
18. J. Rundqvist, J. H. Hoh, D. B. Haviland, *Langmuir* **2006**, *22*, 5100.
19. A. del Campo, E. Arzt, *Chemical Reviews* **2008**, *108*, 911.
20. D. V. Nicolau, T. Taguchi, H. Taniguchi, S. Yoshikawa, *Langmuir* **1999**, *15*, 3845.
21. C. K. Harnett, K. M. Satyalakshmi, H. G. Craighead, *Applied Physics Letters* **2000**, *76*, 2466.
22. C. M. Kolodziej, H. D. Maynard, *Chemistry of Materials* **2011**, *24*, 774.
23. S. H. Emami, R. Salovey, T. E. Hogen-Esch, *Journal of Polymer Science Part A: Polymer Chemistry* **2002**, *40*, 3021.
24. P. Krsko, S. Sukhishvili, M. Mansfield, R. Clancy, M. Libera, *Langmuir* **2003**, *19*, 5618.
25. K. L. Christman, E. Schopf, R. M. Broyer, R. C. Li, Y. Chen, H. D. Maynard, *Journal of the American Chemical Society* **2008**, *131*, 521.
26. G. Dos Reis, F. Fenili, A. Gianfelice, G. Bongiorno, D. Marchesi, P. E. Scopelliti, A. Borgonovo, A. Podestà, M. Indrieri, E. Ranucci, P. Ferruti, C. Lenardi, P. Milani, *Macromolecular Bioscience* **2010**, *10*, 842.
27. R. Chantiwas, S. Park, S. A. Soper, B. C. Kim, S. Takayama, V. Sunkara, H. Hwang, Y.-K. Cho, *Chemical Society Reviews* **2011**, *40*, 3677.
28. H. Saavedra, M., T. J. Mullen, P. Zhang, D. C. Dewey, S. A. Claridge, P. S. Weiss, *Reports on Progress in Physics* **2010**, *73*, 036501.
29. T. G. Oyama, T. Hinata, N. Nagasawa, A. Oshima, M. Washio, S. Tagawa, M. Taguchi, *Applied Physics Letters* **2013**, *103*.
30. T. Tanaka, Y. Suzuki, K. Tsuchiya, H. Yajima, *Surface and Coatings Technology* **2013**, *218*, 162.
31. D. G. Castner, B. D. Ratner, *Surface Science* **2002**, *500*, 28.
32. Y. N. Xia, G. M. Whitesides, *Annual Review of Materials Science* **1998**, *28*, 153.
33. A. Mujahid, N. Iqbal, A. Afzal, *Biotechnology Advances* **2013**, *31*, 1435.
34. A. l. Guyomard-Lack, N. Delorme, C. l. Moreau, J.-F. o. Bardeau, B. Cathala, *Langmuir* **2011**, *27*, 7629.

35. D. R. Barbero, M. S. M. Saifullah, P. Hoffmann, H. J. Mathieu, D. Anderson, G. A. C. Jones, M. E. Welland, U. Steiner, *Advanced Functional Materials* **2007**, *17*, 2419.
36. A. Perl, D. N. Reinhoudt, J. Huskens, *Advanced Materials* **2009**, *21*, 2257.
37. H. Schmid, B. Michel, *Macromolecules* **2000**, *33*, 3042.
38. T. Kaufmann, B. J. Ravoo, *Polymer Chemistry* **2010**, *1*, 371.
39. A. L. Hook, N. H. Voelcker, H. Thissen, *Acta Biomaterialia* **2009**, *5*, 2350.
40. B. Lee, T. Nagamune, *Biotechnology and Bioprocess Engineering* **2004**, *9*, 69.
41. Y. Mei, et. al., *Nature Mat*. **2010**, *9*, 768.
42. A. L. Hook, H. Thissen, N. H. Voelcker, *Biomacromolecules* **2009**, *10*, 573.
43. a)L. E. Bertassoni, et. al., *Biofabrication* **2014**, *6*, 024105; b)S. Nara, S. Chameettachal, S. Ghosh, *Materials Technology* **2014**, *29*, B10.
44. R. B. Bass, A. W. Lichtenberger, *Applied Surface Science* **2004**, *226*, 335.
45. a)P. S. Hale, P. Kappen, W. Prissanaroon, N. Brack, P. J. Pigram, J. Liesegang, *Appl. Surf. Sci.* **2007**, *253*, 3746; b)D. Burdinski, M. Saalmink, J. P. W. G. van den Berg, C. van der Marel, *Angew. Chem. Int. Ed.* **2006**, *45*, 4355.
46. W. Inglis, G. H. W. Sanders, P. M. Williams, M. C. Davies, C. J. Roberts, S. J. B. Tendler, *Langmuir* **2001**, *17*, 7402.
47. C. L. Feng, G. J. Vancso, H. Schönherr, *Advanced Functional Materials* **2006**, *16*, 1306.
48. X. Li, S. Hou, X. Feng, Y. Yu, J. Ma, L. Li, *Colloids and Surfaces B: Biointerfaces* **2009**, *74*, 370.
49. C. Williams, Y. Tsuda, B. C. Isenberg, M. Yamato, T. Shimizu, T. Okano, J. Y. Wong, *Advanced Materials* **2009**, *21*, 2161.
50. L. Buzanska, A. Ruiz, et. al., *Acta Neurobiol Exp* **2009**, *69*, 24.
51. C.-C. Lin, C. C. Co, C.-C. Ho, *Biomaterials* **2005**, *26*, 3655.
52. M. R. Burnham, J. N. Turner, D. Szarowski, D. L. Martin, *Biomaterials* **2006**, *27*, 5883.
53. K. G. Sharp, G. S. Blackman, N. J. Glassmaker, A. Jagota, C.-Y. Hui, *Langmuir* **2004**, *20*, 6430.
54. S. S. Williams, S. Retterer, R. Lopez, R. Ruiz, E. T. Samulski, J. M. DeSimone, *Nano Letters* **2010**, *10*, 1421.
55. K. Glasmastar, J. Gold, A.-S. Andersson, D. S. Sutherland, B. Kasemo, *Langmuir* **2003**, *19*, 5475.
56. B. A. Langowski, K. E. Uhrich, *Langmuir* **2005**, *21*, 6366.
57. Y.-J. Fu, H.-z. Qui, K.-S. Liao, S. J. Lue, C.-C. Hu, K.-R. Lee, J.-Y. Lai, *Langmuir* **2009**, *26*, 4392.
58. R. K. Workman, S. Manne, *Langmuir* **2004**, *20*, 805.
59. P. W. Snyder, M. S. Johannes, B. N. Vogen, R. L. Clark, E. J. Toone, *The Journal of Organic Chemistry* **2007**, *72*, 7459.
60. X.-M. Li, M. Péter, J. Huskens, D. N. Reinhoudt, *Nano Letters* **2003**, *3*, 1449.
61. A. Guyomard-Lack, C. Moreau, N. Delorme, M. Marquis, A. Fang, J. F. Bardeau, B. Cathala, *Colloids and Surfaces B-Biointerfaces* **2012**, *94*, 369.
62. J. P. Bearinger, G. Stone, A. L. Hiddessen, L. C. Dugan, L. Wu, P. Hailey, J. W. Conway, T. Kuenzler, L. Feller, S. Cerritelli, J. A. Hubbell, *Langmuir* **2008**, *25*, 1238.
63. J. P. Bearinger, G. Stone, L. C. Dugan, B. El Dasher, C. Stockton, J. W. Conway, T. Kuenzler, J. A. Hubbell, *Molecular & Cellular Proteomics* **2009**, *8*, 1823.
64. S. Y. Chou, P. R. Krauss, P. J. Renstrom, *Science* **1996**, *272*, 85.
65. H. Schift, S. Bellini, J. Gobrecht, F. Reuther, M. Kubenz, M. B. Mikkelsen, K. Vogelsang, *Microelectronic Engineering* **2007**, *84*, 932.
66. L. J. Guo, *Advanced Materials* **2007**, *19*, 495.
67. Q. B. Xu, B. T. Mayers, M. Lahav, et. al., *J. Am. Chem. Soc.* **2005**, *127*, 854.
68. A. Bietsch, B. Michel, *J. of Appl. Phys*. **2000**, *88*.
69. T. Ohtake, K.-I. Nakamatsu, S. Matsui, H. Tabata, T. Kawai, *Journal of Nanoscience and Nanotechnology* **2006**, *6*, 2187.
70. D. Falconnet, D. Pasqui, S. Park, R. Eckert, H. Schift, J. Gobrecht, R. Barbucci, M. Textor, *Nano Letters* **2004**, *4*, 1909.

71. S. Y. Chou, C. Keimel, J. Gu, Nature **2002**, 417, 835.
72. J. D. Hoff, L.-J. Cheng, E. Meyhöfer, L. J. Guo, A. J. Hunt, Nano Letters **2004**, 4, 853.
73. P. J. Yoo, W.-S. Choe, Y. H. Kim, Y. M. Lee, Materials Express **2011**, 1, 51.
74. R. Yang, B.-R. Lu, J. Wan, S.-Q. Xie, Y. Chen, E. Huq, X.-P. Qu, R. Liu, Microelectronic Engineering **2009**, 86, 1379.
75. X. Liang, S. Y. Chou, Nano Letters **2008**, 8, 1472.
76. a)H.-C. Scheer, H. Schulz, T. Hoffmann, C. M. Sotomayor Torres, Journal of Vacuum Science & amp; Technology B 1998, 16, 3917; b)H. Schulz, M. Wissen, H. C. Scheer, Microelectronic Engineering **2003**, 67–68, 657.
77. C. Acikgoz, M. A. Hempenius, J. Huskens, G. J. Vancso, European Polymer Journal **2011**, 47, 2033.
78. M. Colburn, S. C. Johnson, M. D. Stewart, S. Damle, T. C. Bailey, B. Choi, M. Wedlake, T. B. Michaelson, S. V. Sreenivasan, J. G. Ekerdt, C. G. Willson, Vol. 3676, **1999**, pp. 379.
79. B. K. Lee, T. Kawai, B. H. Chung, Macromolecular Bioscience **2011**, 11, 600.
80. S. Xie, R. Luttge, Microelectronic Engineering **2014**, 124, 30.
81. A. Gaston, A. Z. Khokhar, L. Bilbao, V. Sáez-Martínez, A. Corres, I. Obieta, N. Gadegaard, Microelectronic Engineering **2010**, 87, 1057.
82. S. Takei, Japanese Journal of Applied Physics **2014**, 53, 02BD15.
83. A. Cattoni, J. Chen, D. Decanini, J. Shi, A. M. Haghiri-Gosnet, Soft UV nanoimprint lithography: a versatile tool for nanostructuration at the 20 nm scale, InTech, **2011**.
84. B. Farshchian, A. Amirsadeghi, S. M. Hurst, J. Wu, J. Lee, S. Park, Microelectronic Engineering **2011**, 88, 3287.
85. L. Wang, J. Ren, X. Han, et. al., IEEE Photonics Journal **2012**, 4, 920.
86. K. De Vos, I. Bartolozzi, E. Schacht, P. Bienstman, R. Baets, Opt. Exp. **2007**, 15, 7610.
87. N. Koo, M. Otto, J. W. Kim, J.-H. Jeong, H. Kurz, Microelectronic Engineering **2011**, 88, 1033.
88. J. P. Rolland, B. W. Maynor, L. E. Euliss, A. E. Exner, G. M. Denison, J. M. DeSimone, Journal of the American Chemical Society **2005**, 127, 10096.
89. E. Nuxoll, Advanced Drug Delivery Reviews **2013**, 65, 1611.
90. M. C. Parrott, J. C. Luft, J. D. Byrne, J. H. Fain, M. E. Napier, J. M. DeSimone, Journal of the American Chemical Society **2010**, 132, 17928.
91. C.-H. Choi, J.-H. Lee, T.-S. Hwang, C.-S. Lee, Y.-G. Kim, Y.-H. Yang, K. Huh, Macromolecular Research **2010**, 18, 254.
92. a)J.-H. Lee, H.-E. Kim, J. H. Im, Y. M. Bae, J. S. Choi, K. M. Huh, C.-S. Lee, Colloids and Surfaces B: Biointerfaces **2008**, 64, 126; b)A.-K. Marel, S. Rappl, A. Piera Alberola, J. O. Rädler, Macromolecular Bioscience **2013**, 13, 595; c)H.-W. Shim, J.-H. Lee, T.-S. Hwang, Y. W. Rhee, Y. M. Bae, J. S. Choi, J. Han, C.-S. Lee, Biosensors and Bioelectronics **2007**, 22, 3188.
93. Y. S. Kim, K. Y. Suh, H. H. Lee, Applied Physics Letters **2001**, 79, 2285.
94. V. N. Truskett, M. P. C. Watts, Trends in Biotechnology **2006**, 24, 312.
95. C. Gao, B. Wang, J. Feng, J. Shen, Macromolecules **2004**, 37, 8836.
96. Y. Lu, W. Hu, Y. Ma, L. Zhang, J. Sun, N. Lu, J. Shen, Macromolecular Rapid Communications **2006**, 27, 505.
97. L. Han, J. Wu, T. Ren, Z. Mao, Y. Guo, C. Gao, Chinese Journal of Chemistry **2014**, 32, 66.
98. H. Sugimura, N. Nakagiri, Thin Solid Films **1996**, 281–282, 572.
99. G. Binnig, C. F. Quate, C. Gerber, *Phys. Rev. Lett.* **1986**, *56*, 930.
100. R. Garcia, R. V. Martinez, J. Martinez, *Chemical Society Reviews* **2006**, *35*, 29.
101. W.-K. Lee, P. E. Sheehan, *Scanning* **2008**, *30*, 172.
102. N. Delorme, A. Fery, *Phys. Rev. E* **2006**, *74*, 030901.
103. K. O. Kongshaug, H. Steen, *Surface Science* **2008**, *602*, 3051.
104. B. Cappella, H. Sturm, *Journal of Applied Physics* **2002**, *91*, 506.
105. H. J. Mamin, D. Rugar, *Applied Physics Letters* **1992**, *61*, 1003.
106. K. Wadu-Mesthrige, S. Xu, N. A. Amro, G.-y. Liu, *Langmuir* **1999**, *15*, 8580.

107. B. W. Muir, A. Fairbrother, T. R. Gengenbach, F. Rovere, M. A. Abdo, K. M. McLean, P. G. Hartley, *Advanced Materials* **2006**, *18*, 3079.
108. R. D. Piner, J. Zhu, F. Xu, S. Hong, C. A. Mirkin, *Science* **1999**, *283*, 661.
109. J. Jang, G. C. Schatz, M. A. Ratner, *Phys. Rev. Lett.* **2003**, *90*, 156104.
110. a)J. Jang, G. C. Schatz, M. A. Ratner, *Phys. Rev. Lett.* **2004**, *92*, 085504; b)P. E. Sheehan, L. J. Whitman, *Phys. Rev. Lett.* **2002**, *88*, 156104.
111. B. Pattier, J.-F. Bardeau, M. Edely, A. Gibaud, N. Delorme, *Langmuir* **2008**, *24*, 821.
112. S. Kramer, R. R. Fuierer, C. B. Gorman, *Chem. Rev.* **2003**, *103*, 4367.
113. a)A. Noy, A. E. Miller, J. E. Klare, B. L. Weeks, B. W. Woods, J. J. DeYoreo, *Nano Letters* **2001**, *2*, 109; b)X. Zhou, X. Liu, Z. Xie, Z. Zheng, *Nanoscale* **2011**, *3*, 4929.
114. D. S. Ginger, H. Zhang, C. A. Mirkin, *Angew. Chem. Int. Ed.* **2004**, *43*, 30.
115. a)R. G. Sanedrin, L. Huang, J.-W. Jang, J. Kakkassery, C. A. Mirkin, *Small* **2008**, *4*, 920; b) T. Rakickas, E. M. Ericsson, Ž. Ruželė, B. Liedberg, R. Valiokas, *Small* **2011**, *7*, 2153; c)P. L. Stiles, *Nature Methods* **2010**, *7*.
116. G. Liu, Y. Zhou, R. S. Banga, R. Boya, K. A. Brown, A. J. Chipre, S. T. Nguyen, C. A. Mirkin, *Chem. Sci*. **2013**, *4*, 2093.
117. J.-W. Jang, *Current Applied Physics* **2014**, *14*, 790.
118. S. Turri, L. Torlaj, M. Levi, *Macromolecular Rapid Communications* **2010**, *31*, 1373.
119. R. Suriano, S. Biella, F. Cesura, M. Levi, S. Turri, *Applied Surface Science* **2013**, *273*, 717.
120. E. J. Irvine, A. Hernandez-Santana, K. Faulds, D. Graham, *Analyst* **2011**, *136*, 2925.
121. H. Li, Q. He, X. Wang, G. Lu, C. Liusman, B. Li, F. Boey, S. S. Venkatraman, H. Zhang, *Small* **2011**, *7*, 226.
122. F. Huo, Z. Zheng, G. Zheng, L. R. Giam, H. Zhang, C. A. Mirkin, *Science* **2008**, *321*, 1658.
123. Z. Zheng, W. L. Daniel, L. R. Giam, F. Huo, A. J. Senesi, G. Zheng, C. A. Mirkin, *Angewandte Chemie* **2009**, *121*, 7762.
124. D. J. Eichelsdoerfer, K. A. Brown, M. X. Wang, C. A. Mirkin, *The Journal of Physical Chemistry B* **2013**, *117*, 16363.
125. Z. Xie, C. Chen, X. Zhou, T. Gao, D. Liu, Q. Miao, Z. Zheng, *ACS Applied Materials & Interfaces* **2014**.
126. X. Zhou, X. Wang, Y. Shen, Z. Xie, Z. Zheng, *Angewandte Chemie International Edition* **2011**, *50*, 6506.
127. H. Clausen-Schaumann, M. Grandbois, H. E. Gaub, *Advanced Materials* **1998**, *10*, 949.
128. C. Nakamura, C. Miyamoto, I. Obataya, S. Takeda, M. Yabuta, J. Miyake, *Biosensors and Bioelectronics* **2007**, *22*, 2308.
129. M. Ganesh, J. Nachman, Z. Mao, A. Lyons, M. Rafailovich, R. Gross, *Biomacromolecules* **2013**, *14*, 2470.
130. D. Bullen, C. Liu, *Sensors and Actuators A: Physical* **2006**, *125*, 504.
131. C. D. O'Connell, M. J. Higgins, R. P. Sullivan, S. E. Moulton, G. G. Wallace, *Small* **2014**, ASAP.

# Chapter 8
# Inkjet Printing of Biomolecules for Biorecognition

**Terence G. Henares, Kentaro Yamada, Koji Suzuki and Daniel Citterio**

## 8.1 Introduction of Inkjet Printing Technology

### *8.1.1 Background*

Inkjet printing is undoubtedly the most familiar and most widely applied technology for personal office desktop printing nowadays. It can be stated without exaggerating that the arrival of this technology has revolutionized the possibilities of desktop printing in many aspects, but in particular when it comes to color printing. In contrast to the previously dominant desktop printing technologies (e.g., ink ribbon-based dot-matrix printing), inkjet printing made it possible not only to print simple text but also to instantly reproduce digital color graphics and photographs in astonishingly high quality. Before the implementation of personal desktop inkjet printers, color printing of similarly high resolution was to a large extent unaffordable for the common user. The benefits of inkjet printers, that we take for granted in our daily use nowadays, are the result of a continuous technical development, which has started in 1949 with the filing of the first patent application regarding a practical inkjet device [1]. However, several decades of further research and development were necessary, before the first successful and affordable mass-marketed desktop inkjet printer became available from Hewlett-Packard (HP) in 1984 [2].

In terms of technical functionality, an inkjet printer is straightforwardly simple. It is an electronic device enabling the direct deposition of very small droplets of liquids (inks) onto a well-defined and user-controlled position of a substrate. As implied by the name of the technology, the ink droplets are ejected (jetted) from a small nozzle of the printhead onto a specifically determined position of the substrate. In contrast to several other deposition methods for liquid droplets, this process is performed without any physical contact between the printhead and the substrate.

D. Citterio (✉) · T. G. Henares · K. Yamada · K. Suzuki
Department of Applied Chemistry, Keio University, 3-14-1 Hiyoshi, Kohoku-ku, Yokohama 223-8522, Japan
e-mail: citterio@applc.keio.ac.jp



J. Rodríguez-Hernández, A. L. Cortajarena (eds.), *Design of Polymeric Platforms for Selective Biorecognition,* DOI 10.1007/978-3-319-17061-9_8

Therefore, inkjet printing is referred to as a noncontact liquid dispensing method. Furthermore, compared with most other major printing techniques currently in use (e.g., flexography, gravure printing, offset printing, screen printing), the inkjet printing process is fully digitally controlled, and allows for the "direct transfer" of electronically stored information onto a print substrate. It does not require the costly and time-consuming conversion of electronically stored data into printing plates or screens, before transferring it to the substrate. On the other hand, a graphical image printed by inkjet technology is made up of large numbers of individually deposited ink droplets. Similar to the case of the former ink ribbon-based dot-matrix printers, such a "dot-by-dot" image buildup process is more time consuming compared to plate- or screen-based ink deposition, where a complete image can be transferred to the substrate in a single step. As a consequence, inkjet printing can currently not and will probably never compete with other major printing methods in terms of speed when it comes to the reproduction of large numbers of identical prints. But its digital feature with the possibility to directly transfer an image onto a substrate allows for a very high degree of flexibility. This is particularly advantageous in printing of multiple items in lower number of replicates, in industrial prototyping applications, or for marking and coding of objects with continuously changing patterns [3].

Although most readers will immediately associate the inkjet technology with personal office use, industry-related applications actually go further back in history than the currently best-known and widely spread desktop printing. The technology was first routinely used for marking and coding of products, in what Martin and coworkers refer to as the first generation of commercial inkjet applications [3]. Since every pattern or code deposited on a product or package is unique, inkjet printing without the need for printing plates is advantageous compared to other printing methods. In addition, the noncontact characteristics allow for larger distances between printhead and print substrates which is useful in the setup of industrial production lines. Personal office desktop printers are regarded as the second generation of commercial inkjet applications. Their popularity in relation to cost/performance ratio is currently unbeaten. Only more recently, the enormous potential of inkjet printing has been discovered for industrial applications going beyond the reproduction of text and images on paper, films, or other substrates in what is now referred to as the third generation of commercial inkjet applications. The technology has evolved into full-scale industrial mass production. A popular example is the fabrication of color filters for light emitting diodes and large flat-panel color displays [4]. Another relatively recent but rapidly growing addition to the fields of application for inkjet printing technology is the domain of printed electronics [5].

In this chapter, however, focus is set on a different but equally promising and comparably new application of inkjet printing technology, the printing of biomolecules. In this case, inkjet printers with the ability to reproducibly deposit known and small volumes of liquids onto specific user selectable spots on a substrate can be regarded as accurate tools for liquid dispensing, which are highly important in the fields of chemistry, biology, or life sciences. In this context, inkjet printing is competing with alternative liquid dispensing methods, such as pipetting, contact printing, and pneumatic dispensing, among others [6].

In the following section, the basic mechanic principles of the most commonly applied inkjet printing methods are shortly introduced. This is important in order to understand not only the great potential but also the challenges faced when using inkjet printing as a liquid dispensing method for the deposition of biomolecules on a substrate targeting selective biorecognition.

### *8.1.2 Technical Principles of Inkjet Printing*

Commonly applied inkjet printing technologies are divided into two main categories known as "continuous inkjet printing" (CIJP) and "drop-on-demand" (DOD) inkjet printing (Fig. 8.1). Historically, continuous inkjet technology is the older of the two. Its basic working principle is schematically illustrated in Fig. 8.2: a jet of ink liquid ejected from the printhead nozzle by pressure is broken-up into a stream of small droplets by application of a mechanical disturbance pattern of a specific frequency (e.g., by vibration of a piezoelectric actuator). Selected drops within this stream are subsequently electrically charged while passing through an electrostatic field between two charging electrodes. Further along the drops' flight path is a second set of electrodes with an applied high voltage electric field, resulting in the selective deflection of electrically charged drops only. In most printing systems, the deflected charged drops are guided towards the printing substrate, whereas the uncharged drops fly straight into an ink collection system for reuse. In the simplest practical implementation of this technology, electronically stored digital data is converted into graphical data on the substrate by switching between charged and uncharged ink drops. In more advanced systems, varying the charge of the drops

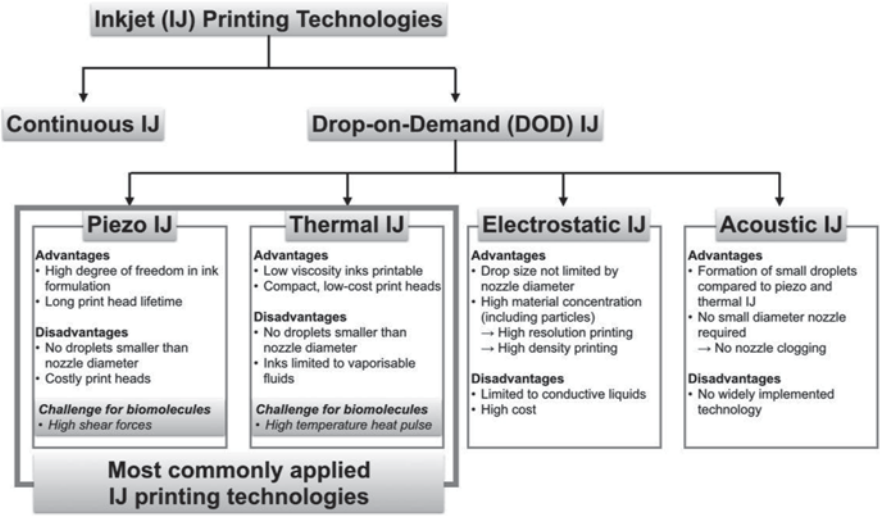


**Fig. 8.1** Overview of major inkjet printing technologies

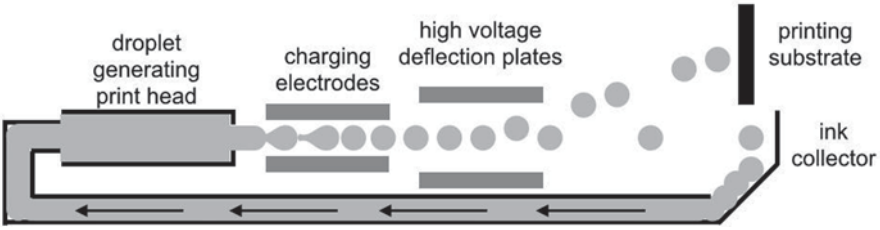


**Fig. 8.2** Schematic representation of the continuous inkjet printing principle

results in different deflection angles and correspondingly in different places of drop impact on the substrate. The continuous inkjet printing mechanism requires the created drops to become electrically charged and therefore, poses restrictions on the choice of printable fluids. In addition, the achievable printing resolution is comparably low. An advantage of the technology is the possibility of achieving high drop firing frequencies (typically around 80–100 kHz, but reaching values up 1 MHz) [7], which result in comparably high printing speeds, and high drop velocities (typically around 20 m/s) [8]. These characteristics allow for larger distances between the printhead and the substrate [9].

The newer and currently most widely applied principle in inkjet printing is the drop-on-demand (DOD) technology. In contrast to the previously described continuous inkjet approach, where a continuous stream of drops is digitally controlled to split into drops reaching the substrate and drops being recycled, DOD printing is based on the control of the drop formation itself. As indicated by its name, drops of ink are ejected from the printhead nozzle only on demand. The first big advantage of this method is the absence of the necessity to create electrically charged ink droplets that strongly expands the choice of potential ink fluids. The second significant advantage is the elimination of the ink recycling system, since all of the created ink droplets are targeted at the substrate. A drawback in comparison with continuous inkjet printing is the significantly lower maximum achievable drop firing frequency of 0–25 kHz [10], with maximum values up to only 100 kHz [8], resulting in reduced printing speeds. The reason for this difference is the fact that a single cycle consisting of drop ejection and subsequent ink refill of the firing chamber has to be completed before the process can be repeated. Furthermore, typical drop velocities for DOD inkjet printing are in the order of 10 m/s which is lower than in the case of continuous inkjet printing. As shown in Fig. 8.1, DOD inkjet printing technologies are commonly further subdivided into four major subgroups (piezoelectric, thermal, electrostatic, and acoustic inkjet printing), named according to the mechanisms used for droplet formation. In the following, all of the four mechanisms are shortly introduced for the sake of completeness. However, focus is set on piezoelectric and thermal inkjet printing, since those two technologies are by far the most technically matured and dominant in current applications. Table 8.1 summarizes major characteristics and physical parameters associated with these two important inkjet printing technologies. Generally, piezoelectric technology is dominating in the industrially related inkjet printing market, whereas thermal inkjet printing has become the major

**Table 8.1** Typical values/ranges of physical parameters for piezoelectrically and thermally actuated DOD inkjet printing

| Parameter[a] | Piezoelectric IJ | Thermal IJ | References |
|---|---|---|---|
| Nozzle diameter (μm) | 20–30 | | [14] |
| Drop diameter in flight (μm) | 15–55 | | [8] |
| Drop volume (pL) | Typically 10–20, minimal 1, maximal 5000 | | [10, 14] |
| Drop velocity (m/s) | 3–15 | | [8] |
| Firing frequency (kHz) | Maximum values up to 100, commonly 0–25 | | [8,10] |
| Ink viscosity (cP) | Minimal 5–10<br>typically < 20 | Minimal 1–1.5<br>typically < 3 | [15–17] |
| Ink surface tension (mN/m) | Typically 28–40 | | [18] |
| Shear rate ($s^{-1}$) | $2 \times 10^4$–$2 \times 10^6$ | $10^4$ | [11, 10] |

[a] The listed values and ranges are significantly varying depending on the literature references and on the printing equipment applied. Therefore, they should be regarded as guidelines, rather than strict requirements

technology in consumer desktop printing. In the inkjet-based deposition of biomolecules, DOD piezoelectric and thermal inkjet printing are currently the only routinely applied technologies, with the piezoelectric approach leading in terms of number of application examples. One reason for this bias towards piezoelectric methods is probably simply their dominance in the industrial inkjet printing sector, although other factors eventually play a role, as will be shown later on in this chapter. On the other hand, no reports on biomolecule-related applications of continuous inkjet printing can be found in the literature, most probably because of the significantly less economical use of ink.

#### 8.1.2.1 Piezoelectric Inkjet Printing

In the piezoelectric inkjet printing mechanism, a drop of ink is ejected from the printhead nozzle by fast and reversible deformation of the firing chamber (Fig. 8.3a). This deformation on a sub-micrometer scale is achieved by applying an electronic signal (voltage pulse) on a piezoelectric actuator surrounding the firing chamber, resulting in a pressure wave propagating towards the nozzle at the chamber exit. The shape of the voltage pulse, characterized by its slope (voltage increase with time), amplitude (maximum voltage), and length, allows to control the ink ejection process. Depending on ink parameters, such as viscosity and surface tension, different pulse shapes are required. However, in general, piezoelectric inkjet printing is characterized by a high degree of freedom in ink formulation. The possibility of having multiple voltage pulse parameters to adapt besides the physical properties of the ink is certainly a big advantage of the technology. A drawback is the fact

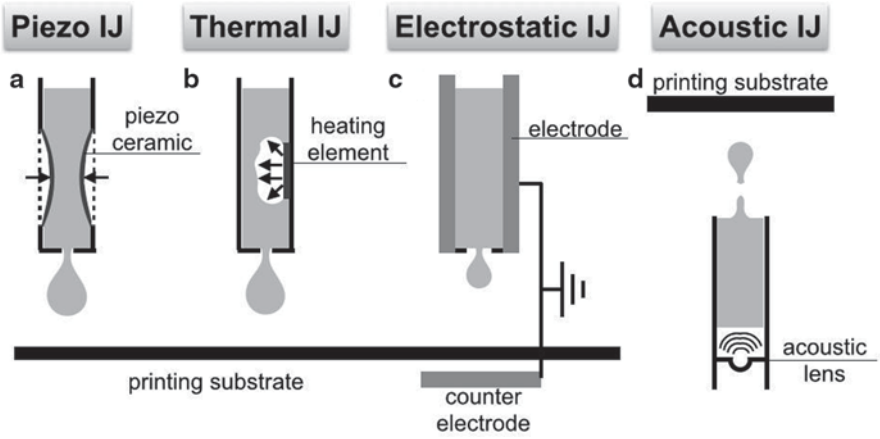


**Fig. 8.3** Schematic representation of the major drop-on-demand (DOD) inkjet printing technologies

that the minimally achievable drop size is limited by the diameter of the printhead nozzle. A factor that has to be considered in the case of working with ink compositions containing biomolecules are the significant shear rates that are experienced by the liquid (Table 8.1). Although shear stress is not unique to piezoelectric inkjet printing and occurs in all jetting methods with sudden mechanical stress applied to the ink liquid, it tends to be higher compared to other printing technologies. The reason for this is the fact that piezoelectric printing generally requires liquids of a higher viscosity (Table 8.1) compared with, for example, the thermal inkjet printing method described in the next section.

### 8.1.2.2 Thermal Inkjet Printing

In thermal inkjet printing, drop generation in the firing chamber occurs by the creation of a rapidly expanding vapor bubble, which results in the displacement of ink from the nozzle (Fig. 8.3b). The bubble is created by local heating and vaporization of ink by means of a heating element located inside the printhead's firing chamber. Upon elimination of the heat pulse after drop ejection, the vapor bubble rapidly collapses creating a vacuum that is filled by drawing in ink from the ink reservoir, after which the system is ready for the next firing cycle. The requirement to locally vaporize the ink fluid poses restrictions on the applicable fluids. Water is the material of choice for the formulation of thermal inkjet printing ink compositions. Generally, a heat pulse in the order of typically around 200–300 °C is applied. At first sight, this high temperature pulse might certainly be regarded as detrimental for the use in combination with comparably heat-sensitive biomolecules. However, it should be noted that the duration of this pulse is in the order of around 2 μs [11]. In addition,

a high gradient of decreasing temperature from the surface of the heating element into the bulk of ink liquid is assumed, so that in fact the temperature experienced by the majority of biomolecules in the liquid volume is far below the 200–300 °C applied for the heat pulse. In fact, it has been stated that only about 1 % of the ink volume of the firing chamber is exposed to high temperature, whereas the bulk of the fluid remains at merely around 10 °C above ambient temperature [12]. The drop ejection method applied in thermal inkjet printing technology allows to work with ink liquids of very low viscosities (Table 8.1) that results in lower shear rates experienced in the ink liquid. As in the case of piezoelectric inkjet printing, the minimally achievable drop size for thermal inkjet printing is equally limited by the diameter of the printhead nozzle.

#### 8.1.2.3 Electrostatic Inkjet Printing

In this technology, a voltage is applied between the printhead nozzle and an electrode located behind the printing substrate (Fig. 8.3c). Droplets are created by pulling out the liquid under the influence of the resulting electrostatic field. A great advantage of the method is the possibility to create liquid droplets that are smaller than the aperture of the printhead nozzle which is generally not possible in the case of piezoelectrically or thermally actuated drop generation. This feature is potentially of high interest when working with liquids containing solid particles or relatively high concentrations of dissolved materials. The option to create small droplets, but at the same time being able to use printhead nozzles with sufficiently large diameter to prevent particle-induced clogging, is of high relevance. However, the limitation to the use of conductive liquids as ink carriers is a disadvantage preventing the more widespread development and use of the technology. As a consequence, the costs for implementing electrostatic inkjet printing methods are currently comparably high.

#### 8.1.2.4 Acoustic Inkjet Printing

In this version of inkjet printing technology, liquid drops are generated by the use of focused, high-intensity sound beams directed to free liquid surfaces through an acoustic lens (Fig. 8.3d). The sound waves traveling towards the liquid–air interface cause the formation of a mound of liquid and ultimately a droplet breaking free. In principle, this method does not require an actual nozzle and therefore, features similar advantages to electrostatic inkjet printing in the sense that there is no need to worry about printhead nozzle clogging even when using concentrated ink liquids or inks with a high content of solid particles. At the same time, the diameters of ejected drops can be as small as 5 μm [13] which can neither be achieved by piezoelectric nor thermal inkjet printing. Unfortunately, however, acoustic inkjet printing technology currently remains a minor technology.

## 8.2 General Considerations for Inkjet Printing of Biomolecules

It is important to keep in mind that inkjet printing technology has not been specifically developed for the application to biomolecules such as nucleic acids and proteins. When compared to constituents of inks for ordinary graphical printing applications (organic and inorganic pigments, organic dyes, etc.), biomolecules are of much more fragile nature. The preservation of their structure and function is generally dependent on several environmental factors such as temperature, solvent, and pH. In this context, the abovementioned high temperature heat pulse applied for drop ejection in thermal inkjet printing is, at first sight, recognized as the most obvious major concern. However, in addition, most biomolecules can be regarded as relatively large macromolecular compounds, in contrast to low-molecular weight colorants used in graphical printing inks. The mechanical forces encountered in both piezoelectric and thermal inkjet printing (e.g., shear forces, high acceleration rates, ink compression upon ejection, high speed droplet impact on the printing substrate, etc.), all have sufficient potential to break or deform larger 3D molecular structures common for biomolecules. For this reason, there is no "safe-zone" in terms of choice of inkjet printing technology (piezoelectric or thermal). As shown in the following example of selected applications, an experimental evaluation is required from case to case. The trend for piezoelectric actuation to dominate the field of bio-ink printing is probably more historically related than caused by biomolecule stability issues.

It is also not possible to define a list of biomolecules suitable or unsuitable for deposition by inkjet printing. In all cases, it will be the combination of three major factors responsible for success or failure of the inkjet printing approach: (1) selection of the printing technology and droplet ejection pulse parameters; (2) choice of ink solvent and additives; and (3) printing substrate. Among those three factors, the ink composition probably offers most options for adaptation and optimization, but at the same time can also be a major source of trouble. As shown in the following sections, certain ink additives can have a positive influence on the stability of biomolecules during the printing process. However, their effect on the printing performance in terms of reliability and reproducibility is not always positive and has therefore to be individually evaluated. In many cases, compromises between biomolecule solubility and stability as well as ink jettability have to be made. In terms of ink solvent, water (mostly pH buffered) is the most obvious choice when working with biomolecules. Interestingly, although its use is less often reported for the deposition of biomolecules, thermal inkjet printing technology has, from its beginning, been much more suitable to handle purely aqueous liquids, compared with piezoelectrically actuated printing. Actually, many industrial-use piezoelectric printheads have been originally incompatible with water-based ink formulations, although this deficiency is now mostly overcome driven by market demands [9].

The printing substrate also plays an essential role in the overall printing process, not only in relation to the more obvious print resolution and quality but also to biomolecule stability. The influence on resolution and quality is not limited to working

with biomolecules, but is common to all inkjet printing processes in general. Print resolution and quality are not determined by the ink droplet size alone. They depend, to a large extent, on the spreading of the ink after drop impact on the substrate, which is primarily determined by the substrate surface energy in relation to the surface tension of the ink. Other relevant parameters include the liquid penetration into or adsorption onto the substrate and the evaporation rate of the ink solvent. The latter, on the other hand, depends on environmental factors such as temperature and humidity. More limited to the inkjet printing of biomolecules is the influence of the print substrate on the biomolecule activity. Although primarily evaluated in relation to the inkjet deposition of living cells, it has been shown that softer and more viscous substrate surfaces can reduce the impact forces acting on droplets, however, at the cost of decreasing resolution [12].

One of the motivations to use inkjet printing for the deposition of biomolecules onto a solid substrate is the ability to achieve high patterning densities (e.g., for DNA microarrays). With presently commercially accessible standard technology (excluding customized systems), droplet sizes down to 1 pL are becoming routinely achievable for optimized ink compositions. In combination with an optimized printing substrate and very precise substrate positioning control, this translates into reproducibly deposited spots of about 30 μm diameter under standard operation conditions, with sizes as low as 10 μm for highly controlled laboratory environments [9]. In the case of using self-aligned printing approaches that rely on selective de-wetting of low surface energy areas, features of below 100 nm have been achieved by inkjet printing alone [19]. However, this has been successfully demonstrated for the printing of electronic features, it has to the best of our knowledge not been realized for biomolecules.

Another point to consider is the selection of the inkjet printer for the deposition of biomolecules. The first and biggest distinction is between the affordable consumer desktop printers and the much more expensive research-use inkjet material printers specially dedicated to non-graphical printing applications. When it comes to thermal actuation, consumer desktop printers are currently the only option. At present, Canon and HP are the dominating manufacturers of thermal inkjet printers. In the case of piezoelectrically operated desktop printers, Epson and Brother are probably the biggest players in the global market at this time. One significant disadvantage when working with desktop printers in terms of convenience is the fact that, depending on the country, empty (virgin) ink cartridges are often not easily available. Therefore, the user is required to disassemble and clean the originally provided ink tanks, before being able to work with self-made bio-inks. A further potential disadvantage of desktop printers is the substrate feeding mechanism which is primarily designed for handling paper. Difficulties can occur with thicker and less flexible materials, unless a printer with a direct CD/DVD print option is used. In addition, it is probably needless to say that the degree of freedom and the reproducibility of substrate positioning can easily become an issue, the latter in particular if multiple print runs are required. Finally, all desktop printers are essentially “black box” systems with limited user control. A big advantage of all consumer desktop printers is that they come equipped with at least four ink tanks (black, cyan, yellow, magenta), thus theoretically allowing the simultaneous use of multiple inks [6].

Inkjet printing systems dedicated to research laboratory use are generally operating with piezoelectric actuation. In contrast to the consumer desktop printers, they offer a high degree of user-controllable features such as a choice of printhead nozzle diameters, the possibility to heat nozzle and substrate stage, visual confirmation of ink droplet ejection, and control of piezo-pulse voltage and duration.

With any type of inkjet printing equipment, there is always a risk of clogging the small printhead nozzle apertures. For this reason, an inkjet printing ink should always be passed through a filter with pore sizes below 1 μm (ideally around 200 nm) before filling a printer ink tank. As long as all used compounds are of sufficient solubility in the chosen ink system, the risk can be minimized. However, in the case of formation of precipitates or aggregates, clogging of the printhead is highly likely. In particular when working with inks containing particulate matter, dispersion stability is a very important factor. As a general "rule of thumb," it is advised to limit the size of particles in inkjet printing inks to a value not exceeding 1/100 times the diameter of the chosen printhead nozzle [15]. This generally corresponds to particle sizes of $\leq$300 nm.

## 8.3 Inkjet Printing of Nucleic Acids

### *8.3.1 Introduction*

Nucleic acids (DNA, RNA) play vital roles in the conservation of gene information and protein synthesis. Since the discovery of the double helix structure of DNA by Watson and Crick, DNA sequencing has attracted much attention as a fundamental approach for the analysis of specific gene information. Especially the comparative study of DNA sequences is motivated by multiple objectives (e.g., elucidation of the function of specific genes, disease-associated gene expression). In addition to DNA sequencing, the quantification of nucleic acids in biological samples is a valuable analytical approach providing information on gene expression levels. Simultaneous detection and quantification of multiple nucleic acids is of high interest for example for the analysis of gene mutations, the study of gene expression levels in cells, and its application to drug development, among others. In order to detect an exhausting number of DNAs in a single experiment, DNA arrays have been prevalently employed since the late 1980s. This very important type of selective biorecognition platforms is manufactured by immobilizing various single strand DNA sequence probes onto a solid support to capture and detect target DNAs by employing the well-known preferential binding between complementary DNA single strands. To obtain high-density DNA arrays, several technologies to deliver small amounts of probes onto a substrate have been developed so far [20–24]. Currently, photolithography [25, 26], pin spotting [27], and inkjet printing [28, 29] are representative methods applied in commercial manufacturing, with other types of deposition techniques being reported (maskless photolithography [30], electronic addressing

[31, 32], etc.). Among them, owing to its noncontact, fine, and precise patterning capability, inkjet printing technology is applied for the deposition of DNA on solid supports via two strategies: direct spotting of DNA and in situ synthesis of oligonucleotides on the solid substrate. In this section, the inkjet printing of nucleic acids is mainly described from the point of view of DNA microarray fabrication.

### *8.3.2 Common Microarraying Technologies*

As mentioned above, several methods exist to deposit nucleic acids on a solid support for preparing DNA arrays. Primary approaches and their features are summarized in Table 8.2. The combination of photolithography and solid-phase synthesis of oligonucleotides was first introduced by Affymetrix [25] and has become one of

**Table 8.2** Major approaches to nucleic acid microarraying

| Arraying technology | Applicable materials | Substrate contact | Advantages | Disadvantages |
|---|---|---|---|---|
| Photolithography [25, 26] | DNA nucleotides | No | Achievable high density | Requirement of UV source and specific photomasks<br>Risk of straying UV irradiation to nearby areas<br>Limitation of oligonucleotide length (ca. 25-mer) |
| Maskless photolithography [30] | DNA nucleotides | No | Achievable high density<br>Flexible sequence design | Requirement of UV source and sophisticated instruments<br>Limitation of oligonucleotide length (ca. 25-mer) |
| Pin spotting [27] | Complete DNA | Yes | Low fabrication cost per spot | High risk of contamination of the printing device<br>Damage of the spotter in every printing cycle |
| Inkjet printing [28, 29] | Complete DNA<br>DNA nucleotides | No | Flexible sequence design<br>Low risk of contamination | Difficult to clean the nozzle completely<br>Risk of nozzle clogging |
| Electro addressing [31] | Complete DNA<br>DNA nucleotides | No | Fast hybridization time<br>Controllable hybridization stringency | Employment of sophisticated semiconductor devices<br>Requirement of labeling of substrate and probes |

the most familiar arraying techniques. It involves the delivery of DNA nucleotides (monomers) protected by photochemically cleavable groups, followed by local UV illumination through photomasks for deprotection. In this approach, $4^n$ different sequences of n-mer oligonucleotides can be created by 4n chemical cycles. The method provides high-density arrays (400,000 probes on 1.6 $cm^2$) [26], but can be time consuming to obtain long oligonucleotides, because of its serial procedure. In addition, it is comparably costly to design new sequences owing to the requirement of the corresponding number of different photomasks. On the other hand, an alternative photopolymerization approach has been developed by a group at the University of Wisconsin, where a computer connected to a digital micromirror array was employed to control the reflection of UV light from the light source to replace the photomasks [30].

A Stanford University group first demonstrated the deposition of pre-synthesized DNA onto a solid support by contact printing methods [27]. The contact dispensing systems involve the direct contact between the substrate and the ink-loaded dispenser such as microspotting pins, tweezers, and microstamps [22]. Their simple principles based on reciprocating movement of the dispenser between sample reservoir and printing matrix yield reproducible results with comparably little maintenance. Furthermore, the length of nucleic acids to be delivered is not limited. However, the limited fabrication throughput, the achievable density, and the fear of contamination through direct contact of dispenser and substrate are potentially problematic.

In contrast, inkjet printing technology is prevalently utilized as the most common approach in noncontact dispensing. As outlined before, inkjet printing technology allows handling of very tiny droplets of as small as nanoliter to picoliter volumes with good accuracy, and thus, is ideal for obtaining quantitative, high-density, reproducible arrays. Although inkjet printing has shortages in terms of the restricted choice of "ink" compositions and durability of the dispenser (i.e., print head), the fine tunability of droplet volumes by the applied voltage (piezoelectric actuation) or temperature gradient (thermal actuation) and the achievable high resolution features have motivated academic research and commercialization. Furthermore, the flexibility in spatial control significantly facilitates the creation of different DNA sequences at each spot, and leads to the preparation of arbitrarily designed DNA microarrays. As a consequence, Agilent has adopted this technology for manufacturing both custom and catalogue-order arrays.

### *8.3.3 Inkjet Printing of Nucleic Acid Arrays*

Inkjet printing technology enables two approaches for arraying nucleic acids on a solid support (typically glass slide, silicon wafer): (1) printing of complete DNAs (pre-synthesized or PCR amplified), and (2) in situ synthesis of oligonucleotides by delivering DNA nucleotides (monomers) (Fig. 8.4).

The feasibility of inkjet printing of pre-synthesized or preliminarily PCR-amplified DNA sequences has been first demonstrated in the 1990s. In one of the earlier reports, Schober et al. employed a piezoelectric inkjet dispenser (Microdrop,

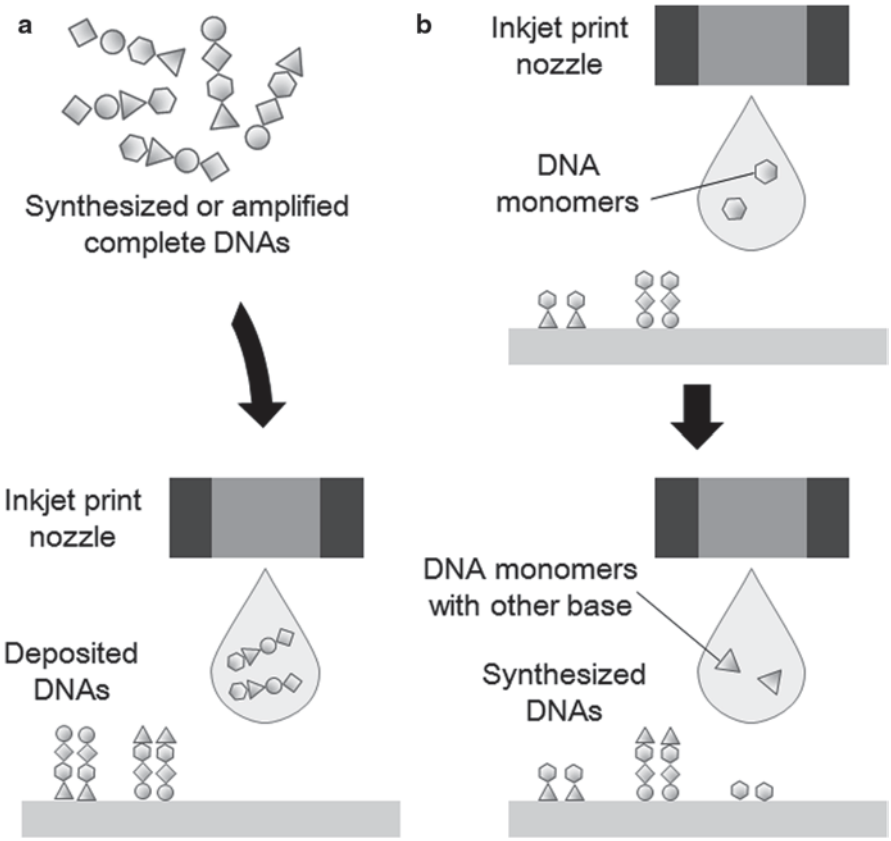


**Fig. 8.4** Two approaches to obtain DNAs on a solid substrate: **a** deposition of complete DNA, **b** in situ synthesis by DNA nucleotide (monomer) printing

Norderstedt, Germany) as an alternative to pipetting small volumes of biological samples with high speed and high accuracy in 1993 [33]. They reproducibly handled volumes from a few nanoliters to as small as 5 pL with high frequency (10,000 drops per second), which surpassed piston-operated pumps, the conventional dispensing systems for biological samples at the time. By using this piezoelectrically actuated system, primary biological samples including DNA and RNA, and even enzymes and cells were successfully dispensed. Surprisingly, in spite of the high acceleration (100,000 g) encountered during the ejection process, no differences were confirmed in gel electrophoresis performed for RNA and DNA samples before and after being subject to the printing process. In 2000, Okamoto et al. first succeeded in printing a microarray of pre-synthesized 18-mer oligonucleotides onto a glass surface by using a modified personal desktop Canon Bubble Jet printer (BJ-600) equipped with a standard ink cartridge [28]. The optimal "ink" composition was evaluated regarding volatility, solubility, wettability, viscosity, and surface tension, and empirically an aqueous solution of glycerol, urea, thiodiglycol (these three

serve as wetting agents), and acetylenol (reduction of viscosity) was chosen as the solvent for DNA printing. The use of ethanol (approx. 10% v/v) as an additive to reduce viscosity and surface tension of inks containing biological samples, which improves the printing reliability by facilitating the wetting of the internal capillary of the ink cartridge, is also possible [34]. Particularly, the viscosity of the ink is a crucial parameter in handling fragile biological samples, because it determines the shear stress experienced by the ink during the droplet ejection process. Although exposure to heat (200–300 °C) and shear rate ($10^4$ $s^{-1}$) were a concern in terms of possible DNA degradation, ejected DNAs of 10–300 base pairs (bp) in length and 0.02–1.6 mg $mL^{-1}$ in concentration remained intact. Quite the contrary, the authors found an advantage of heating the DNA-containing ink. They assumed that the high temperature and the presence of urea in the ink induced DNA denaturation, providing the reaction energy required for a high rate of DNA binding to the glass substrate surface (completed within 30 min). The robustness of DNA compared to other biological substances such as proteins is attributed to its 3D structure. Hydrogen bonds formed between base pairs of complementary DNA strands determine its architecture univocally without bending or folding. On the other hand, proteins are much more challenging to inkjet print without ruining their higher-order structures (see the following section for details about inkjet printing of proteins).

The power of inkjet printing of nucleic acids is particularly revealed in inkjet-based solid-phase synthesis of DNA, which is another powerful technique to align DNAs on a solid support. It involves in situ DNA synthesis on a print medium in a manner similar to the photolithographic approach by delivering DNA nucleotides (monomers). In this approach, DNA nucleotides (typically phosphoramidite monomers) of the four bases are selectively and precisely deposited only onto the desired spots from independent nozzles. Typical inkjet-based in situ DNA synthesis using phosphoramidite protection chemistry is schematically depicted in Fig. 8.5. This method eliminates the requirement of photomasks for spatial control and enables designing of more than tens of thousands of sequences with a single inkjet printer by simply modifying the printing pattern using computer software. Despite the disadvantage that the obtainable length of DNA is shorter than in the case of the abovementioned pre-synthesized DNA printing, this approach possesses significant merits over the complete DNA printing method: (1) theoretically, any sequence can be obtained by one printer without replacing ink cartridges, (2) DNA sequences can be stored as electronic data files instead of frozen DNA libraries. Although several routes of solid phase DNA synthesis have already been reported in the 1980s [35–37], transfer to inkjet printing was first demonstrated in 1996. A research group at the University of Washington attempted the delivery of DNA monomers onto a silicon dioxide wafer patterned by using a self-made piezoelectrically actuated inkjet pump. Though the performance of the DNA array itself has not been specified, the throughput achieved with this approach allowed for the arraying of 100,000 arbitrary 25-mers within only 2 h [38]. A next step in the evolution of this technology was triggered in 2001 by research groups at Rosetta Inpharmatics and Agilent Technologies, two primary inkjet-printed DNA array manufacturers. Following the first in situ DNA synthesis on a glass support employing a self-made inkjet device,

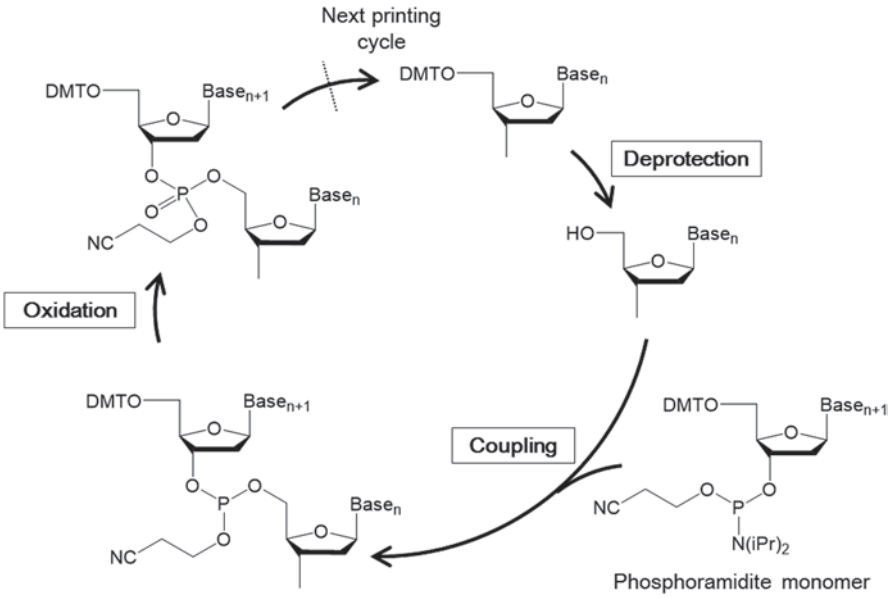


**Fig. 8.5** Typical in situ synthesis cycle employing phosphoramidite chemistry. *DMT* dimethoxytrityl protection for the hydroxyl group

this method was further optimized and validated. The combination of standard phosphoramidite DNA synthesis and commercially supplied inkjet printer heads (product name not specified) enabled the creation of 25,000 different 60-mers on a $25 \times 75$ mm$^2$ glass support with stepwise synthetic yields (one cycle in the process depicted in Fig. 8.5) of 94–98 % [29]. This amount of simultaneously arrayed oligonucleotides covers the estimated number of 20,000–25,000 human genes [39]. At present, the stepwise synthetic yield has been improved to values as high as 99.5 %, and longer DNAs became obtainable with smaller failure rates (successful synthesis rate has risen from 20 to 60 % in the case of 100-mers) [40]. The versatility of the present method is accelerated by the introduction of an open-source inkjet arrayer in 2004. In spite of the strong potential of inkjet-based in situ DNA synthesis, information on this technology accessible to the general research community (not inkjet-related enterprises) was relatively limited compared to other arraying technologies. As for the pin printing method, the arrayer design was released earlier in 1998, which fell in the middle of the Human Genome Project. Thus, it became widely and readily available and triggered multiple research efforts and product developments in the field of microarrays. In this context, The Institute for Systems Biology came up with thePiezoelectric Oligonucleotide Synthesizer and Microarrrayer (POSaM), a piezoelectric inkjet dispenser assembled from mostly off-the-shelf components except for circuit boards and some other minor components [41]. This system is capable of printing 9800 different oligonucleotides on an 8 cm$^2$ area of modified glass and of handling up to 27 slides in parallel. The printhead used is fed by six ink

channels (four phosphoramidite monomers, ethylthiotetrazole as an activator, and optional linker or modified base), and dispenses droplet volumes as small as 6 pL with 100 μm in dropped feature size and 280 μm in dropping space. In addition to the construction of an easily accessible inkjet arrayer, the same work describes some important efforts to fabricate high quality microarrays. First, suitable ink solvents were newly investigated, and a 1:1 mixture of methyl glutaronitrile (MGN) and 3-methoxypropionitrile (3MP) was found to be optimal in terms of volatility, solubility, and surface tension. Acetonitrile is commonly used in automated phosphoramidite synthesis, but its high volatility is disadvantageous to provide proper reaction sites for coupling and results in the reduction of synthetic yield. Furthermore, it can cause clogging of the print head by forming phosphoramidite precipitates during long period storage. Hence, propylene carbonate was chosen as an alternative solvent to accommodate in situ oligonucleotide synthesis by inkjet printing, but a relatively low synthetic yield of 94–98 % for each step significantly affects the array quality in this serial procedure. By dissolving the nucleotides in the 1:1 mixture of MGN and 3MP, the synthesis efficiency was increased to 97.1 ± 1.2 %, which is comparable to acetonitrile (97.2 ± 1.5 %) and superior to propylene carbonate (93.0 ± 1.3 %) [41]. Second, a laser diode droplet detector was incorporated into the system as an effective measure to monitor nozzle ejection failures. Successful droplet ejection is confirmed based on light beam scattering by droplets, detected by digitally converted photodiode signals (Fig. 8.6). Failing nozzles are omitted from use depending on the ejection status checked at the beginning of each printing cycle, and the software recalculates the most efficient printing path, accordingly. Detection and elimination of defective ejection is critical in preparing arrays reproducibly, since otherwise the entire array might be compromised. In addition to this function, the system allows for environmental control (humidity, inert gas supply) and precise motion control features. Despite the high setup costs ($ 34,000), the POSaM system has various advantageous characteristics for flexibly designing high quality inkjet-printed DNA arrays.

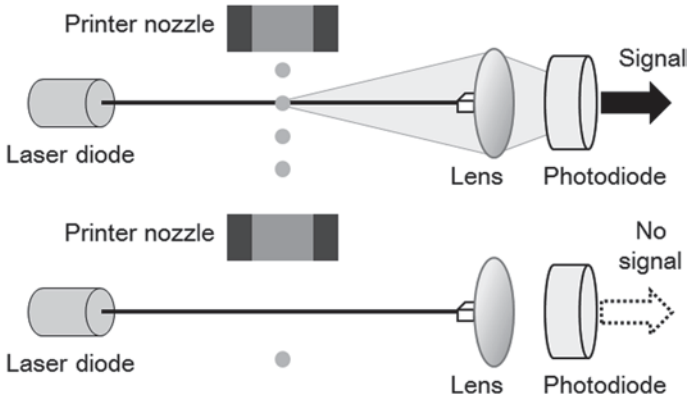


**Fig. 8.6** Droplet monitoring system in a POSaM: **a** normal ejection, **b** defective ejection. (Adapted from reference [41] (http://genomebiology.com/2004/5/8/R58); © 2004 Lausted et al.; licensee BioMed Central Ltd)

### 8.3.4 Inkjet Deposition of Nucleic Acids for Miniaturized Devices

In the future, inkjet-based deposition of nucleic acids will probably play an increasingly active part in developing novel miniaturized analytical devices, rather than in the already technically mature preparation of DNA microarrays.

One early example of applying inkjet printing of DNA for such objective is the fabrication of cantilever sensors. An IBM research group has reported on the functionalization of gold-coated cantilevers with thiol-linked 12-mer oligonucleotides for sequence-specific detection of DNAs using a piezoelectric inkjet dispenser MD-P-705-L (Microdrop, Norderstedt, Germany) [42]. A total of 100–300 nL droplets (corresponding to diameters of 60–80 μm in air) of three different 12-mer oligonucleotides were spotted onto a cantilever array (250 μm pitch), as small as 500 μm in length and 100 μm in width without cross-contamination between adjacent cantilevers.

Yasui et al. applied a piezoelectric inkjet system to inject DNA samples into a microchip device for electrophoresis [43]. With the objective of avoiding denaturation of DNA, they employed a piezo-based injector (Pulse Injector from Cluster Technology Co., Ltd.), and succeeded in handling DNAs up to 3000 bp at a concentration of 4.9 ng/mL. Generally, cleavage is much easier to occur for long DNA molecules. Indeed, in a cleavage study by gel electrophoresis, they confirmed a tailed band in the case of λDNA (48,502 bp) after the injection process, while 250 and 1000 bp DNAs showed bands identical to those of a control sample (not subjected to the inkjet process).

Although the factors determining the maximum printable oligonucleotide length are not fully investigated (e.g., influence of DNA concentration, stress experienced in the droplet ejection process, etc.), the possibility to precisely and reproducibly handle small volumes of relatively long nucleic acid solutions is definitely helpful in developing miniaturized analytical platforms such as microfluidic or nanofluidic devices. Such miniaturized analysis systems are now of great interest especially in medical diagnostic fields, because they are fast, enable the reduction of analytical sample volumes, and material costs for fabrication.

### 8.3.5 Substrates for Nucleic Acid Immobilization

Immobilization of nucleic acids has been attempted for several purposes such as the manufacturing of microarrays and the development of sensors. Some examples of substrates used for immobilizing nucleic acids are listed in Table 8.3. Owing to their widespread availability, robustness, ease of derivatization, and low intrinsic fluorescence, glass microscope slides have been widely used and represent the most common platform for microarrays. In some cases, more sophisticated platforms like quartz glass, silicon wafers, and gold-coated surfaces are applied. These surfaces are normally pretreated to bear functional moieties for coupling with DNAs or their monomers by well-established chemistries (e.g., amine–epoxy, gold–thiol, avidin–biotin linkages) described in detail elsewhere [21, 44]. Figure 8.7 shows an example

**Table 8.3** Substrates for inkjet printing of nucleic acids

| Substrate | Substrate modification | Immobilization principle of DNA |
|---|---|---|
| Microscopic glass slide [30, 41, 45] | Hydroxylation[a] [30]<br>Epoxydation [41]<br>Aminization[a] [45] | Covalent linkage |
| Quartz glass [28] | 1) Amination<br>2) Maleimidation | Covalent linkage (maleimide-thiol DNA) |
| Silicon wafer [29, 38] | Hydroxylation[b] | Covalent linkage (hydroxyl group-phosphoramidite) |
| Nitrocellulose [47] | Baking[c] at 80 °C | Hydrophobic interaction |
| Nylon membrane [47, 48] | Baking[c] at 80 °C<br>Blocking[c] treatment | Electrostatic adsorption |
| Zetaprobe membrane[d] [48] | Blocking[c] treatment | Electrostatic adsorption |
| Gold thin film [42] | Au coating of substrate | Gold-thiol linkage |
| Cyclic olefin copolymer [51] | Silicon oxide sputtering | Covalent linkage (hydroxyl group-phosphoramidite) |

[a] Fluorination was performed to prepare discrete spots by utilizing the difference of surface tensions
[b] Perfluorination was performed for the same purpose as described above
[c] Run after DNA print
[d] Nylon-based membrane with high mechanical strength and positive charge derived from quaternary amine groups (provided by Bio-Rad)

of droplets of phosphoramidite nucleotides in 1:1 3MP:MGN POSaM printed onto a standard epoxysilane-modified glass slide surface [41]. The hydrophobic nature of the silanized glass surface and the hydrophilic ink droplets results in the formation of "virtual reaction wells" for in situ DNA synthesis. To improve the homogeneity of inkjet-printed DNAs, the patterning of round-shaped areas occasionally called "surface tension wells" on the print support has been proposed [38, 45, 46]. The surface tension well is surrounded by highly hydrophobic zones (typically a fluorinated surface obtained by photolithography) and acts as a discrete hydrophilic coupling reaction site. This feature contributes to the improvement of print spot quality, depending on the surface tension of the printing ink or the precision of the inkjet printer. Lausted and co-workers compared spot alignment and spot morphology printed by a POSaM onto two kinds of substrates: (1) untreated glass slides and

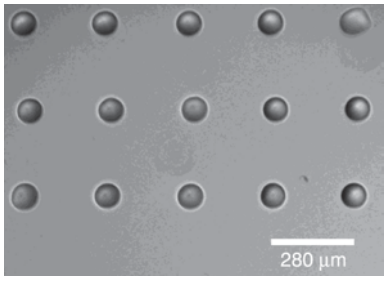


**Fig. 8.7** Virtual reaction wells on silanized glass (phosphoramidites and tetrazole dissolved in 1:1 3MP:MGN), (From reference [41]. (http://genomebiology.com/2004/5/8/R58); © 2004 Lausted et al.; licensee BioMed Central Ltd)

(2) hydrophobic silicon slides with predefined hydrophilic wells (Lumera-patterned silicon). In the latter substrate, hydroxyl group-rich regions are circularly surrounded by a polydimethylsiloxane (PDMS) surface. Spots on this substrate are perfectly round shaped with uniform diameters. On the other hand, spots on the untreated glass slide show somewhat inhomogeneous shapes, and incorrect positioning.

Porous materials have also been studied as solid supports for inkjet printing of nucleic acids. For instance, nitrocellulose and nylon membranes are known as common membrane supports for the blotting of nucleic acids and proteins. They possess a fibrous structure with micropores of 0.45 μm in diameter and negatively or positively charged surfaces derived from nitrate groups and quaternary ammonium groups, respectively. Nucleic acids with their negatively charged phosphate groups strongly adsorb onto nylon membranes electrostatically. Some groups attempted transferring DNA samples onto these supports by using commercial personal desktop inkjet printers. DNA solution was filled into emptied and cleaned ink cartridges and printed on membranes fed into a thermal inkjet printer. Labeled cDNAs [47] and PCR-amplified DNA [34] were transferred onto nitrocellulose, nylon membrane, and Zetaprobe membrane (high-strength cationized nylon membrane with high-density quaternary amine charge; commercial product of Bio-Rad), respectively and sequence-specific hybridization signals were successfully observed. Furthermore, it has been indicated that Zetaprobe membranes showed less nonspecific background binding and higher signal in comparison to common nylon membranes in a fluorescence-based hybridization test [48]. These membranes are commercially available and compatible with common vertical loading inkjet printers, thus are easily accessible alternatives for the inkjet-based fabrication of DNA hybridization assays. However, employing fibrous materials as arraying substrates is challenging mainly due to two reasons: first, it is difficult to obtain high-density arrays because droplets after impact on the substrate are likely to spread automatically via capillary forces. This can be avoided by prepatterning porous materials in a similar manner to "surface tension wells." Various approaches for hydrophobic patterning of porous materials (filter paper, chromatography paper, etc.) have been developed so far [49], but almost all of them are not resistant to organic solvents, hence considerably limiting the available DNA "ink" composition. Second, in situ DNA synthesis yields achievable in fibrous networks might be quite low due to limited contact between reactants. This means that quantitative DNA arrays with various sequences are virtually unrealizable on such substrates.

Only comparatively recently, synthetic polymeric materials have been successfully applied as a substrate for in situ DNA synthesis by inkjet printing. Interest in polymeric platforms is particularly driven by the fact that the traditional glass or silicon substrates are not easily adaptable for the integration into microfluidic systems [50]. Saaem et al. employed cyclic olefin copolymer (COC) as inexpensive, yet physically, chemically, and optically preferable substrate for DNA microarrays. They succeeded in preparing spot arrays onto an originally highly hydrophobic and chemically inert COC surface by sputtering a silicon dioxide thin film onto microwells created by photolithography (Fig. 8.8). Then, DNA synthesis was performed in each well by delivering phosphoramidite nucleotide monomers using a POSaM.

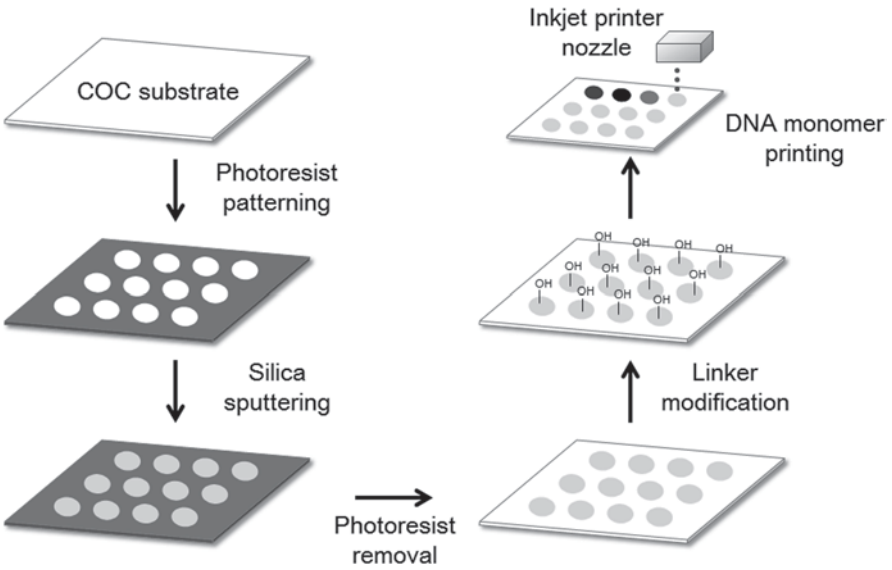


**Fig. 8.8** Procedure of in situ DNA synthesis on polymer substrate by inkjet printing

Resulting array features and oligonucleotide density were comparable to typical glass (50 μm spot diameter in 100 μm pitch and approximately 0.8–1.2 molecules per $\mu m^2$ [51]). It has to be noted, however, that this approach required the local chemical conversion of the substrate surface from its original synthetic polymeric state into a glasslike structure. To the best of our knowledge, an inkjet printing-based approach to in situ DNA synthesis on an unmodified synthetic polymeric platform has yet to be demonstrated.

## 8.4 Inkjet Printing of Proteins

### *8.4.1 Introduction*

Development of a printing strategy that could deposit multiple different proteins, such as enzymes and antibodies, as biorecognition elements on a common polymeric surface without loss of activity and structural integrity is essential in the advancements of a plethora of applications such as drug screening, clinical diagnostics, environmental monitoring, food analysis, biomarker discovery, tissue engineering, and proteomics research [16, 52, 53]. Proteins are biomacromolecules with primary structure composed of a repertoire of amino acids linked together by peptide bonds. This linearly chained protein structure assembles to form the secondary structure which is either helical, globular, or sheet folded through intramolecular hydrogen bonding. Then, the interaction of the secondary structures could mold the functional tertiary structure of the protein [54]. In contrast to the much more stable structures

of nucleic acids, the fragility of the protein structure is not trivial in the area of protein immobilization. Even a slight change in the 3D protein structure could have a significant effect on its function. Usually proteins are operated at their optimum condition to preserve the 3D structure and conformation. Some of the factors that could affect the protein structure in an aqueous solution are temperature, pressure, pH, ionic strength, and organic modifier. In case of protein immobilization, the surface property of the solid material could also induce a change in the protein structure. Therefore, proper handling is critical to achieve an active printed protein on any solid substrate, including polymeric platforms.

The noncontact characteristic of inkjet printing technology makes it potentially a material deposition technique that could gently deliver delicate proteins on a material surface. The mechanism of ink jetting has been discussed thoroughly further above. Essentially, the protein ink solution in the printer cartridge experiences a microsecond pressure pulse and is ejected through the orifice of the printhead nozzle onto the printing substrate located at a distance of 1–5 mm. In terms of versatile protein printing on different polymeric platforms, the inkjet approach is highly suitable for biomolecule deposition due to the following reasons: (1) the contactless operation could significantly minimize protein denaturation; (2) the miniscule picoliter droplet ejection may lead to minimal consumption of precious protein reagent; (3) the highly position-specific printing could lead to precise and reproducible protein immobilization; and (4) the multi-cartridge system of commercial office desktop inkjet printers could potentially lead to high-throughput multiplexing and cost-effective, mass producible protein immobilization.

In this section, focus is directed towards the inkjet deposition of enzymes or antibodies on various substrates with emphasis on polymeric platforms. This also includes some discussion on surface modification and mechanisms of protein immobilization to achieve a surface for successful selective biorecognition. A brief description on the nature of enzymes or antibodies is given to understand the importance of the protein immobilization. Figure 8.9 shows a schematic general overview of this section. Basically, the stability, sensitivity, and structural integrity of protein molecules are dependent on three basic factors—printer actuation, ink formulation, and nature of the substrate surface. Research work devoted to investigating factors that affect the protein stability and activity will also be discussed. Eventually, an outlook on the future direction of this field will be presented.

### *8.4.2 Inkjet Printing of Enzymes*

Enzymes are protein molecules that function based on the activity of the catalytic site and retention of its conformation. In general, the enzyme structure is a combination of hydrophobic amino acid (e.g., phenylalanine, tyrosine) core region and basic (e.g., lysine, arginine) or acidic (e.g., aspartic acid and glutamic acid) hydrophilic amino acid outer surface structure [55]. As a consequence, enzymes are amphiphilic biomaterials that could act both as hydrophobe and hydrophile with a net surface charge depending on the solution pH and isoelectric point. Various types of

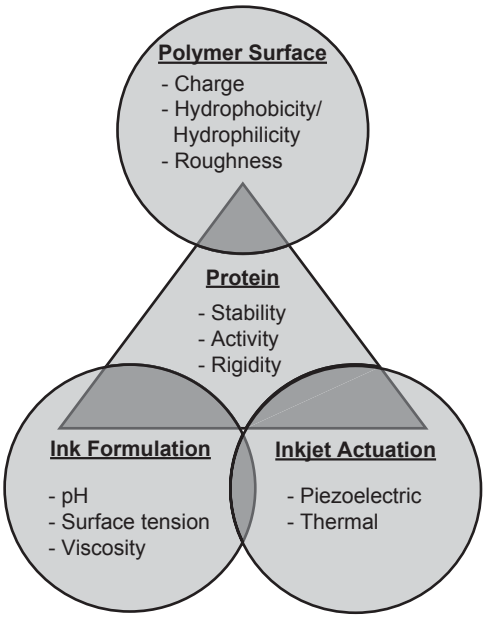


**Fig. 8.9** Overview of the factors affecting the inkjet printing of proteins

non-covalent interactions are involved to preserve the active form of the enzyme, such as hydrogen bonding, van der Waals forces, salt bridges, and hydrophobic interactions. Moreover, the rigidity of an enzyme, which is dependent on the protein structural flexibility, has also an important role on its stability. Hard enzymes have a rigid structure that could maintain the conformation upon adsorption to a surface. On the contrary, significant loss in activity could be observed for a soft enzyme due to disruption of the non-covalent interactions [56]. These characteristics of enzymes are important to have a well-thought approach on how to print them on a polymeric platform.

In 1988, Kimura et al. have successfully demonstrated the first inkjet printing of multiple enzymes, such as glucose oxidase (GOx) and urease, on a silicon wafer surface by creating a glutaraldehyde-crosslinked enzyme membrane for ion-sensitive field effect transistor (ISFET) application [57]. The native silicon wafer surface was used without further treatment. They have incorporated bovine serum albumin (BSA) in the ink formulation to minimize the denaturation of the GOx or urease. Also, the glutaraldehyde molecule may have increased the rigidity of the enzyme structure that led to maintaining its activity and at the same time created an entrapped enzyme within the predominantly BSA-crosslinked membrane. Figure 8.10a shows the experimental setup of the first inkjet printer with a single cartridge used for enzyme printing. Both the X-Y stage and pulse generator were controlled by the computer. It is important to note that the protein droplet-impact position was guided by the microscope and not initiated by the computer software. A photograph of the actual pattern of protein membranes on an ISFET device is depicted in Fig. 8.10b. By confirming an electrochemical response of the device

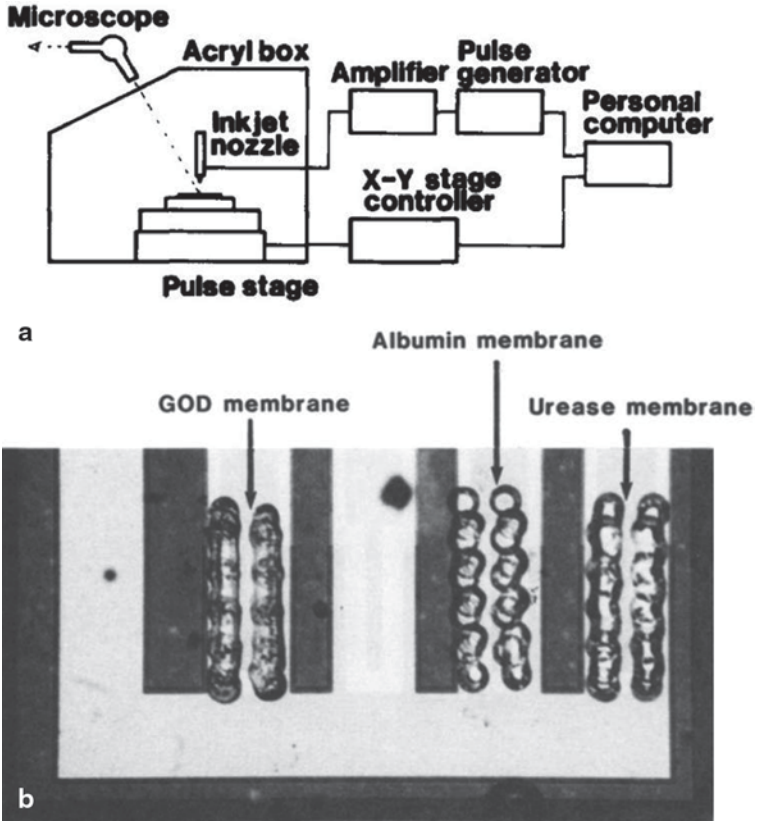


**Fig. 8.10** First demonstration of protein printing by inkjet technology: **a** inkjet printer setup; **b** protein membranes deposited on an ISFET device. Reprinted from Kimura et al. (1988) Biosensors 4:41–52, Copyright (1988), with permission from Elsevier [57]

to glucose and urea, it was indirectly proven that such enzyme deposition strategy could preserve the activity of GOx and urease. Indeed, the inkjet printing technology was in its infancy during that time and its potential for high-resolution printing and mass production has not been realized.

By 2000, inkjet printing technology has matured significantly and commercially available office desktop printers have been exploited for enzyme immobilization. Roda et al. were among the first to demonstrate such use of an office desktop inkjet printer by depositing horseradish peroxidase (HRP) on various solid supports such as conventional cellulose paper with different weights (30–80 g/m$^2$), cellulose filter paper, nylon sheet, photographic gelatin paper, tissue paper, and inkjet transparency film [58]. The printed HRP was simply adsorbed on the surface of the polymeric material and evaluated by chemiluminescence (CL) detection. Among the polymeric platforms, it was the lightest conventional cellulose paper (30 g/m$^2$) that resulted in the maximum CL intensity with the shortest diffusion time of the CL substrate. Figure 8.11 shows the effect of the spot diameter and activity of the HRP enzyme

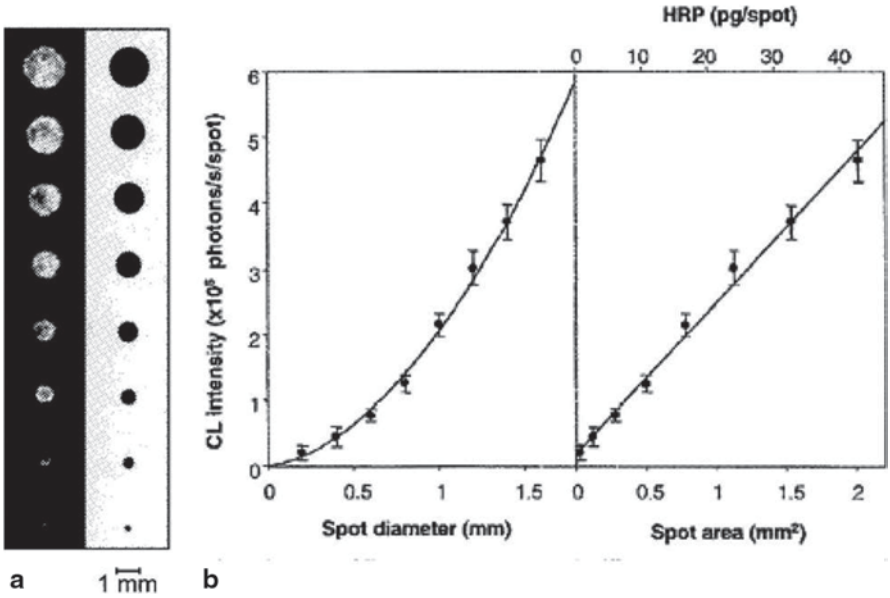


**Fig. 8.11** **a** Left part shows the chemiluminescence signal and right part shows the deposition pattern of an array of HRP spots with different diameters on conventional cellulose paper. **b** Correlation of the chemiluminescence signal and spot diameter, spot area, and amount of HRP. Reprinted from reference [58] Roda et al. (2000), Protein microdeposition using a conventional inkjet printer. Biotechniques 28:492–496 © 2000 BioTechniques. Used by Permission

deposited on the cellulose paper surface. Based on this early work, the feasibility of enzyme deposition using conventional inkjet printing on various material surfaces was realized. The delay in the advancement of protein printing by inkjet technology was probably due to its digital printing nature which relies on the development of both the software and hardware to achieve an efficient transfer of computer graphics onto the printing substrate.

Most of the current investigations on enzyme stability during inkjet printing are focusing on actuation-related parameters (e.g., ink compression [59], shear rate [60], and thermal effect [61]), and ink formulation (e.g., viscosity modifier [62]). Nishioka et al. have studied the effect of inkjet printing on the HRP enzyme by exposing the protein to various compression rates (85 V applied on a piezoceramic between 14 and 70 μs) generated by piezo-actuation [59]. They have demonstrated that compression of the ink liquid could have a direct effect on the HRP activity. Commercial desktop inkjet printers have a drop velocity of about 10 m/s, which creates a condition of high compression rate, thus possibly affecting the stability of the enzyme. However, the use of sugars like trehalose/glucose as ink additives could act as cushion, through extensive hydrogen bonding, to protect the protein from such pressure pulse. In a different report, it was shown that the shear effect of piezoelectric inkjet printing on GOx has no significant effect on the secondary and tertiary structures of the protein, but degradation in enzyme activity was observed

[60]. The authors hypothesized that low level of structural distortion could have affected the active site and the enzyme–substrate interaction. In case of thermal inkjet printing of enzymes, it seems natural to assume that loss in enzyme activity may occur due to high temperature (200–300 °C) exposure in the printhead's firing chamber during vapor bubble formation. Interestingly, based on the work of Khan et al., such effect was insignificant at least when printing an HRP enzyme [61]. This could be due to the following reasons: (a) as already mentioned above, the exposure time of the ink to high temperature is only in the order of a few microseconds and (b) assuming the distance of the printhead and substrate is about 2 mm and the drop velocity is 10 m/s, it takes about 200 μs for the droplet to reach the substrate surface being at room temperature. The remaining heat confined in the droplet could be absorbed by the paper cellulose which has a high heat capacity [2]. Therefore, the overall exposure time to high temperature is probably too short to induce damage on the enzyme activity. On the other hand, the influence of ink viscosity modifiers has been investigated by exposing the HRP enzyme to a number of polymers with different molecular weights, and functional and ionizable groups [62]. Using a piezoelectric inkjet printer for HRP printing, it was concluded that carboxymethyl cellulose, among other polymers, was found to maintain the enzyme activity at a viscosity similar to commercially available inkjet inks (2–9 cP). Here, it is important to keep in mind that the balance between jetting parameters and ink formulation should always be considered when printing an enzyme. This has been pointed out by Arrabito et al. [63], who demonstrated that an increasing amount of glycerol in the ink may support a uniform protein pattern and enzyme stability, but at the same time may also result in higher shear rates on the protein that may eventually affect the enzyme activity.

Table 8.4 shows some of the current reports on enzyme deposition by inkjet printing on various substrate material surfaces. Thermal- and piezoelectric-actuated inkjet printers are both used for enzyme immobilization. Apparently, piezoelectric actuation is utilized more often than the thermally actuated jetting. Although there is a report on insignificant loss in enzyme activity using thermal inkjet printing [61], the piezoelectric approach is probably assumed to offer a more gentle way of actuation, since the bio-ink solution is not exposed to extreme heat. However, it is important to remember that piezoelectric actuation requires higher ink viscosity (5–10 cP) than the thermal inkjet printing (1–1.5 cP) (Table 8.1), which means that an enzyme in ink formulations for piezo-based printers could experience higher shear stress during jetting. Both piezoelectric and thermal actuation have their own advantages and disadvantages, and they always require an optimization of their parameters to achieve a successful enzyme deposition. Moreover, a number of enzymes and polymeric materials have been used for inkjet printing (Table 8.4). The generally used polymeric substrates are cellulosic filter papers, glass, and plastics (e.g., polystyrene, polypropylene, and polyethylene terephthalate (PET)). These are low-cost and readily available materials. Adsorption is perhaps the most convenient method of enzyme immobilization to the majority of these surfaces. This is mainly because of its simplicity by directly printing on the polymer surface without any chemical modification or treatment. Since proteins are amphiphilic biomaterials, their surface

**Table 8.4** Enzyme immobilization on various materials by inkjet printing

| Substrate material | Enzyme | Inkjet actuation | Base ink for enzyme | Enzyme immobilization | References |
|---|---|---|---|---|---|
| Si wafer | Glucose oxidase (GOx), Urease | Piezoelectric | 10 mM HEPES buffer (pH 7.5), 3–5% bovine serum albumin (BSA) | Entrapment | [57] |
| Filter paper or plastic | Horseradish peroxidase (HRP) | Thermal | 0.1 M Tris-HCl buffer (pH 8.6), 1.5 mM sodium dodecyl sulfate (SDS), 10 mM NaCl | Adsorption | [58] |
| Plastic | Peroxidase | Piezoelectric | Buffer, trehalose/glucose | Adsorption | [59] |
| Glass | GOx | Thermal | 0.1 M Phosphate buffer (pH 6.5), 1.5 mM EDTA, 10% glycerol | Adsorption | [67] |
| Glass | GOx | Piezoelectric | Vinylacetate/ethylene copolymer | Adsorption | [68] |
| Glass | HRP | Thermal | 0.1 M Phosphate buffer (pH 6.5), 1.5 mM EDTA, 10% glycerol | Adsorption | [69] |
| Polyvinylidene difluoride | Trypsin, PNGase F | Piezoelectric | 25 mM Ammonium bicarbonate, 10% 2-propanol | Adsorption | [70] |
| Silicon dioxide | GOx | Piezoelectric | 0.05 M Phosphate buffer (pH 6.5), 0–50% glycerol | Covalent | [63] |
| Filter paper | ALP/HRP | Thermal | 0.1 M Phosphate buffer (pH 6.0)/1 M diethanolamine buffer, 0.5 $MgCl_2$ | Adsorption | [61] |
| Filter paper | AChE | Piezoelectric | 100 mM Tris buffer (pH 8) | Entrapment | [65] |
| Plastic | GOx, glutamate and glucose dehydrogenase | Piezoelectric | Phosphate buffered saline (PBS) | Adsorption | [60] |
| Filter paper, electrospun poly-(ε-caprolactone) | HRP | Thermal/ Piezoelectric | 0.1 M Phosphate buffer (pH 6) | Adsorption | [64] |
| Screen-printed carbon paste | Urease | Piezoelectric | 0.1 M Phosphate buffer (pH 7.12), 0.1% glycerol, 0.01% Triton X-100 | Adsorption | [71] |
| Polyethylene terephthalate (PET) | GOx, HRP | Piezoelectric | PEDOT/PSS in water | Adsorption | [72] |

**Table 8.4** (continued)

| Substrate material | Enzyme | Inkjet actuation | Base ink for enzyme | Enzyme immobilization | References |
|---|---|---|---|---|---|
| Filter paper | Tyrosinase | Piezoelectric | 0.1 M Phosphate buffer (pH 6.5) | Entrapment | [66] |
| Silicon dioxide | CY3A4 | Piezoelectric | 0.1 M Phosphate buffer, 30% glycerol | Adsorption | [73] |
| Filter paper | AChE | Piezoelectric | Tris buffer, 30% glycerol, 0.1% Triton X-100 | Entrapment | [74] |
| PET | GOx | Piezoelectric | 20 mM Acetate buffer (pH 5.5) | Adsorption | [75] |
| Screen-printed carbon electrode | GOx or HRP | Piezoelectric | Polypyrrole in water | Adsorption | [76] |

*AChE* acetylcholine esterase

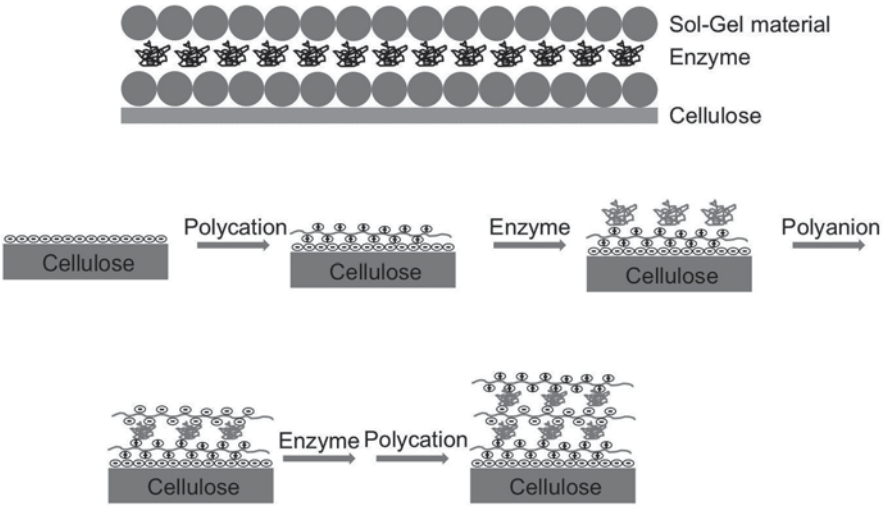


**Fig. 8.12** Enzyme entrapment by **a** sol–gel material (adapted with permission from Hossain SMZ et al. (2009) Anal Chem 81:5474–5483. Copyright (2009) American Chemical Society [65]). **b** Layer-by-layer method (adapted with permission from Alkasir et al. (2012) Anal Chem 84:9729–9737. Copyright (2012) American Chemical Society [66])

adhesion is governed by either hydrophobic (van der Waals forces) or hydrophilic (hydrogen bonding/electrostatic) interactions or their combination. However, one of the important requirements to achieve an optimal surface wetting and efficient adhesion of the protein is to have an ink with lower surface tension than the surface energy of the substrate material [64]. A surfactant such as Triton X-100, a nonionic molecule and mild detergent, is an example of a reagent that could lower the surface tension of the ink formulation. At least when included in an ink formulation containing acetylcholine esterase (AChE), 0.1 wt% Triton X-100 had no effect on the activity of printed AChE [65]. Furthermore, an approach to increase the surface energy of a substrate for printing is a surface pretreatment or modification. Sequential printing of reagents involving sol–gel applications or layer-by-layer (LbL) deposition are some of the interesting approaches that have been explored to modify the surface property of the substrate for a more stable protein immobilization [65, 66]. For sol–gel printing, the silica sol was printed separately from the enzyme solution (Fig. 8.12a) to avoid the gelation to occur in the nozzle of the inkjet printer. It was confirmed that the sol–gel-based ink was deposited on the surface and that enzyme entrapment was effective. In a different approach, LbL deposition of chitosan and sodium alginate with tyrosinase enzyme sandwiched in between layers was accomplished by inkjet printing (Fig. 8.12b). Initially, pentabasic sodium triphosphate (NaTPP) was adsorbed on the filter paper to act as a cross-linker and stabilizer of cationic chitosan. This type of enzyme immobilization provided a biocompatible microenvironment and electrostatic anchoring for the enzyme, which led to a stable bioactive structure on the filter paper surface. Given the proper rheological properties of the bio-ink, both sol–gel enzyme deposition and LbL approach could provide simple fabrication, enzyme-friendly microenvironment, retention of activity, and potential for mass production.

### 8.4.3 Inkjet Printing of Antibodies

Antibodies, also known as immunoglobulins, are large glycoprotein molecules that have high specificity for their antigens which could be a protein, polysaccharide, or lipid. Their basic structure is almost Y-shaped, with two arms composed of pairs of heavy and light polypeptide chains and a trunk made up of a pair of heavy polypeptide chains [77, 78]. The pairs of polypeptide chains are covalently connected by disulfide bonds. This covalent bond controls the structural rigidity and flexibility of the antibody. Antibody–antigen interactions are an extremely important form of biorecognition and are used in various applications such as medical, clinical, pharmaceutical, and proteomics. However, most antibodies are expensive and available in extremely low amounts. A microarray format is the commonly used type of analytical device to maximize the use of miniscule amounts of antibodies on a given substrate surface. Therefore, inkjet printing can offer a convenient and practical solution to the task of dropping a picoliter amount of expensive antibodies in a small, defined region of a substrate surface.

In 1995, Nilsson et al. reported the concept of thin-layer immunoaffinity chromatography, which was an early demonstration of piezoelectric antibody inkjet printing onto a pre-activated nylon membrane for the analysis of the disease biomarker C-reactive protein (CRP) [79]. A monoclonal antibody (Mab) in three different concentrations was printed in a line configuration and formed three selective biorecognition zones (Fig. 8.13). The immunocomplex solution of CRP antigen-Mab-coated latex traveled across the membrane, and then formed blue-colored lines due to sandwich immunocomplexes formed with the printed antibody in the biorecognition zones. This result proved the feasibility of inkjet printing of antibodies on a

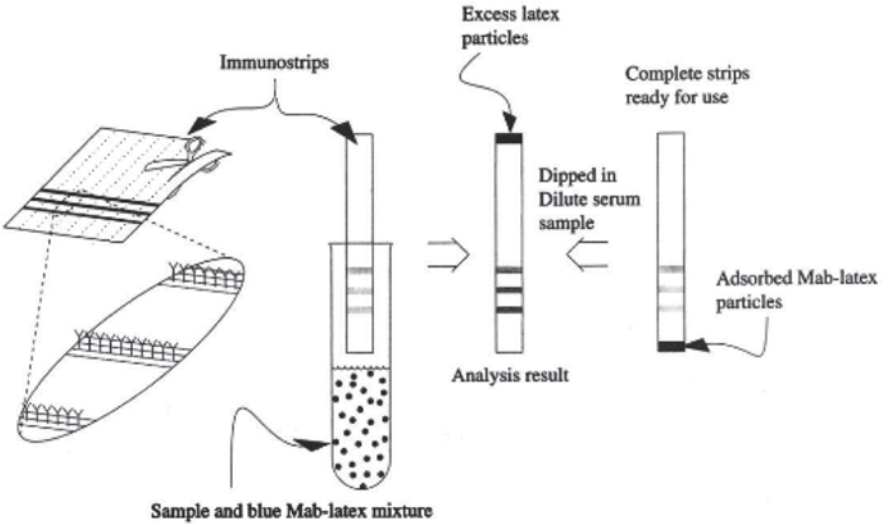


**Fig. 8.13** Line pattern deposition of antibodies on a nylon membrane by a customized inkjet printer. Reprinted with permission from Nilsson et al. (1995) Anal Chem 67:3051–3056. Copyright (1995) American Chemical Society [79]

polymeric support. However, it was only around 2008 that research publications about antibody inkjet printing revived the interest in the topic among the academic community. Historically, the antibody microarray technology is an offshoot of the DNA microarray technology, which was already mature in the early 1990s. This DNA microarray technology was directly translated to fabricate antibody microarrays. Therefore, there was not much research output and efforts only focused on the routine implementation of the commercially available microarrays. Recently, there are demands for the development of antibody microarrays to be more cost-effective and easy to fabricate while maintaining throughput and minimal reagent consumption. Commercially available office desktop inkjet printers could be a potential solution to this challenge. Lonini et al. have used both HP Deskjet 5740 (thermal) and EPSON Stylus c46 (piezoelectric) to investigate the effect of these office printers on immunoglobulin dispensing for an immunoassay [80]. They compared both manual and inkjet printer-based deposition of antibodies on a plastic microwell plate. The use of the piezoelectric printer resulted in a more convenient operation, and comparable immunoassay results with the manually dispensed antibodies were achieved. Meanwhile, the thermally actuated printer did not allow for a reproducible deposition of the antibodies. This result suggests that the piezoelectric actuation is preferred over the thermal actuation.

Table 8.5 describes some of the recent developments in antibody microarray fabrication by using piezoelectric inkjet printers. Apparently, piezo-actuation is the favored mode of fluid dispensing for antibodies, as briefly discussed above. Besides the ink formulation and printer actuation, the surface property of the polymer substrate is also an important factor to consider when printing an antibody. Depending on the surface, the antibody could interact through adsorption, covalent binding, molecular recognition, or entrapment in a porous material (Fig. 8.14). Representative reports are shown in Table 8.5. Molecular recognition requires an initial deposition of a biorecognition element such as avidin or streptavidin to be able to immobilize the biotinylated antibodies. This manner of immobilization allows efficient orientation of antibodies to easily form an immunocomplex. Unlike enzyme printing, which utilizes adsorption as the main method of immobilization, the recent trend in antibody immobilization is through covalent bonding. This is probably due the nature of the related application. Printed antibodies are generally used in biosensors that require multiple bioassay steps such as immunoreaction and washing. This operation necessitates fluid handling with flowing liquids; thus, it may be important that antibodies are permanently attached on the substrate material. Although it is common practice to allow antibodies to be adsorbed on substrates like nitrocellulose, it has been observed that covalent immobilization allows a more wash-stable protein pattern, since fluid movement might promote desorption of molecules from the surface. Moreover, covalent immobilization offers an opportunity to control the proper orientation of antibodies for the immunoreaction.

Polymer substrates used for antibody microarray fabrication can be divided into two types: porous and nonporous materials. Glass and polystyrene are the most generally accepted nonporous substrates, since they are easily available and inexpensive. Mujawar et al. have investigated the effect of changing the surface

**Table 8.5** Antibody immobilization by inkjet printing on various materials

| Substrate material | Antigen | Inkjet actuation | Base ink for antibody | Surface attachment | References |
|---|---|---|---|---|---|
| Pre-activated nylonmembrane | C-reactive protein | Piezoelectric | 0.1 M Tris-HCl, 30% sucrose, 0.15 M NaCl, 0.5% PVA, 0.25% Tween 20 | Covalent | [79] |
| Avidin-coated glass slide | Cholera toxin, S. enterotoxin B, ricin, B. globigili | Thermal | 10 mM Phosphate buffer, 10 mM NaCl, 10 mM sucrose, 0.1% bovine serum albumin (BSA) | Molecular recognition | [85] |
| Filter paper | Human and mouse IgG | Piezoelectric | Water | Adsorption | [86] |
| Glass slide | Cytokines, breast cancer bio-markers, cancer-related protein | Piezoelectric | 0.65% Alginate solution, 10% glycerol | Entrapment | [82] |
| Cyclic olefin copolymer | Procollagen type 1 C-peptide | Piezoelectric | 10 mM Phosphate buffered saline (PBS), 1% BSA | Covalent | [87] |
| Nitrocellulose-coated glass slide | Rabbit IgG, goat IgG, chicken IgY, human IL-4 | Piezoelectric | 0.05% Triton X-100 | Adsorption | [84] |
| Nanofibrillated cellulose film | Human IgG | Piezoelectric | 10 mM Phosphate buffer | Covalent | [88] |
| Cyclic olefin copolymer | Calprotectin | Piezoelectric | Phosphate buffer | Covalent | [89] |
| Cyclic olefin copolymer | Interleukin-6, tumor necrosis factor α | Piezoelectric | Phosphate buffer | Covalent | [90] |
| Poly(methyl methacrylate) | C-reactive protein | Piezoelectric | PBS, 0.1% Tween 20, 10% sucrose | Covalent | [91] |
| Nitrocellulose membrane | Pathogenic DNA | Piezoelectric | PBS | Adsorption | [92] |

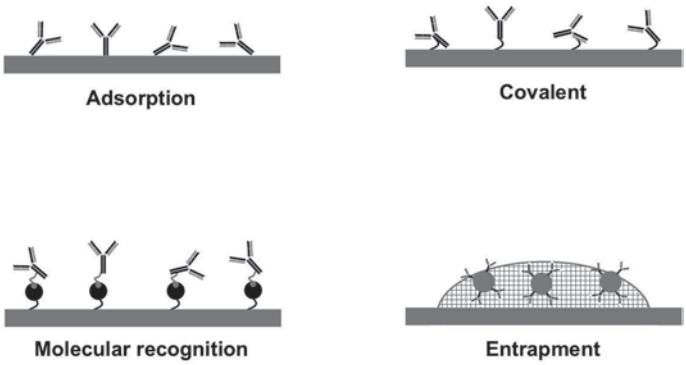


**Fig. 8.14** Different types of immobilization for antibodies dispensed by inkjet printing

hydrophobicity on the spot morphology of inkjet-printed biotinylated IgG on both substrates [81]. For this purpose, they have treated the surface with various silanization reagents to vary the contact angle ($\theta$). Based on a nucleic acid immunoassay for the detection of *Staphylococcus aureus*, excellent spot uniformity and good signal-to-noise ratio were achieved with contact angles of $\theta \sim 65°$ and $\theta \sim 75°$ for untreated glass and polystyrene, respectively. On the contrary, to improve the binding capacity, assay sensitivity, and mass transport, 3D porous network materials have been exploited. In this case, the porosity of the material creates an opportunity for short diffusion path lengths and fast interaction between biomaterials. Such work has been demonstrated by Li et al., where they created a 3D antibody microarray by physical entrapment of the antibodies within a highly porous alginate gel that is spotted on a glass slide [82]. This was achieved through sequential reagent printing using an inkjet printer. Nitrocellulose membranes, on the other hand, are widely used porous materials for biochip fabrication. This material has a successful history of use as an adsorbent for Western-blot analysis which allows the measurement of antibody–antigen interactions [83]. Therefore, such application could easily be adapted to antibody microarray fabrication. Commercially available nitrocellulose coated-glass slides have been used to print a NanoProbeArray by a piezo-actuated inkjet printer for the analysis of ultra-low volumes of protein samples [84].

Microfluidic technology plays an active role in influencing a change in antibody microarray devices from a slide format to a microchip format. The microfluidic chip could offer minimal consumption of samples and reagents, short analysis time, integration of other operational steps, and facile fluid handling [93]. The antibodies could be printed in the microchip channels (millimeter length, millimeter to submillimeter width, and micrometer height) of various polymeric substrates such as filter paper, COC, and poly(methyl methacrylate) (PMMA). Abe et al. pioneered the fabrication of microfluidic paper-based analytical devices by inkjet etching [94]. Basically, the paper substrate is coated with polystyrene, and the hydrophilic channel is created by etching away the polymer using toluene as the ink. Then, the antibodies are inkjet printed on two different zones of the paper microfluidic immunosensor to form the control and test lines [86]. Figure 8.15 shows the simple

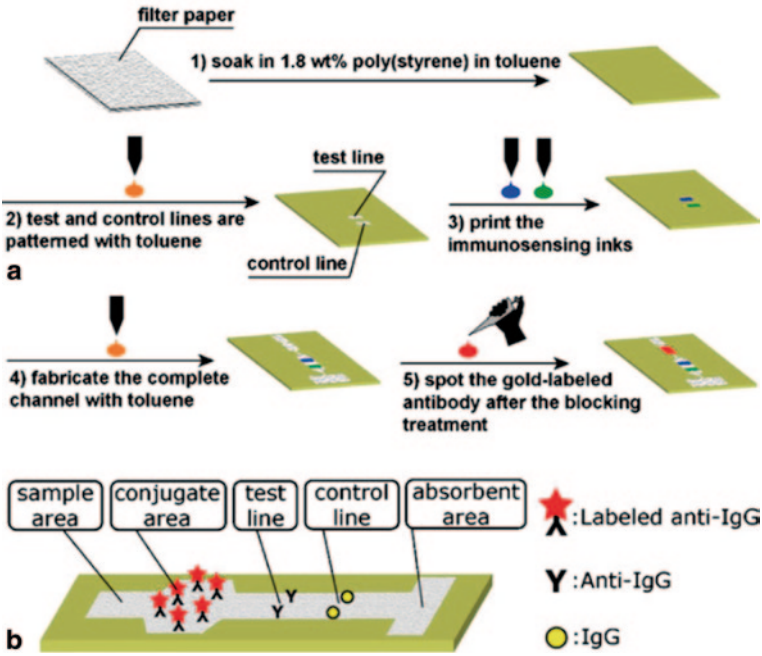


**Fig. 8.15** **a** Fabrication process of an inkjet-printed microfluidic immunosensing strip. **b** Schematic representation of the finalized strip. With kind permission from Springer Science+Business Media: Abe et al. (2010) Inkjet-printed paperfluidic immuno-chemical sensing device. Anal Bioanal Chem 398:885–893 (reference [86])

fabrication concept of the microfluidic paper-based immunosensor and the deposition of antibodies. This approach has been used for simultaneous multianalyte sensing of two different antigens and pH. Successful demonstration of a qualitative sandwich immunoassay was achieved by showing the difference in response of the test and control lines after sample introduction. Inkjet printing of antibodies on microchannels of nonporous polymer substrates has also been demonstrated. In this case, the mode of antibody immobilization is covalent. This is due to the fluid flow characteristic of the microchip and the absence of a 3D network where antibodies could anchor. Therefore, a wash-stable antibody pattern on polymer substrates is desirable. COC has been used as a substrate for a microchip immunosensor array with antibodies deposited through inkjet printing [87, 89, 90]. Surface modification of COC was done by treating it with p-nitrophenyl ester, which can covalently bind with the amino group of the antibody. Moreover, an aldehyde-functionalized PMMA surface has been used as a substrate for an inkjet-printed antibody. The surface functionalization of PMMA has been achieved through sequential treatment with plasma, polyethyleneimine, and glutaraldehyde (Fig. 8.16). The aldehyde reacts with the primary amine of the antibody to form a stable covalent bond on the surface of PMMA. This surface modification strategy is quite common for antibody immobilization.

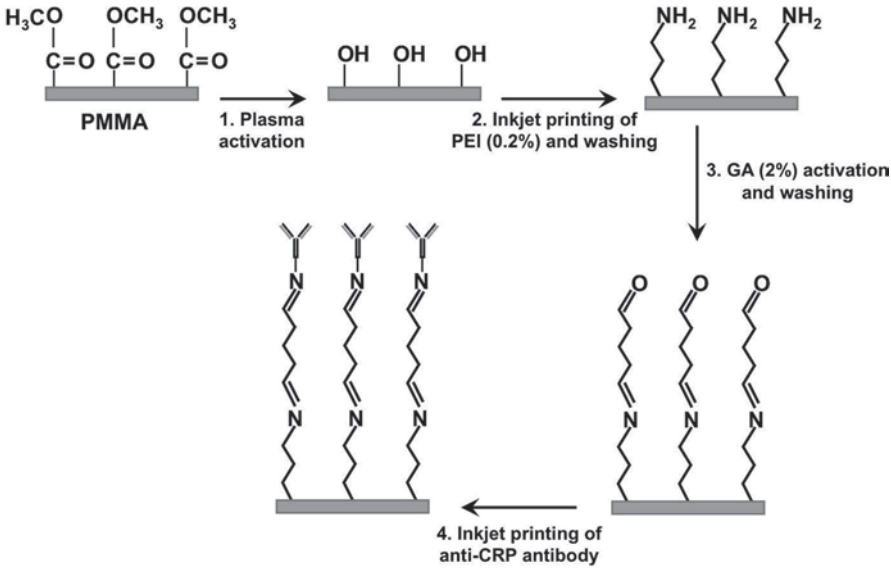


**Fig. 8.16** Covalent immobilization of an inkjet-printed antibody array on poly(methyl methacrylate)

## 8.5 Summary and Future Trends

Starting from around 2000, scientific reports of inkjet printing applied for the deposition of biomolecules with the purpose of fabricating analytical devices based on biorecognition are becoming increasingly numerous. Some applications of inkjet printing of biomolecules have matured close to industrial routine, but others are still in their infancy. While some systems are very robust and reliable for everyday use, others require a highly controlled laboratory environment.

Inkjet printing of nucleic acids has so far been explored mainly for the purpose of DNA microarray fabrication and most attention has been paid to obtain high-quality and high-density arrays. The application of the inkjet technology for the fabrication of other types of analytical devices is still comparatively scarce, despite the method's high potential. Now that manufacturing of DNA microarrays by inkjet printing has evolved into an almost mature technology already commercialized by some manufacturers, the inkjet printing of nucleic acids can be expected to become increasingly applied for the development of other miniaturized analytical tools. Especially miniaturized sensing devices, which enable cost-reduced analysis from low sample volumes, will be of great importance in various fields such as medical diagnosis, and food quality or environmental monitoring, among others. Inkjet printing technology is a prospective approach to handle small amounts of DNAs with the precision required for developing such devices, but at the same time at lowest possible costs.

The inkjet printing of proteins such as enzymes and antibodies on various polymeric surfaces to form selective biorecognition elements is another important

technology that may have high societal impact. It has the potential to facilitate efficient and effective advancements in different areas of research for instance medical and clinical diagnostics, food science, and environmental analysis, among others.

The deposition of enzymes on polymer surfaces by inkjet printing is still considered to be in its early development. This can easily be concluded from the type of examples discussed in this text (e.g., Table 8.4), where most of the enzymes used were either GOx or HRP, which are considered to be comparably stable and widely applied "model enzymes." Currently ongoing research work is still mainly focused on the effect of inkjet actuation and ink formulation on the activity of the enzyme. A good balance between these two inkjet parameters is essential for a successful enzyme immobilization. Keeping the enzyme in its active form is a major consideration to further develop other immobilization strategies. Given the fact that digital inkjet printing itself is an almost mature technology and that the basic factors regarding enzyme handling by inkjet methods are mostly understood as shown by various research reports, it is apparent to print other important enzymes with relevance to the above-mentioned research areas which could become a significant direction for future efforts. Allowing this development to be driven by the requirement for the analysis of real samples from hospitals, food markets, rivers, and other relevant sources will further push the exploitation of inkjet technology towards more practical applications.

Antibodies are more rigid proteins than the enzymes, since they do not rely on the fragile active catalytic site, but rather on polypeptide chains linked by disulphide bonds. Most of the research work demonstrated is related to the antibody immobilization on various polymeric supports. A key to antibody immobilization is to allow its proper orientation for an effective immunoreaction. This can be achieved by either covalent or biomolecular recognition immobilization strategies. It may be concluded from the examples provided in this text (e.g., Table 8.5) that many of the listed applications target the analysis of disease biomarkers. Those are generally more relevant analytes than the ones addressed by inkjet-printed enzyme-based systems, which probably indicates that the inkjet deposition of antibodies is already in a more advanced state of development.

In general, many recent research reports point to a continuing trend to move from a slide format of assay to a microfluidic chip format. The combination of inkjet printing and microfluidic technologies could certainly lead to more efficient and cost-effective fabrication of a broad range of microfluidic analytical devices. In terms of polymeric substrates applied for these purposes, cellulosic paper and COC seem to be most promising at this time.

## References

1. Elmqvist R (1949) Measuring instrument of the recording type. US Patent 2,566,443
2. Le HP (1998) Progress and trends in ink-jet printing technology. J Imaging Sci Technol 42:49–62
3. Martin GD, Hoath SD, Hutchings IM (2008) Inkjet printing—the physics of manipulating liquid jets and drops. Journal of Physics: Conference Series 105:012001

4. Sirringhaus H, Kawase T, Friend RH, Shimoda T, Inbasekaran M, Wu W, Woo EP (2000) High-resolution inkjet printing of all-polymer transistor circuits. Science 290:2123–2126
5. Teichler A, Perelaer J, Schubert US (2013) Inkjet printing of organic electronics—comparison of deposition techniques and state-of-the-art developments. J Mat Chem C 1:1910–1925
6. Komuro N, Takaki S, Suzuki K, Citterio D (2013) Inkjet printed (bio)chemical sensing devices. Anal Bioanal Chem 405:5785–5805
7. Cooley PW, Wallace DB, Antohe BV (2001) Applications of ink-jet printing technology to BioMEMS and microfluidic systems. Proc SPIE 4560:177–188
8. Castrejon-Pita JR, Baxter WRS, Morgan J, Temple S, Martin GD, Hutchings IM (2013) Future, opportunities and challenges of inkjet technologies. Atomization Spray 23:541–565
9. Hudd A (2010) Inkjet printing technologies. In: Magdassi S (ed) The chemistry of inkjet inks. World Scientific, Singapore, pp 3–18
10. Delaney JT, Smith PJ, Schubert US (2009) Inkjet printing of proteins. Soft Matter 5:4866–4877
11. Setti L, Piana C, Bonazzi S, Ballarin B, Frascaro D, Fraleoni-Morgera A, Giuliani S (2004) Thermal inkjet technology for the microdeposition of biological molecules as a viable route for the realization of biosensors. Anal Lett 37:1559–1570
12. Tirella A, Vozzi F, De Maria C, Vozzi G, Sandri T, Sassano D, Cognolato L, Ahluwalia A (2011) Substrate stiffness influences high resolution printing of living cells with an ink-jet system. J Biosci Bioeng 112:79–85
13. Hadimioglu B, Elrod SA, Steinmetz DL, Lim M, Zesch JC, Khuri-Yakub BT, Rawson EG, Quate CF (1992) Acoustic ink printing. In: Ultrasonics Symposium, 1992. Proceedings IEEE 1992, pp 929–935
14. Weng B, Shepherd RL, Crowley K, Killard AJ, Wallace GG (2010) Printing conducting polymers. Analyst 135:2779–2789
15. Magdassi S (2010) Ink requirements and formulations guidelines. In: Magdassi S (ed) The chemistry of inkjet inks. World Scientific, Singapore, pp 19–41
16. Di Risio S, Yan N (2010) Bioactive paper through inkjet printing. J Adhes Sci Technol 24:661–684
17. De Gans BJ, Duineveld PC, Schubert US (2004) Inkjet printing of polymers: State of the art and future developments. Adv Mater 16:203–213
18. Monton MRN, Forsberg EM, Brennan JD (2012) Tailoring sol-gel-derived silica materials for optical biosensing. Chem Mater 24:796–811
19. Sele CW, von Werne T, Friend RH, Sirringhaus H (2005) Lithography-free, self-aligned inkjet printing with sub-hundred-nanometer resolution. Adv Mater 17:997–1001
20. Hwang SY, Lim G (2000) DNA chip technologies. Biotechnol Bioprocess Eng 5:159–163
21. Pirrung MC (2002) How to make a DNA chip. Angew Chem Int Edit 41:1267–1289
22. Barbulovic-Nad I, Lucente M, Yu S, Mingjun Z, Wheeler AR, Bussmann M (2006) Bio-microarray fabrication techniques—A review. Crit Rev Biotechnol 26:237–259
23. Sassolas A, Leca-Bouvier BD, Blum LJ (2008) DNA biosensors and microarrays. Chem Rev 108:109–139
24. Meyer R, Giselbrecht S, Rapp BE, Hirtz M, Niemeyer CM (2014) Advances in DNA-directed immobilization. Curr Opin Chem Biol 18:8–15
25. Pease AC, Solas D, Sullivan EJ, Cronin MT, Holmes CP, Fodor SP (1994) Light-generated oligonucleotide arrays for rapid DNA sequence analysis. P Natl Acad Sci USA 91:5022–5026
26. Lockhart DJ, Dong H, Byrne MC, Follettie MT, Gallo MV, Chee MS, Mittmann M, Wang C, Kobayashi M, Norton H, Brown EL (1996) Expression monitoring by hybridization to high-density oligonucleotide arrays. Nat Biotech 14:1675–1680
27. Schena M, Shalon D, Davis RW, Brown PO (1995) Quantitative monitoring of gene expression patterns with a complementary DNA microarray. Science 270:467–470
28. Okamoto T, Suzuki T, Yamamoto N (2000) Microarray fabrication with covalent attachment of DNA using Bubble Jet technology. Nat Biotech 18:438–441
29. Hughes TR, Mao M, Jones AR, Burchard J, Marton MJ, Shannon KW, Lefkowitz SM, Ziman M, Schelter JM, Meyer MR, Kobayashi S, Davis C, Dai H, He YD, Stephaniants SB, Cavet G, Walker WL, West A, Coffey E, Shoemaker DD, Stoughton R, Blanchard AP, Friend SH, Linsley PS (2001) Expression profiling using microarrays fabricated by an ink-jet oligonucleotide synthesizer. Nat Biotech 19:342–347

30. Singh-Gasson S, Green RD, Yue Y, Nelson C, Blattner F, Sussman MR, Cerrina F (1999) Maskless fabrication of light-directed oligonucleotide microarrays using a digital micromirror array. Nat Biotech 17:974–978
31. Gilles PN, Wu DJ, Foster CB, Dillon PJ, Chanock SJ (1999) Single nucleotide polymorphic discrimination by an electronic dot blot assay on semiconductor microchips. Nat Biotech 17:365–370
32. Egeland RD, Southern EM (2005) Electrochemically directed synthesis of oligonucleotides for DNA microarray fabrication. Nucleic Acids Res 33:e125
33. Schober A, Gunther R, Schwienhorst A, Doring M, Lindemann BF (1993) Accurate high-speed liquid handling of very small biological samples. Biotechniques 15:324–329
34. Allain L, Askari M, Stokes D, Vo-Dinh T (2001) Microarray sampling-platform fabrication using bubble-jet technology for a biochip system. Fresen J Anal Chem 371:146–150
35. Beaucage SL, Caruthers MH (1981) Deoxynucleoside phosphoramidites—A new class of key intermediates for deoxypolynucleotide synthesis. Tetrahedron Lett 22:1859–1862
36. Moore MF, Beaucage SL (1985) Conceptual basis of the selective activation of bis(dialkylamino)methoxyphosphines by weak acids and its application toward the preparation of deoxynucleoside phosphoramidites in situ. J Org Chem 50:2019–2025
37. Froehler BC, Ng PG, Matteucci MD (1986) Synthesis of DNA via deoxynucleoside H-phosphonate intermediates. Nucleic Acids Res 14:5399–5407
38. Blanchard AP, Kaiser RJ, Hood LE (1996) High-density oligonucleotide arrays. Biosens Bioelectron 11:687–690
39. Human Genome Sequencing C (2004) Finishing the euchromatic sequence of the human genome. Nature 431:931–945
40. LeProust E (2008) Agilent's microarray platform: How high-fidelity DNA synthesis maximizes the dynamic range of gene expression measurements. http://www.chem.agilent.com/library/applications/5989-9159en_lo.pdf.
41. Lausted C, Dahl T, Warren C, King K, Smith K, Johnson M, Saleem R, Aitchison J, Hood L, Lasky SR (2004) POSaM: a fast, flexible, open-source, inkjet oligonucleotide synthesizer and microarrayer. Genome Biol 5:R58
42. Bietsch A, Zhang J, Hegner M, Lang HP, Gerber C (2004) Rapid functionalization of cantilever array sensors by inkjet printing. Nanotechnology 15:873–880
43. Yasui T, Inoue Y, Naito T, Okamoto Y, Kaji N, Tokeshi M, Baba Y (2012) Inkjet injection of DNA droplets for microchannel array electrophoresis. Anal Chem 84:9282–9286
44. Dufva M (2005) Fabrication of high quality microarrays. Biomol Eng 22:173–184
45. Butler JH, Cronin M, Anderson KM, Biddison GM, Chatelain F, Cummer M, Davi DJ, Fisher L, Frauendorf AW, Frueh FW, Gjerstad C, Harper TF, Kernahan SD, Long DQ, Pho M, Walker JA, Brennan TM (2001) In situ synthesis of oligonucleotide arrays by using surface tension. JACS 123:8887–8894
46. Lausted CG, Warren CB, Hood LE, Lasky SR (2006) Printing Your Own Inkjet Microarrays. In: Alan K, Brian O (eds) Methods in Enzymology, vol 410. Academic Press, pp 168–189
47. Goldmann T, Gonzalez JS (2000) DNA-printing: utilization of a standard inkjet printer for the transfer of nucleic acids to solid supports. J Biochem Bioph Methods 42:105–110
48. Allain LR, Stratis-Cullum DN, Vo-Dinh T (2004) Investigation of microfabrication of biological sample arrays using piezoelectric and bubble-jet printing technologies. Anal Chim Acta 518:77–85
49. Yetisen AK, Akram MS, Lowe CR (2013) Paper-based microfluidic point-of-care diagnostic devices. Lab Chip 13:2210–2251
50. Zhao Z, Peytavi R, Diaz-Quijada GA, Picard FJ, Huletsky A, Leblanc É, Frenette J, Boivin G, Veres T, Dumoulin MM, Bergeron MG (2008) Plastic polymers for efficient DNA microarray hybridization: Application to microbiological diagnostics. J Clin Microbiol 46:3752–3758
51. Saaem I, Ma K-S, Marchi AN, LaBean TH, Tian J (2010) In situ synthesis of DNA microarray on functionalized cyclic olefin copolymer substrate. ACS Appl Mater Interfaces 2:491–497
52. Phizicky E, Bastiaens PIH, Zhu H, Snyder M, Fields S (2003) Protein analysis on a proteomic scale. Nature 422:208–215

53. Romanov V, Davidoff SN, Miles AR, Grainger DW, Gale BK, Brooks BD (2014) A critical comparison of protein microarray fabrication technologies. Analyst 139:1303–1326
54. Lumry R, Eyring H (1954) Conformation changes of proteins. J Phys Chem 58:110–120
55. Talbert JN, Goddard JM (2012) Enzymes on material surfaces. Colloid Surface B 93:8–19
56. Xie Y, An J, Yang G, Wu G, Zhang Y, Cui L, Feng Y (2014) Enhanced enzyme kinetic stability by increasing rigidity within the active site. J Biol Chem 289:7994–8006
57. Kimura J, Kawana Y, Kuriyama T (1988) An immobilized enzyme membrane fabrication method using an ink jet nozzle. Biosensors 4:41–52
58. Roda A, Guardigli M, Russo C, Pasini P, Baraldini M (2000) Protein microdeposition using a conventional ink-jet printer. Biotechniques 28:492–496
59. Nishioka GM, Markey AA, Holloway CK (2004) Protein damage in drop-on-demand printers. JACS 126:16320–16321
60. Cook CC, Wang T, Derby B (2010) Inkjet delivery of glucose oxidase. Chem Commun 46:5452–5454
61. Khan MS, Li X, Shen W, Garnier G (2010) Thermal stability of bioactive enzymatic papers. Colloid Surface B 75:239–246
62. Di Risio S, Yan N (2007) Piezoelectric ink-jet printing of horseradish peroxidase: Effect of Ink viscosity modifiers on activity. Macromol Rapid Commun 28:1934–1940
63. Arrabito G, Musumeci C, Aiello V, Libertino S, Compagnini G, Pignataro B (2009) On the relationship between jetted inks and printed biopatterns: Molecular-thin functional microarrays of glucose oxidase. Langmuir 25:6312–6318
64. Khan MS, Fon D, Li X, Tian J, Forsythe J, Garnier G, Shen W (2010) Biosurface engineering through ink jet printing. Colloid Surface B 75:441–447
65. Hossain SMZ, Luckham RE, Smith AM, Lebert JM, Davies LM, Pelton RH, Filipe CDM, Brennan JD (2009) Development of a bioactive paper sensor for detection of neurotoxins using piezoelectric inkjet printing of sol-gel-derived bioinks. Anal Chem 81:5474–5483
66. Alkasir RSJ, Ornatska M, Andreescu S (2012) Colorimetric paper bioassay for the detection of phenolic compounds. Anal Chem 84:9729–9737
67. Setti L, Fraleoni-Morgera A, Ballarin B, Filippini A, Frascaro D, Piana C (2005) An amperometric glucose biosensor prototype fabricated by thermal inkjet printing. Biosens Bioelectron 20:2019–2026
68. Turcu F, Hartwich G, Schäfer D, Schuhmann W (2005) Ink-jet microdispensing for the formation of gradients of immobilised enzyme activity. Macromol Rapid Commun 26:325–330
69. Setti L, Fraleoni-Morgera A, Mencarelli I, Filippini A, Ballarin B, Di Biase M (2007) An HRP-based amperometric biosensor fabricated by thermal inkjet printing. Sensor Actuat B-Chem 126:252–257
70. Kimura S, Kameyama A, Nakaya S, Ito H, Narimatsu H (2007) Direct on-membrane glycoproteomic approach using MALDI-TOF mass spectrometry coupled with microdispensing of multiple enzymes. J Proteome Res 6:2488–2494
71. Suman, O'Reilly E, Kelly M, Morrin A, Smyth MR, Killard AJ (2011) Chronocoulometric determination of urea in human serum using an inkjet printed biosensor. Anal Chim Acta 697:98–102
72. Yun YH, Lee BK, Choi JS, Kim S, Yoo B, Kim YS, Park K, Cho YW (2011) A glucose sensor fabricated by piezoelectric inkjet printing of conducting polymers and bienzymes. Anal Sci 27:375–379
73. Arrabito G, Galati C, Castellano S, Pignataro B (2013) Luminometric sub-nanoliter droplet-to-droplet array (LUMDA) and its application to drug screening by phase I metabolism enzymes. Lab Chip 13:68–72
74. Wang J, Bowie D, Zhang X, Filipe C, Pelton R, Brennan JD (2014) Morphology and entrapped enzyme performance in inkjet-printed sol–gel coatings on paper. Chem Mater 26:1941–1947
75. Talbert JN, He F, Seto K, Nugen SR, Goddard JM (2014) Modification of glucose oxidase for the development of biocatalytic solvent inks. Enzyme Microb Technol 55:21–25

76. Weng B, Morrin A, Shepherd R, Crowley K, Killard AJ, Innis PC, Wallace GG (2014) Wholly printed polypyrrole nanoparticle-based biosensors on flexible substrate. J Mat Chem B 2:793–799
77. Pauling L (1940) A theory of the structure and process of formation of antibodies. JACS 62:2643–2657
78. Grossberg AL, Stelos P, Pressman D (1962) Structure of fragments of antibody molecules as revealed by reduction of exposed disulfide bonds. P Natl Acad Sci USA 48:1203–1209
79. Nilsson S, Lager C, Laurell T, Birnbaum S (1995) Thin-layer immunoaffinity chromatography with bar code quantitation of c-reactive protein. Anal Chem 67:3051–3056
80. Lonini L, Accoto D, Petroni S, Guglielmelli E (2008) Dispensing an enzyme-conjugated solution into an ELISA plate by adapting ink-jet printers. J Biochem Bioph Methods 70:1180–1184
81. Mujawar LH, Norde W, van Amerongen A (2013) Spot morphology of non-contact printed protein molecules on non-porous substrates with a range of hydrophobicities. Analyst 138:518–524
82. Li H, Leulmi RF, Juncker D (2011) Hydrogel droplet microarrays with trapped antibody-functionalized beads for multiplexed protein analysis. Lab Chip 11:528–534
83. Towbin H, Staehelin T, Gordon J (1979) Electrophoretic transfer of proteins from polyacrylamide gels to nitrocellulose sheets: procedure and some applications. P Natl Acad Sci USA 76:4350–4354
84. Nagaraj VJ, Eaton S, Wiktor P (2011) NanoProbeArrays for the analysis of ultra-low-volume protein samples using piezoelectric liquid dispensing technology. JALA 16:126–133
85. Delehanty JB, Ligler FS (2002) A microarray immunoassay for simultaneous detection of proteins and bacteria. Anal Chem 74:5681–5687
86. Abe K, Kotera K, Suzuki K, Citterio D (2010) Inkjet-printed paperfluidic immuno-chemical sensing device. Anal Bioanal Chem 398:885–893
87. Yatsushiro S, Akamine R, Yamamura S, Hino M, Kajimoto K, Abe K, Abe H, Kido J-i, Tanaka M, Shinohara Y, Baba Y, Ooie T, Kataoka M (2011) Quantitative analysis of serum procollagen type I C-terminal propeptide by immunoassay on microchip. PLoS ONE 6:e18807
88. Orelma H, Filpponen I, Johansson L-S, Österberg M, Rojas OJ, Laine J (2012) Surface functionalized nanofibrillar cellulose (NFC) film as a platform for immunoassays and diagnostics. Biointerphases 7:61
89. Kido J-i, Abe K, Yatsushiro S, Bando M, Hiroshima Y, Nagata T, Ooie T, Tanaka M, Kataoka M (2012) Determination of calprotectin in gingival crevicular fluid by immunoassay on a microchip. Clin Biochem 45:1239–1244
90. Abe K, Hashimoto Y, Yatsushiro S, Yamamura S, Bando M, Hiroshima Y, Kido J-I, Tanaka M, Shinohara Y, Ooie T, Baba Y, Kataoka M (2013) Simultaneous immunoassay analysis of plasma IL-6 and TNF-α on a microchip. PLoS ONE 8:e53620
91. Feyssa B, Liedert C, Kivimaki L, Johansson L-S, Jantunen H, Hakalahti L (2013) Patterned immobilization of antibodies within roll-to-roll hot embossed polymeric microfluidic channels. PLoS ONE 8:e68918
92. Mujawar L, Moers A, Norde W, van Amerongen A (2013) Rapid mastitis detection assay on porous nitrocellulose membrane slides. Anal Bioanal Chem 405:7469–7476
93. Henares TG, Mizutani F, Hisamoto H (2008) Current development in microfluidic immunosensing chip. Anal Chim Acta 611:17–30
94. Abe K, Suzuki K, Citterio D (2008) Inkjet-printed microfluidic multianalyte chemical sensing paper. Anal Chem 80:6928–6934

# Chapter 9
# Honeycomb Structured Films Prepared by Breath Figures: Fabrication and Application for Biorecognition Purposes

**Alexandra Muñoz-Bonilla and Juan Rodríguez-Hernández**

## 9.1 Generalities. Introduction to the Breath Figures Mechanism

A breath figure (BF) is the water droplet array that is formed when moisture comes in contact with a cold substrate, for instance upon breathing. This phenomenon, well known since the beginning of the nineties, started to get a great attention with the work reported by Francois et al. in 1994 [1]. They discovered the formation of highly ordered porous films when a drop of polymer solution was cast under a moist airflow. Over the past two decades this method, named BF approach, has been extensively utilized as a versatile templating method for the fabrication of porous polymeric films [2–6]. This approach presents several important advantages over other existing procedures to fabricate porous films, such as lithography. First, the self-removal of the water droplets template makes this method very simple, low-cost, and reduces production time. And second with the versatility of the method, as will be discussed throughout this chapter, the pore size, distribution, shape, chemical functionality, and other aspects of the pattern can be easily controlled and adjusted by simply varying experimental conditions such as temperature, humidity, polymer concentration, type of polymer, etc. It is noticeable to remark that all of these topological, morphological, and functional characteristics of the film strongly influence its interactions with biomolecules, cells, or microorganisms, and these porous platforms may open new prospects for biomedical perspectives and applications.

J. Rodríguez-Hernández (✉)
Chemistry and Properties of Polymeric Materials Department, Institute of Polymer Science and Technology (ICTP-CSIC), C/Juan de la Cierva 3, 28006 Madrid, Spain
e-mail: jrodriguez@ictp.csic.es

A. Muñoz-Bonilla
Departamento de Química-Física Aplicada, Facultad de Ciencias, Universidad Autónoma de Madrid, C/Francisco Tomás y Valiente 7, Cantoblanco, 28049 Madrid, Spain



J. Rodríguez-Hernández, A. L. Cortajarena (eds.), *Design of Polymeric Platforms for Selective Biorecognition,* DOI 10.1007/978-3-319-17061-9_9

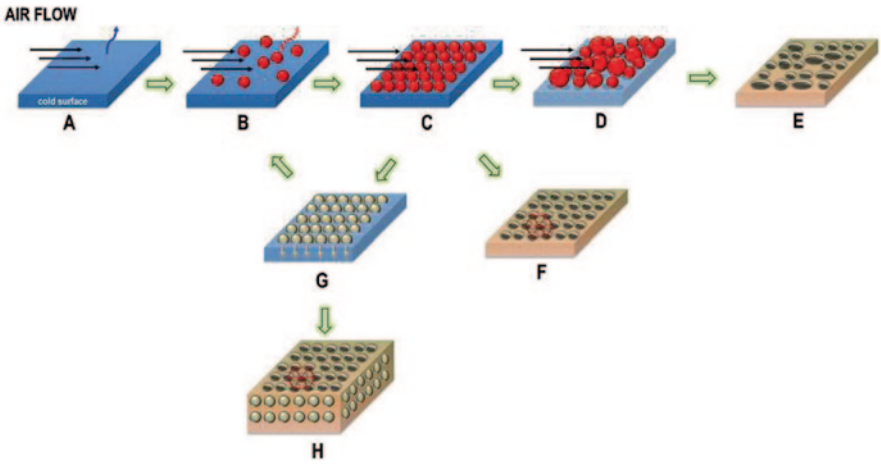


**Fig. 9.1** Schematic representation showing the mechanism of breath figures pattern formation. (Reproduced with permission from reference [3])

In this context, this chapter aims to give an extended overview of the BF approach beginning with the mechanism and all the parameters involved in the process, recent advances on the preparation of more sophisticated structures, and to finish with the applications in biorecognition processes.

The main steps involved in the BF mechanism are well established today and from a practical point of view the procedure is quite simple. Typically, a drop of a polymeric solution is placed onto a substrate under humid environment and then the BF film is produced as follows (Fig. 9.1): (A) the endothermic evaporation of the solvent provokes a decrease of the solvent temperature, resulting in the water condensation onto the solution surface; (B) an initial heterogeneous nucleation forms water droplets on the surface, followed by the growth of the isolated droplets at expense of the vapor of the surrounding atmosphere; (C) a complete coverage of the surface generally provides a hexagonal closed packed array of water droplets. At this stage different situations can take place. When the solvent evaporation finishes before the beginning of the coalescence of the water droplets, a monolayer of regular ordered pores is formed after the complete evaporation of the water droplets (F). In contrast, if the first layer of condensed droplets sinks into the solution and the coagulation is prevented (G), a new layer of water droplets can condense on the surface. The result of this repetitive process before the complete evaporation of the solvent is the formation of multilayer of pores (H). In general, the prompt precipitation of a polymer layer around the water droplets prevents their coagulation allowing the formation of these ordered structures. However, if the stabilization of the droplets is not well achieved, coagulation of droplets can proceed (D), resulting in a disordered array of pores after the complete evaporation of solvent and water (E).

## 9.2 Topographical Modifications Using the Breath Figures Approach

### *9.2.1 General Strategies for the Fabrication of Honeycomb Films*

As aforementioned the preparation process involves the evaporation of a polymer solution on a surface in humid environment. To do this, several approaches have been explored (Fig. 9.2) in order to control some of the variables and render highly regular porous structures. In a typical procedure, a droplet of a polymer solution is cast onto a solid substrate which was placed in a sealed chamber controlling the relative humidity (Fig. 9.2i) by saturated salt solutions [7] or nitrogen bubbled through distilled water [8]. Alternatively to this static process, moisture can also be supplied by directing airflow over the substrate [9]. Here, in addition to the relative humidity, the airflow rate, as well as the distance and angle of the air current strongly influence the final pore structures. Slight modifications of this basic procedure have been introduced with the aim of improving the order of the honeycomb structure. For example, by using a cold stage during the casting process, the temperature of the solution is decreased inducing in this way, an increase in the condensation and

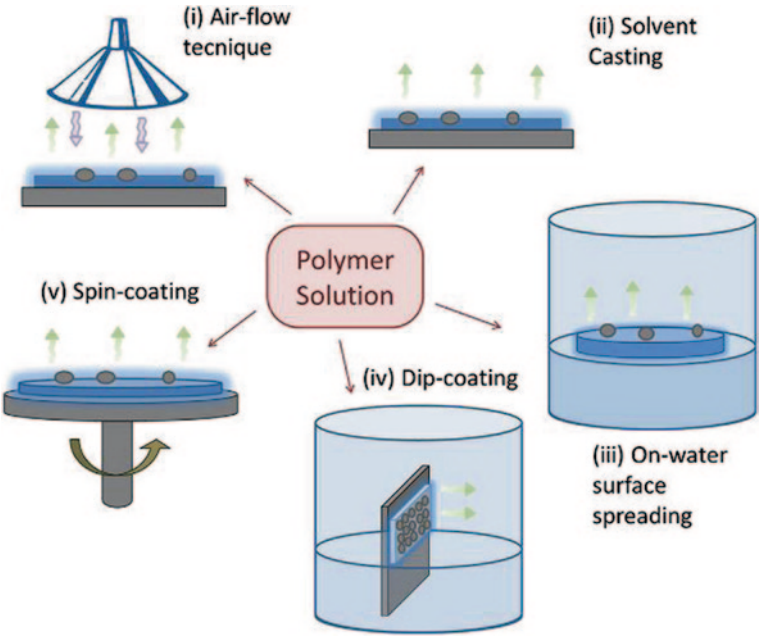


**Fig. 9.2** Instrumental setup for the preparation of honeycomb-structured porous films via: *i* airflow technique; *ii* solvent casting; *iii* on-water surface spreading; *iv* dip coating, and *v* spin coating. (Reprinted with permission from reference [3])

also in the viscosity, facts that favor highly ordered structures [10]. Besides, the BF technique can be combined with spin coating methodology to a priori fabricate large uniform areas of porous structures [11]. Normally, high spinning rates lead to more regular structures with smaller pore sizes [12]. However, spin coating generally conducts to elongated pores and less-ordered patterns in comparison with drop casting or airflow techniques. Dip coating was also successfully combined with BF under high humid environment [13, 14]. In this case, the formation mechanism might vary due to the vertical position of the support and the liquid surface. As described up to now in this section, honeycomb structures are mainly formed on solid support; therefore, there is a solid layer behind the porous structures. Nevertheless, the preparation of honeycomb films at the air–water interface, by the so-called "on water spreading" method, has also been reported [15]. This approach consists of the deposition of a polymer solution on water surface and the formation of a self-standing honeycomb mesh after the evaporation of the casting solvent.

In addition, other less conventional BF approaches have been introduced providing a wide variety of BF patterns that expand the applicability of the methodology and give insights into the formation mechanism. For example honeycomb-structured films are generated from a polymer solution in which water is directly added into the solution. Two possibilities are considered; on one hand, using water-miscible solvent [16] and on the other hand, the homogenization of the system by sonication [17].

Recently, there is an emerging interest in the fabrication of BF in nonaqueous vapor such as ethanol, methanol, or acetone, often called "reverse breath figures" approach [18, 19]. Moreover, this methodology offers the possibility to be formed on nonplanar surfaces which is of great interest for certain applications. This last approach will be discussed in more extend in Sect. 4.

### *9.2.2 Control of the Pore Characteristics: Dimensions, Surface Distribution, and Preparation of Ordered Hexagonal Patterns*

In all of the above described strategies the quality and the properties of the BF patterns are highly affected by the experimental conditions (humidity, temperature, type of solvent, etc.) and other parameters related to polymer structure, such as its nature, architecture, and molecular weight. As a consequence, the porous patterns produced by BF methodology can vary from totally disorder structures to highly regular hexagonal arrays, depending on the experimental parameters. Besides, the dimension of the pores can be tuned in a controlled manner, ranging from 0.2 to 20 μm, as well as the formation of a single monolayer or multilayered pores. The control of the pattern characteristics is crucial for the applicability of these films as platforms for biorecognition purpose because the dimensions of the cavities, regularity of the structure, and roughness are variables, in addition to the chemical

functionality, that significantly affect the interactions between the surface and the biomolecules, cells, and microorganisms. The most important experimental parameters influencing the pore size and distribution are briefly discussed as follows.

- *Relative humidity.* The size of the pores usually increases in a progressive manner with the humidity [20]. However, very high humidity may result in the coalescence of water droplets yielding irregular patterns, especially when amphiphilic structures are used [21].
- *Solvent.* In general, highly regular porous patterns are obtained with nonpolar and highly volatile solvents, such as carbon disulfide and chloroform. The volatility also influences the pore size, decreasing the diameter with higher volatile solvent [22]. The density of the solvent [23] and the evaporation rate [24] seem to affect the formation of mutilayers.
- *Concentration.* The concentration of the solution is an important variable for the film quality, the pore size, and the formation of multilayers, and needs to be optimized for each system. Normally, the pore size increases as the concentration decreases [22].
- *Temperature*. A decrease in temperature reduces the evaporation rate of the solvent leading to bigger pore sizes [25].
- *Substrate.* The surface where the polymer solution is deposited plays a key role. An increase in the wetting of solution on the substrates enhances regularity of the structure [26]. The simple modification of the surface wettability can even allow the preparation of square pore arrays [27].
- *Polymer.* The properties of the polymers strongly determine the characteristics and quality of the final films. The molecular weight, topography, end-groups, and the hydrophilic/hydrophobic character affect the chain flexibility and also the precipitation and stabilization of the water droplets. The role of the polymer employed will be discussed in detail in Sect. 3.2.

### *9.2.3 Approaches to Modify the Morphology of the Pores*

It is also of great importance to control the pore morphology since this characteristic determines the final application of the films. In particular, the pore morphology has a significant influence on the adhesion of cells and microorganisms on the film surface. Typically, honeycomb-like distribution of spherical cavities is obtained by BF approach. As described above, the regularity, pore size, and the distance between pores can be varied. In addition, the morphology of the pore can be tuned introducing some modifications in the formation process or using post-modification approaches. The different strategies used can be grouped as follows (see Fig. 9.3):

- Shrinking is a facile mechanical processing method that has been used to modify the morphology of the pores. In this approach, the BF film is transferred on a thermally shrinkable substrate and then the system is shrunk by heating on a hot

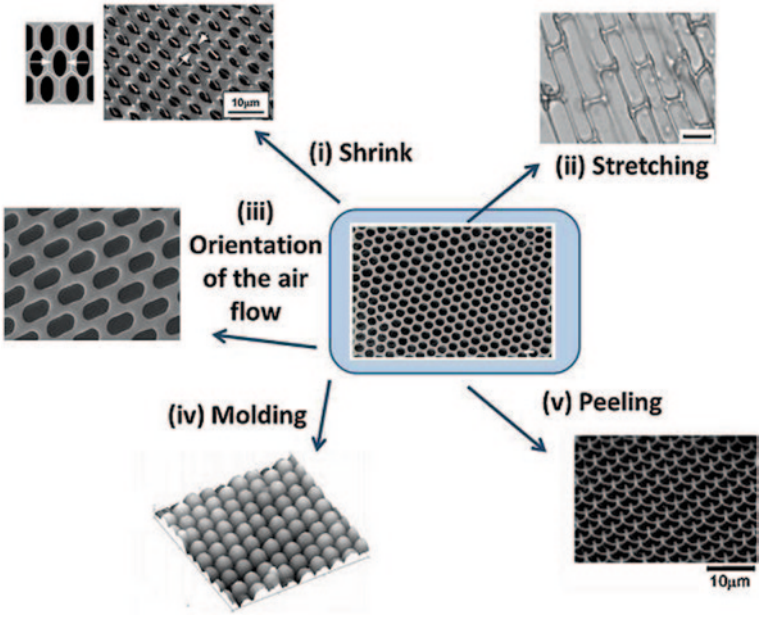


**Fig. 9.3** Schematic illustration of the different approaches used to modify the shape of the pores: *i* shrinking, *ii* stretching, *iii* variation of the orientation of the airflow during the water condensation process, *iv* use of the pores as templates to create the complementary patterns, and *v* pincushion structure. (Reproduced with permission from reference [3])

stage above the $T_g$ of the substrate but below the $T_g$ of the BF film. Alternatively, semicrystalline polymer can be directly used as shrinkable honeycomb patterned film. In both cases the process causes the deformation of the circular pores to ellipsoidal, rectangular, or even triangular pits.

- Stretching is another mechanical way to control the shape and size of the honeycomb cavities. Elongated hexagons, rectangles, squares, and triangles can be obtained by stretching honeycomb films, consisting of viscoelastic polymers such as poly(ε-caprolactone), in different directions [28].
- Variation of the airflow orientation. Airflow normal to the surface provides circular pores whereas elliptic pores with different aspect ratios can be obtained by changing the direction and velocity of airflow during the BF formation [29].
- Molding. Microlens arrays, that is, the complementary patterns of BF structure are easily created by molding in poly(dimethylsiloxane) (PDMS) using standard curing processes [30].
- Peeling. A pincushion structure can be obtained by simply peeling of the top layer of the honeycomb structured surface with adhesive tape. The resulting structure exhibits interesting superhydrophobic properties when highly hydrophobic polymers are employed [31].

## 9.3 Modulation of the Surface Functionality of the Porous Interfaces

### *9.3.1 General Considerations*

Initially, the fabrication of porous structured films by the BF approach focused on the use of polymers based on polystyrene (PS). Progressively, other polymeric structures have been introduced to improve the physical properties (i.e., mechanical, optical, etc.) as well as to introduce additional functionalities, thus extending the applicability of the patterned films. The incorporation of functional groups able to participate in biological events via specific interactions makes this honeycomb structured films very attractive in biomedical and biological applications as supports for biomolecular recognition purpose.

An additional advantage of this BF process, besides the control of the topography, is the possibility to control the distribution of the chemical functionality within the patterned film. As will be described in this section, the functional groups involved for instance, in biorecognition events can be located specifically in different position of the film, i.e., homogeneously distributed in the whole film, exclusively on the top surface, within the cavities, on the edge of the pores, etc. (Fig. 9.4).

The simple case is the use of a single functional homopolymers that produce honeycomb films with the functionality homogeneously distributed (Fig. 9.4a). However, amphiphilic macromolecules are the most typical polymeric structures

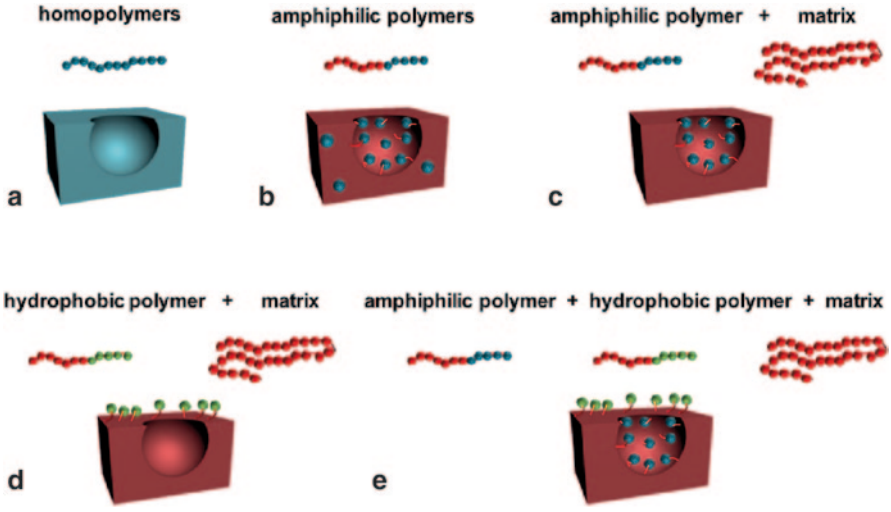


**Fig. 9.4** In situ methods to obtain functional surfaces by using the breath figures approach: **a** using homopolymers; **b** using amphiphilic copolymers; **c** blending homo and amphiphilic copolymers; **d** mixing homo and hydrophobic polymers, and **e** ternary blends of amphiphilic, hydrophobic polymers and homopolymer matrix

employed in the BF process, either end-functionalized polymer or copolymers. In this particular case, the cavities formed on the surface are enriched in polar groups as a consequence of the formation mechanism of the BF that is based on the precipitation of the polymers around the water droplets, implying the orientation of the hydrophilic groups preferably to the wall of the holes finally obtained at the end of the process. Despite this preferential distribution of the polar segments within the pores, these polar and functional groups are also found in the rest of the film (Fig. 9.4b). As an alternative the use of blends has been explored allowing the specific distribution of the different components exclusively within or out of the holes. This is because the condensation of water droplets directs the phase separation of the blend components during the BF process and as a result their final distribution in the structured film. Typically, a small amount of polymer bearing specific functional moieties is mixed with a hydrophobic polymer matrix as major component. This strategy not only reduces the amount of functional polymer, often the expensive component, required for the fabrication of the pattern but also offers great versatility in terms of functional groups and in their distribution within the film. When an amphiphilic or hydrophilic copolymer is utilized as minor component in the blend, a BF film composed of the polymer matrix with holes enriched in the copolymer is obtained (Fig. 9.4c). On the contrary if a hydrophobic polymer is added to the matrix, this minor component will be located out of the cavities in the resulting film (Fig. 9.4d). A more complex option is the use of ternary blends, direct the distribution of two different functionalities in the same structured film, i.e., inside the hydrophilic compound and outside the hydrophobic compound (Fig. 9.4e).

All these strategies described in the preceding allow the control of the functionality during the BF formation, thus in situ functionalization. On the other hand, the post-modification of the chemical composition of these polymer surfaces is also feasible. A diversity of approaches has been employed such as layer by layer, chemical reactions, grafting techniques, and many others. This ex situ functionalization covers some of the limitations of in situ methods because it allows the incorporation of chemical groups incompatible with the BF process (for instance due to solubilization problems). As the topography of the honeycomb films depends on the initial polymeric solution, the post-modification can be an alternative to preserve the desirable BF pattern, varying only the functionality.

In the next section examples of each strategies used to control the functionality of the honeycomb structured films will be discussed.

## *9.3.2 In situ Functionalization of the Porous Film. Design of the System*

### 9.3.2.1 Homopolymers

As mentioned, PS was the reference polymer in the beginning of the BF development [1, 23]. Styrenic polymers are of great interest from the biomedical perspective

because they are probably the most commonly used material for in vitro cell based research and microbiology as plasticware such as culture flasks, cell culture dishes, microplates, etc. Elastomeric PDMS [32] is also extensively used in biomedical applications and in microfluidic, and allows the successful preparation of BF patterns. Honeycomb films directly prepared from poly(lactic acid) [8] and polycaprolactone [33] due to their biodegradability and adequate mechanical properties find applications in tissue engineering. Moreover, films with uniform pore structure can be equally achieved from naturally occurring polymers like silk fibroin [34] and cellulose [17] and used as cell culture substrates because of their biocompatibility, high clarity, and mechanical strength. Other classical homopolymers such as optical-grade poly(methyl methacrylate) (PMMA) [35] and polycarbonate [36] also produce highly ordered BF patterns and are attractive for certain uses. Furthermore, thermally and chemically stable polymers such as poly(phenylene oxide) provides robust patterns with possibilities as membrane material [37].

#### 9.3.2.2 Amphiphilic Polymers

With the aim to generate well-ordered BF with hydrophilic moieties distributed mainly inside the cavities, amphiphilic polymeric structures are usually employed. Typically, polymers with hydrophilic end groups are designed for this purpose using living polymerization techniques. Nitroxide mediated radical polymerization provides 2,2,6,6-tetramethyl-1-piperidinyloxyl (TEMPO) terminated polymers, i.e., PS, in which the end groups can be easily converted in a following step into hydrophilic groups such as p-toluenesulfonate piperidinium [38], carboxyl, amino, hydroxyl, and boron-dipyrromethene (BODIPY) [39]. Reversible addition fragmentation chain transfer (RAFT) polymerization has also been used as a versatile method to synthesize polymers with end functional groups to prepare honeycomb structured interfaces. As an example, carboxy-terminated PS and PS with a polar head of glucose synthesized via RAFT have been employed to form films with bioactive sites within the holes [40].

Following with the design of amphiphilic structure for the fabrication of BF films, the use of block copolymers is of particular interest, not only because they contain much more functional groups per macromolecule than the end functionalized polymers but also for their capacity to self-assemble forming micelles able to better stabilize the condensed water droplets. In addition, as will be discussed in successive sections, they can help the formation of hierarchical structured films, thanks to this self-assembly ability. The design of the block copolymer in terms of hydrophilic/hydrophobic balance is crucial for the optimization of the obtained BF structures because it strongly affects the quality of the film and the pore size. Regular honeycomb structured films having pores enriched in hydrophilic segments have been prepared from a variety of amphiphilic block copolymers most of them based on PS as hydrophobic segments, and including as polar block, stimuli responsive polymers, [41] photoluminescent polymers, [42] polymers mimicking cell membrane like poly(acryloyl phosphorylcholine), [43] and also structures able

to participate in biorecognition processes such as glycopolymers [44, 45]. In the particular case of glycopolymers, highly regular structures are usually obtained from the more hydrophobic acetylated forms, thus a posterior deacetylation step is needed for the specific interactions with proteins. In addition to block copolymers, statistical, graft, star, hyperbranched, and comb-like amphiphilic structures have been extensively used [46, 47].

#### 9.3.2.3 Blends of Polymers

As aforementioned the use of polymeric blends presents numerous advantages over the simple use of amphiphilic polymer system. First, it was demonstrated that when an amphiphilic polymer with high content in hydrophilic segment is mixed with a hydrophobic polymer such as PS, the regularity of the resulting structure importantly improves [45]. Indeed, highly regular honeycomb can be obtained from deacetylated glycopolymers when they are mixing with hydrophobic homopolymers [47]. Another advantage of using blends is, as commented, the preferential distribution of the hydrophilic component inside the cavities. In this concern, Rodríguez-Hernández and coworkers have extensively worked using different systems of polymeric blends. First amphiphilic glycopolymers, based unprotected 2-[(D-glucopyranosyl)aminocarbonyloxy] ethyl acrylate and either PS [48] or MMA [7] were mixed with high molecular weight PS and PMMA, respectively, and the resulting holes in both cases were largely concentrated in glycopolymer. A more complex amphiphilic structure was incorporated into a homopolymer matrix, i.e., triblock copolymer of poly(2,3,4,5,6-pentafluorostyrene)-*b*-polystyrene-*b*-poly[poly(ethylene glycol) methyl ether methacrylate] (PS5F-*b*-PS-*b*-PPEGMA), containing both hydrophilic and high hydrophobic segments [11]. Directed by the hydrophilic block the copolymer rearranges into the cavities, as expected. Nevertheless, as a result of its particular structure this system facilitates the reversible modulation of the surface functionality, changing from holes with hydrophilic character under humid conditions to hydrophobic fluorinated holes in dry air. Conversely, regular porous films were prepared from blends consisting in a totally high hydrophobic copolymers of PS5F-*b*-PS and high molecular weight PS homopolymer [49]. Contrary to when amphiphilic copolymers were used, the fluorinated copolymer is located, in this case homogeneously distributed, along the whole surface of the film as a consequence of the reorientation towards the solution–air interface. Increasing complexity of the system ternary blends of high molecular weight PS and two block copolymers, one hydrophobic, PS5F-*b*-PS and one amphiphilic, PS-*b*-PPEGMA, were employed to obtain BF patterns with special distribution of the component [50]. Therefore, the amphiphilic copolymer is completely segregated into the cavities whereas the PS5F-*b*-PS tends to migrate onto the top surface of the film.

On the other hand, blends of incompatible homopolymers also provide interesting results by the combination of the BF and the phase separation processes, giving place to singular functional distribution [51] or even hierarchical structures [52].

#### 9.3.2.4 Blends of Inorganic Compounds and Polymers: Hybrid Structures

Similarly to the addition of an amphiphilic polymer into a hydrophobic homopolymer, inorganic compounds have been introduced into the polymeric solution to obtain hybrid material with additional properties. Commonly the inorganic component, especially nanoparticles, is mixed with a polymer solution, and then the porous film is prepared from this solution following a standard BF process. The nanoparticles spontaneously can self-assemble at the polymer solution–water droplet interface, stabilizing the water droplets, the so-called pickering emulsion effect, thus directing the nanoparticles inside the holes of the resulting microstructured arrays.

Russell et al. [53] were the pioneers in the fabrication of hybrid BF films, in particular they prepared microporous films decorated with ligand stabilized cadmium selenide nanoparticles. The preferential segregation was confirmed by confocal fluorescence microscopy and transmission electron microscopy (TEM). Later other inorganic materials have been reported to form hybrid BF films including zeolites, [54] polyoxometalate, [55] carbon nanotubes, fullerene, and gold nanoparticles [56].

An alternative to create honeycomb structured films with embedded inorganic compounds involves the in situ generation of the particles. This approach has been utilized to form titania particles inside the cavities of PS film from a chloroform solution of PS and titanium tetrachloride ($TiCl_4$) cast on glass support [57]. The condensed water droplets hydrolyze the $TiCl_4$ during the formation of the film given the corresponding titania particles inside the holes.

### *9.3.3 Post-modification of the Chemical Composition of the Porous Film*

Ex situ functionalization by post-modification expands the variety of functional groups that can be incorporated into the honeycomb structured films prepared by BF. In this case, it is essential to control the penetration or not of the reaction solution into the pores to allow the modification reaction inside or outside the cavities. This is because the air entrapped in the pores results in low wettability and superhydrophobic films (Cassie–Baxter state), and the post modification in the interior of the cavities usually becomes rather difficult. On the other hand, when the droplet is able to wet the whole surface, penetrating inside the pores (Wenzel model) the modification can be obtained exclusively within the cavities or simultaneously with the external surface, depending on the initial functional distribution.

For instance porous films have been obtained from polystyrene-*b*-poly(N, N-dimethylaminoethyl methacrylate) (PS-*b*-PDMAEMA), and then in a posterior step the PDMAEMA segment was quaternized [58]. This approach was chosen instead of the directly use of quaternized polymer in the formation of the BF because the latest strategy conducts to larger pores. In addition, the authors attempt to introduce negatively charged silica nanoparticles into the cationic pores driven by electrostatic attraction. However, the air entrapped in the pores prevents the assembly of the particles into the cavities. A facile solution was the use of ethanol dispersion instead of water to favor the wetting of the pores reaching high filling ratio.

A variety of chemical reactions have also been carried out inside the pores, as an example cavities enriched in amine groups were prepared from a mixture of PS and amino-functionalized PS to modify the surface functionality within the pores in a posterior stage [59]. Thus, bovine serum albumin was attached to the amino-terminated pore surface using an intermediated step glutaraldehyde as a very effective protein crosslinker.

In contrast, the selective functionalization of the external surface in BF films while maintaining the functionality inside the pores is reported. To achieve this, polymeric films were prepared from blends of fluorinated copolymer, PS5F-*b*-PS, and PS matrix [49]. The diblock copolymer resulted to be homogeneously distributed along the whole surface of the films, showing a Cassie–Baxter wetting behavior. This feature allows the chemical modification of the *para*-fluorine groups (via thiol-*para* fluorine "click" reaction) of the copolymer located in the external surface rather than in the interior of the pores.

Besides chemical reaction with low molecular weight molecules, other approaches have been employed such including methods, mainly to modify the pores of the film. Controlled radical polymerization techniques permit to incorporate a wide variety of well-defined polymers by either "grafting onto" or "grafting from" approaches. Atom transfer radical polymerization (ATRP) has been employed to grow polymers from the surface of the pores. As an example, films with porous enriched in hydroxyl groups were fabricated from amphiphilic block copolymers of styrene and 2-hydroxyethyl methacrylate [60]. Then the ATRP initiator 2-bromoisobutyryl bromide was introduced by reaction with these hydroxyl groups, and the surface initiated ATRP can be successfully conducted from the surface. RAFT polymerization is equally used to graft polymer chains into the honeycomb structured films. In a simple approach, amphiphilic copolymers also containing 2-hydroxyethyl methacrylate prepared via RAFT were employed to form the films [61]. As the RAFT groups were located mainly inside the pores after the film formation, they were utilized as grafting points for the further RAFT polymerization of *N*-*iso*-propylacrylamide (NIPAm). This strategy presents as an advantage that does not need previous modification or initiator immobilization.

Layer by layer method has also been utilized to modify the functionality of the BF films with polymeric chains. Different polyelectrolytes such as alginate and chitosan were specifically deposited inside positively charged pores of films based on quaternized PS-*b*-PDMAEMA by using layer-by-layer self-assembly approach [62].

## 9.4 Preparation of Adaptive Porous Films and Sophisticated Structures

### *9.4.1 Preparation of Porous Films with Adaptive Properties*

This section will provide a brief overview of the most recent strategies that have been followed to fabricate more sophisticated interfaces either introducing active

polymers to produce "smart surfaces" or producing rather complex patterns exhibiting order at different length scales based on the BF approach.

Stimuli responsive polymers offer unique opportunities to reduce the gap between synthetic and living systems. In effect, in living systems, the most important substances are able to adapt themselves depending on the external environment, thus enabling biological processes to occur in a controlled manner [63]. Since material interfaces are clearly involved in multiple processes depending on the final application a large effort has been realized in the fabrication of interfaces having adaptive polymers [64].

As has been detailed above, the preparation of porous interfaces by using the BF approach allows us to have a precise control over the surface functionality inside, outside, and both inside–outside the pores. Thus, the BF method is an interesting approach for the introduction of adaptive polymers that may vary back and forth depending on the external environment in particular surface regions. Different polymers have been described to be sensitive to a particular stimulus. Among the polymers that may induce changes in their properties we can find biologically responsive polymers which respond among others to glucose, enzymes, or antigens present in the environment [63]. Also, field responsive polymers have been extensively employed for their response to environmental pH, temperature, electric and magnetic fields, photoresponsive, or even polymers exhibiting large changes in their behavior in response to ultrasounds.

In the case of porous films prepared by the BF approach up to now most of the studies have been focused on the use of pH, temperature, or UV sensitive polymers. For instance, pH responsive polymers have been employed by Hu et al. [41] who described the use of polystyrene-*b*-poly(acrylic acid) (PS-*b*-PAA) diblock copolymers to fabricate microporous thin films with tunable surface properties. The surface composition and thus the wettability were variable when the films were immersed in aqueous solutions with variable pH. This group observed exceptionally large variations in the contact angle between hydrophobic and superhydrophilic character as a consequence of the microstructure of the films. Moreover, an increase in the pH augments the degree of dissociated carboxylic acid groups and produces a faster transformation between these two states.

Orlov et al. [65] described the fabrication of thin film membranes with pore sizes depending on variations of the environmental pH. For that purpose, poly(2-vinylpyridine) partially quaternized with 1,4-diiodobutane (qP2VP) and unreacted 1,4-diiodobutane (DIB) were spin coated under controlled humidity. After formation of the porous structure, the membranes were cross-linked with DIB and became insoluble, i.e., stable to solvents. The resulting cross-linked membranes exhibit a pH-dependent swelling, giving place to variations in the pore diameter (Fig. 9.5).

More recently, Escalé et al. [66] reported the fabrication of smart porous honeycomb patterned films by using a pH responsive block copolymer, i.e., polystyrene-*b*-poly(4-vinylpyridine) (PS-*b*-P4VP). The P4VP block is hydrophobic at pH values above the $pK_a$ ($pK_{a(P4VP)} = 5.2$) and hydrophilic below the $pK_a$. In these films reversible variations on the contact angle values between ~90° and ~72° for basic and acidic conditions, respectively, were observed.

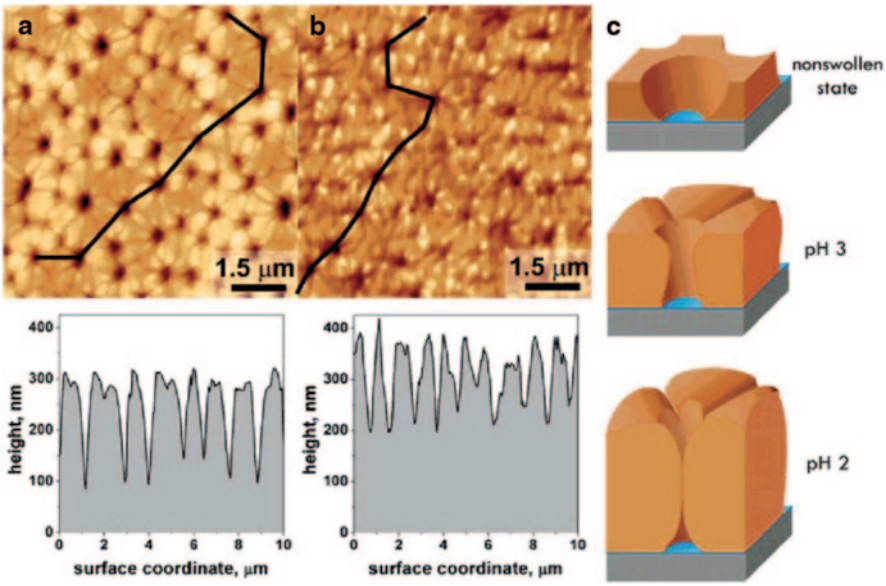


**Fig. 9.5** **a**, **b** Scanning probe microscopy (SPM) topography images with the corresponding cross-sectional profiles of the cross-linked quaternizes poly(2-vinyl pirrolidone) (qP2VP) film under acidic water of pH 3 (a) and pH 2 (b). The film was spin-coated at RH of 55 % from the solution with the 1,4-diodobutane (DIB) concentration of 2 % vol. onto a Si wafer modified with a bromoundecyldimethylchlorosilane monolayer and annealed at 120 °C under vacuum for 48 h. The quaternization degree of qP2VP after the temperature annealing is 23 %. The lines show the location of the cross-sectional profiles. **c** Schematic cross-sectional profiles of a pore in the dry and swollen states as a function of the pH. (Reproduced with permission from reference [65])

Whereas in the above mentioned examples the honeycomb structures were prepared by using directly the pH responsive polymer, Stenzel et al. [61] proposed an alternative to this approach consisting in the chemical post modification of the microporous films. In particular, they propose the use of a thermoresponsive polymer, PNIPAm. Upon modification of the pores, the contact angles at temperatures above and below the lower critical solution temperature (LCST) of the PNIPAm, 25–35 °C, were performed to compare the grafted and non-grafted surfaces and analyze the thermoresponsive behavior of the films. They concluded that at room temperature the grafted films show a decrease in the contact angle with increasing molecular weight of the grafted chains. Moreover, an increase on the temperature increases the hydrophobicity of the films (about 7–10°) which illustrates the typical thermoresponsive behavior of the PNIPAm chains around the LCST.

In addition to pH and temperature responsive polymers, UV-responsive polymers were recently employed to prepare porous films. Bormashenko et al. reported a single-step technique that permits the formation of microscaled thermally stable honeycomb pattern reliefs with reversible wettability [67]. They described the formation of micrometrically scaled honeycomb polysulfone (PSF) and poly(ether

sulfone) (PESF) films. Upon UV irradiation, the apparent contact angles decrease indicating a transition from the Cassie to the Wenzel wetting regime. In spite of the generally admitted irreversibility of this transition, the initial contact angle values were recovered upon heating the UV-irradiated honeycomb. Moreover, several UV-irradiation/heating cycles demonstrated the reversibility of the wettability.

Not only the use of stimuli responsive polymers produces surfaces that respond to the external environment, but also the exposure to the films to selective solvent atmosphere can turn the topography of the surface. An example of topographical changes was reported by Han et al. [68]. These authors described the formation of an ordered array of holes combining the BF approach and the phase separation of polymer blends composed of P2VP and PS. The surface topography changes in a reversible manner between an ordered honeycomb structure and hexagonal islands when treated with different solvents.

In addition to the topography modifications when changing the solvent atmosphere, Muñoz-Bonilla et al. described the changes on the surface topography by changing the relative humidity of the environment [11, 48]. Authors described the use of hydrophilic blocks, PPEGMA, or glycopolymers, able to absorb water molecules in a high relative humid atmosphere. As a consequence, the exposure of the patterned films to soft annealing under water vapor provokes the swelling of the hydrophilic blocks which are concentrated within the pore. Thus, the surface topography changes from holes to island-like patterns. Moreover, the honeycomb structure can be recovered upon annealing to dry air.

### *9.4.2 Preparation of Sophisticated Structures Using the BF Approach*

Variations over the surface features lead, for instance, to more complex ordered structures that may play a key role on the recognition processes at interfaces. These have been obtained by using different alternatives that, in some particular cases, may provide ordered interfaces at different length scales, i.e., hierarchically structured honeycomb films [69, 70].

Hierarchically ordered porous structures can be obtained combining the microscale ordered porous films obtained by using the BF approach with the self-assembly at the nanometer scale when block copolymers are employed. This strategy, used for several groups, has been first reported by Hakayama and Horiuchi [71]. They synthesized a semi rod-coil block copolymer of styrene and isoprene with oligothiophene-modified side chains (POTI), PS-*b*-POTI. By solvent casting, the block copolymer can form organized structures on three different length scales as a result of the different processes taking place simultaneously. At lower length scale, we have to mention that the oligothiophene forms molecularly orientated smectic A liquid crystalline structures in POTI nanophase separated domains. In a higher level of order the PS and POTI blocks self-assembled in nanodomains perpendicular to the substrate with a periodicity of approximately 50 nm. Finally, the solvent

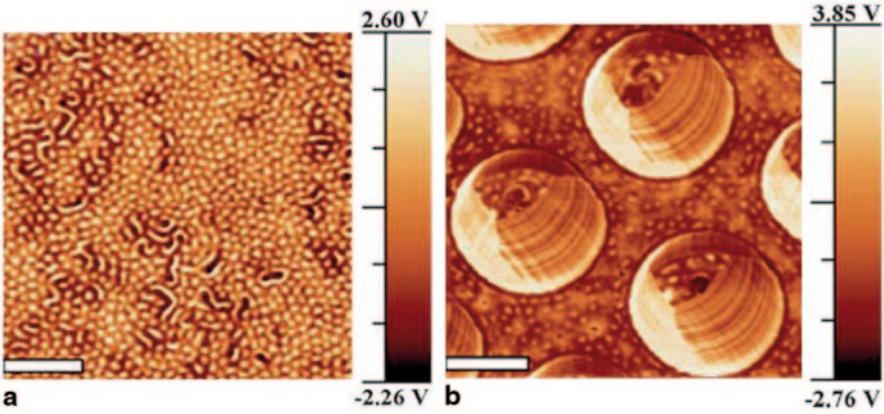


**Fig. 9.6** Atomic force microscopy (AFM) phase images of **a** PnBA-*b*-PS diblock copolymer continuous film and, **b** PnBA-*b*-PS diblock copolymer honeycomb film. (scale bar represents 500 nm). (Reproduced with permission from reference [72])

evaporation entails the production of mono (2D) and multilayered (3D) microporous films with pore sizes ranging between 1.2 and 4.5 μm.

Using amphiphilic block copolymers, more precisely polystyrene-*b*-poly(N, N-dimethylacrylamide), PS-*b*-PDMAm, Stenzel et al. [21] produced multiscale honeycomb structures composed of micrometer-size pores in which additional nanoscale pores could be observed in the hexagonal micron-sized porous array. This is a direct consequence of the block copolymer rearrangement around the water droplets due to the hydrophilicity of the PDMAm block during the water condensation. Hence, the resulting micrometer-size pores should possess a hydrophilic surface. In addition, due to the interactions of the hydrophilic block copolymer with the humidity, water could penetrate into the micelles formed by self-assembly of the block copolymer at the pore wall, leading to water swollen particles. Moreover, the water uptake into the micelle can be correlated with the size of the nano-sized pores found at the surface after drying.

Billon et al. [72] employed other block copolymers, i.e., poly(*n*-butyl acrylate)-*b*-polystyrene (PnBA-*b*-PS) or poly(*tert*-butyl acrylate)-*b*-polystyrene. These block copolymers self-assemble both in hexagonal cylinder packing and lamellar assemblies depending on the block composition (Fig. 9.6a). As a consequence of the use of these block copolymers, the preparation of the films under humid conditions allowed them to obtain films exhibiting order at two different length scales. On the one hand, micrometer sized pores at the surface due to the water condensation were obtained. On the other hand, the nanostructures formed by the self-assembly of the block copolymers were retained in the material (Fig. 9.6b).

Alternatively to use pure block copolymer other groups have employed blends of different copolymers and homopolymers. Compared to the above mentioned approaches, this methodology requires a limited amount of block copolymer

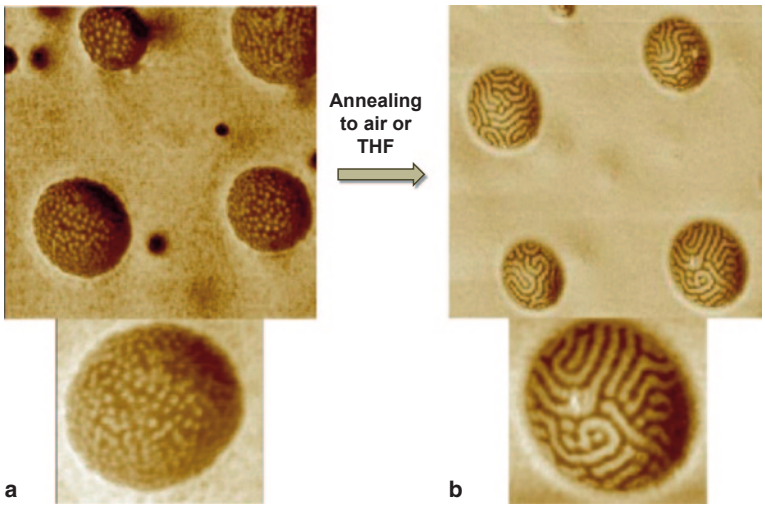


**Fig. 9.7** Atomic force microscopy (AFM) phase images of internal structure evolution of the holes of polymer film having 10 wt% of $PS5F_{21}$-*b*-$PS_{31}$-*b*-$PPEGMA_{38}$ and 90% of PS. **a** After spin coating at 57% of relative humidity; **b** after annealing at 80 °C during 2 days. Image sizes: *Top* 3 × 3 μm; *bottom* 500 × 500 nm. (Reproduced with permission from reference [73])

which needs more complicated synthetic methods. Furthermore, the distribution of the block copolymer is guided by the BF mechanism. For instance, BF with nanostructured pores were prepared by using blends of a ABC triblock copolymer, (PS5F-*b*-PS-*b*-PPEGMA) and a PS homopolymer [73]. During the evaporation process the block copolymer is directed towards the condensed water droplet due to the affinity of the hydrophilic block. As a consequence, the surface spatial distribution of the block copolymers at the surface is localized in the areas where the water droplet was formed. The rest of the surface is mainly composed by the homopolymer (Fig. 9.7). Then, the micro-size cavities are enriched in block copolymers which self-assemble in nanostructured micellar array. Additionally, the pore nanostructure can be tuned changing from micelles to lamellar phase by simply annealing or exposing the film to Tetrahydrofurane (THF) vapor.

More recently, ternary blends have been reported producing novel and intriguing surface patterns. For instance, the mixing of PS matrix with two block copolymers, PS5F-*b*-PS and PS-*b*-PPEGMA, conducts to hierarchically structured porous films with two different nanostructured areas [50]. The condensation of water droplets during the casting process directs the phase separation of the two block copolymers and their spatial distribution. Whereas the fluorinated copolymer was homogeneously distributed in the PS matrix and on the film surface, the amphiphilic PS-*b*-PPEGMA copolymer was located in the edge of the holes. As a result of the self-assembly of the distinct block copolymers two nanostructures were formed inside and outside the pores.

Finally, in some selected cases, demixing of polymer blend solutions on structured substrates can also be employed to create multiscale ordered surfaces. For that purpose, Boneberg et al. [74] blended two components, poly(2-vinylpyridine) (PVP) and PS, already known to form ordered porous films by phase separation [68] and used a substrate with micrometer patterned hydrophilic/hydrophobic areas. The authors prepared the films under a high relative humidity (~50% R.H.) that improves further the demixing of the components [75]. As a result of the surface energy patterns the PVP and PS are demixed and distributed in specific areas depending on their affinity for the substrate. Moreover, the relative humidity not only enhances the demixing between the two homopolymers but also favors the water condensation to occur in both phases, i.e., the PVP and PS domains produce pores with dimension below 30 nm. After the demixing process, PS and PVP could be selectively removed without altering the other polymer and revealing a polymer pattern formed by alternating micrometer size layers of polymer with nanopores.

Hierarchical hybrid nanoparticle-polymer porous assemblies have been obtained by self-assembly of nanoparticles at the polymer solution–water droplet interface. The first example was reported by Russell et al. [76]. In this work, BF were prepared by casting a chloroform solution of PS using tri-*n*-octylphosphine oxide (TOPO)-stabilized CdSe nanoparticles. According to the authors the TOPO-CdSe nanoparticles segregate to the interface and form a uniform layer before the evaporation of the solvent. Other nanoparticles have been employed by Hao's group [77, 78] who described how gold nanoparticles accumulate at the water–chloroform interface, thus forming a protective barrier stabilizing the templating water droplets and preventing the water droplets from coagulation. As a consequence, when the solvent is evaporated, the excess of gold nanoparticles aggregated under the monolayer of pores. Hierarchically, honeycomb hybrid films have also been prepared via BF from metal oxide nanoparticles such as ZnO or $SiO_2$ previously modified by surface initiated polymerizations [79]. The pore sizes of the films can be tuned depending on the polymer attached to the nanoparticles.

On the other hand, hierarchical multiscale structures in the micrometer and/or submicrometer scale are also of broad interest and can be prepared via BF using different approaches. Mixing immiscible polymers, for instance PS and PVP, Lu and Ge [52] obtained hexagonal patterned porous surfaces in which the pores are filled at the bottom. Due to its hydrophobicity, PS forms the wall of the pores. On the contrary, PVP hygroscopic and hydrophilic polymer enriches the water droplet/PS phase, thus, upon evaporation the PVP is deposited within the pore. In order to pattern and functionalize the hierarchical pores with well-defined multi-scale features the authors embossed the films using a PDMS stamp (see Fig. 9.8). Moreover, these porous structures can be employed as template to prepare microstructures of negative PDMS replicas.

Raczkowska et al. [80] also prepared hierarchical ordered films from blends of polar PMMA and non polar PS. Spin coating of the blends under an appropriate relative humidity produced macrophase separated domains and simultaneously droplet-like patterns selectively in the domains rich in the polar polymer. Submi-

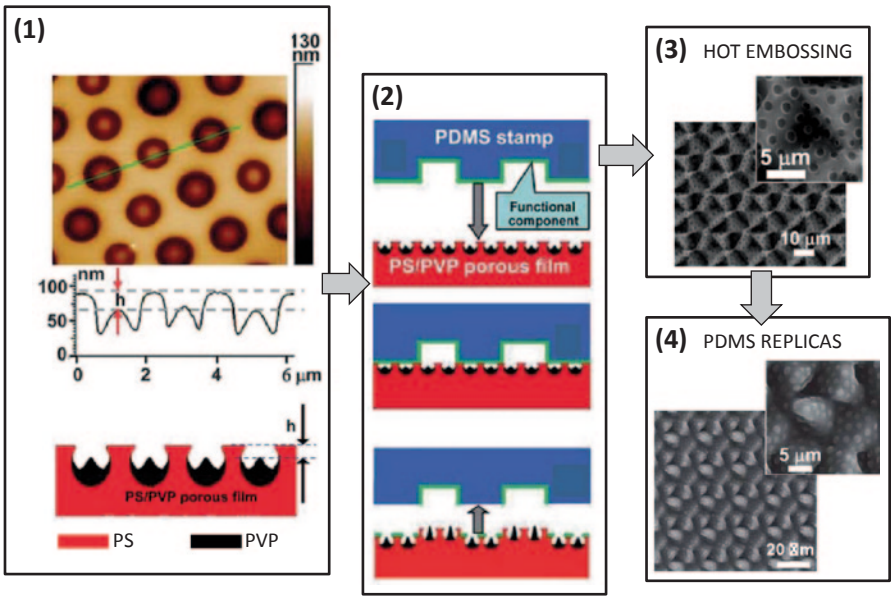


**Fig. 9.8** Formation of multiscale structures by using immiscible PS and PVP. The immiscibility between both homopolymers added to the different hydrophilicity produces hierarchical ordered patterns where the PVP is located inside the pore and the PS at the pore wall. In addition, embossing can produce an additional level of order at the micrometer length-scale as well as replicas. (Reproduced with permission from reference [52])

crometer pores decorated large PMMA-rich surface regions thus resulting in hierarchical film morphology.

In contrast to the previous cases carried out in planar films, porous honeycomb materials with hierarchical surface features formed in nonplanar surfaces have been reported by Connal and Qiao [81]. The authors prepared core cross-linked star (CCS) polymers based on PDMS, PMMA, poly(methyl acrylate), poly(*tert*-butyl acrylate), and poly(ethyl acrylate) [82]. The polymers were employed for the preparation of macroporous materials with two levels of ordered surface features by casting the star PDMS solution onto a TEM grid. As a consequence one level of ordered surface features is originated from the contours of the TEM grid while the second level is obtained by the condensation of water vapor. The concept has been extended to other types of substrates thus giving a variety of porous surfaces with doughnut, golf balls, and hollow porous pockets shapes [83]. These hierarchically structured films were additionally employed as templates so that by replica molding the negative structures can be produced.

Similarly, two levels of order were obtained by the same group combining the BF approach with photocross-linking strategies [82]. A CCS star polymer based on poly(methyl acrylate) modified at the chain ends with 9-anthracene carbonyl chloride was cast under flow of humid air forming porous, micro-structured films. The 9-anthracene groups introduce the ability to reversibly cross-link the micro-

structured film when irradiated with long wave UV (>350 nm) and the reaction can be reversed upon exposure to short-wave UV light (<300 nm). Hence, in addition to the structural micrometer size pores, larger scale (several hundreds of microns) surface patterns due to the mask employed (TEM grids) were obtained.

Whereas, the polymers employed by Qiao et al. concerned only stars with low $T_g$ (below 48 °C), Li et al. [84] studied the construction of macroporous polymeric films on various nonplanar substrates with static breath figure (BF) technique, using linear polymers with high $T_g$. For this purpose, two kinds of linear polymers with high $T_g$, PS-*b*-PAA, and PS without polar end groups, were employed to prepare 3-dimensional macroporous films on different nonplanar substrates. Contrary to previous works, this group concluded that neither $T_g$ nor molecular topography of polymers is the key factors during the formation of 3D macroporous film on nonplanar substrate. Instead, the authors claim that the morphology of the substrate influences the shape and the arrangement of macropores.

Membranes for advanced filtration (also known as microsieves) composed by a hierarchical pore structure have been prepared by Goedel et al. [85]. The strategy concerns the creation of BF patterns within layers of polymer solutions that are spread out on top of structured supports, e.g., spherical glass beads. Instead of using a planar support the spreading of the polymer solution is done on a support decorated with protrusions. Finally, the vitrified polymer layer obtained upon evaporation of the solvent can be separated from the substrate thus leading to a polymer membrane with a hierarchical structure. This multiscale ordered structure consists, then, of an ultrathin active separation layer with submicrometer pores and a supporting layer with larger pores.

Finally, the construction of hierarchical structures by combination of electrospinning or electrospraying and BF has been first reported by Kwak et al. [86]. Recently Han et al. [87] and Karimi et al. [88] prepared PS fibers with uniform nanopores distributed. By adjusting parameters such as the solvent, polymer concentration, humidity, or the electrospinning temperature, the authors prepared multiscale structures based on fibers with diameters in the micrometer size with nanopores at their surface. The formation of the nanopores requires a high humidity and the employment of a volatile solvent, e.g., THF.

## 9.5 Application of Breath Figures in Biorecognition Processes

The development of platforms for biorecognition purposes requires an appropriate control of both the surface features and the chemical composition of the interface. In this sense, BF technique has been proposed as a very simple and versatile method to fabricate functional micropatterned substrates with potential in biorecognition processes. It is today well established that, among others, the depth and the average pore size of the microporous films are factors which influence the attachment of microorganisms and cells to solid substrates [69, 70] and these parameters can be modulated using the BF approach. Moreover, as depicted above, a wide variety

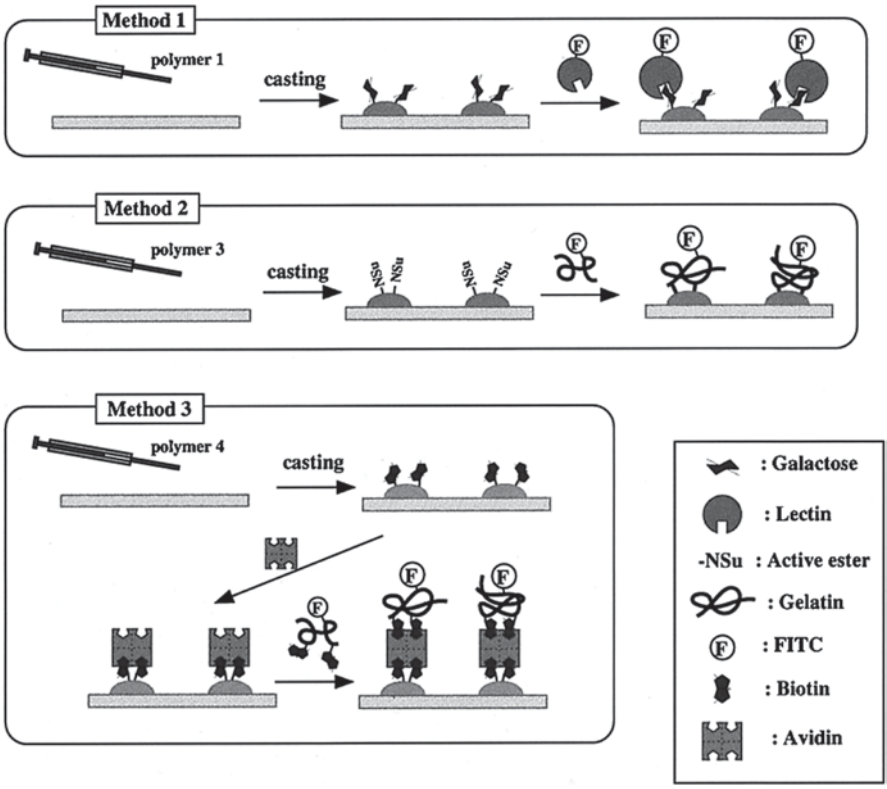


**Fig. 9.9** Schematic representation of the procedures for introduction cell adhesive ligands onto honeycomb-patterned films. (Reproduced with permission from reference [89])

of polymers can be used as precursors, including biocompatible and biodegradable polymers. Thus, this section will provide a thorough overview about the recent achievements in the use of porous polymeric films for the development of different recognition systems.

One of the pioneers in this area was the group of Nishida [89] who extensively used honeycomb patterned films for bio-related purposes. Among their findings, this group described different approaches that can lead to the preparation of porous films having cell attaching ligands. The ligands were introduced at the surface of the pore wall by using three different approaches as depicted in Fig. 9.9. In the first method, the functionalized honeycomb films were obtained directly by casting the solution of the amphiphilic polymer containing ligand. The second method concerns the preparation of the honeycomb films using an amphiphilic copolymer that possesses several moieties able to be post-modified. Thus, the inner part of the pore can be modified, for instance, introducing covalently the ligand to the polymer honeycomb pattern. Finally, they additionally described the preparation of surface modified porous films via specific interaction between Biotin and Avidin (method 3).

The strategy depicted below has also been employed by other authors to functionalize the porous surfaces with saccharides (including glucose or mannose) moieties [40, 47] taking advantage of their protein-specific binding ability. One of the most explored functional polymers used in the BF technique are amphiphilic glycopolymers which may provide honeycomb structured porous films with bioactivity. In this concern, different molecular architectures have been employed such as linear statistical copolymers, block copolymers, or graft copolymers.

Honeycomb patterned films have been, for example, prepared from solutions of comb-like copolymers of polystyrene-*b*-poly((2-,3-,4-,6-tetra-O-acetyl-β-D-glucosyloxy)ethyl methacrylate) [44]. Furthermore, the functionality of the structures and their biological activity were tested by taking advantage of a largely extended biorecognition model, i.e., the study of the specific recognition of immobilized saccharides to fluorescent-labeled lectins. The films obtained from the acetylated polymer do not result in the interaction with Concanavalin A (Con A) but are significantly visible after deprotection. Besides, in this article random copolymers and comb-like structures were studied and compared with the block glycopolymer. Only the acetylated comb-like structure, similarly to the diblock copolymer, can form honeycomb patterned films. Also Ting et al. [47] and Escalé et al. [45] reported the ability of different architectures such as block, statistical, and gradient glycopolymers to form bioactive honeycomb porous surfaces. In these works, copolymers of 2-(2′,3′,4′,6′-tetra-O-acetyl-β-D-galactosyloxy)ethyl acrylate and styrene were synthesized and later were deprotected. The deacetylated copolymers produced slight irregular arrays, and also a second porosity was observed. They concluded that a higher hydrophobic fraction compared to the hydrophilic fraction is required to form regular arrays. In effect, the use of amphiphilic block copolymer with a large hydrophilic fraction reduces the surface tension of the water droplets which coagulate with neighboring droplets, resulting in large disordered pores. With the purpose of improving the regularity, the hydrophobic fraction was augmented in the polymer solution and star PS homopolymer was added. In this case, highly ordered hexagonal array was obtained and at the same time glycopolymer segments were mainly localized inside the pores. This was confirmed by molecular recognition experiments and visualized by fluorescence microscopy, where fluorescein isothiocyanate conjugated peanut agglutinin (PNA), a β-galactose specific binding protein, was preferentially located inside the pores.

As described above, the mixing of hydrophobic homopolymers such as PS with the amphiphilic polymers allows the improvement of the regularity of the porous structured films because the hydrophobicity of the system increases. In addition, the use of polymeric blends consisting of functional polymers embedded into polymer matrix directs the preferential location of certain functionalities inside the cavities [90]. By using this approach, Muñoz-Bonilla et al. prepared regularly patterned polymer surfaces from blends of PS and a statistical glycopolymer, poly(styrene-*co*-2-[(D-glucopyranosyl)aminocarbonyloxy]ethyl acrylate) [48]. The resulting holes were highly concentrated in glycopolymer, employing only 10 wt% of glycopolymer in the mixture, as a consequence of the interactions between the polar glycomonomer units and condensed water droplets. Moreover, soft annealing in humid air

allows preferential swelling in this area due to the hygroscopic character of the carbohydrate groups, as shown by atomic force microscopy (AFM) thus changing the surface morphology between pores and hills. The functionalization of the pores as well as the ability to interact with proteins, have also been studied by fluorescence microscopy, using fluorescent labeled lectins. This approach was later extended to other polymeric systems. For instance, regularly patterned polymer surfaces have also been achieved using mixtures of PMMA and random or block copolymers based on MMA and 2-[(D-glucopyranosyl)aminocarbonyloxy] ethyl acrylate [7].

An alternative strategy to include saccharide moieties in the pores and avoid the possibility of having coagulation concerns the post-modification of the pores by additional polymerization steps using the chemical groups at the pore wall as initiators or by simple chemical reactions for instance using click chemistry. For example, ATRP has been employed to graft glycopolymer chains onto the holes of the honeycomb patterned films. In this case, an ATRP initiator, 2-bromoisobutyryl bromide, was immobilized inside the cavities of the films to further grow the glycopolymer chain by surface initiated ATRP from the pore walls of the honeycomb structures [60]. The specific recognition to Con A lectin proved the site-directing grafting on honeycomb porous films. Equally, RAFT polymerization was used as strategy to graft thermo-responsive glycopolymers onto honeycomb structured films [91]. Based on the later, porous films were obtained from poly(styrene-*co*-maleic anhydride), and then the films were cross-linked with 1,8-diaminooctane. The excess of diamine was used to attach the RAFT agent for the subsequent controlled copolymerization of NIPAm and a glycomonomer from the surface. In this way the resulting porous films showed specific and temperature-dependent recognition to Con A lectin.

By the previously mentioned approaches, i.e., including a functional additive or by post-modification, the hydrophilic additive directs the formation of pores and simultaneously is reoriented towards the pore surface. Therefore, the functionalization typically occurs in the pore wall. However, recent approaches have been developed to modify the surface of the film while maintaining the pore surface unmodified. For that purpose, de León et al. [49] described the preparation of porous films using blends of PS and PS-*b*-PS5F by the BF approach. The diblock copolymer resulted to be homogeneously distributed along the whole surface of the films not only in the pore wall but also the solution/air interface. In effect, the low surface energy of the fluorinated block induces the surface segregation of the block copolymer, thus a surface enrichment is observed in the areas where the solution was exposed to air. As a consequence of the presence of fluorinated groups at the surface, these films exhibit a particular wetting behavior that can be described by the Cassie state, i.e., the water droplet only wets the surface but not the pore. This particular effect permits to modify selectively the chemical composition of the film surface whilst the interior of the pores does not vary. In particular, the modification strategy resorts to the use of click chemistry. Thus, thiolated glucose molecules were attached specifically to the poly(2,3,4,5,6-pentafluorostyrene) domains via thiol-*para* fluorine "click" reaction. The use of a fluorescent labeled Con A, i.e., Con A-FITC, permitted to determine the position within the film where the protein

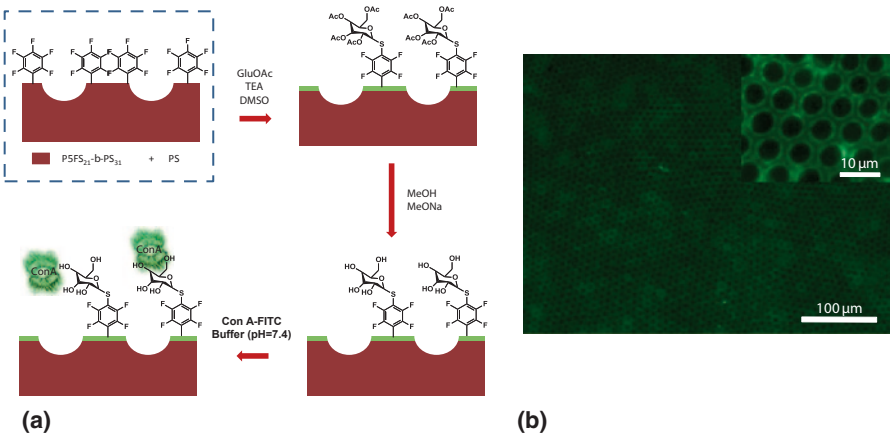


**Fig. 9.10** **a** Scheme of the procedure followed to modify selectively the surface of the films while maintaining the composition of the pores. **b** Fluorescence microscopy images of a porous film containing 50 wt% of $PS_{31}$-*b*-$P5FS_{21}$ and 50% homopolystyrene (prepared from polymer solutions with concentration of 20 mg/mL and casted from $CS_2$ at 98% RH) after "click" reaction with the GluOAc, deprotection of the acetyl groups, and incubation with Con A-FITC lectin. (Reproduced with permission from reference [49])

has been immobilized. As depicted in Fig. 9.10, Con A lectin is distributed homogeneously along the entire surface outside the pores.

Immobilization of the biomolecules outside the pores have also been carried out using incompatible ternary blends consisting of high molecular weight PS, an amphiphilic block copolymer, $PS_{40}$-*b*-$P(PEGMA300)_{48}$, and a fluorinated homopolymer, $P5FS_{21}$.[51] In these blends two simultaneously occurring processes, i.e., the BF mechanism and the phase separation process, lead to rather intriguing morphologies. More interestingly, as schematically depicted in Fig. 9.11, both the amphiphilic block copolymer and the fluorinated polymer were mainly located in the cavities. Above a certain percentage of relative humidity, honeycomb structured films were obtained in which the block copolymer is distributed on the edge of the pore as a result of the affinity by the condensing water droplet and the coffee stain effect. Moreover, thiolated glucose molecules were specifically attached to the $P5FS_{21}$ domains via thiol-*para* fluorine "click" reaction. Subsequently, the immobilized glucose moieties were able to bind lectins, in particular ConA-FITC. The successful binding of the Con A was demonstrated by the fluorescence, observed exclusively at the areas where $P5FS_{21}$ domains are located.

In addition to the extended glucose-Con A model system for biorecognition, other systems have been recently developed for the recognition of small molecules. In particular, Stenzel et al. [92] uses the biotin-streptavidin system to obtain patterns of proteins on the pores. For this purpose, the group took advantage of the self-assembly process that occurs during the BF formation, i.e., the reorientation of polar groups of a polystyrene-block-poly(acrylic acid) (PS-*b*-PAA) block copolymer towards the inner part of the pore to covalently modify the acid groups with biotin.

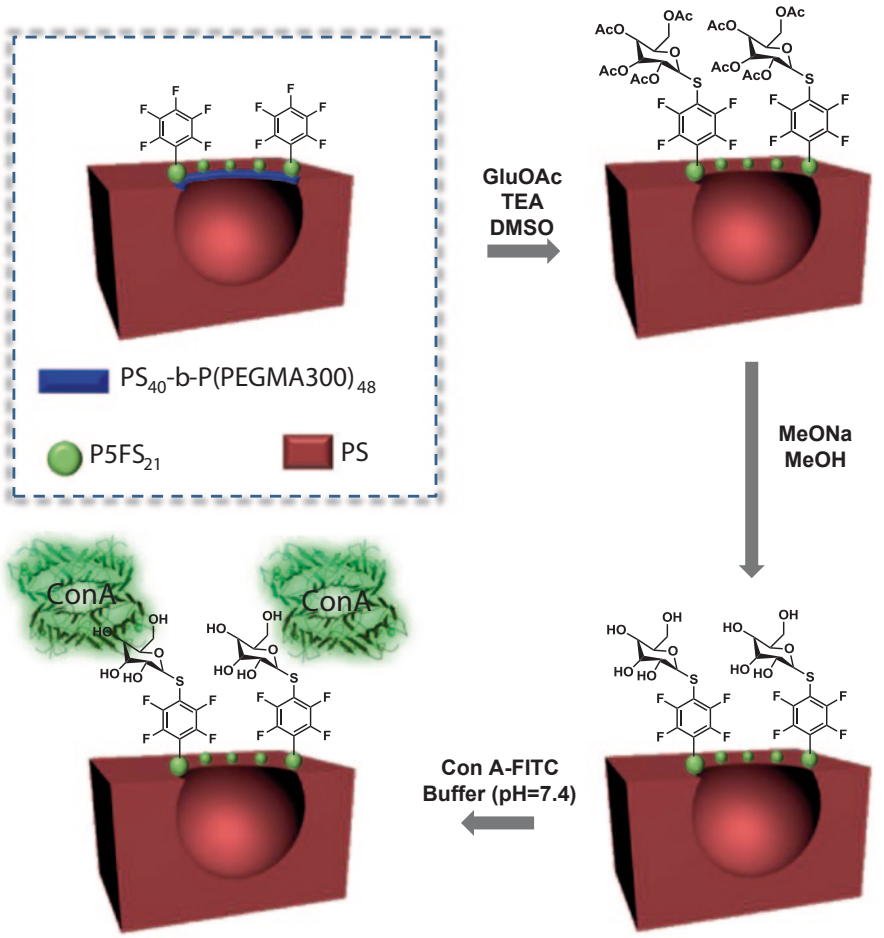


**Fig. 9.11** Schematic representation of the approach employed to incorporate glucose moieties and, subsequently, Con A onto the microstructured films

Honeycomb structured films have been recently employed by Wan et al. for glucose sensing [93]. The strategy is based on the use of porous films modified with phenylboronic acid (PBA) functional groups which are known to be molecular receptors able to bind reversibly cis-diol moieties. Among the applications of PBAs for sensing different compounds (such as carbohydrates, nucleotides, coenzymes, and other biological compounds) [94–96], the authors employed porous surfaces modified with PBA for detection of glucose. The approach is schematically shown in Fig. 9.12 (above). First of all, the evaporation of the copolymer, i.e., a PBA containing block copolymer, polystyrene-*b*-poly(acrylic acid-*co*-acrylamidophenylboronic acid) [PS-*b*-P(AA-*co*-AAPBA)] using a volatile solvent mixture leads to highly ordered macroporous films. Then, Alizarin Red S (ARS) was immobilized at the pore wall as evidenced by fluorescence spectroscopy. This is a direct conse-

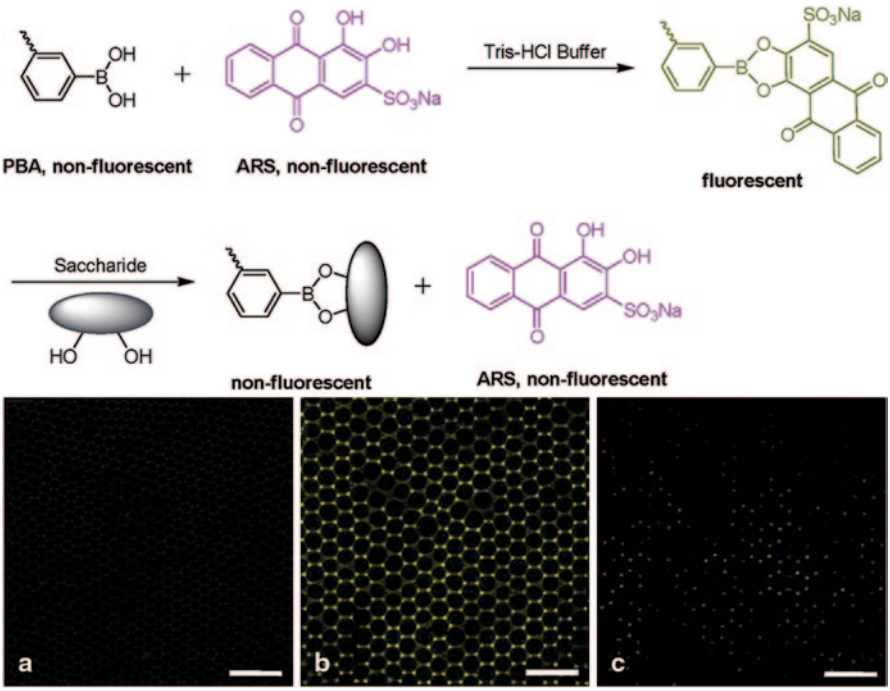


**Fig. 9.12** *Above*: schematic illustration of the interaction among Alizarin Red S (ARS), saccharide, and phenylboronic acid (PBA). *Below*: fluorescence images of **a** $PS_{141}$-*b*-$PAA_{14}$ porous film, **b** ARS-immobilized B3honeycomb-patterned porous films, and **c** sample in part b being exposed to 1 M of glucose solution. Scale bar: 10 μm. (Reproduced with permission from reference [93])

quence of the particular distribution of the PBA groups contained in the copolymer during the evaporation. The surfaces having ARS immobilized exhibit fluorescence that is not found in free ARS. More interestingly, in the presence of glucose ARS is replaced and the fluorescence disappeared.

In addition to the above mentioned examples devoted to the study of recognition of small molecules including saccharides and proteins, functionalized porous interfaces have been employed to either favor or limit anchoring different types of cells including bacteria. Stenzel et al. [97] have prepared honeycomb structured porous films for cell culturing applications from a conducting block copolymer composed of PS and polypyrrole-templated poly(acrylic acid). This group employed conducting polymers that are utilized in biological systems because the stimulation with electrical currents is known to be beneficial for the cell's growth. Among their finding they demonstrated that the porosity of the films clearly influenced both the attachment and proliferation of fibroblast cells, increasing the cell attachment as the pore size decreases. In addition, the obtained samples exhibited almost no inhibition of cell growth, indicating their biocompatibility and negligible toxicity.

Similarly, by using poly(glycine ethyl ester-*co*-alanine ethyl ester) phosphazene (PGAP), Duan et al. [98] prepared honeycomb films and exposed them to osteoblast

culture. They reported that although the initial cell attachment and proliferation on PGAP films were inferior to those obtained using conventional poly(lactic-*co*-glycolic acid) films, P-containing PGAP was a sort of bone-binding bioactive polymer. Honeycomb-patterned PGAP films have accordingly enhanced protein adsorption and apatite deposition in simulated body fluid and showed great advantages in promoting osteogenous differentiation.

In addition to the variation of the chemical structure, depicted above, the formation of microporous films with different shapes and dimensions also influenced the adhesion of cells. In particular, extensive work has been carried out to determine how the morphology affects the function of different types of cells (hepatocytes, endothelial, and neural projenitor cells) and can be controlled by manipulating the size of the micropores on the honeycomb films [15, 99–104].

For that purpose, Nishikawa et al. [28] employed an amphiphilic copolymer and a viscoelastic polymer, in this particular case poly(ε-caprolactone) (PCL). The viscoelastic properties of PCL allow the honeycomb films to be stretched. As a consequence, the isotropic hexagonal arrays were transformed into anisotropic alignment. The shape of the pores has been proved to play a crucial role among others on the cell adhesion processes. A similar matrix, i.e., PCL containing an amphiphilic copolymer has been employed by Tsuruma et al. to evidence the role of the presence of pores and their particular dimensions on the differentiation process [105]. These authors concluded that the differentiation of neural stem cells (NSC) was controlled by manipulating the pore size on honeycomb films. The highest suppression of NSC differentiation was observed on films with 3 μm pore specifically [106].

This group also obtained porous films with uniform pore size which can attach leukocytes and provide the complete selective separation of the leukocyte from the whole blood, depending on pore structure in terms of size and depth [100]. In addition, they also have cultured hepatocytes on honeycomb-patterned polymer films to investigate the influence of the honeycomb pattern on the cell adhesion, actin organization, and hepatic function [102]. The hepatocytes cultured on the honeycomb film were formed in a spherical shape with actin filaments localized inside the edge of the spheroid, in contrast to those cultured on flat surface where hepatocytes were flattened and the actin filaments appeared in the spreading regions. This is critical for the applicability of the materials because the spheroids cells expressed a higher level of liver specific function than the cells on the flat films. The same group examined the influence of the honeycomb pattern and pore size on the behavior of vascular endothelial cells. Again the morphology of the cells changed from culturing in a flat surface to honeycomb films, where the smallest pore size induced the highest cell proliferation [103]. They also demonstrated that the surface topography of the films made from poly(ε-caprolactone) and amphiphilic copolymer can affect the mesenteric-visceral adipocytes function, facilitating the long-term culture [107]. Moreover, as mentioned above neural cells were used to investigate the effect of the honeycomb film on the neural network, where the morphologies of neurons changed by varying the pore size of the honeycomb patterned films [101, 105]. In particular, the highest suppression of neural stem cell differentiation was observed on honeycomb film with 3 μm pore specifically. Besides, honeycomb poly(ε-caprolactone)

films were fabricated using the BF method without the addition of any surfactant [108]. The cell adhesion, spreading, proliferation, differentiation, and gene expression of mouse preosteoblastic MC3T3-E1 cell were significantly enhanced. In addition, when the pore diameter decreases this effect was more remarkable.

Yamamoto et al. [33] demonstrated that films with BF patterned (modified with fibronectin) result in increased expression of focal adhesion kinase autophosphorylated at the tyrosine residue, a crucial signal transduction protein that mediates cell adhesion, growth, and proliferation. The surface characteristic influences the adsorption of the fibronectin and, consequently, the adhesion of the cells guided by the corresponding receptor. The use of peptides to make porous films is also an attractive approach for tissue engineering applications as a scaffold to grow adherent cells [109]. The honeycomb porous scaffolds were formed by a combination of BF and self-assembly of small peptide diphenylalanine building blocks where human embryo skin fibroblast can grow.

Honeycomb patterned films enhanced cell adhesion but they have also been studied as adhesion barriers. To reduce postoperative adhesion, fibrinolytic agents or anticoagulants among others have been used. Nevertheless, these agents alone cannot completely prevent adhesion and physical barriers have been employed to reduce the adhesion formation by separating the gliding surfaces during the healing process. Fukuhira et al. [110] studied the potential of a honeycomb patterned poly(lactic acid) film as an adhesion barrier to reduce postoperative adhesion using an in vitro bioadhesive test. The honeycomb structure of the films prevents the migration of fibroblasts to the other side of the film thus allowing them to function as a physical barrier.

More recently, a selective modification of the pore inner part using appropriate polypeptide sequences permitted the use of these surfaces as scaffolds for pattern and display of active biomolecules, as ordered templates for both specific recognition processes and for the micropatterning of bacterial cells. A straightforward functionalization step, using 1-Ethyl-3-(3-dimethylaminopropyl)carbodiimide (EDC) as activating agent, permits to modify only the pore surface with different polypeptide sequences. In particular, different experiments were carried out using Magainin I peptide to selectively recognize bacteria membranes and thus immobilize them into the pores. As depicted in Fig. 9.13, the design of the pore dimensions having average pore sizes of 5 μm permits to bind single bacteria with similar dimensions at the inner pore interface [111].

## 9.6 Summary and Conclusions

In this chapter, we described the advantages and capabilities of the BF approach to create functional bioactive structured porous materials. First of all, in comparison with other templating approaches, the use of BF presents interesting opportunities. Since the requirement of a template that needs to be removed is avoided, the method can be employed with a large variety of polymeric materials, which

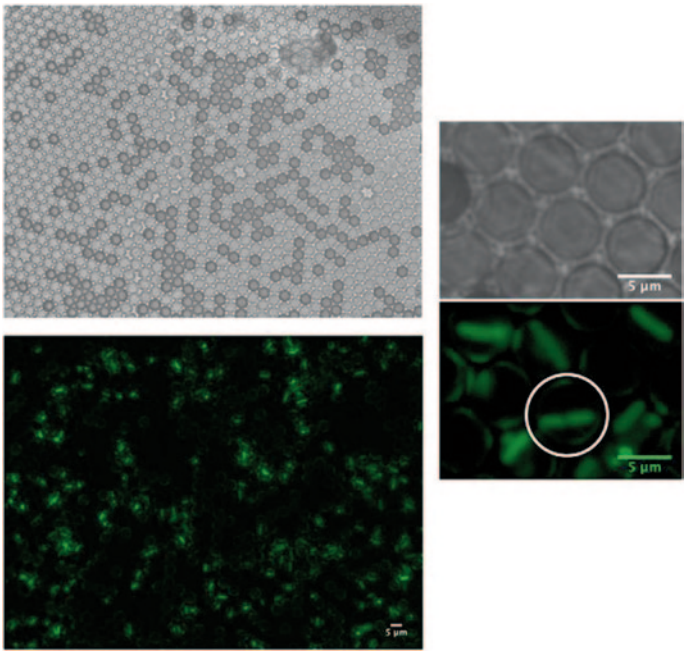


**Fig. 9.13** Immobilization of fluorescent bacteria in the porous surfaces. *Top panels*: Optical microscope images of the polymer surfaces in which a rather regular pattern of pores can be observed. *Bottom panels*: Fluorescent image of the surfaces with the immobilized bacteria. (Reproduced with permission from reference [111])

makes the methodology fast and inexpensive. Moreover, porous films with variable pore sizes and shapes have been reported highlighting the versatility of this approach.

Taking advantage of the mechanism of BF formation different strategies allowed the control over the chemical distribution of the functional groups at the surface. Thus, the pore surface, the film surface, or both simultaneously can be precisely controlled. As a consequence and mainly based on post-modification reactions the BF approach permits the use of a range of chemistries to immobilize biomolecules including saccharides, peptides sequences, or proteins. Thus, this patterning methodology may be of interest in view of contribution in the understanding of a variety of biological processes including the biology of cells that requires, for instance, the investigation of isolated cells.

Even if this chapter is mainly concerned with the preparation of functional surfaces with biorecognition capabilities, it has to be mentioned that this method has opened a general interest and its use has been extended to a large scientific community in the frontiers of chemistry, materials, physics, biology, and medicine among others.

In effect, the features discussed, i.e., control of topography, possibility of having stimuli-responsive behavior and the multiscale order within the porous films, make the systems interesting for a broad variety of applications ranging from electronics and optics to the elaboration of biomaterials or control of the wettability to produce superhydrophobic films.

**Acknowledgements** A M.-B. and JRH acknowledge financial support by the MINECO (Projects MAT2010-17016, MAT2010-21088-C03-01, and COST Action MP0904 SIMUFER). A M.-B. gratefully acknowledges the MINECO for her Juan de la Cierva postdoctoral contract.

## References

1. Widawski, G., M. Rawiso, and B. François, *Self-organized honeycomb morphology of star-polymer polystyrene films*. Nature, 1994. **369**(6479): p. 387–389.
2. Bunz, U.H.F., *Breath Figures as a Dynamic Templating Method for Polymers and Nanomaterials*. Advanced Materials, 2006. **18**(8): p. 973–989.
3. Muñoz-Bonilla, A., M. Fernández-García, and J. Rodríguez-Hernández, *Towards hierarchically ordered functional porous polymeric surfaces prepared by the breath figures approach*. Progress in Polymer Science, 2013.
4. Bai, H., et al., *Breath figure arrays: Unconventional fabrications, functionalizations, and applications*. Angewandte Chemie—International Edition, 2013. **52**(47): p. 12240–12255.
5. Escalé, P., et al., *Recent advances in honeycomb-structured porous polymer films prepared via breath figures*. European Polymer Journal, 2012. **48**(6): p. 1001–1025.
6. Hernández-Guerrero, M. and M.H. Stenzel, *Honeycomb structured polymer films via breath figures*. Polymer Chemistry, 2012. **3**(3): p. 563–577.
7. de León, A.S., et al., *Breath figures method to control the topography and the functionality of polymeric surfaces in porous films and microspheres*. Journal of Polymer Science Part A: Polymer Chemistry, 2012. **50**(5): p. 851–859.
8. Zhao, B., et al., *Water-assisted fabrication of honeycomb structure porous film from poly(l-lactide)*. Journal of Materials Chemistry, 2006. **16**(5): p. 509–513.
9. Yabu, H., et al., *Preparation of Honeycomb-Patterned Polyimide Films by Self-Organization*. Langmuir, 2003. **19**(15): p. 6297–6300.
10. Angus, S.D. and T.P. Davis, *Polymer Surface Design and Infomatics: Facile Microscopy/Image Analysis Techniques for Self-Organizing Microporous Polymer Film Characterization*. Langmuir, 2002. **18**(24): p. 9547–9553.
11. Muñoz-Bonilla, A., et al., *Engineering polymer surfaces with variable chemistry and topography*. Journal of Polymer Science Part A: Polymer Chemistry, 2009. **47**(9): p. 2262–2271.
12. Pilati, F., et al., *Design of surface properties of PET films: Effect of fluorinated block copolymers*. Journal of Colloid and Interface Science, 2007. **315**(1): p. 210–222.
13. Roszol, L.s., et al., *Micropatterned Polyvinyl Butyral Membrane for Acid–Base Diodes*. The Journal of Physical Chemistry B, 2010. **114**(43): p. 13718–13725.
14. Mansouri, J., E. Yapit, and V. Chen, *Polysulfone filtration membranes with isoporous structures prepared by a combination of dip-coating and breath figure approach*. Journal of Membrane Science, 2013. **444**(0): p. 237–251.
15. Nishikawa, T., et al., *Fabrication of honeycomb film of an amphiphilic copolymer at the air–water interface*. Langmuir, 2002. **18**(15): p. 5734–5740.
16. Park, M.S. and J.K. Kim, *Breath Figure Patterns Prepared by Spin Coating in a Dry Environment*. Langmuir, 2004. **20**(13): p. 5347–5352.
17. Kasai, W. and T. Kondo, *Fabrication of Honeycomb-Patterned Cellulose Films*. Macromolecular Bioscience, 2004. **4**(1): p. 17–21.

18. Ding, J., et al., *Breath figure in non-aqueous vapor*. Soft Matter, 2013. **9**(2): p. 506–514.
19. Xiong, X., et al., *Microsphere Pattern Prepared by a "Reverse" Breath Figure Method*. Macromolecules, 2009. **42**(23): p. 9351–9356.
20. Zhang, R., et al., *Fabrication of honeycomb polyvinyl butyral film under humidity provided by super saturated salt solutions*. Journal of Applied Polymer Science, 2012. **124**(1): p. 495–500.
21. Wong, K.H., et al., *Honeycomb structured porous films from amphiphilic block copolymers prepared via RAFT polymerization*. Polymer, 2007. **48**(17): p. 4950–4965.
22. Han, X., et al., *Formation of honeycomb films based on a soluble polyimide synthesized from 2,2'-bis[4-(3,4-dicarboxyphenoxy)phenyl]hexafluoropropane dianhydride and 3,3'-dimethyl-4,4'-diaminodiphenylmethane*. Journal of Applied Polymer Science, 2008. **107**(1): p. 618–623.
23. Srinivasarao, M., et al., *Three-Dimensionally Ordered Array of Air Bubbles in a Polymer Film*. Science, 2001. **292**(5514): p. 79–83.
24. Billon, L., et al., *Tailoring Highly Ordered Honeycomb Films Based on Ionomer Macromolecules by the Bottom-Up Approach*. Macromolecules, 2008. **42**(1): p. 345–356.
25. Bormashenko, E., S. Balter, and D. Aurbach, *On the Nature of the Breath Figures Self-Assembly in Evaporated Polymer Solutions: Revisiting Physical Factors Governing the Patterning*. Macromolecular Chemistry and Physics, 2012. **213**(16): p. 1742–1747.
26. Ferrari, E., P. Fabbri, and F. Pilati, *Solvent and Substrate Contributions to the Formation of Breath Figure Patterns in Polystyrene Films*. Langmuir, 2011. **27**(5): p. 1874–1881.
27. Cai, Y. and B.-m. Zhang Newby, *Porous Polymer Films Templated by Marangoni Flow-Induced Water Droplet Arrays*. Langmuir, 2009. **25**(13): p. 7638–7645.
28. Nishikawa, T., et al., *Micropatterns Based on Deformation of a Viscoelastic Honeycomb Mesh*. Langmuir, 2003. **19**(15): p. 6193–6201.
29. Li, J., et al., *Ordered Honeycomb-Structured Gold Nanoparticle Films with Changeable Pore Morphology: From Circle to Ellipse*. Langmuir, 2005. **21**(5): p. 2017–2021.
30. Yabu, H. and M. Shimomura, *Simple Fabrication of Micro Lens Arrays*. Langmuir, 2005. **21**(5): p. 1709–1711.
31. Yabu, H., et al., *Superhydrophobic and Lipophobic Properties of Self-Organized Honeycomb and Pincushion Structures*. Langmuir, 2005. **21**(8): p. 3235–3237.
32. Shojaei-Zadeh, S., S.R. Swanson, and S.L. Anna, *Highly uniform micro-cavity arrays in flexible elastomer film*. Soft Matter, 2009. **5**(4): p. 743–746.
33. Yamamoto, S., et al., *Effect of honeycomb-patterned surface topography on the adhesion and signal transduction of porcine aortic endothelial cells*. Langmuir, 2007. **23**(15): p. 8114–8120.
34. Galeotti, F., et al., *Precise surface patterning of silk fibroin films by breath figures*. Soft Matter, 2012. **8**(17): p. 4815–4821.
35. Peng, J., et al., *Formation of Regular Hole Pattern in Polymer Films*. Macromolecular Chemistry and Physics, 2003. **204**(1): p. 125–130.
36. Zhao, B., et al., *Fabrication of honeycomb ordered polycarbonate films using water droplets as template*. Thin Solid Films, 2007. **515**(7–8): p. 3629–3634.
37. Tian, Y., et al., *The formation of honeycomb structure in polyphenylene oxide films*. Polymer, 2006. **47**(11): p. 3866–3873.
38. Yunus, S., et al., *A Route to Self-Organized Honeycomb Microstructured Polystyrene Films and Their Chemical Characterization by ToF-SIMS Imaging*. Advanced Functional Materials, 2007. **17**(7): p. 1079–1084.
39. Galeotti, F., et al., *Self-Functionalizing Polymer Film Surfaces Assisted by Specific Polystyrene End-Tagging*. Chemistry of Materials, 2010. **22**(9): p. 2764–2769.
40. Stenzel, M.H., T.P. Davis, and A.G. Fane, *Honeycomb structured porous films prepared from carbohydrate based polymers synthesized via the RAFT process*. Journal of Materials Chemistry, 2003. **13**(9): p. 2090–2097.
41. Wang, C.Y., et al., *Fabrication of highly ordered microporous thin films by PS-b-PAA self-assembly and investigation of their tunable surface properties*. Journal of Materials Chemistry, 2008. **18**(6): p. 683–690.

42. Bolognesi, A., et al., *Nanophase Separation in Polystyrene-Polyfluorene Block Copolymers Thin Films Prepared through the Breath Figure Procedure*. Langmuir, 2009. **25**(9): p. 5333–5338.
43. Stenzel, M.H. and T.P. Davis, *Biomimetic Honeycomb-Structured Surfaces Formed from Block Copolymers Incorporating Acryloyl Phosphorylcholine*. Australian Journal of Chemistry, 2003. **56**(10): p. 1035–1038.
44. Ke, B.B., et al., *Controlled synthesis of linear and comb-like glycopolymers for preparation of honeycomb-patterned films*. Polymer, 2010. **51**(10): p. 2168–2176.
45. Escalé, P., et al., *Synthetic route effect on macromolecular architecture: from block to gradient copolymers based on acryloyl galactose monomer using RAFT polymerization*. Macromolecules, 2011. **44** (15): p. 5911–5919.
46. Dong, W., et al., *Honeycomb-Structured Microporous Films Made from Hyperbranched Polymers by the Breath Figure Method*. Langmuir, 2008. **25**(1): p. 173–178.
47. Ting, S.R.S., et al., *Lectin recognizable biomaterials synthesized via nitroxide-mediated polymerization of a methacryloyl galactose monomer*. Macromolecules, 2009. **42**(24): p. 9422–9434.
48. Muñoz-Bonilla, A., et al., *Fabrication of honeycomb-structured porous surfaces decorated with glycopolymers*. Langmuir, 2010. **26**(11): p. 8552–8558.
49. de Leon, A.S., et al., *Control of the chemistry outside the pores in honeycomb patterned films*. Polymer Chemistry, 2013. **4**(14): p. 4024–4032.
50. de León, A.S., et al., Hierarchically structured multifunctional porous interfaces through water templated self-assembly of ternary systems. Langmuir, 2012.
51. De León, A.S., et al., *Fabrication of structured porous films by breath figures and phase separation processes: Tuning the chemistry and morphology inside the pores using click chemistry*. ACS Applied Materials and Interfaces, 2013. **5**(9): p. 3943–3951.
52. Ge, W. and C. Lu, *Hierarchical honeycomb patterns with tunable microstructures: Controllable fabrication and application as replication templates*. Soft Matter, 2011. **7**(6): p. 2790–2796.
53. Böker, A., et al., *Hierarchical nanoparticle assemblies formed by decorating breath figures*. Nature Materials, 2004. **3**(5): p. 302–306.
54. Vohra, V., et al., *Multilevel Organization in Hybrid Thin Films for Optoelectronic Applications*. Langmuir, 2009. **25**(20): p. 12019–12023.
55. Sun, H., H. Li, and L. Wu, *Micro-patterned polystyrene surfaces directed by surfactant-encapsulated polyoxometalate complex via breath figures*. Polymer, 2009. **50**(9): p. 2113–2122.
56. Nurmawati, M.H., et al., *Hierarchical Self-Organization of Nanomaterials into Two-Dimensional Arrays Using Functional Polymer Scaffold*. Advanced Functional Materials, 2008. **18**(20): p. 3213–3218.
57. Li, X., et al., *A Bottom-Up Approach To Fabricate Patterned Surfaces with Asymmetrical TiO2 Microparticles Trapped in the Holes of Honeycomblike Polymer Film*. Journal of the American Chemical Society, 2011. **133**(11): p. 3736–3739.
58. Ke, B.-B., et al., *Tunable Assembly of Nanoparticles on Patterned Porous Film*. Langmuir, 2010. **26**(20): p. 15982–15988.
59. Zhang, Y. and C. Wang, *Micropatterning of Proteins on 3D Porous Polymer Film Fabricated by Using the Breath-Figure Method*. Advanced Materials, 2007. **19**(7): p. 913–916.
60. Ke, B.-B., L.-S. Wan, and Z.-K. Xu, *Controllable construction of carbohydrate microarrays by site-directed grafting on self-organized porous films*. Langmuir, 2010. **26**(11): p. 8946–8952.
61. Hernandez-Guerrero, M., et al., *Grafting thermoresponsive polymers onto honeycomb structured porous films using the RAFT process*. Journal of Materials Chemistry, 2008. **18**(39): p. 4718–4730.
62. Ke, B.B., et al., *Selective layer-by-layer self-assembly on patterned porous films modulated by Cassie-Wenzel transition*. Physical Chemistry Chemical Physics, 2011. **13**(11): p. 4881–4887.

63. Roy, D., J.N. Cambre, and B.S. Sumerlin, *Future perspectives and recent advances in stimuli-responsive materials*. Progress in Polymer Science, 2010. **35**(1–2): p. 278–301.
64. Liu, F. and M.W. Urban, *Recent advances and challenges in designing stimuli-responsive polymers*. Progress in Polymer Science, 2010. **35**(1–2): p. 3–23.
65. Orlov, M., et al., *pH-responsive thin film membranes from poly(2-vinylpyridine): water vapor-induced formation of a microporous structure*. Macromolecules, 2007. **40**(6): p. 2086–2091.
66. Escalé, P., et al., *pH sensitive hierarchically self-organized bioinspired films*. Macromolecular Rapid Communications, 2011. **32**(14): p. 1072–1076.
67. Bormashenko, E., et al., *Single-step technique allowing formation of microscaled thermally stable polymer honeycomb reliefs demonstrating reversible wettability*. Polymers for Advanced Technologies, 2011. **22**(1): p. 94–98.
68. Cui, L., et al., *Polymer surfaces with reversibly switchable ordered morphology*. Langmuir, 2005. **21**(25): p. 11696–11703.
69. Su, B.-L., C. Sanchez, and X.-Y. Yang, Insights into Hierarchically Structured Porous Materials: From Nanoscience to Catalysis, Separation, Optics, Energy, and Life Science, in Hierarchically Structured Porous Materials. 2011, Wiley-VCH Verlag GmbH & Co. KGaA. p. 1–27.
70. Zhu, H.X., T.X. Fan, and D. Zhang, On the Optimal Mechanical Properties of Hierarchical Biomaterials, in Hierarchically Structured Porous Materials. 2011, Wiley-VCH Verlag GmbH & Co. KGaA. p. 621–631.
71. Hayakawa, T. and S. Horiuchi, *From angstroms to micrometers: self-organized hierarchical structure within a polymer film*. Angewandte Chemie, 2003. **115**(20): p. 2387–2391.
72. Escalé, P., et al., *Hierarchical structures based on self-assembled diblock copolymers within honeycomb micro-structured porous films*. Soft Matter, 2010. **6**(14): p. 3202–3210.
73. Muñoz-Bonilla, A., et al., *Self-organized hierarchical structures in polymer surfaces: self-assembled nanostructures within breath figures*. Langmuir, 2009. **25**(11): p. 6493–6499.
74. Geldhauser, T., et al., *Influence of the relative humidity on the demixing of polymer blends on prepatterned substrates*. Macromolecules, 2009. **43**(2): p. 1124–1128.
75. Hecht, U., C.M. Schilz, and M. Stratmann, *Influence of relative humidity during film formation processes on the structure of ultrathin polymeric films*. Langmuir, 1998. **14**(23): p. 6743–6748.
76. Boker, A., et al., *Hierarchical nanoparticle assemblies formed by decorating breath figures*. Nature Materials, 2004. **3**(5): p. 302–306.
77. Samanta, S., et al., *Multifunctional porous poly(vinylidene fluoride)-graft-poly(butyl methacrylate) with good Li + ion conductivity*. Macromolecular Chemistry and Physics, 2011. **212**(2): p. 134–149.
78. Ma, H., et al., *Fabrication of freestanding honeycomb films with through-pore structures via air/water interfacial self-assembly*. Chemical Communications, 2011. **47**(4): p. 1154–1156.
79. Deleuze, C., et al., *Hierarchically structured hybrid honeycomb films via micro to nanosized building blocks*. Soft Matter, 2012. **8**(33): p. 8559–8562.
80. Madej, W., et al., *Breath figures in polymer and polymer blend films spin-coated in dry and humid ambience*. Langmuir, 2008. **24**(7): p. 3517–3524.
81. Connal, L.A. and G.G. Qiao, *Preparation of porous poly(dimethylsiloxane)-based honeycomb materials with hierarchal surface features and their use as soft-lithography templates*. Advanced Materials, 2006. **18**(22): p. 3024–3028.
82. Connal, L.A., et al., *Fabrication of reversibly crosslinkable, 3-dimensionally conformal polymeric microstructures*. Advanced Functional Materials, 2008. **18**(20): p. 3315–3322.
83. Connal, L.A. and G.G. Qiao, *Honeycomb coated particles: porous doughnuts, golf balls and hollow porous pockets*. Soft Matter, 2007. **3**(7): p. 837–839.
84. Ding, J., et al., *Constructing honeycomb micropatterns on nonplanar substrates with high glass transition temperature polymers*. Journal of Colloid and Interface Science, 2012. **380**: p. 99–104.

85. Greiser, C., S. Ebert, and W.A. Goedel, *Using breath figure patterns on structured substrates for the preparation of hierarchically structured microsieves*. Langmuir, 2008. **24**(3): p. 617–620.
86. Kwak, G., et al., *Nanoporous, honeycomb-structured network fibers spun from semiflexible, ultrahigh molecular weight, disubstituted aromatic polyacetylenes: Superhierarchical structure and unique optical anisotropy*. Chemistry of Materials, 2006. **18**(23): p. 5537–5542.
87. Zheng, J., et al., *Construction of hierarchical structures by electrospinning or electrospraying*. Polymer, 2012. **53**(2): p. 546–554.
88. Fashandi, H. and M. Karimi, *Pore formation in polystyrene fiber by superimposing temperature and relative humidity of electrospinning atmosphere*. Polymer, 2012. **53**(25): p. 5832–5849.
89. Nishida, J., et al., *Preparation of self-organized micro-patterned polymer films having cell adhesive ligands*. Polymer Journal, 2002. **34**(3): p. 166–174.
90. Stenzel-Rosenbaum, M.H., et al., *Porous polymer films and honeycomb structures made by the self-organization of well-defined macromolecular structures created by living radical polymerization techniques*. Angewandte Chemie International Edition, 2001. **40**(18): p. 3428–3432.
91. Min, E.H., et al., *Thermo-Responsive Glycopolymer Chains Grafted onto Honeycomb Structured Porous Films via RAFT Polymerization as a Thermo-Dependent Switcher for Lectin Concanavalin A Conjugation*. Journal of Polymer Science Part a-Polymer Chemistry, 2010. **48**(15): p. 3440–3455.
92. Min, E., K.H. Wong, and M.H. Stenzel, *Microwells with Patterned Proteins by a Self-Assembly Process Using Honeycomb-Structured Porous Films*. Advanced Materials, 2008. **20**(18): p. 3550–3556.
93. Chen, P.-C., et al., *Honeycomb-Patterned Film Segregated with Phenylboronic Acid for Glucose Sensing*. Langmuir, 2011. **27**(20): p. 12597–12605.
94. Wang, B., et al., *Glucose-Responsive Micelles from Self-Assembly of Poly(ethylene glycol)-b-Poly(acrylic acid-co-acrylamidophenylboronic acid) and the Controlled Release of Insulin*. Langmuir, 2009. **25**(21): p. 12522–12528.
95. Liu, Y., et al., *Specific Detection of d-Glucose by a Tetraphenylethene-Based Fluorescent Sensor*. Journal of the American Chemical Society, 2010. **133**(4): p. 660–663.
96. Matsumoto, A., R. Yoshida, and K. Kataoka, *Glucose-Responsive Polymer Gel Bearing Phenylborate Derivative as a Glucose-Sensing Moiety Operating at the Physiological pH*. Biomacromolecules, 2004. **5**(3): p. 1038–1045.
97. Beattie, D., et al., *Honeycomb-structured porous films from polypyrrole-containing block copolymers prepared via RAFT polymerization as a scaffold for cell growth*. Biomacromolecules, 2006. **7**(4): p. 1072–1082.
98. Duan, S., et al., *Osteocompatibility evaluation of poly(glycine ethyl ester-co-alanine ethyl ester)phosphazene with honeycomb-patterned surface topography*. Journal of Biomedical Materials Research Part A, 2013. **101A**(2): p. 307–317.
99. Nishikawa, T., et al., *Honeycomb-patterned thin films of amphiphilic polymers as cell culture substrates*. Materials Science and Engineering: C, 1999. **8–9**(0): p. 495–500.
100. Tanaka, M., et al., *Design of novel biointerfaces (II). Fabrication of self-organized porous polymer film with highly uniform pores*. Bio-Medical Materials and Engineering, 2004. **14**(4): p. 439–446.
101. Tsuruma, A., et al., *Morphological changes in neurons by self-organized patterned films*. e-Journal of Surface Science and Nanotechnology, 2005. **3**.
102. Tanaka, M., et al., *Control of hepatocyte adhesion and function on self-organized honeycomb-patterned polymer film*. Colloids and Surfaces A: Physicochemical and Engineering Aspects, 2006. **284–285**: p. 464–469.
103. Tanaka, M., et al., *Effect of pore size of self-organized honeycomb-patterned polymer films on spreading, focal adhesion, proliferation, and function of endothelial cells*. Journal of Nanoscience and Nanotechnology, 2007. **7**(3): p. 763–772.

104. Yamamoto, S., et al., *Relationship between adsorbed fibronectin and cell adhesion on a honeycomb-patterned film*. Surface Science, 2006. **600**(18): p. 3785–3791.
105. Tsuruma, A., et al., *Control of neural stem cell differentiation on honeycomb films*. Colloids and Surfaces A: Physicochemical and Engineering Aspects, 2008. **313–314**: p. 536–540.
106. Arai, K., et al., *Effect of pore size of honeycomb films on the morphology, adhesion and cytoskeletal organization of cardiac myocytes*. Colloids and Surfaces A: Physicochemical and Engineering Aspects, 2008. **313–314**(0): p. 530–535.
107. Sato, T., et al., *Effect of honeycomb-patterned surface topography on the function of mesenteric adipocytes*. Journal of Biomaterials Science, Polymer Edition, 2010. **21**: p. 1947–1956.
108. Wu, X. and S. Wang, *Regulating MC3T3-E1 Cells on Deformable Poly(epsilon-caprolactone) Honeycomb Films Prepared Using a Surfactant-Free Breath Figure Method in a Water-Miscible Solvent*. Acs Applied Materials & Interfaces, 2012. **4**(9): p. 4966–4975.
109. Du, M., et al., *Honeycomb self-assembled peptide scaffolds by the breath figure method*. Chemistry—A European Journal, 2011. **17**(15): p. 4238–4245.
110. Fukuhira, Y., et al., *Prevention of postoperative adhesions by a novel honeycomb-patterned poly(lactide) film in a rat experimental model*. Journal of Biomedical Materials Research Part B-Applied Biomaterials, 2008. **86B**(2): p. 353–359.
111. Sanz de Leon, A., J. Rodriguez-Hernandez, and A.L. Cortajarena, *Honeycomb patterned surfaces functionalized with polypeptide sequences for recognition and selective bacterial adhesion*. Biomaterials, 2013. **34**(5): p. 1453–60.

# Chapter 10
# Polymer Brushes with Precise Architectures for Molecular Biorecognition

**Mónica Pérez-Perrino, Serena Molina and Rodrigo Navarro**

## 10.1 Introduction

In several biomedical devices, such as biosensors, microarrays, there is an increasing demand for the selective identification of specific biomolecules in extremely complex mixtures, such as blood, urine, plasma, saliva, etc. In those mixtures of biological molecules, their identification and quantification are based on selective molecular recognition processes, which take place on several platforms, biosensors, or microarrays. The development of these devices has attracted substantial interest from researchers from several scientific disciplines—biology, chemistry, and physics, to name a few. Due to the ability of these systems to analyze a large number of interesting biomolecules in parallel, such as nucleic acids, peptides, proteins, or carbohydrates, the researchers can extract valuable information, which can further be used for the development of new drug targets, or to identify biomarkers or specific altered genes. Nowadays, the recent developments in these research areas allow for the prediction of individual drug responsiveness, and the personalization of therapeutic strategies.

Another important research line in biorecognition processes is based on the preparation and development of smart surfaces that can mimic the dynamic properties of extremely complex biological systems. Therefore, these surfaces could be able to modulate biomolecular activity, protein immobilization, and cell adhesion and its migration. For instance, during a tissue regeneration process, the adhesion and interaction of cells with their extracellular environment is mainly governed by cell–cell and cell–extracellular matrix connections. Due to the extremely complex nature

R. Navarro (✉) · S. Molina
Macromolecular Department, Institute of Polymer Science and Technology (ICTP-CSIC), Juan de la Cierva, 3, 28006 Madrid, Spain
e-mail: rnavarro@ictp.csic.es

M. Pérez-Perrino
Glycosystems Laboratory, Instituto de Investigaciones Químicas (IIQ), CSIC-Universidad de Sevilla, Av. Américo Vespucio 49, 41092 Seville, Spain



J. Rodríguez-Hernández, A. L. Cortajarena (eds.), *Design of Polymeric Platforms for Selective Biorecognition,* DOI 10.1007/978-3-319-17061-9_10

of these interactions, the researchers have developed extracellular matrix (ECM) model systems, which significantly reduce the complex character of these interactions but are able to mimic to a certain degree the in vivo situation. The introduction of specific biomolecular cues, which mimic certain aspects of the structure or function of natural ECM by selective recognition processes, allows the opportunity to simplify and control the cell interactions with their environments. This finally leads to an understanding of the nature and magnitude of those interactions that occur in biological processes. The chemistry used for the immobilization of bioprobe target molecules on the substrate plays a significant role in the success of any experiment. Various types of functional surfaces, such as self-assembled monolayers, polymer networks, or polymer brushes, are generally used as functional scaffolds for the chemical immobilization of biomolecules.

This chapter highlights the recent developments in surface science and polymer brush technology with applications in biomolecular recognition and their use in sensing, with a particular attention on their relevance for biological applications. The main aim of this chapter is to describe how polymer brushes can be tailored to optimize the selective interaction between incoming guest biomolecules in solution and their corresponding host molecules, which are bound to those polymeric brush layers. This significant chapter begins with a brief, but essential, introduction of polymer brush technology, followed by another short discussion about nonspecific adsorption of proteins. From there on, the following sections will be devoted to recent advancements in designing and fabricating brush scaffolds that can interact specifically with biomolecules for cell adhesion and attachment of biomolecules (protein, carbohydrate molecules).

## 10.2 Synthesis of Polymer Brushes

Research in surface-grafted polymers has fascinated physicists, chemists, and biologists for their synthetic approaches, characterization methods and biomedical applications for nearly half a century. These surface-anchored macromolecular architectures, in which the polymeric assemblies are tethered at one end to a solid substrates, are referred to as polymer brushes [1].

Initially, much of the scientific interest in polymer surfaces and interfaces originated from their importance for different technological aspects, such as wettability, absorption, or recognition of biomolecules, among other examples. For several years now research in polymer science has spread out to several material science and engineering disciplines, especially in biotechnology [2]. The introduction and advent of new polymerization techniques that allow for the preparation of tailor-made polymer brushes have significantly accelerated this tendency. Less-demanding synthetic protocols facilitating scientific community-wide access to a macromolecular design toolkit so far believed to be exclusive domain of polymer chemists. [3, 4] During the 1970s, the immobilization of target biomolecules onto polymer thin films prompted and attracted much attention because it made possible

to immobilize bioactive molecules (proteins, enzymes, nucleic acids) and design-functionalized polymer coatings for suitable biomedical devices (microarrays, biosensors). This in turn fostered the possibility to screen complex mixtures of proteins with its concomitant expansion in polymer science for biorecognition processes. More recently, functional polymer brushes have been extensively utilized, as reactive scaffolds for molecule biorecognition, due to their robustness, high versatility, and flexibility to create tailor-made polymer thin films. The development of macromolecular surface chemistry allows for the control of the polymeric thickness, grafting density, and chemical composition of the surface or interphase. The architecture of surface-grated polymer coating can also be controlled and even addressed using rather simple and well-known experimental settings.

Basically, surface-confined macromolecular films can typically be prepared by two main routes, physisorption or covalent attachment. The physical adsorption (physisorption) of end-capped functionalized polymer chains onto a surface can be applied from solution or chemical vapor deposition. This "grafting to" approach requires the tethering of preformed polymer chains onto the substrate. Due to the strong development of synthetic protocols, this strategy, in principle, is easy to perform from a chemical point of view; however, it often suffers from low grafting densities. It should be noted that this complication inherent to "grafting to" processes is due to kinetic and thermodynamic factors. With increasing coverage of the surface with grafted chains, the polymer concentration at the interface quickly becomes larger than the concentration of polymer in solution. The incoming polymer chains must diffuse against this concentration gradient that constantly increases with increasing grafting density of the already attached polymer chains. Owing to this steric repulsion, this diffusion process slows down the immobilization reaction at the surface further as the grafting reaction proceeds. Thus, the rate of the reaction levels off rather quickly and further polymer chains are linked to the substrate only at an extremely slow rate due to this kinetic hindrance. It should also be noted that the attachment of free chains to a strongly covered surface becomes unfavorable also for thermodynamic reasons. At high grafting densities, the surface-attached polymer chains are in a rather stretched conformation due to the presence of strong segment–segment interactions. This leads to an entropy loss state during this conformational rearrangement; however, this is only compensated by the establishment of one chemical bond, namely the one connecting the polymer to the surface. Hence, the higher the graft density of the chains at the surface, the stronger will be the entropy penalty and this rapidly precludes the attachment of further chains.

On the other hand, the *grafting from* strategy allows the formation of polymeric chains from a substrate which has previously been decorated with initiator molecules. The polymer chains grow directly from the reactive sites of the decorated surface. This so-called surface-initiated polymerization (SIP) has been used to prepare thick polymer films that are covalently tethered to the substrate with high graft density. This approach presents a strong control over the molecular architecture of polymer films because it can be implemented with almost all available polymerization techniques, free and controlled radical polymerization, such as reversible addition fragmentation transfer (RAFT) [5–7], nitroxide-mediated polymerization

(NMP) [8], atom transfer radical polymerization (ATRP) [3, 9, 10], anionic and cationic polymerization, and ring-opening polymerization [11–13], just to name a few examples.

Regardless of the synthetic route, another appealing aspect of surface-tethered polymer films is that they are fully compatible with a wide range of technologically relevant substrates, going far beyond the classical silicon wafer, gold nanoparticles, and porous membranes. The resulting polymer brush layers possess properties that suffer significantly from the underlying substrates.

## 10.3 Nonspecific Adsorption on Surfaces

The adsorption of biological material (proteins, cells) physically onto surfaces without specific receptor recognition is called *nonspecific adsorption*. This type of contamination strongly affects the efficacy and reliability, increasing undesirable features such as high background noise or *false* positive. The study and development of strategies for controlling the interface between surfaces and biological materials present an important issue in a wide range of settings, for instance, medical devices, biosensors, contact lenses, as well as polymeric membranes for water treatments. Polymer brushes appear as promising and attractive candidates for tailor-made surfaces with nonspecific biofouling resistance. Controlling the surface-initiation polymerization with "living" polymerization techniques, thickness, composition, and architecture of polymer brush coatings are well-defined. Hydrophilic polymer brushes can easily form ultrathin hydrated coatings that provide an effective enthalpic and entropic barrier to nonspecific protein adsorption [14, 15]. It is well accepted that proteins adsorb onto a hydrophilic polymer brush, and water molecules can easily release into the bulk. As a consequence, the surface-tethered chains will be compressed. The increase of enthalpy due to chain dehydration and the decrease in entropy due to chain compression (even though the later term may be small) are both unfavorable and provide the thermodynamic basis for non-biofouling properties of the coating.

Non-biofouling polymer brushes can be subdivided into two groups. The first group is obtained by neutral monomers and the second class is obtained using zwitterionic monomers.

### *10.3.1 Neutral Non-biofouling Polymer Brushes*

Probably one of the most used materials for biofouling resistance is Poly(ethylene glycol) (PEG) because of its well-known capacity to resist nonspecific adhesion and its nontoxic and nonimmunogenic character. A PEGylated brush surface is typically prepared by a "grafting to" approach, in which an end-capped functional PEG chain is able to bind specifically with the surface. Different synthetic strategies have been described. [16] The second class of PEGylated surfaces is based on PEG-containing

monomers. This second approach has been widely used by different researchers, where monomers with PEG side-chain were efficiently polymerized by several controlled radical polymerization techniques (ATRP [17], NMP, etc.). Andruzzi et al. [18] described the preference for nitroxide-mediated CRP over ATRP due to the fact that the former process is free of metal catalysts. The metal traces could trigger undesired side effects in many biological applications.

In these PEGylated surfaces, the non-biofouling properties are mainly determined by the brush thickness, grafting density [19], and the length of the PEG side chains. With regard to the length of PEG-side chains, copolymers brushes of 2-(2-methoxyethoxy) ethyl methacrylate ($MEO_2MA$) and oligo(ethylene glycol) methacrylate (OEGMA) have become more important because of their thermoresponsive property under physiological conditions. The lower critical solution temperature (LCST) observed in these systems can be easily adjusted by changing the composition of the copolymer chains [20]. Laschewsky et al. [21], for example, demonstrated the attachment, proliferation, and detachment of 3T3 mouse fibroblasts onto these biocompatible copolymer brushes. The behavior was controlled by temperature cycles around the LCST of the macromolecular platform. In a similar fashion, Dey et al. described the use of these thermorresponsive copolymer brushes as responsive platforms for culturing mouse embryonic stem cells (mESCs) and the control of their attachment/detachment to the substrate [22]. Wei et al. demonstrated the ability of these surfaces to confer an osteogenetic capacity to the modified substrates [23]. While it can be argued that PEGylated surfaces have become a first choice strategy for avoiding nonspecific adsorption on surface coatings, concern exists that these PEGylated surfaces can also increase complement activation and induce a specific recognition of their corresponding antibodies (anti-PEG IgM) [24–28].

Another important issue is related to the long-term stability of non-biofouling polymer brushes, because this aspect determines the lifetime of biomedical devices. Merssersmith et al. [29] studied the influence of the PEG side chain length over fibroblasts immobilization during 80 days. During the first three weeks, all brushes effectively prevented cell attachment. However, after that, the influence of the chain length became evident; the shortest chains showed their non-biofouling capacity for 28 days, the other two types of PEG-chains were stable for more than 35 days. For the longest chains, a cell monolayer was formed after 11 weeks. These findings suggested that the loss of non-biofouling properties could be due to the degradation of the ethylene glycol side chains, detachment of grafted PEG chains from the surface, or hydrolysis of the binding group to the surface.

Recently, Kitano et al. [30] prepared a polymer brush with pendent D-glucosylurea groups (Poly(glucosylureaethyl methacrylate), PolyGUMA)) that was obtained by RAFT polymerization of GUMA monomer on a glass substrate. Their findings have indicated that the PolyGUMA brush layer was significantly resistant against nonspecific adsorption of albumin and lysozyme. Furthermore, the adhesion of cells, such as HEPG2 and HEK93, was strongly suppressed by the presence of this brush coating. The glucosylurea group might be quite useful to provide a neutral non-biofouling surface in biomedical fields.

### *10.3.2 Charged Non-biofouling Polymer Brushes*

In addition to the neutral polymer brushes discussed in the previous section, a second major class of non-biofouling polymer brushes present charges in their chemical structure. In principle, two types of charged monomers can be described: pH-dependent and pH-independent monomer types.

For pH-independent types, several researchers have extensively studied the non-biofouling properties of monomers bearing positive and/or negative charges, such as ammonium, phosphonium, and sulfonate groups. Polymeric materials with quaternary ammonium groups have been widely used as effective antibacterial agents. In principle, the lethal action of these polycationic disinfectants involves a sequence of steps that include a primary interaction with the bacterial cell surface (they are usually negatively charged) followed by diffusion through the cell wall. These processes lead to the binding to the cytoplasmic membrane, which in turn promotes the disruption of the cytoplasmic membrane. In the case of polycationic polymer brushes, the interaction with the cell surface is expected to take place to a greater extent than that of monomeric cationic units because of the much higher density of the surface-grafted polymers. Within this framework, interesting research has been undertaken by Feng et al. [31] who tried to gain insight into the rational design of polymer brushes as nonthrombogenic polymeric coatings. To this end, a biomimetic monomer (2-methacryloyloxyethyl phosphorylcholine (MPC)) was polymerized from $SiO_x$ at room temperature using the ATRP approach. Phosphorylcholine is the major component outer surface of the erythrocyte membrane. The findings of this study demonstrated the effectiveness of these biomaterial coatings reducing nonspecific adsorption of proteins, cells, bacteria, and platelets. In other studies on these biomimetic monomers, the adsorption of binary (fibrinogen/lysozyme) protein mixtures was evaluated. The results indicated that the adsorbed protein ratio was equal to the feed concentration, suggesting that this biopolymer material shows the same efficiency in preventing the adsorption of small (lysozyme) and large (fibrinogen) proteins. Furthermore, protein adsorption has been carried out in the outermost layer so that the penetration through the graft layer to the silicon interface was avoided. For this type of surface, an increase in the polymer thickness and grafting density produces an increase in the hydrophilicity (measured by water contact angle), what leads to improved protein resistance, as was the case of PEGylated polymer brushes described above.

A well-studied polymeric system is based on the cationic 2-(methacryloyloxy ethyl trimethylammonium chloride) (METAC). In this system in charge repulsion of the chains and excluded volume effects from solvation dominate in the absence of electrolyte, causing the surface to be hydrophilic, what implies improved non-biofouling properties. However, when electrostatic screening of the cationic charges takes place in the electrolyte solution, the polymer chains collapse into a more entropically favorable coiled conformation [32, 33].

Not only positive charges can present an antifouling character, there are other functional groups bearing negative charges that also present a marked antifouling character. Huck's group has investigated sulfopropyl methacrylate brushes

containing silver cations [34]. While this $Ag^+$ loaded system was effective for preventing bacterial colonization, a subsequent paper showed that the effective silver concentrations were also cytotoxic towards mammalian cells. One aspect when using ions as killing agent is in their ability to leach out of the brush. While this phenomenon does create a zone of inhibition around the substrate, which might be useful in some applications and can be controlled by using different types of silver compounds, other situations will call for a well-controlled area of biocide activity. In these cases, biocide agents other than ions must be used. In another study, Bernard et al. [35] prepared surface-grafted copolymers bearing 3-sulfopropyl methacrylate potassium salt and (2-methacryloyloxy)ethyl) trimethylammonium chloride moieties. The copolymer brushes were prepared by a surface-initiated ATRP process. The non-biofouling character of these copolymers was demonstrated.

Polymer brushes bearing betaine containing monomeric structures have been widely used as active non-biofouling coatings. Monomers, such as sulfobetaine methacrylate or carboxybetaine methacrylate, were easily polymerized using a surface-initiated controlled radical polymerization approach. Polymer brushes with sulfobetaine units have been demonstrated to withstand nonspecific adsorption of fibrinogen even under conditions of high ionic strength conditions at 37ºC and pH values ranging from 5 to 11 [36]. At pH values below 5, some fibrinogen adsorption occurred even though the polymer brushes display a very hydrophilic surface at that pH. The increased nonspecific adsorption at these low pH values was attributed to protein denaturation.

Other example of sulfo-derivate monomers with non-biofouling properties are based on sulfonated sugar residues that mimic the natural heparin. Heparin is a highly sulfonated glycosaminoglycan and commonly used for modifiying blood-containing surfaces (in vivo and in vitro). Ayeres et al. [37] have synthetized polymer brushes with nonthrombogenic character, using ATRP methods. The sulfonated polymer brush coating exhibited better assay performance in these blood component assays than the unsulfonated sugar functionalized surface-tethered chains in all tests performed. The results also described that the sulfonated brushes reduced the production of complement factor products C3a, C4a, and C5a, in comparison to the control and pristine surfaces.

In addition to the charged polymer brushes, the second class of monomers is pH-dependent. Interesting research has been carried out by Murata et al. [38] to gain insight into the rational design of poly(quaternary ammonium) brushes to be used as antimicrobial polymeric coatings on inorganic surfaces. To this end, poly(2-dimethylamino-ethyl methacrylate) (PDMAEMA) brushes displaying precise control over molecular weight and grafting density were quaternized with alkyl bromides to obtain polymer brushes bearing quaternary ammonium groups, a surface with antimicrobial activity. The experimental evidence indicates that surface charge density is a critical element for attaining macromolecular surfaces displaying maximum kill efficiency. In this context, they showed that short chains with high grafting density and long chains with low grafting density are equally effective against *Escherichia coli*.

Patrucco et al. made use of Poly(Glycerol monomethacrylate-*co*-Dimethylamino ethyl methacrylmide) P(GM-co-DMAEMA) brushes to tune cellular adhesion for tissue substrates [39]. The researchers modified tissue culture PS with a macroinitiator, and then grew the copolymers in varying compositional ratios. PGM prevents cell adhesion by creating a non-biofouling surface, whereas DMAEMA will promote cell adhesion at physiological pH values. Their results demonstrate that PGM homopolymer is a nontoxic and nonadhesive material for cell growth. Unfortunately, the group could not determine the composition of the P(GM-co-DMAEMA) copolymers. Nonetheless, the cells show morphologies similar to the ones that have come in contact with adhesive after exposure to the copolymer brushes.

Madkour et al. [40] reported another route to biocidal activity using butoxycarbonyl-aminoethylmethacrylate (Boc-AEMA) brushes. After growth and removing the protecting group, the surface-grafted polymer coating presented its amino groups as pendant side chains. Brushes with thicknesses between 3 and 50 nm and a broad range of grafting densities killed 100 % *E. coli* and *Staphylococcus* bacteria exposed to the biocidal surface.

## 10.4 Cell Adhesive Surfaces

Nowadays, the development of novel and alternative strategies for controlling the interface between cells and materials is important in a wide range of settings. For instance, in tissue engineering and regenerative medicine the surface of artificial biomaterials plays a key role in guiding and directing cellular behavior and function. This branch of bioengineering has emerged as an important field of research over the past decade and promises to revolutionize medical treatments [41]. The cell adhesion process is mainly governed by extremely complex cell–cell and cell–environment interactions. In order to induce the adhesion of cells onto surfaces or scaffolds, biospecific cues must be immobilized and accessible because they can mimic the structure of natural ECM by their selective biorecognition. It is well known that polymer brushes have played a keystone in bringing the potential of tissue engineering technology and other biomedical disciplines to fruition. Considering the cell-adhesion issue, this type of surfaces can be subdivided into three groups:

A). Non-biofouling polymer brushes that contain an extracellular matrix (ECM) protein of a cell adhesion peptide derived thereof.
B). Patterned non-biofouling polymer brushes that have been used to control geometrically the cell adhesion process.
C). Thermo-responsive polymer brushes that possess a lower critical solution temperature (LCST) and can be thermally triggered to change from a hydrophobic cell adhesive state to a hydrophilic non-biofouling state.

Each of these classes will be discussed in more detail below.

### 10.4.1 Polymer Brushes Functionalized with ECM Peptide/Protein

The decoration of substrate surfaces with a surface-grafted non-biofouling polymer layer that contains bioactive short peptide sequences leads to an efficient cell adhesion by specific cell surface biorecognition. Probably one of the most widely used cell attachment peptides is based on the *arginine-glycine-aspartic acid* (RGD) sequence, because it is found in numerous adhesive proteins and is believed to be the main domain binding to the integrins on the cell membranes [42]. Klok et al. explored the functionalization of polymer brushes with RGD peptide in order to promote endothelialization of blood-contacting biomaterials. Poly (2-hydroxyethyl methacrylate) or Poly(poly(ethylene glycol) methacrylate) (PPEGMA) were used as macromolecular platforms suppressing nonspecific adhesion of proteins and cells and exposing hydroxyl groups for further conjugation of RGD-containing peptide ligands. Their findings demonstrated a clear improvement over neat polymer brushes, because human umbilical vascular endothelial cells (HUVECs) were able to adhere and spread rapidly on the RGD-bearing surface as well as to retain homeostasis when exposed to shear stresses that simulated arterial blood flow. Furthermore, the authors also observed differences in size and morphology of focal adhesions between HUVECs immobilized on PHEMA and PPEGMA brushes. These differences were attributed to the length of the ethylene glycol spacer and hydrophilicity of the PPEGMA brushes, which ultimately leads to increased ligand mobility and reduced recognition efficiency. This group has described the synthesis of these RGD-bearing PPEGMA on polyethylene, which is a non-biofouling surface and widely used in the biotechnological industry [43]. Recently, these authors have also reported osteoblast adhesion studies, applying the same attractive strategy [44]. The RGD sequences were incorporated on poly(2-hydroxyethyl methacrylate-co-2-(methacryloyloxy) ethyl phosphate) (P(HEMA-co-MEP)) brushes. The RGD units have improved osseointegration of osteoblast cells and the phosphate groups were able to mimic the function of naturally bonded extracellular matrix-phosphorylated protein. Navarro et al. [45] immobilized RGD on the PMAA brushes and explored the effect of the spatial arrangement of the RGD sequence along the polymer brush on the adhesion of MG63 osteoblasts. The incorporation of this bioactive peptide was carried out using an EDC/NHS protocol. Whether the RGD sequence was situated at the outer most layer or at greater depth (about 15 nm) had very little influence on cell density and viability, however, the cell morphology was affected. On samples decorated with RGD moieties on the surface, the authors observed that cells spread well with marked focal adhesion points at the periphery of the cytoplasm, whereas in the case of samples where RGD was situated in deeper layers, cells were found to adopt a rounded morphology and focal adhesion concentrated towards the internal part of the cell. The change of the cellular morphology was probably due to the fact that the cells tended to reach the RGD units. (Fig. 10.1)

The functionalization of PMAA with RGD units was also carried out by Metters et al. [46], who studied the cell adhesion of 3T3 fibroblast on such reactive surfaces.

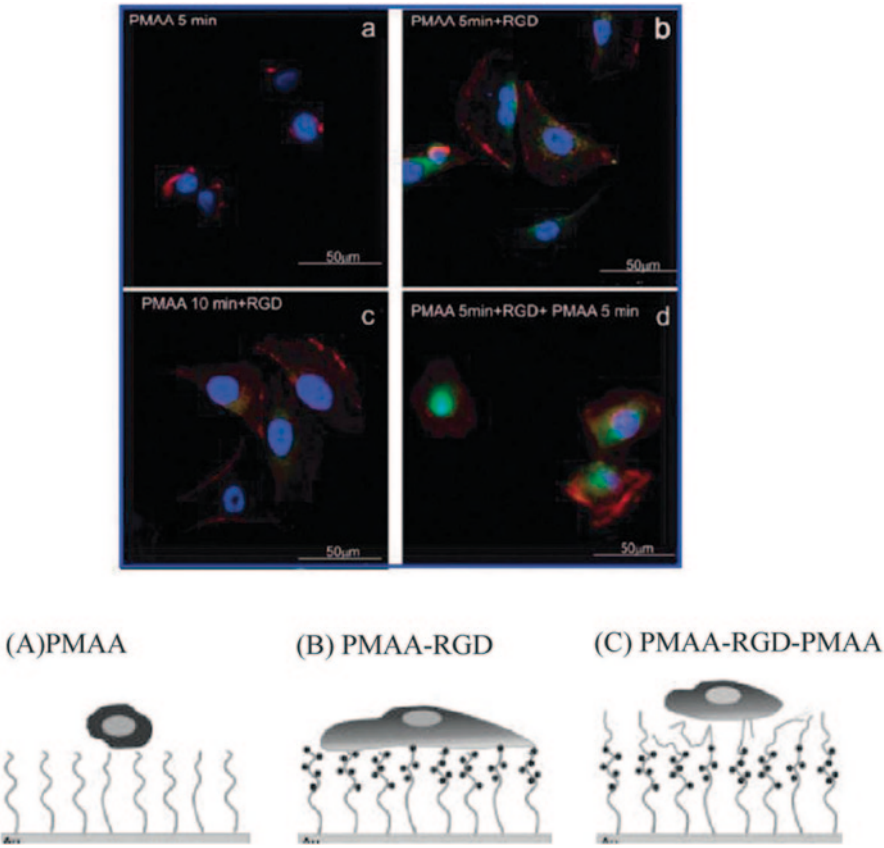


**Fig. 10.1** (*top panel*) Immunofluorescence images of MG63 cells on various types of surfaces. (*bottom* panel) the morphological changes of MG63 cells on a pure PMAA brush layer without RGD units, and with RGD at different depths. ©2008 American Chemical Society

This type of cells was also studied on PPEGMA modified with RGD sequences [47]. It will be interesting to follow the progress of RGD-functional biomaterials in in vivo studies. While promising examples exist [48], other reports [49] showed RGD-functional quantum dots being taken up primarily through the liver, spleen, and bone-marrow rather than tumors that should over express RGD receptors. Furthermore, it is well known that platelets also bind the RGD sequence through glycoprotein receptors [50, 51]. Petrie et al. have studied the immobilization of this bioactive peptide and glycoprotein ($\alpha_5\beta_1$-integrin) on clinical-grade titanium implants with a non-biofouling surface-grafted PEG coating [52]. Their results have demonstrated that the immobilization of a specific fibronectin fragments enhanced osteoblast differentiation and improved functional implant osseointegration compared to RGD-functionalized or pristine Ti-substrates. Later on, the same group has decorated [53] Ti-surfaces with another bioactive peptide motif, which also induces

cell adhesion. Recently, He et al. [54] have immobilized this peptide sequence on Polyvinylidene fluoride (PVDF) films. These surfaces were initially activated with poly(glycidyl methacrylate) chains using an ATRP polymerization process, starting from secondary fluorine atoms. After the incorporation of azide groups, by ring opening of oxirane rings, the RGD sequences were efficiently immobilized on PVDF films by a "click-chemistry" protocol. The as-synthetized PVDF-g-PGMA-click-RGD surfaces were found to promote the cell attachment and proliferation of adipose-derived stem cells (ASCs), as compared to the pristine PVDF and PGMA-grafted film surfaces. In addition, the in vitro cell studies have also demonstrated that the cell proliferation rate and coverage of this type of cells on decorated surfaces are correlated to the surface concentration of the RGD moieties.

Many adhesive proteins present in extracellular matrices and in the blood contain arginine-glycine-aspartic acid (RGD) as their cell recognition site [55, 56]. Hence, short synthetic peptides containing the RGD sequence have been also used to improve the cell attachment properties of biomaterials. However, the RGD peptide adhesion ligand for members of the integrin family of cell-surface receptors is found in most cells and hence is not cell-specific. On the other hand, the Arg-Glu-Asp-Val (REDV) peptide sequence is known to be selective for endothelial cells (ECs) [57] as it is specifically recognized by integrin α4β1, which is expressed in abundance by ECs but not by other cell types. The decoration of titanium surfaces with this type of active oligopeptide was carried out by Choong et al. [58], who studied the cell adhesion of human umbilical vascular endothelial cells (HUVECs) by selective biorecognition of REDV sequences. The polymer brush chains were obtained by ATRP polymerization using a DOPA-modified surface and the immobilization of peptide groups was carried out by the activation of –OH groups with carbonyldiimidazol (CDI). The findings of this study showed that the proliferation and attachment of HUVECs were substantially improved by the conjugation of PEG brush chains with REDV units, while no significant effects were observed for other types of cells (mesenchymal stem cells, MSCs), what confirms the bioselective recognition of REDV for the integrin α4β1 presented in HUEVCs. The authors have also studied the platelets adhesion with these REDV-decorated surfaces. The immobilization of this peptide increases the hemocompatibility of the surface materials.

Other peptide motif might be used to achieve the adhesion of specific cell lines by bioselective recognition. This is the case of the GFOGER sequence (where O stands for hydroxyproline) that represents the minimal binding site in collagen and is specifically recognized by the integrins $\alpha_2\beta_1$ and $\alpha_1\beta_1$. The peptide molecule was efficiently grafted to a 2-glucanoamidoethyl methacrylate (GAMA) polymer brush, which has been previously synthetized by surface-initiated atom transfer radical polymerization (SI-ATRP). The results showed that a tethered GFOGER-containing peptide polymer brushes induced confluent well-spread osteoblast cells with improved bone formation and differentiation, whereas pristine poly(GAMA) brushes prevent cell adhesion. [59]

The wide variety of immobilized biomolecules which lead to cell-adhesion are also based on the use of adhesive proteins such as fibrinogen [60] (FNG), fibronectin [52] (FN), vitronectin (VN), and von Willebrand factor (vWF). They are normal

components of blood plasma and may adsorb on biomaterial surfaces after surgical interventions inserting implants and scaffolds for tissue engineering. In these ECM proteins, an RGD motif is easily found and biorecognized by a set of integrin family proteins. As mentioned above, the specific interactions of these ECM proteins and integrins, by the recognition of the RGD unit, are known to trigger a cascade of overlapping reactions, including cell attachment, cell spreading, or cytoskeletal reorganization.

Alternatively, other bioactive cues have been also proposed for cell adhesion, for instance insulin. The immobilized insulin could also enhance proliferation and cell growth rather than facilitate cell adherence in the presence of serum proteins [61]. The immobilized insulin molecules sufficiently, and continuously stimulate their receptors and downstream signal transduction proteins without internalization of ligand-receptor complexes. Without serum, insulin is insufficient for stimulating cell growth, even in the presence of a cell-adherent protein.

Other target biomolecules are based on cell-surface saccharides, which also play an important role in numerous biological phenomena [62, 63]. High-surface carbohydrate density is a prerequisite for mimicking the multivalent interaction, or "glycoside cluster effect." A facile method for the construction of biosurfaces with high glycosyl density was reported by W. Song et al. [64] A silicon surface was first covered with polymer brushes containing "clickable" alkyne pendant groups prepared by SI-ATRP, and then a microwave assisted CuAAC reaction was adopted for immobilizing azido biomolecules onto the brushes. The authors investigated the interaction between these modified silicon wafers and two kinds of bacteria, *E. coli* and *S. aureus*. Their results showed that these carbohydrate-decorated surfaces maintained their functionalities and can be used to mimic cell surfaces by specific recognition of mannose units. Recently, Chernyy et al. [65] studied the morphology of human hepatocellular carcinoma cancer cells (HepG2) on the synthesized poly(LAMA) (poly(2-lactobionamidoethyl methacrylate)) brush on silicon wafer and glass slides. ToF-SIMS imaging of HepG2 cells on the poly(LAMA) brush revealed that the proteins were concentrated along the cell periphery whereas the protein distribution was uniform when a glass substrate is used.

### *10.4.2 Patterned Non-biofouling Polymer Brushes*

The combination of polymer brushes with lithographic techniques enables the creation of complex surfaces displaying compositionally controlled patterned domains. In order to make these scaffolds more similar to the extracellular matrix (ECM), it is important to take into consideration a huge number of cellular interactions, recognition sites, and communication events that takes place between the cell and the surrounding media. The position and orientation of immobilized peptides or proteins within these surface-grafted polymer layers have marked effects on the biorecognition, which allow the integrin receptors on the cell membrane to recognize the peptide sequences to promote the cell adhesion processes. For instance, there is evidence that topographical features such as grooves, ridges, and curvature

can easily induce an oriented cell adhesion, its subsequent proliferation, and even the cell morphology, exhibiting the shape of a micropatterned surface. It should be also possible to modify the patterned surface of the polymer brush with different micropattering techniques in order to improve features of the polymer brush as functionalized scaffold.

Cell adhesion and its subsequent proliferation onto functionalized surface materials can also be guided by specific cell surface receptor interactions with geometrically patterned polymer brushes. Chilkoti et al. [66], for example, have created a micropatterned PEG surface-grafted chain with circular and striped shapes using microcontact printing techniques. Then, during the incubation process the fibronectin was selectively adsorbed in those areas that were not covered with polymer chains, leading to spatial control of cell adhesion. Ober et al. [67], for example, have studied the localization of antidinitrophenyl-immunoglobulin-E sensitized RBL mast cells on patterned OligoPEG-modified polystyrene brushes with different feature sizes. Cell adhesion to these substrates was mediated by dinitrophenyl-bovine serum albumin (DNP-BSA), which was preadsorbed on areas not covered by the non-biofouling polymer brush. Linear patterns with feature sizes of 50 and 90 μm and a spacing of 50 μm showed a high degree of spatial control over cell adhesion. On patterns with a line width of 10 μm and a spacing of 30 μm, however, some regions showed cells located on the PEG surface between the DNP-BSA lines. This was attributed either to imperfections in the patterning process or to binding of cell across the DNP-BSA lines.

Photochemical reactions that go along with the change of shape/size of a molecule may also result in a stimuli-responsive behavior of the polymer brushes. The most commonly used feature is a cis–trans isomerization of an azobenzene molecule. Taking advantage of the change of the molecular dimensions in azobenzene, Kessler et al. [68] reported the control of cell adhesion properties of the RGD-functionalized surfaces. The azobenzene derivative was incorporated into the RGD tripeptide and tethered to a poly(methyl methacrylate) (PMMA) surface. Such photoswitchable brushes exhibited enhanced cell adhesion in the trans-azobenzene configuration. However, the surfaces irradiated at 366 nm showed a reduced cell plating efficiency as a result of the shortening of the distances from RGD to the surface due to the formation of an azobenzene cis isomer. This example demonstrates how biorecognition processes can be strongly affected with the accessibility and availability of target molecules.

### *10.4.3 Thermoresponsive Polymer brushes*

It is well known that poly(N-isopropylacrylamide) (PNIPAM) is a water-soluble thermo-responsive polymer that has been widely used in the preparation of stimuli-responsive cell culture surfaces for regulating cell adhesion and detachment [69–71]. According to its chemical composition, it exhibits a so-called lower critical solution temperature (LCST) of about 32ºC in an aqueous medium. Below the LCST, the PNIPAM chains adopt a random coil conformation (brush conformation

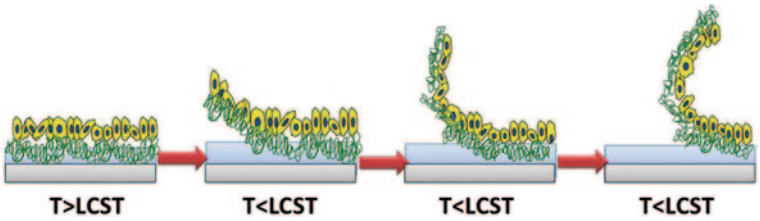


**Fig. 10.2** Schematic cartoon of cell-sheet detachment using temperature control from a thermoresponsive coating. From Nash et al. [69] © 2012 The Royal Society of Chemitry

and hydrophilic state), however, above the LCST the polymer chains exhibit a collapsed globular conformation (hydrophobic state). PNIPAM polymer brushes have been applied as supports for culturing and harvesting of cells enabling effective detachment of the intact cell sheets upon only small temperature variations [72–75]. Further developments on these surfaces are based on the immobilization of biospecific cues, such as collagen [76] and RGD-peptide sequence [71], on the PNIPAMm-grafted surfaces, which improve cell adhesion and proliferation above the LCST without destroying the cell detachment properties at lower temperatures (Fig. 10.2). This attractive switch of affinity between cells and PNIPAMm surfaces is mainly due to the fact that the surface swelling, wettabilities, and modulus of the PNIPAM surfaces can be changed by the temperature. The cell adhesion and detachment properties of PNIPAM-based polymer brushes can be tuned by engineering the architecture and composition of the brushes. Above the LCST of PNIPAM, the grafted polymeric chains collapse and the recognition of peptide units can take place, inducing cell attachment, spreading, and proliferation onto these surfaces. Below the LCST, hydrated polymer chains soften, expand, and swell, shielding the immobilized biomolecules from access, reducing the cell-surface attachment tension, and mechanically disrupting the cell-surface contacts [71, 77].

There are no functional groups in PNIPAM brushes to be used to tether biomolecules, however, RGD motifs or insulin have been immobilized on PNIPAM-*b*-PAA brushes through the reaction of the activated carboxylate of the PAA units and the $–NH_2$ groups in RGD or in the protein. The higher the content of the immobilized target biomolecules on the PNIPAM-grafted surfaces, the higher the density of the attached cells on the surface. However, too high contents of immobilized collagen [77] may weaken the interactions between the PNIPAM brush and the attached cells, hindering the complete recovery of the cell sheet. In this research line, Kröger et al. [78] have described theoretically the mechanism of biorecognition of integrin proteins with RGD units, which have been previously grafted to a PNIPAM brush. They have presented theoretical considerations concerning the grafting density of RGD units and their distribution throughout these surface-tethered chains to enable cell adhesion at 37ºC and efficient detachment at temperatures below LCST. These recent developments are directed towards cell sheet-based regenerative medicine and bring better control over the adhesive properties of this thermoresponsive active surface. Based on tissue regeneration processes, thermoactive surface-grafted chains that are able to discriminate between living and dead cells

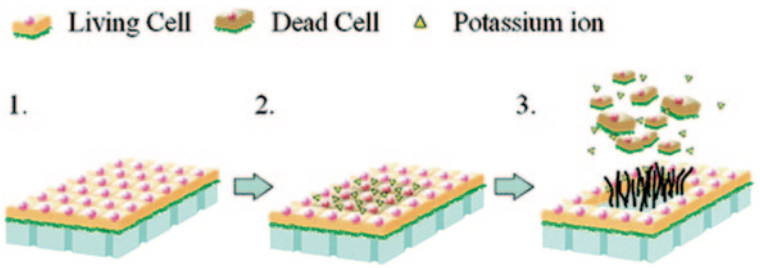


**Fig. 10.3** Selective release process of dead cells by recognition of potassium cations released from dead cells. From Yamaguchi et al. [79] © 2005 American Chemical Society

have been developed during the last decade. To distinguish between cells, the cell culture surface recognizes potassium ions which are released only from dead cells. As recognition sites of released ions grafted crown ether receptors were used, which favor the formation of a hydrated polymeric surface, what in turn leads to selective release of dead cells [79]. (Fig. 10.3)

However, the main drawback of this thermoresponsive polymer is that it is not bioinert and could induce cellular cytotoxicity, due to formation of cooperative hydrogen-bonding interactions with proteins [80, 81]. Random copolymers of di(ethylene glycol) methacrylate and oligo(ethylene glycol) methacrylate prepared via controlled radical polymerization are a promising alternative candidates to PNIPAM. According to the content of oligoPEG units, the cloud point of these copolymers can be varied between 30 and 39°C. Laschewsky et al. [21] have described that those polymers allowed for the spreading and adhesion of fibroblasts at 37ºC, but a cell sheet was obtained at 25°C due to the cell-repellent character of those surfaces at this given temperature. Later on, Wei et al. [23] have proposed the introduction of fibronectin (FN) and recombinant human bone morphogenetic protein-2 into these thermo-responsive polymer brushes to induce the adhesion of MC3T3 cells.

Alternatively, Idota et al. [82] have designed temperature-responsive glycopolymer brushes to investigate the effect of the grafting architectures of the copolymer on the selective adhesion and collection of hypatocytes (Fig. 10.4). The galactose/lactose-specific lectin RCA120 and HepG2 cells were used to test for specific recognition of the polymer brushes containing galactose residues over the lower critical solution temperatures. This morphology can be extended to the preparation of smart bioactive interfaces with diverse architectures and to cell screening.

## 10.5 Antimicrobial and Antibacterial Coatings

Bacteria adsorption or microorganism–surface interactions constitute the acute biological response to biomedical materials. The design of tailor-made surfaces that can prevent those processes may be able to improve the performance of a range of biomedical devices. In this regard, the design and development of methodologies

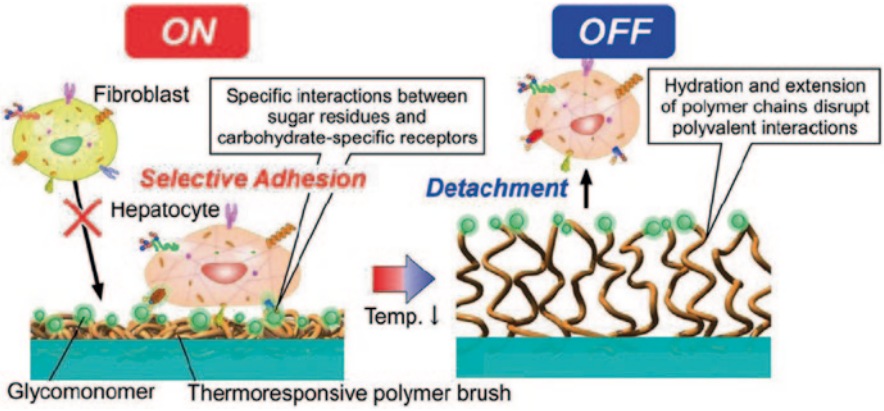


**Fig. 10.4** Schematic of an "on-off" switchable surface trap for selective adhesion/detachment of hepatocyte using a termo-responsive glycopolymer brush. From Idota et al. [82] © 2012 IOPScience

that can specifically focus the action of antimicrobial agents on the polymeric surface is very attractive. Based on this issue, *antimicrobial peptides* (AMPs) are an attractive alternative to classical antimicrobial drugs and antibiotics, due to their broad spectrum activity, relatively nontoxic nature towards host cells and are effective at low concentrations [83–85]. These natural oligopeptides, which are components of the immune natural defense system of various living organisms, exert their activity by creating pores or structural defects in the bacteria cell membranes. The novel strategies describe the protocols to immobilize those peptides on the polymer brush keeping its accessibility and its activity towards the surrounding bacterial cells. Gao and co-workers [86] have immobilized the antimicrobial peptide Tet213 (KRWWKWWRRC) onto a Titanium surface, which has been decorated with amino-functionalized copolymer brushes. The binding of AMPs to surface-grafted chains was carried out by a selective and specific reaction between the maleimide groups and thiol moieties of the cysteine residue AMPs. Their findings revealed that the interplay between grafting and peptide density determines the optimum antimicrobial properties of the peptide-modified polymer brush against *Pseudomonas aeruginosa*. These authors have also immobilized other AMPs (Tet-20, Tet-1010) on the copolymer brushes. Their results have demonstrated the potent antimicrobial activity of those AMPs [87]. These Ti-surfaces decorated with Tet-subunits were nontoxic to mammalian cells; they improve slightly the cell adhesion process compared to pristine polymer brushes.

It is well known that the incorporation of Vancomycin into a biopassive polymer backbone leads to a system where this biopeptide has remained active after immobilization, but its incorporation has compromised the biopassive properties of the coating. Wach et al. [88] involved the attachment of Vancomycin to anachelin chromophores through a PEG-chain linker. The binding to the surface was achieved by the anachelin chromophore, which strongly interacts with $TiO_2$

surfaces. Vancomycin unit provides to this surface a marked antimicrobial activity. Several researchers have immobilized other natural antimicrobial peptides such as Magainin I [89–91] and Gentamicin [92, 93].

## 10.6 Immobilization of Proteins

Polymer brushes from immobilized proteins have received much attention as shown by the considerable number of recent reviews [94, 95]. After the binding to these scaffolds, the tethered proteins must preserve their biological functions [76, 96–98]. The versatile structure, chemistry as well as tunable mechanical properties [99] of polymer brushes make these scaffolds very attractive candidates to bind and immobilize proteins. Polymer brushes were used as supports for immobilization of different proteins, which makes them of interest in different scientific fields, for instance, protein microarrays, preparation of microreactors, microfluidic devices, or biosensors to name a few. Polymer brushes also offer high rates of loading and protection from denaturation relative to other scaffolds for proteins. The chemical strategies to bind proteins are subdivided into two categories: (1) non-covalent protein binding and (2) covalent protein immobilization

### *10.6.1 Non-covalent Protein Immobilization*

Several strategies have been extensively developed to bind proteins through non-covalent interactions. Considering the scope of this chapter, we will only consider strategies based on specific interactions such as metal-coordination or receptor-ligand interactions. The controlled nonspecific interactions allow control over the orientation of the immobilized proteins, which becomes especially advantageous for microarray applications.

Metal ion affinity interactions, in particular using nitrilotriacetate (NTA) metal ion-complexes, have extensively been used to prepare protein binding polymer brushes. The tetradentate ligand nitriloacetate (NTA) can easily form hexagonal complexes with different metal ions, leaving two binding sites available for chelation with a histidine residue. Several research groups have found an attractive utility of NTA-metal ion complexes due to the fact that the selectivity of the binding process can be tuned by varying the metal ion and the controlled orientation of bound proteins onto a polymer layer. Moreover, due to the strong coordination of, for example, histidine residues to the metal complex, the presence of water is not problematic. Finally, using appropriate competitive ligands, such as EDTA, bound proteins can be released and the polymer brush layer regenerated by loading with the appropriate metal ion.

Polymer brushes decorated with NTA-Cu(II) complexes have demonstrated to bind proteins. The metal ion is able to recognize specific areas of proteins, which are rich in histidine residues. The imidazole moiety of this amino acid participates

in the coordination to the metal center. Bruening et al. have extensively studied the binding of several proteins onto polymer brushes [100–102]. Their findings suggest that protein binding is mainly governed by the number of histidine residues in the protein and their accessibility. Several strategies for protein purification are based on this methodology. The authors have also found that the binding capacity of these NTA-Cu(II)-complex-decorated surfaces was higher than the surfaces activated with standard agents, due to the high stability of this complex against side reactions such as hydrolysis. The binding of bovine serum albumin (BSA) onto Poly(2-(methacryloyloxy)ethyl succinate), PMES brushes increase with their thickness, however, the system reaches a plateau value of 7.2 μg/cm$^2$. According to this finding, the immobilization of protein occurs not only at the brush surface but can also take place at deeper layers.

The versatility of NTA allows for the use of alternative metal ions such as Nickel, Iron, or Cobalt. The binding of an imidazole unit of a histidine derivate to Ni(II) is weaker than that of a NTA-Cu(II) complex. Due to this issue, several reports describe the use of this metal ion for oligohistidine-protein purification. Porous membranes [103, 104] or magnetic nanoparticles [105] were functionalized with NTA-Ni(II) complexes which have been grafted onto polymer brushes. These functional polymeric supports were able to purify oligohistidine-tagged proteins with a purity > 99 % directly from cell extracts or a mixture of proteins. An alternative metallic center is Fe(III): brush layers decorated with NTA-Fe(III) complexes reduce the detection limit of phosphopeptide until 15 fmol. This enhancement is based on a selective and efficient enrichment of the phosphopeptides due to the recognition of these moieties with the immobilized ligands. [106]

Recently, other research groups also exploited alternative ligands to form highly selective protein adsorbers by non-covalent recognition interactions, for instance, iminodiacetic acid (IDA) units. Zhao et al. [107] have immobilized Glucoamylase, as a model enzyme, onto grafted Poly(glycidyl methacrylate) polymer chains. PGMA brushes were first functionalized with iminodiacetic acid (IDA) units and Cu(II) ions, in which this enzyme could also be tethered *via* specific metal ion interactions. Applying this novel approach, the authors could control the orientation of the enzyme and their findings have demonstrated that the enzyme immobilization was faster, which would lead to a reduced activity loss. The bound glucoamylase showed better pH, temperature, and thermal stabilities than its free state.

The third type of non-covalent interactions used for the selective immobilization of proteins is based on the biorecognition of biotin by (strept)avidin. This interaction is one of the strongest non-covalent bindings known in nature. With this strategy, avidin is covalently grafted to surface-tethered polymer chains and different biotin-tagged molecules are then immobilized through this almost non-reversible avidin-biotin recognition. Based on this strong specific interaction, the functionality of the grafted biomolecules is expected to be better preserved than by direct covalent binding methods. Ober et al. [108] have demonstrated that biotinylated BSA that was previously grafted onto a PAA brush could be used to immobilize streptavidin by this specific non-covalent interaction. BSA linkages can simultaneously block the nonspecific interactions of the remaining unreacted carboxylic groups on

PAA and this protein as a polypeptide may also offer a biocompatible environment for immobilizing other biomolecules. This novel method can be readily expanded to immobilize a range of antigens or ligands for advanced biomedical applications. Yang et al. [109] have reported a photolithographic process for micropatterning of two-component biomolecules using two types of polymer brushes, (poly(sodium acrylate), and poly(glycidyl methacrylate)). Biotin was selectively grafted to the epoxy groups in the PGMA domains, while immunoglobulin (IgG) was immobilized onto the PAA domains. In each domain, the grafted biotin and immobilized IgG were able to specifically recognize their corresponding target protein, avidin, and anti-Ig, respectively. Site-specific biotinylation of proteins to surfaces is a key task for implementing biomedical assays [110, 111]. Depending on the applied biotinylation method, proteins can be immobilized in a random or oriented fashion. Proteins randomly biotinylated at the free amine groups were compared to oriented proteins, site specifically biotinylated at the hinge region, far from the specific center of the proteins in order to avoid side effects on the immobilized protein.

Special mention deserves the strategies specifically developed for non-covalent immobilization of antibodies. Immobilization of pristine antibodies can be carried out by an intermediate protein directly attached to the surface-tethered layer, such as protein A and protein G. Both proteins present strong specific interactions to several antibodies because of five and two binding domains specific to the Fc part of the antibodies, respectively. Ishihara et al. [112] optimized the approach by forming highly organized aggregates of Staphylococcol protein A (SpA) and antibody. In this work also, the activity of immobilized antidody by adding its corresponding antigen was studied. The SpA was immobilized onto a high brush density of a phospholipid polymer in order to reduce undesired denaturation. The binding process was based on the selective oxidation of the tyrosine motif from SpA by the Tyrosinase enzyme, leading to an oxidized tyrosine, which can further bind to the amino group from the polymeric layer. The corresponding SpA-functionalized surface was, then, decorated with an antibody by the non-covalent recognition process described above. The results of this study suggested that the oriented antibodies showed a strong affinity for antigens compared with the partially or randomly oriented antibodies.

Following this strategy, Ober et al. [113] have recently immobilized one type of antibody by the specific recognition of its corresponding hapten. In this case, the authors have first introduced 2,4-dinitrophenol (DNP) onto a polymer brush, which reveals a high affinity and specificity to anti-DNP antibodies. The developed sensor platform is based on the antibody-catalyzed water oxidation pathway, in which the binding antibodies catalyze the production of hydrogen peroxide ($H_2O_2$) from water and singlet oxygen ($O_2$*), which is generated by a photosensitizer. Another tag used for non-covalent binding of antibodies is Digoxigenin [114]. This steroid presents a high affinity and specificity to anti-digoxigenin antibodies, which are frequently used in a variety of biological immune-assays, such as ELISA.

Alternative target biocues for non-covalent binding of proteins are based on carbohydrate recognition processes. Yu et al. [115] prepared three novel glycocomonomers containing α-mannoside, α-galactoside, and α-glucoside units which were used for the synthesis of artificial glycocalyx. The glycocalyx is a “carbohydrate-rich

coat" on the external surface of the plasma membrane of cells. The specific interactions of glycocalyx with proteins present in the surrounding environments are important recognition events that regulate a myriad of biological and pathological processes. These glycopolymer brushes showed ultralow adsorption of bovine serum albumin (BSA) and fibrinogen (Fb) and retained specific lectin recognition capacity. Specific protein interaction studies with Concanavalin A, which is a lectin that specifically binds α-mannose and α-glucose units, showed the importance to preserve the carbohydrate structure in its natural form in order to enhance the specific protein interactions. In a later study [116], their interaction with blood was also examined and it was found that the nature of the sugar group (Glc, Man, or Gal) has an effect on the amount and type of plasma proteins being adsorbed, with glucose-functionalized brushes leading to the lowest adsorption. Bian [117] et al. reported an example of glycan arrays decorated with Concanavalin A, creating glycan-functionalized polymer brushes with pendant carbohydrate side groups by the thiol-acrylate photopolymerization. The results of this study have demonstrated that polymer brushes are better polymer scaffolds than their counterpart SAM decorated with α-mannosides and α-glucosides. The authors have also concluded that these glycan arrays may be a new tool to study the role of multivalency on carbohydrate recognition.

### *10.6.2 Covalent Protein Binding*

In principle, covalent immobilization provides probably the best entry point, which combines longevity of the protein-functionalized surfaces with a high sensitivity due to a desired specific orientation. Therefore, a lot of efforts are currently undertaken to investigate and improve this area, including both well-known reactions of naturally present moieties and the developments of tailor-made surfaces and modifications thereof. The formation of a robust link between the polymer brush chain and the protein allows for the use of stronger experimental conditions, such as intensive washing; however one should also take care of these conditions so that they do not denaturalize the immobilized proteins. The covalent binding of proteins has become an attractive way to fabricate robust and selective protein microchips. In early stages for protein immobilization, the deployed chemistry has been limited to classical organic reactions via functional groups such as amino, hydroxyl, etc.

Gautrot et al. [118] have extensively studied the binding of Streptavidin to Poly(oligo(ethylene glycol) methacrylate) (POEGMA) brushes using ten different coupling agents and studying which coupling conditions leads to the highest Streptavidin loading efficiency. Their findings have demonstrated that Disuccinimidyl carbonate (DSC) was the most efficient and reliable coupling agent. This agent has created N-hydroxysuccinimide (NHS ) carbonate units at hydroxyl-terminated polymer chains, which have further reacted with the primary amines of streptavidin. The hydroxyl groups could also react with Carbonyldiimidazole (CDI), leading to imidazole carbamate moieties, which react readily with free amino groups of biomolecules (Streptavidin) to form stable carbamate linkages. The tendency

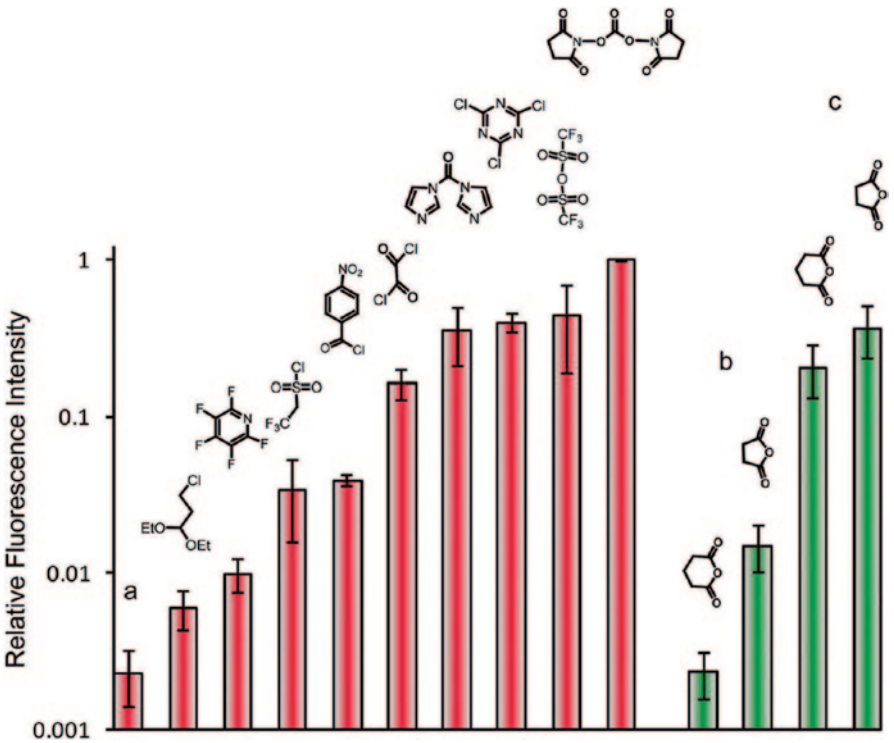


**Fig. 10.5** SA immbolibilization levels on PEGylated brushes using a range of coupling agents. *Red* bars (10 leftmost): end-capped hydroxyl brushes were directly activated with the corresponding coupling agent depicted. *Green* bars (4 rightmost): end-capped hydroxyl brushes activated firstly with anhydride (glutaric or succinic) and then incubated with SA. From Gautrot et al. [118] © 2009 American Chemical Society

of hydrolysis of the imidazole moiety is very low when compared to NHS units. Therefore, they appear as a good candidate for coupling biomolecules in an aqueous buffer solution. The authors have also activated the hydroxyl-terminated groups with anhydrides, leading to the formation of end-capped carboxylate groups, which later on could easily bind amino groups of biomolecules using the well-known EDC/NHS protocol (Fig. 10.5).

Epoxide groups are very attractive grafting points for the covalent binding of proteins because they can react irreversibly with different nucleophiles. Poly(glycidyl methacrylate) brushes have been extensively used for the immobilization of proteins [119]. However, their main drawback is that this polymer is not water soluble what strongly reduces the field of possible applications. In order to overcome this problem, several authors have proposed the copolymerization of glycidyl methacrylate with hydrophilic comonomers such as 2,3-hydroxypropyl methacrylate or 2-hydroxypropyl acrylamide.

The attractive chemistry of active esters, CDI, and epoxide moieties have extensively been used for the covalent binding of proteins by reacting hydroxyl or amine groups contained in a large number of natural amino acids. However, these approaches present some limitations related to the nonselective interactions between functional groups and the lack of control over the orientation of the immobilized protein. In order to improve the chemoselectivity of the covalent immobilization reactions and the orientation of the proteins, several strategies have been addressed. One strategy is based on the cysteine residue. This nonessential amino acid is much lower abundant compared to, for instance, its counter-partner serine and contains a thiol group in its side chain. This side chain thiol can further undergo a variety of interesting coupling reactions, for example, Michael addition. Piehler et al. [120] have efficiently bound Ribonuclease barnase to PEGylated surface, which has been activated by the incorporation of maleimido-moieties that can specifically recognize free thiol groups. The maleimide unit reacts faster than other Michael acceptors, such as vinyl sulfone, acrylates, or acrylamides, and the coupling reactions can also be performed in slightly acidic conditions (pH 6–7). When proteins containing a single reactive moiety are used, this method allows for the control of the binding orientation of the target protein.

Another strategy for the conjugation to cysteine units involves the formation of disulfide bonds. To this end, the thiol group of the cysteine moiety of the incoming protein is reacted with an activated disulfide group of the polymer brush layer. A thiol-disulfide displacement leads to a new disulfide bond connecting the incoming protein with the brush chains. An advantage of this strategy is that the activated disulfide can selectively react with biothiols under a broad pH range (pH 3–10). One of the most widely used active disulfide is *o*-pyridiyl disulfide because it presents an efficient reaction towards biothiols, and the leaving group (2-mercaptopyridine) can no longer participate in the thiol-disulfide interchange reaction. In line with this strategy, Iwasaki et al. [121, 122] successfully immobilized the antibody fragment (Fab 0) onto Phosphorylcholine copolymer brushes. This antibody fragment comes from the Y-shaped IgG protein, and its thiol group is at the opposite side of the antigen-binding domain. Therefore, this thiol-disulfide displacement approach could be used to covalently immobilize those fragments with an appropriate orientation keeping the antigen-binding domain still accessible.

Another possibility to covalently immobilize proteins on polymer brush layer involves the use of the intein-associated protein splicing process. This strategy is based on a mechanism known from nature and called *native chemical ligation* (NCL), in which cysteine presents an important role. It was initially developed for the preparation of peptides as alternative candidates for the solid-phase peptide synthesis. This approach enables the chemoselective coupling of two unprotected peptides by the participation of Coenzyme A (CoA). At the beginning of the reaction, the C-terminal of a free peptide reacts with another peptide end-capped with a cysteine residue, leading to a thioester-linked product. This intermediate presents a spontaneous rearrangement, forming a native peptide bond at the ligation site. Piehler et al. [123] have reported an approach for efficient site-specific protein immobilization based on enzymatic phosphopantethinyl transfer (PPT) from

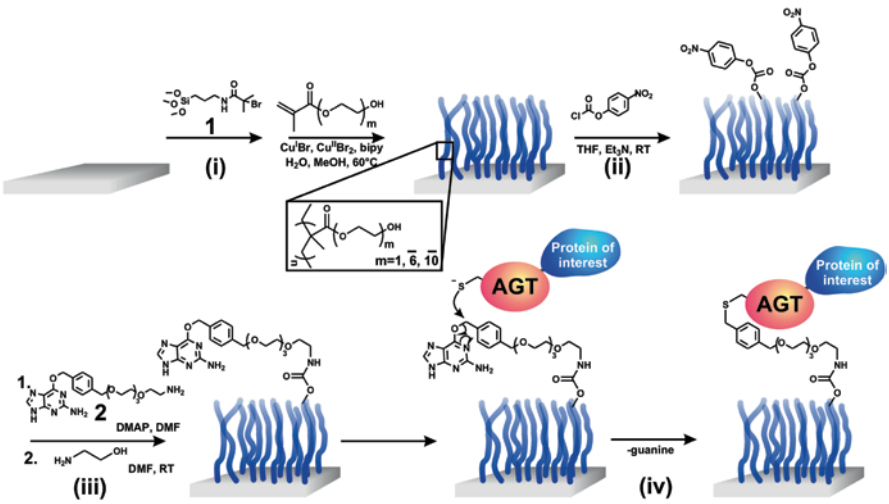


**Fig. 10.6** Schematic illustration of immobilization of AGT fusion proteins onto polymer brush layer by benzylguanine-displacement. From Klok et al. [76] © 2005 American Chemical Society

coenzyme A (CoA)-functionalized glass-type surfaces to specific peptide tags. These reactions are highly specific and can efficiently be performed without prior purification of the proteins, allowing for the selective immobilization of proteins from crude mixtures onto decorated-CoA surfaces. In this work, the authors first coupled the CoA motif onto dense PEGylated polymer brushes, by the reaction of the CoA thiol group with maleimide units situated on the PEG chains. Then, the CoA can specifically recognize the serine residue from the incoming protein. Later, the NCL process leads to a covalent binding between incoming protein and the PEGylated surface. The findings of this study concluded that, compared to the other biochemical and enzymatic immobilization processes, this approach offers the advantage of relatively rugged coupling protocols and compatibility with nearly all proteins. This method, therefore, will be a valuable tool for covalent functional protein immobilization in several demanding bioanalytical and biophysical applications such as label-free biosensor detection, single-molecule force spectroscopy, and fluorescence imaging techniques.

Another interesting pathway to covalently immobilize proteins on polymer brushes involves the use of fusion constructs of the protein of interest and an enzyme. This strategy [76] was inspired by the natural chemoselectivity of enzymes, which took advantage of the ability of O-6-alkylguanine-DNA alkyltransferase (AGT) to transfer the benzyl group of O 6-benzylguanine (BG) to one of its cysteine residues. (Fig. 10.6) In this approach, the protein of interest was initially fused to an AGT tag [124, 125], and subsequently those units were biorecognized by the BG-motifs situated onto the polymer brush chains. As the bioconjugation occurred exclusively via the reaction of the AGT tag, immobilization could be carried out directly from the crude cell lysates without the need for separate purification steps.

The mild procedure left the fusion protein intact and free to react with its substrate. Furthermore, the density of the protein on the polymer brush surface could be varied by changing the grafting density of BG. Currently, three other tags are used for the covalent binding of proteins: the CLIP tag [126], the tetracysteine tag [127], and Indole-3-butyric acid [128]. One could see that these tags could also be employed for bioconjugation using the same strategy.

## 10.7 Conclusions and Outlook

Biomolecule recognition is the keystone for the development of biosensors, biochips, and other applications in biomedical fields. The continuous design of tailor-made polymeric surfaces, especially polymer brushes, is of particular importance for biomolecule recognition. Due to the growing progress in polymerization toolkits, highly sophisticated polymer brushes decorated with target biomolecules can be obtained with less demanding synthetic protocols. This chapter has summarized the recent research activities in the recognition of biomolecules using polymer brush layers. The different topics, mainly cell adhesion and immobilization of proteins, for biorecognition have been reviewed in detail. The work reviewed has shown that functional polymer brushes are versatile and powerful spacers for the immobilization of target biomolecules to maximize their properties. Hopefully, this chapter will trigger fresh and novel strategies in polymer surface science and inspire further interest in restoring polymer brushes as appropiate scaffolds.

Although tremendous progress has been carried out in polymer science, many challenging problems remain, such as the design of novel strategies to optimize the grafting density of the active cues at the surface and to immobilize specifically certain target biomolecules under mild conditions, what becomes especially important for those biomolecules with a marked low thermal or photochemical stability. The random distribution of biocues around the polymer-grafted chains affects the recognition processes, leading to a reduced activity and sensitivity of biomolecules. Therefore, the ever increasing demands for sensitivity should direct future efforts towards the development of controlled and oriented binding of biomolecules. These requirements are particularly important for antibody immobilization. Currently, methodologies are effective but also limited given the heterogeneous nature of such surfaces.

## References

1. Advincula, R. C.; Brittain, W. J.; Caster, K. C.; Rühe, J. *Polymer brushes*; Wiley Online Library 2004.
2. Goddard, J. M.; Hotchkiss, J. Polymer surface modification for the attachment of bioactive compounds. *Progress in Polymer Science* **2007**, *32* (7), 698–725.
3. Matyjaszewski, K. Atom transfer radical polymerization (ATRP): current status and future perspectives. *Macromolecules* **2012**, *45* (10), 4015–4039.

4. Matyjaszewski, K.; Davis, T. P. *Handbook of radical polymerization*; Wiley Online Library2002.
5. Olivier, A.; Meyer, F.; Raquez, J.-M.; Damman, P.; Dubois, P. Surface-initiated controlled polymerization as a convenient method for designing functional polymer brushes: From self-assembled monolayers to patterned surfaces. *Progress in Polymer Science* **2012**, *37* (1), 157–181.
6. Gregory, A.; Stenzel, M. H. Complex polymer architectures via RAFT polymerization: From fundamental process to extending the scope using click chemistry and nature's building blocks. *Progress in Polymer Science* **2012**, *37* (1), 38–105.
7. Lowe, A. B.; McCormick, C. L. Reversible addition–fragmentation chain transfer (RAFT) radical polymerization and the synthesis of water-soluble (co) polymers under homogeneous conditions in organic and aqueous media. *Progress in Polymer Science* **2007**, *32* (3), 283–351.
8. Wang, L.; Broadbelt, L. J. Explicit sequence of styrene/methyl methacrylate gradient copolymers synthesized by forced gradient copolymerization with nitroxide-mediated controlled radical polymerization. *Macromolecules* **2009**, *42* (20), 7961–7968.
9. Siegwart, D. J.; Oh, J. K; Matyjaszewski, K. ATRP in the design of functional materials for biomedical applications. *Progress in Polymer Science* **2012**, *37* (1), 18–37.
10. Choi, J.; Hui, C. M.; Pietrasik, J.; Dong, H.; Matyjaszewski, K.; Bockstaller, M. R. Toughening fragile matter: mechanical properties of particle solids assembled from polymer-grafted hybrid particles synthesized by ATRP. *Soft Matter* **2012**, *8* (15), 4072–4082.
11. Higaki, Y.; Okazaki, R; Takahara, A. Semirigid Biobased Polymer Brush: Poly(α-methylene-γ-butyrolactone) Brushes. *ACS Macro Letters* **2012**, *1* (9), 1124–1127.
12. Haque, H. A.; Kakehi, S.; Hara, M.; Nagano, S.; Seki, T. High-Density Liquid-Crystalline Azobenzene Polymer Brush Attained by Surface-Initiated Ring-Opening Metathesis Polymerization. *Langmuir* **2013**, *29* (25), 7571–7575.
13. Duran, H.; Yameen, B.; Khan, H. U.; Förch, R.; Knoll, W. Surface-initiated ring opening polymerization of N-carboxy anhydride of benzyl-l-glutamate monomers on soft flexible substrates. *Reactive and Functional Polymers* **2013**, *73* (3), 606–612.
14. Jeon, S.; Lee, J.; Andrade, J.; De Gennes, P. Protein—surface interactions in the presence of polyethylene oxide: I. Simplified theory. *Journal of Colloid and Interface Science* **1991**, *142* (1), 149–158.
15. Li, L.; Chen, S.; Zheng, J.; Ratner, B. D.; Jiang, S. Protein adsorption on oligo (ethylene glycol)-terminated alkanethiolate self-assembled monolayers: the molecular basis for nonfouling behavior. *The Journal of Physical Chemistry B* **2005**, *109* (7), 2934–2941.
16. Roosjen, A.; Norde, W.; van der Mei, H.; Busscher, H. Characterization of polymer surfaces and thin films. *Prog Colloid Polym Sci* **2006**, *132*, 138–144.
17. Ma, H.; Wells, M.; Beebe, T. P.; Chilkoti, A. Surface-Initiated Atom Transfer Radical Polymerization of Oligo (ethylene glycol) Methyl Methacrylate from a Mixed Self-Assembled Monolayer on Gold. *Advanced Functional Materials* **2006**, *16* (5), 640–648.
18. Youngblood, J. P.; Andruzzi, L.; Ober, C. K.; Hexemer, A.; Kramer, E. J.; Callow, J. A.; Finlay, J. A.; Callow, M. E. Coatings based on side-chain ether-linked poly (ethylene glycol) and fluorocarbon polymers for the control of marine biofouling. *Biofouling* **2003**, *19* (S 1), 91–98.
19. Tugulu, S.; Klok, H.-A. Stability and nonfouling properties of poly (poly (ethylene glycol) methacrylate) brushes under cell culture conditions. *Biomacromolecules* **2008**, *9* (3), 906–912.
20. Jonas, A. M.; Glinel, K.; Oren, R.; Nysten, B.; Huck, W. T. Thermo-responsive polymer brushes with tunable collapse temperatures in the physiological range. *Macromolecules* **2007**, *40* (13), 4403–4405.
21. Wischerhoff, E.; Uhlig, K.; Lankenau, A.; Börner, H. G.; Laschewsky, A.; Duschl, C.; Lutz, J. F. Controlled Cell Adhesion on PEG-Based Switchable Surfaces. *Angewandte Chemie International Edition* **2008**, *47* (30), 5666–5668.
22. Dey, S.; Kellam, B.; Alexander, M. R.; Alexander, C.; Rose, F. R. Enzyme-passage free culture of mouse embryonic stem cells on thermo-responsive polymer surfaces. *Journal of Materials Chemistry* **2011**, *21* (19), 6883–6890.

23. Ren, X.; Wu, Y.; Cheng, Y.; Ma, H.; Wei, S. Fibronectin and bone morphogenetic protein-2-decorated poly (OEGMA-r-HEMA) brushes promote osseointegration of titanium surfaces. *Langmuir* **2011**, *27* (19), 12069–12073.
24. Arima, Y.; Toda, M.; Iwata, H. Complement activation on surfaces modified with ethylene glycol units. *Biomaterials* **2008**, *29* (5), 551–560.
25. Hamad, I.; Hunter, A.; Szebeni, J.; Moghimi, S. M. Poly (ethylene glycol) s generate complement activation products in human serum through increased alternative pathway turnover and a MASP-2-dependent process. *Molecular immunology* **2008**, *46* (2), 225–232.
26. Ishida, T.; Kashima, S.; Kiwada, H. The contribution of phagocytic activity of liver macrophages to the accelerated blood clearance (ABC) phenomenon of PEGylated liposomes in rats. *Journal of Controlled Release* **2008**, *126* (2), 162–165.
27. Ishida, T.; Kiwada, H. Accelerated blood clearance (ABC) phenomenon upon repeated injection of PEGylated liposomes. *International journal of pharmaceutics* **2008**, *354* (1), 56–62.
28. Kidane, A.; Park, K. Complement activation by PEO-grafted glass surfaces. *Journal of biomedical materials research* **1999**, *48* (5), 640–647.
29. Fan, X.; Lin, L.; Messersmith, P. B. Cell fouling resistance of polymer brushes grafted from Ti substrates by surface-initiated polymerization: effect of ethylene glycol side chain length. *Biomacromolecules* **2006**, *7* (8), 2443–2448.
30. Kitano, H.; Liu, Y.; Tokuwa, K.-i.; Li, L.; Iwanaga, S.; Nakamura, M.; Kanayama, N.; Ohno, K.; Saruwatari, Y. Polymer brush with pendent glucosylurea groups constructed on a glass substrate by RAFT polymerization. *Eur. Polym. J.* **2012**, *48* (11), 1875–1882.
31. Feng, W.; Brash, J.; Zhu, S. Atom-transfer radical grafting polymerization of 2-methacryloyloxyethyl phosphorylcholine from silicon wafer surfaces. *Journal of Polymer Science Part A: Polymer Chemistry* **2004**, *42* (12), 2931–2942.
32. Kügler, R.; Bouloussa, O.; Rondelez, F. Evidence of a charge-density threshold for optimum efficiency of biocidal cationic surfaces. *Microbiology* **2005**, *151* (5), 1341–1348.
33. Azzaroni, O.; Moya, S.; Farhan, T.; Brown, A. A.; Huck, W. T. Switching the properties of polyelectrolyte brushes via "hydrophobic collapse". *Macromolecules* **2005**, *38* (24), 10192–10199.
34. Döbbelin, M.; Arias, G.; Loinaz, I.; Llarena, I.; Mecerreyes, D; Moya, S. Tuning Surface Wettability of Poly (3-sulfopropyl methacrylate) Brushes by Cationic Surfactant-Driven Interactions. *Macromolecular Rapid Communications* **2008**, *29* (11), 871–875.
35. Bernards, M. T.; Cheng, G.; Zhang, Z.; Chen, S.; Jiang, S. Nonfouling polymer brushes via surface-initiated, two-component atom transfer radical polymerization. *Macromolecules* **2008**, *41* (12), 4216–4219.
36. Chang, Y.; Liao, S.-C.; Higuchi, A.; Ruaan, R.-C.; Chu, C.-W; Chen, W.-Y. A highly stable nonbiofouling surface with well-packed grafted zwitterionic polysulfobetaine for plasma protein repulsion. *Langmuir* **2008**, *24* (10), 5453–5458.
37. Ayres, N.; Holt, D.; Jones, C.; Corum, L.; Grainger, D. Polymer brushes containing sulfonated sugar repeat units: synthesis, characterization, and in vitro testing of blood coagulation activation. *Journal of Polymer Science Part A: Polymer Chemistry* **2008**, *46* (23), 7713–7724.
38. Murata, H.; Koepsel, R. R.; Matyjaszewski, K.; Russell, A. J. Permanent, non-leaching antibacterial surfaces—2: How high density cationic surfaces kill bacterial cells. *Biomaterials* **2007**, *28* (32), 4870–4879.
39. Patrucco, E.; Ouasti, S.; Vo, C. D.; De Leonardis, P.; Pollicino, A.; Armes, S. P.; Scandola, M.; Tirelli, N. Surface-initiated ATRP modification of tissue culture substrates: poly (glycerol monomethacrylate) as an antifouling surface. *Biomacromolecules* **2009**, *10* (11), 3130–3140.
40. Madkour, A. E.; Dabkowski, J. M.; Nüsslein, K.; Tew, G. N. Fast disinfecting antimicrobial surfaces. *Langmuir* **2008**, *25* (2), 1060–1067.
41. Langer, R. Editorial: tissue engineering: perspectives, challenges, and future directions. *Tissue engineering* **2007**, *13* (1), 1–2.
42. Hersel, U.; Dahmen, C.; Kessler, H. RGD modified polymers: biomaterials for stimulated cell adhesion and beyond. *Biomaterials* **2003**, *24* (24), 4385–4415.
43. Lavanant, L.; Pullin, B.; Hubbell, J. A.; Klok, H. A. A Facile Strategy for the Modification of Polyethylene Substrates with Non-Fouling, Bioactive Poly (poly (ethylene glycol) methacrylate) Brushes. *Macromol. Biosci.* **2010**, *10* (1), 101–108.

44. Paripovic, D.; Hall-Bozic, H.; Klok, H.-A. Osteoconductive surfaces generated from peptide functionalized poly (2-hydroxyethyl methacrylate-co-2-(methacryloyloxy) ethyl phosphate) brushes. *Journal of Materials Chemistry* **2012**, *22* (37), 19570–19578.
45. Navarro, M.; Benetti, E. M.; Zapotoczny, S.; Planell, J. A.; Vancso, G. J. Buried, covalently attached RGD peptide motifs in poly (methacrylic acid) brush layers: The effect of brush structure on cell adhesion. *Langmuir* **2008**, *24* (19), 10996–11002.
46. Harris, B. P.; Kutty, J. K.; Fritz, E. W.; Webb, C. K.; Burg, K. J.; Metters, A. T. Photopatterned polymer brushes promoting cell adhesion gradients. *Langmuir* **2006**, *22* (10), 4467–4471.
47. Singh, N.; Cui, X.; Boland, T.; Husson, S. M. The role of independently variable grafting density and layer thickness of polymer nanolayers on peptide adsorption and cell adhesion. *Biomaterials* **2007**, *28* (5), 763–771.
48. Schaffner, P.; Meyer, J.; Dard, M.; Nies, B.; Verrier, S.; Kessler, H.; Kantlehner, M. Induced tissue integration of bone implants by coating with bone selective RGD-peptides in vitro and in vivo studies. *Journal of Materials Science: Materials in Medicine* **1999**, *10* (12), 837–839.
49. Cai, W.; Chen, K.; Li, Z.-B.; Gambhir, S. S.; Chen, X. Dual-function probe for PET and near-infrared fluorescence imaging of tumor vasculature. *Journal of Nuclear Medicine* **2007**, *48* (11), 1862–1870.
50. Springer, T. A.; Zhu, J.; Xiao, T. Structural basis for distinctive recognition of fibrinogen γC peptide by the platelet integrin αIIbβ3. *The Journal of cell biology* **2008**, *182* (4), 791–800.
51. Zhang, J.; Krajden, O.; Kainthan, R.; Kizhakkedathu, J.; Constantinescu, I.; Brooks, D.; Gyongyossy-Issa, M. Conjugation to hyperbranched polyglycerols improves RGD-mediated inhibition of platelet function in vitro. *Bioconjugate chemistry* **2008**, *19* (6), 1241–1247.
52. Petrie, T. A.; Raynor, J. E.; Reyes, C. D.; Burns, K. L.; Collard, D. M.; García, A. J. The effect of integrin-specific bioactive coatings on tissue healing and implant osseointegration. *Biomaterials* **2008**, *29* (19), 2849–2857.
53. Raynor, J. E.; Petrie, T. A.; Fears, K. P.; Latour, R. A.; García, A. s. J.; Collard, D. M. Saccharide polymer brushes to control protein and cell adhesion to titanium. *Biomacromolecules* **2009**, *10* (4), 748–755.
54. He, F.; Luo, B.; Yuan, S.; Liang, B.; Choong, C.; Pehkonen, S. O. PVDF film tethered with RGD-click-poly (glycidyl methacrylate) brushes by combination of direct surface-initiated ATRP and click chemistry for improved cytocompatibility. *RSC Advances* **2014**, *4* (1), 105–117.
55. Ruoslahti, E.; Pierschbacher, M. D. New perspectives in cell adhesion: RGD and integrins. *Science* **1987**, *238* (4826), 491–497.
56. LeBaron, R. G.; Athanasiou, K. A. Extracellular matrix cell adhesion peptides: functional applications in orthopedic materials. *Tissue engineering* **2000**, *6* (2), 85–103.
57. Ji, Y.; Wei, Y.; Liu, X.; Wang, J.; Ren, K.; Ji, J. Zwitterionic polycarboxybetaine coating functionalized with REDV peptide to improve selectivity for endothelial cells. *Journal of Biomedical Materials Research Part A* **2012**, *100* (6), 1387–1397.
58. Liu, Y.; Tan, T. T. Y.; Yuan, S.; Choong, C. Multifunctional P (PEGMA)–REDV conjugated titanium surfaces for improved endothelial cell selectivity and hemocompatibility. *Journal of Materials Chemistry B* **2013**, *1* (2), 157–167.
59. Raynor, J. E.; Petrie, T. A.; Fears, K. P.; Latour, R. A.; García, A. J.; Collard, D. M. Saccharide polymer brushes to control protein and cell adhesion to titanium. *Biomacromolecules* **2009**, *10* (4), 748–755.
60. Liu, W.; Li, Y.; Wang, T.; Li, D.; Fang, L.; Zhu, S.; Shen, H.; Zhang, J.; Sun, H; Yang, B. Elliptical Polymer Brush Ring Array Mediated Protein Patterning and Cell Adhesion on Patterned Protein Surfaces. *ACS applied materials & interfaces* **2013**, *5* (23), 12587–12593.
61. Hatakeyama, H.; Kikuchi, A.; Yamato, M.; Okano, T. Influence of insulin immobilization to thermoresponsive culture surfaces on cell proliferation and thermally induced cell detachment. *Biomaterials* **2005**, *26* (25), 5167–5176.
62. Flitsch, S. L.; Ulijn, R. V. Sugars tied to the spot. *Nature* **2003**, *421* (6920), 219–220.
63. Ise, H.; Kobayashi, S.; Goto, M.; Sato, T.; Kawakubo, M.; Takahashi, M.; Ikeda, U.; Akaike, T. Vimentin and desmin possess GlcNAc-binding lectin-like properties on cell surfaces. *Glycobiology* **2010**, *20* (7), 843–864.

64. Song, W.; Xiao, C.; Cui, L.; Tang, Z.; Zhuang, X.; Chen, X. Facile construction of functional biosurface via SI-ATRP and "click glycosylation". *Colloids and Surfaces B: Biointerfaces* **2012**, *93*, 188–194.
65. Chernyy, S.; Jensen, B. E.; Shimizu, K.; Ceccato, M.; Pedersen, S. U.; Zelikin, A. N.; Daasbjerg, K.; Iruthayaraj, J. Surface grafted glycopolymer brushes to enhance selective adhesion of HepG2 cells. *Journal of Colloid and Interface Science* **2013**, *404*, 207–214.
66. Ma, H.; Hyun, J.; Stiller, P.; Chilkoti, A. "Non-Fouling" Oligo (ethylene glycol)-Functionalized Polymer Brushes Synthesized by Surface-Initiated Atom Transfer Radical Polymerization. *Advanced Materials* **2004**, *16* (4), 338–341.
67. Andruzzi, L.; Senaratne, W.; Hexemer, A.; Sheets, E. D.; Ilic, B.; Kramer, E. J.; Baird, B.; Ober, C. K. Oligo (ethylene glycol) containing polymer brushes as bioselective surfaces. *Langmuir* **2005**, *21* (6), 2495–2504.
68. Auernheimer, J.; Dahmen, C.; Hersel, U.; Bausch, A.; Kessler, H. Photoswitched cell adhesion on surfaces with RGD peptides. *Journal of the American Chemical Society* **2005**, *127* (46), 16107–16110.
69. Nash, M. E.; Healy, D.; Carroll, W. M.; Elvira, C.; Rochev, Y. A. Cell and cell sheet recovery from pNIPAm coatings; motivation and history to present day approaches. *Journal of Materials Chemistry* **2012**, *22* (37), 19376–19389.
70. Nash, M. E.; Carroll, W. M.; Foley, P. J.; Maguire, G.; O'Connell, C.; Gorelov, A. V.; Beloshapkin, S.; Rochev, Y. A. Ultra-thin spin coated crosslinkable hydrogels for use in cell sheet recovery—synthesis, characterisation to application. *Soft Matter* **2012**, *8* (14), 3889–3899.
71. Ebara, M.; Yamato, M.; Aoyagi, T.; Kikuchi, A.; Sakai, K.; Okano, T. Temperature-responsive cell culture surfaces enable "on-off" affinity control between cell integrins and RGDS ligands. *Biomacromolecules* **2004**, *5* (2), 505–510.
72. Xu, F.; Zhong, S.; Yung, L.; Tong, Y.; Kang, E.-T.; Neoh, K. Thermoresponsive comb-shaped copolymer-Si (100) hybrids for accelerated temperature-dependent cell detachment. *Biomaterials* **2006**, *27* (8), 1236–1245.
73. Xu, F.; Zhong, S.; Yung, L.; Kang, E.; Neoh, K. Surface-active and stimuli-responsive polymer-Si (100) hybrids from surface-initiated atom transfer radical polymerization for control of cell adhesion. *Biomacromolecules* **2004**, *5* (6), 2392–2403.
74. Fujita, H.; Shimizu, K.; Nagamori, E. Application of a cell sheet–polymer film complex with temperature sensitivity for increased mechanical strength and cell alignment capability. *Biotechnology and bioengineering* **2009**, *103* (2), 370–377.
75. Mazumder, M.; Fitzpatrick, S. D.; Muirhead, B.; Sheardown, H. Cell-adhesive thermogelling PNIPAAm/hyaluronic acid cell delivery hydrogels for potential application as minimally invasive retinal therapeutics. *Journal of Biomedical Materials Research Part A* **2012**, *100* (7), 1877–1887.
76. Tugulu, S.; Arnold, A.; Sielaff, I.; Johnsson, K.; Klok, H.-A. Protein-functionalized polymer brushes. *Biomacromolecules* **2005**, *6* (3), 1602–1607.
77. Xu, F.; Zheng, Y.; Zhen, W.; Yang, W. Thermoresponsive poly (N-isopropyl acrylamide)-grafted polycaprolactone films with surface immobilization of collagen. *Colloids and Surfaces B: Biointerfaces* **2011**, *85* (1), 40–47.
78. Halperin, A.; Kröger, M. Thermoresponsive cell culture substrates based on PNIPAM brushes functionalized with adhesion peptides: theoretical considerations of mechanism and design. *Langmuir* **2012**, *28* (48), 16623–16637.
79. Okajima, S.; Sakai, Y.; Yamaguchi, T. Development of a Regenerable Cell Culture System That Senses and Releases Dead Cells. *Langmuir* **2005**, *21* (9), 4043–4049.
80. Vihola, H.; Laukkanen, A.; Valtola, L.; Tenhu, H.; Hirvonen, J. Cytotoxicity of thermosensitive polymers poly (N-isopropylacrylamide), poly (N-vinylcaprolactam) and amphiphilically modified poly (N-vinylcaprolactam). *Biomaterials* **2005**, *26* (16), 3055–3064.
81. Keerl, M.; Smirnovas, V.; Winter, R.; Richtering, W. Interplay between hydrogen bonding and macromolecular architecture leading to unusual phase behavior in thermosensitive microgels. *Angewandte Chemie* **2008**, *120* (2), 344–347.

82. Idota, N.; Ebara, M.; Kotsuchibashi, Y.; Narain, R.; Aoyagi, T. Novel temperature-responsive polymer brushes with carbohydrate residues facilitate selective adhesion and collection of hepatocytes. *Science and Technology of Advanced Materials* **2012**, *13* (6), 064206.
83. Hancock, R. E.; Sahl, H.-G. Antimicrobial and host-defense peptides as new anti-infective therapeutic strategies. *Nature biotechnology* **2006**, *24* (12), 1551–1557.
84. Onaizi, S. A.; Leong, S. S. Tethering antimicrobial peptides: current status and potential challenges. *Biotechnology advances* **2011**, *29* (1), 67–74.
85. Scott, M. G.; Dullaghan, E.; Mookherjee, N.; Glavas, N.; Waldbrook, M.; Thompson, A.; Wang, A.; Lee, K.; Doria, S.; Hamill, P. An anti-infective peptide that selectively modulates the innate immune response. *Nature biotechnology* **2007**, *25* (4), 465–472.
86. Gao, G.; Yu, K.; Kindrachuk, J.; Brooks, D. E.; Hancock, R. E.; Kizhakkedathu, J. N. Antibacterial surfaces based on polymer brushes: investigation on the influence of brush properties on antimicrobial peptide immobilization and antimicrobial activity. *Biomacromolecules* **2011**, *12* (10), 3715–3727.
87. Gao, G.; Lange, D.; Hilpert, K.; Kindrachuk, J.; Zou, Y.; Cheng, J. T.; Kazemzadeh-Narbat, M.; Yu, K.; Wang, R.; Straus, S. K. The biocompatibility and biofilm resistance of implant coatings based on hydrophilic polymer brushes conjugated with antimicrobial peptides. *Biomaterials* **2011**, *32* (16), 3899–3909.
88. Wach, J. Y.; Bonazzi, S.; Gademann, K. Antimicrobial surfaces through natural product hybrids. *Angewandte Chemie International Edition* **2008**, *47* (37), 7123–7126.
89. Glinel, K.; Jonas, A. M.; Jouenne, T.; Leprince, J.; Galas, L.; Huck, W. T. Antibacterial and antifouling polymer brushes incorporating antimicrobial peptide. *Bioconjugate chemistry* **2008**, *20* (1), 71–77.
90. Blin, T.; Purohit, V.; Leprince, J.; Jouenne, T.; Glinel, K. Bactericidal microparticles decorated by an antimicrobial peptide for the easy disinfection of sensitive aqueous solutions. *Biomacromolecules* **2011**, *12* (4), 1259–1264.
91. Peyre, J.; Humblot, V.; Méthivier, C.; Berjeaud, J.-M.; Pradier, C.-M. Co-Grafting of Amino–Poly (ethylene glycol) and Magainin I on a TiO2 Surface: Tests of Antifouling and Antibacterial Activities. *The Journal of Physical Chemistry B* **2012**, *116* (47), 13839–13847.
92. Muszanska, A. K.; Nejadnik, M. R.; Chen, Y.; van den Heuvel, E. R.; Busscher, H. J.; van der Mei, H. C.; Norde, W. Bacterial adhesion forces with substratum surfaces and the susceptibility of biofilms to antibiotics. *Antimicrobial agents and chemotherapy* **2012**, *56* (9), 4961–4964.
93. Zhang, F.; Shi, Z.; Chua, P.; Kang, E.; Neoh, K. Functionalization of titanium surfaces via controlled living radical polymerization: from antibacterial surface to surface for osteoblast adhesion. *Industrial & Engineering Chemistry Research* **2007**, *46* (26), 9077–9086.
94. Barbey, R.; Lavanant, L.; Paripovic, D.; Schüwer, N.; Sugnaux, C.; Tugulu, S.; Klok, H.-A. Polymer brushes via surface-initiated controlled radical polymerization: synthesis, characterization, properties, and applications. *Chemical reviews* **2009**, *109* (11), 5437–5527.
95. Azzaroni, O. Polymer brushes here, there, and everywhere: Recent advances in their practical applications and emerging opportunities in multiple research fields. *Journal of Polymer Science Part A: Polymer Chemistry* **2012**, *50* (16), 3225–3258.
96. Lane, S. M.; Kuang, Z.; Yom, J.; Arifuzzaman, S.; Genzer, J.; Farmer, B.; Naik, R.; Vaia, R. A. Poly (2-hydroxyethyl methacrylate) for enzyme immobilization: impact on activity and stability of horseradish peroxidase. *Biomacromolecules* **2011**, *12* (5), 1822–1830.
97. Dai, J.; Bao, Z.; Sun, L.; Hong, S. U.; Baker, G. L.; Bruening, M. L. High-capacity binding of proteins by poly (acrylic acid) brushes and their derivatives. *Langmuir* **2006**, *22* (9), 4274–4281.
98. Ionov, L.; Houbenov, N.; Sidorenko, A.; Stamm, M.; Minko, S. Stimuli-responsive command polymer surface for generation of protein gradients. *Biointerphases* **2009**, *4* (2), FA45–FA49.
99. Tranchida, D.; Sperotto, E.; Staedler, T.; Jiang, X.; Schönherr, H. Nanomechanical Properties of Oligo (ethylene glycol methacrylate) Polymer Brush-Based Biointerfaces. *Advanced Engineering Materials* **2011**, *13* (10), B369–B376.

100. Dai, J.; Bao, Z.; Sun, L.; Hong, S. U.; Baker, G. L.; Bruening, M. L. High-Capacity Binding of Proteins by Poly(Acrylic Acid) Brushes and Their Derivatives. *Langmuir* **2006**, *22* (9), 4274–4281.
101. Jain, P.; Dai, J.; Baker, G. L.; Bruening, M. L. Rapid Synthesis of Functional Polymer Brushes by Surface-Initiated Atom Transfer Radical Polymerization of an Acidic Monomer. *Macromolecules* **2008**, *41* (22), 8413–8417.
102. Sun, L.; Dai, J.; Baker, G. L.; Bruening, M. L. High-Capacity, Protein-Binding Membranes Based on Polymer Brushes Grown in Porous Substrates. *Chemistry of Materials* **2006**, *18* (17), 4033–4039.
103. Jain, P.; Sun, L.; Dai, J.; Baker, G. L.; Bruening, M. L. High-Capacity Purification of His-tagged Proteins by Affinity Membranes Containing Functionalized Polymer Brushes. *Biomacromolecules* **2007**, *8* (10), 3102–3107.
104. Jain, P.; Vyas, M. K.; Geiger, J. H.; Baker, G. L.; Bruening, M. L. Protein Purification with Polymeric Affinity Membranes Containing Functionalized Poly(acid) Brushes. *Biomacromolecules* **2010**, *11* (4), 1019–1026.
105. Xu, F.; Geiger, J. H.; Baker, G. L.; Bruening, M. L. Polymer Brush-Modified Magnetic Nanoparticles for His-Tagged Protein Purification. *Langmuir* **2011**, *27* (6), 3106–3112.
106. Wang, W.-H.; Dong, J.-L.; Baker, G. L.; Bruening, M. L. Bifunctional polymer brushes for low-bias enrichment of mono- and multi-phosphorylated peptides prior to mass spectrometry analysis. *Analyst* **2011**, *136* (18), 3595–3598.
107. Zhao, G.; Wang, J.; Li, Y.; Huang, H.; Chen, X. Reversible immobilization of glucoamylase onto metal–ligand functionalized magnetic FeSBA-15. *Biochemical Engineering Journal* **2012**, *68*, 159–166.
108. Dong, R.; Krishnan, S.; Baird, B. A.; Lindau, M.; Ober, C. K. Patterned biofunctional poly (acrylic acid) brushes on silicon surfaces. *Biomacromolecules* **2007**, *8* (10), 3082–3092.
109. Tang, S. C.; Xie, J. Y.; Huang, Z. H.; Xu, F. J.; Yang, W. UV-Induced Grafting Processes with In Situ Formed Photomask for Micropatterning of Two-Component Biomolecules. *Langmuir* **2010**, *26* (12), 9905–9910.
110. Reichel, A.; Schaible, D.; Al Furoukh, N.; Cohen, M.; Schreiber, G.; Piehler, J. Noncovalent, site-specific biotinylation of histidine-tagged proteins. *Analytical chemistry* **2007**, *79* (22), 8590–8600.
111. Trilling, A. K.; Beekwilder, J.; Zuilhof, H. Antibody orientation on biosensor surfaces: a minireview. *Analyst* **2013**, *138* (6), 1619–1627.
112. Tajima, N.; Takai, M; Ishihara, K. Significance of Antibody Orientation Unraveled: Well-Oriented Antibodies Recorded High Binding Affinity. *Analytical chemistry* **2011**, *83* (6), 1969–1976.
113. Welch, M. E.; Ritzert, N. L.; Chen, H.; Smith, N. L.; Tague, M. E.; Xu, Y.; Baird, B. A.; Abruña, H. D.; Ober, C. K. A Generalized Platform for Antibody Detection using the Antibody Catalyzed Water Oxidation Pathway. *Journal of the American Chemical Society* **2014**.
114. Neuert, G.; Albrecht, C.; Pamir, E.; Gaub, H. Dynamic force spectroscopy of the digoxigenin–antibody complex. *FEBS letters* **2006**, *580* (2), 505–509.
115. Yu, K.; Kizhakkedathu, J. N. Synthesis of functional polymer brushes containing carbohydrate residues in the pyranose form and their specific and nonspecific interactions with proteins. *Biomacromolecules* **2010**, *11* (11), 3073–3085.
116. Yu, K.; Lai, B. F.; Kizhakkedathu, J. N. Carbohydrate structure dependent hemocompatibility of biomimetic functional polymer brushes on surfaces. *Advanced healthcare materials* **2012**, *1* (2), 199–213.
117. Bian, S.; Zieba, S. B.; Morris, W.; Han, X.; Richter, D. C.; Brown, K. A.; Mirkin, C. A.; Braunschweig, A. B. Beam pen lithography as a new tool for spatially controlled photochemistry, and its utilization in the synthesis of multivalent glycan arrays. *Chemical Science* **2014**, *5* (5), 2023–2030.
118. Trmcic-Cvitas, J.; Hasan, E.; Ramstedt, M.; Li, X.; Cooper, M. A.; Abell, C.; Huck, W. T.; Gautrot, J. E. Biofunctionalized protein resistant oligo (ethylene glycol)-derived polymer brushes as selective immobilization and sensing platforms. *Biomacromolecules* **2009**, *10* (10), 2885–2894.

119. Yuan, L.; Hua, X.; Wu, Y.; Pan, X.; Liu, S. Polymer-Functionalized Silica Nanosphere Labels for Ultrasensitive Detection of Tumor Necrosis Factor-alpha. *Analytical chemistry* **2011**, *83* (17), 6800–6809.
120. Piehler, J.; Brecht, A.; Valiokas, R.; Liedberg, B.; Gauglitz, G. A high-density poly (ethylene glycol) polymer brush for immobilization on glass-type surfaces. *Biosensors and Bioelectronics* **2000**, *15* (9), 473–481.
121. Iwasaki, Y.; Omichi, Y.; Iwata, R. Site-specific dense immobilization of antibody fragments on polymer brushes supported by silicone nanofilaments. *Langmuir* **2008**, *24* (16), 8427–8430.
122. Iwata, R.; Satoh, R.; Iwasaki, Y.; Akiyoshi, K. Covalent immobilization of antibody fragments on well-defined polymer brushes via site-directed method. *Colloids and Surfaces B: Biointerfaces* **2008**, *62* (2), 288–298.
123. Waichman, S.; Bhagawati, M.; Podoplelova, Y.; Reichel, A.; Brunk, A.; Paterok, D.; Piehler, J. Functional immobilization and patterning of proteins by an enzymatic transfer reaction. *Analytical chemistry* **2010**, *82* (4), 1478–1485.
124. Kindermann, M.; George, N.; Johnsson, N.; Johnsson, K. Covalent and selective immobilization of fusion proteins. *Journal of the American Chemical Society* **2003**, *125* (26), 7810–7811.
125. Keppler, A.; Gendreizig, S.; Gronemeyer, T.; Pick, H.; Vogel, H; Johnsson, K. A general method for the covalent labeling of fusion proteins with small molecules in vivo. *Nature biotechnology* **2003**, *21* (1), 86–89.
126. Gautier, A.; Juillerat, A.; Heinis, C.; Corrêa Jr, I. R.; Kindermann, M.; Beaufils, F.; Johnsson, K. An engineered protein tag for multiprotein labeling in living cells. *Chemistry & biology* **2008**, *15* (2), 128–136.
127. Griffin, B. A.; Adams, S. R.; Tsien, R. Y. Specific covalent labeling of recombinant protein molecules inside live cells. *Science* **1998**, *281* (5374), 269–272.
128. Alves, N. J.; Kiziltepe, T.; Bilgicer, B. Oriented surface immobilization of antibodies at the conserved nucleotide binding site for enhanced antigen detection. *Langmuir* **2012**, *28* (25), 9640–9648.

# Chapter 11
# Microfluidic Systems with Functional Patterned Surface for Biomedical Applications

**Kin Fong Lei, I-Chi Lee and Tim C. Lei**

## 11.1 Introduction

In the past decades, microfluidics system, also called "lab-on-chip (LOC)," "biochip," or "micro-total-analysis-system (μTAS)," has been rapidly developed, and a number of biomedical applications have been demonstrated using microfluidic technology [1–4]. It is a very exciting multidisciplinary topic of the combination of engineering and life science. One of the objectives of the development is to substitute the bioanalytical equipment performing in a conventional laboratory to an automated and miniaturized device operating in a remote environment. A total solution starting from sample pretreatment, sample/reagent manipulation, separation, reaction, detection, to analytical result display can be automatically conducted in a single compact device. Due to their miniaturization and automation, there are a number of advantages of using microfluidic systems such as less sample/reagent consumption, reduced risk of contamination, less cost per analysis, lower power consumption, faster analysis, enhanced sensitivity and specificity, and higher reliability.

The development of microfluidic technology began from micro-electromechanical system (MEMS) manufacturing infrastructure, which is silicon-based fabrication process. Beside the conventional surface microfabrication technique, high-aspect ratio fabrication processes were specifically developed for MEMS such

K. F. Lei (✉)
Graduate Institute of Medical Mechatronics, Chang Gung University,
259 Wen-Hwa 1st Road, Kwei-Shan, Tao-Yuan, Taiwan 333
e-mail: kflei@mail.cgu.edu.tw

Department of Mechanical Engineering, Chang Gung University, Kwei-Shan, Tao-Yuan, Taiwan

I.-C. Lee
Graduate Institute of Biochemical and Biomedical Engineering,
Chang Gung University, Kwei-Shan, Tao-Yuan, Taiwan

T. C. Lei
Department of Electrical Engineering, University of Colorado Denver, Denver, USA



J. Rodríguez-Hernández, A. L. Cortajarena (eds.), *Design of Polymeric Platforms for Selective Biorecognition,* DOI 10.1007/978-3-319-17061-9_11

as deep reactive ion etching (DRIE), LIGA, and substrate bonding techniques [5–7]. Based on the well-established silicon microfabrication process and extensive studies of silicon property, development of microfluidic technology has rapidly grown and silicon-based microfluidic systems have been demonstrated on various fluidic functions [8–11]. However, most of the biological activities are commonly represented by optical signals. Silicon substrate is not optically transparent and may be limited to be used in the biomedical applications. Hence, glass and polymer materials were introduced for the substrates of microfluidic systems. Polymer materials include polymethylmethacrylate (PMMA), polystyrene (PS), polycarbonate (PC), and polydimethylsiloxane (PDMS) and they are less expensive, flexible, optical transparent, and biocompatible. Some newly developed fabrication techniques were proposed such as soft lithography, hot embossing, injection molding, and low-temperature polymer bonding [12–16]. Currently, glass and polymer materials are the most widely used substrates for the development of microfluidic systems [17–19], and a lot of excellent demonstrations have been reported for diagnostic applications [1, 20]. These systems are much more automated and miniaturized and may achieve the objective of substitution of bioanalytical equipment performing in a conventional laboratory. But for the applications specifically aimed at rapid diagnostics, they are still not readily accessible to untrained personnel and are not appropriate for remote environment [21]. Most recently, paper has been proposed to be an alternative material used for the substrates of the microfluidic systems. It has the advantages of low cost, biocompatibility, disposability, and passive aqueous transportation and was suggested to be suitable for rapid diagnostics in remote environment [22]. The paper-based microfluidic systems can be realized by patterning sheets of paper into hydrophilic channels bounded by hydrophobic barriers based on the technologies of photolithography [23, 24], wax printing [25, 26], polydimethylsiloxane (PDMS) printing [27], and plasma treatment [28]. Based on these fabrication techniques, a number of biomedical applications have been demonstrated including colorimetric bio-assays [22, 29–30], electrochemical bio-assays [23, 31, 32], and paper-based enzyme-linked immunosorbent assay (ELISA) [33–36]. Conclusively, a board spectrum of materials and fabrication techniques have been used and developed for the microfluidic systems. The technology is mature to design and fabricate automated and miniaturized devices for various applications.

A wide range of biomedical applications have been implemented to the microfluidic systems, such as DNA analysis [37–42], immunoassay [43–47], and cell analysis [48–52]. These demonstrations showed the power of microfluidic technology and its capability of performing complex analytical problems. In addition, in order to have more specific functions in microfluidic systems, surface modifications were introduced to improve the performance of the systems. The aim of this chapter focuses some of the recent developments of functional patterned surfaces in microfluidic systems. In-depth discussions of the surface modification technologies and their applications of fluid manipulation, suppression of biomolecule adsorption, control of cellular behavior, and biosensing are respectively included. The current excellent integration of microfluidic technology and surface chemistry suggests a solid foundation for the development of practical biomedical applications.

## 11.2 Modification of Surface Wetting Property

Surface wetting property can be modified to become hydrophobic or hydrophilic. Hydrophobic surfaces can be produced by coating hydrophobic non-polar molecules on top of them. With the hydrophobic coating, water on the surface exhibits a high contact angle $\theta$, as illustrated in Fig. 11.1a. The determination of the contact angle is based on the result of the mechanical equilibrium of a droplet resting on a solid surface [53]. This is the action of three surface tensions: $\gamma_{LG}$ at the interface of the liquid and gas; $\gamma_{SL}$ at the interface of the solid and liquid; and $\gamma_{SG}$ at the interface of the solid and gas. In contrast, hydrophilic surface is the surface modified by hydrophilic molecules which attract water. That is, water on hydrophilic surface exhibits a low contact angle, as illustrated in Fig. 11.1b. In general, if the water contact angle is larger than 90°, the solid surface is considered as hydrophobic, and if the water contact angle is smaller than 90°, the solid surface is considered to be hydrophilic. Surface wetting property can be modified by coating a layer of self-assembled monolayer (SAM). In the following, applications of fluid manipulation and suppression of bimolecular absorption through controlling the surface wetting property are discussed in this section.

### *11.2.1 SAM Coating*

SAM of an organic molecule is a molecular assembly formed spontaneously on a surface. In some cases, SAM consists of head group, tail, and functional end group, as illustrated in Fig. 11.2. The head group has a strong affinity to the substrate and anchoring the molecule to the surface. Common head groups include thiols, silanes, and phosphonates. SAM can be created by first chemisorping the molecules to the substrate with the head groups through vapor or lipid phase deposition. A slow reorganization of the tails of the molecules after the deposition forms the SAM coating. Finally, substrate surface is covered in a single monolayer. Depending on

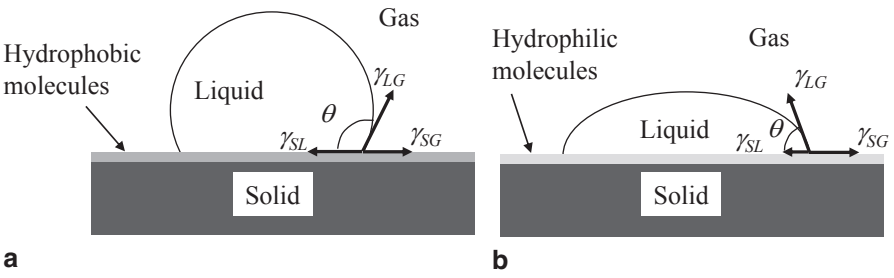


**Fig. 11.1** Illustration of surface wetting property. **a** Water on hydrophobic surface. **b** Water on hydrophilic surface

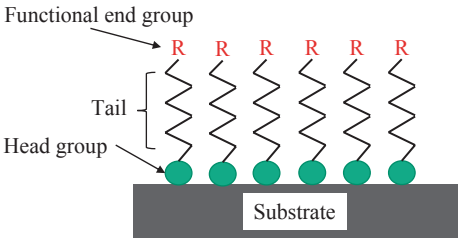


**Fig. 11.2** Representation of an SAM structure

the molecular property of the SAM, either hydrophobic or hydrophilic surface can therefore be created.

Silicon and glass surfaces consist of siloxane (Si-O-Si) bonds, which can rapidly acquire silanol (Si-OH) groups after contacting with water or atmospheric moisture. These –OH groups are polar and therefore make the surface hydrophilic [54]. Typically, a bare glass surface has a water contact angle of around 70–80°. To further enhance the hydrophilic property of the surface, SAM can be coated, and the water contact angle of the SAM-treated surface can be achieved to be as low as 40°. Example of the widely used hydrophilic molecule immobilized on glass substrate is 2-methoxy(polyethylenoxy)propyl trichlorosilane (PEG-silane). In contrast, octadecyltrichlorosilane (OTS) is the most commonly used hydrophobic molecule to change the substrate to be hydrophobic. The water contact angle of an OTS-treated surface is typically around 110°. A silicon or a glass surface can be dipped into an organic solvent dissolved with SAM molecules, such as hexadecane (HD) or dichloromethane. Illustration of the process is shown in Fig. 11.3. The trichlorosilane ($HSiCl_3$) group of the SAM molecules acts as the polar end of an amphiphilic molecule and attracts a layer of water to be bound to the silanol groups of the silicon or glass surface. Upon contact with water, the molecule is hydrolyzed with the elimination of HCl. The –OH groups of the molecules are then created hydrogen bonds with the silanol groups at the substrate surface with the elimination of $H_2O$. Finally, SAM can be coated on the entire substrate surface to modify the substrate surface wetting property.

PDMS is also a widely used material for the development of microfluidic systems. Original PDMS surface is hydrophobic and has a water contact angle of around 110°. To modify PDMS surface to be hydrophilic, plasma activation or SAM coat-

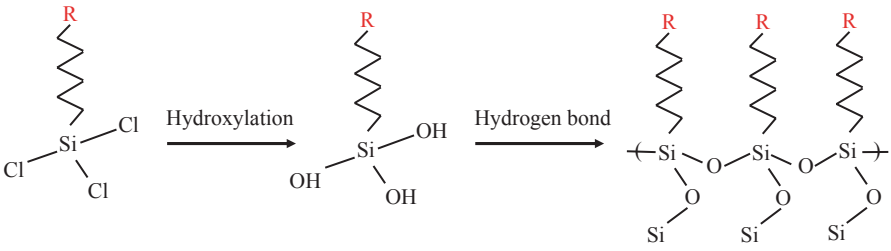


**Fig. 11.3** Formation of SAM molecules on silicon or glass surface

ing can be used. In plasma activation, hydrogen atoms of PDMS are first removed from the polymer chain, and the activated surface reacts with the oxygen or moisture in the air, forming $SiO_2$, Si-OH, or Si-$CH_2$OH groups on the PDMS surface [55, 56]. These polar groups make the surface hydrophilic immediately after the plasma treatment. However, the surface regains its original hydrophobic character after several days. In order to stabilize the surface wetting property, incorporation of monomer molecules, e.g., poly(ethylene glycol) (PEG) and poly(oxyethylene) (POE), can modify the PDMS surface to be hydrophilic. These molecules have polar groups that increase dipole–dipole interactions. The PDMS surface finally has a water contact angle of around 40°. By coating the SAM, the surface wetting property of PDMS material can be modified.

### *11.2.2 Application Examples—Fluid Manipulation*

Fluid manipulation in microfluidic systems can be realized by various fluid components such as micropumps [57, 58] and microvalves [59, 60]. To generate pumping and valving functions, most of these components were composed of moving parts and involved complicated fabrication process. An alternative method was proposed to modify the surface wetting property to induce passive pumping and valving functions. By special arrangement of hydrophilic and hydrophobic surfaces in the microfluidic systems, passive fluid manipulation can be realized without moving parts. To pattern hydrophobic and hydrophilic SAM in microfluidic systems, multistream laminar flow and UV photolithography were respectively proposed [61–63]. The former one was to pattern the surface inside channel networks by combining multistream liquid laminar flow and SAM chemistry. Pressure-sensitive microfluidic gates were demonstrated, and hydrophobic molecules of OTS and heptadecafluoro-1,1,2,2-tetrahydrodecyltrichlorosilane (HFTS) were used to coat on glass surface [62]. Three solutions of HD, OTS in HD, and HFTS in HD were pumped into the channels and maintained under laminar flow for a predetermined period of time, as illustrated in Fig. 11.4a. Hence, SAMs formed on the top and bottom substrates of the channels simultaneously in the areas where OTS and HFTS solutions flowed through, while other areas remained hydrophilic. Once the surface was patterned, aqueous dye solution was pumped along the hydrophilic pathway at three different pressures of spontaneous flow, 26 mm$H_2O$, and 39 mm$H_2O$. As shown in Fig. 11.4b–d, solution was confined to the hydrophilic pathway under spontaneous flow condition and flowed into the hydrophobic regions when pressures exceeded critical values.

Alternatively, patterning the surface by UV photolithography combined with photocleavable SMA of 2,2,3,3,4,4,5,5,6,6,7,7,8,8,8-pentadecafluoro-1-octyl 4-(11-trichlorosilyl-1-oxoundecyloxymethyl)-3-nitrobenzoate (F-SAM) was reported to generate hydrophilic and hydrophobic surface patterns for fabricating microfluidic gates [62]. Upon exposure to UV irradiation, the *o*-nitrobenzyl-oxygen bond in the F-SAM was cleaved and thus the carboxylic acid groups were exposed to the air interface, making the surface hydrophilic. Illustration of photodeprotection

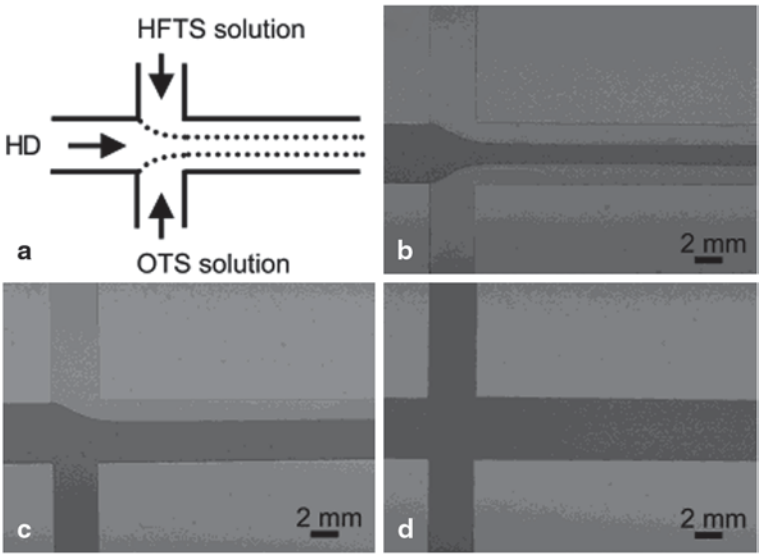


**Fig. 11.4** **a** Schematic illustrations of multistream laminar flow of HD, a solution of OTS in HD, and a solution of HFTS in HD. **b-d** Optical micrograph of an aqueous dye solution flowing **b** along the hydrophilic pathway under spontaneous flow conditions, **c** into the OTS region under a pressure of 26 mm$H_2O$, and **d** into the HFTS region under a pressure of 39 mm$H_2O$. (Reprinted with permission from [62]. Copyright (2003) American Chemistry Society.)

of F-SAM upon exposure to UV irradiation is shown in Fig. 11.5a. The water contact angle on F-SAM-coated cover glass could be adjusted by the UV irradiation time, as shown in Fig. 11.5b. The contact angle decreased rapidly in the beginning but leveled off after 90 min. Thus, patterning different surface wetting properties inside microchannel was demonstrated by different irradiation times on the F-SAM-coated surface. As shown in Fig. 11.6a, regions A and B were irradiated for 120 and 60 min, respectively, resulting in the contact angles of 69° and 76°, respectively. Under spontaneous flow condition, water was confined in region A, as shown in Fig. 11.6b. Increasing water pressure led to water flowing into region B, as shown in Fig. 11.6c, d. As there was no physical wall on the sides of the liquid streams, liquid was referred to as being confined by virtual walls.

### *11.2.3 Application Examples—Suppression of Biomolecule Adsorption*

Hydrophobic surfaces cause adsorption of significant amounts of protein from the surrounding biological environment, resulted in microbial adhesion and biofilm formation. In some cases, the adsorption of nonspecific proteins leads to failure of the

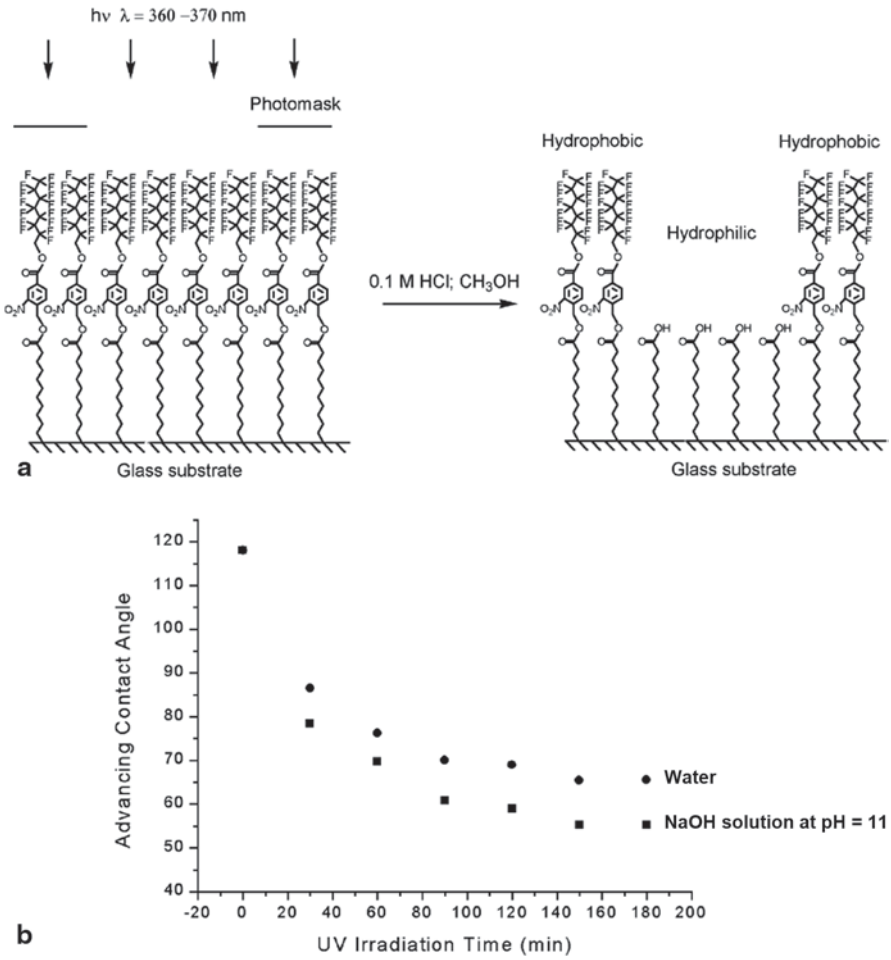


**Fig. 11.5** **a** Photodeprotection of F-SAM upon exposure to UV irradiation. **b** Effect of UV irradiation time on the surface wettability of F-SAM. (Reprinted with permission from [62]. Copyright (2003) American Chemistry Society.)

device [64, 65]. Therefore, it is desirable to modify surfaces of the devices to reduce absorption of proteins and adhesion of cells [66–69]. These were demonstrated by PEG-grafted PDMS surfaces [68]. The monomer of polyethylene glycol diacrylate (PEGDA) was used, and the micropatterned PEGDA-grafted PDMS surface was prepared by photo-induced graft polymerization. After an application of PEGDA on the surface, UV light was irradiated through a photomask with an array of black squares to obtain a completely grafted surface. The PDMS surface was then rinsed and dried. Fluoresceien isothiocyanate-labeled bovine albumin (FITC-BSA) and HepG2 cells were respectively added to the mciropatterned PEGDA-grafted PDMS surfaces and were then incubated. Adsorption of FITC-BSA and HepG2 cells are

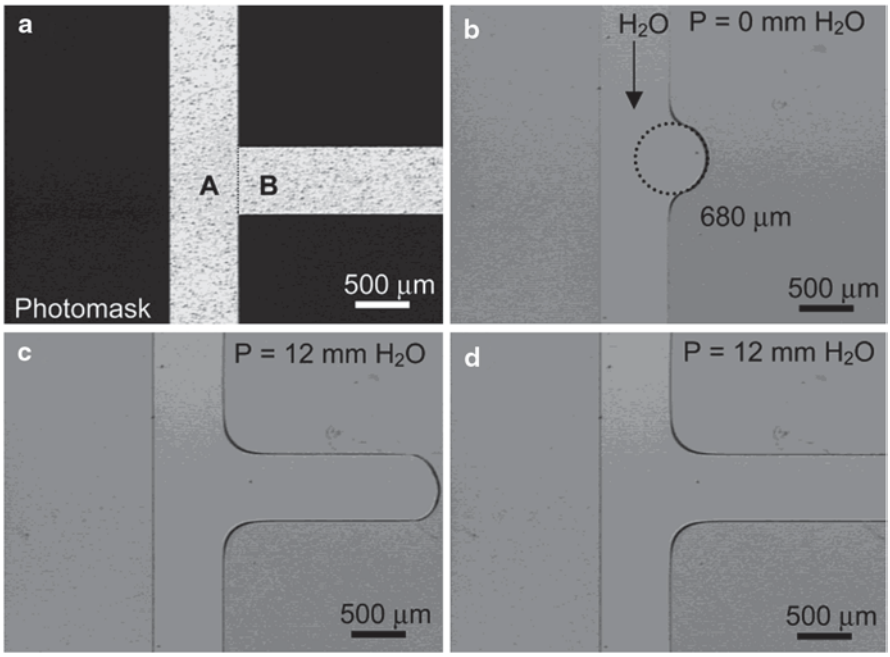


**Fig. 11.6** **a** Optical micrograph of the photomask that was used in patterning surface free energies inside a microchannel. **b** Optical micrograph of a water stream under spontaneous flow condition. **c, d** Optical micrographs of water flow under a pressure of 12 mm $H_2O$ recorded at different times. (Reprinted with permission from [62]. Copyright (2003) American Chemistry Society.)

respectively shown in Fig. 11.7 and Fig. 11.8. The green fluorescence intensity was proportional to the amount of the adsorbed BSA and suggested that the untreated PDMS area adsorbed more proteins than the PEGDA-grafted area. The HepG2 cells were not observed to attach to the PEG-covered area. These results indicated that the PEGDA-grafted layer prevents nonspecific protein adsorption and cell adhesion on PDMS.

A more specific biomedical application requiring suppression of biomolecule adsorption is electrophoretic separations of biological compounds. PDMS microfluidic devices are hampered with unwanted adsorption of biomolecules. Covalent coating of POE molecules of varying chain lengths as well as physical adsorption of triblock-copolymers of Pluronic® F108 and L101 on PDMS surface were performed to compare the electroosmotic mobilities of microchannels [69]. Results revealed that all of the above surface coatings led to reductions of electroosmotic flow. However, molecules with smaller POE tails, such as Si-$POE_{(8)}$ and L101, were the least effective. Molecules with longer POE tails (POE units > 70) are more effective but risk a consequence of lower electroosmotic velocity per unit field strength. Therefore, tailoring POE length may be a good parameter to control electroosmotic velocity in PDMS microchannels.

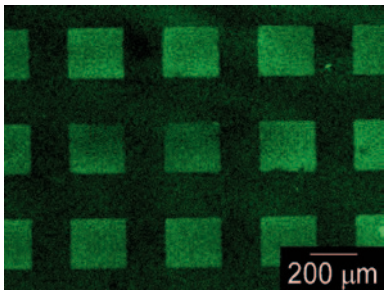


**Fig. 11.7** FITC-BSA adsorption onto the micropatterned PEGDA-grafted PDMS. (Reprinted with permission from [68]. Copyright (2008) Elsevier.)

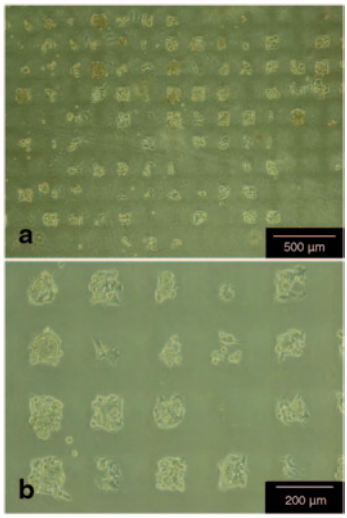


**Fig. 11.8** Optical micrographs of HepG2 cells cultured on the micropatterned PEGDA-grafted PDMS observed through **a** a 4× objective lens and **b** a 10× objective lens. (Reprinted with permission from [68]. Copyright (2008) Elsevier.)

## 11.3 Creation of Cyto-compatible Surfaces

To promote the cell adhesion on the substrate surface, protein and peptide molecules were used as coating materials, such as fibronectin protein [70] and Arg-Gly-Asp (RGD) peptide [71]. Better cell attachment was demonstrated on these immobilized surfaces, but the protein and peptide immobilization processes involve complicated protocol which may lead to uncontrollable surface absorption. Therefore, development of new coating techniques was being pursued to improve cyto-compatibility using extracellular matrix (ECM) components and microstructures. In this section, the use of polyelectrolyte multilayer (PEM) film on solid surfaces to control cellular behaviors is being discussed.

### *11.3.1 PEM Film Coating*

Coating a PEM film on a solid surface relies on nonstochiometric electrostatic interactions and cationic and anionic polyelectrolyte layers are absorbed to the surface

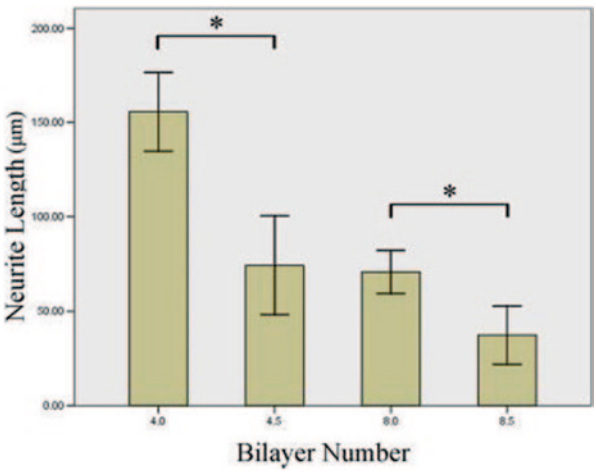


**Fig. 11.9** The neurite length of neurons was compared with $(HA/COL)_n$ films with different terminated outlayers using Student's *t* test in the group of close bilayer numbers. *Error bars* show standard deviation of the mean. $*p < 0.01$. (Reprinted with permission from [75]. Copyright (2006) Wiley Periodicals, Inc.)

alternatively. Poly-$_L$-lysine (PLL) is postively charged and is widely used for promoting cell adhesion to solid surfaces [72, 73]. Poly-$_L$-glutamine acid (PLGA) is negatively charged and is known to be a biodegradable material [74]. Layer-by-layer assembly of PEM film has been demonstrated for the improvement of cytocompatibility and the control of cellular behavior [75–80]. This method provides adjustable film properties in terms of thickness, morphology, and internal molecular structure [81, 82].

### *11.3.2 Application Examples—Control of Cellular Behavior*

Surface morphology of a hyaluronic acid (HA)-based PEM film (bilayer number <9) deposited on the amino-functionalized glass slides was investigated to have a nanoscale roughness ranging from 10 to 100 nm [75]. Primary hippocampal and cortical neural cells were cultured on the HA/Collagen type I (COL) PEM films for 5 days. The statistical results of neurite lengths of the neurons on different bilayer numbers of HA/COL films are shown in Fig. 11.9. The neurite lengths of the COL-terminated films were significantly longer than those of the HA-terminated films where they had a very close bilayer number. However, neurons grown on $(HA/COL)_{4.5}$ and $(HA/COL)_8$ films had no significant difference in neurite lengths. It was pointed out that neurite outgrowth is not simply influenced by the last layer of the PE films but may also be related to the bilayer number and other surface properties.

Moreover, in vitro cultures of neural progenitor cells on PEM films built up by heparin and PLL were also studied to improve cell adhesion and subsequent cellular functions [79]. In this study, neuronal spreading ($\beta$III-Tubulin positive) was observed on both PLL positive controls and PLL-terminating PEM films (Fig. 11.10a–c). Neurites radially elongating and perpendicular side branching at the periphery of outgrowths were observed. For heparin terminating layers, while

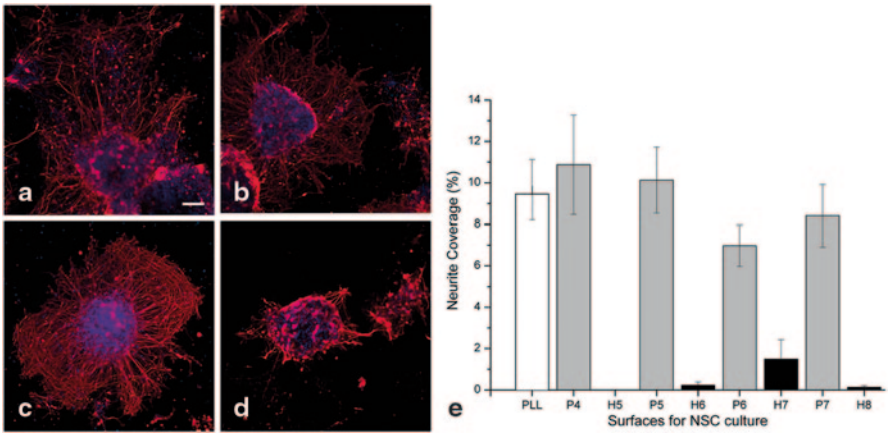


**Fig. 11.10** **a** Cells cultured for 5 days on the PLL positive control, **b** P4, **c** P5, and **d** H6 PEM film surfaces. The cells were stained by *β*III-Tubulin (*red*) for neurons and DAPI (*blue*) for nuclei. *Scale bar* indicates 100 μm in **a-d**. **e** Day 5 neurite coverage (from cell clusters) on the PLL positive control and the PEM films from P4 to H8. *Error bars* show standard deviation of the mean. (Reprinted with permission from [79]. Copyright (2011) American Vacuum Society.)

some cell colonies were seen to adhere, neurite elongations were relatively short and sparse (Fig. 11.10d. Based on the quantified neurite coverage shown in Fig. 11.10e, cell–substrate interactions were significantly improved on the PLL-terminating surfaces. In addition, brain-derived neurotrophic factor (BDNF) was adsorbed onto the PEM film surfaces. This combined chemical and biological effect was then characterized in terms of neurite length along with the full length/truncated isoform 1 tyrosine kinase receptor (TrkB-FL/TrkB-T1) and growth associated protein-43 mRNA levels. Here, the authors reported the differential effect of the adsorbed and soluble BDNF in different concentrations. The adsorbed BDNF promoted the neurite outgrowth and led to elevated, sustained TrkB mRNA levels.

## 11.4 Creation of Biological Specific Surfaces

Microfluidic systems were developed for various automated and miniaturized diagnostic applications [1]. In miniaturized environment, high surface-to-volume ratio can improve the sensitivity of biosensing when comparing to standard well format, but also magnify the effect of nonspecific binding of biomolecules. This is especially important in immunoassays that key reagents such as proteins and enzyme labels can absorb to hydrophobic surfaces, seriously degrading the assay performance. Immunoassay is to measure the presence and the concentration of antibody or antigen in biological liquid. The detection method is generally based on protein binding reaction, which is a specific interaction between an antibody and its antigen. One of the challenges is to immobilize antibodies on the sensing

surface homogeneously and effectively to achieve accurate and sensitive detection. Creating an antibody-immobilized sensing surface to specifically capture a specific antigen is important for the development of the microfluidic biological sensing systems. Hence the concentration of the target antigen in the biological liquid can be measured correctly. Strategies that have been used to attach antibodies on the sensing surface include direct adsorption and covalent attachment to reactive functional groups on the substrate. Direct adsorption is commonly used on hydrophobic polymer surfaces but this technique may not be the most sensitive because of the conformational uncertainty. Therefore, covalent attachment is more preferable to have stable protein immobilization on the sensing surface.

## *11.4.1 Immobilization of Biomolecules*

Surface modification by SAM on solid surfaces was employed to covalently immobilize protein on a surface. The functional end group of SAM can yield a number of active groups like –OH, -$NH_2$, -COOH, and –COOR to attach proteins. Generally, proteins supply the following chemical functionalities on the side chains of their polypeptide backbone: -SH (cystenine), -$NH_2$ (lysine, arginine), -COOH (asparagine, glutamine), -OH (serine), Ph-OH (Ph = phenyl, tyrosine), and imidazole (histidine). In principle, all of them can be used during the direct chemical coupling reaction on specially prepared SAM surfaces. Several strategies on modifying silicon or glass surfaces were developed and are shown in Fig. 11.11: (1) glutaraldehyde (GA)-activated 3-aminopropyltriethoxysilane (APTES) (APTES-GA surface), (2) GA-activated physically adsorbed poly(ethyleneimine) (BPEI) (BPEI-GA surface), (3) GA-activated BPEI covalently attached to 3-glycidoxypropyltrimethoxysilane (GOPS)-silanized surface (GOPS-BPEI-GA surface), (4) GA-activated physically adsorbed poly(ethyleneimine) (LPEI) (LPEI-GA surface), and (5) adsorption of antibodies on a physically adsorbed LPEI layer (LPEI surface) [83]. The detailed procedures of antibody immobilization based on different strategies are included below.

### 11.4.1.1 Immobilization of Antibodies onto APTES-GA Surface

Cleaned silicon or glass substrates are washed with sodium-dried toluene and then immersed in a solution of 10% APTES in dried toluene. Then the reaction mixture is refluxed overnight at room temperature. After removal of the solution, the substrates are rinsed several times with toluene and acetone and dried in an oven at 110 °C for 1 h. The amine groups of the APTES-silanized substrates are reacted with 2.5% v/v GA in buffer for 1 h at room temperature, followed by thorough rinsing with Milli-Q water in order to remove traces of GA to avoid cross-linking after adding antibodies. Antibody (1 mg/mL) in buffer is then added to the GA-activated surfaces to react overnight at 4 °C under gentle shaking. After 12 h, the residual aldehyde groups remained after antibody attachment are blocked with 10 mg/mL of L-lysine. The Schiff bases are reduced with 20 mg/mL $NaBH_3CN$ solution in buf-

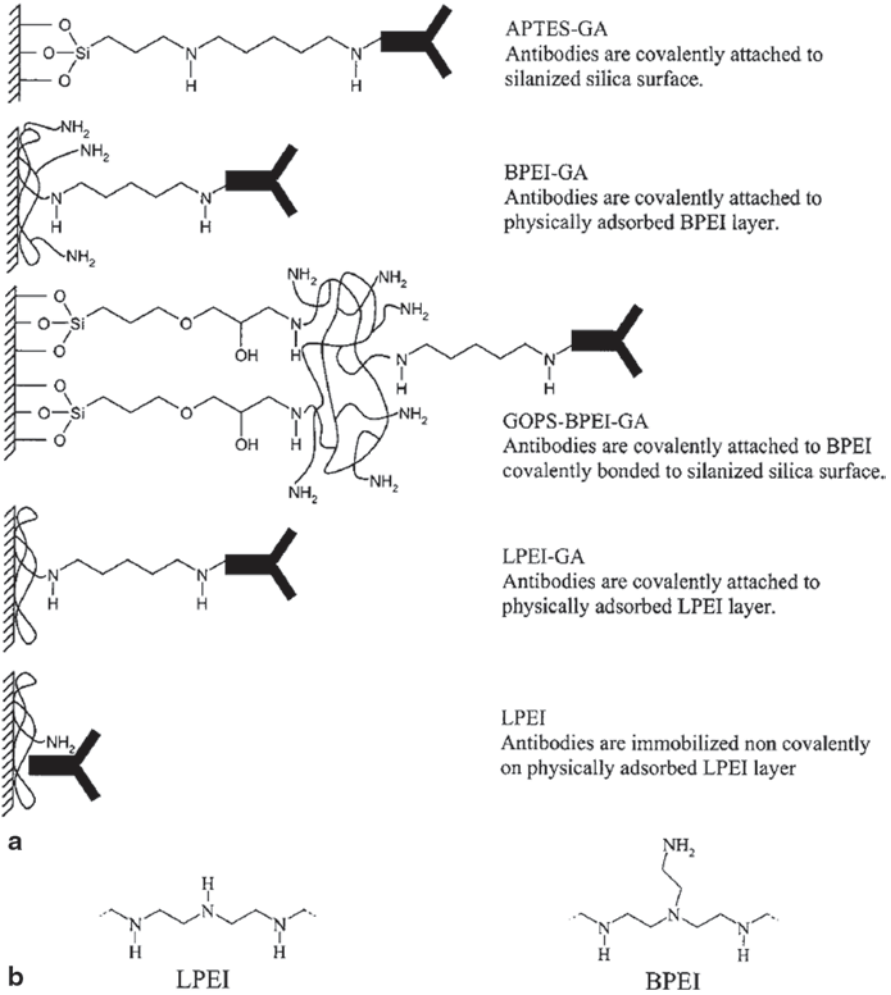


**Fig. 11.11** **a** Structures of the modified surfaces for protein immobilization. **b** Chemical structures of LPEI and BPFI. (Reprinted with permission from [83]. Copyright (2002) American Chemistry Society.)

fer, and the reaction mixture is allowed to proceed for 1–2 h under stirring at room temperature. The substrates are then carefully washed and stored in 0.1 M Tris/HCl buffer at 4 °C until use.

### 11.4.1.2 Immobilization of Antibodies on BPEI-GA Surface

Cleaned substrates are immersed in 0.5 % v/v solution of BPEI in buffer and kept under stirring at room temperature overnight and then thoroughly washed with buf-

fer. To incorporate active aldehyde groups, the substrates are reacted with 2.5% v/v GA in buffer for 2 h at room temperature under stirring. After careful washing with Milli-Q water and buffer, the aldehyde-functionalized surfaces are reacted with antibody solution overnight at 4 °C. Then the residual aldehyde groups on the surfaces are blocked and the Schiff bases reduced as described in Sect. 4.1.1.

#### 11.4.1.3 Immobilization of Antibodies on GOPS-BPEI-GA Surface

The cleaned substrates are reacted with GOPS in dry toluene, containing 2% v/v GOPS and 0.2% triethylamine at room temperature. After 1 h, the GOPS-coated surfaces are rinsed with toluene, then with acetone, and then dried in an oven at 110 °C for 1 h. A solution of 0.5% v/v BPEI in succinate buffer is added, and the reaction mixture is gently shaken for 5 h at room temperature. After careful washing with Milli-Q water, the surfaces are treated with 2.5% v/v GA in buffer. After 2 h, the surfaces are rinsed and then immersed in antibody solution. The reaction is allowed to proceed overnight at 4 °C, after which the surfaces are blocked and reduced as described in Sect. 4.1.1.

#### 11.4.1.4 Immobilization of Antibodies on LPEI-GA Surface

The cleaned substrates are immersed in 0.5% v/v solution of LPEI in buffer and kept under stirring at room temperature overnight and then thoroughly washed with buffer. The GA activation and antibody attachment steps are carried out as described in Sect. 4.1.1.

#### 11.4.1.5 Adsorption of Antibodies on LPEI Surface

The cleaned substrates are immersed in 0.5% v/v solution of LPEI in buffer and kept under stirring at room temperature overnight. The surfaces are then carefully washed with Milli-Q water, immersed in solution of antibodies in buffer, and allowed to proceed overnight at 4 °C.

### *11.4.2 Application Examples—Biosensing*

A miniaturized mosaic immunoassay was proposed based on patterning lines of antigens onto a surface by means of a microfluidic network [84]. Illustration of the strategy is shown in Fig. 11.12. The microfluidic network immobilized a series of antigens as narrow stripes on a planar substrate. After a blocking step, the antigens in each line could be recognized by specific analytes from a sample solution also guided over the substrate with a second microfluidic network. The resulting binding pattern could then be readily evaluated when analytes were tagged or developed by binding

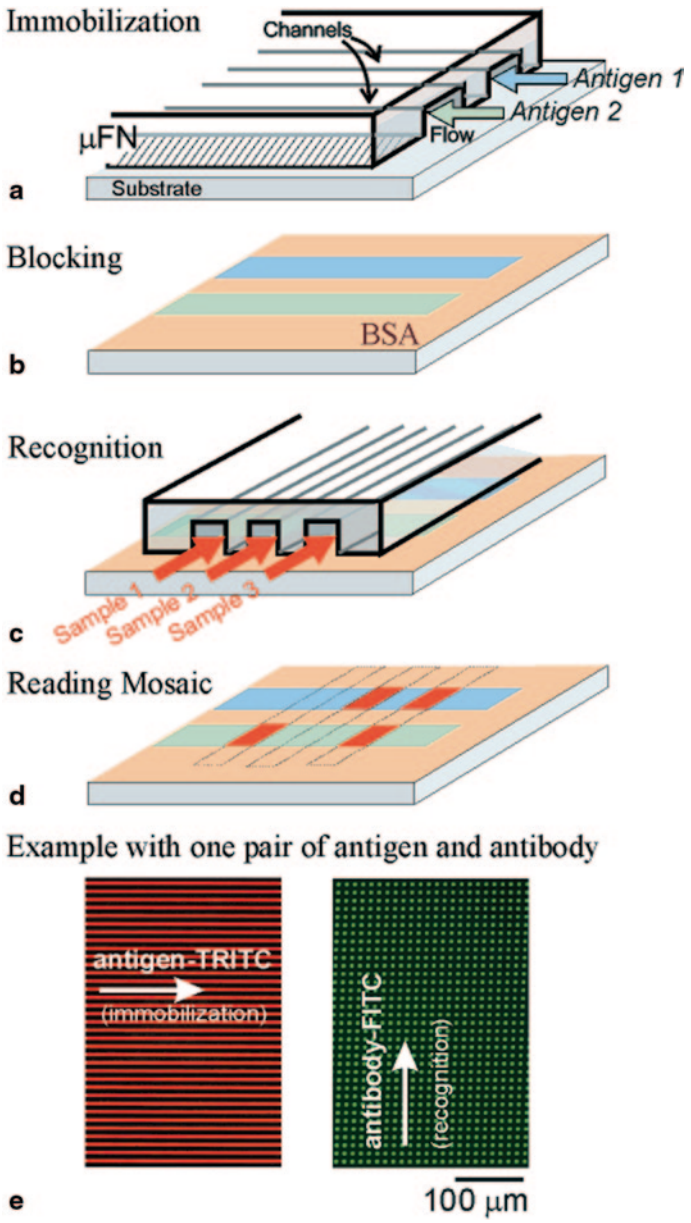


**Fig. 11.12** Strategy for performing a micromosaic immunoassay on a surface with microfluidic network cross-delivery of a series of antigens and one of antibodies. **a** A microfluidic network patterns different antigen molecules along single lines on a substrates. **b** The area of the substrate left unpatterned during (**a**), it is blocked to prevent nonspecific binding of proteins in subsequent steps. **c** Antibodies flowing through the channels of a second microfluidic network locally bind to the patterned antigens. **d** Reading the binding mosaic reveals the amount of antibodies present in the samples. **e** A mosaic can be read using a fluorescence microscope. (Reprinted with permission from [84]. Copyright (2001) American Chemistry Society.)

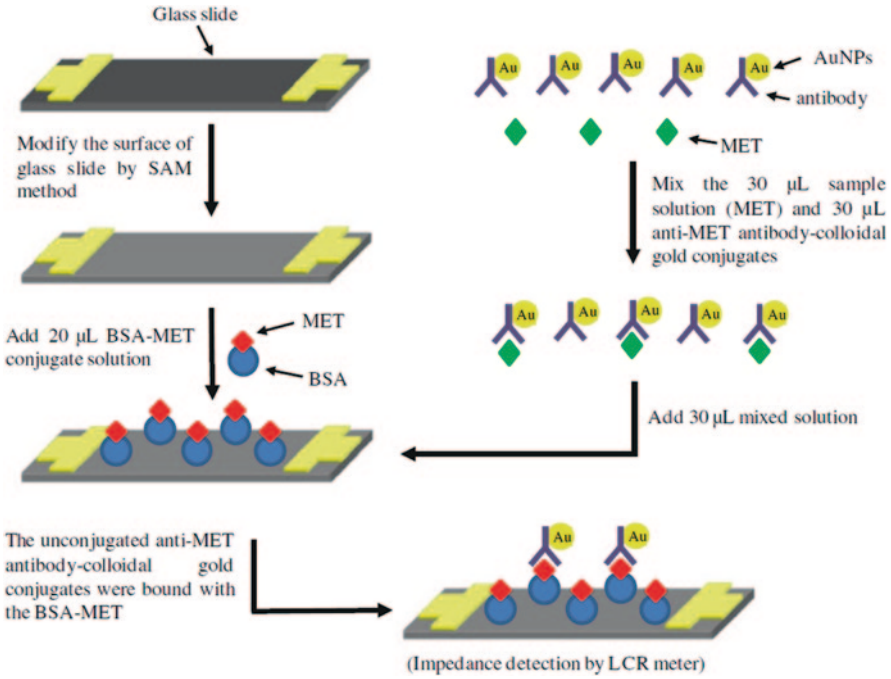


**Fig. 11.13** Principle of the competitive immunoassay method for impedance detection of MET concentration. (Reprinted with permission from [86]. Copyright (2012) Springer.)

a fluorescent- or enzyme-conjugated antibody to the analyte. A mosaic of binding events can readily be measured in one screening using fluorescence. Similarly, large-scale protein microarray was also reported, and surface modification of the biological specific surfaces is one of the key challenges for such development [85].

The abovementioned example was to immobilize antibodies on the planar substrate, and the antigen–antibody interaction was indicated by fluorescent signal. The technique of protein immobilization is also important for specific and sensitive electrical immunoassay measurement. Electrical detection of protein concentration was developed based on the resistance measurement across a pair of indium tin oxide-interdigitated electrodes [44]. Antibody was first immobilized on the electrode surface and gold nanoparticles were then applied to indicate the concentration of the immobilized antibodies. Similar development was reported for methamphetamine (MET) detection [86]. Competitive immunoassay method was used in this study and illustrated in Fig. 11.13. The electrode on SAM modified glass slide was immobilized with bovine serum albumin (BSA)-MET conjugates. After sample solution of MET in urine was mixed with anti-MET antibody-colloidal gold conjugates for 1 min, the mixed solution was applied to the electrode surface, and the residual anti-MET antibody-colloidal gold conjugates were bound with BSA-MET conjugates. Consequently, the impedance across the electrode was measured and represented the concentration of the MET.

## 11.5 Concluding Remarks

Functional patterned surfaces provide a simple approach for selective biorecognition. This chapter reviewed the most commonly used surface modification technologies and their applications of fluid manipulation, suppression of biomolecule adsorption, control of cellular behavior, and biosensing in microfluidic systems. We anticipate that as these manufacturing and surface chemical techniques mature, microfluidic devices will be more widely used for many biomedical screening and diagnostics in the near future.

## References

1. K.F. Lei, Microfluidic systems for diagnostic applications: A review. JALA 2012, 17, 330–347.
2. K.F. Lei, Review on impedance detection of cellular responses in micro/nano environment. Micromachines 2014, 5, 1–12.
3. H. Andersson, A. van den Berg, Microfluidic devices for cellomics: A review. Sens Actuators B 2003, 92, 315–325.
4. C. Zhang, J. Xu, W. Ma, W. Zheng, PCR Microfluidic devices for DNA amplification. Biotech. Advances 2006, 24, 243–284.
5. P. Pal, K. Sato, Various shapes of silicon freestanding microfluidic channels and microstructures in one-step lithography. J. Micromech. Microeng. 2009, 19, 055003–055013.
6. F. Marty, L. Rousseau, B. Saadany, B. Mercier, O. Francais, Y. Mita, T. Bourouina, Advanced etching of silicon based on deep reactive ion etching for silicon high aspect ratio microstructures and three-dimensional micro- and nanostructures. Mciroelectron. J. 2005, 36(7), 673–677.
7. M. Esashi, A. Nakano, S. Shoji, H. Hebiguchi, Low-temperature silicon-to-silicon anodic bonding with intermediate low melting point glan. Sens. Actuators A 1990, 23, 931–934.
8. P. Gravesen, J. Branebjerg, O.S. Jensen, Microfluidics-a review. J. Micromech. Microeng. 1993, 3, 168–182.
9. A. Luque, J.M. Quero, C. Hibert, P. Fluckiger, A.M. Ganan-Calvo, Integrable silicon microfluidic valve with pneumatic action. Sens. Actuators A 2005, 118(1), 144–151.
10. Y. Li, T. Pfohl, J.H. Kim, M. Yasa, Z. Wen, M.W. Kim, C.R. Safinya, Selective surface modification in silicon microfluidic channel for micromanipulation of biological macromolecules. Biomed. Microdevices 2001, 3(3), 239–244.
11. N.R. Harris, M. Hill, S. Beeby, Y. Shen, N.M. White, J.J. Hawkes, W.T. Coakley, A silicon microfluidic ultrasonic separator. Sens. Actuators B 2003, 95, 425–434.
12. Y. Xia, G.M. Whitesides, Soft lithography. Annu. Rev. Mater. Sci. 1998, 28, 153–184.
13. H. Becker, U. Heim, Hot embossing as a method for the fabrication of polymer high aspect ratio structures. Sens. Actuators A 2000, 83(1–3), 130–135.
14. U.M. Attia, S. Marson, J.R. Alcock, Micro-injection moulding of polymer microfluidic devices. Microfluid. Nanofluid. 2009, 7, 1–28.
15. K.F. Lei, S. Ahsan, N. Budraa, W.J. Li, J.D. Mai, Microwave bonding of polymer-based substrates for potential encapsulated micro/nano device fabrication. Sens. Actuators A 2004, 114(2–3), 340–346.
16. C.W. Tsao, D.L. DeVoe, Bonding of thermoplastic polymer microfluidics. Microfluid. Nanofluid. 2009, 6, 1–16.
17. M.A. Unger, H.P. Chou, T. Thorsen, A. Scherer, S.R. Quake, Monolithic microfabricated valves and pumps by multilayer soft lithography. Science 2000, 288, 113–116.

18. H. Becker, L.E. Locascio, Polymer microfluidic devices. Talanta 2002, 56(2), 267–287.
19. B. Kuswandi, Nuriman, J. Huskens, W. Verboom, Optical sensing systems for microfluidic devices: A review. Anal. Chim. Acta 2007, 601(2), 141–155.
20. S.E. McCalla, A. Tripathi, Microfluidic reactors for diagnostics applications. Annu. Rev. Biomed. Eng. 2011, 13, 321–343.
21. G.M. Whitesides, The origins and the future of microfluidics. Nature 2006, 442, 368–373.
22. A.W. Martinez, S.T. Phillips, G.M. Whitesides, Diagnostics for the developing world: microfluidic paper-based analytical devices. Anal. Chem. 2010, 82(1), 3–10.
23. W. Dungchai, O. Chailapakul, C.S. Henry, Electrochemical detection for paper-based microfluidics. Anal. Chem. 2009, 81, 5821–5826.
24. A.W. Martinez, S.T. Philips, B.J. Wiley, M. Gupta, G.M. Whitesides, FLASH: A rapid method for prototyping paper-based microfluidic devices. Lab Chip 2008, 8, 2146–2150.
25. E. Carrilho, A.W. Martinez, G.M. Whitesides, Understanding wax printing: A simple micropatterning process for paper-based microfluidics. Anal. Chem. 2009, 81, 7091–7095.
26. Y. Lu, W. Shi, L. Jiang, J. Qin, B. Lin, Rapid prototyping of paper-based microfluidics with wax for low-cost, portable bioassay. Electrophoresis 2009, 30, 1497–1500.
27. D.A. Bruzewicz, M. Reches, G.M. Whitesides, Low-cost printing of poly(dimethylsiloxane) barriers to define microchannels in paper. Anal. Chem. 2008, 80, 3387–3392.
28. X. Li, J. Tian, T. Nguyen, W. Shen, Paper-based microfluidic devices by plasma treatment. Anal. Chem. 2006, 80, 9131–9134.
29. W. Zhao, M.M. All, S.D. Aguirre, M.A. Brook, Y. Li, Paper-based bioassays using gold nanoparticle colorimetric probes. Anal. Chem. 2008, 80, 8431–8437.
30. A.K. Ellerbee, S.T. Phillips, A.C. Siegel, K.A. Mlrica, A.W. Martinez, et al., Quantifying colorimetric assays in paper-based microfluidic devices by measuring the transmission of light through paper. Anal. Chem. 2009, 81, 8447–8452.
31. D. Zang, L. Ge, M. Yan, X. Song, J. Yu, Electrochemical immunoassay on a 3D microfluidic paper-based device. Chem. Commun. 2012, 48, 4683–4685.
32. Z. Nie, C.A. Nijhuis, J. Gong, X. Chen, A. Kumachev, et al., Electrochemical sensing in paper-based microfluidic devices. Lab Chip 2009, 10, 477–483.
33. C.M. Cheng, A.W. Martinez, J. Gong, C.R. Mace, S.T. Phillips, et al., Paper-based ELISA. Angew. Chem. Int. Ed. 2010, 49, 4771–4774.
34. R.C. Murdock, L. Shen, D.K. Griffin, N. Kelley-Loughnane, I. Papautsky, et al., Optimization of a paper-based ELISA for a human performance biomarker. Anal. Chem. 2013, 85, 11634–11642.
35. H.K. Wang, C.H. Tsai, K.H. Chen, C.T. Tang, J.S. Leou, et al., Cellulose-based diagnostic devices for diagnosing serotype-2 dengue fever in human serum. Adv. Healthcare Mater. 2013, 3(2), 187–196.
36. S. Wang, L. Ge, X. Song, J. Yu, S. Ge, et al., Paper-based chemiluminescence ELISA: lab-on-paper based on chitosan modified paper device and wax-screen-printing. Biosens. Bioelectron. 2012, 31, 212–218.
37. D. Erickson, X. Liu, U. Krull, D. Li, Electrokinetically Controlled DNA hybridization microfluidic chip enabling rapid target analysis. Anal. Chem. 2004, 76, 7269–7277.
38. G.B. Lee, S.H. Chen, G.R. Huang, W.C. Sung, Y.H. Lin, Microfabricated plastic chips by hot embossing methods and their applications for DNA separation and detection. Sens. Actuators B 2001, 75(1–2), 142–148.
39. L. Wang, P.C.H. Li, Microfluidic DNA microarray analysis: A review. Anal. Chim. Acta 2011, 687, 12–27.
40. X. Weng, H. Jiang, D. Li, Microfluidic DNA hybridization assays. Microfluid. Nanofluid. 2011, 11, 367–383.
41. K.F. Lei, H. Cheng, K.Y. Choy, L.M.C. Chow, Electrokinetic DNA concentration in micro systems. Sens. Actuators A 2009, 156, 381–387.
42. Y. He, M. Tsutsui, C. Fan, M. Taniguchi, T. Kawai, Gate manipulation of DNA capture into nanopores. ACS Nano 2011, 5, 8391–8397.
43. A.H. Diercks, A. Ozinsky, C.L. Hansen, J.M. Spotts, D.J. Rodriguez, A. Aderem, A microfluidic device for multiplexed protein detection in nano-liter volumes. Anal. Biochem. 2009, 386, 30–35.

44. K.F. Lei, Quantitative electrical detection of immobilized protein using gold nanoparticles and gold enhancement on a biochip. Meas. Sci. Technol. 2011, 22, 105802.
45. M. Hervas, M.A. Lopez, A. Escarpa, Electrochemical immunosensing on board microfluidic chip platforms. TrAC Trends Anal. Chem. 2012, 31, 109–128.
46. A.H.C. Ng, U. Uddayasankar, A.R. Wheeler, Immunoassays in microfluidic systems. Anal. Bioanal. Chem. 2010, 397, 991–1007.
47. A. Bhattacharyya, C.M. Klapperich, Design and testing of a disposable microfluidic chemiluminescent immunoassay for disease biomarkers in human serum samples. Biomed. Microdevices 2007, 9, 245–251.
48. F.T.G. van den Brink, E. Gool, J.P. Frimat, J. Borner, A. van den Berg, S. Le Gac, Parallel single-cell analysis microfluidic platform. Electrophoresis 2011, 32, 3094–3100.
49. R.N. Zare, S. Kim, Microfluidic platforms for single-cell analysis. Annu. Rev. Biomed. Eng. 2010, 12, 187–201.
50. M.H. Wu, S.B. Huang, G.B. Lee, Microfluidic cell culture systems for drug research. Lab Chip 2010, 10, 939–956.
51. K.F. Lei, P.H.M. Leung, Microelectrode array biosensor for the detection of Legionella pneumophila. Microelectron. Eng. 2012, 91, 174–177.
52. K.F. Lei, M.H. Wu, C.W. Hsu, Y.D. Chen, Real-time and non-invasive impedimetric monitoring of cell proliferation and chemosensitivity in a perfusion 3D cell culture microfluidic chip. Biosens. Bioelectron. 2014, 51, 16–21.
53. A.W. Adamson. Physical Chemistry of Surface, Wiley, New York, 1990.
54. R.K. Iler. The Chemistry of Silica, Wiley, New York, 1979.
55. E.M. Liston, L. Martinu, M.R. Wertheimer, Plasma surface modification of polymers for improved adhesion: a critical review. J Adhesion Sci. Tech. 1993, 7(10), 1091–1127.
56. C. Oehr, Plasma surface modification of polymers for biomedical use. Nucl. Instrum. Meth. Phys. Res. B 2003, 208, 40–47.
57. L.S. Jang, W.H. Kan, Peristaltic piezoelectric micropump system for biomedical applications. Biomed. Microdevices 2007, 9, 619–626.
58. F. Amirouche, Y. Zhou, T. Johnson, Current micropump technologies and their biomedical applications. Microsyst. Tech. 2009, 15, 647–666.
59. S. Zeng, B. Li, X. Su, J. Qin, B. Lin, Microvalve-actuated precise control of individual droplets in microfluidic devices. Lab Chip 2009, 9, 1340–1343.
60. K.W. Oh, C.H. Ahn, A review of microvalves. J Micromech. Microeng. 2006, 16, R13–R39.
61. B. Zhao, J.S. Moore, D.J. Beebe, Surface-directed liquid flow inside microchannels. Science 2001, 291, 1023–1026.
62. B. Zhao, J.S. Moore, D.J. Beebe, Pressure-sensitive microfluidic gates fabricated by patterning surface free energies inside microchannels. Langmuir 2003, 19, 1873–1879.
63. B. Zhao, J.S. Moore, D.J. Beebe, Principles of surface-directed liquid flow in microfluidic channels. Anal. Chem. 2002, 74(16), 4259–4268.
64. H. Chen, M.A. Brook, H. Sheardown, Silicon elastomers for reduced protein adsorption. Biomaterials 2004, 25, 2273–2282.
65. F. Abbasi, H. Mirzadeh, Adhesion between modified and unmodified poly(dimethylsiloxane) layers for a biomedical application. Int. J. Adhes. Adhes. 2004, 24, 247–257.
66. H. Makambe, J.H. Kim, K. Lim, N. Park, J.H. Hahn, Surface modification of poly(dimethyl siloxane) microchannels. Electrophoresis 2003, 24, 3607–3619.
67. S. Pinto, P. Alves, C.M. Matos, A.C. Santos, L.R. Rodrigues, J.A. Texeira, M.H. Gil, Poly(dimethyl siloxane) surface modification by low pressure plasma to improve its characteristics towards biomedical applications. Colloid Surface B 2010, 81, 20–26.
68. S. Sugiura, J. Edahiro, K. Sumaru, T. Kanamori, Surface modification of poly dimethylsiloxane with photo-grafted poly(ethylene glycol) for micropatterned protein adsorption and cell adhesion. Colloids Surface B 2008, 63, 301–305.
69. W. Hellmich, J. Regtmeier, T.T. Duong, R. Ros, D. Anselmetti, A. Ros, Poly(oxyethylene) based surface coatings for poly(dimethylxiloxane) microchannels. Langmuir 2005, 21, 7551–7557.

70. Vassanelli, S.; Fromherz, P. Transistor probes local potassium conductances in the adhesion region of cultured rat hippocampal neurons. J. Neurosci. 1999, 19, 6767–6773.
71. Davis, D. H.; Giannoulis, C. S.; Johnson, R. W.; Desai, T. A. Immobilization of RGD to < 111 > silicon surfaces for enhanced cell adhesion and proliferation. Biomaterials 2002, 23, 4019–4027.
72. V. Gribova, C. Gauthier-Rouviere, C. Albiges-Rizo, R. Auzely-Velty, C. Picart. Effect of RGD functionalization and stiffness modulation of polyelectrolyte multilayer films on muscle cell differentiation. Acta Biomaterialia. 2013, 9, 6468–6480.
73. L. Richert, P. Lavalle, D. Vautier, B. Senger, J.F. Stoltz, P. Schaaf, et al., Cell interactions with polyelectrolyte multilayer films. Biomacromolecules 2002, 3(6), 1170–1178.
74. B. Cao, S. Yan, K. Zhang, Z. Song, X. Chen, L. Cui, et al., Layer-by-layer assembled multilayer films of methoxypoly(ethylene glycol)-block-poly(alpha, l-glutamic acid) and chitosan with reduced cell adhesion. Macromolecular Biosci. 2011, 11(9), 1211–1217.
75. Z.R. Wu, J. Ma, B.F. Liu, Q.Y. Xu, F.Z. Cui, Layer-by-layer assembly of polyelectrolyte films improving cytocompatibility to neural cells. J. Biomed. Mater. Res. A 2007, 81 A, 355–362.
76. L. Richert, P. Lavalle, D. Vautier, B. Senger, J.F. Stoltz, et al., Cell interactions with polyelectrolyte multilayer films. Biomacromolecules 2002, 3, 1170–1178.
77. L. Richert, A. Youri, P. Schaar, J.C. Voegel, C. Picart, pH dependent growth of poly(L-lysine)/poly(L-glutamic) acid multilayer films and their cell adhesion properties. Surf. Sci. 2004, 570, 13–29.
78. L. Richert, A. Schneider, D. Vautier, C. Voduouhe, N. Jessel, et al. Imaging cell interactions with native and crosslinked polyelectrolyte multilayers. Cell Biochem. Biophys. 2006, 44, 273–285.
79. K. Zhou, G.Z. Sun, C.C. Bernard, G.A. Thouas, D.R. Nisbet, et al., Optimizing interfacial features to regulate neural progenitor cells using polyelectrolyte multilayers and brain derived neurotrophic factor. Biointerphases 2011, 6, 187–199.
80. J. Almodóvar, S. Bacon, J. Gogolski, J.D. Kisiday, M.J. Kipper, Polysaccharide-based polyelectrolyte multilayer surface coatings can enhance mesenchymal stem cell response to adsorbed growth factors. Biomacromolecules 2010, 11, 2629–2639.
81. R. A McAloney, M. Sinyor, V. Dudnik, M.C. Goh, Atomic force microscopy studies of salt effects on polyelectrolyte multilayer film morphology. Langmuir 2001, 17, 6655–6663.
82. D. Yoo, S.S. Shiratori, M.F. Rubner, Controlling bilayer composition and surface wettability of sequentially adsorbed multilayers of weak polyelectrolytes. Macromolecules 1998, 31, 4309–4318.
83. J. Yakovleva, R. Davidsson, A. Lobanova, M. Bengtsson, S. Eremin, et al., Microfluidic enzyme immunoassay using silicon microchip with immobilized antibodies and chemiluminescence detection. Anal. Chem. 2002, 74, 2994–3004.
84. A. Bernard, B. Michel, E. Delamarche, Micromosaic Immunoassays. Anal. Chem. 2001, 73, 8–12.
85. M. Schaeferling, S. Schiller, H. Paul, M. Kruschina, P. Pavlickova, et al., Application of self-assembly techniques in the design of biocompatible protein microarray surfaces. Electrophoresis 2002, 23, 3097–3105.
86. C.H. Yeh, W.T. Wang, P.L. Shen, Y.C. Lin, A developed competitive immunoassay based on impedance measurements for methamphetamine detection. Microfluid. Nanofluid. 2012, 13, 319–329.

# Chapter 12
# Biopatterns Created Using Colloidal Templates

**Qin Li, Maria Askildsen and Ehsan Eftekhari**

## 12.1 Introduction

Colloids refer to particles in the size range of a few nanometres to a few micrometres. When the colloidal particles are monodispersed in size, upon favourable conditions, they can spontaneously assemble into ordered assemblies, named 'colloidal crystals'. Colloidal assemblies can be either two-dimensional (2D) or three-dimensional (3D) periodically structured lattices, and they serve as excellent templates for patterning [1]. Colloidal templating is also sometimes referred to as colloidal lithography. 2D hexagonal lattices of colloidal spheres have been successfully demonstrated as physical masks for fabrications of ordered arrays of micro- or nanostructures, whilst 3D colloidal crystals have often been employed as removable templates for highly ordered, macroporous materials with partial photonic bandgaps, which have applications in sensors and optoelectronic devices [2]. In colloidal templating, the most commonly used colloidal particles are either polystyrene (PS) spheres or silica spheres, owing to the well-established synthesis methods for controlling particle size with tight monodispersity and the ease in removal as a template [2].

Colloidal templating is a very versatile technique; the 2D and 3D colloidal crystals can serve as templates for depositing various metals, catalysts, polymers and inorganic materials and forming inversed replica structures [3–6]. Colloidal templating has salient advantages in that it does not require any elaborate lithrography equipment, it is intrinsically a parallel process and can be easily integrated with existing material deposition techniques such as sputtering/evaporation [7], chemical

Q. Li (✉) · M. Askildsen
School of Engineering (Environmental), Griffith University, Nathan, QLD 4111, Australia
e-mail: qin.li@griffith.edu.au

Queensland Micro- and Nanotechnology Centre, Griffith University,
Nathan, QLD 4111, Australia

E. Eftekhari
Queensland Micro- and Nanotechnology Center and School of Engineering, Griffith University,
170 Kessels Rd, 4111 Nathan, QLD, Australia
e-mail: ehsan.eftekhari@griffithuni.edu.au



J. Rodríguez-Hernández, A. L. Cortajarena (eds.), *Design of Polymeric Platforms for Selective Biorecognition,* DOI 10.1007/978-3-319-17061-9_12

vapour deposition [8], reactive ion etching [9], plasma treatment [10] and inkjet printing [11] to produce patterns of desired chemistry.

Self-assembled colloidal templates have been used to successfully pattern and culture cellular structures such as bacteria [12], and human cell cultures [13, 14] by providing an underlying protein pattern. The morphology and growth direction of biological microstructures can also be controlled by the substrate topography—both natural, and synthesized (e.g. fabricated nanostructures)—and is a major area of research in tissue engineering such as scaffold design for regenerative therapies [15]. In those patterning formats, the colloidal assembly can be used either as the direct underlying surface, or a sacrificial template. The formed patterns can be either disconnected or interconnected. Ordered patterns imply uniformity and optimum density, and they are compatible with array systems, and signal read-out platforms. Colloidal crystals also possess special optical features originated from Bragg's diffraction owing to their structural periodicity, which may be exploited particularly in sensing technologies. Moreover, colloidal self-assembly can be combined with supramolecular chemistry [16] or soft lithography [17] for creating hierarchical patterning.

The patterns generated by colloidal templating can be controlled in the range from several nanometres to several micrometres. When the pattern feature size is two or three orders of magnitude larger than proteins themselves, the protein adsorption behaviour is not different from protein adsorption on a non-patterned surface with the same surface chemistry, governed by the same fundamental protein–surface interactions, such as physisorption, chemisorption and bioaffinity. But when the pattern dimensions become comparable to the protein size, the protein–surface interaction can become atypical, which deserves particular attention [18]. We should also be mindful of that, proteins are delicate biomolecules which are prone to denaturation if chemically treated, and this critical factor must be considered when selecting or developing a patterning strategy.

This chapter intends to provide an overview on protein patterning generated by colloidal templating including the fabrications, properties and their applications. It aims to serve as a compendium for researchers and industry readers who are interested in this technology.

## 12.2 Fabrications of Colloidal Crystal Templates

Since the colloidal templates are the basis for this technology, we first introduce the fabrication methodologies for producing the 2D, 3D and hierarchically ordered colloidal crystals.

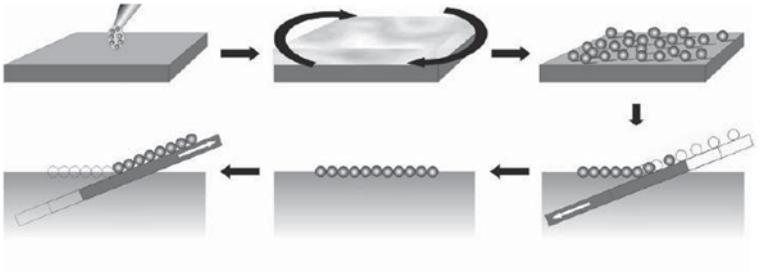

**Fig. 12.1** Monolayer formation at the air–water interface from a spin-coated parent substrate by the SC method [23]

## *12.2.1 2D Colloidal Crystals*

### 12.2.1.1 2D Close Packing

Self-assembling of 2D colloidal crystals (also *colloidal monolayers*) often involves a solvent drying process and an air–water interface; it is highly dependent on the interplay between the capillary forces and DLVO force among the colloidal particles [19]. The fabrication of 2D colloidal crystals can be categorized into two main approaches: (1) direct assembly on targeted substrate materials, or (2) pre-assembly on an intermediate surface, typically at air–water interface, with subsequent transfer onto the target. In the former case, the monolayer is created by either drying a colloidal suspension on a very smooth substrate such as mercury or by vertical lifting deposition [20, 21] or spin coating [22].

Retsch et al. [23] developed a more reproducible method whereby close-packed colloidal 2D crystals were constructed through floatation and re-deposition of PS particles at the air–water interface. As depicted in Fig. 12.1, in this method, a PS colloidal dispersion is first spin-coated onto a solid support termed the 'parent substrate' in a sparsely distributed fashion. After the dispersion is dried, the parent substrate is slowly immersed at a shallow angle in MilliQ water with moderate addition of sodium dodecylsulfate surfactant and/or pH-adjustment, causing the colloidal particles to detach and float at the air–water interface. The detached particles spontaneously self-assemble into a dense monolayer and remain afloat at the interface. A second 'receiving substrate' is then immersed into the water and slowly withdrawn at a shallow angle and collects the floating colloidal monolayer.

The method can produce high quality 2D colloidal crystals with large domain size spanning hundreds of micrometres as shown in Fig. 12.2. Moreover, the 2D assemblies exhibit strong mechanical stability; they can be transferred onto curved receiving surfaces, such as on tubular surface and undulating surfaces such as the ones formed by 2D crystals of different particle sizes as shown in the right panel in Fig. 12.2 [23].

The additional advantage of the method is that the 2D colloidal crystals formed at the air–water interface can be transferred onto both hydrophilic and hydrophobic

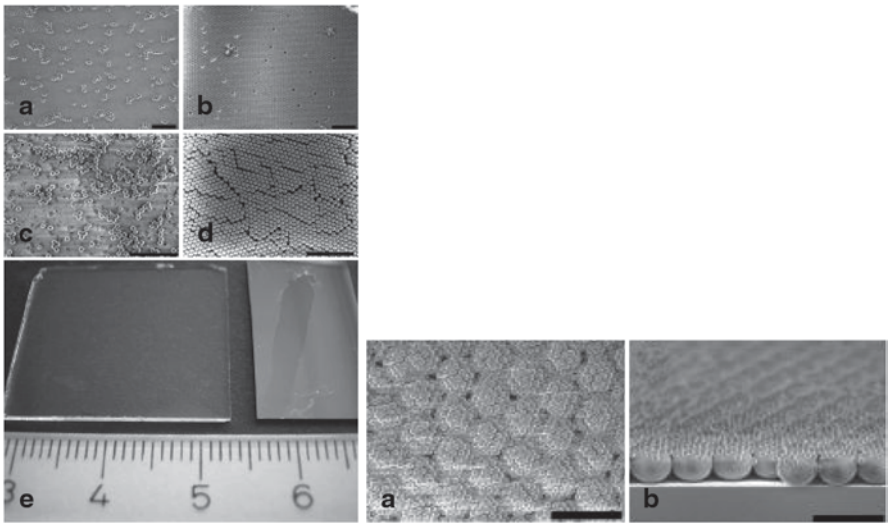


**Fig. 12.2** *Left panel*: Formation of highly ordered, hexagonally close-packed monolayers (**b** and **d**) by floatation of sparsely distributed colloids of 1116 (**a**) and 182 nm (**c**), respectively. **e** shows a comparison of the 182 nm particles distribution on the parent substrate (*left*) versus a resultant close packed monolayer after floating (*right, dark grey* patch). *Scale bars* are 10 μm for **a** and **b**, and 2 μm for **c** and **d**. *Right panel*: stacking of PS monolayers of different particle size [23]

surfaces, as shown in the schematics in Fig. 12.3. This significantly enhances the versatility of this facile method.

#### 12.2.1.2 Non-close 2D Ordered Packing

Non-close packed 2D arrays provide further flexibility in controlling pattern size, shape and inter-distance. Strategies have been developed to overcome the predestined hexagonal close packing structure governed by the thermodynamics. Zhou et al. [24] have invented a layer by layer method to produce non-close 2D

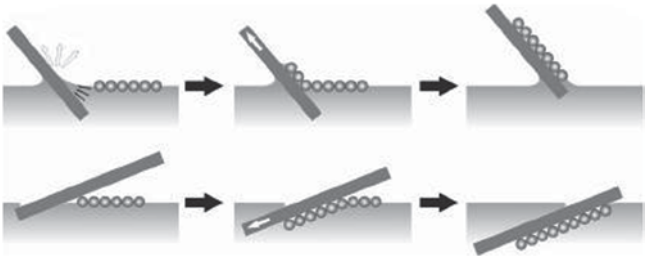

**Fig. 12.3** Scheme: Transfer of a floating monolayer onto a hydrophilic (*top row*) and hydrophobic (*bottom row*) substrate

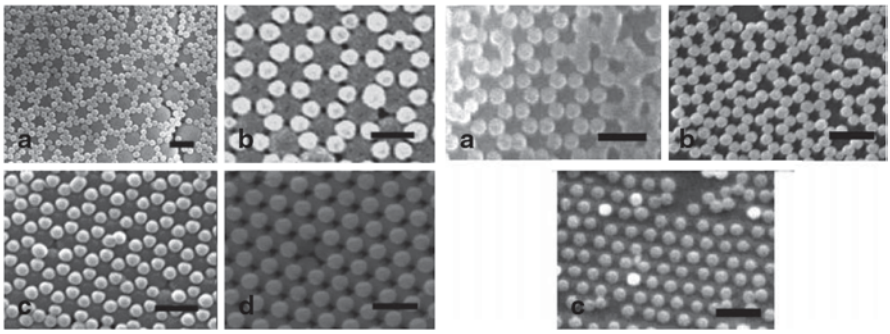


**Fig. 12.4** *Left panel*: Silica monolayer patterns fabricated on PS colloidal films with size ratios of 0.28 (**a**), 0.4 (**b**), 0.48 (**c**) and 0.68 (**d**); *Right panel*: Remaining silica monolayer after removing the underlying PS colloidal films with size ratios of 0.4 (**a**), 0.48 (**b**) and 0.68 (**c**). The scale bar indicates 1 μm in all images [24]

packing, whereby a PS colloidal monolayer is first deposited on a glass substrate, followed by a second silica sphere layer deposited by vertical deposition, and subsequently heat treatment to remove the bottom PS layer. Figure 12.4 displays the SEM images of the structures after the bilayer formation and the following heat treatment.

Non-close packed 2D arrays can also be obtained by shrinking the size of colloidal spheres of the 2D hexagonal close packing. Vogel et al. [25, 26] have demonstrated that non-close packed 2D arrays can be used in combination with plasma etching to form the non-close 2D ordered packing. In their study, the non-close 2D packing enabled an inclined Au sputtering process to create novel nanostructures such as arrays of gold crescents, which showed heightened sensitivity in biosensing due to enhanced plasmonic effect.

#### 12.2.1.3 2D Binary Colloidal Crystals

Singh et al. [27] have recently successfully fabricated 2D binary colloidal crystals with the two sizes of particles truly on the same plane. A modified Denkov 2D colloidal crystallization [28] was developed, whereby the colloidal solution of multicomponent colloids was confined inside a rubber ring placed on a hydrophilic surface to grow [10]. The schematic in Fig. 12.5 demonstrates the versatility of this binary colloidal monolayer in changing the chemical pattern geometry by using different composite binary colloidal assemblies (BCAs) as lithographic masks, and they can be utilized to adsorb proteins selectively after surface modification. Different chemical, micro- and nanopatterns can be created by exposing the templates to sputter-coating processes. Gold sputtering was chiefly employed in this study owing to its good compatibility with biomolecules.

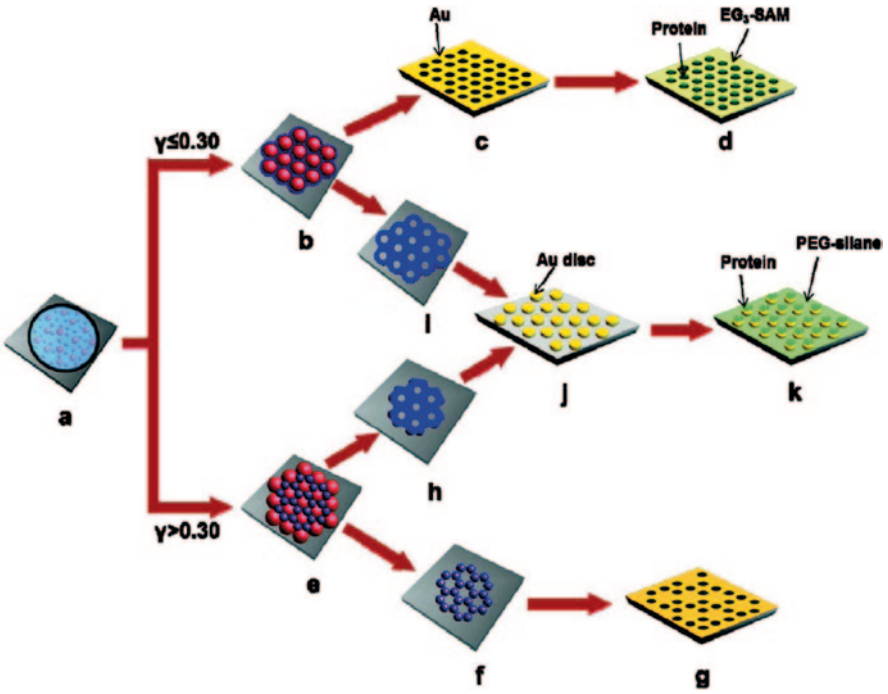


**Fig. 12.5** Schematic illustration showing the generation of different chemical patterns from low and high size ratio BCAs, and subsequent protein patterning after surface modification of the patterned surface. **a** A mixed suspension of different sizes of colloidal particles is spread inside a rubber ring. **b**, **e** BCAs form after complete evaporation of the solvent. **c** Au sputtering over the colloidal mast and the removal of particles by sonication or lift-off yield chemically patterned surfaces. **f** Heating the composite template made from PS and SiO2 particles for 5–10 min at 100°C and removal of SiO2 particles by H. **g** Au deposition over the mast generates a chemical pattern comprising six holes arranged in hexagonal fashion. **h**, **i** Heating the composite masks for longer duration (20–45 min) at 120°C and removal of silica particles by HF. **j** Au deposition and subsequent removal of PS particles yield disk-like gold patterns. **d**, **k** The chemical modification of the patterned surface with protein resistant molecules guides the specific adsorption of the protein to unmodified regions [27]

#### 12.2.1.4 Other Unconventional Patterns

The growth of thin film colloidal crystals can be influenced by substrate patterning. Key parameters influencing crystal formation include confining cell thickness, and the surface profile of the patterned substrate. Using the corrugated surface of commercially-available recordable DVDs as a wedge cell template, Ramiro-Manzano, Bonet [29] studied the growth of PS colloidal crystals. The researchers found that groove size, substrate pitch, cell thickness value and particle-to-substrate relative size dictated the deposited crystal configuration. For particles with size in order of the groove width, increasing cell thickness resulted in spherical particle distribution going from linear rows (i.e. reported ‘zigzag angle of 180 degrees’) to 60 degrees ‘zigzag’, and eventually to triangular arrangement of close-packed spheres as more

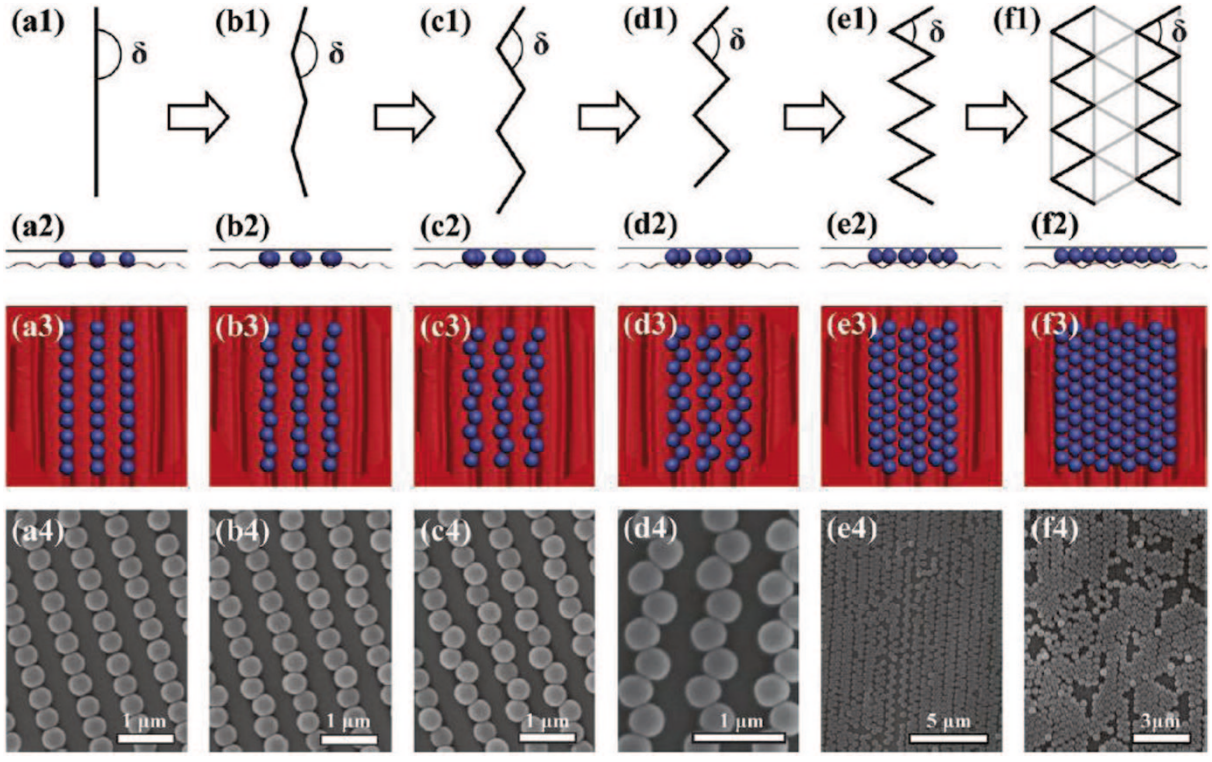


**Fig. 12.6** SEM images (*bottom row*) of different particle orderings, the cell thickness increasing from the *left* to the *right* side of the panel. Side (*second row*) and top (*third row*) views of the ordering model showing the sphere distribution in the grooves. The *first row* shows how the zigzag angle of particle strips changes from180° (**a**) to 60° (**e**). **f** A triangular arrangement of close-packed spheres. The particle size is 380 nm [29]

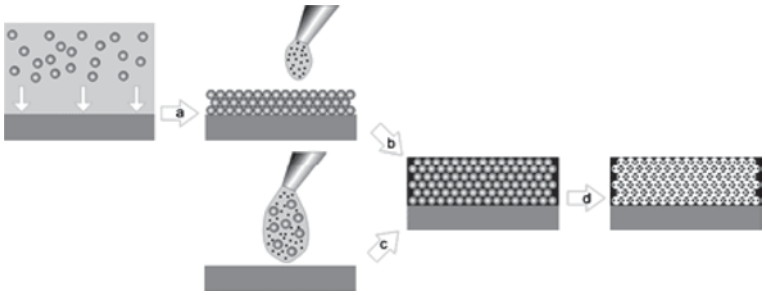


**Fig. 12.7** Scheme of general preparation routes to 3D macroporous networks by colloidal crystal templating [32]

spheres are spatially accommodated and filling fraction is maximized (Fig. 12.6). When spherical particles of diameters larger than the corrugated groove width were used, the patterned surface could still influence particle ordering with a transitioning sequence of buckling, triangular and HCP observed—similar to that reported in non-patterned wedge cells. While localized dislocations and defects occurred, long-range patterning was essentially maintained [29]. The principles and techniques explored therefore provide opportunities to create large domain colloidal crystal arrangements of varying configurations based on tailored substrate structures using different colloidal particle sizes for applications where large surfaces areas or functional sites are required.

### *12.2.2 3D Colloidal Crystals*

In comparison, the formation of 3D colloidal crystals is more straightforward and can be facilitated by a rich variety of methods, such as sedimentation in a force field, packing in a confined space, controlled evaporation including vertical lifting deposition [30] and horizontal deposition [31]. The most common type of colloidal crystals formed by self-assembly of monodisperse particles has a face-centred cubic (*fcc*) lattice symmetry with the highest crystalline packing density of 74 % volume filling. Various operational parameters can be tuned in each process for controlling the film thickness.

3D colloidal crystals are often employed as templates for 3D macroporous networks. It is typically achieved by infiltrating the targeted precursor material into the interstitial voids of the colloidal crystal template, followed by solidification and subsequent template removal. The contact points between templating particles lead to orifices between the spherical voids in the resulting replica and consequently results in an open, fully continuous 3D network, often referred to as ‘inverse opals’.

The inverse opals can be formed in two principal ways, as illustrated in Fig. 12.7 [32]:

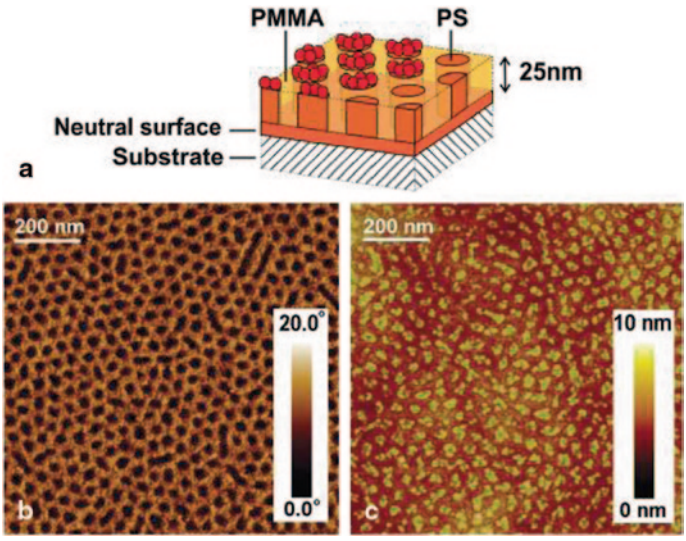


**Fig. 12.8** **a** Schematic drawing of the PS-b-PMMA pattern on a neutral surface with proteins adsorbed on the PS domains. **b** AFM phase image showing the PS-PMMA ordered pattern. **c** AFM topography image showing that the IgG proteins are selectively adsorbed on the PS domains [34, 35]

a. Infiltration with a second material, which can be polymer precursors, or sol-gel precursors, or a dispersion of nanoparticles, into the interstices of the colloidal template, followed by polymerization, solidification and template removal;
b. Codeposition of the colloidal templates together with the matrix material, typically in the form of nanoparticles, followed by template removal.

### *12.2.3 Hierarchically Ordered Colloidal Crystals (HOCCs)*

HOCCs are self-organized structures combining features of several hierarchical ordering characteristic length scales. Yang et al. [17] have first demonstrated this concept by combining copolymer templating (~10 nm), latex sphere templating (~100 nm) and micromolding (~µm) for the fabrication of hierarchically ordered porous oxides. HOCCs offer great potential for the design of new materials and devices for a broad range of applications due to the interconnected pores at different length scales, increased specific surface area, higher density of reactive sites and simultaneous patterning on surface [16].

Taking the colloidal particle size as the reference point, the larger length scale features can be conveniently introduced by incorporating mature microfabrication techniques, such as soft lithography through PDMS stamping, or photolithography, or silane chemistry combined with photolithography, whereas novelties often emerge from the pursuit of introducing additional features on the nanoscale. The

meso- and micro-size features can be introduced by surfactants, amphiphilic block copolymers, multi-size colloidal particles, anisotropic colloidal particles, ionic liquids and pre-functionalized constituent particles. Here we highlight the block copolymer co-assembly and multi-size colloidal particles co-assembly, due to their close pertinence to protein patterning. A more comprehensive account on HOCCs can be found in [33].

a. Block copolymer surface templating

Among those nanoscopic patterning methods, block copolymers is particularly relevant to protein patterning, because the phase separation as a result of the copolymer self-assembly can induce regular patterns that would have contrast in affinity to proteins or protein linker molecules [34, 35]. For example, polystyrene-*b*-poly(methyl methacrylate) can form cylindrical patterns with a PS domain size of tens of nanometres, which would favour protein adsorption, as shown in Fig. 12.8.

Fu et al. have introduced PS-*b*-PMMA copolymer in silica inverse opals using solution wetting [36]. Different from the previous studies, they succeeded in inducing the copolymer self-assembly along the inner surface of the inverse opal structure, instead of filling the pore volumes. The study showed a unique behaviour of copolymer self-assembly on a highly curved spherical surface with significant boundary constraints.

The study showed that the coexistence of polymer/silica and polymer/vacuum interfaces in the shells of the hollow spheres plays a synergetic role in block copolymer patterning, which can be adjusted by changing the commensurability between the block copolymer period and the shell geometry. Due to the confinement effect, the geometry and feature size of the copolymer patterns can be tuned by the pore size of the inverse opal as wells as the molecular size of the copolymer, as demonstrated by their SEM images and the cartoon schematics in Fig. 12.9 They further demonstrated a hierarchical patterning of gold and palladium nanoparticles in the PS-b-poly(2 vinylpyridine) copolymer coated silica opal as shown in Fig. 12.9.

b. Multiple-size particle templating

Binary colloidal crystal (bCC) structures form when two species of colloidal particles in dispersion co-crystallize. Earlier fabrication processes of bCC structures were based on layer-by-layer deposition methods where a monolayer is initially prepared and subsequent monolayers are deposited on top containing different sized spheres. The resulting arrangement is that of stacked 2D monolayers, rather than a complete 3D binary structure.

An alternative approach to bCC fabrication was achieved by Wang et al. [37] using a simplified vertical lifting co-deposition method under thermodynamically non-equilibrium conditions. In this method, a mixed colloidal suspension is deposited onto a solid lifting support by vertical lifting action. Co-crystallization of large and small particles occurs due to kinetically controlled liquid flux-induced particle packing [37]. In the study, two experimental parameters were varied and their effect explored—(1) the size ratio of particles, $\gamma_{S/L}$ and (2) the relative concentration, $\phi_{S/L}$, where the subscripts S and L denote the small and large particles, respectively. The

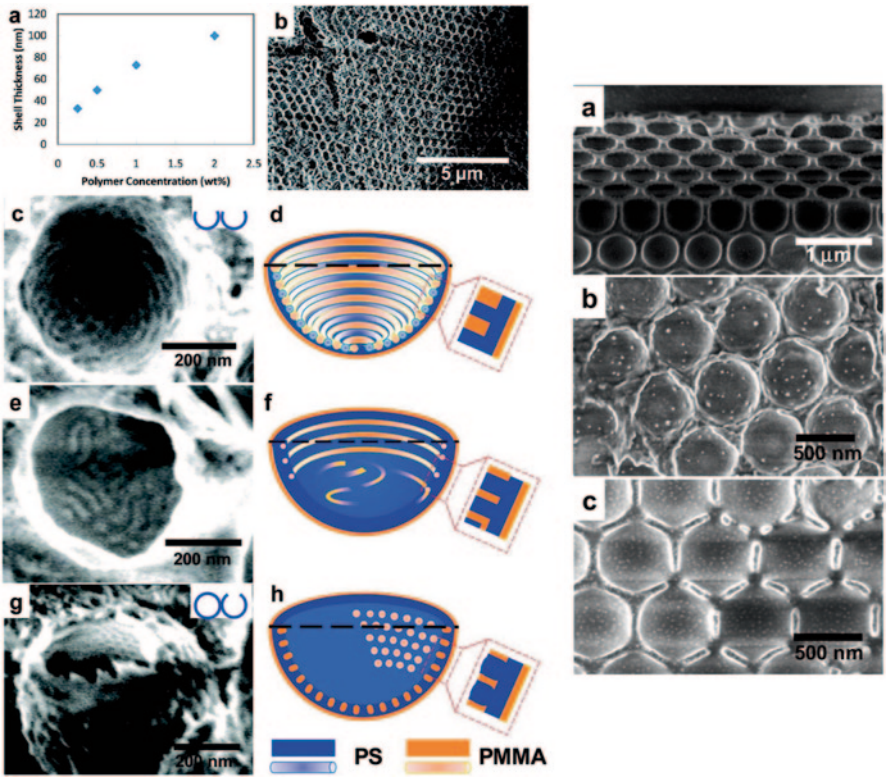


**Fig. 12.9** *Left panel*: **a** Concentration dependence of shell thickness and the SEM images of, after removal of silica templates, **b** the 3D arrays of hollow PS-b-PMMA spheres and the annealed hollow spheres of **c** $S_{326}$-PMMA301, **e** $S_{450}$-MMA182 and **g** $S_{1037}$-MMA322. The PS-rich domains appear bright and the PMMA-rich domains appear dark in the SEM images. The schemes in **d**, **f** and **h** represent the schematic cross-section view of the nanostructured shells observed in **c**, **e** and **g**. *Right panel*: SEM images of Au/PS-P2VP hemisphere array with silica templates (side view) (**a**); before (**b**) and after annealing at 200°C for 24 h and with subsequent removal of silica templates (**c**)

lattice geometry commonly formed was found to be the close-packed face-centred cubic lattice (fcc) with tetrahedral or octahedral interstitial sites as illustrated in the schematic shown in Fig. 12.10. Figure 12.10 also presents the morphology of the 3D binary colloidal crystals when size ratio and relative concentration were varied.

The deposition method was simplified by Wang et al. [38] by a horizontal deposition method as illustrated by the schematic in Fig. 12.11. It was found that in horizontal deposition, the evaporation-induced liquid flux is fast enough to move the homogenously distributed binary colloids to the drying edge without allowing them to segregate, thereby forming uniform binary crystal structures.

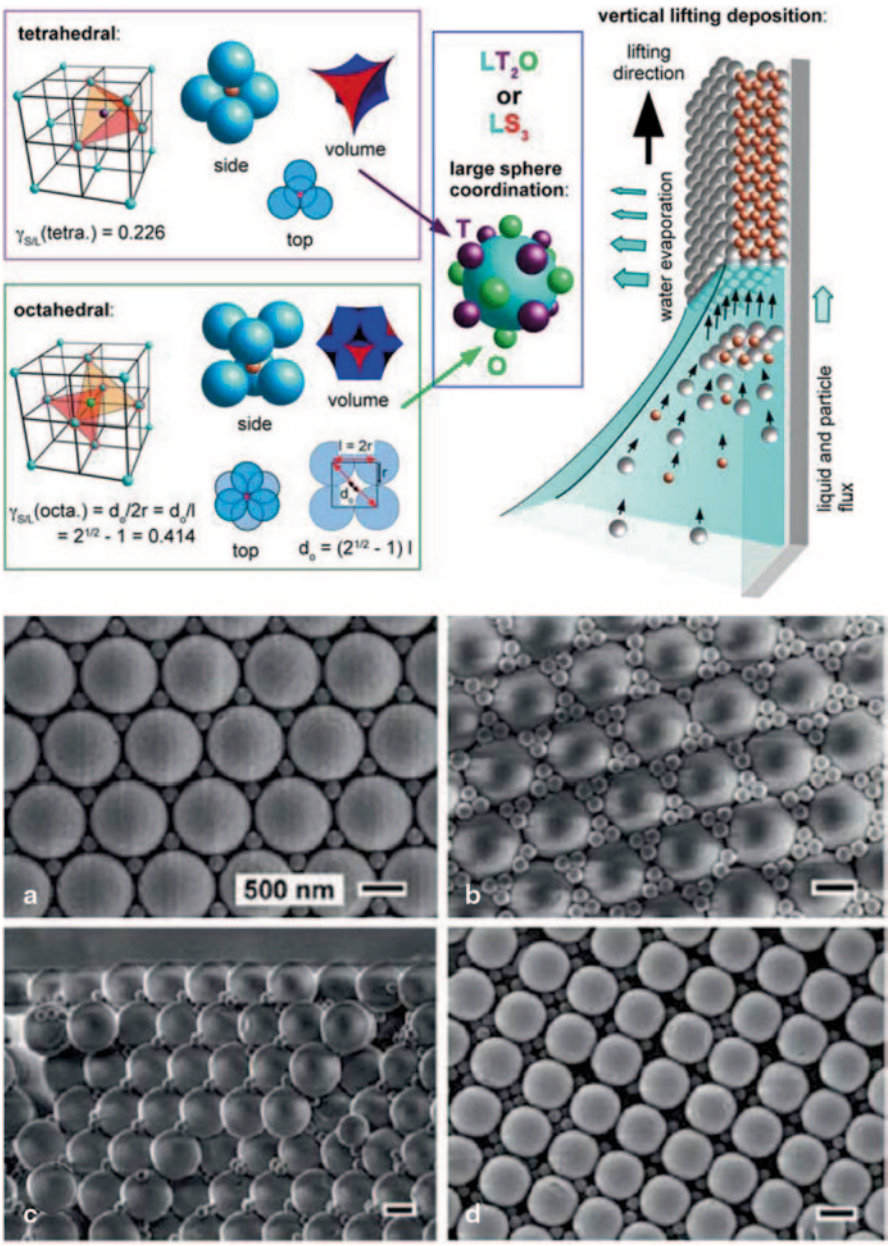


**Fig. 12.10** *Left Panel*: *Left*: analysis of the fcc lattice geometry of large particles in *blue* with interstitial sites (tetrahedral in *purple*, *left-top* and octahedral in *green*, *left-bottom*) for accommodation of small particles. *Right*: schematic representation of the particle transfer and crystallization mechanism during vertical lifting deposition. *Right panel*: *Top view* onto a binary colloidal crystal of large (dL = 839 nm, $\phi$L = 0.01) and small (dS = 187 nm, $\phi S = 2.0 \times 10^{-4}$) with $\gamma$S/L = 0.223, NS/NL = 1.80. **b** Concentration of small particles $\phi S = 3.84 \times$ 10-4, NS/NL = 3.43. **c** Side view of a fracture through **a**. **d** Region with a square lattice geometry at small particle concentration of $\phi S = 3.07 \times 10^{-4}$, NS/NL = 2.77

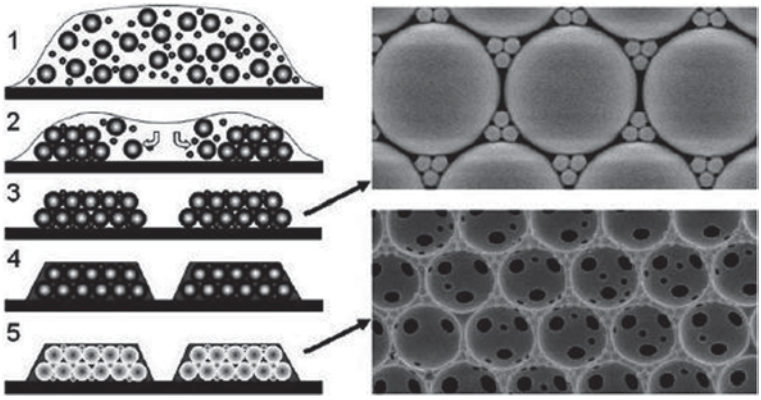


**Fig. 12.11** Horizontal deposition method for fabrications of HOCCs

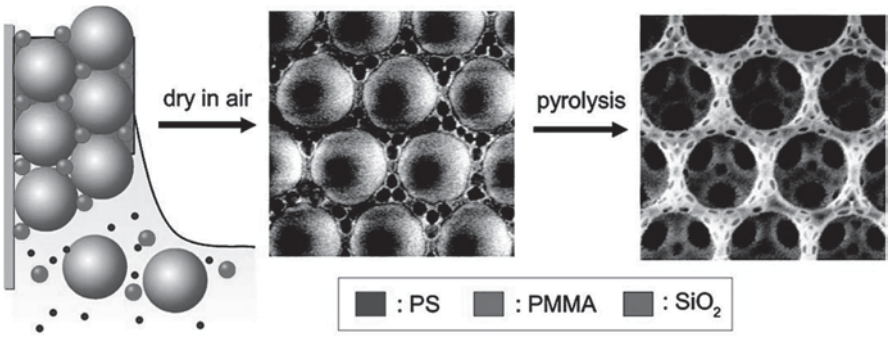


**Fig. 12.12** Schematic and SEM image of multiple-size particle templating of hierarchically ordered binary colloidal particles [39]

Wang et al. [39] further demonstrated another important extension of this methodology, whereby they mixed three different types of colloids which are also of different size, namely 489 nm PS particles, 80 nm PMMA spheres and 12 nm silica nanoparticles. By a single stroke of vertical deposition, the three constituents co-crystalized into colloidal crystal formation, which is dominated by the large particle-induced periodicity with intermediate and small size particles filling the interstitial voids in an ordered fashion, as shown in Fig. 12.12.

### *12.2.4 Template Removal*

In most cases in colloidal templating, the colloidal templates need to be removed after the desired patterns are formed. In 2D colloidal templating, the most frequently used method is the physical lift-off approach, which can be simply assisted by a piece of scotch tape. For 3D colloidal templating, particularly in inverse opal

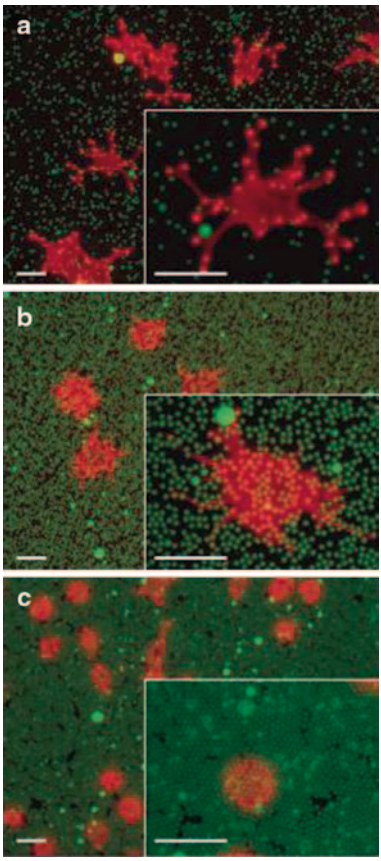


**Fig. 12.13** Spreading and morphology of fibroblast cells on different densities of colloidal particles. Fibroblasts attached and spread on particles presenting immobilized FN (*green*). Actin filaments in the cells were stained with rhodamine-phalloidin (*red*). Cell morphologies differ with particle organization. **a** Array with a sparse distribution of particles, 10.2 % surface coverage, 2.19 μ particle spacing. **b** Array of intermediate density, 42.5 % coverage, 0.59 μ particle spacing. **c** Close-packed array of particles, 96.5 % coverage. All scale *bars* are 25 μm

formation, the templates can be selectively removed by solvents, e.g. HF or NaOH solutions for removing silica colloids and toluene, tetrahydrofuran (THF) for removing PS colloids, or by heat treatment for removing the organic phase.

## 12.3 Protein Patterning Generated by Colloidal Templating

### *12.3.1 2D Patterning*

#### 12.3.1.1 Self-Assembly of Protein Coated Colloids

Carbeck and co-workers [14] have presented a straightforward approach to employ colloidal templating for patterning proteins. They used the streptavidin–biotin linking strategy to coat streptavidin-functionalized colloids with adhesion protein

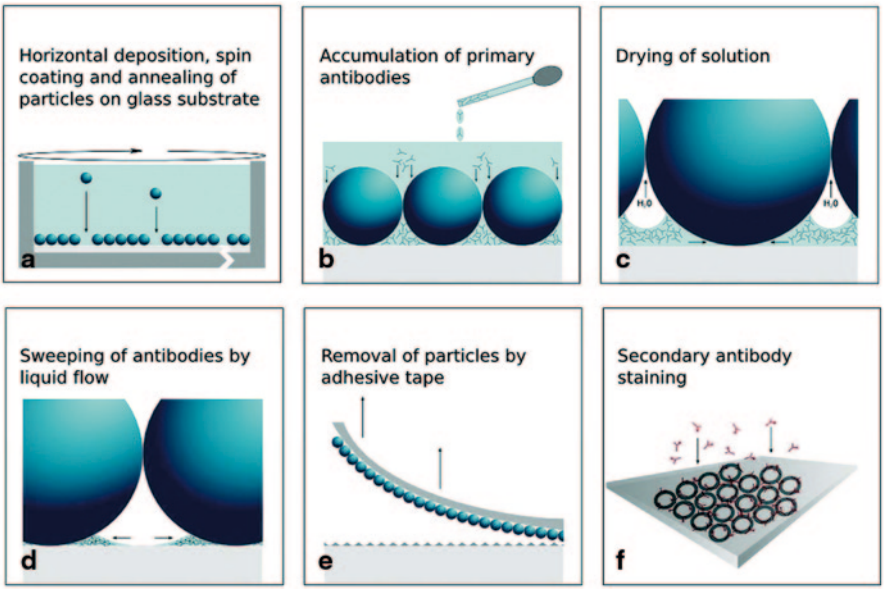


**Fig. 12.14** Schematic drawing details the key steps in fabricating the protein annuli arrays [40]

fibronectin (FN) conjugated with biotin, followed by assembling the FN-coated colloids into 2D array by an electric-field assisted deposition. They then cultured fibroblast cells on colloidal arrays of different densities and used such a colloidal-templated protein patterns to study the biophysics underlying cell growth as shown in Fig. 12.13. They have demonstrated that colloidal assembly can control the composition of biomolecules on three different length scales, namely the size of individual particles, the spacing between particles and the length scale of the patterned area on a substrate.

#### 12.3.1.2 2D Array Patterning

For developing biosensors for high-throughput protein and pathogen screening technologies, annulus-shaped protein structures are highly interesting, because the well-like structure comprised of protein is likely to enhance protein–protein interactions, thereby improve the detection sensitivity to antigens. Wolf and Li [40] have combined colloidal templating with drying lithorgraphy [41] and produced large-scale (~$cm^2$) 2D arrays of antibodies against Escherichia coli K12 and enhanced green fluorescent protein (eGFP) on versatile glass surfaces.

As illustrated by the Schematic in Fig. 12.14, the steps for generating this antibody annuli array include (a). 2D colloidal crystal template formation; (b). applying antibody solution (in PBS ); (c). bulk solution drying; (d). sphere-substrate contact

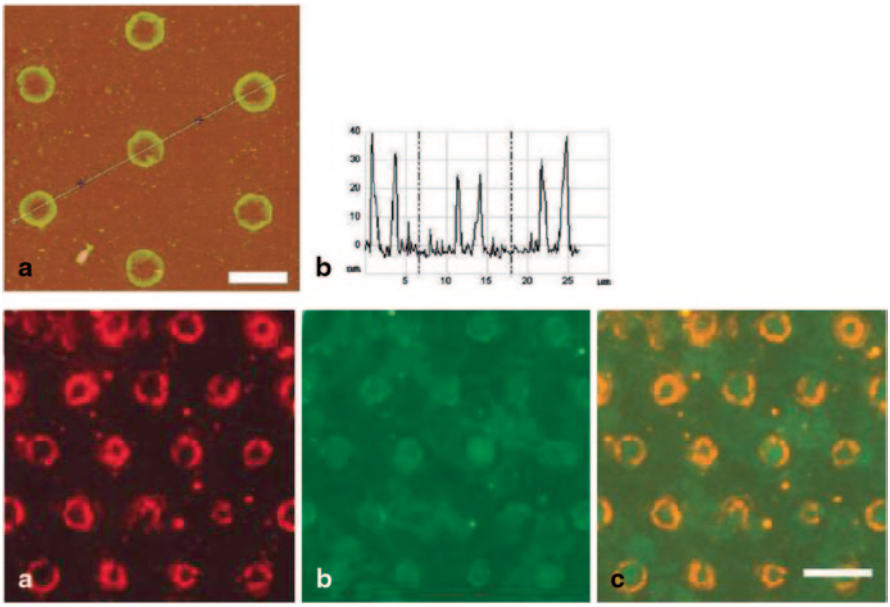


**Fig. 12.15** *Top row*: The AFM topography images of the protein annuli hexagonal array. *Bottom row*: Fluorescence microscopy images of a hexagonal annulus structure. **a** Anti-GFP Dy Light 549-labelled antibodies (Ab1.3). **b** GFP bound to Ab1.3. **c** Overlay of **a** and **b**. The scale *bar* is 20 μm [40]

area drying, which is the key step for the annulus shape formation; (e). removal of colloidal template by adhesive tape lift-off.

As shown by the AFM image of the proteins-assembled annulus, the ring structure is defined by the original contact area between the colloids and substrate. Therefore, the annuli array is a direct replica of the 2D hexagonal colloidal assembly. As depicted in Step D in the Scheme, as the final stage of protein solution drying process, the protein molecules are swept around the bottom of the spheres, as the capillary contact lines recede. Therefore, the size of the rings is defined by the colloidal particle size and the sphere-substrate contact area. AFM imaging also reveals that the height of the annuli is in the range of 25–40 nm, which corresponds to two to three layers of antibodies. Fluorescence microscopy analysis displayed in Fig. 12.15 bottom row shows the red annuli arrays for anti-GFP DyLight 549-labelled antibodies, and their retained specific binding affinity to GFP.

Wolf and Li's study showed that the evaporation rate is a critical factor in the formation of the antibody annuli; accelerated drying by providing a vacuumed environment or elevated temperature did not result in similar ordered ring structures. It was also found that both the solvent and the antibody concentration play important roles on protein arrangement in the drying process. It appeared that the addition of surfactant Tween20 is also crucial for the protein sweeping process to take place, otherwise, the proteins would simply form connected network covering areas which

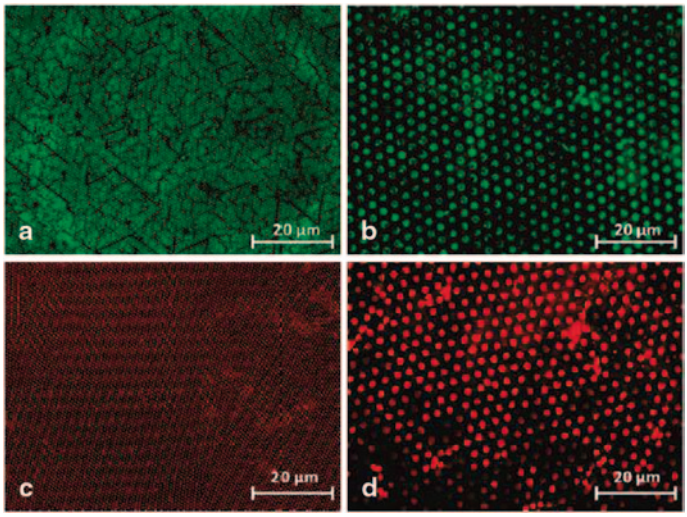


**Fig. 12.16** FM images demonstrate a specific adsorption of R-BSA on unmodified glass regions on different chemical patterns generated from: **a** 2 µm COOH-PS/200 nm NH2-PS, scale bar = 20 µm, **b** 5 µm plain-SiO2/500 nm NH2-PS (j5 µm = $1.4 \times 10^{-3}$ and j500 nm = $1.1 \times 10^{-4}$), scale bar = 20 µm. FM images showing fluorescent signals from dislike Au features on the glass substrate produced from BCA masks: **c** 2 µm plain-SiO2/200 nm NH2-PS, scale bar = 20 µm; **d** 5 µm plain-SiO2/500 nm NH2-PS, Scale bar = 20 µm [27]

are not protected by the colloidal particles. Two possible reasons were attributed to this observation: (a). the protein mobility on glass surface may be increased by the presence of the surfactant; (b). the meniscus between the template spheres break earlier in the presence of surfactants due to reduced surface tension, facilitating the formation of disconnected ring structure. In addition, there is a working range for the protein concentration; too low or too high would result in no pattern formation or too high a 'protein blanket' over the non-protected surface.

As the study has demonstrated, such protein annuli array patterns are robust; they did not show any sign of degradation after rewetting, for instance, by the aqueous secondary antibody solution. The authors concluded that the proteins are strongly bound to the glass substrate and connected to each other simply by the drying procedure while retaining their bioactivity. The subject of protein folding during drying in air itself is highly complex, which deserves particular attention in protein patterning. The annulus shape of this protein pattern provides a 3D extension based on the 2D colloidal templating, which is envisaged to have a significant advantage in antigen and cell binding due to the entrapment effect.

#### 12.3.1.3 Patterning Based on 2D Binary Colloidal Assembly

As laid out in earlier section, variations in size and spacing of colloidal particles in the binary colloidal assembly (BCA) allow for tunable chemical patterns to be formed. Singh et al. [27] have demonstrated that arrays of disc-like patterns, with disc diameter in the range of hundreds of nanometres to a few μm and lateral distance ranging on the same order, can be formed by using BCAs comprised of large and small particles as masks for Au sputtering. The method is simple and versatile.

Singh et al. [27] further demonstrated that the patterns were capable of allowing selective protein adsorption to the unmodified regions. The patterns formed by Au sputtering for 10 min using a BCA mask were exposed to tetramethylrhodamine-labelled bovine serum albumin (R-BSA). The patterns were then examined by fluorescent microscopy (FM) as shown in Fig. 12.16, which shows that the fluorescent signals are mostly due to R-BSA specifically adsorbing onto the unmodified $SiO_2$ regions within the patterned surface.

### *12.3.2 3D Protein Templating*

There are at least two modes in 3D protein patterning via colloidal templating. The first type is based on 3D colloidal crystal structure, which provides a homogenous distribution of proteins in a 3D ordered porous network, whereas the second type is related to transforming colloidal particles into vehicles for proteins, which is fundamental to a range of biomedical applications.

#### 12.3.2.1 Protein Patterning via 3D Colloidal Crystals

The macroporous network derived from colloidal templates attracts particular interest from a chemo/biosensing perspective, due to its combinatorial advantages: in addition to the enormous surface area provided by the porous structure for immobilizing the target analytes, the ordered porous structure can also act as the transducer that converts the binding event into an optical signal, following Bragg's equation for the adsorption maxima [5].

For immobilizing proteins in the porous network, various strategies have been developed. Depending on the chemistry nature of the porous network, different protein linking molecules/elements can be first introduced on the surface via silane chemistry [42], or esterification reaction [43], or incorporation of protein-binding metals [44]. Protein functionalized 3D inverse opals have been demonstrated as effective label-free antigen–antibody sensor [44, 45].

Xia and coworkers [46, 47] have employed surface-functionalized inverse opals as a novel class of scaffolds with uniform and controllable pore sizes for tissue engineering to provide better nutrient transport, a uniform cell distribution and an adjustable microenvironment for cell differentiation. In a recent study [46], they reported that a truly 3D microenvironment can be created inside a pore by fur-

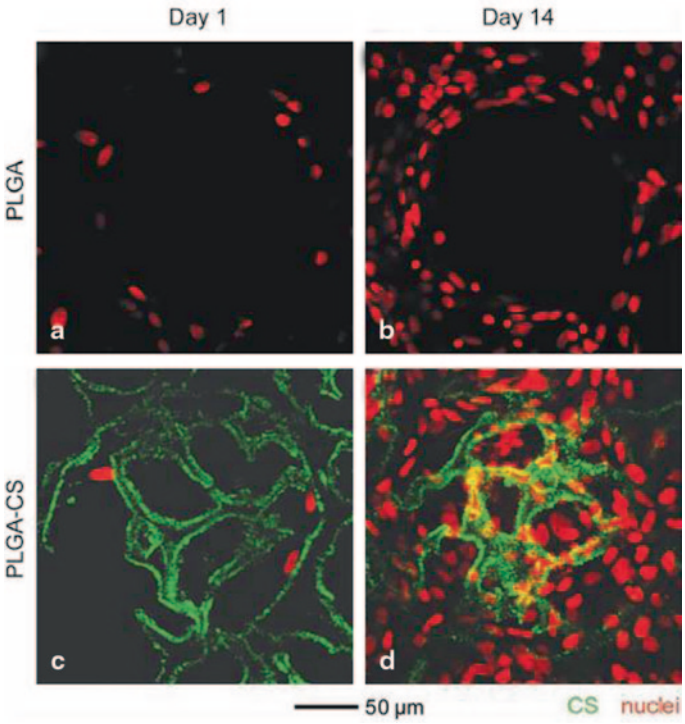


**Fig. 12.17** Confocal fluorescence micrographs showing cell proliferation in the scaffolds. The focal depth was ~50 µm from the surface of the scaffold, and the layer thickness was ~5 µm. **a, b** The cells only proliferated along the walls of the pores in a PLGA scaffold and still could not completely fill the void space of a pore after 14 d of culture. **c, d** The cells were able to attach to the microstructures inside the pores of a PLGA-chitosan scaffold and could also populate the centre region of the pore. Here, CS was prelabelled with fluorescein isothiocyanate and nuclei were stained with PI [46]

ther functionalizing the as-prepared inverse opal scaffold with chitosan by freeze-drying. The resultant inverse opal scaffold with hierarchically structured pores enhanced both cell proliferation and tissue infiltration. It can be envisioned that the 3D microenvironment can be further improved by introducing patterned protein on pore surfaces to mimic the in vivo cell environment (Fig. 12.17).

#### 12.3.2.2 3D Protein Patterning via Colloidal Templating

3D protein assemblies can be prepared by repeated deposition of biotin–protein conjugate pairs operating as binding mediators between layers, or self-assembly techniques involving hybrid protein-polyelectrolyte multilayer films and protein–colloid multilayers. One of the earlier studies into the use of colloidal particles for controlled fabrication of protein multilayers was conducted by Caruso and Möh-

wald [48]. In this study, a layer-by-layer self-assembly strategy was employed to construct protein-shell structures onto colloids. To facilitate protein adsorption, polyelectrolytes were placed in suspension with PS particles to produce coated polyelectrolyte-colloid particles. Protein layers were then constructed by alternating adsorption of the polyelectrolyte-coated PS particles with protein solution and with polyelectrolyte solution of opposite charge to previous layers thereby facilitating film growth by exploiting electrostatic interactions. After each deposition of either protein or polyelectrolyte, samples were centrifuged and washed to remove supernatant. Using this method, Caruso and Möhwald [48] succeeded in creating multilayer protein films comprising of fluorescein isoticyanate-labelled bovine serum albumin (FITC-BSA) and immunoglobulin G (IgG). Operating on the same basic strategy and principles as Caruso and Möhwald [48], Caruso and Schüler [49] formed glucose oxidase and horseradish peroxidase enzyme multilayers on polyelectrolyte-coated PS colloidal particles.

## 12.4 Conclusions

Chemically patterned surfaces with multiple feature length scales for selective immobilization of biomolecules are instrumental for the development of biosensors and bioanalytics, drug screening, tissue engineering and fundamental studies of cell biology. Colloidal templating based on self-assembly of colloidal particles provides an important technique that can create a feature size ranging from tens of nanometres to several μm in either 2D array or ordered 3D spatial configuration. As illustrated by the examples presented in this chapter, colloidal self-assembly can be tuned in various ways to create different types of patterns. Moreover, colloidal templating has significant advantages in that it does not require elaborate equipment, and being an intrinsic parallel process, the technique can be easily integrated with main stream materials deposition facilities such as sputtering/evaporation, chemical vapour deposition, reactive ion etching, plasma treatment, spotting and inkjet printing. Therefore, it is a promising technique in the development of proteometrics and bioanalysis.

## References

1. Deckman, H.W. and J.H. Dunsmuir, *NATURAL LITHOGRAPHY*. Applied Physics Letters, 1982. **41**(4): p. 377–379.
2. Gates, B., S.H. Park, and Y.N. Xia, *Tuning the photonic bandgap properties of crystalline arrays of polystyrene beads by annealing at elevated temperatures*. Advanced Materials, 2000. **12**(9): p. 653- +.
3. Holtz, J.H. and S.A. Asher, *Polymerized colloidal crystal hydrogel films as intelligent chemical sensing materials*. Nature, 1997. **389**(6653): p. 829–832.
4. Kulinowski, K.M., et al., *Porous metals from colloidal templates*. Advanced Materials, 2000. **12**(11): p. 833–838.

5. Li, Q., et al., *Porous Networks Through Colloidal Templates*. Topics in Current Chemistry, 2009. **287**: p. 135–180.
6. Marquez, M. and B.P. Grady, *The use of surface tension to predict the formation of 2D arrays of latex spheres formed via the Langmuir-Blodgett-like technique*. Langmuir, 2004. **20**(25): p. 10998–11004.
7. Wright, J.P., et al., *Ultraflat ternary nanopatterns fabricated using colloidal lithography*. Advanced Materials, 2006. **18**(4): p. 421- +.
8. Trujillo, N.J., S.H. Baxamusa, and K.K. Gleason, *Grafted Functional Polymer Nanostructures Patterned Bottom-Up by Colloidal Lithography and Initiated Chemical Vapor Deposition (iCVD)*. Chemistry of Materials, 2009. **21**(4): p. 742–750.
9. Choi, D.G., et al., *Colloidal lithographic nanopatterning via reactive ion etching*. Journal of the American Chemical Society, 2004. **126**(22): p. 7019–7025.
10. Singh, G., et al., *Highly Ordered Nanometer-Scale Chemical and Protein Patterns by Binary Colloidal Crystal Lithography Combined with Plasma Polymerization*. Advanced Functional Materials, 2011. **21**(3): p. 540–546.
11. Hou, J., et al., *Bio-Inspired Photonic-Crystal Microchip for Fluorescent Ultratrace Detection*. Angewandte Chemie-International Edition, 2014. **53**(23): p. 5791–5795.
12. Yi, D.K., et al., *Colloid Lithography-Induced Polydimethylsiloxane Microstructures and their Application to Cell Patterning*. Biotechnology Letters, 2006. **28**(3): p. 169–173.
13. Wang, Y.C., et al., *Stretched inverse opal colloid crystal substrates-induced orientation of fibroblast*. Biomedical Materials, 2010. **5**: p. 035011.
14. Gleason, N.J., et al., *Patterning Proteins and Cells Using Two-Dimensional Arrays of Colloids*. Langmuir, 2003. **19**(3): p. 513–518.
15. Curtis, A. and M. Riehle, *Tissue engineering: the biophysical background*. Physics in Medicine and Biology, 2001. **46**(4): p. R47.
16. Jonas, U., et al., *Colloidal assemblies on patterned silane layers*. Proceedings of the National Academy of Sciences of the United States of America, 2002. **99**(8): p. 5034–5039.
17. Yang, P.D., et al., *Hierarchically ordered oxides*. Science, 1998. **282**(5397): p. 2244–2246.
18. Ekblad, T. and B. Liedberg, *Protein adsorption and surface patterning*. Current Opinion in Colloid & Interface Science, 2010. **15**(6): p. 499–509.
19. Li, Q., et al., *The forces at work in collodial self-assembly: a review on fundamental interactions between collodial particels*. Asia-Pacific Journal of Chemical Engineering, 2008. **3**(3): p. 255–268.
20. Dimitrov, A.S. and K. Nagayama, *Continuous Convective Assembling of Fine Particles into Two-Dimensional Arrays on Solid Surfaces*. Langmuir, 1996. **12**(5): p. 1303–1311.
21. Yoshimura, H., et al., *Two-dimensional crystallization*. Nature, 1993. **361**(6407): p. 26–26.
22. Wang, D.Y. and H. Mohwald, *Rapid fabrication of binary colloidal crystals by stepwise spin-coating*. Advanced Materials, 2004. **16**(3): p. 244- +.
23. Retsch, M., et al., *Fabrication of Large-Area, Transferable Colloidal Monolayers Utilizing Self-Assembly at the Air/Water Interface*. Macromolecular Chemistry and Physics, 2009. **210**(3–4): p. 230–241.
24. Zhou, Z., et al., *Fabrication of binary colloidal crystals and non-close-packed structures by a sequential self-assembly method*. Langmuir, 2007. **23**(3): p. 1473–1477.
25. Vogel, N., et al., *Plasmon Hybridization in Stacked Double Crescents Arrays Fabricated by Colloidal Lithography*. Nano Letters, 2011. **11**(2): p. 446–454.
26. Vogel, N., et al., *Laterally Patterned Ultraflat Surfaces*. Small, 2009. **5**(7): p. 821–825.
27. Singh, G., et al., *Large-area protein patterns generated by ordered binary colloidal assemblies as templates*. ACS nano 2011. **5**(5): p. 3542.
28. Denkov, N.D., et al., *MECHANISM OF FORMATION OF 2-DIMENSIONAL CRYSTALS FROM LATEX-PARTICLES ON SUBSTRATES*. Langmuir, 1992. **8**(12): p. 3183–3190.
29. Ramiro-Manzano, F., et al., *Colloidal Crystal Thin Films Grown into Corrugated Surface Templates*. Langmuir, 2010. **26**(7): p. 4559–4562.
30. Xia, Y.N., et al., *Monodispersed colloidal spheres: Old materials with new applications*. Advanced Materials, 2000. **12**(10): p. 693–713.

31. Yan, Q.F., Z.C. Zhou, and X.S. Zhao, *Inward-growing self-assembly of colloidal crystal films on horizontal substrates*. Langmuir, 2005. **21**(7): p. 3158–3164.
32. Li, Q., et al., *Porous Networks Through Colloidal Templates*, in *Templates in Chemistry Iii*, P. Broekmann, K.H. Dotz, and C.A. Schalley, Editors. 2009, Springer-Verlag Berlin: Berlin. p. 135–180.
33. Li, Q. and E. Eftekhari, *Hierarchically Ordered Colloid Chrystals: Fabrication, Structures, and Functions*, in *Nanostructures: Properties, Production Methods and Applications*, Y. Dong, Editor. 2013, Nova Science Publishers, Inc.: Hauppauge, NY, USA. p. 169–181.
34. Lau, K.H.A., et al., *Self-assembly of Protein Nanoarrays on Block Copolymer Templates*. Advanced Functional Materials, 2008. **18**(20): p. 3148–3157.
35. Li, Q., et al., *The Effect of Fluid Flow on Selective Protein Adsorption on Polystyrene-block-Poly(methyl methacrylate) Copolymers*. Langmuir, 2009. **25**(20): p. 12144–12150.
36. Fu, J., et al., *3D Hierarchically Ordered Composite Block Copolymer Hollow Sphere Arrays by Solution Wetting*. Langmuir, 2010. **26**(14): p. 12336–12341.
37. Wang, J., et al., *Structural and optical characterization of 3D binary colloidal crystal and inverse opal films prepared by direct co-deposition*. Journal of Materials Chemistry, 2008. **18**(9): p. 981.
38. Wang, L., et al., *Binary Colloidal Crystals Fabricated with a Horizontal Deposition Method*. Langmuir, 2009. **25**(12): p. 6753–6759.
39. Wang, J., et al., *Preparation of multilayered trimodal colloid crystals and binary inverse opals*. Journal of the American Chemical Society, 2006. **128**(49): p. 15606–15607.
40. Wolf, C. and Q. Li, *Tunable Two-Dimensional Array Patterning of Antibody Annuli through Microsphere Templating*. Langmuir, 2010. **26**(14): p. 12068–12074.
41. Vakarelski, I.U., et al., *Assembly of Gold Nanoparticles into Microwire Networks Induced by Drying Liquid Bridges*. Physical Review Letters, 2009. **102**(5): p. 4.
42. del Campo, A., et al., *Surface modification with orthogonal photosensitive silanes for sequential chemical lithography and site-selective particle deposition*. Angewandte Chemie-International Edition, 2005. **44**(30): p. 4707–4712.
43. Cassagneau, T. and F. Caruso, *Inverse opals for optical affinity biosensing*. Advanced Materials, 2002. **14**: p. 1629–1633.
44. Qian, W.P., et al., *Three-dimensionally ordered macroporous polymer materials: An approach for biosensor applications*. Langmuir, 2002. **18**(11): p. 4526–4529.
45. Choi, E., et al., *Label-free specific detection of immunoglobulin G antibody using nanoporous hydrogel photonic crystals*. Sensors and Actuators B-Chemical, 2013. **180**: p. 107–113.
46. Zhang, Y., S.W. Choi, and Y.N. Xia, *Modifying the Pores of an Inverse Opal Scaffold With Chitosan Microstructures for Truly Three-Dimensional Cell Culture*. Macromolecular Rapid Communications, 2012. **33**(4): p. 296–301.
47. Zhang, Y.S., S.W. Choi, and Y.N. Xia, *Inverse opal scaffolds for applications in regenerative medicine*. Soft Matter, 2013. **9**(41): p. 9747–9754.
48. Caruso, F. and H. Möhwald, *Protein Multilayer Formation on Colloids through a Stepwise Self-Assembly Technique*. Journal of the American Chemical Society, 1999. **121**(25): p. 6039–6046.
49. Caruso, F. and C. Schüler, *Enzyme Multilayers on Colloid Particles: Assembly, Stability, and Enzymatic Activity*. Langmuir, 2000. **16**(24): p. 9595–9603.

# Chapter 13
# Electrochemical Approaches for Molecular Surface Imprinting of Polymers Toward Fully Synthetic Receptors for Selective Recognition of Proteins

**Frieder W. Scheller, Aysu Yarmana and Róbert E. Gyurcsányic**

## 13.1 Introduction

Molecular recognition and catalytic conversion of the target molecules by antibodies and enzymes take place in so-called paratopes or catalytic centers, which comprise typically 10–15 amino acids. Nucleic acids not only bind to complementary single stranded nucleic acids by base pairing (hybridization), but also interact with highly specific proteins, e.g., transcription factors, and low-molecular weight molecules and also with ions. These biomolecules are used as recognition elements in biosensors. Still, the analytical use of bioreceptors can be restricted by incompatibility with the analysis conditions and their limited stability. Obviously, they have been optimized by nature to perform a given task in the milieu of a living organism and not for integration and use in an analytical device. Therefore, there is a strong motivation toward developing synthetic receptors, which through finely tailored chemical–physical properties are expected not only to overcome the limitations of receptors of biological origin, but also to enable better analytical performance of the relevant sensing devices as well as reproducible and cost-effective fabrication. As alternatives to "natural receptors" APTAMERS [1, 2] have been generated from both natural and synthetic [3] nucleotides by combinatorial approaches using "evolution in the test tube." Beside obvious advantages of aptamers deriving from their in-vitro generation, small molecular weight, and the option of tuning their chemical–physical properties by chemical synthesis, the possibility of counterselection by

F. W. Scheller (✉) · A. Yarmana
Fraunhofer Institute for Biomedical Engineering IBMT, 14476 Potsdam, Germany
e-mail: fschell@uni-potsdam.de

Institute of Biochemistry and Biology, University of Potsdam, Karl-Liebknecht-Str. 24–25, 14476 Potsdam, Germany

R. E. Gyurcsányic
Department of Inorganic and Analytical Chemistry, MTA-BME "Lendület" Chemical Nanosensors Research Group, Budapest University of Technology and Economics, Szt. Gellért tér 4, Budapest, 1111 Hungary



J. Rodríguez-Hernández, A. L. Cortajarena (eds.), *Design of Polymeric Platforms for Selective Biorecognition,* DOI 10.1007/978-3-319-17061-9_13

screening out sequences binding to critical interferents or to the sample matrix, was shown to result in aptamers with enhanced selectivities applicable in real samples [4]. A similar generic template-based, but fully synthetic approach was introduced to shape selective recognition sites in polymers to obtain molecularly imprinted polymers (MIPs) that will be the focus of this perspective article.

## 13.2 The Concept of Molecular Imprinting

In order to create artificial binders, synthetic polymers are "imprinted" by the analyte during the polymer formation as conceptualized by Wulff, Shea, and Mosbach [5, 6, 7]. The recognition sites are generally formed by copolymerizing a functional and a cross-linking monomer in the presence of the target analyte, which acts as a template. In the prepolymerization mixture, the target interacts by covalent (preorganized approach) or noncovalent (self-assembly approach) bonds with the functional monomers and this arrangement is fixed during copolymerization. After polymerization the template molecules are removed, providing binding sites, which are ideally complementary in size and shape to the template facilitating their preferential rebinding (Fig. 13.1).

A comprehensive definition of molecular imprinting was attempted by Whitecombe and coworkers [8] as: *The construction of ligand selective recognition sites in synthetic polymers where a template (atom, ion, molecule, complex or a molecular, ionic or macromolecular assembly, including micro-organisms) is employed in order to facilitate recognition site formation during the covalent assembly of*

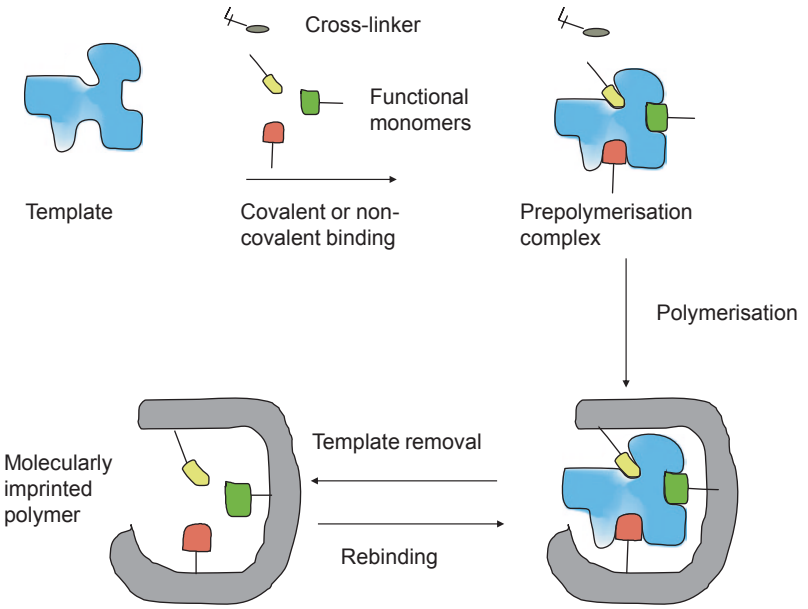


**Fig. 13.1** Workflow of MIP preparation (Scheller and Yarman 2012 permission by Springer)

*the bulk phase by a polymerization or polycondensation process, with subsequent removal of some or all of the template being necessary for recognition to occur in the spaces vacated by the templating species*.

Even smart nano-environments were obtained by cell-imprinted substrates based on mature and dedifferentiated stem cells as templates. Stem cells seeded on these cell-imprinted substrates were driven to adopt the specific shape and molecular characteristics of the cell types, which had been used as template for the cell-imprinting. This method might pave the way for a reliable, efficient, and cheap way of controlling stem cell differentiation [9].

The benefits of this universal approach are mainly related to the synthetic nature of MIPs, i.e., excellent chemical and thermal stability associated with reproducible, cost-effective fabrication compared to biological molecules [10]. Therefore, they have found applications as stationary phase in chromatography [11], in solid-phase extraction, environmental and clinical analysis, and also as recognition elements in sensors [12].

Beside affinity interactions, the catalytic concept of catalytically active antibodies (abzymes) has also been transferred to the totally synthetic MIPs. In analogy to the generation of abzymes, stable analogues of the postulated transition state (TSA) of the catalyzed reaction are used as the template to mimic the active center of the enzyme. [13, 14]. Another approach is the incorporation of transition metals or mimics of the catalytic center of enzymes. [15, 16].

Among the different formats for the preparation of MIPs, bulk polymerization is the most frequently used. This technique produces monolithic structures, which are then grounded and sieved. The most common functional monomers applied in thermal or photopolymerization are methacrylic acid, vinylimidazole, vinylpyridine, and their derivatives [17]. However, these materials show slow binding kinetics. To overcome these drawbacks a variety of more efficient approaches and formats have been developed that include: suspension, emulsion, or precipitation polymerization, which lead to the formation of micro- or nanobeads [18]. MIP nanomaterials such as nanoparticles, nanospheres; MIP nanomaterial composites [16]; self-assembled monolayers of thiols [19] and spreader-bar technique [20] have been developed.

### *13.2.1 Electrochemical MIP-based Sensors*

For sensor applications the MIPs have to be immobilized on a transducer surface. This can be done by physical confinement such as drop-coating, spin coating, or spray coating, layer-by-layer-approach [21, 22] or by chemical attachment, e.g., by grafting and by preparation of composite membranes. Obviously, the direct in-situ synthesis of MIPs directly onto the transducer surface is preferred in most cases as the shortest route to functional sensors [23]. Among various surface confinement methods electropolymerization is particularly an elegant way to prepare MIPs, as highly reproducible film thickness can be obtained by controlling the charge passed during the electropolymerization. Different types of electroactive monomers or monomer mixtures have been applied for the imprinting of low or high molecular

weight substances leading either to electrically insulating or conducting polymers. Nonconducting films offer an inherent electrochemical transduction scheme: an electroactive template can be measured by diffusion through the pores formed by the MIP process. For electro-inactive targets indirect measurement by using redox probes such as ferricyanide, or competitive assays can be applied. Upon filling of imprinted cavities by template molecules, the signal due to a redox probe is suppressed.

## *13.2.2 MIPs for Selective Recognition of Proteins*

The development of MIPs for protein (or biomacromolecules in general) is probably one of the most promising and highly challenging research area in MIP development. "Plastic antibodies" with similar performance as their biological counterparts (e.g., antibodies), but less prone to environmental effects and extended shelf lights, would clearly have a major impact on diagnostic devices and bioaffinity assays. In contrast to the results in generating MIPs for low-molecular-weight compounds, molecular imprinting is still facing challenges in terms of selective biomacromolecular recognition. Despite of the obvious need for robust selective synthetic receptors/sorbents for biomacromolecules it was reported that less than 2% of the MIP literature involves macromolecular imprinting [24]. The bulk synthesis method used to fabricate MIPs for low-molecular-weight compounds, is hardly applicable to macromolecules due to their hindered mobility in the highly reticulated polymeric networks. Thus, in the worst case the macromolecules become entrapped in the polymeric material with both their removal and rebinding prohibited. Therefore, the essential prerequisite of generating macromolecular imprints should be clear to create accessible binding sites amenable for free exchange of the target between the MIP and the sample phase, i.e., to have them confined to the surface of the MIPs. Surface imprinting by reducing the contact area between macromolecular targets and bulk polymeric material is advantageous also in terms of free accessibility and low nonspecific adsorption. In this respect, the following new approaches of electrochemical surface imprinting of polymers for selective recognition of macromoleculecules have been introduced by the authors.

### 13.2.2.1 Template Synthesis by Using Sacrificial Microreactors

The fabrication strategy used the polycarbonate (PC) membranes with cylindrically shaped pores of 8 μm in diameter as sacrificial microreactors [25]. The hypothesis was that if target proteins are immobilized on the inner wall of the pores, the confined growth of an electrically conducting polymer in the pores and subsequent removal of the membrane will result in microrods bearing on their surface the molecular imprint of the respective protein. The microrods were made by the electrosynthesis of the electrically conductive polymer, poly-3,4-ethylenedioxythiophene (PEDOT), doped with polystyrene sulfonate (PSS), which offers the advantage of controlled deposition and growth of the polymer chains coupled with mild synthesis

conditions, high stability, and compatibility with aqueous media. Furthermore, PEDOT/PSS was reported to have an inherently high biocompatibility owing to its structural similarity with natural compounds such as melanin. The proof of concept was used with avidin as a model protein owing to its high stability, the availability of fluorescently labeled derivatives, and the prospect of easily changing the template protein on the nanopore surface, based on linking their biotinylated derivatives, to the surface-adsorbed avidin. The surface-imprinted conducting polymer microrods were shown to selectively recognize the template protein, as demonstrated by competitive binding assays using fluorescence detection. The concept has been transferred also to smaller diameter pores; however, in this case the obtained polymeric nanorods got detached from the electrode surface during the washing step [26]. Thus to enable their easier handling, nanoparticles with magnetite core and PSS shell having a hydrodynamic diameter of 100 nm were used as anionic dopants during electrosynthesis of PEDOT. This concept has been used later for the fabrication of MIP-covered catalytic micromotors that were able to capture and transport target protein molecules in biological samples and as such to selectively extract and preconcentrate proteins [27].

#### 13.2.2.2 Surface Imprinting Based on Photolitographically Made Sacrificial Reactors

The authors further improved the previously described strategy by replacing nanoporous PC membranes with photolitographically made sacrificial reactors from PC. The novel fabrication methodology is not only compatible with large-scale fabrication technologies, but also offers the possibility of patterning multiple recognition sites for various proteins on an imaging surface plasmon resonance chip, enabling the direct, label-free detection of selective recognition events [28]. The procedure was based on forming 5-µm wide and 2-µm deep microchannels from AZ® Photoresist on the Au substrate and then depositing PC within the channels by spin coating. After subsequent removal of the photoresist, the model protein, avidin, was adsorbed on the walls of the PC microchannels. Thus, the electrodeposition of PEDOT and dissolution of the sacrificial PC bands results in SPR chips with micropatterned polymer bands possessing the complementary imprint of the target protein on their lateral surface.

#### 13.2.2.3 Nanosphere Lithography

Target molecule-nanoparticle conjugates are deposited in a compact monolayer on the electrode surface followed by electropolymerization of the functional electroactive monomers. The film is grown in thicknesses that are smaller than the radius of the nanosphere to avoid impeding the removal of the particles. Avidin-latex nanoparticle conjugates deposited on the surface of gold-coated quartz crystals were used for proof of principle. The removal of the nanoparticles facilitated by the use of a cleavable protein-nanosphere linkage resulted in 2D arrays of periodic complementary size cavities. Nanogravimetric measurements demonstrated that the

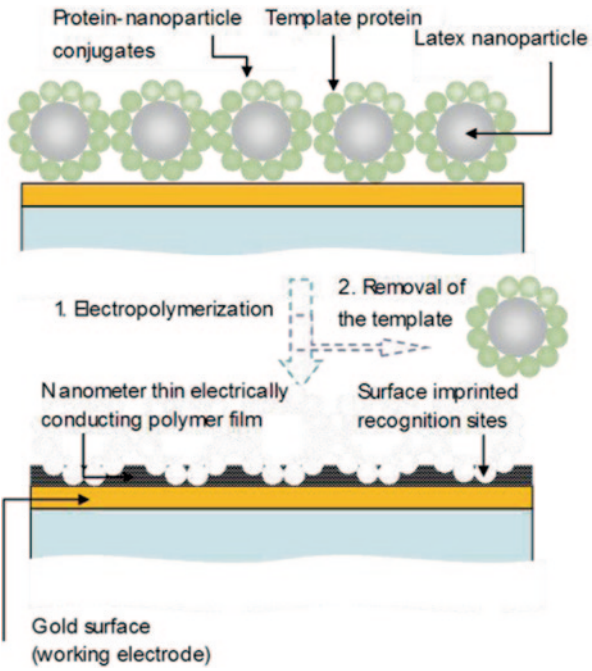


**Fig. 13.2** Schematic of the concept to generate surface imprinted polymers for selective recognition of macromolecules by nanosphere lithography with protein modified nanoparticles

imprinting proceeds further at molecular level with the avidin coating of the particle generating selective recognition sites on the surface of the PEDOT/PSS film [29] (Fig. 13.2).

#### 13.2.2.4 Vectorial Epitope Imprinting

Vectorial epitope imprinting uses a linear template (e.g., peptide from the C- or N-terminus), instead of using the whole protein. The cysteine-terminated template is self-assembled on a gold surface in an ordered submonolayer. A polymer film is grown between the template molecules by electropolymerization, with its thickness matching the thickness of the template layer (ca. 3–4 nm). After template removal by electrochemical stripping, a thin polymer film is obtained with a high density of vectorially imprinted surface sites for recognition of the template peptide and the protein it was derived from. Such imprinted sensing layers are compatible with SPR, QCM, or electrochemical detection [30].

#### 13.2.2.5 En Route Towards Protein/MIP Hybrids

A novel strategy to prepare a surface-confined molecularly imprinted polymer film directly on a transducer surface for protein sensing is achieved by combining

interaction with a natural binding receptor and binding to a fully synthetic MIP: a thiolated oligoethyleneglycol/mannose conjugate is first self-assembled on the transducer surface. Then the carbohydrate binding protein, concanavalin A (ConA), is "vectorially" immobilized as a submonolayer on the underlying mannose modified surface. Afterward, an ultrathin polyscopoletin film with the thickness comparable to that of the protein is electrodeposited on the top. The resulting functional material shows an approximately 20-fold higher affinity than that obtained from the mannose self-assembled monolayer. In comparison to the nonimprinted film, the MIP reveals 8.6 times higher binding capacity toward the target protein ConA. High discrimination toward the target protein's homologues (i.e., peanut lectin, soybean lectin, and lentil lectin) shows size and shape specificity of the imprint. This result shows a synergism between binding to the natural sugar ligand and the noncovalent interactions within the MIP cavities [31] (Fig. 13.3).

So far the catalytic activity of MIPs has in general been lower than those of their biological counterparts. Hybrids which are composed of a biocatalyst and a MIP may combine the advantages of both components. Recently, a novel combination of a molecularly imprinted electropolymer with the minienzyme-microperoxidase-11 (MP-11) or horseradish peroxidase (HRP) as a catalyst was reported (Yarman et al. 2012). The indicator electrode is covered with a product-imprinted electropolymer which is formed by anodic oxidation of an o-phenylenediamine/resorcinol mixture. The peroxide-dependent conversion of the analgetic drug aminopyrine ocurred in a layer on top of a product-imprinted electropolymer on the indicator electrode. The lower limit of detection for aminopyrine is 190 nM and interference from ascorbic is completely suppressed by the action of the MIP layer and oxidation with perox-

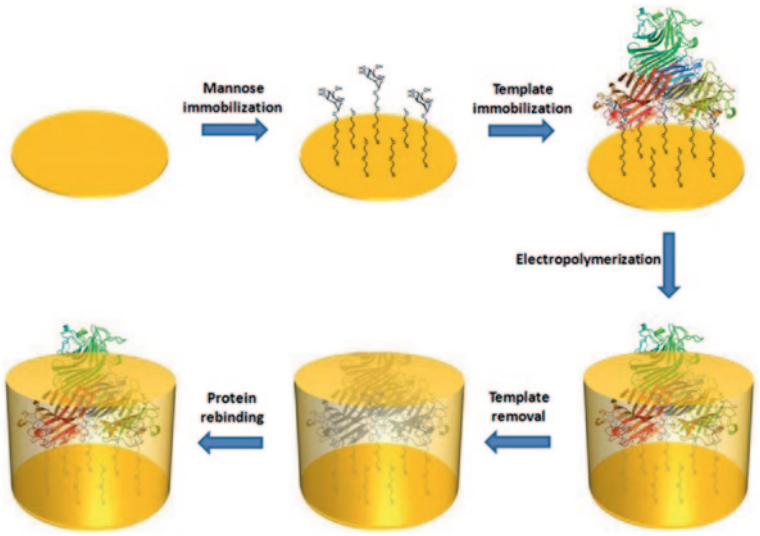


**Fig. 13.3** Workflow of MIP preparation of the SAM/MIP hybrid

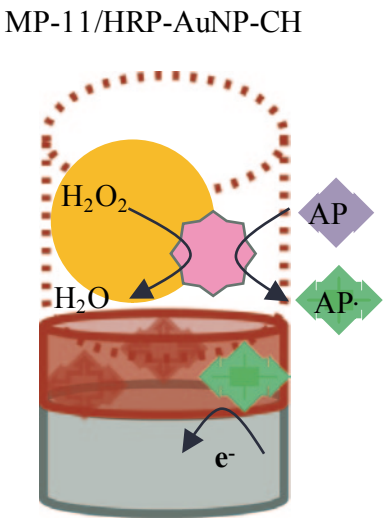


**Fig. 13.4** Structure of the sensor for aminopyrine which combines enzymatic substrate conversion with a MIP

ide. An advantage of this new hierarchical structure is the separation of MIP formation by electropolymerization and immobilization of the catalyst [32] (Fig. 13.4).

This combination has the potential to be transferred to other enzymes, e.g., Cytochrome P450, opening up a way to measure other clinically important analyte. Furthermore, integration of enzymatic substrate conversion, process control, and product separation may be accomplished by such hybrids.

## 13.3 Conclusions

Surface imprinting is a major enabling strategy for the generation of protein selective MIPs. Surface imprinting combined with electrochemical polymerization offers a particularly versatile synthetic approach with a high level of control over the polymer layer thicknesses and morphologies. The paradox that needs to be addressed, which nature has solved by evolution for biological receptors, is that proper recognition sites need building blocks rich in complementary functionalities to their target; however, on the other hand such units are likely to generate high levels of nonspecific binding. At present one of the challenge is to find the electroactive monomers best suited for the selective recognition of a given protein target. As with aptamers where the use of hydrophobic synthetic nucleotides led to a dramatic increase of the binding affinities, the MIPs would also gain from a rational selection of the functional monomers. Finally for an efficient development high throughput methods are required to enable rapid screening of monomers and template mixtures as well as synthesis conditions.

**Acnowledgements** REGy gratefully acknowledges the support of the Lendület program of the Hungarian Academy of Sciences. FWS and AY gratefully acknowledge the financial support of

BMBF (03IS 2201A) of Germany. This research forms part of UniCat, a Cluster of Excellence in the field of catalysis that is coordinated by the Technical University of Berlin and supported financially by the Deutsche Forschungsgemeinschaft (DFG) within the framework of the German Excellence Initiative (EXC 314).

## References

1. Ellington, A.D., Szostak, J.W. (1990) In vitro selection of RNA molecules that bind specific ligands. Nature, 346:818–822.
2. Tuerk, C., Gold, L. (1990) Systematic evolution of ligands by exponential enrichment: RNA ligands to bacteriophage T4 DNA polymerase. Science 249:505–510.
3. Kimoto, M., Yamashige, R., Matsunaga, K.-I., Yokoyama, S., Hirao, I. (2013) Generation of high-affinity DNA aptamers using an expanded genetic alphabet. Nat. Biotech. 31:453–457.
4. Lautner, G., Balogh, Z., Bardoczy, V., Meszaros, T., Gyurcsanyi, R.E. (2010) Aptamer-based biochips for label-free detection of plant virus coat proteins by SPR imaging. Analyst, 135: 918–926.
5. Wulff, G. and Sarhan, A. (1972) The Use of Polymers with Enzyme-Analogous Structures for the Resolution of Racemates. Angew Chem Int. Ed. Engl., 11:341–344.
6. Shea, K.J. and Thompson, E.A. (1978) Template Synthesis of Macromolecules. Selective Functionalization of an Organic Polymer. *J. Org. Chem.*, 43:4253–4255.
7. Arshady, R. and Mosbach K. (1981) 'Synthesis of Substrate-selective Polymers by Host-Guest Polymerization', Makromol. Chem., 182:687–692.
8. Alexander, C., Andersson, H.S., Andersson, L.I., Ansell, R.J., Kirsch, N., Nicholls, I.A., O'Mahony, J., Whitcombe, M.J. (2006) Molecular imprinting science and technology: a survey of the literature for the years up to and including 2003. J. Mol. Recognit. 19: 106–180.
9. Mahmoudi, M., Bonakdar, S., Shokrgozar, M. A., Aghaverdi, H., Hartmann, R., Pick, A., Witte G., Parak, W. J. (2013). Cell-Imprinted Substrates Direct the Fate of Stem Cells. *ACS nano*, *7*:8379–8384.
10. Piletsky, S. and Turner, A. (2006) A New Generation of Chemical Sensors Based on MIPs', in Piletsky S and Turner A, *Molecular Imprinting of Polymers*, Georgetown, TX, USA, Landes Bioscience.
11. Sellergen, B. and Shea, K.J. (1993) Influence of polymer morphology on the ability of imprinted network polymers to resolve enantiomers. *J. Chromatogr. A*, 635:31–49.
12. Haupt, K and Mosbach, K. (2000) 'Molecularly Imprinted Polymers and Their Use in Biomimetic Sensors', *Chem Rev*, 100, 2495–2504.
13. Wulff, G. (1995) Molekulares Prägen (Imprinting) in vernetzten Materialen mit Hilfe von Matrizenmolekülen-auf dem Weg zu künstlichen Antikörpern. *Angew. Chem.*, 107: 1958–1979.
14. Lettau, K., Warsinke, A., Katterle, M., Danielsson, B., Scheller, F.W. (2006) A Bifunctional Molecularly Imprinted Polymer (MIP): Analysis of Binding and Catalysis by a Thermistor. *Angew. Chem. Int. Ed. Engl.* 45:6986–6990.
15. Lakshmi, D., Bossi, A., Whitcombe, M.J., Chianella, I., Fowler, S.A., Subrahmanyam, S., Piletska, E.V., Piletsky, S.A. (2009) Electrochemical Sensor for Catechol and Dopamine Based on Catalytic Molecularly Imprinted Polymer-Conducting Polymer Hybrid Recognition Element. *Ana.l Chem.*, 81:3576–3584.
16. Díaz-Díaz, G., Antuña-Jiménez, D., Blanco-López, M.C., Lobo-Castañón, M.J., Miranda-Ordieres, A.J., Tuñón-Blanco, P. (2012) New materials for analytical biomimetic assays based on affinity and catalytic receptors prepared by molecular imprinting. *Trends. Anal. Chem*, 33: 68–80.
17. Whitcombe, M.J., Rodriguez, M.E., Villar, P., Vulfson, E.N. (1995) A New Method for the Introduction of Recognition Site Functionality into Polymers Prepared by Molecular Imprinting: Synthesis and Characterization of Polymeric Receptors for Cholesterol. *J. Am. Chem. Soc.* 117:7105–7111.

18. Ansell, R. J. and Mosbach K. (1997) 'Molecularly imprinted polymers by suspension polymerisation in perfluorocarbon liquids, with emphasis on the influence of the porogenic solvent', J. Chromatog.r A, 787, 55–66.
19. Chou, L.C.-S. and Liu, C.-C. (2005) Development of a molecular imprinting thick film electrochemical sensor for cholesterol detection. Sensor. Actuat. B-Chem. 110:204–208.
20. Mirsky, V.M., Hirsch, T., Piletsky, S. A., Wolfbeis, O.S. (1999) A Spreader-Bar Approach to Molecular Architecture: Formation of Stabil Artificial Chemoreceptors. *Angew. Chem. Int. Ed. Engl.* 38:1108–1110.
21. Merkoçi, A. and Alegret S. (2002) 'New materials for electrochemical sensing IV. Molecular imprinted polymers. *Trends Anal. Chem.* 21:717–725.
22. Malitesta, C., Mazotta, E., Picca, R.A., Poma, A., Chianella, I., Piletsky, S.A. (2012) MIP sensors: the electrochemical approach. *Anal. Bioanal. Chem*, 402:1827–1846.
23. Syritski, V., Reut, J., Menaker, A., Gyurcsanyi, R.E., Oepik, A. (2008) Electrosynthesized molecularly imprinted polypyrrole films for enantioselective recognition of L-aspartic acid. Electrochim. Acta. 53:2729–2736.
24. Kryscio, D.R., Peppas, N.A. (2012) Critical review and perspective of macromolecularly imprinted polymers. Acta Biomater., 8:461–473.
25. Menaker, A., Syritski, V., Reut, J., Opik, A., Horvath, V., Gyurcsanyi, R.E. (2009) Electrosynthesized Surface-Imprinted Conducting Polymer Microrods for Selective Protein Recognition. Adv. Mater. 21:2271–2275.
26. Ceolin, G., Orban, A., Kocsis, V., Gyurcsanyi, R.E., Kezsmarki, I., Horvath, V. (2013) Electrochemical template synthesis of protein-imprinted magnetic polymer microrods. J. Mater. Sci. 48:5209–5218.
27. Orozco, J., Cortés, A., Cheng, G., Sattayasamitsathit, S., Gao, W., Feng, X., Shen, Y., Wang, J. (2013) Molecularly Imprinted Polymer-Based Catalytic Micromotors for Selective Protein Transport. J. Am. Chem. Soc., 135: 5336–5339.
28. Lautner, G., Kaev, J., Reut, J., Opik, A., Rappich, J., Syritski, V., Gyurcsanyi, R.E. (2011) Selective Artificial Receptors Based on Micropatterned Surface-Imprinted Polymers for Label-Free Detection of Proteins by SPR Imaging. Adv. Funct. Mater. 21: 591–597.
29. Bognar, J., Szucs, J., Dorko, Z., Horvath, V., Gyurcsanyi, R.E. (2013) Nanosphere Lithography as a Versatile Method to Generate Surface-Imprinted Polymer Films for Selective Protein Recognition. Adv. Funct. Mater. 23:4703–4709.
30. Dechtrirat, D., Jetzschmann, K.J., Stöcklein, W.F.M., Scheller, F.W., Gajovic-Eichelmann, (2012) Protein Rebinding to a Surface-Confined Imprint. Adv. Funct. Mater. 22:5231–5237.
31. Dechtrirat, D., Gajovic-Eichelmann, N., Bier, F. F., & Scheller, F. W. (2013). Hybrid Material for Protein Sensing Based on Electrosynthesized MIP on a Mannose Terminated Self-Assembled Monolayer. Adv. Funct. Mater. 24:233–2239.
32. Yarman, A. And Scheller, F.W. (2013) Coupling biocatalysis with molecular imprinting in a biomimetic sensor. *Angew Chem Int. Ed. Engl.*, 52(44):11521–11525.

# Chapter 14
# Bio-nanostructured Interfaces Fabricated by Scanning Probe Nanolithography (SPN)

**Juan Rodríguez-Hernández**

## 14.1 Introduction

Biomolecular patterning at the nanoscale is currently a very active field that combines the know-how of two different fields: biology and nanotechnology. The interest in the preparation of nanoscale features at surfaces relies on their wide range of applications in different areas, including physical science and life science. In particular, the immobilization of biomolecules having nanometer resolution has been pursued for their interest in fundamental studies in molecular and cell biology or to prepare platforms with different biomedical applications such as molecular diagnostics just to mention a few of them.

In particular, as depicted by Christman et al. [1, 2], in the case of proteins, the ability to spatially orient and anchor them at the nanoscale affords useful materials in such applications as biosensors, biomaterials, and tissue engineering. Several major advantages are derived from this control of the protein distribution at the surface at the nanometer scale. For instance, protein nanoarrays offer the possibility to achieve greater sensitivity in diagnostic tests since the disease progression is often connected with single proteins [3]. In addition, further miniaturization from protein microarrays to nanoarrays may allow for the discovery of currently undetectable disease markers [3]. Moreover, provided the possibility to have multifunctional surfaces with a large variety of different proteins, the detection of thousands of biomarkers could be performed on one single chip [4–7].

Scanning probe nanolithography (SPN) has its origin in 1981 and since then this technique has been used to gain knowledge of surface structures and molecular organization in different fields, including physics, chemistry, and biology, and has been later expanded to other areas of science and technology [8]. In addition, SPN is today a largely extended technique for fabrication of nanoscale structures,

J. Rodríguez-Hernández (✉)
Department of Chemistry and Properties of Polymers, Institute of Polymer Science and Technology (ICTP-CSIC), C/Juan de la Cierva 3, 28006 Madrid, Spain
e-mail: jrodriguez@ictp.csic.es



J. Rodríguez-Hernández, A. L. Cortajarena (eds.), *Design of Polymeric Platforms for Selective Biorecognition*, DOI 10.1007/978-3-319-17061-9_14

especially for directly inducing selective modifications on a surface with a precise localization of the defined pattern [9].

SPN takes advantage of a sharp tip to either build or destruct the interface to produce different surface patterns. The tip is connected to one of the following equipments: scanning tunneling microscope (STM), atomic force microscope (AFM), scanning electrochemical microscope (SECM), or scanning near-field optical microscope (SNOM) [10]. These techniques offer remarkable versatility and permit both a precise spatial fabrication and simultaneously the possibility to image the patterned surfaces at the nanometer or molecular scale. Moreover, in addition to the ultrahigh resolution they do not require the use of particular masks or templates. Finally, their relatively low cost and capability to operate in ambient conditions is worth mentioning.

In this chapter, we will review the main strategies employed to produce nanometer-scale surface patterns by using scanning probe techniques focusing on the fabrication of nanostructured interfaces with biomolecules capable of acting in recognition processes.

## 14.2 Methodologies for Generating Nanoscale Features

A significant effort has been carried out to develop different methodologies in order to generate nanoscale features. These include bottom-up self-assembly approaches [11–18], redox control [19], conductive AFM [20], scanning-near field photolithography [21], and stamping techniques, such as nanoimprint lithography [22, 23], just to mention a few of them. Other alternatives resort to the combination of several patterning methodologies. For instance, Falconnet et al. produced protein patterns combining nanoimprint lithography and molecular self-assembly [24]. Within this context, in this chapter, we will highlight and analyze those methodologies that involve the use of AFM tips to create biomolecular nanopatterns.

In comparison with other methods, to pattern biomolecules at the nanometer scale, scanning probe approaches can be carried out under ambient conditions to permit the formation of high-resolution patterns, and the pattern to be fabricated can be easily modified and adapted for a particular demand. Moreover, in the case of dip-pen nanolithography (DPN), there exist a variety of “inks” that can be employed. Therefore, the surface chemistry can be easily modified. The major challenges remaining for these approaches are related to the small area that can be patterned and that the process can be rather slow. The latter can be, at least to some extent, overcome by using arrays of multiple tips that reduce the patterning time. In order to summarize the capabilities of SPN techniques that include DPN, nanografting, and nanoshaving, Table 14.1 contains the main advantages and limitations of directly related approaches: electron beam lithography, nanocontact printing, or nanoimprint lithography.

**Table 14.1** Nanoscale-patterning methods using biomolecules. (Reproduced with permission-from reference [25])

| Technique | Advantages | Limitations |
|---|---|---|
| Electron beam lithography(EBL) | Maskless, stampless<br>High resolution<br>Arbitrary pattering with different shapes and sizes | Slow (serial process) Complicated, expensive (requiring equipment, clean room and vacuum condition) Small area patterning |
| Nanocontact printing(NCP) | Simple (direct patterning)<br>Parallel, cheap<br>Fast process<br>Large area patterning | Preparing nanoscale stamp with high feature density Mechanical stability of stamp<br>Diffusion of SAM inks |
| Nanoimprint lithography (NIL) | Large area patterning with a high throughput and low cost<br>Parallel | Stress and wear of mold<br>Use of polymer<br>Slow (molding, demolding, and etching process) |
| Nanografting/nanoshaving | High resolution, ambient.<br>Quick change of fabricated patterns | Small area patterning |
| Dip-pen nanolithography(DPN) | High resolution, ambient Variety of inks usable Parallelization possible | Slow (serial process)<br>Small area patterning |

## 14.3 Tip-based Nanofabrication Approaches

Tip-based nanofabrication refers to those techniques that employ a functionalized cantilever-tip or an array of cantilever-tips to perform the surface patterning. Initially, these techniques resorted to what has been named "destructive" SPL, i.e., the materials at the surface are either removed or modified by applying external mechanical, thermal, electrical, or optical energy through the scanning probe [26]. Typical examples include plowing through the first of two resist layers on an arbitrary substrate and following with a development step [27–29], nanoshaving and nanografting [30, 31], thermomechanical indentation [32], thermochemical nanolithography (TCNL) [33–35], electrostatic nanolithography [36, 37], electrochemical oxidation [38–40], and scanning near-field optical lithography (SNOM) [41–43]. More recently, other alternatives considered the possibility to place materials onto a surface, "constructive" SPL for instance by using the probe wetted with a particular ink as a "pen." This methodology was first described by Mirkin et al. [44, 45] and today other variations have been developed further by combining the DPN with additional stimuli such as forces, [46], heat [47], or electric fields [48].

These techniques have been employed for different materials; however, the preparation of polymeric nanostructures has received particular attention. Thus, SPL has extended their use for multiple polymer-based applications including the preparation of polymer resists for nanofabrication, the preparation of polymeric carriers for functional materials, nanopatterning of electronically active polymers, or the fabrication of polymer brush nanostructures [10].

### 14.3.1 Dynamic Plowing Lithography

Dynamic plowing lithography (DPL) consists of surface modification by indenting the material with a vibrating tip using an AFM working in the tapping mode [27–29]. The tapping mode is required since a permanent contact with the substrate (contact mode of the SFM) restricts the tip movement to directions close to the cantilever axis due to frictional forces. Equally, other directions can lead to a cantilever torsion and thus produce irregularities in the final pattern. By using these conditions, this method provides a lithography technique that is nearly free from problems due to cantilever torsion and permits us to image the modified surface without any further modification.

DPL has been employed to pattern semiconductor crystals and oxide layers. However, the tip rapidly degraded since the hardness of both the material and the tip are in a similar range. Nevertheless, this approach appeared to be interesting when the pattern transfer and the lithography process are separated. More precisely, we can plow first a thin polymer layer (Fig. 14.1 left) and then transfer the pattern by a wet chemical etchant, which does not significantly affect the polymer thin film.

### 14.3.2 Nanoshaving/Nanografting

Nanoshaving works in a similar fashion as plowing lithography. However, in this case a resist material is mechanically removed by an AFM tip for creating nanometer-scale patterns on surfaces [30]. In this technique, the immediate removal of the displaced compound requires additionally the suppression of readsorption [31]. On the other hand, nanografting operates on a matrix monolayer immersed in a solution containing the desired molecules different from the matrix. In this situation, as the AFM tip plows through the matrix monolayer, the matrix molecules are removed and replaced by these reactive molecules in solution [30]. As an example Liu et al. [31] succeeded to pattern self-assembled monolayers (SAMs) using mixtures of thiols with various chain lengths. As a consequence, nanografting can create both positive and negative patterns, depending upon the relative chain length between the new and matrix adsorbates [49, 50] (Fig. 14.2).

### 14.3.3 Thermomechanical or Thermochemically Induced Nanopatterns [33, 34]

Thermomechanical writing was first reported by Mamin and Rugar [32, 51]. They employed an infrared laser focused on an AFM tip, which is in contact with a transparent polymethyl methacrylate (PMMA) substrate. The laser beam heated the AFM tip and the later softens the PMMA in the contact region. The heated tip causes very local heating of the polymer material above its softening temperature,

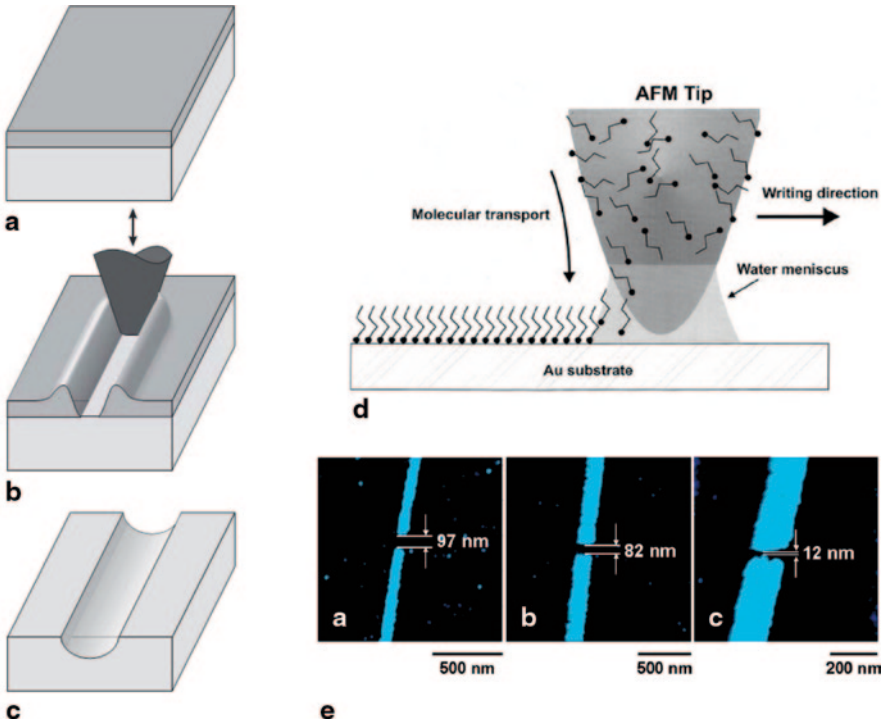


**Fig. 14.1** *Left*: Example of "destructive" tip-nanofabrication. Scheme of a nanoscale line produced with a SFM: **a)** Substrate with a polymer coating of a few nanometers thickness. **b)** Plowing of a furrow into the polymer layer with the vibrating tip of the SFM along a desired line. **c)** Transfer of the line by etching the substrate in the furrow and removing the masking layer (shown here). Reproduced with permission from ref. [29]. *Right*: example of "constructive" tip-nanofabrication. **d)** A schematic diagram of the DPN process where the ink molecules transfer from an AFM probe to the substrate surface [44]. **e)** TMAFM topographic images of etched MHA/Au/Ti/SiOx/Si nanogaps [45].

which effectively acts as the switch to turn on the writing process [11]. As a consequence, applying a controlled pressured allowed to create a pit. The pits range in size from several hundred angstroms to 1 m, depending on the size of the laser pulse and the loading force on the tip. As a consequence, this technique has been proposed, among others for ultrahigh storage density permitting store, read back, and erase data in very thin polymer films [52]. More recently, thermomechanical writing has been improved and used for other purposes [53–56].

TCNL employs a resistively heated AFM cantilever to induce chemical reactions in a nanometer-scale position, thus, inducing changes on the surface functionality of thin polymer films or SAMs [35]. The basis for achieving a high degree of spatial resolution is the sharp thermal gradient in the vicinity of the warmed tip and the kinetics of the chemical reaction that are known to increase exponentially with

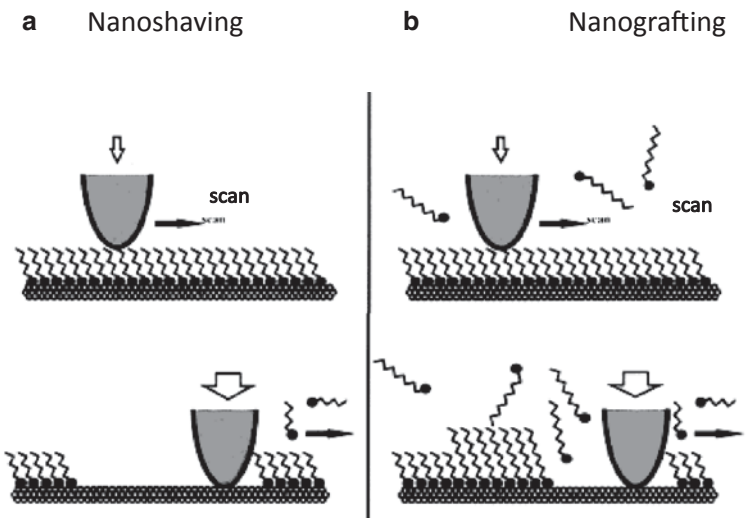


**Fig. 14.2** Schematic diagrams to produce nanopatterns either by nanoshaving or by nanografting. (Reproduced with permission from reference [31])

temperature. An illustrative example of this approach has been reported by Gotsmann et al. [34] who employed a reversible cross-linking that allows the thin film to exist in two different chemical states: a low-temperature state of high-molecular-weight material and a high-temperature state of low-molecular-weight molecules (see Scheme 14.1).

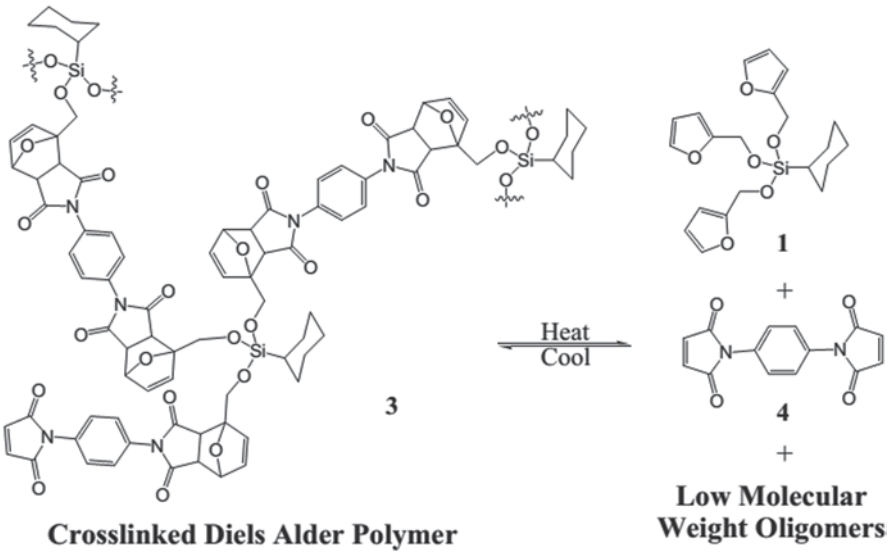


**Scheme 14.1** Reversible Diels–Alder (DA) reaction for depolymerization of cross-linked thin films on heating and re-cross-linking of the low-molecular-weight products on cooling. (Reproduced with permission from ref. [34])

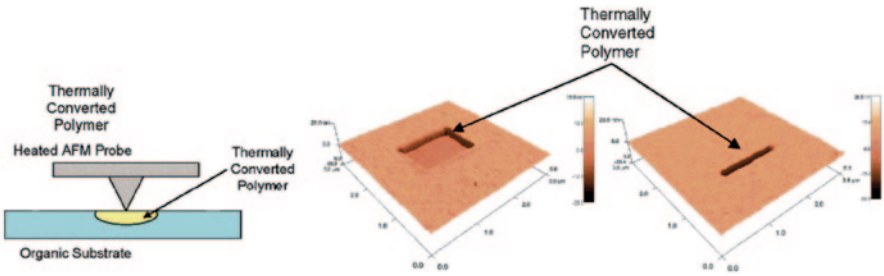


**Fig. 14.3** Local thermal writing into the organic substrate using a heated AFM cantilever tip. *Left*: Thermal writing process. *Middle* and *right*: Thermally induced writing using a conjugated polymer made by click chemistry at the micrometer and submicrometer scale. The recessed regions are the locations where the heated AFM tip has scanned over the polymer film and locally induced cycloaddition. Reproduced with permission from ref. [33]. *AFM* atomic force microscope

Finally, thermochemical nanopatterning can be associated with thermomechanical lithography. As a consequence, both surface structure and functionality can be simultaneously varied. For instance, Bakbak et al. [33] described an interesting approach in which the heating of a tip directed the synthesis of conjugated fluorescent polymers. In particular, they employed the thermal and Cu-catalyzed 1, 3-dipolar cycloadditions of terminal diynes with aromatic diazides. In addition, they reported the fabrication of nanostructured organic semiconductors by nanoscale thermal processing of annealed diazide/dialkyne thin films with a heated AFM cantilever tip (Fig. 14.3).

### *14.3.4 Electrostatic Nanolithography*

As has been described among others by Heminghaus et al. [57] and Schaffer et al. [58], strong field gradients can produce forces that overcome the surface tension in thin liquid films, inducing an instability. In this situation, electrostatic and/or van der Waals pressure overcomes Laplace pressure; a film heated above the glass-transition temperature (Tg) becomes highly unstable with regard to small perturbations, thus leading to particular surface features [36]. More precisely, the dynamic instability of a dielectric liquid in a strong electric field ($10^{7}$–$10^{8}$Vm$^{-1}$) has been implemented for polymer melts, and a wide range of architectures with submicrometer features (~100 nm) have been created [58]. Within this context, AFM-assisted electrostatic lithography (AFMEN) generates nanometer-scale features (1–50 nm) by simply biasing (0–20 V) a highly conductive tip across a thin polymer film. The features of the nanopatterns created from polymer films depend on the type of polymer used, the applied bias, and speed of the AFM tip. Figure 14.3 shows the nanolines drawn on a PMAA thin film at different voltages varying from −4 to −11 V at an AFM tip speed of 0.5 ms$^{-1}$.The observed line widths are 62, 78, 113, 135, and 172 nm. Whereas at low negative potential, i.e., the first two lines drawn at −4 and −5 V, are all raised patterns, an increase in the bias applied induced the formation of grooved patterns (last two lines drawn at −9 and −11 V) (Fig. 14.4).

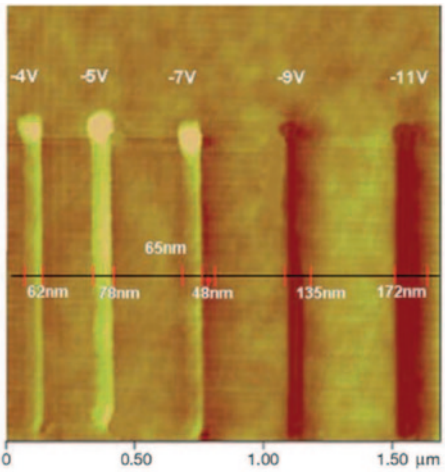


**Fig. 14.4** AFM image of the nanolines drawn with a tip speed of 0.5 $mms^{-1}$ at different applied voltages. (Reproduced with permission from ref. [37]). *AFM* atomic force microscope

### *14.3.5 Electrochemical Oxidation [38–40]*

In a parallel fashion to what has been depicted below, Sagiv and co-workers were pioneer in the use of bias voltage pulses applied to a conductive SFM tip to chemically modify the surface by inducing the electrochemical conversion of surface-exposed terminal groups of an SAM. Thus, this strategy served to create chemical functionalities introduced directly onto a surface with precise distribution. The authors reported different chemical patterns using, for instance, nonadecyltrichlorosilane (NTS) monolayers with terminal vinyl groups on the surface or chemically inert *n*-octadecyltrichlorosilane (OTS) monolayers [59–61]. Particularly interesting is the latter where by applying a surface voltage the authors detected the presence of acid groups on the patterned monolayer and revealed that the monolayer was preserved during the electrooxidation process (Fig. 14.5). Moreover, these acid groups can be employed to carry out further functionalization steps [62]. A review covering further details of this technology has been already published [38].

### *14.3.6 Scanning Near-field Optical Lithography (SNOM)*

The basic idea behind near-field optical methods is to avoid the normal diffraction limited far-field imaging by taking advantage of evanescent components of a point-like light source [41–43, 63]. Since evanescent waves decay exponentially with the distance to the surface and dominate in the near field zone, SNOM requires operation in a region where probe-sample distance remains below the excitation wavelength. By using these conditions, the lateral resolution achieved with this method is

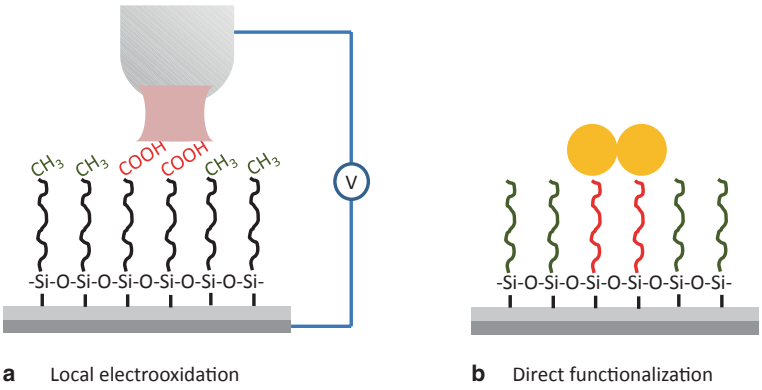


**Fig. 14.5** **a** The local electrooxidation of *n*-octadecyltrichlorosilane monolayers induces the formation of carboxylic acid end groups, which can be used for **b** the direct attachment of functional materials (*yellow* circle; *red*: COOH-functionalized monolayer; *green*: nonfunctionalized monolayer). (Reproduced with permission from ref. [62])

largely below the diffraction limit for microscopic imaging. The shear-force method is suitable for conductive as well as for nonconductive samples, such as conventional photoresists.

### *14.3.7 Dip-pen Nanolithography (DPN)*

DPN was introduced in 1999 by Mirkin and co-workers [44]. They reported that water can be either transported from an AFM tip to a substrate or from the substrate to the tip, depending on the properties of each [64]. Based on these findings, the authors developed strategies to deposit different compounds on solid surfaces. In DPN the AFM tip is coated with a liquid thin layer composed of solvent and what has been named "ink." The AFM tip delivers the molecular ink directly to a specific region of a target substrate by simple contact with the surface. Typically, the "inks" used in DPN form a monolayer on the substrate as a consequence of the chemical reaction between the ink and the surface [65] and thus the choice of a particular ink is determined by the substrate employed [9]. Inks can vary from organic reactive molecules, such as silanes, alkynes, thiols, and silazanes (e.g., 1-octadecane-thiol or ODT) to inorganics, such as oxides, metals, and magnetic compounds (e.g., gold nanoparticles) to biomolecules such as peptides, DNA, and proteins (e.g., thioredoxin) [66]. In comparison with previous methodologies DPN can be employed under ambient conditions. However, as depicted by Ginger et al. the optimal conditions for this technique require the use of a chamber with controlled humidity [65].

**Table 14.2** Techniques developed to immobilize biomolecules at the micro-/nanoscale

| Deposition method | Best resolution | Ink | Substrate | Reference |
|---|---|---|---|---|
| Microcontact printing | 500 nm<br>19 m | IgG protein<br>Lipid bilayers | | [76]<br>[77] |
| Optical lithography | 8 m<br>500 nm | Alkanethiols<br>Streptavidin | | [78]<br>[2] |
| Scanning probe lithography | 30 nm lines<br>45 nm dots | Collagen<br>IgG protein | Gold | [79]<br>[80] |
| Surface-patterning tool | 2–3 m dots<br>150 nm lines | Cy3-streptavidin<br>Quantum dots conjugated to streptavidin | | [81] |
| Microspotters | 30 m dots | IgG protein and oligonucleotides | Glass | [82, 83] |
| Nanopipettes | 440 nm dots<br>510 nm dots | IgG protein<br>Biotylinated DNA | Glass | [84] |
| Nanofountain probe | 40 nm lines<br>200–300 nm dots<br>200–300 nnm dots | MHA<br>DNA<br>IgG protein | Gold | [85, 86] |

## 14.4 Immobilization of Biomolecules onto Surfaces Through Nanolithography

A large number of biomolecules such as DNA, RNA, virus, or proteins have been immobilized onto surfaces with nanometer precision by using different SPN approaches. The targeted applications pursued for the immobilized surfaces varied from proteomics and genomics, clinical-based diagnostics to studies devoted to protein profiling or the screening of drug candidates [66–69]. Other biological and biomedical applications include the elaboration of nanobiochips and nanobiosensors, tissue engineering, and molecular and cell biology [1, 70–75].

As has been reported by Mendes et al. [26], the immobilization of biomolecules requires accomplishing several additional issues. Immobilized biomolecules require to be placed in a precise position (shape and distance between them has to be controlled) with nanometer-scale resolution. Equally, the immobilized biomolecules should not be degraded or damaged during the immobilization process so that the native biological properties remain identical. (Table 14.2)

As depicted above, several approaches using the tip-based technology are excellent candidates to immobilize biomolecules at the micro-/nanometer scale. Herein, we will focus on the most extended methodologies to immobilize biomolecules for biorecognition purposes that include DPN, nanoshaving, and nanografting. As will be depicted in detail, DPN and nanografting can be achieved by using two alternatives either by directly writing/grafting the desired biomolecule or by pre-patterning the surface with an organic molecule showing high biomolecule affinity. Moreover, as depicted in Fig. 14.6, the patterning process can be followed by a second patterning step where, for instance, free surface can be completed with a second molecule.

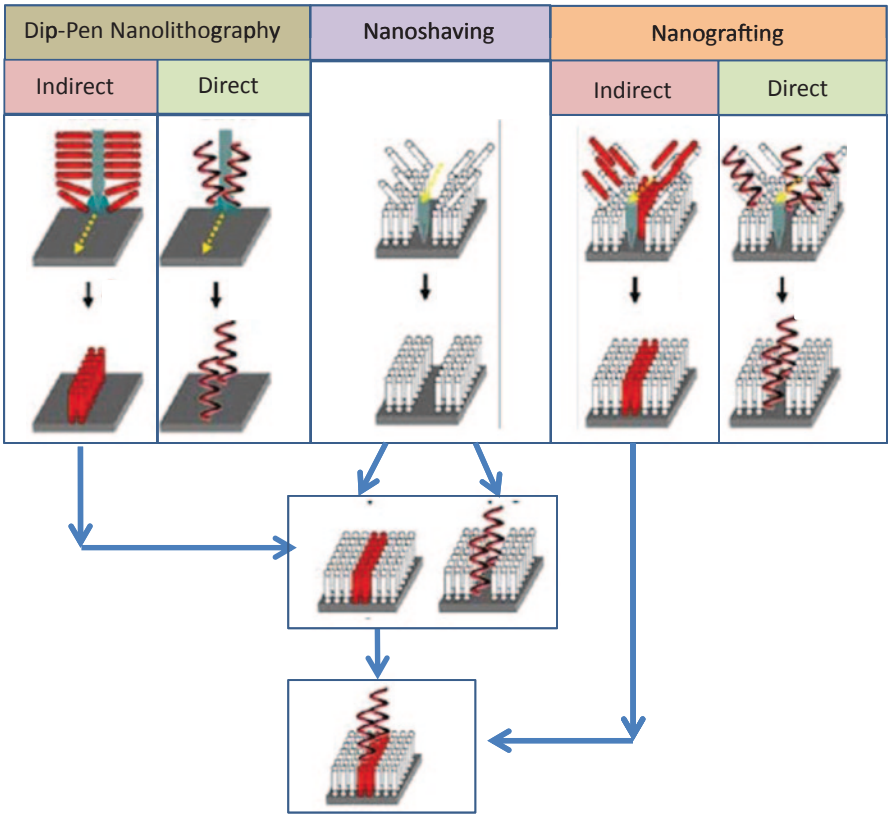


**Fig. 14.6** Schematic representation of the different scanning probe lithographic techniques employed to indirectly or directly immobilize biomolecules on surfaces at nanometer-scale resolution. Whereas in the direct approach, the biomolecules are directly deposited onto the substrate, in the indirect approach, the nanopatterns created by the different lithographic techniques are used in a second stage (i.e., post-patterning process) as templates to immobilize the biomolecules onto surfaces. (Figure adapted from ref. [26])

### *14.4.1 Biomolecules Deposited by Dip-pen Nanolithography (DPN)*

In DPN the tip is wetted with the biomolecule solution and is employed to deliver the material to a particular surface by bringing the tip in contact with the substrate. DPN utilizes the water meniscus formed between an AFM tip and a substrate to transfer ink molecules onto surfaces. As a consequence, patterns with resolutions ranging from few microns down to ~10 nm can be fabricated. The high resolution obtained offers a large increase in the areal density of the deposited motifs. According to Zhang et al. [65] (depicted in Fig. 14.7), the increase in density could reach 10,000- to 100,000-fold the values obtained with other methodologies such as

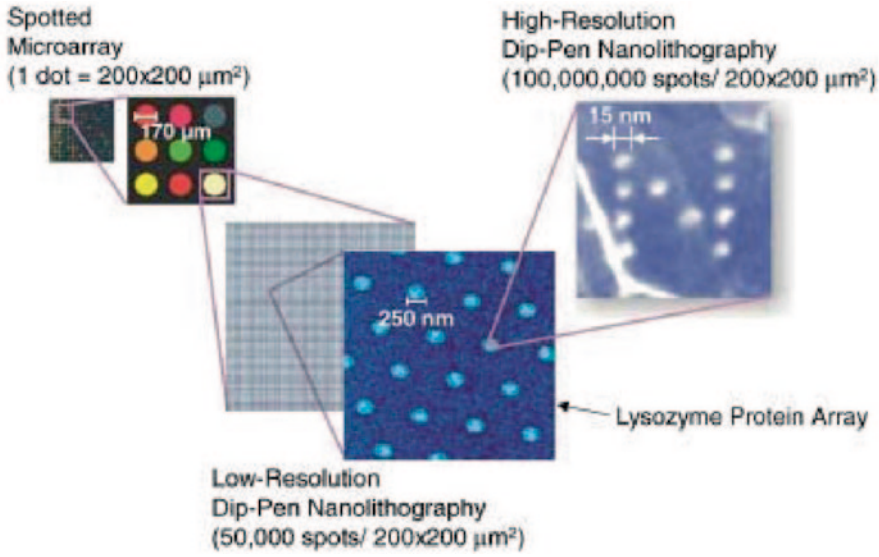


**Fig. 14.7** Schematic illustration of the power of DPN resolution in the context of biomolecular nanoarray fabrication. (Reproduced with permission from ref. [65])

robotic spotting or photolithographic technology. Two main factors will influence the resolution of the final pattern obtained. On the one hand the size of the meniscus affects the size of the pattern created. Xie et al. [64] estimated that smaller meniscus allows higher resolution. However, when the meniscus is too small, it becomes unstable and fluctuates in shape, with fluctuations that are larger in magnitude than its average width. The meniscus size is not only dependent on the tip sharpness but also on other parameters including the humidity, wettability of the tip, and distance to the surface. On the other hand, the diffusion constants of the molecules being deposited also play a key role in pattern formation [44, 87]. For detailed information on the DPN methodology the reader is referred to several reviews that have covered the most recent advances [1, 26, 65, 88].

As depicted in Fig. 14.6, DPN can be carried out using two different methodologies. The direct method involves the deposition of the biomolecule directly onto the surface. In the indirect method, the immobilization of biomolecules is accomplished in two separate steps. In the first step biomolecule-adherent organic molecules are deposited from the solution. The second step concerns the adsorption of the biomolecule from the solution onto those areas where the organic molecule has been deposited (Fig. 14.8).

DPN has been employed for a variety of applications ranging from the construction of building nanostructured materials with DPN to the elaboration of DPN-patterned etch resists [65, 66]. Nevertheless, a major field of application of this technique concerns the controlled biomolecule deposition onto surfaces. In particular, DPN has been employed for the fabrication of micro- and nanoarrays of patterned biomolecules such as DNA or proteins in order to control the biorecognition pro-

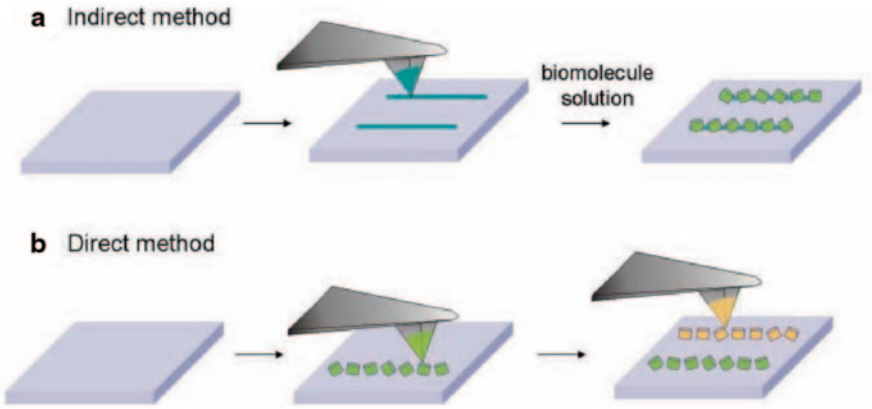


**Fig. 14.8** Schematic representation of **a** indirect and **b** direct dip-pen nanolithography (DPN) method for patterning biomolecules [88]

cesses from the molecular to the cellular level. Equally, several studies have been concerned with the surface immobilization of virus and cells [89].

#### 14.4.1.1 Direct DPN Nanolithography

Direct DPN has been employed to construct among others protein and DNA nanostructures which have exhibited a potential for different purposes such as screening of drug candidates and studying of protein expression profiling. DPN is a simple and straightforward way for creating protein and DNA patterns since features can be directly written onto the surface. Significantly, this method avoids the complications associated with nonspecific binding.

However, in general, the use of DPN to direct-write biomolecules requires the modification of the surface of commercially available AFM tips obtained upon several steps. For instance, as depicted in Fig. 14.9, this functionalization has been achieved by immersing the gold-coated cantilever in a solution of a symmetric 11-mercapto-undecylpenta(ethylene glycol)disulfide (PEG) [80] in order to prevent protein adhesion on the backside of the tip. After this step, the tip is coated with gold by means of thermal evaporation methods. The cantilevers with the gold-coated tips were immersed in thiotic acid. As a result, the hydrophilic tips with the carboxylic acid-terminated SAMs favor the protein adsorption on the tip surface. Upon functionalization of the tip and protein adsorption, the biomolecule can be directly deposited onto the solid surface. By using this methodology, Lee et al. [68] succeeded in the preparation of nanostructures of lysozyme (Lyz) and rabbit immunoglobulin-gamma (IgG) nanodot arrays constructed in a direct-write fashion. In further studies, the same group employed DPN for the construction of an angiogenin protein nanoarray. In particular, they studied the immobilization of angiogenin and their recognition activity with integrin $\alpha_v\beta_3$ used as model protein.

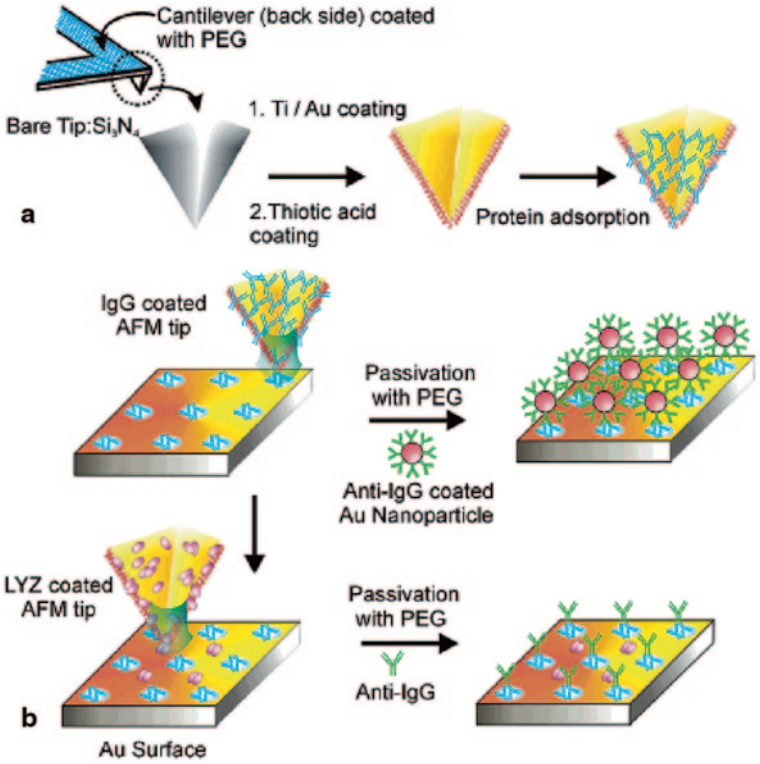


**Fig. 14.9** Strategies for: **a** Tip Modification using a Ti/Au coating followed by a thiolic acid and the protein adsorption. **b** Scheme for the protein patterning using two different alternatives. On the first approach, upon coating with the IgG the surface is passivated and the biorecognition permits the immobilization of the anti-IgG-coated nanoparticles. The second strategy refers to a multistep procedure to pattern different proteins, i.e., IgG and lysozyme (Lyz) [80]

Other examples in which proteins were directly deposited on surfaces include thiolated collagen and collagen-like peptides onto gold surfaces [79]. The authors were able to print collagen and a collagen-like peptide down to 30–50 nm line widths. Moreover, the direct deposition methodology preserved the triple-helical structure and biological activity of collagen. In addition, this approach permits the formation of characteristic higher levels of structural organization. The sensitivity of these types of biological molecules to thermally induced structural changes (e.g., denaturation) makes the DPN lithographic method ideal in comparison to harsher techniques such as ion-beam-based lithography. According to the authors, the specific nanopatterned arrays of collagen might be used to induce an assembly network of collagen scaffoldings to mediate cell attachment processes, organized as optical gratings because of their ability to form liquid crystalline phases, and as guest–host systems for other biological or nonbiological components. The “direct-write” capability of biologically relevant molecules, while preserving their structure and

functionality, provides tremendous flexibility in future biological device applications and in proteomics arrays, as well as a new strategy to study the important hierarchical assembly processes of biological systems.

More recently, De Yoreo's group has shown that it is possible to generate nanoscale patterns of human chorionic gonadotropin (HCG) antibody [90]. In their approach, the protein was tagged with a specific fluorophore, so that the pattern can be easily identified and verified using optical imaging. More precisely, they fabricated patterns of HCG antibody tagged with tetramethylrhodamine (TMR) dye on the glass surface. The glass surface was pretreated with 3-glycidoxypropyltrimethoxysilane to introduce the epoxy groups that facilitate protein adhesion to the surface.

Direct dip-pen nanolithography was employed also by Demers et al. [65, 91] to pattern modified oligonucleotides on metals (gold) and insulators (silicon oxide). The first step requires the surface modification of a silicon nitride AFM cantilever with 3'-aminopropyltrimethoxysilane that promotes reliable adhesion of the DNA ink to the tip surface thus improving control over DNA patterning. In particular, the authors employed hexanethiol-modified oligonucleotides to directly pattern gold substrates with features ranging from 50 nm to several micrometers in size. The thiol group assures the chemisorption of the DNA into the underlying Au surface. Further hybridization experiments by using the anchored DNA require the passivation of the surface towards complementary DNA. For that purpose, the patterned surfaces with oligonucleotides were immersed in an ethanol solution of 1-octadecanethiol that coats the unpatterned gold surface with a hydrophobic monolayer. Finally, by using oligonucleotide-modified gold nanoparticles, the authors demonstrated that the immobilized DNA retained its highly specific recognition properties.

Due to the nanometric precision of DPN, this approach is an interesting alternative to fabricate not only patterns with nanometer-size resolution (as depicted above) but also go a step further in order to create biological nanoarrays. DPN is one technique that has shown particular promise in this area, allowing one to prepare standardized multicomponent arrays of biomolecules that can retain their biorecognition properties once transferred to a surface [44, 65, 80, 89, 92–96]. These arrays have been employed, among others, for the detection of proteins, DNA, and other small molecules and exhibit several advantages over typical microarrays. First, as mentioned above, nanoarrays created by DPN are 10,000–100,000 times denser that microarrays. Therefore, smaller areas are required to identify the same number of targets and smaller sample is required [66]. Moreover, a larger number of targets can be screened in a shorter period of time and due to the minimum area of the nanoarray a target can be detected at very low concentrations. In addition, cDNA and oligonucleotide arrays permit to quantify both gene expression and genomic structure (e.g., through single-nucleotide-polymorphism (SNP) detection). This unique feature has induced their extensive use among others in oncology [97], for the elucidation of the roles of genes in the pathogenesis of infectious diseases [98], in neurology for the evaluation of a large amount of genes [99], and the study of genomic structures and gene expression [98, 100].

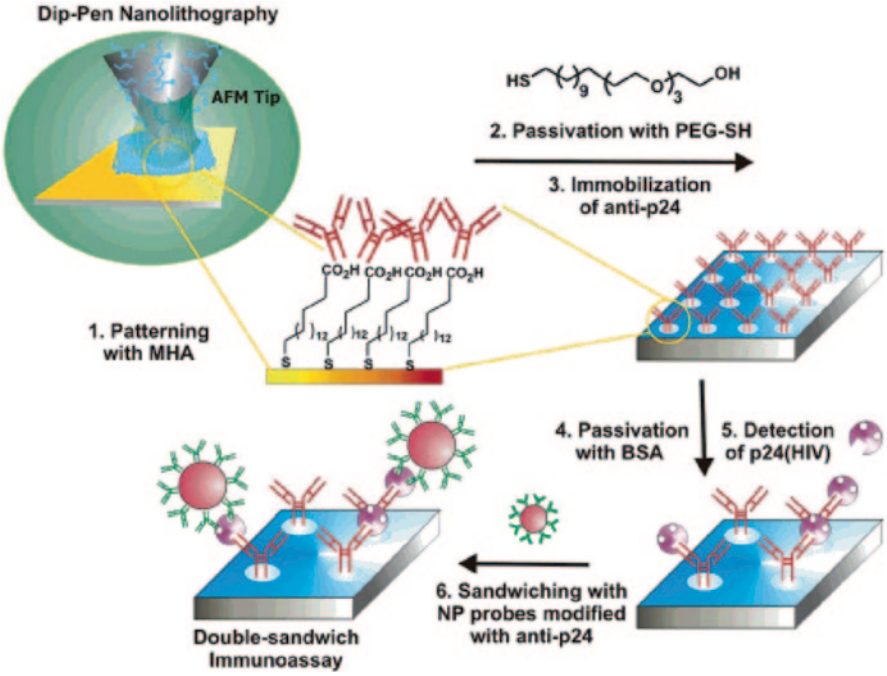


**Fig. 14.10** Schematic representation of the immunoassay format used to detect HIV-1 p24 antigen with anti-p24 antibody nanoarray. (Reproduced with permission,reference [101])

Nanoarrays have been applied, for instance, in the detection of human immunodeficiency virus type 1 in plasma [101]. Lee et al. used DPN to generate nanoscale patterns of antibodies against the HIV-1 p24 antigen on a gold surface. They succeeded in the preparation of feature sizes that were less than 100 nm, while preserving the activity of the antibody. As depicted in Fig. 14.10, HIV-1 p24 antigen in plasma was hybridized to the antibody array in situ, and the bound protein was hybridized to a gold antibody-functionalized nanoparticle probe for signal enhancement. According to the authors, measurable amounts of HIV-1 p24 antigen in plasma obtained from men with less than 50 copies of RNA per ml of plasma (corresponding to 0.025 pg/ml) were achieved, which is evidence that the nanoarray-based assay can exceed the limit of detection of conventional enzyme-linked immunosorbent assay (ELISA)-based immunoassays by more than 1000-fold.

#### 14.4.1.2 Indirect DPN Nanolithography

As mentioned, indirect DPN requires first the immobilization of small organic molecules with high affinity for the biomolecule of interest. Thus, in a second step, the biomolecule can be immobilized onto the organic molecules through specific interactions. Examples of the use of this approach are the use of electrostatic interactions

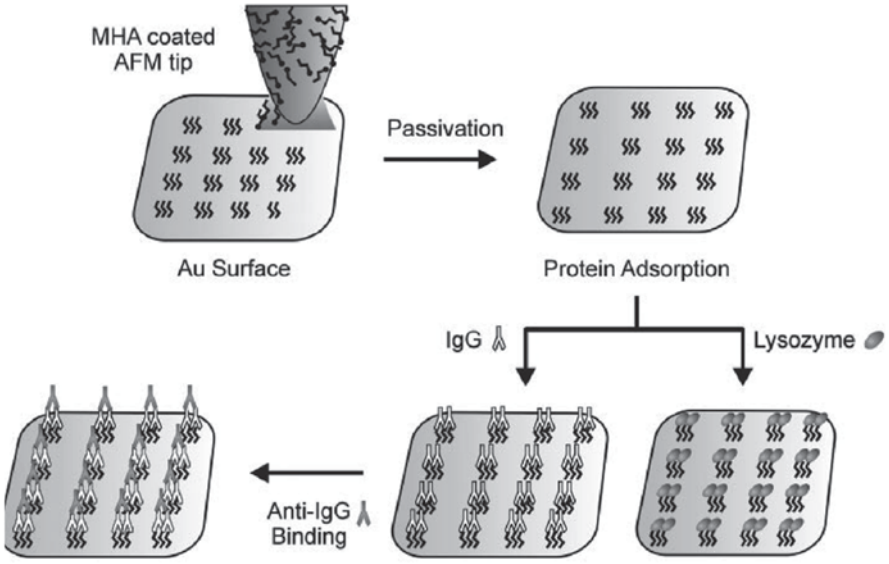


**Fig. 14.11** Diagram of proof-of-concept experiments in which proteins were adsorbed on DPN-generated MHA patterns (1) MHA deposited from AFM tip onto surface, (2) passivation, (3) protein adsorption, (4) antibody recognition. (Reproduced with permission from ref. [105])

that have been successfully exploited to immobilize the negatively charged DNA [102, 103] and negatively charged membrane protein complexes onto protonated amino-terminated nanotemplates generated by DPN [104].

The indirect approach was first employed by Lee and coworkers [105] following the procedure illustrated in Fig. 14.11. In order to fabricate the protein array in a first step, the patterning 16-mercaptohexadecanoic acid (MHA) was carried out on a gold thin-film substrate in the form nanometer-size dots or grids. Then, the areas surrounding these features required to be passivated with 11-mercaptoundecyl-tri(ethylene glycol) by placing a droplet of the surfactant on the patterned area. Finally, the proteins were absorbed on the preformed MHA patterns by immersing the substrate in a solution containing the desired protein. The final pattern is a consequence of the high affinity for carboxylic acid-terminated monolayers at pH 7 and a relatively weak affinity for surfaces coated with 11-mercaptoundecyl-tri(ethylene glycol).

Moreover, this group evaluated the biorecognition capabilities of the nanoarrays by treating the surface with anti-IgG. Their findings show that regardless of the orientations of the IgG within the nanoscopic features, the proper orientation can be adopted under these conditions to react with the anti-IgG in a complex protein solution. Thus, the proteins maintained biological activity after adsorption.

In addition to protein arrays, other groups have been involved in the preparation of DNA nanoarrays by indirect DPN. Nyamjav and Ivanisevic [102, 103], based on the conventional molecular combing technique, succeeded in the preparation of long DNA molecules onto derivatized surfaces with three different shapes: dots,

squares, and lines [106, 107]. For that purpose, they fabricated surface templates composed of positively and negatively charged regions by pattering a polyelectrolyte "ink" (poly(allylamine hydrochloride)—PAH) on $SiO_x$. The affinity of the DNA for the positively charged areas allowed them to deposit the DNA strands on the areas modified with PAH.

The examples above describe employed electrostatic interactions to immobilize biomolecules onto the surface. However, molecular recognition-mediated coupling can be also applied for the same purpose. In this concern, Hyun et al. [93] also described an indirect approach for the fabrication of patterned protein nanostructures with feature sizes of the order of 200 nm based on molecular recognition processes. For that purpose, the authors immobilized first an SAM of 16-mercaptohexadecanoic acid (MHA) onto gold and the unpatterned regions were passivated with a protein-resistant oligoethylene glycol-terminated alkanethiol SAM. The carboxylic functional groups served to, in a following step, anchor covalently an amine-terminated biotin derivative with the chemically activated MHA SAM nanopattern. The authors described also the biorecognition capabilities of the surface by using streptavidin. The surface was incubated with streptavidin to form streptavidin nanostructures, mediated by molecular recognition between biotin and streptavidin. The resulting streptavidin nanopattern provides a universal platform for molecular recognition-mediated protein immobilization because of the ubiquity of biotin-tagged molecules.

### *14.4.2 Biomolecules Deposited by Nanoshaving*

Nanoshaving, involves the precise removal by using an AFM tip of a pre-deposited monolayer. The removed areas can be used in a second step to anchor the desired biomolecule. Thus, in general, nanoshaving is combined with SAMs as nanometer thickness resists indirect immobilization of biomolecules onto surfaces [108].

Nanoshaving was used by Banerjee et al. [109] to direct the assembly of thiolated peptide nanotubes. In their strategy (depicted in Fig. 14.12), 1-octadecanethiol was used as a mask to prevent the nonspecific nanotube attachment and it was first self-assembled on the flat Au substrate. Then, the octadecanethiol SAM was shaved by an $Si_3N_4$ tip, thus, exposing Au regions. After the Au regions were drawn, the substrate was extensively washed. Then, the thiolated nanotubes were attached to the patterned Au pads on the substrate. After these substrates were washed thoroughly, the thiolated nanotube was observed to attach selectively to the Au areas via the thiol–Au interaction.

Following a similar approach in later studies, they extended the concept to the preparation of patterned surfaces based on biological molecular recognition. The authors introduced a new type of building block, antibody nanotubes, and demonstrated anchoring them to complementary antigen arrays via antibody–antigen recognition [110]. The array of antigens was written by nanoshaving the alkylthiol SAM-coated Au substrates using the tip of an AFM. Then, the antigens were immobilized onto the shaved regions of the alkylthiol SAMs with the AFM tip. Finally,

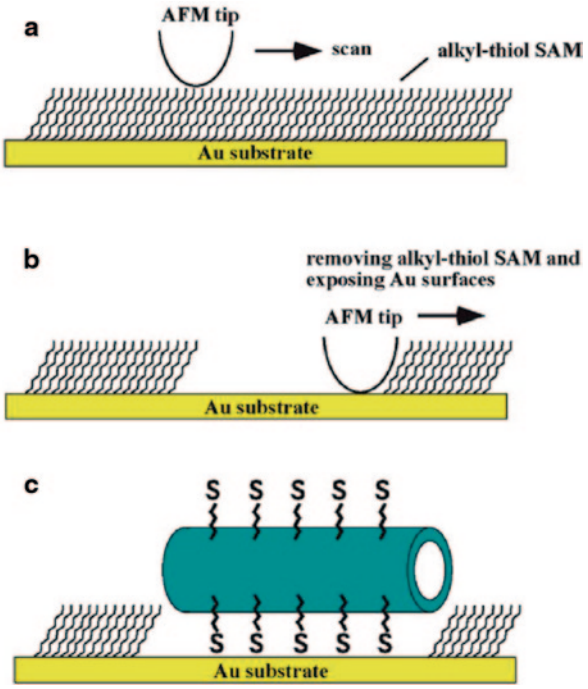


**Fig. 14.12** Schematic diagram of thiolated peptide nanotube assembly on the Au trench arrays. **a** Self-assembly of alkylthiols on Au substrates. **b** Shaving trenches on the alkylthiol SAM by using the AFM tip. **c** Location-specific immobilization of the thiolated peptide nanotube onto the patterned Au trenches. (Reproduced with permission from ref. [109])

the antibody nanotubes were selectively attached onto the antigen regions. Later, to test the feasibility of antibody nanotubes for real applications in device fabrications by assembling them into more complex configurations, they explored the possibility to anchor multiple types of antibody nanotubes onto their respective complementary binding areas. To prove this hypothesis, they anchored selectively two types of nanotubes coated with different antibodies onto their complementary antigen areas, patterned by AFM tips (Fig. 14.13).

### *14.4.3 Biomolecules Deposited by Nanografting*

Nanografting which is, at least to some extent, an extension of the above depicted nanoshaving, has been also extensively employed to create nanometer-size patterns onto SAMs. Similar to dip-pen nanolithography, nanografting can be carried out either using a direct or an indirect strategy. The direct approach involves the immobilization of the biomolecules onto the areas in which the SAM has been removed. This strategy requires the modification of the biomolecules with the appropriate functional groups (typically thiol) to be anchored to the surface. DNA and proteins have been deposited on gold surfaces using direct nanografting.

The indirect nanografting approach is schematically depicted in Fig. 14.14 [1]. By using the AFM tip, molecules anchored to particular positions at the surface are first removed (B). Then, the addition of new molecules can be absorbed on the

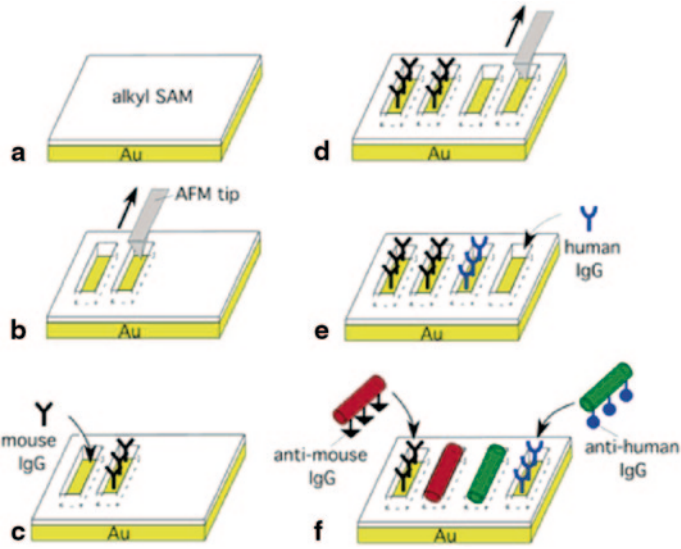


**Fig. 14.13** Schematic diagram to assemble anti-mouse IgG-coated nanotubes and antihuman IgG-coated nanotubes onto their antigen-patterned substrates via biological recognition. **a** Self-assembly of alkylthiol monolayers on Au substrates. **b** Shaving trenches on the alkylthiol SAM by using the AFM tip. **c** Deposition of mouse IgG on the shaved trenches. **d** Shaving another array of trenches on the alkylthiol SAM by using the AFM tip. **e** Deposition of human IgG on the shaved trenches. **f** Location-specific immobilization of Alexa Fluor 546-labeled anti-mouse IgG nanotubes onto the mouse IgG trenches and FITC-labeled antihuman IgG nanotubes onto the human IgG trenches via their biological recognition. (Reproduced with permission from ref. [111])

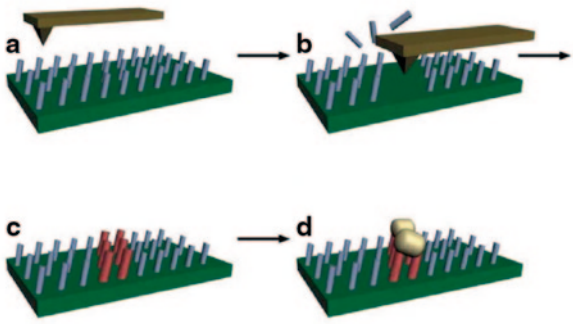


**Fig. 14.14** Schematic of nanografting. An AFM tip is first used to scrape away patterns on an existing protein-resistant SAM *(A–B)*, which are then replaced by new protein-adherent SAM molecules from solution *(C)*. Proteins then adsorb to the grafted patterns *(D)*. (Reproduced with permission from [1])

available areas. The new molecules can have, for instance, affinity for a biomolecule so that the latter can be immobilized in a further step. This approach has been, among others, employed to pattern proteins by partial substitution of a protein-resistant SAM by a protein-adherent SAM.

The direct nanografting approach has been employed by Liu et al. [112] who assessed the application of nanografting in patterning single-stranded DNA (ssDNA).

They demonstrated that both the orientation and packing of the oligonucleotides within the patterns can be directly determined in situ using AFM. More interestingly, in their experiments they evaluated the accessibility of the oligonucleotides within the patterns by using DNase I enzyme digestion.

Proteins have also been deposited on solid surfaces using direct nanografting, typically using gold surfaces by means of thiol–gold interactions. The use of nanografting to pattern proteins was introduced by Liu in 1997. They demonstrated the advantages of this technique that permits, among others, the coupling of a protein to a surface without disturbing its tertiary structure [30]. The basic idea of their work relies on the use an AFM tip to disturb the original molecules (e.g., thiols on gold) from a specified area of a monolayer, thereby enabling different thiol molecules from a contacting solution to self-assemble by diffusion or exchange into the exposed gold sites. This strategy has been later followed by Hu and coworkers [113] and Case et al. [114] to pattern gold surfaces with proteins. Whereas Hu et al. [113] employed parallel three-helix bundle metalloproteins to orient vertically on a gold surface, Case et al. [114] reported the nanografting of de novo four-helix bundle proteins engineered to contain a Gly-Gly-Cys linker at its C-terminus.

Indirect nanografting involves the modification of the SAM monolayer, with other molecules exhibiting either higher or lower affinity by the biomolecules that will be absorbed in a further step. Several groups have employed this alternative to prepare nanopatterns on solid surfaces [30, 50, 115–119]. One of the most illustrative examples has been reported by Zhou et al. [116]. In their work, the authors tested three differently charged nanoscale features prepared by sequential nanografting of 6-mercaptohexan-1-ol, N-(6-mercapto)hexylpyridinium bromide, and 3-mercaptopropionic acid into a SAM. By using these charged/neutral surfaces, they studied the immobilization of three proteins (lysozyme, rabbit IgG, and bovine carbonic anhydrase (II)) onto these differently charged nanopatches as a function of the surface charge, additionally depending on the pH. At pH 4.5, all three proteins adsorbed onto the charged nanosurfaces. At higher pH, the proteins behaved differently, depending on the pH and relative surface charge of the nanosurface. Moreover, they developed an approach (depicted in Fig. 14.15) that combines electrostatic immobilization and specific protein–protein interactions to fabricate multiple layered (protein G/rabbit IgG/anti-IgG) three-dimensional (3D) protein nanostructures, demonstrating that the combination of nanografting, electrostatic immobilization, and specific protein interaction is a powerful tool for construction of novel 3D protein surface nanostructures.

### *14.4.4 Other Alternatives*

In addition, other alternatives to pattern bioactive molecules on planar surfaces have been reported that result from the combination of at least two of the approaches depicted above. As an illustrative example we would like to mention the work of Sun et al. [21] who fabricated of biological nanostructures by scanning near-field

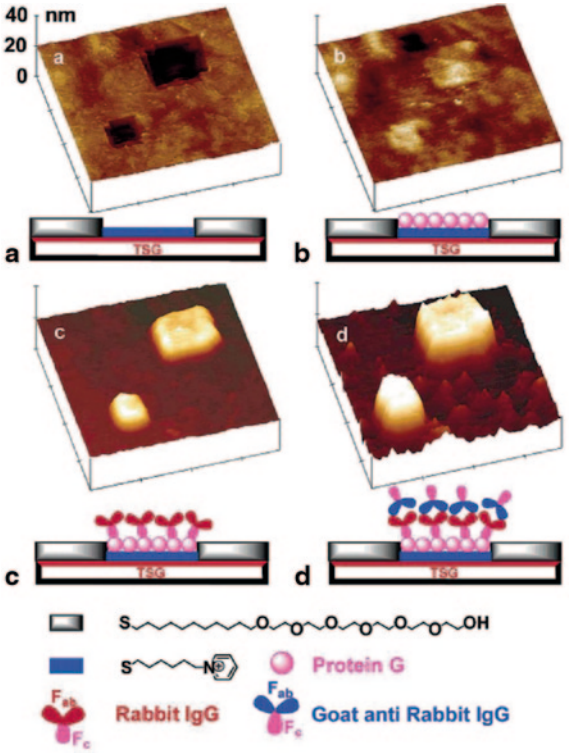


**Fig. 14.15** 3D AFM topographic images and schemes (below) showing the process of creating and growing the 3D protein nanostructures by electrostatic immobilization and biospecific interaction. All of the images have the same scan sizes ($2 \times 2$ μm$^2$) and have the same z-scale. **a** Two nanopatches ($200 \times 200$ and $400 \times 400$ nm$^2$) created by nanografting of MHP into the SAM of $C_{11}EG_6$ had a depth of 2 nm. **b** After incubation of the surface with protein G (0.1 mg/mL in PBS, 20 min), the patches were filled by protein G and transformed into plateaus with an average height of ca. 1 nm. **c** After a treatment of the surface with rabbit IgG (0.1 mg/mL in PBS, 30 min), the height of the protein nanofeatures increased to 8–9 nm. **d** After subsequent treatment of the surface with goat anti-rabbit IgG (0.1 mg/mL in PBS, 30 min), the height of the protein nanofeatures increased to 19–20 nm. (Reproduced with permission from [116])

photolithography of chloromethylphenylsiloxane (CMPS) monolayers. They evidenced that this approach can be applied to other systems, and demonstrated its utility for the fabrication of functional molecular nanostructures (Fig. 14.16). More precisely, the process developed by the authors involved 244-nm exposure of the CMPS SAM to create nanoscale patterns of surface carboxylic acid functional groups. Then, the carboxylic groups were employed to attach different biomolecules by their conversion to the N-hydroxysuccinimidyl ester and reaction of the active ester. According to the authors, the resulting patterns were activated readily under ambient conditions using simple, widely applicable coupling chemistries to facilitate the formation of patterned nanoparticle, protein, and DNA structures.

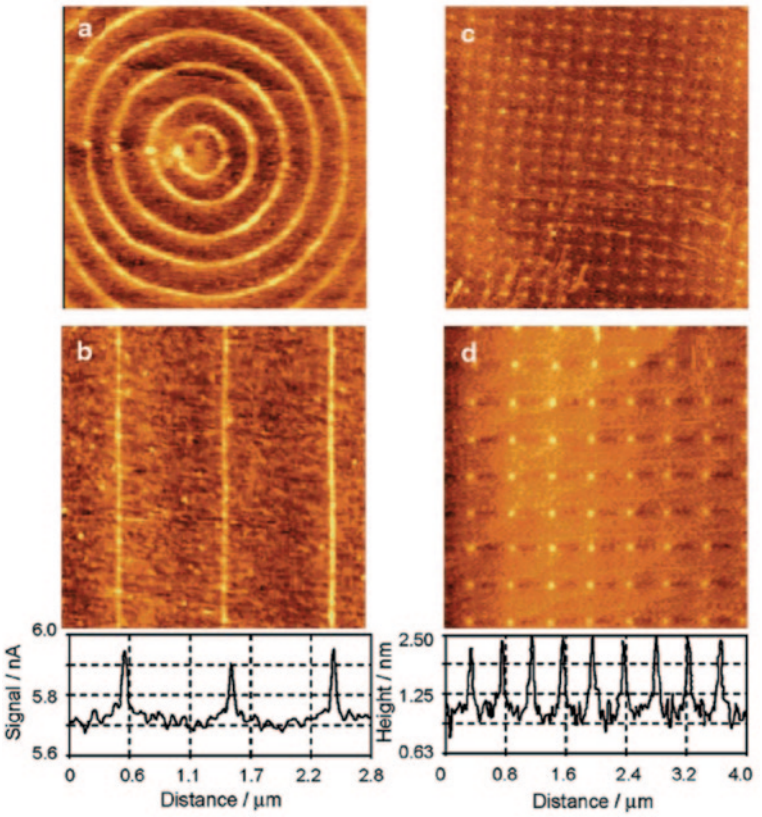


**Fig. 14.16** *Left*: friction force microscopy images of nanopatterns. *Right*: topographical images of nanopatterned surfaces following incubation with calf thymus DNA. Image sizes: **a** $4.0 \times 4.0$ m$^2$; **b** $2.8 \times 2.8$ m$^2$; **c** $8.0 \times 8.0$ m$^2$; **d** $4.0 \times 4.0$ m$^2$. Reproduced with permission from [21]

## 14.5 Summary and Conclusions

In this chapter, we provided a general overview of the scanning probe nanopatterning (SPN) approaches focusing on their capabilities to fabricate biopatterned surfaces. First, we introduced the different approaches developed in order to obtain nanoscale resolution patterns and placed SPN within this context highlighting their advantages and limitations. Then, the basic principles of each technique developed from a common tip-based approach have been discussed. Finally, we selected those approaches that have been employed to a larger extent to pattern biomolecules on surfaces and pay special attention in those cases in which the patterned biomolecule is able to participate in biomolecular recognition processes. In particular, DPN, nanoshaving, and nanografting due to their unique resolution and the possibility to be carried out under ambient conditions have been extensively used to fabricate bio-nanopatterned surfaces. Table 14.3 summarizes the most extended approaches

**Table 14.3** Summary of the biomolecules employed and the highest resolution obtained by using scanning probe lithography and references. (Reproduced with permission from [26])

| | DPN | | Nanoshaving | Nanografting | |
|---|---|---|---|---|---|
| | Indirect | Direct | | Indirect | Direct |
| Patterned biomolecules | DNA, peptides, proteins, virus | DNA, peptides, proteins | Peptides, proteins | Proteins | DNA, proteins |
| Highest resolution | ~85 nm | 30 nm | 150 nm | 10 nm | 10 nm |
| Examples | IgG protein dot features [120] | Collage-like peptide lines [79] | IgG protein lines [111] | Lysozyme protein lines [117, 118] | DNA lines [112, 121] |

to pattern biomolecules by using scanning probe microscopes, highlighting the type of molecule immobilized onto the surface, the highest resolution achieved for each technique, and we gave particular examples.

SPN with their simplicity and unique resolution is currently an interesting tool to study the new properties of materials at the nanoscale. Their range of applications in a variety of fields includes microelectronics, optics, medicine, and biology. In particular, bionanopatterning of surface which is an active field in the biotechnology and nanotechnology interface has been highlighted for its potential applications ranging from molecular diagnostics to fundamental studies in molecular and cell biology [26]. However, in order to enlarge the range of applications, several challenges still need to be resolved including the possibility to pattern multiple biomolecule nanoarrays or the patterning speed.

**Acknowledgments** The author would like to thank the financial support by the MINECO (Projects MAT2010-17016, MAT2013-47902-C2-1-R).

## References

1. Christman KL, Enriquez-Rios VD, Maynard HD. Nanopatterning proteins and peptides. Soft Matter. 2006;2:928–39.
2. Christman KL, Requa MV, Enriquez-Rios VD, Ward SC, Bradley KA, Turner KL, et al. Submicron Streptavidin Patterns for Protein Assembly. Langmuir. 2006;22:7444–50.
3. Silzel JW, Cercek B, Dodson C, Tsay T, Obremski RJ. Mass-sensing, multianalyte microarray immunoassay with imaging detection. Clinical Chemistry. 1998;44:2036–43.
4. Bussow K, Konthur Z, Lueking A, Lehrach H, Walter G. Protein array technology. Potential use in medical diagnostics. American journal of pharmacogenomics: genomics-related research in drug development and clinical practice. 2001;1:37–43.
5. Eickhoff H, Konthur Z, Lueking A, Lehrach H, Walter G, Nordhoff E, et al. Protein array technology: the tool to bridge genomics and proteomics. Advances in biochemical engineering/biotechnology. 2002;77:103–12.
6. Walter G, Bussow K, Lueking A, Glokler J. High-throughput protein arrays: prospects for molecular diagnostics. Trends in Molecular Medicine. 2002;8:250–3.
7. Wilson DS, Nock S. Recent developments in protein microarray technology. Angewandte Chemie-International Edition. 2003;42:494–500.

8. Lee W-K, Sheehan PE. Scanning probe lithography of polymers: Tailoring morphology and functionality at the nanometer scale. Scanning. 2008;30:172–83.
9. Tseng AA, Notargiacomo A, Chen TP. Nanofabrication by scanning probe microscope lithography: A review. Journal of Vacuum Science & Technology B. 2005;23:877–94.
10. Xie Z, Zhou X, Tao X, Zheng Z. Polymer Nanostructures Made by Scanning Probe Lithography: Recent Progress in Material Applications. Macromolecular Rapid Communications. 2012;33:359–73.
11. Groll J, Albrecht K, Gasteier P, Riethmueller S, Ziener U, Moeller M. Nanostructured ordering of fluorescent markers and single proteins on substrates. Chembiochem. 2005;6:1782–7.
12. Valsesia A, Colpo P, Meziani T, Lisboa P, Lejeune M, Rossi F. Immobilization of antibodies on biosensing devices by nanoarrayed self-assembled monolayers. Langmuir. 2006;22:1763–7.
13. Denis FA, Hanarp P, Sutherland DS, Dufrene YF. Nanoscale chemical patterns fabricated by using colloidal lithography and self-assembled monolayers. Langmuir. 2004;20:9335–9.
14. Michel R, Reviakine I, Sutherland D, Fokas C, Csucs G, Danuser G, et al. A novel approach to produce biologically relevant chemical patterns at the nanometer scale: Selective molecular assembly patterning combined with colloidal lithography. Langmuir. 2002;18:8580–6.
15. Cai YG, Ocko BM. Large-scale fabrication of protein nanoarrays based on nanosphere lithography. Langmuir. 2005;21:9274–9.
16. Agheli H, Malmstrom J, Larsson EM, Textor M, Sutherland DS. Large area protein nanopatterning for biological applications. Nano Letters. 2006;6:1165–71.
17. Yan H, Park SH, Finkelstein G, Reif JH, LaBean TH. DNA-templated self-assembly of protein arrays and highly conductive nanowires. Science. 2003;301:1882–4.
18. Park SH, Yin P, Liu Y, Reif JH, LaBean TH, Yan H. Programmable DNA self-assemblies for nanoscale organization of ligands and proteins. Nano Letters. 2005;5:729–33.
19. Lee CS, Baker SE, Marcus MS, Yang WS, Eriksson MA, Hamers RJ. Electrically addressable biomolecular functionalization of carbon nanotube and carbon nanofiber electrodes. Nano Letters. 2004;4:1713–6.
20. Gu JH, Yam CM, Li S, Cai CZ. Nanometric protein arrays on protein-resistant monolayers on silicon surfaces. Journal of the American Chemical Society. 2004;126:8098–9.
21. Sun SQ, Montague M, Critchley K, Chen MS, Dressick WJ, Evans SD, et al. Fabrication of biological nanostructures by scanning near-field photolithography of chloromethylphenylsiloxane monolayers. Nano Letters. 2006;6:29–33.
22. Hoff JD, Cheng LJ, Meyhofer E, Guo LJ, Hunt AJ. Nanoscale protein patterning by imprint lithography. Nano Letters. 2004;4:853–7.
23. Truskett VN, Watts MPC. Trends in imprint lithography for biological applications. Trends in Biotechnology. 2006;24:312–7.
24. Falconnet D, Pasqui D, Park S, Eckert R, Schift H, Gobrecht J, et al. A novel approach to produce protein nanopatterns by combining nanoimprint lithography and molecular self-assembly. Nano Letters. 2004;4:1909–14.
25. Kim DC, Kang DJ. Molecular Recognition and Specific Interactions for Biosensing Applications. Sensors. 2008;8:6605–41.
26. Mendes PM, Yeung CL, Preece JA. Bio-nanopatterning of surfaces. Nanoscale Research Letters. 2007;2:373–84.
27. Sohn LL, Willett RL. Fabrication of nanostructures using atomic-force-microscope-based lithography. Applied Physics Letters. 1995;67:1552–4.
28. Heyde M, Rademann K, Cappella B, Geuss M, Sturm H, Spangenberg T, et al. Dynamic plowing nanolithography on polymethylmethacrylate using an atomic force microscope. Review of Scientific Instruments. 2001;72:136–41.
29. Kunze U, Klehn B. Plowing on the sub-50nm scale: Nanolithography using scanning force microscopy. Advanced Materials. 1999;11:1473–5.
30. Xu S, Liu GY. Nanometer-scale fabrication by simultaneous nanoshaving and molecular self-assembly. Langmuir. 1997;13:127–9.
31. Liu GY, Xu S, Qian YL. Nanofabrication of self-assembled monolayers using scanning probe lithography. Accounts of Chemical Research. 2000;33:457–66.

32. Mamin HJ, Rugar D. THERMOMECHANICAL WRITING WITH AN ATOMIC FORCE MICROSCOPE TIP. Applied Physics Letters. 1992;61:1003–5.
33. Bakbak S, Leech PJ, Carson BE, Saxena S, King WP, Bunz UHF. 1,3-dipolar cycloaddition for the generation of nanostructured semiconductors by heated probe tips. Macromolecules. 2006;39:6793–5.
34. Gotsmann B, Duerig U, Frommer J, Hawker CJ. Exploiting chemical switching in a Diels-Alder polymer for nanoscale probe lithography and data storage. Advanced Functional Materials. 2006;16:1499–505.
35. Szoszkiewicz R, Okada T, Jones SC, Li T-D, King WP, Marder SR, et al. High-speed, sub-15nm feature size thermochemical nanolithography. Nano Letters. 2007;7:1064–9.
36. Lyuksyutov SF, Vaia RA, Paramonov PB, Juhl S, Waterhouse L, Ralich RM, et al. Electrostatic nanolithography in polymers using atomic force microscopy. Nature Materials. 2003;2:468–72.
37. Jegadesan S, Sindhu S, Valiyaveettil S. Easy writing of nanopatterns on a polymer film using electrostatic nanolithography. Small. 2006;2:481–4.
38. Wouters D, Hoeppener S, Schubert US. Local Probe Oxidation of Self-Assembled Monolayers: Templates for the Assembly of Functional Nanostructures. Angewandte Chemie-International Edition. 2009;48:1732–9.
39. Jang SY, Marquez M, Sotzing GA. Rapid direct nanowriting of conductive polymer via electrochemical oxidative nanolithography. Journal of the American Chemical Society. 2004;126:9476–7.
40. Jagadesan S, Advincula RC, Valiyaveettil S. Nanolithographic electropolymerization of a precursor polymer film to form conducting nanopatterns. Advanced Materials. 2005;17:1282- +.
41. Wegscheider S, Kirsch A, Mlynek J, Krausch G. SCANNING NEAR-FIELD OPTICAL LITHOGRAPHY. Thin Solid Films. 1995;264:264–7.
42. Naber A, Kock H, Fuchs H. High-resolution lithography with near-field optical microscopy. Scanning. 1996;18:567–71.
43. Sun SQ, Chong KSL, Leggett GJ. Nanoscale molecular patterns fabricated by using scanning near-field optical lithography. Journal of the American Chemical Society. 2002;124:2414–5.
44. Piner RD, Zhu J, Xu F, Hong SH, Mirkin CA. "Dip-pen" nanolithography. Science. 1999;283:661–3.
45. Zhang H, Chung SW, Mirkin CA. Fabrication of sub-50-nm solid-state nanostructures on the basis of dip-pen nanolithography. Nano Letters. 2003;3:43–5.
46. Amro NA, Xu S, Liu GY. Patterning surfaces using tip-directed displacement and self-assembly. Langmuir. 2000;16:3006–9.
47. Sheehan PE, Whitman LJ, King WP, Nelson BA. Nanoscale deposition of solid inks via thermal dip pen nanolithography. Applied Physics Letters. 2004;85:1589–91.
48. Maynor BW, Filocamo SF, Grinstaff MW, Liu J. Direct-writing of polymer nanostructures: Poly(thiophene) nanowires on semiconducting and insulating surfaces. Journal of the American Chemical Society. 2002;124:522–3.
49. Xu S, Laibinis PE, Liu GY. Accelerating the kinetics of thiol self-assembly on gold—A spatial confinement effect. Journal of the American Chemical Society. 1998;120:9356–61.
50. Xu S, Miller S, Laibinis PE, Liu GY. Fabrication of nanometer scale patterns within self-assembled monolayers by nanografting. Langmuir. 1999;15:7244–51.
51. Mamin HJ, Terris BD, Fan LS, Hoen S, Barrett RC, Rugar D. High-density data storage using proximal probe techniques. Ibm Journal of Research and Development. 1995;39:681–99.
52. Vettiger P, Cross G, Despont M, Drechsler U, Durig U, Gotsmann B, et al. The "millipede"—Nanotechnology entering data storage. IEEE Transactions on Nanotechnology. 2002;1:39–55.
53. Dryakhlushin VF, Klimov AY, Rogov VV, Shashkin VI, Sukhodoev LV, Volgunov DG, et al. Development of contact scanning probe lithography methods for the fabrication of lateral nano-dimensional elements. Nanotechnology. 2000;11:188–91.
54. Bae JH, Ono T, Esashi M. Scanning probe with an integrated diamond heater element for nanolithography. Applied Physics Letters. 2003;82:814–6.

55. Gotsmann B, Duerig U. Nano-thermomechanics: Fundamentals and application in data storage devices. Applied Scanning Probe Methods Iv: Industrial Applications. 2006:215–49.
56. Lantz MA, Gotsmann B, Durig UT, Vettiger P, Nakayama Y, Shimizu T, et al. Carbon nanotube tips for thermomechanical data storage. Applied Physics Letters. 2003;83:1266–8.
57. Herminghaus S. Dynamical instability of thin liquid films between conducting media. Physical Review Letters. 1999;83:2359–61.
58. Schaffer E, Thurn-Albrecht T, Russell TP, Steiner U. Electrically induced structure formation and pattern transfer. Nature. 2000;403:874–7.
59. Maoz R, Frydman E, Cohen SR, Sagiv J. Constructive nanolithography: Site-defined silver self-assembly on nanoelectrochemically patterned monolayer templates. Advanced Materials. 2000;12:424- +.
60. Maoz R, Frydman E, Cohen SR, Sagiv J. "Constructive nanolithography": Inert monolayers as patternable templates for in-situ nanofabrication of metal-semiconductor-organic surface structures—A generic approach. Advanced Materials. 2000;12:725- +.
61. Maoz R, Cohen SR, Sagiv J. Nanoelectrochemical patterning of monolayer surfaces: Toward spatially defined self-assembly of nanostructures. Advanced Materials. 1999;11:55–61.
62. Hoeppener S, Maoz R, Sagiv J. Constructive microlithography: Electrochemical printing of monolayer template patterns extends constructive nanolithography to the micrometer-millimeter dimension range. Nano Letters. 2003;3:761–7.
63. Dunn RC. Near-field scanning optical microscopy. Chemical Reviews. 1999;99:2891- +.
64. Xie XN, Chung HJ, Sow CH, Wee ATS. Nanoscale materials patterning and engineering by atomic force microscopy nanolithography. Materials Science and Engineering: R: Reports. 2006;54:1–48.
65. Ginger DS, Zhang H, Mirkin CA. The evolution of dip-pen nanolithography. Angewandte Chemie-International Edition. 2004;43:30–45.
66. Salaita K, Wang Y, Mirkin CA. Applications of dip-pen nanolithography. Nature Nanotechnology. 2007;2:145–55.
67. Tseng AA, Jou S, Notargiacomo A, Chen TP. Recent developments in tip-based nanofabrication and its roadmap. Journal of Nanoscience and Nanotechnology. 2008;8:2167–86.
68. Lee M, Kang DK, Yang HK, Park KH, Choe SY, Kang C, et al. Protein nanoarray on Prolinker ™ surface constructed by atomic force microscopy dip-pen nanolithography for analysis of protein interaction. Proteomics. 2006;6:1094–103.
69. Vega RA, Shen CKF, Maspoch D, Robach JG, Lamb RA, Mirkin CA. Monitoring single-cell infectivity from virus-particle nanoarrays fabricated by parallel dip-pen nanotithography. Small. 2007;3:1482–5.
70. Niemeyer CM, Mirkin CA. Nanobiotechnology: Concepts, Applications and Perspectives: Wiley; 2004.
71. Kambhampati D. Protein Microarray Technology: Wiley; 2006.
72. Zheng GF, Patolsky F, Cui Y, Wang WU, Lieber CM. Multiplexed electrical detection of cancer markers with nanowire sensor arrays. Nature Biotechnology. 2005;23:1294–301.
73. Shekhawat G, Tark SH, Dravid VP. MOSFET-embedded microcantilevers for measuring deflection in biomolecular sensors. Science. 2006;311:1592–5.
74. Cui Y, Wei QQ, Park HK, Lieber CM. Nanowire nanosensors for highly sensitive and selective detection of biological and chemical species. Science. 2001;293:1289–92.
75. Demidov VV. Nanobiosensors and molecular diagnostics: a promising partnership. Expert Review of Molecular Diagnostics. 2004;4:267–8.
76. Bernard A, Renault JP, Michel B, Bosshard HR, Delamarche E. Microcontact Printing of Proteins. Advanced Materials. 2000;12:1067–70.
77. Hovis JS, Boxer SG. Patterning Barriers to Lateral Diffusion in Supported Lipid Bilayer Membranes by Blotting and Stamping. Langmuir. 2000;16:894–7.
78. Tarlov MJ, Burgess DRF, Gillen G. UV photopatterning of alkanethiolate monolayers self-assembled on gold and silver. Journal of the American Chemical Society. 1993;115:5305–6.

79. Wilson DL, Martin R, Hong S, Cronin-Golomb M, Mirkin CA, Kaplan DL. Surface organization and nanopatterning of collagen by dip-pen nanolithography. Proceedings of the National Academy of Sciences of the United States of America. 2001;98:13660–4.
80. Lee K-B, Lim J-H, Mirkin CA. Protein Nanostructures Formed via Direct-Write Dip-Pen Nanolithography. Journal of the American Chemical Society. 2003;125:5588–9.
81. Vengasandra SG, Lynch M, Xu JT, Henderson E. Microfluidic ultramicroscale deposition and patterning of quantum dots. Nanotechnology. 2005;16:2052–5.
82. Belaubre P, Guirardel M, Leberre V, Pourciel JB, Bergaud C. Cantilever-based microsystem for contact and non-contact deposition of picoliter biological samples. Sensors and Actuators a-Physical. 2004;110:130–5.
83. Belaubre P, Guirardel M, Garcia G, Pourciel JB, Leberre V, Dagkessamanskaia A, et al. Fabrication of biological microarrays using microcantilevers. Applied Physics Letters. 2003;82:3122–4.
84. Rodolfa KT, Bruckbauer A, Zhou DJ, Schevchuk AI, Korchev YE, Klenerman D. Nanoscale pipetting for controlled chemistry in small arrayed water droplets using a double-barrel pipet. Nano Letters. 2006;6:252–7.
85. Kim KH, Moldovan N, Ke C, Espinosa HD, Xiao X, Carlisle JA, et al. Novel ultrananocrystalline diamond probes for high-resolution low-wear nanolithographic techniques (vol 1, pg 866, 2005). Small. 2005;1:912-.
86. Kim K-H, Sanedrin RG, Ho AM, Lee SW, Moldovan N, Mirkin CA, et al. Direct delivery and submicrometer Patterning of DNA by a nanofountain probe. Advanced Materials. 2008;20:330- +.
87. Hong SH, Zhu J, Mirkin CA. Multiple ink nanolithography: Toward a multiple-pen nanoplotter. Science. 1999;286:523–5.
88. Wu C-C, Reinhoudt DN, Otto C, Subramaniam V, Velders AH. Strategies for Patterning Biomolecules with Dip-Pen Nanolithography. Small. 2011;7:989–1002.
89. Smith JC, Lee K-B, Wang Q, Finn MG, Johnson JE, Mrksich M, et al. Nanopatterning the Chemospecific Immobilization of Cowpea Mosaic Virus Capsid. Nano Letters. 2003;3: 883–6.
90. Noy A, Miller AE, Klare JE, Weeks BL, Woods BW, DeYoreo JJ. Fabrication of luminescent nanostructures and polymer nanowires using dip-pen nanolithography. Nano Letters. 2002;2:109–12.
91. Demers LM, Ginger DS, Park SJ, Li Z, Chung SW, Mirkin CA. Direct patterning of modified oligonucleotides on metals and insulators by dip-pen nanolithography. Science. 2002;296:1836–8.
92. Jung H, Kulkarni R, Collier CP. Dip-Pen Nanolithography of Reactive Alkoxysilanes on Glass. Journal of the American Chemical Society. 2003;125:12096–7.
93. Hyun J, Ahn SJ, Lee WK, Chilkoti A, Zauscher S. Molecular Recognition-Mediated Fabrication of Protein Nanostructures by Dip-Pen Lithography. Nano Letters. 2002;2:1203–7.
94. Hyun J, Kim J, Craig SL, Chilkoti A. Enzymatic nanolithography of a self-assembled oligonucleotide monolayer on gold. Journal of the American Chemical Society. 2004;126:4770–1.
95. Agarwal G, Sowards LA, Naik RR, Stone MO. Dip-pen nanolithography in tapping mode. Journal of the American Chemical Society. 2003;125:580–3.
96. Agarwal G, Naik RR, Stone MO. Immobilization of histidine-tagged proteins on nickel by electrochemical dip pen nanolithography. Journal of the American Chemical Society. 2003;125:7408–12.
97. Schulze A, Downward J. Navigating gene expression using microarrays—a technology review. Nature Cell Biology. 2001;3:E190–E5.
98. Kato-Maeda M, Gao Q, Small PM. Microarray analysis of pathogens and their interaction with hosts. Cellular Microbiology. 2001;3:713–9.
99. Marciano PG, Eberwine JH, Raghupathi R, McIntosh TK. The assessment of genomic alterations using DNA arrays following traumatic brain injury: a review. Restorative Neurology and Neuroscience. 2001;18:105–13.

100. Bier FF, Kleinjung F. Feature-size limitations of microarray technology—a critical review. Fresenius Journal of Analytical Chemistry. 2001;371:151–6.
101. Lee K-B, Kim E-Y, Mirkin CA, Wolinsky SM. The Use of Nanoarrays for Highly Sensitive and Selective Detection of Human Immunodeficiency Virus Type 1in Plasma. Nano Letters. 2004;4:1869–72.
102. Nyamjav D, Ivanisevic A. Alignment of long DNA molecules on templates generated via dip-pen nanolithography. Advanced Materials. 2003;15:1805–9.
103. Nyamjav D, Ivanisevic A. Templates for DNA-templated Fe3O4 nanoparticles. Biomaterials. 2005;26:2749–57.
104. Valiokas R, Vaitekonis A, Klenkar G, Trinkunas G, Liedberg B. Selective recruitment of membrane protein complexes onto gold substrates patterned by dip-pen nanolithography. Langmuir. 2006;22:3456–60.
105. Lee KB, Park SJ, Mirkin CA, Smith JC, Mrksich M. Protein nanoarrays generated by dip-pen nanolithography. Science. 2002;295:1702–5.
106. Woolley AT, Kelly RT. Deposition and characterization of extended single-stranded DNA molecules on surfaces. Nano Letters. 2001;1:345–8.
107. Monson CF, Woolley AT. DNA-templated construction of copper nanowires. Nano Letters. 2003;3:359–63.
108. Kaholek M, Lee WK, LaMattina B, Caster KC, Zauscher S. Fabrication of stimulus-responsive nanopatterned polymer brushes by scanning-probe lithography. Nano Letters. 2004;4:373–6.
109. Banerjee IA, Yu LT, MacCuspie RI, Matsui H. Thiolated peptide nanotube assembly as arrays on patterned Au substrates. Nano Letters. 2004;4:2437–40.
110. Nuraje N, Banerjee IA, MacCuspie RI, Yu LT, Matsui H. Biological bottom-up assembly of antibody nanotubes on patterned antigen arrays. Journal of the American Chemical Society. 2004;126:8088–9.
111. Zhao ZY, Banerjee PA, Matsui H. Simultaneous targeted immobilization of anti-human IgG-coated nanotubes and anti-mouse IgG-coated nanotubes on the complementary antigen-patterned surfaces via biological molecular recognition. Journal of the American Chemical Society. 2005;127:8930–1.
112. Liu M, Amro N, Chow C, Liu G-y. Production of Nanostructures of DNA on Surfaces. Nano letters. 2002;2:863–7.
113. Hu Y, Das A, Hecht MH, Scoles G. Nanografting de novo proteins onto gold surfaces. Langmuir. 2005;21:9103–9.
114. Case MA, McLendon GL, Hu Y, Vanderlick TK, Scoles G. Using nanografting to achieve directed assembly of de novo designed metalloproteins on gold. Nano Letters. 2003;3:425–9.
115. Kenseth JR, Harnisch JA, Jones VW, Porter MD. Investigation of approaches for the fabrication of protein patterns by scanning probe lithography. Langmuir. 2001;17:4105–12.
116. Zhou DJ, Wang XZ, Birch L, Rayment T, Abell C. AFM study on protein immobilization on charged surfaces at the nanoscale: Toward the fabrication of three-dimensional protein nanostructures. Langmuir. 2003;19:10557–62.
117. Wadu-Mesthrige K, Xu S, Amro NA, Liu GY. Fabrication and imaging of nanometer-sized protein patterns. Langmuir. 1999;15:8580–3.
118. Wadu-Mesthrige K, Amro NA, Garno JC, Xu S, Liu GY. Fabrication of nanometer-sized protein patterns using atomic force microscopy and selective immobilization. Biophys J. 2001;80:1891–9.
119. Liu GY, Amro NA. Positioning protein molecules on surfaces: A nanoengineering approach to supramolecular chemistry. Proceedings of the National Academy of Sciences of the United States of America. 2002;99:5165–70.
120. Lee KB, Kim EY, Mirkin CA, Wolinsky SM. The use of nanoarrays for highly sensitive and selective detection of human immunodeficiency virus type 1in plasma. Nano Letters. 2004;4:1869–72.
121. Liu MZ, Amro NA, Chow CS, Liu GY. Production of nanostructures of DNA on surfaces. Nano Letters. 2002;2:863–7.

# Chapter 15
# Selective Biorecognition on Polymer Surfaces: Remarks and Future Trends

**Juan Rodríguez-Hernández and Aitziber L. Cortajarena**

In spite of the limitations in comparison with natural occurring recognition processes, chemists, physicists and biologists have been extensively involved in the design of platforms that take advantage of well-known particular biorecognition processes in order to employ them for multitude of applications. These include a broad range of fields ranging from the design and fabrication of micro/nanosensors by immobilizing proteins and DNA to other such as drug screening, tissue engineering or proteomics research.

This book covered selected examples of the most recent advances concerning the immobilization of bioactive molecules highlighting their role as intermediates in biorecognition processes. These latest developments have overcome serious drawbacks from precedent works in the field. However, it is worth to mention and present some issues that still remain challenging.

A primary challenge in developing biorecognition surfaces is the design of biorecognition layers that possess the desirable properties of biocompatibility, stability, and binding specificity and reversibility. For instance, performing reliable label-free biosensing in real-world samples requires a surface chemistry platform that combines high binding capacity with preservation of the specificity and activity of the biorecognition elements (e.g. antibodies or DNA) [1].

The large number of desirable characteristics required for such an interface entails the elaboration of sophisticated materials in which the topography, the chemistry and the surface distribution of the later need a thorough control. Technological advances permit now the elaboration of surfaces with nano- and micro-structured

J. Rodríguez-Hernández (✉)
Department of Chemistry and Properties of Polymers, Institute of Polymer Science and Technology (ICTP-CSIC), Juan de la Cierva 3, 28006 Madrid, Spain
e-mail: rodriguez@ictp.csic.es

A. L. Cortajarena
Instituto Madrileño de Estudios Avanzados en Nanociencia (IMDEA-Nanociencia), CNB-CSIC-IMDEA Nanociencia Associated Unit "Unidad de Nanobiotecnología", 28049 Cantoblanco, Madrid, Spain
e-mail: aitziber.lopezcortajarena@imdea.org



J. Rodríguez-Hernández, A. L. Cortajarena (eds.), *Design of Polymeric Platforms for Selective Biorecognition,* DOI 10.1007/978-3-319-17061-9_15

domains and also the variation of the chemical composition of such structures. However, in order to approach the high complexity existing in living systems the combination of nano- and microstructures and the possibility to include several functionalities appears to be crucial. Designing robust and reliable surface platforms that meet the aforementioned properties and allow their use for various biorecognition elements and samples continues to be one of the major challenges for further development, for instance, of analytical biosensors.

The recent technological advances, both in instrumentation and surface structural and chemical characterization, together with the latest progresses in macromolecular engineering have enabled the preparation of biomolecule surface patterns with nanometer scale resolution. The ability to site-specifically patterned biomolecules with spatial resolution achieving the single protein level is a key challenge for biophysical cell studies, microarray analytics, tissue engineering, therapeutics and high-density biosensor applications [2]. In addition, particular interest has been highlighted towards understanding fundamental concepts of biorecognition processes at the molecular level in biological systems. In nature, many biological interactions rely on the specific placement of single biomolecules or small clusters of biomolecules exhibiting features in the sub-50 nm regime to dictate and direct complex processes. Biorecognition platforms can be used to get insight into the function of complex biomolecular machines [3, 4].

Biorecognition at surfaces and in particular on polymeric surfaces is a research area that in spite of the extensive current interest is still in its infancy. Several aspects remains not completely understood. For instance, how the surface might affect the structure of the biomolecules, the ligand mass transport, the binding kinetics and, therefore, the recognition process compared to the recognition in solution are aspects that require further studies. Another key point is the selection of the recognition systems to be employed. The application of surface with biorecognition capabilities is limited by the existence of target analytes that could be prepared by separation, purification that in turn requires efficient preparation protocols [5]. Nowadays, scientists generally apply mostly solid commercially available biorecognition molecules such as biotin–streptavidin, or antibodies. However, there are many biorecognition systems that can be tailored with optimized properties for different applications. The development of research fields such as protein engineering, will make other recognition systems widely available.

## 15.1 Tendencies

Among the extensive current research several aspects can be highlighted that may set the path for the near future developments.

The current need of rapid, robust and inexpensive methods for sensing and diagnostic purposes has focused the attention of researchers on the development of new molecular recognition probes among others for sensing applications. Within this context for example, aptamers are excellent candidates from several points of

view. First of all, aptamer generation has been achieved for a wide variety of targets including small molecules, proteins, viruses and cells. In addition, variable experimental conditions other than the physiological can be employed so that salt conditions, temperature or pH can be varied and still preserve their biorecognition capability. In many biological molecules, changes on the pH, temperature or ionic strength might lead to an irreversible denaturation of the biomolecule. Aptamers hold promise as an attractive alternative to other molecular recognition elements, such as antibodies.

On the other hand focusing on proteins, the most extended biorecogniton domains, there is a great challenge in the protein engineering field in order to design novel recognition domains and fine-tune the structure, stability and binding properties of these modules. We have shown the state of the art research and how new proteins with recognition functions can be generated. The advances on this field towards a full control of the design and molecular recognition and the bioinspired engineering of biomolecules with tailored properties will open the door to any potential application. There is a need not only for the development of the field but also for the translation of the current advances in protein design into other areas of research and technology to make novel optimized molecules available for technological applications.

Finally, the growth of multidisciplinary research teams will open the door to extend the use of more sophisticated recognition systems in a broader number of applications. The combination of state of the art techniques for both the production of patterned polymeric platforms and the engineering of biomolecular biorecognition, emerges as the path for the smart design of advanced biorecognition platforms.

In summary, biorecognition at surfaces and in particular using polymeric platforms is a growing field with a large number of current applications and emerging ones. The technology that allows the fabrication of biorecognition platforms has greatly advanced in recent years, as reviewed in this book. The integration of recent developments from diverse research fields is the current challenge and will clearly be valuable for ensuring the translation of this research into advanced devices.

## References

1. Vaisocherova, H., et al., *Functionalized ultra-low fouling carboxy- and hydroxy-functional surface platforms: functionalization capacity, biorecognition capability and resistance to fouling from undiluted biological media*. Biosensors & Bioelectronics, 2014. **51**: p. 150–157.
2. Tran, H., K.L. Killops, and L.M. Campos, *Advancements and challenges of patterning biomolecules with sub-50 nm features*. Soft Matter, 2013. **9**(29): p. 6578–6586.
3. Otten, M., et al., *From genes to protein mechanics on a chip*. Nature Methods, 2014. **11**(11): p. 1127–1130.
4. Mertens, J., et al., *Stepwise motion of a microcantilever driven by the hydrolysis of viral ATPases*. Nanotechnology, 2012. **23**(1).
5. Castillo, J., et al., *Biosensors for life quality—Design, development and applications*. Sensors and Actuators B-Chemical, 2004. **102**(2): p. 179–194.